frontiers | Research Topics

55th Anniversary of Ivan Barnes: Microbial communities of serpentinite-hosted ecosystems

Edited by
Nancy Merino, Shino Suzuki, Marianne Quéméneur, Gaël Erauso and Penny Lea Morrill

Published in
Frontiers in Microbiology

ISSN 1664-8714
ISBN 978-2-8325-4459-4
DOI 10.3389/978-2-8325-4459-4

About Frontiers

Frontiers is more than just an open access publisher of scholarly articles: it is a pioneering approach to the world of academia, radically improving the way scholarly research is managed. The grand vision of Frontiers is a world where all people have an equal opportunity to seek, share and generate knowledge. Frontiers provides immediate and permanent online open access to all its publications, but this alone is not enough to realize our grand goals.

Frontiers journal series

The Frontiers journal series is a multi-tier and interdisciplinary set of open-access, online journals, promising a paradigm shift from the current review, selection and dissemination processes in academic publishing. All Frontiers journals are driven by researchers for researchers; therefore, they constitute a service to the scholarly community. At the same time, the *Frontiers journal series* operates on a revolutionary invention, the tiered publishing system, initially addressing specific communities of scholars, and gradually climbing up to broader public understanding, thus serving the interests of the lay society, too.

Dedication to quality

Each Frontiers article is a landmark of the highest quality, thanks to genuinely collaborative interactions between authors and review editors, who include some of the world's best academicians. Research must be certified by peers before entering a stream of knowledge that may eventually reach the public - and shape society; therefore, Frontiers only applies the most rigorous and unbiased reviews. Frontiers revolutionizes research publishing by freely delivering the most outstanding research, evaluated with no bias from both the academic and social point of view. By applying the most advanced information technologies, Frontiers is catapulting scholarly publishing into a new generation.

What are Frontiers Research Topics?

Frontiers Research Topics are very popular trademarks of the *Frontiers journals series*: they are collections of at least ten articles, all centered on a particular subject. With their unique mix of varied contributions from Original Research to Review Articles, Frontiers Research Topics unify the most influential researchers, the latest key findings and historical advances in a hot research area.

Find out more on how to host your own Frontiers Research Topic or contribute to one as an author by contacting the Frontiers editorial office: frontiersin.org/about/contact

55th Anniversary of Ivan Barnes: Microbial communities of serpentinite-hosted ecosystems

Topic editors

Nancy Merino — Physical and Life Sciences Directorate, Lawrence Livermore National Laboratory (DOE), United States

Shino Suzuki — Institute of Space and Astronautical Science, Japan Aerospace Exploration Agency, Japan

Marianne Quéméneur — UMR7294 Institut Méditerranéen d'océanographie (MIO), France

Gaël Erauso — Aix-Marseille Université, France

Penny Lea Morrill — Memorial University of Newfoundland, Canada

Citation

Merino, N., Suzuki, S., Quéméneur, M., Erauso, G., Morrill, P. L., eds. (2024). *55th Anniversary of Ivan Barnes: Microbial communities of serpentinite-hosted ecosystems*. Lausanne: Frontiers Media SA. doi: 10.3389/978-2-8325-4459-4

Table of contents

frontiers | Frontiers in Microbiology

TYPE Original Research
PUBLISHED 09 March 2023
DOI 10.3389/fmicb.2023.1093372

OPEN ACCESS

EDITED BY
Penny Lea Morrill,
Memorial University of Newfoundland, Canada

REVIEWED BY
Mark Alexander Lever,
The University of Texas at Austin, United States
Jeffrey M. Dick,
Central South University, China

*CORRESPONDENCE
Lauren M. Seyler
✉ auren.seyler@stockton.edu

SPECIALTY SECTION
This article was submitted to Frontiers in Microbiology Microbiological Chemistry and Geomicrobiology, a section of the journal Frontiers in Microbiology

RECEIVED 08 November 2022
ACCEPTED 23 January 2023
PUBLISHED 09 March 2023

CITATION
Seyler LM, Kraus EA, McLean C, Spear JR, Templeton AS and Schrenk MO (2023) An untargeted exometabolomics approach to characterize dissolved organic matter in groundwater of the Samail Ophiolite. *Front. Microbiol.* 14:1093372. doi: 10.3389/fmicb.2023.1093372

An untargeted exometabolomics approach to characterize dissolved organic matter in groundwater of the Samail Ophiolite

Lauren M. Seyler[1,2,3]*, Emily A. Kraus[4,5], Craig McLean[6], John R. Spear[4], Alexis S. Templeton[7] and Matthew O. Schrenk[1,8]

[1]Department of Earth and Environmental Sciences, Michigan State University, East Lansing, MI, United States, [2]Biology Program, School of Natural Sciences and Mathematics, Stockton University, Galloway, NJ, United States, [3]Blue Marble Space Institute of Science, Seattle, WA, United States, [4]Department of Civil and Environmental Engineering, Colorado School of Mines, Golden, CO, United States, [5]Department of Environmental Engineering, University of Colorado, Boulder, Boulder, CO, United States, [6]Massachusetts Institute of Technology, Cambridge, MA, United States, [7]Department of Geological Sciences, University of Colorado, Boulder, Boulder, CO, United States, [8]Department of Microbiology and Molecular Genetics, Michigan State University, East Lansing, MI, United States

The process of serpentinization supports life on Earth and gives rise to the habitability of other worlds in our Solar System. While numerous studies have provided clues to the survival strategies of microbial communities in serpentinizing environments on the modern Earth, characterizing microbial activity in such environments remains challenging due to low biomass and extreme conditions. Here, we used an untargeted metabolomics approach to characterize dissolved organic matter in groundwater in the Samail Ophiolite, the largest and best characterized example of actively serpentinizing uplifted ocean crust and mantle. We found that dissolved organic matter composition is strongly correlated with both fluid type and microbial community composition, and that the fluids that were most influenced by serpentinization contained the greatest number of unique compounds, none of which could be identified using the current metabolite databases. Using metabolomics in conjunction with metagenomic data, we detected numerous products and intermediates of microbial metabolic processes and identified potential biosignatures of microbial activity, including pigments, porphyrins, quinones, fatty acids, and metabolites involved in methanogenesis. Metabolomics techniques like the ones used in this study may be used to further our understanding of life in serpentinizing environments, and aid in the identification of biosignatures that can be used to search for life in serpentinizing systems on other worlds.

KEYWORDS

metabolomics, serpentinization, metagenomics, DOM, alkaliphiles, methanogenesis, biosignatures

Introduction

Serpentinization is the geochemical process by which ultramafic rock reacts with water, resulting in the production of serpentine minerals and hydrogen gas (H_2) (Sleep et al., 2004). High concentrations of H_2 can further drive the reduction of dissolved inorganic carbon (DIC) to reduced carbon compounds including formate, methane, and carbon monoxide (McCollom and Seewald, 2001; Charlou et al., 2002; Proskurowski et al., 2008; McCollom, 2013). Chemolithotrophic microorganisms are able to use the products of these reactions as sources of carbon and reducing power (Schrenk et al., 2004, 2013; McCollom, 2007; Amend et al., 2011; Brazelton et al., 2011, 2012, 2013; Lang et al., 2012; Cardace et al., 2015). Serpentinization may be a widespread process in other locations in our solar system, including the subsurface of Mars, Enceladus, and Europa, making it a potential source of chemical disequilibria that may be harnessed by extraterrestrial life (Schulte et al., 2006; Vance et al., 2007; Klein et al., 2019; McCollom et al., 2022). Environments associated with serpentinization host microbial communities capable of a variety of metabolic strategies, including methanogenesis (Miller et al., 2016; Brazelton et al., 2017; Rempfert et al., 2017; Fones et al., 2019; Kraus et al., 2021), methane oxidation (Miller et al., 2016; Brazelton et al., 2017; Seyler L. M. et al., 2020; Kraus et al., 2021), acetogenesis (Brazelton et al., 2012; Rempfert et al., 2017; Suzuki et al., 2018; Fones et al., 2019; Seyler L. M. et al., 2020; Coleman et al., 2022), and sulfate reduction (Sabuda et al., 2020; Glombitza et al., 2021; Nothaft et al., 2021; Templeton et al., 2021). However, the highly alkaline conditions resulting from the serpentinization reaction, coupled with the precipitation of available DIC to calcite at high pH (Barnes et al., 1978), creates a challenging environment for microbial life (Schrenk et al., 2013). The physiological strategies used by microbial communities to overcome these challenges are not well understood.

Metabolomics is a rapidly advancing tool in the field of microbial ecology (Bauermeister et al., 2021; Oyedeji et al., 2021; van Santen et al., 2021). The detection and annotation of metabolites using mass spectrometry has allowed researchers to demonstrate the existence of complete metabolic pathways not commonly detected by genome annotation (Tang et al., 2009), to describe the function of theoretical pathways (Peyraud et al., 2009), and to discover entirely novel pathways (Fürch et al., 2009; Liu et al., 2016). When integrated with other -omics approaches, including metagenomics and metatranscriptomics, metabolomics is a powerful tool for describing metabolic activity in microbial communities (Turnbaugh and Gordon, 2008; Beale et al., 2016; Porcar et al., 2018). Metabolomic profiling of microbial communities in extreme (e.g., hyperalkaline) environments can assist in understanding the metabolic pathways used by microbial communities to adapt to extreme conditions, and the mechanisms and degree to which metabolites may be preserved under these conditions (Blachowicz et al., 2019). Metabolomics thus holds great potential in the search for biomarkers with astrobiological applications (Seyler L. et al., 2020).

The extracellular mixture of compounds that constitutes the dissolved organic matter pool contains growth factors, substrates, and chemical signals that represent the fundamental relationship between microbes and their environment (Kujawinski, 2011; Douglas, 2020). Most primary metabolites tend to be retained within cells due to their charge at physiological pH values (Bar-Even et al., 2011). These metabolites are usually involved in multiple metabolic pathways and are common across clades of organisms (Peregrín-Alvarez et al., 2009). Secondary metabolites, however, are often more species-specific, and more likely to diffuse into the surrounding environment (Breitling et al., 2013; Covington et al., 2016). Secreted metabolites also act as a chemical language for microorganisms, whose transmission is in constant flux due to evolutionary and environmental pressures (Soldatou et al., 2019; Douglas, 2020). The secretion of metabolites into the surrounding environment is a clear reflection of microbial activity, as the production of these compounds relies on the functional operation of metabolic pathways (Kell et al., 2005). Exometabolomics, or "metabolomic footprinting" (Kell et al., 2005), thus allows for the direct characterization of the molecular interaction between microbes and their environment (Sogin et al., 2019, Douglas, 2020). Metabolomics techniques, in conjunction with metagenomic data, have previously been used to describe the pool of intracellular and extracellular metabolites produced by microbial communities in the Coast Range Ophiolite Microbial Observatory (CROMO), a series of wells that provide access to a serpenization-influenced aquifer in the Coast Range of northern California (Seyler L. M. et al., 2020).

In this study, we used exometabolomics to characterize dissolved organic matter derived from microbial metabolic activity in the Samail Ophiolite groundwaters in the Sultanate of Oman, which is the largest and best exposed ophiolite in the world. The Samail Ophiolite consists of a large (~15,000 km^3) block of ocean crust and upper mantle (Nicolas et al., 2000) that was rapidly emplaced onto the Arabian continental plate approximately 70 million years ago (Glennie and Clarke, 1973; Coleman, 1981; Tilton et al., 1981; Hacker et al., 1996). Here, mafic and ultramafic rocks that once underwent alteration in seafloor hydrothermal systems continue to be altered by active serpentinization on the continent (Canovas et al., 2017; Keleman et al., 2021). We used an untargeted metabolomics approach (Patti et al., 2012) to characterize compounds in the dissolved organic matter (DOM) pool of groundwaters collected from varied geochemical conditions. Metagenomic data acquired from biomass filtered from the same samples was used to verify the annotation of metabolomic features. To our knowledge, this is the first such study attempting to describe biomolecules that make up the DOM pool in the Samail Ophiolite groundwater.

Materials and methods

Site description

The Samail Ophiolite provides a complete cross-section through 7 km of oceanic crust and 15 km of underlying upper mantle rocks (Boudier and Coleman, 1981; Coleman and Hopson, 1981; Lippard et al., 1986; Glennie, 1996; Nicolas et al., 2000). Partially serpentinized peridotite in the ophiolite actively undergoes hydration and carbonation reactions at low temperatures (≤60?), producing hyperalkaline fluids enriched in dissolved methane and hydrogen gas in the subsurface (Barnes et al., 1978;

Neal and Stanger, 1983, 1985; Clark and Fontes, 1990; Kelemen and Matter, 2008; Kelemen et al., 2011, 2013; Paukert et al., 2012; Streit et al., 2012; Miller et al., 2016). The ophiolite's size, exposure, and accessibility create unique opportunities for studying a broad range of geologic and hydrologic conditions supporting subsurface microbial life (Rempfert et al., 2017). Previous geochemical studies of the Samail Ophiolite groundwater observed a strong partitioning between two subgroups of peridotite-hosted fluids and classified them as "Type I/alkaline" (pH 8–10) or "Type II/hyperalkaline" (pH > 10), while wells positioned at the "contact" between peridotite and gabbro displayed more geochemical variability (Rempfert et al., 2017; **Supplementary Figure 1**). Alkaline waters have greater availability of oxidants and DIC and more meteoric influences than hyperalkaline, while contact waters appear to be a mixture of the two (Nothaft et al., 2021). We continue to use these designations to refer to well types throughout this study.

Sampling

In February 2017, a submersible pump was used to collect water samples from five previously drilled wells in the Samail Ophiolite (**Table 1**). Approximately 100 L of flush water were pumped from at least 20 M below the air-water interface in each well prior to sample collection. Sample volume varied according to the amount of water that could be acquired from each well while continuously pumping: 20 L were collected from NSHQ14, 7 L from WAB71, 18 L from WAB55, 4 L from WAB104, and 20 L from WAB105. Each sample was filtered through 0.3 μM glass fiber filters in a muffled stainless steel inline filter holder using PTFE tubing. Approximately 30 ml filtrate was quenched and stored in liquid nitrogen for transport back to the laboratory, where total organic carbon analysis was performed on a Shimadzu total organic carbon analyzer. The rest of the filtrate was acidified to pH 3 using concentrated HCl for solid phase extraction in the field. Biomass for DNA extraction was collected using in-line 0.2 μM polycarbonate filters as described previously (Fones et al., 2019). A total of 10 ml samples of unfiltered waters from each well were preserved in the field for enumeration of planktonic cells by adding formaldehyde to a final concentration of 10% vol/vol, and transported back to the laboratory for direct cell counting *via* 4′,6-diamidino-2-phenylindole (DAPI) staining on black polycarbonate 0.2 μM filters. Water temperature, conductivity, pH, oxidation-reduction potential (ORP), and dissolved oxygen concentration were measured during sampling using a Hach HQ40D Portable Multi Meter (Fones et al., 2019).

Metabolomics

Dissolved organics were captured from the acidified filtrate on a solid phase extraction Bond Elut-PPL cartridge (Agilent, Santa Clara, CA, USA) (Dittmar et al., 2008; Fiore et al., 2015; Seyler L. M. et al., 2020). 1/8″ × 1/4″ PTFE tubing was used to pull the supernatant into the cartridge to minimize the possibility of contamination from plastic leaching, and discarded flow-through was removed *via* Viton tubing with a peristaltic pump (flow rate not exceeding 40 ml/min). The cartridges were then rinsed with at least two cartridge volumes of 0.01 M HCl to remove salt, and the sorbent dried with air for 5 min. Dissolved organic matter (DOM) was eluted with 2 ml 100% methanol *via* gravity flow into muffled amber glass vials. These extracts were then shipped back to the laboratory at Michigan State University, where they were dried down *via* vacuum centrifugation, and resuspended in 495 μL 95:5 water:acetonitrile and 5 μL 5 μg/ml biotin-(ring-6,6-d_2) standard (Rabinowitz and Kimball, 2007; Fiore et al., 2015). This protocol was repeated for 4 L milliQ water as an extraction blank. In addition, an extraction solvent blank was run consisting of 495 μL of 95:5 water:acetonitrile plus 5 μL 5 μg/ml biotin-(ring-6,6-d_2).

Samples were analyzed *via* quadrupole time-of-flight liquid chromatography tandem mass spectrometry (QToF-LC/MS/MS) on a Waters Xevo G2-XS UPLC/MS/MS instrument at the MSU Metabolomics Core facility. Each sample was separated chromatographically in an Acquity UPLC BEH C18 column (1.7 μM, 2.1 mm × 50 mm) using a polar/non-polar gradient made up of 10 mm TBA and 15 mm acetic acid in 97:3 water:methanol (solvent A), and 100% methanol (solvent B). The gradient was run at 99.9/0.1 (% A/B) to 1.0/99.0 (% A/B) over 9 min, held an additional 3 min at 1.0/99.0 (% A/B), then reversed to 99.9/0.1 (% A/B) and held another 3 min. At a rate of 400μL/min, the sample was fed into a quadrupole time-of-flight mass spectrometer using a Waters Xevo G2-XS MS/MS in negative ion mode using a data independent collection method (m/z acquisition range 50–1,500 Da). Mass spec data were then imported into Progenesis QI software for statistical analysis and correlation. Quality control was performed by checking ion intensity maps and producing alignments of all sample runs. An aggregate data set was then created from the aligned runs to produce a map of compound ions that was applied to each sample for peak matching. Compound ions were deconvoluted and ion abundance measurements normalized so that runs could be compared. This approach yielded a table of peak areas that are identified by a unique mass to charge (m/z) and retention time (rt) pair referred to as features. Multivariate statistics was then performed on the data including principal components

TABLE 1 Geochemical data of wells sampled for metabolomics.

Site	UTM easting	UTM northing	Lithology	Pump depth (m)	pH	T (°C)	Cond (μS/cm)	ORP (mV)	Cell counts (per ml)	TOC (mg/L)	SPE volume (L)	TOC of sample (mg)
NSHQ14	675,495	2,529,716	Peridotite	50	11.1	34.4	493	−415	3.04E + 05	1.4470	20	28.94
WAB71	670,322	2,533,981	Peridotite	50–70	10.6	34.5	1803	−86	2.79E + 05	2.5130	7	17.591
WAB55	634,777	2,506,101	Contact	30	9.2	34.7	1171	110	6.79E + 04	0.3560	18	6.408
WAB104	643,099	2,541,124	Peridotite	70	8.5	33.4	493	180	2.38E + 05	0.6146	20	12.292
WAB105	644,678	2,536,524	Peridotite	50	8.3	31.6	448	178	1.80E + 05	0.5756	4	2.3024

analysis and correlation analysis. A table of relative abundances of features was generated for further analysis. Features found in the blanks were subtracted from the sample data (Broadhurst et al., 2018). In order to be considered present in a sample, a feature had to have at least a two-fold greater abundance in the sample than in both blanks. Features were putatively annotated in Progenesis QI against the ChemSpider database using mass, charge, retention time, and fragmentation spectra. Further annotation of features was achieved using mummichog (Li et al., 2013), which predicts functional activity by compiling metabolic networks using mass spec data. Whenever possible, we used autonomous METLIN-Guided In-source Fragment Annotation (MISA) (Domingo-Almenara et al., 2019), an algorithm that compares detected features against low-energy fragments from MS/MS spectra in the METLIN database (Smith et al., 2005), to increase our confidence in the putative annotation of representative metabolites; however, most of the putative metabolites did not have MS/MS spectral data available in the database. Raw spectrometry data are available in the MetaboLights database (Haug et al., 2020) under study identifier MTBLS6081.

Metagenome binning

DNA extraction, generation of sequencing libraries, and analysis of metagenomic sequence data, including binning, was described previously (Fones et al., 2019; Kraus et al., 2021).

Bins were taxonomically classified using GTDB-Tk (Chaumeil et al., 2020). Bin quality was assessed using CheckM version 1.0.11 (Parks et al., 2015); bins with 50% or greater completion were selected for further downstream analyses. The relative abundance of each bin in the metagenomes was calculated using a competitive recruitment approach. A bowtie2 index was built from a concatenated file of all bin contigs using bowtie2-build (Langmead and Salzberg, 2012). Quality-filtered metagenome reads were mapped against the bin bowtie2 index using bowtie2 with the –no-unal flag. The resulting SAM files (containing only the reads which mapped) were converted to BAM files, then BamM[1] was used to remove all alignments with <95% identity and <75% alignment coverage. The number of reads in each remaining BAM file was counted using Binsanity-profile (v0.3.3) (Graham et al., 2017). The read counts were then used to calculate the normalized relative fraction of the metagenomes that mapped to the bins using the following equation:

$$\frac{\frac{Reads}{bp}\,per\ genome}{\sum \frac{Reads}{bp}\,all\ genome} \times \frac{\sum Recruited\ reads\ to\ genomes}{total\ reads} \times 100$$

Z-scores of the normalized relative fractions were calculated using the average and sample standard deviation of the relative fraction of each bin across all metagenomes. The bin relative abundance data was run through the Non-negative Matrix Factorization (NMF) package (Gaujoux and Seoighe, 2010) in R to run a standard non-negative matrix factorization algorithm based on the Kullback–Leibler divergence (Brunet et al., 2004). This algorithm generated a heatmap of the bins across samples and a dendrogram using a Pearson correlation distance function. Bins that were representative of particular wells or geochemical conditions were selected using the method defined by Carmona-Saez et al. (2006). MetaSanity (Neely et al., 2020) was used to annotate functional orthologies against the KEGG database (Kanehisa and Goto, 2000); these annotations were run through KEGGDecoder (Graham et al., 2018) to determine the completeness of metabolic pathways of interest. Genes and pathways not detected by KEGGDecoder were searched for in the bins using protein sequences available in UniProt (UniProt Consortium, 2021) and the Conserved Domain Database (Lu et al., 2020), the MUSCLE alignment tool (Edgar, 2004), and the hmmsearch function in HMMER v 3.3.2 (Eddy, 2008).

Cross-referencing metabolomic and metagenomic data

Metabolomic feature abundance and bin abundance were standardized for ordination according to Legendre and Gallagher (2001) using the decostand function in the R vegan package (v2.4-2).[2] Regularized Discriminant Analysis (RDA) was performed on the standardized data using the klaR package (v0.6-14).[3] These RDAs were then subjected to Procrustes rotation using function Procrustes with symmetric scaling.

Feature annotations acquired using mummichog were cross-referenced with intermediate compounds from pathways identified in representative bins. As for the bins, NMF analysis was performed, and a heatmap of features across samples and a dendrogram using a Pearson correlation distance function were generated. Features that were representative of particular wells or geochemical conditions were extracted using the procedure described by Kim and Park (2007).

Results

Total organic carbon (TOC) was highest in WAB71 (2.5130 mg/L), followed by NSHQ14 (1.4470 mg/L), WAB104 (0.6146 mg/L), WAB105 (0.5756 mg/L), and WAB55 (0.3560 mg/L) (**Table 1**). A total of 2,483 features were detected in the mass spectrometry data across all wells (**Supplementary Table 1**). Principal coordinate analysis of the mass spectrometry data grouped WAB71, WAB55, WAB104, and WAB105 together and set NSHQ14 apart from the other wells (**Figure 1**). A Pearson correlation of feature abundance across wells followed by NMF analysis of feature abundance using the standard algorithm (Brunet et al., 2004) and a factorization rank of three clustered the wells into three "levels": NSHQ14, WAB71, and the alkaline/contact wells (WAB104, WAB105, WAB55) (**Figure 2**). A factorization rank of two resulted in WAB71 being clustered with WAB104, WAB105, and WAB55 (data not shown). NMF analysis also identified features which were representative of (i.e., most abundant in and most likely to be found in) each level. In our analyses, 48 features were designated as representative of NSHQ14, only one

1 https://github.com/Ecogenomics/BamM

2 https://www.rdocumentation.org/packages/vegan

3 https://www.rdocumentation.org/packages/klaR

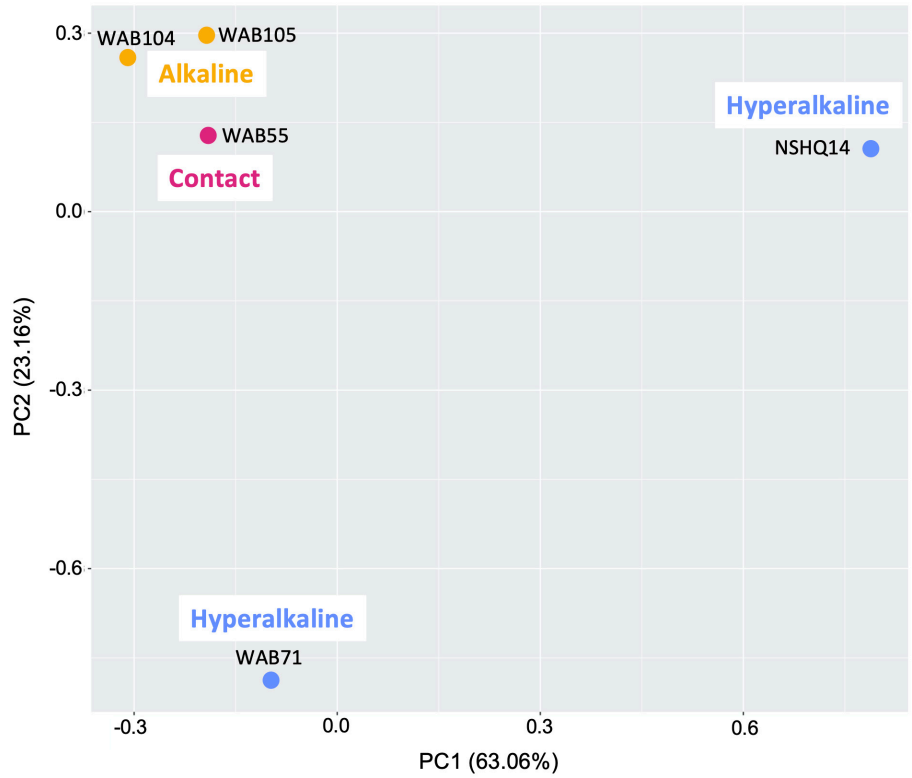

FIGURE 1
Principal component analysis comparing metabolomes of five sampled wells and blanks. The gray area is a cloud of all metabolomic features across all samples.

of which could be annotated by mummichog; two features were representative of WAB71, neither of which could be annotated by either Progenesis QI or mummichog; and the remaining wells had 90 representative features, eight of which could be annotated by mummichog (**Supplementary Table 2**). We also searched the mass spectrometry data for features which were only detected in one well (unique features). NSHQ14 had the greatest number (200) of unique features, WAB71 had 49, WAB104 had 15, WAB105 had five, and WAB55 had no unique features; none of these unique features could be annotated by either Progenesis QI or mummichog (data not shown).

In contrast to the metabolomic features, metagenomic bins tended to cluster by well (**Figure 3**). NMF analysis clustered the bins according to fluid type, and identified bins which were representative of (i.e., most abundant in and most likely to be found in) the hyperalkaline (NSHQ14 and WAB71), alkaline (WAB104 and WAB105), or contact (WAB55) wells. Superimposing the ordination plots of feature abundance and bin abundance data using Procrustes analysis showed that variance in the DOM pool could be attributed to variance in bin abundance and that the wells clustered according to fluid type (Procrustes sum of squares = 0.5033, correlation coefficient = 0.7048, $p = 0.375$), with the exception of WAB71, whose DOM pool clustered with the alkaline wells (**Figure 4**). Procrustes analysis also distinguished the DOM pool of WAB55 from those of NSHQ14 and WAB71, WAB 104, and WAB105 (**Figure 4**).

A total of 1,625 of the 2,483 features in the mass spectrometry data were putatively annotated by Progenesis QI, by matching feature mass to compounds in the ChemSpider database. After removing features that appeared in the extraction blanks, the list of features was reduced to 953, 206 of which could be annotated by Progenesis QI. In contrast, 119 of these 953 features were able to be annotated by mummichog, which annotates metabolomic data by using network analysis and metabolite prediction to resolve ambiguity in metabolite annotation. Because Progenesis QI relies on mass matches to the ChemSpider database, which includes synthetic and theoretical compounds in addition to naturally-occurring metabolites, we primarily relied on the mummichog annotations for our analyses (We have included the Progenesis QI annotations of representative compounds in **Supplementary Table 2**). We cross-referenced metabolic pathways annotated in the representative bins by KEGGDecoder with the features that could be annotated by mummichog to select features in the data on which to further focus our analyses. We then used the MetaCyc database (Caspi et al., 2014) to identify specific reaction pathways involving these metabolites and confirmed the presence of the relevant genes in the annotated MAGs. Pathways of interest and their annotated features in the mass spectrometry data are outlined below.

Carbohydrates and organic acids

Putative annotations of mass spectrometry features included glycan sugars (L-fuculose, L-rhamnose, L-rhamnulose) and their degradation products (L-fucono-1,5-lactone and 2-dehydro-3-deoxy-L-rhamnonate), sugar alcohols, polysaccharides, butanoate,

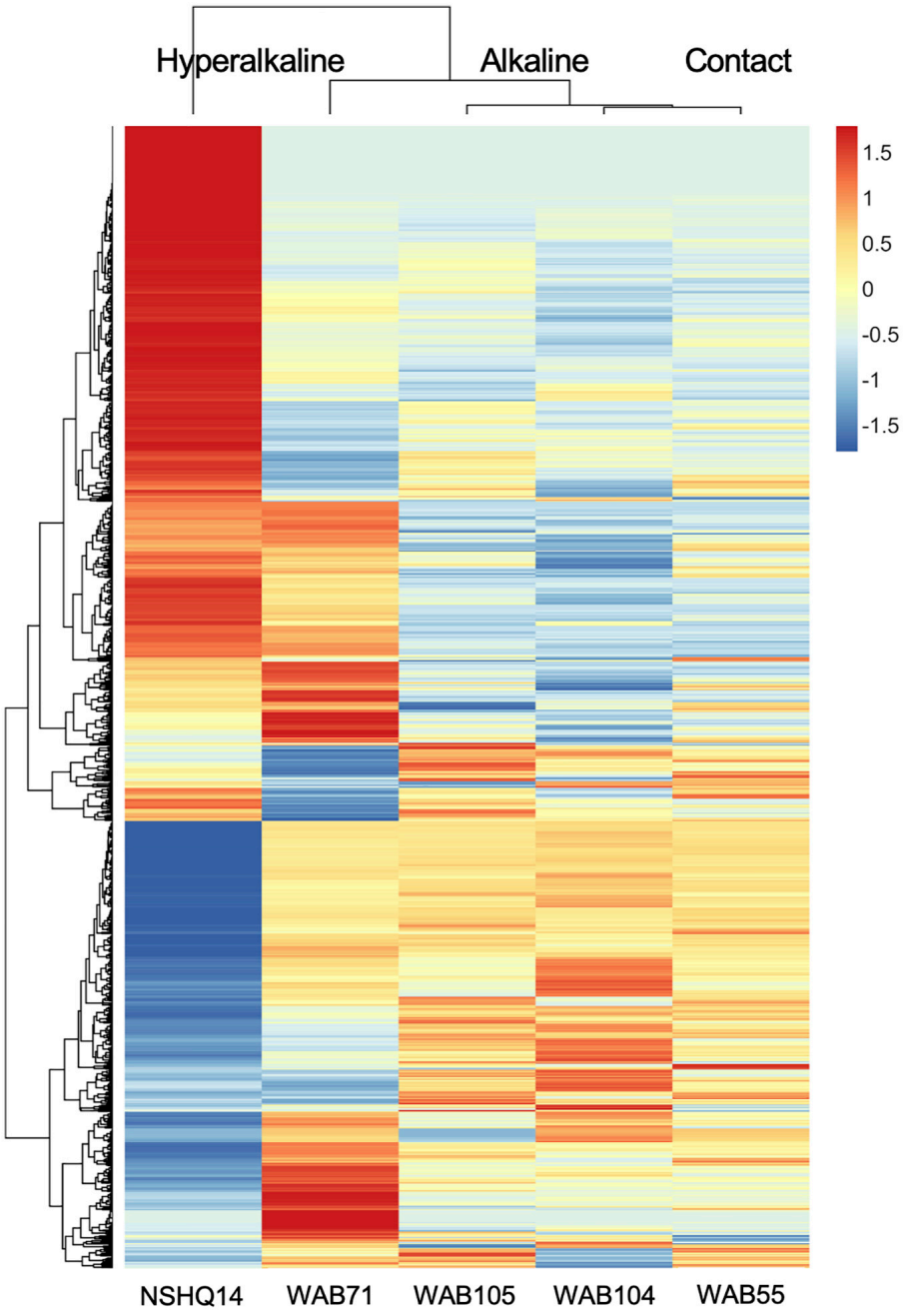

FIGURE 2
Z-scores of metabolomic feature abundance across wells clustered using a Pearson correlation, indicate peaks in the mass spectrometry data are differentially more abundant in some wells than in others. In particular, NSHQ14 had many unique features, most of which could not be identified.

and isocitrate (Figure 5). We further confirmed the annotation of isocitrate using MISA.

Isocitrate was more abundant in the hyperalkaline wells than in the contact or alkaline wells. Isocitrate is an intermediate of multiple metabolic pathways, most notably the citric acid (TCA) cycle, the reverse TCA (rTCA) carbon fixation pathway, the glyoxylate cycle, and coenzyme B biosynthesis in methanogens. A partial TCA cycle was annotated in nearly every bin generated from the metagenomic data, but the rTCA pathway was not identified in any of the bins (Figure 6). The glyoxylate cycle, which uses five of the eight enzymes of the TCA cycle to synthesize macromolecules from two-carbon compounds (e.g., acetate), was annotated in 25 bins, three of which were representative bins of the alkaline wells, three which were representative of the contact well, and one which was representative of the hyperalkaline wells (Figure 6). A complete pathway for coenzyme B biosynthesis was detected in only one bin, a *Methanobacterium* that was representative of NSHQ14 (Figure 6).

Butanoate was also most abundant in the hyperalkaline wells. Butanoate may be produced by the fermentation of pyruvate, but while fermentation pathways were found in 31 (23 representative) bins (Figure 6), the complete set of enzymes required for pyruvate

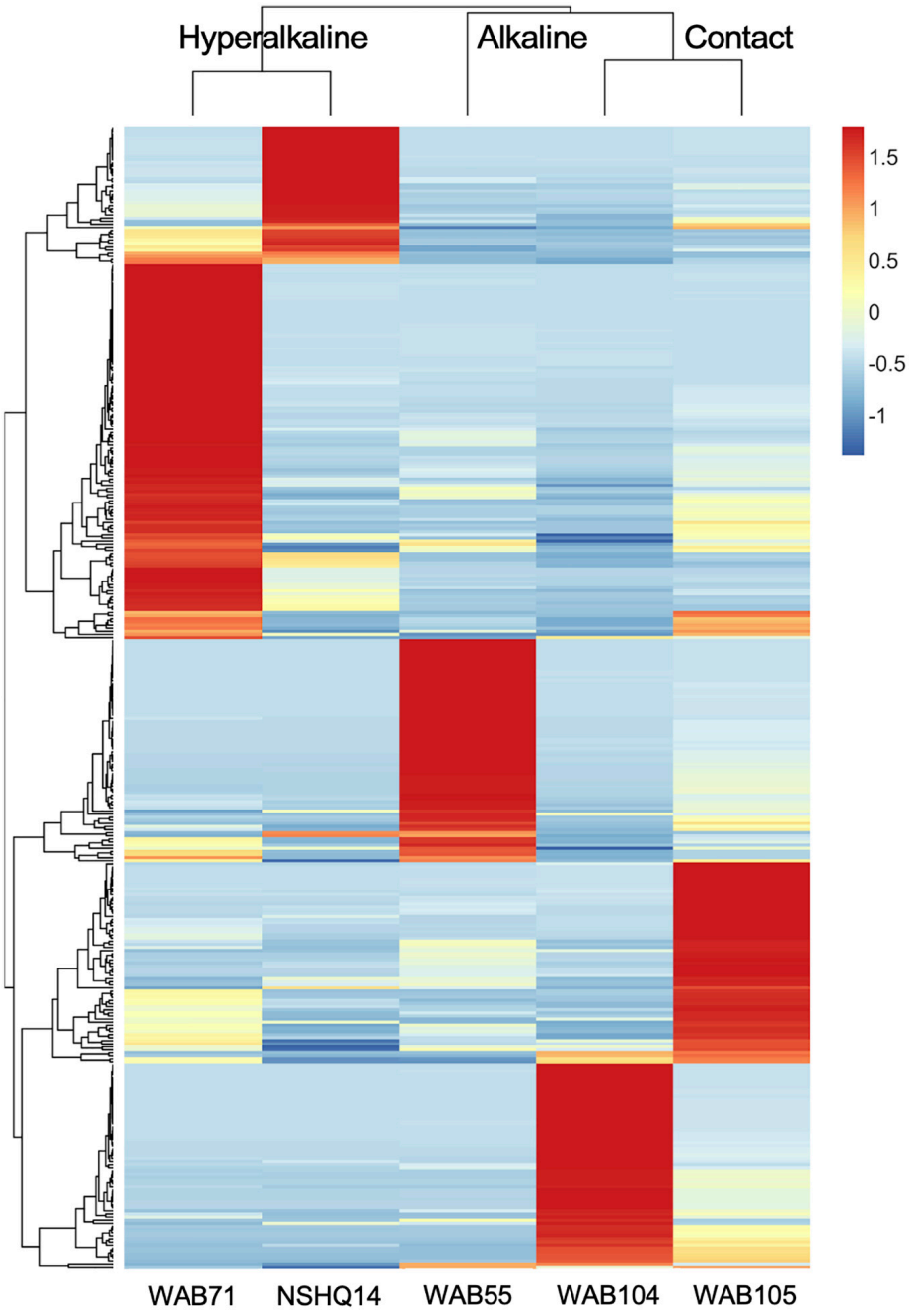

FIGURE 3
Z-scores of bin abundance across wells, clustered using a Pearson correlation. Wells clustered according to fluid type: hyperalkaline (NSHQ14 and WAB71), alkaline (WAB104 and WAB105), and contact (WAB55). WAB71 had the greatest number of bins which were more abundant in this well than any other well, while NSHQ14 had the fewest.

fermentation to butanoate were not detected in any of the bins (Supplementary Table 3).

A complete pathway for L-fuculose or L-rhamnose degradation was not annotated in any of the bins (Supplementary Table 3). The gene for D-threo-aldose 1-dehydrogenase, which produces L-fucono-1,5-lactone during L-fucose degradation, was only annotated in three bins, but the gene for L-fuconolactonase, which further degrades L-fucono-1,5-lactone to L-fuconate, was annotated in fifteen bins (Supplementary Table 3). Similarly, the gene for the L-rhamnonate dehydratase enzyme that produces 2-dehydro-3-deoxy-L-rhamnonate was only annotated in two bins, but the enzyme that acts on this product, 2-dehydro-3-deoxy-L-rhamnonate dehydrogenase, was annotated in seven bins (Supplementary Table 3).

Chitobiose, a disaccharide produced by the hydrolysis of chitin, was also annotated in the mass spectrometry data (Figure 5). MISA further confirmed the annotation of chitobiose; however, we question the validity of the annotation as the peaks eluted very far apart, suggesting that they did not arise from the same parent molecule (Supplementary Figure 1). Genes

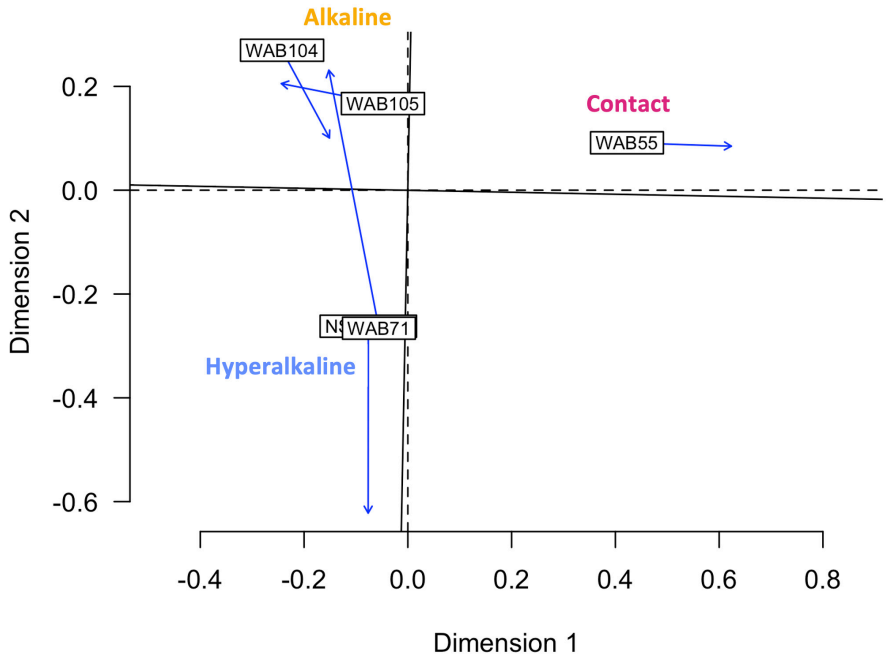

FIGURE 4
Procrustes analysis in which the metabolomic feature abundance and bin abundance ordinations are optimally superimposed through rotating and rescaling, showing that metabolomic feature abundance and bin abundance are correlated. Hyperalkaline wells and alkaline wells cluster together, while the contact well is distinct from both. Labeled boxes indicate the position of the samples in the first ordination, and arrows point to their positions in the target ordination. The dashed lines represent the axes of the first ordination (bin abundance); the solid lines represent the axes of the target ordination (metabolomic feature abundance).

for chitinase and diacetylchitobiose deacetylase, enzymes that hydrolyze chitin and chitobiose, were identified in 11 and 16 bins, respectively, though only two bins contained both (Figure 6). Beta-*N*-acetylhexosaminidase, an exoglycosidase that catalyzes the hydrolysis of chitobiose, was detected in 54 out of 128 total bins, 14 of which were representative bins (six of the seven alkaline representative bins, three hyperalkaline representative bins, and five contact representative bins) (Figure 6). Genes for enzymes involved in the catabolism of other polysaccharides, including alpha-amylase, glucoamylase, beta-glucosidase, D-galacturonate epimerase, D-galacturonate isomerase, oligogalacturonide lyase, and pullulanase were also detected in the metagenomic data, and tended to be associated with bins that displayed the greatest abundance in the hyperalkaline wells (Supplementary Table 3).

Methanogenesis/propanoate degradation

Five features were putatively annotated as either *cis*-homoaconitate, an intermediate in coenzyme B biosynthesis, or *cis*-2-methylaconitate/2-methyl-trans-aconitate, intermediates in propanoate degradation to pyruvate and succinate *via* the 2-methylcitrate cycle (Figure 5). These features were more abundant (by up to eight orders of magnitude) in the hyperalkaline wells compared to the contact and alkaline wells. An intermediate of coenzyme M production, (2R)-phosphosulfolactate, was also putatively annotated in the mass spectrometry data and was detected in all of the wells, though it was most abundant in the alkaline wells and was designated a representative feature of the alkaline/contact wells by NMF analysis (Figure 5). A feature putatively annotated as 2-hexaprenyl-6-methoxyphenol, an intermediate in methanogenesis from methoxylated aromatic compounds, was almost exclusively found in NSHQ14 (Figure 5). The enzyme that produces this intermediate has not been characterized.

Complete pathways for methanogenesis *via* CO_2 and coenzyme M reduction to methane were found in two out of the 128 bins analyzed (Figure 6; Fones et al., 2019). Both of these bins were taxonomically annotated as Euryarchaeota belonging to the Methanobacteriales; one bin was designated a representative bin for NSHQ14, and was one of the most abundant bins in that well (Figure 6; Fones et al., 2019). Both bins also contained the acetoclastic methanogenesis pathway, as well as a nearly complete pathway for methanogenesis from methoxylated aromatic compounds, except for the gene for the first enzyme in the pathway, *mtoB* (Figure 6 and Supplementary Table 3). The *mtoB* gene was detected in 51 other bins; 80% of these bins displayed the greatest abundance in the hyperalkaline or contact wells (Supplementary Table 3). A complete 2-methylcitrate cycle for propanoate degradation was detected in four bins, including a representative bin of WAB71 (a member of the Microtrichales) and a representative bin of WAB105 (*Acinetobacter junii*) (Figure 6).

Porphyrins, pigments, and quinones

Fourteen features in the mass spec data were annotated as intermediates of pigment, porphyrin, and quinone biosynthesis

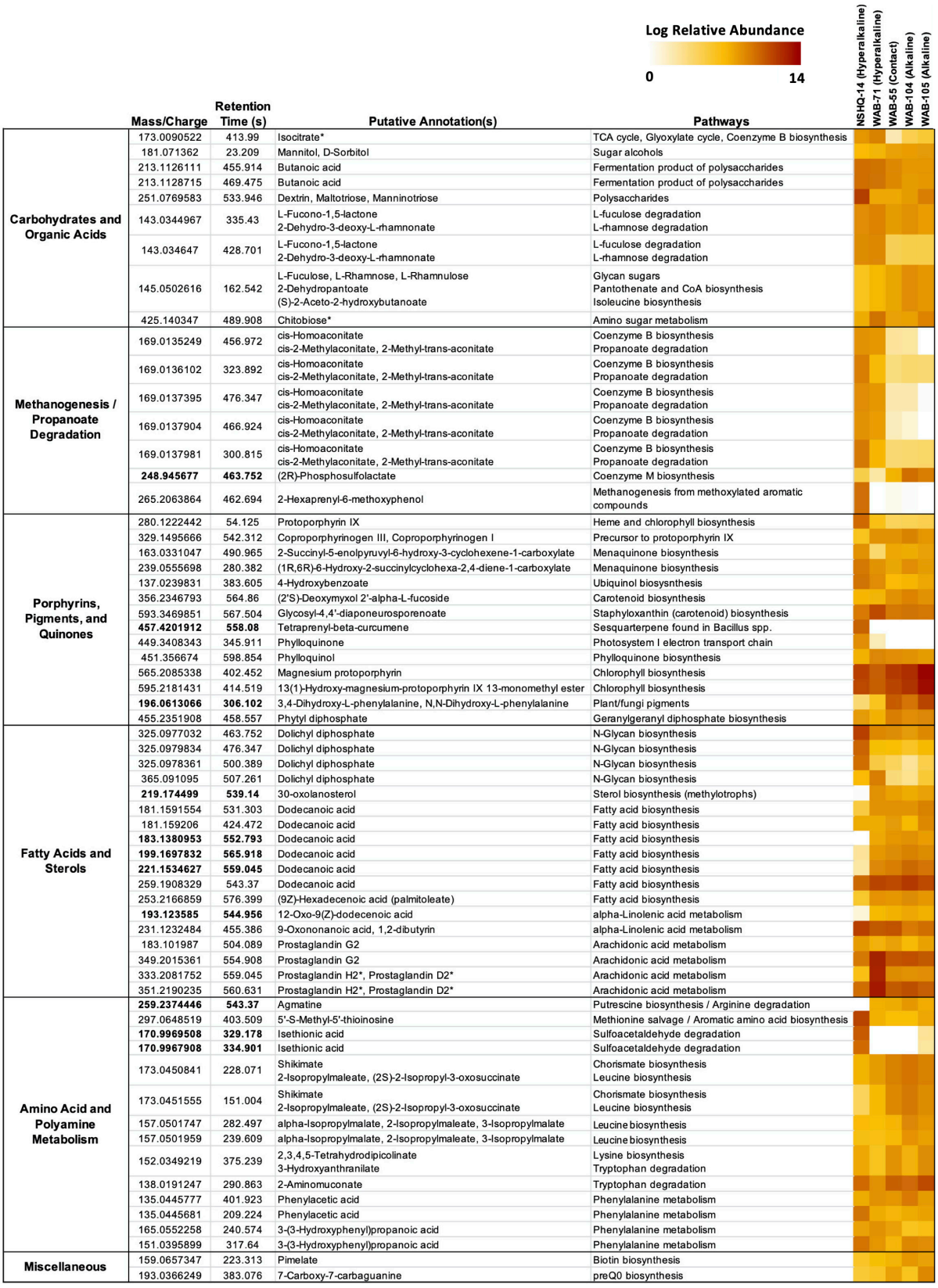

	Mass/Charge	Retention Time (s)	Putative Annotation(s)	Pathways
Carbohydrates and Organic Acids	173.0090522	413.99	Isocitrate*	TCA cycle, Glyoxylate cycle, Coenzyme B biosynthesis
	181.071362	23.209	Mannitol, D-Sorbitol	Sugar alcohols
	213.1126111	455.914	Butanoic acid	Fermentation product of polysaccharides
	213.1128715	469.475	Butanoic acid	Fermentation product of polysaccharides
	251.0769583	533.946	Dextrin, Maltotriose, Manninotriose	Polysaccharides
	143.0344967	335.43	L-Fucono-1,5-lactone 2-Dehydro-3-deoxy-L-rhamnonate	L-fuculose degradation L-rhamnose degradation
	143.034647	428.701	L-Fucono-1,5-lactone 2-Dehydro-3-deoxy-L-rhamnonate	L-fuculose degradation L-rhamnose degradation
	145.0502616	162.542	L-Fuculose, L-Rhamnose, L-Rhamnulose 2-Dehydropantoate (S)-2-Aceto-2-hydroxybutanoate	Glycan sugars Pantothenate and CoA biosynthesis Isoleucine biosynthesis
	425.140347	489.908	Chitobiose*	Amino sugar metabolism
Methanogenesis / Propanoate Degradation	169.0135249	456.972	cis-Homoaconitate cis-2-Methylaconitate, 2-Methyl-trans-aconitate	Coenzyme B biosynthesis Propanoate degradation
	169.0136102	323.892	cis-Homoaconitate cis-2-Methylaconitate, 2-Methyl-trans-aconitate	Coenzyme B biosynthesis Propanoate degradation
	169.0137395	476.347	cis-Homoaconitate cis-2-Methylaconitate, 2-Methyl-trans-aconitate	Coenzyme B biosynthesis Propanoate degradation
	169.0137904	466.924	cis-Homoaconitate cis-2-Methylaconitate, 2-Methyl-trans-aconitate	Coenzyme B biosynthesis Propanoate degradation
	169.0137981	300.815	cis-Homoaconitate cis-2-Methylaconitate, 2-Methyl-trans-aconitate	Coenzyme B biosynthesis Propanoate degradation
	248.945677	**463.752**	(2R)-Phosphosulfolactate	Coenzyme M biosynthesis
	265.2063864	462.694	2-Hexaprenyl-6-methoxyphenol	Methanogenesis from methoxylated aromatic compounds
Porphyrins, Pigments, and Quinones	280.1222442	54.125	Protoporphyrin IX	Heme and chlorophyll biosynthesis
	329.1495666	542.312	Coproporphyrinogen III, Coproporphyrinogen I	Precursor to protoporphyrin IX
	163.0331047	490.965	2-Succinyl-5-enolpyruvyl-6-hydroxy-3-cyclohexene-1-carboxylate	Menaquinone biosynthesis
	239.0555698	280.382	(1R,6R)-6-Hydroxy-2-succinylcyclohexa-2,4-diene-1-carboxylate	Menaquinone biosynthesis
	137.0239831	383.605	4-Hydroxybenzoate	Ubiquinol biosysnthesis
	356.2346793	564.86	(2'S)-Deoxymyxol 2'-alpha-L-fucoside	Carotenoid biosynthesis
	593.3469851	567.504	Glycosyl-4,4'-diaponeurosporenoate	Staphyloxanthin (carotenoid) biosynthesis
	457.4201912	**558.08**	Tetraprenyl-beta-curcumene	Sesquarterpene found in Bacillus spp.
	449.3408343	345.911	Phylloquinone	Photosystem I electron transport chain
	451.356674	598.854	Phylloquinol	Phylloquinone biosynthesis
	565.2085338	402.452	Magnesium protoporphyrin	Chlorophyll biosynthesis
	595.2181431	414.519	13(1)-Hydroxy-magnesium-protoporphyrin IX 13-monomethyl ester	Chlorophyll biosynthesis
	196.0613066	**306.102**	3,4-Dihydroxy-L-phenylalanine, N,N-Dihydroxy-L-phenylalanine	Plant/fungi pigments
	455.2351908	458.557	Phytyl diphosphate	Geranylgeranyl diphosphate biosynthesis
Fatty Acids and Sterols	325.0977032	463.752	Dolichyl diphosphate	N-Glycan biosynthesis
	325.0979834	476.347	Dolichyl diphosphate	N-Glycan biosynthesis
	325.0978361	500.389	Dolichyl diphosphate	N-Glycan biosynthesis
	365.091095	507.261	Dolichyl diphosphate	N-Glycan biosynthesis
	219.174499	**539.14**	30-oxolanosterol	Sterol biosynthesis (methylotrophs)
	181.1591554	531.303	Dodecanoic acid	Fatty acid biosynthesis
	181.159206	424.472	Dodecanoic acid	Fatty acid biosynthesis
	183.1380953	**552.793**	Dodecanoic acid	Fatty acid biosynthesis
	199.1697832	**565.918**	Dodecanoic acid	Fatty acid biosynthesis
	221.1534627	**559.045**	Dodecanoic acid	Fatty acid biosynthesis
	259.1908329	543.37	Dodecanoic acid	Fatty acid biosynthesis
	253.2166859	576.399	(9Z)-Hexadecenoic acid (palmitoleate)	Fatty acid biosynthesis
	193.123585	**544.956**	12-Oxo-9(Z)-dodecenoic acid	alpha-Linolenic acid metabolism
	231.1232484	455.386	9-Oxononanoic acid, 1,2-dibutyrin	alpha-Linolenic acid metabolism
	183.101987	504.089	Prostaglandin G2	Arachidonic acid metabolism
	349.2015361	554.908	Prostaglandin G2	Arachidonic acid metabolism
	333.2081752	559.045	Prostaglandin H2*, Prostaglandin D2*	Arachidonic acid metabolism
	351.2190235	560.631	Prostaglandin H2*, Prostaglandin D2*	Arachidonic acid metabolism
Amino Acid and Polyamine Metabolism	**259.2374446**	**543.37**	Agmatine	Putrescine biosynthesis / Arginine degradation
	297.0648519	403.509	5'-S-Methyl-5'-thioinosine	Methionine salvage / Aromatic amino acid biosynthesis
	170.9969508	**329.178**	Isethionic acid	Sulfoacetaldehyde degradation
	170.9967908	**334.901**	Isethionic acid	Sulfoacetaldehyde degradation
	173.0450841	228.071	Shikimate 2-Isopropylmaleate, (2S)-2-Isopropyl-3-oxosuccinate	Chorismate biosynthesis Leucine biosynthesis
	173.0451555	151.004	Shikimate 2-Isopropylmaleate, (2S)-2-Isopropyl-3-oxosuccinate	Chorismate biosynthesis Leucine biosynthesis
	157.0501747	282.497	alpha-Isopropylmalate, 2-Isopropylmaleate, 3-Isopropylmalate	Leucine biosynthesis
	157.0501959	239.609	alpha-Isopropylmalate, 2-Isopropylmaleate, 3-Isopropylmalate	Leucine biosynthesis
	152.0349219	375.239	2,3,4,5-Tetrahydrodipicolinate 3-Hydroxyanthranilate	Lysine biosynthesis Tryptophan degradation
	138.0191247	290.863	2-Aminomuconate	Tryptophan degradation
	135.0445777	401.923	Phenylacetic acid	Phenylalanine metabolism
	135.0445681	209.224	Phenylacetic acid	Phenylalanine metabolism
	165.0552258	240.574	3-(3-Hydroxyphenyl)propanoic acid	Phenylalanine metabolism
	151.0395899	317.64	3-(3-Hydroxyphenyl)propanoic acid	Phenylalanine metabolism
Miscellaneous	159.0657347	223.313	Pimelate	Biotin biosynthesis
	193.0366249	383.076	7-Carboxy-7-carbaguanine	preQ0 biosynthesis

FIGURE 5
Features cross-referenced between KEGG results and mummichog annotations. Features are grouped by putative annotation/function. Diagnostic features appear in bold. Feature annotations confirmed by MISA are indicated with an asterisk (*). Feature abundance is expressed as the log of the normalized relative abundance.

pathways (Figure 5). A feature putatively annotated as protoporphyrin IX, a central metabolite in the production of heme and chlorophyll, was detected in all wells and was particularly abundant (3–5 orders of magnitude greater) in NSHQ14 (Figure 5). Another feature, putatively annotated as coproporphyrinogen III (a precursor to protoporphyrin IX) was detected in every well but displayed the lowest abundance in NSHQ14, by more than two orders of magnitude (Figure 5). Complete pathways for the biosynthesis of heme from glutamate and/or glutamyl-tRNA were annotated in bins detected in every well; however, bins containing complete or nearly complete (≥90%) heme pathways were generally more abundant in the hyperalkaline and contact wells (Figure 6).

Three features annotated as intermediates in ubiquinol (4-hydroxybenzoate) and menaquinone synthesis (2-succinyl-5-enolpyruvyl-6-hydroxy-3-cyclohexene-1-carboxylate and (1R,6R)-6-hydroxy-2-succinylcyclohexa-2,4-diene-1-carboxylate, intermediates in the synthesis of menaquinol and phylloquinol from isochorismate) were detected in all of the wells but were most abundant in NSHQ14 (Figure 5). Genes for the enzymes

FIGURE 6
(Continued)

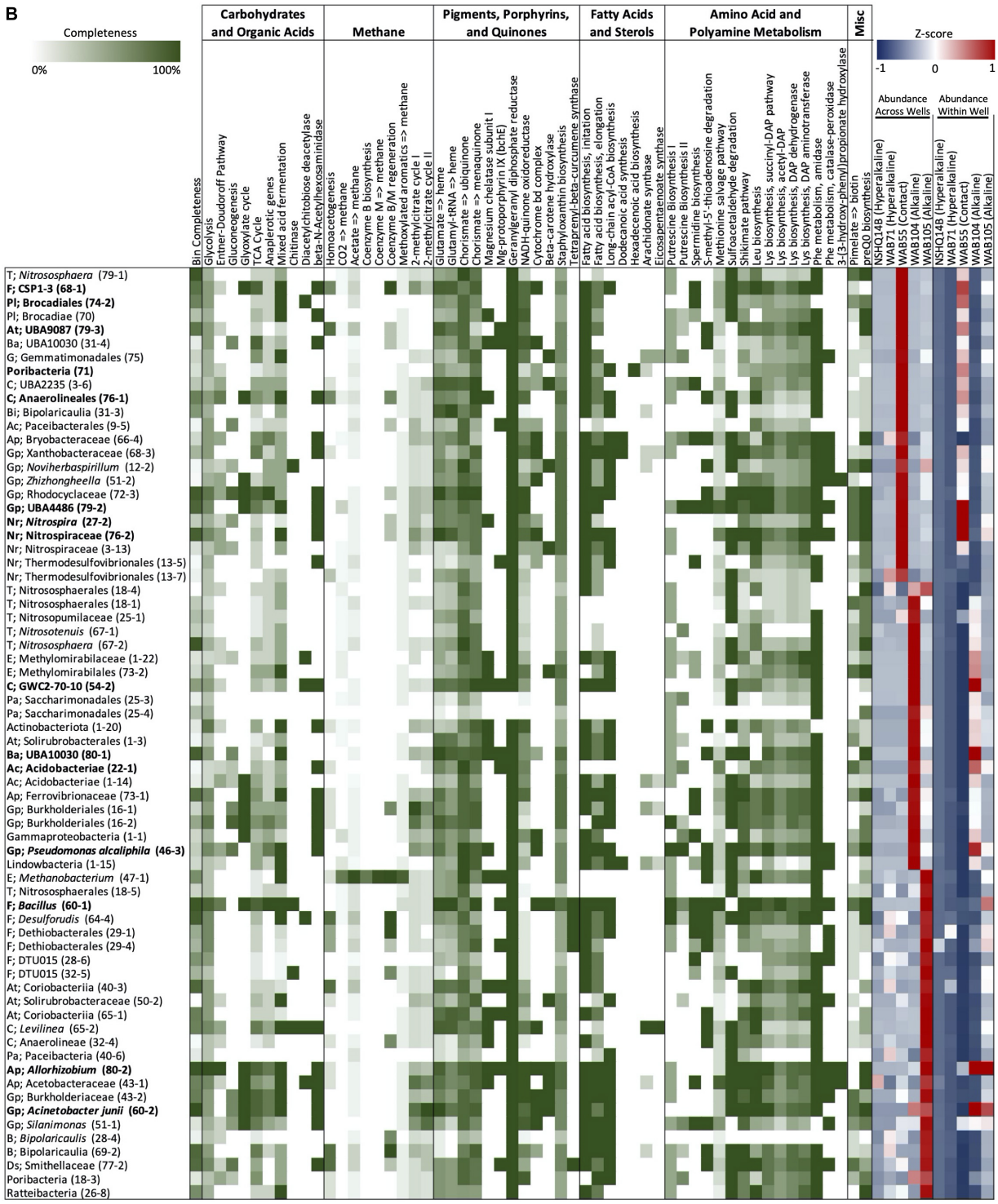

FIGURE 6
(A,B) Metabolic genes and pathways of interest, annotated in each bin using KEGGDecoder and HMMER. Percentage completion of each pathway is indicated in shades of green. Z-scores of bin abundance within each well and across all wells are indicated in a blue/red heatmap at the top of the figure (negative z-scores in blue, positive z-scores in red).

that produce these intermediates were detected in 14, 11, and 6 bins, respectively; these bins tended to be most abundant in the hyperalkaline or contact wells (Supplementary Table 3). The complete pathway for ubiquinone biosynthesis was detected in thirteen bins, including two representative bins of NSHQ14 (*Methanobacterium* and *Pseudomonas*) and two representative bins of WAB104 (a member of the Acidobacteria, and *Pseudomonas alcaliphila*) (Figure 6). The complete pathway for menaquinone biosynthesis was detected in eleven bins, including a representative bin of every well except NSHQ14 (although one representative bin

of that well, a member of the Moorellia, had 90% of the pathway) (Figure 6). The most commonly found cytochrome genes in the bins encoded for the cytochrome bd complex and NADH-quinone oxidoreductase. A total of 41 of the 128 bins contained ≥90% of the genes encoding one or both of these cytochromes (Figure 6).

Features putatively annotated as (2′S)-deoxymyxol 2′-alpha-L-fucoside and glycosyl-4,4′-diaponeurosporenoate, metabolites produced in the biosynthesis of the carotenoids myxol 2′-dimethyl-fucoside and staphyloxanthin, respectively, were also detected in all the wells (Figure 5). The biosynthesis of (2′S)-deoxymyxol 2′-alpha-L-fucoside is a multi-step reaction that has not been fully characterized, but we were able to annotate the enzyme that catalyzes the conversion of (2′S)-deoxymyxol 2′-alpha-L-fucoside to myxol 2′-dimethyl-fucoside, beta-carotene hydroxylase, in 18 bins (Figure 6). Genes in the pathway for staphyloxanthin biosynthesis were annotated in nearly every bin, but the complete pathway was only detected in one bin, a member of the Anaerolineales that was most abundant in WAB71 (Figure 6).

A feature found exclusively in NSHQ14 and designated as a representative feature of that well was putatively annotated as tetraprenyl-beta-curcumene, an intermediate in the biosynthesis of a sesquiterpene found in *Bacillus* spp. (Figure 5). The gene for tetraprenyl-beta-curcumene synthase was detected in seven bins, two of which were most abundant in WAB71, and the rest of which were most abundant in WAB105 (Figure 6).

Two features that were among the most abundant features in the mass spec data were annotated as intermediates of chlorophyll metabolism: magnesium protophorin and 13(1)-hydroxy-magnesium-protoporphyrin IX 13-monomethyl ester (Figure 5). Other putatively annotated features associated with photosynthesis and chlorophyll metabolism include phylloquinone, phytyl diphosphate, and phylloquinol (Figure 5). A feature annotated as either 3,4-dihydroxy-L-phenylalanine or N,N-dihydroxy-L-phenylalanine, precursors to pigments/cytochromes in fungi and plants, was also detected in all of the wells and was a representative feature of the alkaline/contact wells (Figure 5). Most of these features were relatively more abundant in the alkaline and contact wells. However, the feature putatively annotated as phylloquinone was exclusively detected in the hyperalkaline wells and was particularly abundant in NSHQ14 (Figure 5). Because the pathway for phylloquinol/phylloquinone synthesis and menaquinol synthesis involve the same/highly homologous enzymes, we could not distinguish between these pathways in the bins.

The complete pathway for chlorophyll biosynthesis was not detected in any bin (Supplementary Table 3). However, genes for two enzymes in this pathway, magnesium chelatase subunit I and anaerobic magnesium-protoporphyrin IX monomethyl ester cyclase, were annotated in 27 bins and 29 bins, respectively (Figure 6). Magnesium chelatase is a three-subunit enzyme responsible for inserting a Mg^{+2} into protoporphyrin IX in the first step of chlorophyll biosynthesis; genes for the other two subunits (H and D) were found in two and five bins, respectively, and none of the bins contained the genes for all three subunits of the enzyme (Supplementary Table 3). Anaerobic magnesium-protoporphyrin IX monomethyl ester cyclase produces 13(1)-hydroxy-magnesium-protoporphyrin IX 13-monomethyl ester in the chlorophyll biosynthesis pathway found in anaerobic photosynthetic bacteria. None of the bins contained the complete suite of genes required for photosynthesis, but two bins (one diagnostic) in the alkaline wells did contain the genes for an anoxygenic type-II reaction center (Supplementary Table 3). Thirteen bins contained the genes for the RuBisCo enzyme, nine of which also contained the complete Calvin–Benson–Bassham pathway for carbon fixation, but none of which included the anoxygenic type-II reaction center (Supplementary Table 3).

A feature putatively annotated as phytyl diphosphate, an intermediate of geranylgeranyl diphosphate biosynthesis, was also detected in all the wells. Geranylgeranyl diphosphate is a precursor to phylloquinol, chlorophyll, archaeol, and multiple pigments across all domains of life.

Fatty acids and sterols

Eighteen features were annotated as fatty acids and intermediates in fatty acid pathways, five of which were designated characteristic features of the alkaline and contact wells by NMF analysis. These included four peaks annotated as dolichyl diphosphate, lipids involved in N-glycan production in archaea, which were detected in all the wells but were most abundant in NHSQ14 and WAB71. We also detected a feature putatively annotated as 12-oxo-9(Z)-dodecenoic acid (an intermediate of alpha-linolenic acid metabolism), a feature putatively annotated as 30-oxolanosterol (an intermediate of sterol biosynthesis in methylotrophs), and three features annotated as dodecanoic acid (Figure 5). There were also three features found in all the wells but particularly abundant in WAB71, which were annotated as prostaglandins by mummichog. MISA further confirmed the annotation of the latter two features as prostaglandin H2 or prostaglandin D2 (Figure 5 and Supplementary Figure 1). However, we suspect that this annotation is incorrect and that these features are more likely intermediates or secondary metabolites of arachidonic acid and/or eicosapentaenoic acid (see section "Discussion").

Genes for polyunsaturated fatty acid (PUFA) synthases (arachidonate and/or eicosapentaenoate synthase) were annotated in 18 of the bins analyzed in this study; however, a complete PUFA synthase operon (*pfaABCD*) was only found in two bins, one taxonomically annotated as belonging to the genus *Bellilinea* and the other as genus *Levilinea*, which are in the family Anaerolineaceae (phylum Chloroflexota, class Anaerolineae, order Anaerolineales) (Figure 6 and Supplementary Table 3). The *pfaE* gene that encodes the phosphopantetheinyl transferase required for catalytic activation of acyl carrier protein domains was not present in these bins, but was found in two other bins belonging to phylum Chloroflexota, class Dehalococcoidia (Supplementary Table 3). Genes for fatty acid synthesis initiation and elongation (*fabB, fabD, fabF, fabG, fabH, fabI, fabZ*) and long chain acyl-CoA biosynthesis (*ACSL, fadD*), which produce the precursors to arachidonate and eicosapentaenoate, were annotated in all but two of the representative bins (Figure 6).

Amino acid and polyamine metabolism

Thirteen features were putatively annotated as intermediates of amino acid/polyamine biosynthesis or degradation pathways

(Figure 5). Most of these features were detected in all of the wells, with a few exceptions. A feature annotated as agmatine, an intermediate of arginine degradation and putrescine/spermidine biosynthesis, was present in every well except NSHQ14, and was designated a representative feature of the alkaline/contact wells by NMF analysis (Figure 5). Complete putrescine biosynthesis pathways were annotated in 12 bins; interestingly, nearly half of these bins displayed the greatest abundance in NSHQ14 (Figure 6). Conversely, a feature annotated as 5′-S-methyl-5′-thioinosine, a metabolite produced by the deamination of 5′-methylthioadenosine (an intermediate of the methionine salvage cycle and spermidine biosynthesis), was detected in all the wells but was particularly abundant in NHSQ14 (Figure 5). The gene for enzyme that performs the deamination reaction, 5-methylthioadenosine/S-adenosylhomocysteine deaminase, was detected in 50 of the 128 bins analyzed in this study, including four representative bins of NSHQ14, one representative bin of WAB71, three representative bins of WAB55, two representative bins of WAB104, and one representative bin of WAB105 (Figure 6). This enzyme has also been implicated in the recycling of 5′-deoxyadenosine and the biosynthesis of aromatic amino acids in methanogens (Miller et al., 2014). The methionine salvage cycle is also linked to the production of putrescine and spermidine. Only four bins contained ≥90% of the methionine salvage pathway, but 60 bins contained the portion of the pathway that results in 5′-methylthioadenosine/spermidine biosynthesis (Figure 6).

Two representative features of NSHQ14 were putatively annotated as isethionic acid, a product of sulfoacetaldehyde degradation. These features were found only in NSHQ14 and WAB105, but at eight orders of magnitude greater abundance in the former versus the latter well (Figure 5). Sulfoacetaldehyde is both a product of taurine degradation and an intermediate of coenzyme M biosynthesis. The gene for NADH-dependent sulfoacetaldehyde reductase, the enzyme that catalyzes the conversion of sulfoacetaldehyde to isethionic acid, was detected in 77 bins, including four representative bins from NSHQ14, one from WAB71, five from WAB55, three from WAB104, and two from WAB105 (Figure 6).

Two features annotated as either shikimate, 2-isopropylmaleate, or (2S)-2-isopropyl-3-oxosuccinate were detected in all of the wells but were most abundant in the alkaline and contact wells (Figure 5). Shikimate is an intermediate of the shikimate pathway for the production of chorismate, a precursor to aromatic amino acid and menaquinone/ubiquinone biosynthesis. 2-Isopropylmaleate and (2S)-2-Isopropyl-3-oxosuccinate are intermediates of leucine biosynthesis. Two other features, annotated as alpha-isopropylmalate/2-isopropylmaleate/3-isopropylmalate, all of which are intermediates in leucine biosynthesis, were also detected in all the wells but most abundant in the alkaline wells (Figure 5). Complete shikimate and leucine biosynthesis pathways were detected in bins in every well (Figure 6). Nine of the 15 representative bins of the contact and alkaline wells contained one or both of these pathways, but only one of the eight representative hyperalkaline bins contained these pathways (Figure 6).

Other putatively annotated features related to amino acid metabolism include intermediates of lysine biosynthesis (2,3,4,5-tetrahydrodipicolinate), tryptophan degradation (3-hydroxyanthranilate and 2-aminomuconate), and phenylalanine metabolism [phenylacetic acid and 3-(3-hydroxyphenyl)propanoic acid] (Figure 5). Lysine biosynthesis pathways were detected in multiple bins (Figure 6). The complete pathway for tryptophan degradation *via* 3-hydroxyanthranilate to 2-aminomuconate was annotated in only one bin, which was taxonomically annotated as a member of the Bipolaricaulia (Supplementary Table 3). This bin was more abundant in WAB105 than any other well, but had a low relative abundance compared to other bins in that well. The gene *amiE*, which encodes the amidase enzyme that converts 2-phenylacetamide to phenylacetic acid, was detected in almost every bin; the gene *katG*, which encodes the catalase-peroxidase enzyme that converts phenylalanine to 2-phenylacetamide was detected in 43 bins (Figure 6). The enzyme in phenylalanine metabolism that produces 3-(3-hydroxyphenyl)propanoic acid has not been characterized, but the gene for 3-(3-hydroxy-phenyl)propionate hydroxylase, which converts 3-(3-hydroxy-phenyl)propionate acid to 3-(2,3-dihydroxyphenyl)propanoate in the same pathway, was detected in seven bins, only one of which was designated a representative bin of a well (WAB105) (Figure 6).

Miscellaneous

A feature putatively annotated as pimelate, a precursor of biotin, was detected in every well, with a slightly greater relative abundance in the alkaline wells (Figure 5). The complete pathway for biotin synthesis from pimelate was annotated in only one bin, a member of the Thermodesulfovibrionales that displayed the greatest relative abundance in WAB71 (Figure 6). Twenty-one bins possessed four out of the five genes necessary for the pathway but were missing the gene for the enzyme 6-carboxyhexanoate-CoA ligase (*bioW*), which initiates the pathway by converting pimelate to pimeloyl-CoA (Supplementary Table 3). Two other bins contained this gene but otherwise lacked the complete pathway (Supplementary Table 3). The mechanism for the biosynthesis of pimelate is currently unknown, though it is speculated to begin with malonyl-CoA (Manandhar and Cronan, 2017). This same study found that deletion of the *bioW* gene results in a biotin auxotrophic phenotype in *Bacillus subtilis*.

Another feature, putatively annotated as 7-carboxy-7-carbaguanine (the precursor to preQ0 in preQ0 biosynthesis), was also detected in every well but was most abundant in WAB55 and WAB105 (Figure 5). A total of 36 bins contained the complete pathway for preQ0 biosynthesis, including one representative bin for NSHQ14, four representative bins for WAB55, two representative bins for WAB104, and three representative bins for WAB105 (Figure 6).

Representative and abundant bins

Bins we identified as representative of alkaline wells belonged to the Bacillales (family Bacillaceae), Rhizobiales (family Rhizobiaceae), Pseudomonadales (*Acinetobacter junii* and *Pseudomonas alcaliphila*), Acidobacteria, Bacteroidota (UBA10030), and Chloroflexota A (Figure 6). The most

abundant bins in the alkaline wells also included members of the Thaumarchaeota, Actinobacteriota, Methylomirabilota, and Saccharimonadales (**Figure 6**). Representative hyperalkaline bins included members of the Thermodesulfovibrionales, Bipolaricaulia (formerly candidate phylum OP1), Chloroflexota (Dehalococcoidia), Moorellia, Methanobacteriales, Microtrichales, Gemmatimonadetes, and Pseudomonadales (*Pseudomonas aeruginosa*) (**Figure 6**). Members of the Deinococcales, Burkholderiales, and Nitrospirales were also among the most abundant bins in the hyperalkaline wells (**Figure 6**). Bins representative of WAB55 (the only contact well sampled in this study) included Nitrospirales, Brocadiales, Chloroflexota (Anaerolineales), Gammaproteobacteria (UBA4486), Firmicutes (CSP1-3), and Poribacteria (**Figure 6**). A complete list of the bins, including bin completeness, contamination, strain heterogeneity, and phylogenetic classification, is presented in **Supplementary Table 4**.

Discussion

Previous studies have demonstrated clear trends correlating microbial diversity and metabolic capability to rock/fluid type in the Samail Ophiolite (Rempfert et al., 2017; Fones et al., 2019, 2021; Kraus et al., 2021). The chemistry of the subsurface fluids reflects both hydrologic context (i.e., the extent of equilibration with the atmosphere or host rock, or potential for mixing with other fluids) and the geology of the host rock (Rempfert et al., 2017; Leong et al., 2021). Multitracer experiments indicate that the higher pH (>9.3) fluids are older than their less alkaline counterparts, and their chemistry reflects a greater extent of serpentinization in the host rock (Paukert Vankeuren et al., 2019). Microbial community composition correlates with fluid geochemistry, with gabbro and alkaline peridotite fluids displaying a greater richness of microorganisms than the low-diversity communities found in hyperalkaline peridotite (Rempfert et al., 2017). Due to the covariance of multiple geochemical parameters, it is difficult to determine which of these parameters drives these correlations (Rempfert et al., 2017). Here, we present a broad snapshot of the DOM pool in the Samail Ophiolite groundwater and identify some of the secondary metabolites produced by the microbial communities found there. The annotation of these features was supported by comparing putative compounds to the genes identified in the metagenomic bins.

Given that both microbial community structure and protein-coding gene abundance correlate with rock and fluid type (Rempfert et al., 2017; Fones et al., 2019, 2021; Kraus et al., 2021), we hypothesized that DOM composition would likewise correlate to these characteristics. Principal components analysis (**Figure 1**), NMF analysis (**Figure 2**), and procrustes analysis (**Figure 4**) comparing mass spec data across five wells lend support to this hypothesis. The DOM pools of NSHQ14, WAB71, and WAB55 are each distinguished from the other wells in these analyses, while the two alkaline wells analyzed (WAB104 and WAB105) contain DOM pools that are very similar to each other. TOC was highest in the hyperalkaline wells, lower in the alkaline wells, and lowest in the contact wells (**Table 1**). Correlating TOC to cell count resulted in an R^2 value of 0.503, indicating that TOC is only partially driven by the amount of biomass present. Assuming an average carbon content per cell of 65 fg C cell^{-1} in the subsurface (Parkes et al., 1994), intact cells account for 0.00072–0.0025% of TOC; lower estimates of 14 fg C cell^{-1} from subsurface marine sediments (Braun et al., 2016) yield a TOC percentage of 0.00016–0.00054% from intact cells.

We hypothesize that the relative shortage of bioavailable electron acceptors in the hyperalkaline wells leads to dissolved organics being degraded and remineralized more slowly in these environments (Fones et al., 2019). The higher TOC values in the hyperalkaline wells also may reflect the abiotic production of formate and/or small molecular weight organic compounds associated with serpentinization (Proskurowski et al., 2008; McCollom, 2013). For example, the features annotated as butanoic acid, which displayed the greatest abundance in the hyperalkaline wells, may be the result of abiotic organic synthesis (McCollom and Seewald, 2006), as we did not detect the pathway for butanoic acid production *via* fermentation in the metagenomic data. Similarly, relatively high abundances of features annotated as intermediates of propanoate degradation in the hyperalkaline wells raise the intriguing possibility that the abiotic production of propanoate could serve as a carbon source for the microbial communities found there (Shock and Schulte, 1998). Recent carbon analysis of serpentinized rocks obtained in the Oman Drilling Project shows that non-carbonate-carbon loadings are approximately 140–360 ppm (Ternieten et al., 2021). Thus, there may be multiple primary sources of organic carbon in this system: autotrophic carbon fixation and turnover of biomass, heterotrophic utilization of reduced carbon accumulated in the rock during prior water/rock interaction, or ongoing abiotic organic synthesis.

Metagenomic data from the hyperalkaline wells indicates an enrichment of functional genes involved in C1 metabolisms such as CO utilization, methanogenesis, and acetogenesis (Fones et al., 2019; Coleman et al., 2022). Our characterization of the DOC pool generally supports these findings. Features annotated as metabolites associated with methanogenesis tended to display greater relative abundance in the hyperalkaline wells, where both methane and methanogens have been detected by previous studies (Rempfert et al., 2017; Fones et al., 2019; Kraus et al., 2021). The features putatively annotated as intermediates of propanoate degradation (mentioned above) were also putatively annotated as *cis*-homoaconitate (**Figure 5**), an intermediate in the biosynthesis of coenzyme B, which reacts with coenzyme M to release methane during methanogenesis. The detection of isethionic acid in NSHQ14 may be linked to the degradation of sulfoacetaldehyde produced during coenzyme M biosynthesis, while the abundance of dolichyl diphosphate, an intermediate of N-glycan biosynthesis in archaea, may also be a result of the high abundance of methanogenic archaea in NSHQ14 (Fones et al., 2019, 2021).

The feature annotated as isocitrate was three orders of magnitude more abundant in the hyperalkaline wells than in the alkaline wells, and seven orders of magnitude higher in the hyperalkaline wells than in the contact well (**Figure 5**). Isocitrate has been implicated as a metabolic intermediate in some methanogens; for example, Methanosarcinales generates CO_2 and 2-oxoglutarate from isocitrate *via* a partial oxidative TCA cycle (Anderson et al., 2009). This activity may serve as a source of CO_2 for the production of methane by hydrogenotrophic methanogen

such as *Methanobacterium*, which do not contain the pathway for 2-oxoglutarate generation *via* isocitrate (Anderson et al., 2009), but are abundant and active in NSHQ14 (Rempfert et al., 2017; Kraus et al., 2021). A bin annotated as *Methanobacterium* was the most abundant bin in NSHQ14, and designated as a representative bin of NSHQ14 by NMF analysis (**Figure 6**). This bin did not contain the gene for the NAD-dependent isocitrate dehydrogenase required for CO_2 and 2-oxoglutarate generation *via* isocitrate, but 20 other bins did contain this gene, more than half of which were most abundant in the hyperalkaline wells (including one bin belonging to the Moorellia that was designated a representative bin of NSHQ14, and a likely homoacetogen) (**Supplementary Table 3**). A syntrophy relationship may exist between hydrogenotrophic methanogens and bacteria containing the partial oxidative TCA cycle, whereby the CO_2 generated through this pathway fuels methanogenesis. Further studies, perhaps involving tracer/microcosm experiments, will be necessary to confirm if isocitrate generates CO_2 for methanogenesis in the hyperalkaline wells.

Isocitrate is an important central metabolite in many processes, including glyoxylate and dicarboxylate metabolism, 2-oxocarboxylic metabolism, and the biosynthesis of signaling molecules and secondary metabolites. The glyoxylate cycle allows microorganisms to use C2 compounds such as acetate to satisfy cellular carbon requirements when simple sugars such as glucose are not available (Kornberg and Madsen, 1957; LaPorte et al., 1984). Microcosm experiments conducted in parallel to this study found that rates of assimilation/oxidation of acetate were higher than those of bicarbonate and carbon monoxide across all sampled wells, suggesting that acetate may be the preferred source of bioavailable carbon (Fones et al., 2019; Coleman et al., 2022).

Metagenomic data have also shown an enrichment in genes involved in anaerobic metabolisms in hyperalkaline waters, while the alkaline wells were enriched in respiratory and electron transport chain genes (Fones et al., 2019). In contrast to the previously published metagenomic study, we found that features annotated as quinones and their precursors were generally enriched in NSHQ14, and to a lesser extent WAB71, compared to the contact and alkaline wells, with the exception of coproporphyrinogen III and phylloquinol (**Figure 6**). The abundance of these intermediates in the deeper wells may be indicative of slower turnover rates due to the extremophilic nature of this environment, or they may serve as intermediates of a process not yet characterized.

The abundance of features associated with plant and fungi pigments, including chlorophyll, in the alkaline and contact wells may reflect the greater influence of meteoric water in these wells (Nothaft et al., 2021). However, while the complete pathways for chlorophyll biosynthesis were not detected in the metagenomic data, the genes for the production of the intermediates we detected in the metabolome were found in multiple bins (**Figure 6**). In general, features related to the biosynthesis of pigments including carotenoids, quinones, and the chlorophyll intermediates may be linked to oxidative stress. Increased production of carotenoids, for example, has been observed previously in both neutrophilic (Lan et al., 2010) and extremophilic microorganisms (Tian and Hua, 2010; Mandelli et al., 2012) under oxidative stress conditions.

Of particular interest is the detection of several features putatively annotated as prostaglandins. These features were detected in all the wells, but were two to six orders of magnitude more abundant in WAB71 than in the other wells. We immediately questioned the validity of this annotation, as prostaglandins are signaling molecules found in higher eukaryotes. MISA analysis suggested that these features were either prostaglandin H2 or prostaglandin D2, both of which are involved in the human inflammatory response. However, prostaglandin H2 has a half-life of 90–100 s at room temperature (Human Metabolome Database), while prostaglandin D2 is found chiefly in brain and mast cells. These factors make it unlikely that these features are the result of contamination of our samples *via* casual contact. They may be prostaglandins produced by plants, but their abundance in WAB71, one of the most alkaline and least surface-influenced of the wells, makes this likewise unlikely.

We propose that these features may instead be secondary metabolites of arachidonic (ARA) or eicosapentaenoic acid (EPA). These polyunsaturated fatty acids serve as precursors to prostaglandins in higher eukaryotes, but are also found in some (mostly marine) bacteria belonging to the Gammaproteobacteria, Bacteroidetes, and Cyanobacteria. Eicosapentaenoic acid was annotated in the mass spec data during analysis with Progenesis QI, but MISA did not confirm this annotation (data not shown). Bacterial biosynthetic mechanisms of long-chain polyunsaturated fatty acids (LC-PUFAs) are not well understood and the functions of these lipids in bacteria have not been experimentally confirmed (Yoshida et al., 2016). It has been suggested that the primary function of LC-PUFAs is the adjustment of cell membrane fluidity under conditions of low temperature and/or high pressure (Kato and Nogi, 2001). EPA is required for growth at low temperatures and high pressures by some *Shewanella* species (Wang et al., 2004; Kawamoto et al., 2009; Usui et al., 2012), but a study of an EPA-deficient strain of *Photobacterium profundum* showed that monounsaturated or branched chain fatty acids could compensate for the loss of EPA (Allen et al., 1999). EPA and other LC-PUFAs have also been implicated in resistance to reactive oxygen species and oxidative stress (Nishida et al., 2006a,b, 2007, 2010; Okuyama et al., 2008; Tilay and Annapure, 2012).

Four of the bins analyzed in this study contained ≥75% of the protein-coding genes required to produce arachidonate synthase and/or eicosapentaenoate synthase (**Figure 6**). Three of these bins were more abundant in WAB71 than any other well, and included two members of the Chloroflexota, order Anaerolineales (one of which was annotated *Bellilinea* sp.), and one member of the Desulfobacterota, family Desulfomonilaceae. The other bin was most abundant in WAB105, and was also a member of the Anaerolineales, *Levilinea* sp. The gene organization, order of genes, and composition of enzymatic domains in *pfa* gene clusters that produce LC-PUFAs appear to be highly conserved (Okuyama et al., 2007). *Pfa* gene homologs have also been identified in the genomes of 86 bacterial species belonging to 10 phyla, the products of which are largely unknown (Shulse and Allen, 2011). These homologs

can be classified into 20 different gene types, which show a significant correlation with the ecological and physiological characteristics of the bacteria possessing the genes, suggesting that characterizing these secondary lipids may provide valuable insight into the ecological adaptation and evolution of microorganisms (Shulse and Allen, 2011). Lipid biomarkers have previously been characterized in rock samples obtained from the Samail Ophiolite; however, this study did not screen for LC-PUFAs (Newman et al., 2020). The *pfa* genes we detected in these bins may be homologs that produce an as-of-yet uncharacterized fatty acid product (Shulse and Allen, 2011).

Conclusion

Characterization of the DOM pool in the Samail Ophiolite groundwater reveals the presence of numerous metabolic products and intermediates that may provide clues to the survival strategies of microbial communities in environments associated with serpentinization. Among the features we were able to annotate and confirm with metagenomic data, the pigments, porphyrins, fatty acids, sterols, and intermediates/byproducts of pathways associated with methanogenesis (such as coenzyme B and coenzyme M biosynthesis) were the compounds whose abundance was most strongly correlated to fluid type. In particular, pigments are a promising and intriguing biosignature of life in this system, due to both their specificity to particular processes and their longevity in the geological record (Schwieterman et al., 2015).

We chose methods for characterization that we hoped would allow us to capture as many DOM features as possible. These methods naturally have limitations. Many of the metabolic pathways of interest in these wells, in particular those involved with C1 metabolisms, consist of intermediate compounds that are involved in multiple overlapping pathways (Peregrín-Alvarez et al., 2009), many of which are too small to be detected using the liquid chromatography methods used in this study. These compounds are also cycled rapidly and retained within the cell (Bar-Even et al., 2011), precluding them from an exometabolome analysis such as this one. Additionally, many of the features we detected could not be annotated using available metabolite databases- a caveat which reflects both the under-characterization of microbial secondary metabolites on the whole, but also the uniqueness of the environment and the microbial communities that inhabit it. The annotation of features based on mass and fragmentation is also a potential source of error, and structural assignments based on these criteria may not be valid. Metagenomic data can be used to reinforce these annotations but does not provide absolute certainty.

Linking DOM composition to environmental characteristics has exciting implications for the search for potential biomarkers for life fueled by serpentinization, in particular because the greatest numbers of unique features were found in wells that are the most heavily influenced by serpentinization. Metabolomics studies of environments of astrobiological significance, such as serpentinizing rock, hold great promise in the search for biomarkers that may be used as evidence of life on other worlds (Seyler L. et al., 2020). Further efforts to characterize the unique features detected in hyperalkaline fluids in the Samail Ophiolite may thus provide researchers with the means to detect life in serpentinizing systems elsewhere in our Solar System, such as the subsurface of Mars or the icy moons of Jupiter and Saturn. Such techniques hold the possibility of uncovering biomarkers of processes and relationships that are representative of habitats influenced by serpentinization, aiding the search for life in similar environments on other worlds in our Solar System.

Data availability statement

The datasets presented in this study can be found in online repositories. The names of the repository/repositories and accession number(s) can be found below: https://www.mg-rast.org/mgmain.html?mgpage=overview&metagenome=mgm4795806.3, mgm.4795806.3, https://www.mg-rast.org/mgmain.html?mgpage=overview&metagenome=mgm4795807.3, mgm4795807.3, https://www.mg-rast.org/mgmain.html?mgpage=overview&metagenome=mgm4795808.3, mgm4795808.3, https://www.mg-rast.org/mgmain.html?mgpage=overview&metagenome=mgm4795804.3, mgm4795804.3, https://www.mg-rast.org/mgmain.html?mgpage=overview&metagenome=mgm4795810.3, mgm4795810.3, and https://www.ebi.ac.uk/metabolights/MTBLS6081. The data in the MetaboLights database has just been made publicly available.

Author contributions

LS collected the samples, carried out metabolite extractions, and performed metagenomic and metabolomic data analysis. EK performed metagenomic data analysis. CM performed metabolomic data analysis. JS and AT oversaw fieldwork operations. JS, AT, and MS supervised the work. LS wrote the manuscript with input from all authors. All authors contributed to the article and approved the submitted version.

Funding

This work was supported by a grant from the NASA Astrobiology Institute (NNA15BB02A) to AT, JS, Eric Boyd, and MS and the Deep Carbon Observatory - Deep Life Community (#2015-14084) to MS.

Acknowledgments

We thank Kaitlin Rempfert, Eric Ellison, Laura Beuter, and Eric Boyd for assistance with sample collection, Juerg Matter for help with equipment acquisition, permitting, and sample export, and the Ministry of Regional Municipalities and Water Resources in the Sultanate of Oman for allowing sampling and export of well waters.

We also thank A. Daniel Jones and Anthony Schilmiller for their assistance with performing QToF-LC/MS/MS, and Elizabeth Kujawinski for her guidance regarding data analysis and interpretation.

Conflict of interest

The authors declare that the research was conducted in the absence of any commercial or financial relationships that could be construed as a potential conflict of interest.

Publisher's note

All claims expressed in this article are solely those of the authors and do not necessarily represent those of their affiliated organizations, or those of the publisher, the editors and the reviewers. Any product that may be evaluated in this article, or claim that may be made by its manufacturer, is not guaranteed or endorsed by the publisher.

Supplementary material

The Supplementary Material for this article can be found online at: https://www.frontiersin.org/articles/10.3389/fmicb.2023.1093372/full#supplementary-material

SUPPLEMENTARY FIGURE 1
Map of sampled wells in the Samail Ophiolite. Figure adapted from Rempfert et al. (2017).

SUPPLEMENTARY TABLE 1
All features identified as representative of the three well types ("levels") determined by non-negative matrix factorization (NMF) analysis. Annotations acquired by mummichog are included where available. Features highlighted in bold were annotated by Progenesis QI using the ChemSpider Database (**Supplementary Table 2**).

SUPPLEMENTARY TABLE 2
Representative features that could be annotated by Progenesis QI using the ChemSpider database.

SUPPLEMENTARY TABLE 3
KOs for all genes annotated by KEGGDecoder in bins included in this study.

SUPPLEMENTARY TABLE 4
All bins included in this study, including bin completeness, contamination, strain heterogeneity, and phylogenetic annotation.

References

Allen, E. E., Facciotti, D., and Bartlett, D. H. (1999). Monounsaturated but not polyunsaturated fatty acids are required for growth of the deep-sea bacterium *Photobacterium profundum* SS9 at high pressure and low temperature. *Appl. Environ. Microbiol.* 65, 1710–1720. doi: 10.1128/AEM.65.4.1710-1720.1999

Amend, J. P., McCollom, T. M., Hentscher, M., and Bach, W. (2011). Catabolic and anabolic energy for chemolithoautotrophs in deep-sea hydrothermal systems hosted by different rock types. *Geochim. Cosmochim. Acta* 75, 5736–5748. doi: 10.1016/j.gca.2011.07.041

Anderson, I., Ulrich, L. E., Lupa, B., Susanti, W., Porat, I., Hooper, S. D., et al. (2009). Genomic characterization of Methanomicrobiales reveals three classes of methanogens. *PLoS One* 4:e5797. doi: 10.1371/journal.pone.0005797

Bar-Even, A., Noor, E., Flamholz, A., Buescher, J. M., and Milo, R. (2011). Hydrophobicity and charge shape cellular metabolite concentrations. *PLoS Comp. Biol.* 7:e1002166. doi: 10.1371/journal.pcbi.1002166

Barnes, I., O'Neil, J. R., and Trescases, J. J. (1978). Present day serpentinization in New Caledonia, Oman and Yugoslavia. *Geochim. Cosmochim. Acta* 42, 144–145. doi: 10.1016/0016-7037(78)90225-9

Bauermeister, A., Mannochio-Russo, H., Costa-Lotufo, L. V., Jarmusch, A. K., and Dorrestein, P. C. (2021). Mass spectrometry-based metabolomics in microbiome investigations. *Nat. Rev. Microbiol.* 20, 143–160. doi: 10.1038/s41579-021-00621-9

Beale, D. J., Karpe, A. V., and Ahmed, W. (2016). "Beyond metabolomics: a review of multi-omics-based approaches," in *Microbial Metabolomics*, eds D. Beale, K. Kouremenos, and E. Palombo (Cham: Springer), 289–312.

Blachowicz, A., Chiang, A. J., Elsaesser, A., Kalkum, M., Ehrenfreund, P., Stajich, J. E., et al. (2019). Proteomic and metabolomic characteristics of extremophilic fungi under simulated Mars conditions. *Front. Microbiol.* 10:1013. doi: 10.3389/fmicb.2019.01013

Boudier, F., and Coleman, R. G. (1981). Cross section through the peridotite in the Samail Ophiolite. *J. Geophys. Res.* 86, 2573–2592. doi: 10.1029/JB086iB04p02573

Braun, S., Morono, Y., Littman, S., Kuypers, M., Aslan, H., Dong, M., et al. (2016). Size and carbon content of sub-seafloor microbial cells at Landsort Deep, Baltic Sea. *Front. Microbiol.* 7:1375. doi: 10.3389/fmicb.2016.01375

Brazelton, W. J., Mehta, M. P., Kelley, D. S., and Baross, J. A. (2011). Physiological differentiation within a single-species biofilm fueled by serpentinization. *mBio* 2:e00127-11. doi: 10.1128/mBio.00127-11

Brazelton, W. J., Morrill, P. L., Szponar, N., and Schrenk, M. O. (2013). Bacterial communities associated with subsurface geochemical processes in continental serpentinite springs. *Appl. Environ. Microbiol.* 79, 3906–3916. doi: 10.1128/AEM.00330-13

Brazelton, W. J., Nelson, B., and Schrenk, M. O. (2012). Metagenomic evidence for H2 oxidation and H2 production by serpentinite-hosted subsurface microbial communities. *Front. Microbiol.* 2:268. doi: 10.3389/fmicb.2011.00268

Brazelton, W. J., Thornton, C. N., Hyer, A., Twing, K. I., Longino, A. A., Lang, S. Q., et al. (2017). Metagenomic identification of active methanogens and methanotrophs in serpentinite springs of the Voltri Massif, Italy. *PeerJ* 5:e2945. doi: 10.7717/peerj.2945

Breitling, R., Ceniceros, A., Jankevics, A., and Takano, E. (2013). Metabolomics for secondary metabolite research. *Metabolites* 3, 1076–1083. doi: 10.3390/metabo3041076

Broadhurst, D., Goodacre, R., Reinke, S. N., Kuligowski, J., Wilson, I. D., Lewis, M. R., et al. (2018). Guidelines and considerations for the use of system suitability and quality control samples in mass spectrometry assays applied in untargeted clinical metabolomic studies. *Metabolomics* 14:72. doi: 10.1007/s11306-018-1367-3

Brunet, J. P., Tamayo, P., Golub, T. R., and Mesirov, J. P. (2004). Metagenes and molecular pattern discovery using matrix factorization. *Proc. Natl. Acad. Sci. U.S.A.* 101, 4164–4169. doi: 10.1073/pnas.0308531101

Canovas, P. A., Hoehler, T., and Shock, E. L. (2017). Geochemical bioenergetics during low-temperature serpentinization: an example from the Samail ophiolite, Sultanate of Oman. *J. Geophys. Res. Biogeosci.* 122, 1821–1847. doi: 10.1002/2017JG003825

Cardace, D., Meyer Dombard, D. R., Woycheese, K. M., and Arcilla, C. A. (2015). Feasible metabolisms in high pH springs of the Philippines. *Front. Microbiol.* 6:10. doi: 10.3389/fmicb.2015.00010

Carmona-Saez, P., Pascual-Marqui, R., Tirado, F., Carazo, J., and Pascual-Montano, A. (2006). Biclustering of gene expression data by non-smooth non-negative matrix factorization. *BMC Bioinformatics* 7:78. doi: 10.1186/1471-2105-7-78

Caspi, R., Altman, T., Billington, R., Foerster, H., Fulcher, C. A., and Keseler, I. M. (2014). The MetaCyc Database of metabolic pathways and enzymes and the BioCyc collection of Pathway/Genome Databases. *Nucleic Acids Res.* 44, D471–D480. doi: 10.1093/nar/gkv1164

Charlou, J. L., Donval, J. P., Fouquet, Y., Jean-Baptiste, P., and Holm, N. (2002). Geochemistry of high H2 and CH4 vent fluids issuing from ultramafic rocks at the Rainbow hydrothermal field (36 Deg14'N, MAR). *Chem. Geol.* 191, 345–359. doi: 10.1016/S0009-2541(02)00134-1

Chaumeil, P.-A., Mussig, A. J., Hugenholtz, P., and Parks, D. H. (2020). GTDB-Tk: A toolkit to classify genomes with the genome taxonomy database. *Bioinformatics* 36, 1925–1927. doi: 10.1093/bioinformatics/btz848

Clark, I. D., and Fontes, J.-C. (1990). Paleoclimatic reconstruction in northern Oman based on carbonates from hyperalkaline groundwaters. *Quat. Res.* 33, 320–336. doi: 10.1016/0033-5894(90)90059-T

Coleman, R. G. (1981). Tectonic setting for ophiolite obduction in Oman. *J. Geophys. Res.* 86, 2497–2508. doi: 10.1029/JB086iB04p02497

Coleman, R. G., and Hopson, C. A. (1981). Introduction to the Oman Ophiolite special issue. *J. Geophys. Res.* 86, 2495–2496. doi: 10.1029/JB086iB04p02495

Coleman, D. R., Kraus, E. A., Rempfert, K., Templeton, A. S., Spear, J. R., and Boyd, E. S. (2022). Adaptations of deeply-rooted acetogens to serpentinized subsurface fluids. *Proc. Natl. Acad. Sci. U.S.A.* 119:e2206845119. doi: 10.1073/pnas.220684511

Covington, B. C., McLean, J. A., and Bachmann, B. O. (2016). Comparative mass spectrometry-based metabolomics strategies for the investigation of microbial secondary metabolites. *Nat. Prod. Rep.* 34, 6–24. doi: 10.1039/c6np00048g

Dittmar, T., Koch, B., Hertkorn, N., and Kattner, G. (2008). A simple and efficient method for the solid-phase extraction of dissolved organic matter (SPE-DOM) from seawater. *Limnol. Oceanogr. Methods* 6, 230–235. doi: 10.4319/lom.2008.6.230

Domingo-Almenara, X., Montenegro-Burke, J. R., Guijas, C., Majumder, E. L., Benton, H. P., and Siuzdak, G. (2019). Autonomous METLIN-guided in-source fragment annotation for untargeted metabolomics. *Anal. Chem.* 91, 3246–3253. doi: 10.1021/acs.analchem.8b03126

Douglas, A. E. (2020). The microbial exometabolome: ecological resource and architect of microbial communities. *Philos. Trans. R. Soc. Lond. B. Biol. Sci.* 375:20190250. doi: 10.1098/rstb.2019.0250

Eddy, S. R. (2008). A probabilistic model of local sequence alignment that simplifies statistical significance estimation. *PLoS Comp. Biol.* 4:e1000069. doi: 10.1371/journal.pcbi.1000069

Edgar, R. C. (2004). MUSCLE: multiple sequence alignment with high accuracy and high throughput. *Nucleic Acids Res.* 32, 1792–1797. doi: 10.1093/nar/gkh340

Fiore, C. L., Longnecker, K., Kido Soule, M. C., and Kujawinski, E. (2015). Release of ecologically relevant metabolites by the cyanobacterium *Synechococcus elongatus* CCMP 1631. *Environ. Microbiol.* 17, 3949–3963. doi: 10.1111/1462-2920.12899

Fones, E. M., Colman, D. R., Kraus, E. A., Nothaft, D. B., Poudel, S., Rempfert, K. R., et al. (2019). Physiological adaptations to serpentinization in the Samail Ophiolite, Oman. *ISME J.* 13, 1750–1762. doi: 10.1038/s41396-019-0391-2

Fones, E. M., Colman, D. R., Kraus, E. A., Stepanauskas, R., Templeton, A. S., Spear, J. R., et al. (2021). Diversification of methanogens into hyperalkaline serpentinizing environments through adaptations to minimize oxidant limitation. *ISME J.* 15, 1121–1135. doi: 10.1038/s41396-020-00838-1

Fürch, T., Preusse, M., Tomasch, J., Zech, H., Wagner-Döbler, I., Rabus, R., et al. (2009). Metabolic fluxes in the central carbon metabolism of *Dinoroseobacter shibae* and *Phaeobacter gallaeciensis*, two members of the marine *Roseobacter clade*. *BMC Microbiol.* 9:209. doi: 10.1186/1471-2180-9-209

Gaujoux, R., and Seoighe, C. (2010). A flexible R package for nonnegative matrix factorization. *BMC Bioinform.* 11:367. doi: 10.1186/1471-2105-11-367

Glennie, K. W. (1996). The geology of the Oman mountains. *J. Pet. Geol.* 19:125. doi: 10.1111/j.1747-5457.1996.tb00520.x

Glennie, K. W., and Clarke, M. H. (1973). Late *Cretaceous nappes* in Oman Mountains and their geologic evolution. *AAPG Bull.* 57, 5–27. doi: 10.1306/83D912F4-16C7-11D7-8645000102C1865D

Glombitza, C., Putman, L. I., Rempfert, K. R., Kubo, M. D., Schrenk, M. O., Templeton, A. S., et al. (2021). Active microbial sulfate reduction in fluids of serpentinizing peridotites of the continental subsurface. *Commun. Earth Environ.* 2:84. doi: 10.1038/s43247-021-00157-z

Graham, E. D., Heidelberg, J. F., and Tully, B. J. (2017). BinSanity: unsupervised clustering of environmental microbial assemblies using coverage and affinity propagation. *PeerJ* 5:e3035. doi: 10.7717/peerj.3035

Graham, E. D., Heidelberg, J. F., and Tully, B. J. (2018). Potential for primary productivity in a globally-distributed bacterial phototroph. *ISME J.* 12, 1861–1866. doi: 10.1038/s41396-018-0091-3

Hacker, B. R., Mosenfelder, J. L., and Gnos, E. (1996). Rapid emplacement of the Oman ophiolite: thermal and geochronologic constraints. *Tectonics* 15, 1230–1247. doi: 10.1029/96TC01973

Haug, K., Cochrane, K., Nainala, V. C., Williams, M., Chang, J., Jayaseelan, K. V., et al. (2020). MetaboLights: a resource evolving in response to the needs of its scientific community. *Nucleic Acids Res.* 48, D440–D444. doi: 10.1093/nar/gkz1019

Kanehisa, M., and Goto, S. (2000). KEGG: kyoto encyclopedia of genes and genomes. *Nucleic Acids Res.* 28:4. doi: 10.1093/nar/28.1.27

Kato, C., and Nogi, Y. (2001). Correlation between phylogenetic structure and function: examples from deep-sea *Shewanella*. *FEMS Microbiol. Ecol.* 35, 223–230. doi: 10.1111/j.1574-6941.2001.tb00807.x

Kawamoto, J., Kurihara, T., Yamamoto, K., Nagayasu, M., Tani, Y., Mihara, H., et al. (2009). Eicosapentaenoic acid plays a beneficial role in membrane organization and cell division of a cold-adapted bacterium, *Shewanella livingstonensis* Ac10. *J. Bacteriol.* 191, 632–640. doi: 10.1128/JB.00881-08

Keleman, P. B., Leong, J. A., de Obeso, J. C., Matter, J. M., Ellison, E. T., Templeton, A., et al. (2021). Initial results from the Oman drilling project multi-borehole observatory: petrogenesis and ongoing alteration of mantle peridotite in the weathering horizon. *J. Geophys. Res. Solid Earth* 126:e2021JB022729. doi: 10.1029/2021JB022729

Kelemen, P. B., and Matter, J. (2008). *In situ* carbonation of peridotite for CO_2 storage. *Proc. Nat. Acad. Sci. U.S.A.* 105, 17295–17300. doi: 10.1073/pnas.0805794105

Kelemen, P., Rajhi, A. A., Godard, M., Ildefonse, B., Köpke, J., MacLeod, C., et al. (2013). Scientific drilling and related research in the Samail Ophiolite, Sultanate of Oman. *Sci. Dril.* 15, 64–71. doi: 10.2204/iodp.sd.15.10.2013

Kelemen, P. B., Matter, J., Streit, E. E., Rudge, J. F., Curry, W. B., and Blusztajn, J. (2011). Rates and mechanisms of mineral carbonation in peridotite: natural processes and recipes for enhanced, *in situ* CO_2 capture and storage. *Annu. Rev. Earth. Planet. Sci.* 39, 545–576. doi: 10.1146/annurev-earth-092010-152509

Kell, D., Brown, M., Davey, H., Dunn, W. B., Spasic, I., and Oliver, S. G. (2005). Metabolic footprinting and systems biology: the medium is the message. *Nat. Rev. Microbiol.* 3, 557–565. doi: 10.1038/nrmicro1177

Kim, H., and Park, H. (2007). Sparse non-negative matrix factorizations via alternating non-negativity-constrained least squares for microarray data analysis. *Bioinformatics* 23, 1495–1502. doi: 10.1093/bioinformatics/btm134

Klein, F., Grozeva, N. G., and Seewald, J. S. (2019). Abiotic methane synthesis and serpentinization in olivine-hosted fluid inclusions. *Proc. Natl. Acad. Sci. U.S.A.* 116, 17666–17672. doi: 10.1073/pnas.1907871116

Kornberg, H. L., and Madsen, N. B. (1957). Synthesis of C4-dicarboxylic acids from acetate by a glyoxylate bypass of the tricarboxylic acid cycle. *Biochim. Biophys. Acta* 24, 651–653. doi: 10.1016/0006-3002(57)90268-8

Kraus, E. A., Nothaft, D., Stamps, B. W., Rempfert, K. R., Ellison, E. T., Matter, J. M., et al. (2021). Molecular evidence for an active microbial methane cycle in subsurface serpentinite-hosted groundwaters in the Samail Ophiolite, Oman. *Appl. Environ. Microbiol.* 87:e02068-20. doi: 10.1128/AEM.02068-20

Kujawinski, E. B. (2011). The impact of microbial metabolism on marine dissolved organic matter. *Annu. Rev. Mar. Sci.* 3, 567–599. doi: 10.1146/annurev-marine-120308-081003

Lan, L., Murray, T. S., Kazmierczak, B. I., and He, C. (2010). *Pseudomonas aeruginosa* OspR is an oxidative stress sensing regulator that affects pigment production, antibiotic resistance and dissemination during infection. *Mol. Microbiol.* 75, 76–91. doi: 10.1111/j.1365-2958.2009.06955.x

Lang, S. Q., Früh-Green, G. L., Bernasconi, S. M., Lilley, M. D., Proskurowski, G., Méhaya, S., et al. (2012). Microbial utilization of abiogenic carbon and hydrogen in a serpentinite-hosted system. *Geochim. Cosmochim. Acta* 92, 82–99. doi: 10.1016/j.gca.2012.06.006

Langmead, B., and Salzberg, S. (2012). Fast gapped-read alignment with Bowtie 2. *Nat. Methods* 9, 357–359. doi: 10.1038/nmeth.1923

LaPorte, D. C., Walsh, K., and Koshland, D. E. Jr. (1984). The branch point effect. Ultrasensitivity and subsensitivity to metabolic control. *J. Biol. Chem.* 259, 14068–14075. doi: 10.1016/S0021-9258(18)89857-X

Legendre, P., and Gallagher, E. D. (2001). Ecologically meaningful transformations for ordination of species data. *Oecologia* 129, 271–280. doi: 10.1007/s004420100716

Leong, J. A. M., Howells, A. E., Robinson, K. J., Cox, A., Debes, R. V. II, Fecteau, K., et al. (2021). Theoretical predictions versus environmental observations on serpentinization fluids: lessons from the Samail Ophiolite in Oman. *J. Geophys. Res. Solid Earth* 126:e2020JB020756. doi: 10.1029/2020JB020756

Li, S., Park, Y., Duraisingham, S., Strobel, F. H., Khan, N., Soltow, Q. A., et al. (2013). Predicting network activity from high throughput metabolomics. *PLoS Comput. Biol.* 9:e1003123. doi: 10.1371/journal.pcbi.1003123

Lippard, S. J., Shelton, A. W., and Gass, I. G. (1986). *The Ophiolite of Northern Oman*. London: Geological Society.

Liu, X., Lu, Y. F., Guan, X., Zhao, M., Wang, J., and Li, F. (2016). Characterizing novel metabolic pathways of melatonin receptor agonist agomelatine using metabolomic approaches. *Biochem. Pharmacol.* 109, 70–82. doi: 10.1016/j.bcp.2016.03.020

Lu, S., Wang, J., Chitsaz, F., Derbyshire, M. K., Geer, R. C., Gonzales, N. R., et al. (2020). CDD/SPARCLE: the conserved domain database in 2020. *Nucleic Acids Res.* 48, D265–D268. doi: 10.1093/nar/gkz991

Manandhar, M., and Cronan, J. E. (2017). Pimelic acid, the first precursor of the Bacillus subtilis biotin synthesis pathway, exists as the free acid and is assembled by fatty acid synthesis. *Mol. Microbiol.* 104, 595–607. doi: 10.1111/mmi.13648

Mandelli, F., Miranda, V. S., and Rodrigues, E. Z. (2012). Identification of carotenoids with high antioxidant capacity produced by extremophile microorganisms. *World J. Microbiol. Biotechnol.* 28, 1781–1790. doi: 10.1007/s11274-011-0993-y

McCollom, T. M. (2007). Geochemical constraints on sources of metabolic energy for chemolithoautotrophy in ultramafic-hosted deep-sea hydrothermal systems. *Astrobiology* 7, 933–950. doi: 10.1089/ast.2006.0119

McCollom, T. M. (2013). Laboratory simulations of abiotic hydrocarbon formation in Earth's deep subsurface. *Rev. Mineral. Geochem.* 75, 467–494.

McCollom, T. M., Klein, F., and Ramba, M. (2022). Hydrogen generation from serpentinization of iron-rich olivine on Mars, icy moons, and other planetary bodies. *Icarus* 372:114754. doi: 10.1016/j.icarus.2021.114754

McCollom, T. M., and Seewald, J. S. (2001). A reassessment of the potential for reduction of dissolved CO_2 to hydrocarbons during serpentinization of olivine. *Geochim. Cosmochim. Acta* 65, 3769–3778. doi: 10.1016/S0016-7037(01)00655-X

McCollom, T. M., and Seewald, J. S. (2006). Carbon isotope composition of organic compounds produced by abiotic synthesis under hydrothermal conditions. *Earth Planet. Sci. Lett.* 243, 74–84. doi: 10.1016/j.epsl.2006.01.027

Miller, H. M., Matter, J. M., Kelemen, P., Ellison, E. T., Conrad, M. E., Fierer, N., et al. (2016). Modern water/rock reactions in Oman hyperalkaline peridotite aquifers and implications for microbial habitability. *Geochim. Cosmochim. Acta* 179, 217–241. doi: 10.1016/j.gca.2016.01.033

Miller, D., O'Brien, K., Xu, H., and White, R. H. (2014). Identification of a 5'-deoxyadenosine deaminase in Methanocaldococcus janaschii and its possible role in recycling the radical S-adenosylmethionine enzyme reaction product 5'-deoxyadenosine. *J. Bacteriol.* 196, 1064–1072. doi: 10.1128/JB.01308-13

Neal, C., and Stanger, G. (1983). Hydrogen generation from mantle source rocks in Oman. *Earth Planet. Sci. Lett.* 66, 315–320. doi: 10.1016/0012-821X(83)90144-9

Neal, C., and Stanger, G. (1985). "Past and present serpentinisation of ultramafic rocks; an example from the Semail Ophiolite nappe of northern Oman," in *The Chemistry of Weathering*, ed. J. I. Drever (Dordrecht: Springer Netherlands), 249–275.

Neely, C. J., Graham, E. D., and Tully, B. J. (2020). MetaSanity: an integrated microbial genome evaluation and annotation pipeline. *Bioinformatics* 36, 4341–4344. doi: 10.1093/bioinformatics/btaa512

Newman, S. A., Lincoln, S. A., O'Reilly, S., Liu, X., Shock, E. L., Kelemen, P. B., et al. (2020). Lipid biomarker record of the serpentinite-hosted ecosystem of the Samail Ophiolite, Oman and implications for the search for biosignatures on Mars. *Astrobiology* 20, 830–845. doi: 10.1089/ast.2019.2066

Nicolas, A., Boudier, F., Ildefonse, B., and Ball, E. (2000). Accretion of Oman and United Arab Emirates ophiolite- discussion of a new structural map. *Mar. Geophys. Res.* 21, 147–180. doi: 10.1023/A:1026769727917

Nishida, T., Hori, R., Morita, N., and Okuyama, H. (2010). Membrane eicosapentaenoic acid is involved in the hydrophobicity of bacterial cells and affects the entry of hydrophilic and hydrophobic compounds. *FEMS Microbiol. Lett.* 306, 91–96. doi: 10.1111/j.1574-6968.2010.01943.x

Nishida, T., Morita, N., Yano, Y., Orikasa, Y., and Okuyama, H. (2007). The antioxidative function of eicosapentaenoic acid in a marine bacterium, *Shewanella marinintestina* IK-1. *FEBS Lett.* 581, 4212–4216. doi: 10.1016/j.febslet.2007.07.065

Nishida, T., Orikasa, Y., Ito, Y., Yu, R., Yamada, A., Watanabe, K., et al. (2006a). *Escherichia coli* engineered to produce eicosapentaenoic acid becomes resistant against oxidative damages. *FEBS Lett.* 580, 2731–2735. doi: 10.1016/j.febslet.2006.04.032

Nishida, T., Orikasa, Y., Watanabe, K., and Okuyama, H. (2006b). The cell membrane-shielding function of eicosapentaenoic acid for *Escherichia coli* against exogenously added hydrogen peroxide. *FEBS Lett.* 580, 6690–6694. doi: 10.1016/j.febslet.2006.11.030

Nothaft, D. B., Templeton, A. S., Boyd, E. S., Matter, J. M., Stute, M., Paukert Vankeuren, A. N., et al. (2021). Aqueous geochemical and microbial variation across discrete depth intervals in a peridotite aquifer assessed using a packer system in the Samail Ophiolite, Oman. *J. Geophys. Res. Biogeosci.* 126:e2021JG006319. doi: 10.1029/2021JG006319

Okuyama, H., Orikasa, Y., and Nishida, T. (2008). Significance of antioxidative functions of eicosapentaenoic and docosahexaenoic acids in marine microorganisms. *Appl. Environ. Microbiol.* 74, 570–574. doi: 10.1128/AEM.02256-07

Okuyama, H., Orikasa, Y., Nishida, T., Watanabe, K., and Morita, N. (2007). Bacterial genes responsible for the biosynthesis of eicosapentaenoic acid and docosahexanoic acids and their heterologous expression. *Appl. Environ. Microbiol.* 73, 665–670. doi: 10.1128/AEM.02270-06

Oyedeji, A. B., Green, E., Adebiyi, J. A., Ogundele, O. M., Gbashi, S., Adefisoye, M. J., et al. (2021). Metabolomic approaches for the determination of metabolites from pathogenic microorganisms: a review. *Food Res. Int.* 140:110042. doi: 10.1016/j.foodres.2020.110042

Parkes, R. J., Cragg, B. A., Bale, S. J., Getliff, J. M., Goodman, K., Rochelle, P. A., et al. (1994). Deep bacterial biosphere in Pacific Ocean sediments. *Nature* 371, 410–413. doi: 10.1038/371410a0

Parks, D. H., Imelfort, M., Skennerton, C. T., Hugenholtz, P., and Tyson, G. W. (2015). CheckM: assessing the quality of microbial genomes recovered from isolates, single cells, and metagenomes. *Genome Res.* 25, 1043–1055. doi: 10.1101/gr.186072.114

Patti, G. J., Yanes, O., and Siuzdak, G. (2012). Metabolomics: the apogee of the omics trilogy. *Nat. Rev. Mol. Cell. Biol.* 13, 263–269. doi: 10.1038/nrm3314

Paukert, A. N., Matter, J. M., Kelemen, P. B., Shock, E. L., and Havig, J. R. (2012). Reaction path modeling of enhanced *in situ* CO_2 mineralization for carbon sequestration in the peridotite of the Samail Ophiolite, Sultanate of Oman. *Chem. Geol.* 330-331, 86–100. doi: 10.1016/j.chemgeo.2012.08.013

Paukert Vankeuren, A. N., Matter, J. M., Stute, M., and Kelemen, P. B. (2019). Multitracer determination of apparent groundwater ages in peridotite aquifers within the Samail ophiolite, Sultanate of Oman. *Earth Planet. Sci. Lett.* 516, 37–48. doi: 10.1016/j.epsl.2019.03.007

Peregrín-Alvarez, J. M., Sanford, C., and Parkinson, J. (2009). The conservation and evolutionary modularity of metabolism. *Genome Biol.* 10:R63. doi: 10.1186/gb-2009-10-6-r63

Peyraud, R., Kiefer, P., Christen, P., and Vorholt, J. A. (2009). Demonstration of the ethylmalonyl-CoA pathway by using ^{13}C metabolomics. *Proc. Natl. Acad. Sci. U.S.A.* 106, 4846–4851. doi: 10.1073/pnas.0810932106

Porcar, M., Louie, K. B., Kosina, S. M., Van Goethem, M. W., Bowen, B. P., Tanner, K., et al. (2018). Microbial ecology on solar panels in Berkeley, CA, United States. *Front. Microbiol.* 9:3043. doi: 10.3389/fmicb.2018.03043

Proskurowski, G., Lilley, M. D., Seewald, J. S., Früh-Green, G., Olson, E. J., Lupton, J. E., et al. (2008). Abiotic hydrocarbon production at lost city hydrothermal field. *Science* 319, 604–607. doi: 10.1126/science.1151194

Rabinowitz, J. D., and Kimball, E. (2007). Acidic acetonitrile for cellular metabolome extraction from *Escherichia coli*. *Anal. Chem.* 79, 6167–6173. doi: 10.1021/ac070470c

Rempfert, K. R., Miller, H. M., Bompard, N., Nothaft, D., Matter, J. M., Kelemen, P., et al. (2017). Geological and geochemical controls on subsurface microbial life in the Samail Ophiolite, Oman. *Front. Microbiol.* 8:56. doi: 10.3389/fmicb.2017.00056

Sabuda, M. C., Brazelton, W. J., Putman, L. I., McCollom, T. M., Hoehler, T. M., Kubo, M. D. Y., et al. (2020). A dynamic microbial sulfur cycle in a serpentinizing continental ophiolite. *Environ. Microbiol.* 22, 2329–2345. doi: 10.1111/1462-2920.15006

Schrenk, M. O., Brazelton, W. J., and Lang, S. Q. (2013). Serpentinization, carbon, and deep life. *Rev. Mineral. Geochem.* 75, 575–606. doi: 10.2138/rmg.2013.75.18

Schrenk, M. O., Kelley, D. S., Bolton, S. A., and Baroos, J. A. (2004). Low archaeal diversity linked to subseafloor geochemical processes at the Lost City Hydrothermal Field, Mid-Atlantic Ridge. *Environ. Microbiol.* 6, 1086–1095. doi: 10.1111/j.1462-2920.2004.00650.x

Schulte, M., Blake, D., Hoehler, T., and McCollom, T. (2006). Serpentinization and its implications for life on the early Earth and Mars. *Astrobiology* 6, 364–376. doi: 10.1089/ast.2006.6.364

Schwieterman, E. W., Cockell, C. S., and Meadows, V. S. (2015). Nonphotosynthetic pigments as potential biosignatures. *Astrobiology* 15, 341–361. doi: 10.1089/ast.2014.1178

Seyler, L., Kujawinski, E. B., Azua-Bustos, A., Lee, M. D., Marlow, J., Perl, S. M., et al. (2020). Metabolomics as an emerging tool in the search for astrobiologically relevant biomarkers. *Astrobiology* 20, 1251–1261. doi: 10.1089/ast.2019.2135

Seyler, L. M., Brazelton, W. L., McLean, C., Putman, L. I., Hyer, A., Kubo, M. D. Y., et al. (2020). Carbon assimilation strategies in ultrabasic groundwater: clues from the integrated study of a serpentinization-influenced aquifer. *mSystems* 5:e00607-19. doi: 10.1128/mSystems.00607-19

Shock, E. L., and Schulte, M. D. (1998). Organic synthesis during fluid mixing in hydrothermal systems. *J. Geophys. Res.* 103, 28513–28527. doi: 10.1029/98JE02142

Shulse, C. N., and Allen, E. E. (2011). Widespread occurrence of secondary lipid biosynthesis potential in microbial lineages. *PLoS One* 6:e20146. doi: 10.1371/journal.pone.0020146

Sleep, N. H., Meibom, A., Fridriksson, T., and Bord, D. K. (2004). H_2-rich fluids from serpentinization: geochemical and biotic implications. *Proc. Natl. Acad. Sci. U.S.A.* 101, 12818–12823. doi: 10.1073/pnas.0405289101

Smith, C. A., O'Maille, G. O., Want, E. J., Qin, C., Trauger, S. A., Brandon, T. R., et al. (2005). METLIN: a metabolite mass spectral database. *Ther. Drug Monit.* 27, 747–751. doi: 10.1097/01.ftd.0000179845.53213.39

Sogin, E. M., Puskás, E., Dubilier, N., and Liebeke, M. (2019). Marine metabolomics: a method for nontargeted measurement of metabolites in seawater by gas chromatography-mass spectrometry. *mSystems* 4:e00638-19. doi: 10.1128/mSystems.00638-19

Soldatou, S., Eldjarn, G. H., Huerta-Uribe, A., Rogers, S., and Duncan, K. R. (2019). Linking biosynthetic and chemical space to accelerate microbial secondary metabolite discovery. *FEMS Microbiol. Lett.* 366:fnz142. doi: 10.1093/femsle/fnz142

Streit, E., Kelemen, P., and Eiler, J. (2012). Coexisting serpentine and quartz from carbonate-bearing serpentinized peridotite in the Samail Ophiolite, Oman. *Contrib. Mineral. Petrol.* 164, 821–837. doi: 10.1007/s00410-012-0775-z

Suzuki, S., Nealson, N. H., and Ishii, S. (2018). Genomic and in-situ transcriptomic characterization of the candidate phylum NPL-UPL2 from highly alkaline highly reducing serpentinized groundwater. *Front. Microbiol.* 9:3141. doi: 10.3389/fmicb.2018.03141

Tang, Y. J., Yi, S., Zhuang, W.-Q., Zinder, S. H., Keasling, J. D., and Alvarez-Cohen, L. (2009). Investigation of carbon metabolism in "*Dehalococcoides ethenogenes*" strain 195 by use of isotopomer and transcriptomic analyses. *J. Bacteriol.* 191, 5224–5231. doi: 10.1128/JB.00085-09

Templeton, A. S., Ellison, E. T., Glombitza, C., Morono, Y., Rempfert, K. R., Hoehler, T. M., et al. (2021). Accessing the subsurface biosphere within rocks undergoing active

low-temperature serpentinization in the Samail Ophiolite (Oman Drilling Project). *J. Geophys. Res. Biogeosci.* 126:e2021JG006315.

Ternieten, L., Früh-Green, G. L., and Bernasconi, S. M. (2021). Carbon geochemistry of the active serpentinization site at the Wadi Tayin Massif: insights from the ICDP Oman Drilling Project: phase II. *J. Geophys. Res.Solid Earth* 126:e2021JB022712. doi: 10.1029/2021JB022712

Tian, B., and Hua, Y. (2010). Carotenoid biosynthesis in extremophilic Deinococcus-Thermus bacteria. *Trends Microbiol.* 18, 512–520. doi: 10.1016/j.tim.2010.07.007

Tilay, A., and Annapure, U. (2012). Novel simplified and rapid method for screening and isolation of polyunsaturated fatty acids producing marine bacteria. *Biotechnol. Res. Int.* 2012:542721. doi: 10.1155/2012/542721

Tilton, G. R., Hopson, C. A., and Wright, J. E. (1981). Uranium-lead isotopic ages of the Samail ophiolite, Oman, with applications to Tethyan Ocean ridge tectonics. *J. Geophys. Res.* 86, 2763–2775. doi: 10.1029/JB086iB04p02763

Turnbaugh, P. J., and Gordon, J. I. (2008). An invitation to the marriage of metagenomics and metabolomics. *Cell* 134, 708–713. doi: 10.1016/j.cell.2008.08.025

UniProt Consortium (2021). UniProt: The universal protein knowledgebase in 2021. *Nucleic Acids Res.* 49, D480–D489. doi: 10.1093/nar/gkaa1100

Usui, K., Hiraki, T., Kawamoto, J., Kurihara, T., Nogi, Y., Kato, C., et al. (2012). Eicosapentaenoic acid plays a role in stabilizing dynamic membrane structure in the deep-sea piezophile *Shewanella violacea*: a study employing high-pressure time-resolved fluorescence anisotropy measurement. *Biochim. Biophys. Acta* 1818, 574–583. doi: 10.1016/j.bbamem.2011.10.010

van Santen, J. A., Kautsar, S. A., Medema, M. H., and Linington, R. G. (2021). Microbial natural product databases: moving forward in the multi-omics era. *Nat. Prod. Rep.* 38, 264–278. doi: 10.1039/d0np00053a

Vance, S., Harnmeijer, J., Kimura, J., Hussman, H., Demartin, B., and Brown, J. M. (2007). Hydrothermal systems in small ocean planets. *Astrobiology* 7, 987–1005. doi: 10.1089/ast.2007.0075

Wang, F., Wang, P., Chen, M., and Xiao, X. (2004). Isolation of extremophiles with the detection and retrieval of *Shewanella* strains in deep-sea sediments from the west Pacific. *Extremophiles* 8, 165–168. doi: 10.1007/s00792-003-0365-0

Yoshida, K., Hashimoto, M., Hori, R., Adachi, T., Okuyama, H., Orikasa, Y., et al. (2016). Bacterial long-chain polyunsaturated fatty acids: their biosynthetic genes, functions, and practical use. *Mar. Drugs* 14, 94. doi: 10.3390/md14050094

frontiers | Frontiers in Microbiology

TYPE Original Research
PUBLISHED 12 April 2023
DOI 10.3389/fmicb.2023.1138656

OPEN ACCESS

EDITED BY
Gaël Erauso,
Aix-Marseille Université, France

REVIEWED BY
Mark Alexander Lever,
The University of Texas at Austin, United States
William J. Brazelton,
The University of Utah, United States

*CORRESPONDENCE
Eric S. Boyd
✉ eboyd@montana.edu

SPECIALTY SECTION
This article was submitted to Microbiological Chemistry and Geomicrobiology, a section of the journal Frontiers in Microbiology

RECEIVED 05 January 2023
ACCEPTED 27 March 2023
PUBLISHED 12 April 2023

CITATION
Munro-Ehrlich M, Nothaft DB, Fones EM, Matter JM, Templeton AS and Boyd ES (2023) Parapatric speciation of *Meiothermus* in serpentinite-hosted aquifers in Oman. *Front. Microbiol.* 14:1138656. doi: 10.3389/fmicb.2023.1138656

Parapatric speciation of *Meiothermus* in serpentinite-hosted aquifers in Oman

Mason Munro-Ehrlich[1], Daniel B. Nothaft[2], Elizabeth M. Fones[1], Juerg M. Matter[3], Alexis S. Templeton[2] and Eric S. Boyd[1]*

[1]Department of Microbiology and Cell Biology, Montana State University, Bozeman, MT, United States, [2]Department of Geosciences, University of Colorado, Boulder, Boulder, CO, United States, [3]School of Ocean and Earth Science, University of Southampton, Southampton, United Kingdom

The factors that control the distribution and evolution of microbial life in subsurface environments remain enigmatic due to challenges associated with sampling fluids from discrete depth intervals via boreholes while avoiding mixing of fluids. Here, using an inflatable packer system, fracture waters were isolated and collected from three discrete depth intervals spanning >130 m in a borehole intersecting an ultramafic rock formation undergoing serpentinization in the Samail Ophiolite, Sultanate of Oman. Near surface aquifer waters were moderately reducing and had alkaline pH while deeper aquifer waters were reduced and had hyperalkaline pH, indicating extensive influence by serpentinization. Metagenomic sequencing and analysis of DNA from filtered biomass collected from discrete depth intervals revealed an abundance of aerobes in near surface waters and a greater proportion of anaerobes at depth. Yet the abundance of the putatively obligate aerobe, *Meiothermus*, increased with depth, providing an opportunity to evaluate the influence of chemical and spatial variation on its distribution and speciation. Two clades of *Meiothermus* metagenome assembled genomes (MAGs) were identified that correspond to surface and deep populations termed Types I (S) and II (D), respectively; both clades comprised an apparently Oman-specific lineage indicating a common ancestor. Type II (D) clade MAGs encoded fewer genes and were undergoing slower genome replication as inferred from read mapping. Further, single nucleotide variants (SNVs) and mobile genetic elements identified among MAGs revealed detectable, albeit limited, evidence for gene flow/recombination between spatially segregated Type I (S) and Type II (D) populations. Together, these observations indicate that chemical variation generated by serpentinization, combined with physical barriers that reduce/limit dispersal and gene flow, allowed for the parapatric speciation of *Meiothermus* in the Samail Ophiolite or a geologic precursor. Further, *Meiothermus* genomic data suggest that deep and shallow aquifer fluids in the Samail Ophiolite may mix over shorter time scales than has been previously estimated from geochemical data.

KEYWORDS

subsurface, serpentinite, recombination, evolution, geographic isolation, parapatric speciation, dispersal limitation, competitive exclusion

Introduction

The terrestrial subsurface is host to an abundant and active microbial biosphere (McMahon and Parnell, 2014; Bar-On et al., 2018; Magnabosco et al., 2018) that comprises populations of cells inhabiting the pore spaces and (micro)fractures of rocks (Goordial et al., 2021; Fones et al., 2022). A large amount of the habitable subsurface is comprised of mafic and ultramafic igneous rocks. Mafic and ultramafic igneous rocks can undergo the geologic process of serpentinization that can generate H_2 through the oxidation of Fe(II)-containing minerals, such as olivine and brucite (Miller et al., 2017; Ellison et al., 2021). H_2, in turn, can react with CO_2 to generate formate ($HCOO^-$), carbon monoxide (CO), or methane (CH_4) (Seewald et al., 2006; McCollom and Seewald, 2007) that can be used as electron donors and/or carbon sources in microbial metabolism.

Serpentinization also generates highly reducing conditions that can limit the availability of oxidants needed to support microbial metabolism. For example, fracture fluids from rock formations undergoing serpentinization can exhibit oxidation-reduction potentials (*Eh*) as low as −750 mV (Templeton et al., 2021). Available oxidants in waters infiltrating these environments are consumed either abiotically via reactions involving minerals or soluble reductants (e.g., ferrous iron or hydrogen) or biotically by microorganisms. Low oxygen fugacity and oxidant limitation is characteristic of fluids collected from environments undergoing serpentinization (Frost and Beard, 2007; Rempfert et al., 2017; Suzuki et al., 2017; Templeton et al., 2021). In these systems, dissolved O_2 concentrations rarely exceed 40 μM even in the least reacted waters and are below detection in highly reacted waters (Rempfert et al., 2017; Suzuki et al., 2017; Piccoli et al., 2019). Yet, despite the apparent absence of O_2 in reacted waters, putatively obligate aerobes are often detected. For example, sequences related to the obligately aerobic genus of bacteria, *Meiothermus* (Deinococcota), have been detected in subsurface hyperalkaline and suboxic environments, oftentimes in high relative abundance (Chung et al., 1997; López-López et al., 2015; Woycheese et al., 2015). Likewise, fracture waters collected from a variety of depths in numerous wells have been shown to host *Meiothermus* DNA, including circumneutral near-surface waters and the most hyperalkaline and most highly reacted waters in the Samail Ophiolite, Sultanate of Oman (Rempfert et al., 2017; Nothaft et al., 2021).

Multiple reports of the presence of putative aerobes (e.g., *Meiothermus*) in what appear to be otherwise anoxic serpentinite fluids suggest the possibility that aerobes are widespread, can freely disperse among fractures in rocks, and are inactive in reduced portions of the serpentinites only to become active when favorable conditions are encountered. Depending on the time scales over which this occurs, the extent of dispersal could either allow for or fully restrict gene flow/recombination among otherwise isolated populations, allowing for localized speciation among closely related populations. Several recent studies offer differing perspectives on whether dispersal and/or gene flow/recombination are possible in subsurface habitats. A metagenomic analysis of low biomass subseafloor sediment communities in North Pond in the Atlantic Ocean sampled repeatedly (n = 10) over a period of nearly two years showed strain level shifts in the composition of populations comprising those communities (Anderson et al., 2022). Similarly, an analysis of 16S rRNA genes recovered from fluids in three boreholes intersecting a 1,400 m deep hard rock aquifer sampled over a 10 month period revealed substantial changes in community compositions (Zhang et al., 2022). In both studies, the results were interpreted to reflect dispersal of cells through sediment porewaters or fracture networks. In contrast, a recent study of 16S rRNA genes collected from subsurface fluids in the Cedars, a hard rock serpentinite formation located in California, USA, over multiple years concluded that spatial barriers limit dispersal (Putman et al., 2021). Together, these observations raise questions as to the predominant mode of speciation that drives microbial evolution in serpentinite formations, as well as other hard rock subsurface environments.

In 2017, the Oman Drilling Project drilled six new wells to establish a multi-borehole observatory of the serpentinizing subsurface in the Samail Ophiolite. In 2018 and again in 2019, a submersible down borehole packer and pump system was installed in several of the boreholes, including BA1A, a 400 m borehole that primarily intersects dunite nearer to the surface and harzburgite at depth (Lods et al., 2020; Malvoisin et al., 2020). The packer system uses inflatable nitrogen balloons to seal off permeable zones in the bedrock and to identify the primary fractures that allow for fluid flow. In BA1A, these were identified as 0–30 m, 41–65 m, and 108–132 m, with limited connectivity to aquifers below this depth (Lods et al., 2020). By sealing off these discrete intervals, fluids could be sampled while limiting the possibility for mixing of subsurface waters during sampling within the well. Previously reported chemical analyses reveal aquifer waters from the top two depth intervals in BA1A are circumneutral and moderately reducing whereas aquifer waters from the deeper interval are hyperalkaline and highly reducing, consistent with successful segregation of fluid types by the packer system (Nothaft et al., 2021). Furthermore, 16S rRNA gene sequencing of biomass collected from each of the three discrete depth intervals revealed shifts in the composition of the communities from largely aerobic taxa nearer to the surface toward anaerobic, putatively sulfate reducing taxa at depth (Nothaft et al., 2021). Notably, *Meiothermus* sequences were detected at all three sampled depths, but had an order of magnitude higher relative abundance in the 108–132 m interval. This suggests that the presence of *Meiothermus* is unlikely to be due solely to mixing of fluids during sampling and raises the question of how *Meiothermus* withstand the polyextremophilic conditions associated with heavily serpentinized deep subsurface fluids, including an apparent lack of O_2.

Here, we apply metagenomic sequencing to DNA extracted from biomass from each of the three isolated depth intervals (0–30 m, 41–65 m, and 108–132 m) in BA1A to further evaluate controls on the distribution and evolution of microbial life in subsurface environments undergoing serpentinization, with a specific focus on *Meiothermus*. Sequences were assembled, binned into metagenome assembled genomes (MAGs), and *Meiothermus*-affiliated MAGs were identified and curated. *Meiothermus* MAGs were then compared bioinformatically, phylogenetically, and metabolically to identify similarities and differences as a function of depth and extent of serpentinization in the fluids they inhabited. Estimated genome replication rates were calculated for *Meiothermus* MAGs to establish whether those populations are likely in an active state of replication. Single nucleotide variants

(SNVs) were identified to generate high fidelity *Meiothermus* population structures to evaluate patterns in the diversification and gene flow/recombination among depth-resolved populations. Collectively, the results indicate that chemical and physical barriers that limit co-habitation and gene flow/recombination, in combination with gene loss and gain via mobile genetic elements, drove parapatric speciation of *Meiothermus* in the Samail Ophiolite. While gene flow/recombination among depth-resolved populations was limited, it was detected, suggesting that the reduced, hyperalkaline subsurface aquifer waters in the Samail Ophiolite may not be as isolated from the surface aquifer as has been previously estimated based on bulk characterization of the chemistry of fluids [e.g., deep fluids isolated for >20,000 years (Paukert Vankeuren et al., 2019)]. The results are discussed in terms of processes controlling the distribution and evolution of microbial populations in subsurface environments undergoing serpentinization.

Materials and methods

Site description, drilling, and sampling

BA1A is a part of a multi-borehole observatory established by the Oman Drilling Project. Details on drilling are reported previously (Lods et al., 2020; Kelemen et al., 2021; Nothaft et al., 2021) and are further expanded upon in the **Supplementary methods**. Briefly, BA1A is a 400 m deep, 0.152 m diameter well, intersecting fully serpentinized dunite in the upper 250 m and partially serpentinized harzburgite at greater depth (Lods et al., 2020; Kelemen et al., 2021).

A Solexperts packer system (Zurich, Switzerland) that included two inflatable bladders ("packers") and a Grundfos (Bjerringbro, Denmark) model SQE 1–140 submersible pump was installed in BA1A in February 2019, enabling the isolation of discrete depth intervals for hydrological testing (Lods et al., 2020) and microbiological and chemical characterization of groundwaters (Nothaft et al., 2021). Samples of planktonic biomass were collected from discrete depth intervals in February 2019 using the packer system, as described previously (Nothaft et al., 2021). Controls for contamination, both in the form of remnant drilling fluid as well as laboratory contamination and DNA extraction controls, are described in previous studies (Nothaft et al., 2021; Templeton et al., 2021).

DNA extraction and shotgun metagenomic sequencing

Genomic DNA was extracted from filtered biomass with the Qiagen PowerSoil kit (Germantown, MD, USA) and was submitted to the University of Wisconsin Biotechnology Center for library preparation following the Illumina (San Diego, CA, USA) regular fragment (~300 bp) kit and these libraries were shotgun sequenced via the Illumina NovaSeq 6000 (2 × 150 bp) platform. Information on the depth and quality of sequences obtained from the three libraries are reported in **Supplementary Table 1**. Additional details on the DNA extraction can be found in Nothaft et al. (2021) and in the **Supplementary methods**.

Metagenomic sequence assembly, binning, and metagenome assembled genome (MAG) metabolic predictions

DNA was shotgun sequenced, curated, assembled, and binned into MAGs using the same pipeline outlined previously (Fernandes-Martins et al., 2021). Further details regarding assembly and binning can be found in the **Supplementary methods**. MAGs are available from National Center for Biotechnology Information (NCBI) under the BioProject identification number PRJNA918706. The taxonomic affiliations, relative abundances, and completeness/quality of MAGs in each of the three communities are reported in **Supplementary Table 2**.

Metagenome assembled genomes were characterized as corresponding to putatively aerobic or anaerobic cells using the Basic Local Alignment Search Tool (BLASTp) to query MAGs first for homologs of cytochrome *c* oxidase [Cox I and II; Enzyme Category (EC) 7.1.1.9] and cytochrome *bd* complex (CydABX; EC 7.1.1.7), two proteins necessary for aerobic metabolism. Following this, MAGs were uploaded to the Kyoto Encyclopedia of Genes and Genomes (KEGG) server for annotation and pathway prediction. Specifically, orthologs predicted by KEGG to be involved in other (i.e., those not involving O_2) aspects of putative electron transport chains were examined, specifically orthologs of terminal oxidases (e.g., dissimilatory nitrate reductase, dissimilatory bisulfite reductase). The potential for a MAG to correspond to an aerobe or an anaerobe was then cross checked against the metabolism of its closest cultivated relative, as assessed using the Genome Taxonomy Database-Toolkit (GTDB-Tk) (Chaumeil et al., 2019). Further details regarding this approach can be found in the **Supplementary methods**. We also evaluated the potential for alternative O_2-producing biochemical mechanisms in BA1A populations. MAGs were examined for genes encoding enzymes known to produce O_2, including nitric oxide dismutase (Nod; Zhu et al., 2019), superoxide dismutase (SOD; Imlay, 2002), chlorite dismutase (Cld; Hofbauer et al., 2014), and peroxidases/catalases (Cat; Singh et al., 2008) using BLASTp, with characterized proteins as query sequences (**Supplementary Table 3**).

Compilation of *Meiothermus* genomes and MAGs

Metagenome assembled genomes were assigned taxonomy using the GTDB-Tk (Chaumeil et al., 2019). Using this approach, MAGs that showed close affiliation to *Meiothermus* were compiled from BA1A metagenomes, as well as fracture fluid metagenomes from other subsurface locations in the Samail Ophiolite (Fones et al., 2019, 2021). Taxonomic assignments were verified manually via BLASTp analysis of housekeeping genes (e.g., RNA polymerase) against the NCBI non-redundant database.

The size of *Meiothermus* MAGs was estimated by normalizing MAG size to estimated completeness, where completeness was determined as the proportion of housekeeping genes present as

determined by Metawrap (version 1.3) (Uritskiy et al., 2018). The housekeeping genes assumed to be present in a complete genome were expected to be the same as those present in *Meiothermus hypogaeus* the closest relative (~85% ANI) to Oman *Meiothermus* strains. Only MAGs that contained >60 full length housekeeping genes were retained for downstream analysis. This included six *Meiothermus* MAGs from BA1A and twelve *Meiothermus* MAGs from our database of Oman fracture fluid metagenomes (Fones et al., 2019, 2021).

Phylogenomic analyses of *Meiothermus*-affiliated MAGs

The database of Oman *Meiothermus* MAGs was subjected to alignment of housekeeping genes using the GTDB-Tk (Chaumeil et al., 2019). Also included in the alignments were housekeeping genes from eight *Meiothermus* lineages not from Oman (*Meiothermus taiwanensis* GCA_000482765.1, *Meiothermus ruber* GCA_015478585.1, *Meiothermus silvanus* GCF_000092125.1, *Meiothermus rufus* GCF_00042325.1, *Meiothermus cerbereus* GCF_000620065.1, *Meiothermus* sp. Pnk-1 GCF_003226535.1, *Meiothermus* sp. QL-1 GCF_003351145.1, and *Meiothermus hypogaeus* GCF_003574035.1) to be used as an outgroup. The alignment was generated using Clustal Omega (version 1.2.4) (Sievers et al., 2011), and IQtree (version 1.6.12) (Minh et al., 2020) was used to generate the tree specifying the LG substitution model and 1,000 bootstraps. The tree was visualized using the Interactive Tree of Life (iTOL) web platform (version 6) (Letunic and Bork, 2021), which identified two clades of *Meiothermus* that are herein referred to as "Type I surface or (S)" and "Type II deep or (D)."

Additionally, since housekeeping genes could not be retrieved for many other *Meiothermus* MAGs or metagenomic assemblies, RpoB sequences from MAGs closely related to *Meiothermus* and from unbinned metagenomic sequence data from other environmental samples were retrieved (**Supplementary Table 4**), including those from the NCBI non-redundant (NR) database and the sequence read archive (SRA) database. RpoB from *Thermus thermophilus,* a member of the sister genus to *Meiothermus* (Henne et al., 2004), was used to root the phylogeny. The tree was generated and visualized as described above.

Estimation of *Meiothermus* genome replication rates

The Strain level Metagenomic Estimation of Growth (SMEG) program (ver. 1.1.1) was used to infer genome replication rates for MAGs that showed closest affiliation to *Meiothermus* (Emiola et al., 2020). Mauve (ver. 2.4) (Darling et al., 2004) was used to reorder contigs of *Meiothermus*-affiliated MAGs through alignment to the genome of *M. hypogaeus*. The quality of contig realignment was examined by evaluating the depth of mapped raw reads to ensure that they were generally reordered from highest read depth (origin of replication) to lowest read depth (terminus of replication). SMEG then aligned these reordered contigs to determine single nucleotide variants (SNVs) and assigned MAGs into phylogenetic subclusters based on SNV sites. Read coverage for each contig within each MAG at each SNV site was then determined, and the resultant read map coverage ratios were used to estimate genome replication rates.

Assignment and characterization of *Meiothermus* protein clusters

Protein clustering was used to identify protein encoding genes unique to each *Meiothermus* MAG and to facilitate downstream evaluation of SNV profiles. All called proteins for each MAG were subjected to protein clustering using CD-HIT (ver. 4.8.1) (Fu et al., 2012) resulting in clusters of homologous proteins. Additional details regarding the protein clustering approach used herein can be found in the **Supplementary methods**.

Representative sequences from each protein cluster among BA1A *Meiothermus* MAGs were uploaded to KEGG and analyzed using the BlastKOALA annotation pipeline (Kanehisa et al., 2020). This pipeline assigns hierarchical annotations to protein sequences, wherein each uploaded protein sequence is annotated with the closest database protein, and then is placed into a hierarchy of biological pathways. These annotations were collated and compared across the six *Meiothermus* MAGs from BA1A to identify which KEGG orthologs, protein families, and biological pathways were overrepresented in certain MAGs or MAG groupings. Differences between the Type I (S) and Type II (D) clades were investigated, as were differences between more abundant and less abundant (i.e., rare) MAGs.

Identification and curation of single nucleotide variants (SNVs)

Single nucleotide variants were identified in the six high quality BA1A *Meiothermus* MAGs using Instrain (ver. 1.5.5) (Olm et al., 2021). Instrain identifies SNVs in metagenomic data by mapping the trimmed metagenomic reads against a provided reference genome. Since the BA1A *Meiothermus* MAGs are not closely related (<90% ANI) to any published reference genome, each of the six MAGs was used as a reference genome for SNV identification. SNVs were identified among the six MAGs, and these were then curated to identify and remove those that likely result from sequence read errors. Specifically, putative sequence errors were identified by calculating the ANI between sequence read pairs and the reference genome. Read pairs exhibiting pairwise ANI to the reference genome of <90% were discarded. This ensured that read pairs bearing a significant mismatch were not used for SNV calling, as this would likely result in the retrieval of false positive SNVs. The minimum consensus score was set to 90% rather than 95% to account for lower overall quality of metagenomic data relative to genomes from pure cultures.

Single nucleotide variants identified as a consensus SNV [i.e., SNVs where the variant base frequency was present in 40% of mapped reads or more (see below)] were also identified. Consensus SNVs were rare in the BA1A Oman *Meiothermus* MAGs and occurred at a frequency of about 1:25,000 base pairs (bp). Consensus SNVs typically occurred when two or more alleles were present in the population and represent either intra-strain level

genetic heterogeneity or a sequencing artifact. Since there is no definitive way to determine whether these correspond to true allelic heterogeneity or are artifactual, they were discarded without further consideration. Nonetheless, since they are rare, they would have a minimal influence on the outcome of the study.

Single nucleotide variants were further curated by only using trimmed reads that had a mapQ score equal to or exceeding 1.0. The mapQ score is a read quality measurement determined by bowtie during the read mapping step of the pipeline (Langmead and Salzberg, 2012). The mapQ score is also used to validate the consensus base or the most frequent allele at a variable nucleotide site by verifying that it was also the base with the highest average mapQ score across reads exhibiting that base. Finally, a minimum and maximum sequence insert size is used to further curate SNVs. Here, if sequence inserted into the middle of an ORF alignment is too large, the SNVs in that alignment are discarded since the insertion may indicate incorrect alignment of sequences that are separated on the genome. Default parameters of 50 bp and 3× median insert size were used for minimum and maximum sequence insert size, respectively. The total number of SNVs, both inside and outside of ORFs, was determined for each MAG for comparative purposes. However, only SNVs that were within ORFs, as identified by PROKKA, were used for downstream analyses, since these would allow for potential annotation of the encoded proteins. This secondary filtering step was performed to reduce the frequency of false positive SNVs, as the ORFs tended to have much higher read quality than non-coding sequences. Further, SNVs on ORFs are expected to be more informative regarding the functional dynamics of populations and thus more indicative of where selective pressures are acting on the population level genomes.

Curated SNVs among BA1A *Meiothermus* MAGs were collated using the R base package to facilitate downstream comparison. Specifically, a table was uploaded to R that contained (1) each SNV, (2) the nucleotide frequencies of that SNV, (3) the location of that SNV on its ORF, (4) which of the six MAGs contained that SNV, (5) the full nucleotide sequence of the ORF containing that SNV, (6) the inferred amino acid sequence encoded by that ORF, (7) the assigned KEGG ortholog of the inferred protein encoded by that region (where possible), (8) the protein cluster that protein was assigned to, and (9) the KEGG pathways that the protein identified in the preceding step presumably belongs to. This allowed for identification of SNVs shared by multiple MAGs, statistical evaluation of those SNVs, and other relevant analyses within the R statistical platform.

The overall SNV profile was determined for each MAG. Specifically, the total number of SNVs in the MAG was identified, regardless of whether they were on an ORF. Similarly, the number of SNVS in ORFs in those MAGs, the proportion of ORFs in the MAG containing at least one SNV, and the mean and variance of the SNV frequency across the length of the MAG were identified. Student's T-tests were performed to compare total SNVs among pairs of MAGs, SNVs in ORFs among pairs of MAGs, variance in SNVs per ORF among pairs of MAGs, and the total number of ORFs containing at least one SNV across the designations of community (depth from which it was recovered), abundance (rare versus abundant), and phylogeny (shallow clade versus deep clade, as described below).

Characterization of SNVs

The six BA1A *Meiothermus* MAGs were compared to identify SNVs that were shared at the same position within an ORF. Shared SNVs identified in all six MAG populations were presumed to be ancestral SNVs that were likely present in the population of founder cells, or those that first colonized the Samail Ophiolite or its geologic precursor, and whose genomes gave rise to the descendent MAGs identified herein. The distribution of SNVs was examined between Type I (S) and Type II (D) MAGs using a hierarchical approach. First, shared SNVs that are present in more than one MAG were identified. This approach was more facile than alignment-based approaches that are more time and computationally intensive. While the latter would identify many more potential SNVs, it would also increase the identification of false positive SNVs. Consequently, SNVs identified using the approaches reported herein should be regarded as a conservative estimate of the total number. Secondly, shared SNVs with the same substitution (i.e., the same consensus base and same variable base) at the same site on the same protein encoding ORF were identified. The number of shared SNVs across these hierarchical categories was subjected to statistical analysis using the R base package. Student's *t*-tests were used to compare the number of shared SNVs by different MAG pairs or MAG triplets.

Evaluation of the correlation between shared SNV presence and pairwise MAG sequence similarity

To determine if the presence of shared SNVs corresponded to areas of genomes with high similarity, the ANI of pairs of contigs in pairs of MAGs that contained shared SNVs was determined and compared to the average ANI of pairs of contigs of those same pairs of MAGs that lacked shared SNVs. FastANI (version 1.3.2) (Jain et al., 2018) was used to determine the pairwise ANI of every contig pair between MAGs. Contig pairs containing a shared SNV were then identified. The average ANI for contig pairs containing a shared SNV was then determined for each MAG pair and was compared to the average ANI for contig pairs in that MAG pair that did not contain a shared ANI. The length and coverage of contigs containing shared SNVs and those contigs lacking shared SNVs were also compared to ensure that sequence quality and read depth was not a confounding factor in this analysis. No significant difference was observed between contig coverage (i.e., read depth) between the two groups ($P = 0.12$; two tailed t-test). There was a significant difference in length between contig groups ($P < 0.01$; two tailed t-test), but this is likely a consequence of large sample sizes rather than a true difference, as mean contig lengths were similar (84,325 bp for contigs containing shared SNVs, 50,007 bp for those without), as were the standard deviations (73,698 bp for contigs containing shared SNVs, 63,906 bp for those without). However, since contigs containing less than 80% ANI cannot reliably be aligned, the reported similarity values are intended to be comparative, not an absolute measurement of the actual sequence similarity between specific portions of the genome. Nonetheless, due to the large

number of total calculated alignments, the difference in similarity between genomic regions with shared SNVs and those without is expected to be real.

Estimating the likelihood that shared SNVs arose through convergent evolution

To evaluate the likelihood that SNVs arose in *Meiothermus* MAGs convergently rather than being inherited from a common ancestor (allopatry) or through gene flow/recombination between MAGs, a simple site substitution model was developed and employed. For each MAG pair, the number of SNVs occurring at the same site (i.e., on the same residue on the same ORF) was determined by comparing the retrieved SNVs from InStrain for each MAG. The previously discussed protein clustering was used to identify orthologous proteins and the genes encoding them. This protein clustering approach was utilized in place of a much more computationally intense and error prone whole genome alignment-based approach. The number of shared SNVs that would be expected to have the same base substitution (i.e., the same consensus and variant bases) through convergent evolution (i.e., random mutations and not through horizontal or vertical gene flow) was calculated. Here, roughly 12/256 of SNVs are expected to converge on the same substitution at the same site through random mutation alone. The denominator of 256 (i.e., the 256 total possible pairs of base changes) comes from a base at a given position in the MAG (4 bases are possible) and the possibility of a variant base (4 bases are possible) at this position (4 bases × 4 bases or 16 base combinations). The same applies to the second MAG pair, resulting in 16 combinations × 16 combinations or 256 total combinations for the identity of the original base and what it could mutate to at a single position in both MAGs. The numerator is based on the 16 total pairings where both SNVs start and end with the same base. Thus, the likelihood two SNVs arose from the same substitution is (4 bases choose 2 bases)^2 or $(4)^2$ or 16 minus 4 (the four instances where no base change occurs are subtracted out) is 12. The combined likelihood is therefore 12/256.

For triplet sets of MAGs, the number of possible variations is now based on three mutations rather than two. The likelihood that the three MAGs convergently develop the same SNV at the same position is the combined likelihood that the three MAGs experience a mutation from one nucleotide to another nucleotide (i.e., three MAGs experience the same substitution at the same position in an ORF). Consequently, in the absence of gene flow, it is expected that roughly 12/4,096 of SNVs will converge on the same substitution at the same site. The 4,096 denominator comes from a MAG having an original base at a given position and the possibility of a variant base at this position (4 bases × 4 bases or 16 base combinations). The same is true for the second and third MAGs, resulting in a total of 4,096 combinations (16 × 16 × 16). Thus, the likelihood two SNVs arose from the same substitution is (4 bases choose 2 bases)^2 or $(4)^2$ or 16 minus 4 (the four instances where no base change occurs) or 12. The combined likelihood is therefore 12/4,096.

Identification of viral and integrated mobile genetic elements (IMGEs)

To identify the quantity and type of viral elements present in the three BA1A subsurface microbial communities, metagenomes were probed for viral nucleotide sequences using VIBRANT (version 1.2.1) (Kieft et al., 2020), which identifies viral sequences by comparing retrieved metagenomic sequences to the KEGG, protein Family (PFAM), and Virus Orthologous Groups (VOG) databases (Thannesberger et al., 2017; El-Gebali et al., 2018; Kanehisa et al., 2020). Contigs from the six BA1A *Meiothermus* MAGs were submitted to the Mobile Genetic Element finder tool (version 1.0.3) (Johansson et al., 2021) to identify the quantity, location, and type of IMGEs present.

Results

Overview of previous hydrogeochemical work conducted at BA1A

Hydrological experiments, including flowmeter tests under ambient and forced hydraulic conditions, revealed three discrete depth intervals with connectivity to local aquifers in the 400 m deep BA1A well and these intersected different bedrock types, as reported previously (Lods et al., 2020; Kelemen et al., 2021). Briefly, the 0–30 m depth interval (BA1A30) intersected alluvium (well cased to 21 m to isolate this section) and weathered dunite to at least 30 m, whereas the 41–65 m (BA1A65) and the 108–132 m (BA1A132) depth intervals intersected intact dunite. There was no significant connectivity of upper aquifers to aquifers between 132–400 m depth, as assessed in field with a flowmeter (limit of detection of 0.1 L min^{-1}). Field hydraulic tests suggested that waters from the 0–30 m interval may have limited connectivity with those from 41–65 m interval (Lods et al., 2020). Further, it is possible that connectivity exists to the deeper 108–132 m aquifer, although the flow is expected to be substantively less than from the weathered dunite aquifer (0–30 m interval) to the upper (41–65 m) dunite-hosted aquifer (Lods et al., 2020).

The different depth intervals sampled generally corresponded to different geochemical regimes (Lods et al., 2020; Nothaft et al., 2021), with the 0–30 m depth water having a temperature of 34.9°C, a pH of 8.10, a conductivity of 0.458 mS cm^{-1}, and an oxidation reduction potential (*Eh*) of 128 mV (**Table 1**). Similarly, water from the 41–65 m depth interval had a temperature of 35.0°C, a pH of 8.21, a conductivity of 0.402 mS cm^{-1}, and an *Eh* of 120 mV. In contrast, water from the 108–132 m depth interval had a temperature of 36.5°C, a pH of 10.67, a conductivity of 0.871 mS cm^{-1}, and an *Eh* of −249 mV. Thus, waters from 0–30 m and 41–65 m are classified as Mg–HCO_3-type waters (Type I) while waters from 108 to 132 m are classified as Ca–OH-type waters (Type II), according to a previously reported classification scheme (Rempfert et al., 2017). Type II waters have extensively reacted with rock (i.e., dunite) in regions of the subsurface thought to be closed to atmospheric inputs whereas Type I waters may include atmospheric inputs (Rempfert et al., 2017).

TABLE 1 Select geochemical measurements of waters recovered from discrete depth intervals in well BA1A in February 2019 and their inferred water type.

Isolated depth interval (meters below surface)	Water type	pH	Temperature (°C)	Conductivity ($\mu S\ cm^{-1}$)	Redox potential (mV)
0–30	Mg–HCO_3	8.1	34.9	458	127.7
41–65	Mg–HCO_3	8.2	35.0	402	120.3
108–132	Ca–OH	10.6	36.4	950	−310.0

Mg-HCO_3 type fluids are also termed Type I fluids whereas Ca-OH fluids are also termed Type II fluids, based on prior classification schemes (Barnes and O'Neil, 1969; Neal and Stanger, 1985). Values were previously reported in Nothaft et al. (2021).

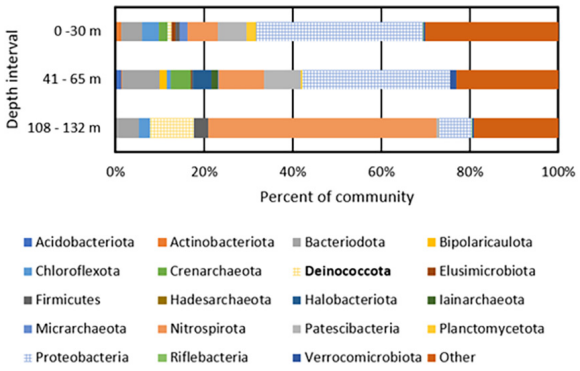

FIGURE 1
Phylum level taxonomic composition of metagenome assembled genomes (MAGs) recovered from BA1A filtered biomass from discrete depth intervals. MAGs that encode homologs of enzymes or enzyme complexes that allow for the respiration of oxygen (Cox I and II, CydABX) are depicted with a grid pattern. Deinococcota, the phylum containing *Meiothermus*, is bolded in the legend.

BA1A taxonomic composition and diversity

A total of 447, 626, and 229 giga base pairs (Gbp) of metagenomic sequence from depth intervals of 0–30 m (BA1A30), 41–65 m (BA1A65), and 108–132 m (BA1A132), respectively, was generated and subjected to assembly and binning (**Supplementary Table 1**). A similar proportion of each of the BA1A30, BA1A65, and BA1A132 communities was binned (77, 80, and 79%, respectively). In BA1A30, a total of 11 high quality MAGs (i.e., MAGs that had at least 90% completeness and less than 5% contamination) were identified. Thirteen high quality MAGs were recovered from BA1A65, and ten high quality MAGs were recovered from BA1A132. The taxonomic compositions of communities were consistent with those of Nothaft et al. (2021) and showed a decreasing proportion of Proteobacteria with depth and an increasing proportion of Nitrospirae and Deinococcota with depth (**Figure 1** and **Supplementary Table 2**).

The most abundant MAGs in BA1A30 were affiliated with *Parvibaculum* (Proteobacteria; 25% of the binned community), *Burkholderia* (Proteobacteria; 8%), Ignavibacteria (5%), Patescibacteria (3%), and *Thermodesulfovibrio* (3%). The composition of BA1A65 was similar to BA1A30 at the phylum level and was dominated by Proteobacteria, including an unclassified Acidoferrobacterales population (9% of the binned community), *Burkholderia* (7%), and *Lysobacter* (6%). Like BA1A30, Ignavibacteria (5% of the binned community) and *Thermodesulfovibrio* (5%) were also detected in the BA1A65 community. A major shift in taxonomic composition was observed in BA1A132, where *Thermodesulfovibrio* comprised nearly 50% of the binned community. *Meiothermus* was also abundant in BA1A132, comprising roughly 10% of the binned community.

Inferred oxygen usage among BA1A populations

Metagenome assembled genomes from the discrete depth intervals sampled in BA1A were examined for protein homologs of cytochrome *c* oxidase [Cox I and II; Enzyme Category (EC) 7.1.1.9] and cytochrome *bd* complex (CydABX; EC 7.1.1.7), known protein complexes involved in the respiration of O_2 (Ludwig, 1987; Jünemann, 1997). MAGs that encoded homologs of one or both complexes were considered as capable of integrating O_2 into their energy metabolism (i.e., obligate aerobes or facultative anaerobes). MAGs that did not encode homologs of these complexes were considered incapable of integrating O_2 in their cellular energy metabolism (i.e., obligate anaerobes). Forty-three and 37% of the binned BA1A30 and BA1A65 populations were determined to be aerobic/facultatively anaerobic, respectively, with the remainder inferred to be strict anaerobes (**Figure 1**). Surprisingly, 20% of the BA1A132 community was determined to be aerobic/facultatively anaerobic based on MAGs encoding Cox; *Meiothermus* comprised 10% of this community. Homologs of proteins that would putatively allow for respiration of additional oxidants (e.g., SO_4^{2-}, S°, Fe(III), NO_3^-) were not identified among BA1A *Meiothermus* MAGs (data not shown). In addition to encoding for Cox, BA1A *Meiothermus* MAGs are closely related (83–85% ANI) to the obligately aerobic cultivar, *Meiothermus hypogaeus* (NCBI taxonomy ID: 884155) (Mori et al., 2012), suggesting a similar O_2-dependent energy metabolism.

To investigate if putative aerobes in BA1A may be capable of generating endogenous O_2 thereby allowing for a high abundance of putative aerobes in an otherwise anoxic environment, MAGs were probed for genes that encode oxygenic proteins including Nod, Cld, SOD, and Cat (see section "Materials and methods"). Homologs of Cld, including both the pentameric and dimeric forms, were the only such proteins identified in BA1A MAGs. One hundred and fourteen Cld sequences among the BA1A MAGs passed the alignment and conserved residue cutoff used to curate homologs (**Supplementary Table 3**). All six *Meiothermus* MAGs

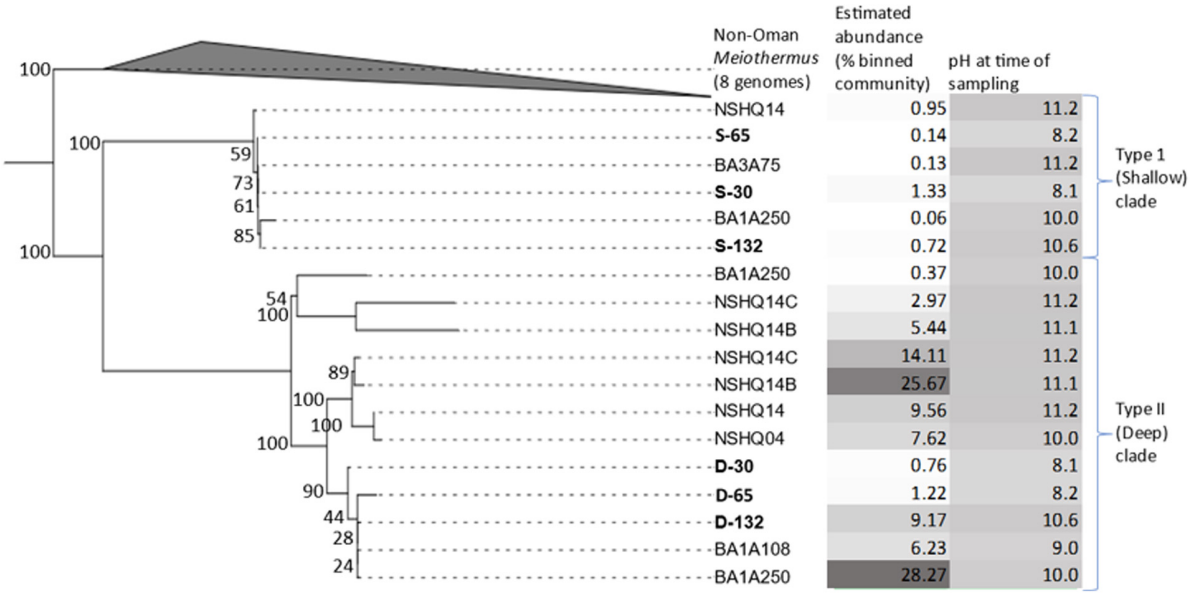

FIGURE 2
Maximum-likelihood phylogenomic reconstruction of a concatenation of 115 housekeeping genes from metagenome assembled genomes (MAGs) recovered from discrete depth intervals in wells BA1A (sampled with packer system), BA1A (sampled using niskin bottles), BA3A (sampled using niskin bottles), or from specified depths (open well pumping) in NSHQ14B (50 m) and NSHQ14C (85 m). Eight genomes of non-Oman *Meiothermus* served as the outgroup. For BA1A samples collected with the packer system, MAGs are labeled as belonging to the Type I surface phylogenetic clade (S) or the Type II deep phylogenetic clade (D) followed by the maximum depth interval (m) from where they were recovered (30, 65, 132). For BA1A and BA3A samples collected with niskin bottles, MAGs are labeled by well followed by depth of recovery. Only MAGs that were most closely related to *Meiothermus* were considered. MAGs obtained from discrete depth intervals isolated by packers in well BA1A that were used for further genomic analyses are in bold. Bootstrap scores are indicated at each node. The relative abundance of MAGs (% of mapped reads) and the pH of fluids at the time of sampling are indicated, with darker colors corresponding to higher values for both parameters.

from BA1A (discussed below) encoded a homolog of Cld, regardless of the depth from which they were recovered.

Meiothermus phylogeny and clade designations

Phylogenomic reconstruction of *Meiothermus* MAGs from BA1A, *Meiothermus* from other wells in the Samail Ophiolite study site, and all *Meiothermus* reference genomes available in the Genome taxonomy database (**Figure 2**) revealed that MAGs from Oman formed a monophyletic clade, with *M. hypogaeus* as the closest non-Oman outgroup. However, *Meiothermus* MAGs from other serpentinizing systems were not yet available to compare phylogenetically to the *Meiothermus* from the Samail Ophiolite. Yet, a single RNA polymerase subunit B (RpoB) sequence from *Meiothermus* was available in the NCBI NR and SRA databases from a metagenome from the Zambales ophiolite (Woycheese et al., 2015). Phylogenetic reconstruction of RpoB homologs from *Meiothermus* MAGs from BA1A, *Meiothermus*-affiliated RpoB from the Zambales ophiolite, and *Meiothermus* RpoB sequences from the NCBI NR and SRA databases revealed the same pattern whereby *Meiothermus* RpoB from the Samail Ophiolite formed a monophyletic lineage, referred to herein as the Oman-specific clade (**Supplementary Figure 1**).

Within the Oman-specific *Meiothermus* clade, MAGs from BA1A partitioned into two distinct sub-clades. Both *Meiothermus* sub-clades were present in all three depth intervals, but they exhibited opposing abundance trends (**Table 2**). Specifically, one *Meiothermus* clade, hence referred to as Type II (D) from the BA1A30 (D-30), BA1A65 (D-65), and BA1A132 (D-132) intervals, increased in abundance as depth increased, whereas the other *Meiothermus* clade, hence referred to as the Type I (S) clade comprising BA1A30 (S-30), BA1A65 (S-65), and BA1A132 (S-132), is most abundant in the BA1A30 community and decreased in abundance with depth. Within clade average nucleotide identity (ANI) was 99.99% for each clade, indicating a single population. However, ANI between MAGs forming Type I (S) and Type II (D) clades averaged 84%, whilst the ANI between Oman-specific *Meiothermus* MAGs and *Meiothermus hypogaeus* varied between 78 and 81%, depending on the MAG.

Meiothermus inferred genome replication rates

To begin to assess whether *Meiothermus* MAGs detected in each depth interval correspond to cells that are likely active or inactive, genome replication rates were estimated using metagenomic sequence data and SMEG calculations. SMEG scores for five of the six high quality *Meiothermus*-affiliated MAGs in BA1A indicate active genome replication, as indicated by a SMEG score exceeding 1.0 (**Table 2**). The sole exception was *Meiothermus* S-132, which belongs to the Type I (S) clade but that was recovered from the BA1A132 community. The other two MAGs that belong to the Type I (S) clade, S-30 and S-65, had SMEG values of 3.019

TABLE 2 Name, estimated abundance, estimated genome size (mega basepairs, Mbp), estimated number of protein coding genes, strain level metagenomic estimation of growth rate (SMEG), and number of single nucleotide variants detected for metagenome assembled genomes (MAGs) recovered from discrete intervals in well BA1A.

Metagenome assembled genome (MAG)	Estimated abundance (% binned community)	Abundance designation	Estimated genome size (Mbp)	Estimated number of protein coding genes	Inferred genome replication rate (SMEG)	Single nucleotide variants
S-30	1.33	Abundant	3.56	3,278	3.02	1,473
S-65	0.14	Rare	3.25	2,953	2.72	5,016
S-132	0.72	Rare	3.71	3,526	1.00	15,560
D-30	0.76	Rare	2.82	2,656	1.06	6,942
D-65	1.22	Abundant	3.12	2,949	1.04	1,335
D-132	9.17	Abundant	3.00	2,869	1.01	2,589
M. hypogaeus	NA	NA	3.70	3,623	NA	NA

MAG names are labeled as belonging to the Type I surface phylogenetic clade (S) or the Type II deep phylogenetic clade (D) followed by the maximum depth interval (m) from where they were recovered (30, 65, 132). MAGs were also empirically defined as abundant versus rare based on read mapping (see section "Materials and methods"). Genome characteristics of the most closely related *Meiothermus* cultivar that is not from Oman, *Meiothermus hypogaeus*, are provided for context. A SMEG score of 1.00 indicates a non-replicating MAG. NA, not available.

and 2.722, respectively. In contrast, MAGs that belong to the Type II (D) clade that were detected in BA1A30 (D-30), BA1A65 (D-65), and BA1A132 (D-132) communities had SMEG values of 1.060, 1.042, and 1.013, respectively. The 95% confidence intervals for all three Type II (D) clades are above one, indicating that these values are significantly different than 1.000 (non-replicating genome). Thus, while the MAGs corresponding to the Type II (D) clade are in a state of active genome replication, they are doing so more slowly than the Type I (S) clade at the 0–30 m and 41–65 m intervals. Further, the Type I (S) *Meiothermus* MAG S-132, recovered from Type II waters, is not in a state of active genome replication.

Meiothermus genome sizes

To further examine differences in the BA1A MAGs that correspond to the Type I (S) and Type II (D) clades, their genome sizes were inferred. The inferred genome size was similar for MAGs from each respective clade (**Table 2**). MAGs belonging to the Type I (S) clade had an estimated genome size of 3.5 Mega-basepairs (mbp), which is comparable to the observed genome sizes of most other described *Meiothermus* species, including the closest non-Oman relative, *M. hypogaeus*, which has an observed genome size of 3.7 mbp (Mori et al., 2012). However, the Type II (D) clade MAGs had much smaller inferred genomes, with an average size of 3.0 mbp.

Protein clustering of BA1A *Meiothermus* MAGs and their inferred metabolism

The larger genome sizes of MAGs that cluster within Type I (S) versus Type II (D) *Meiothermus* clades suggested differences in the functional potential of the associated organisms. To determine the differences in encoded protein content between the six *Meiothermus* MAGs, the inferred proteins encoded in MAGs were subjected to protein clustering and comparative analysis (**Supplementary Table 5**). The 17,477 inferred protein sequences [encoded by genes or open reading frames (ORFs)] among the six BA1A *Meiothermus* MAGs partitioned into 4,114 clusters, 2,169 of which included protein homologs encoded in both the Type I (S) and the Type II (D) clade MAGs. Among the proteins that were shared between the Type I (S) and the Type II (D) clade MAGs are homologs of proteins for complete glycolytic and tricarboxylic acid cycles as well as homologs of bidirectional $NAD^+/NADP^+$-reducing [NiFe]-hydrogenases. Both clades also encoded a homolog of group 1 [NiFe]-hydrogenases, however, they are likely involved in different processes based on phylogenetic relationships of the large subunit with characterized homologs and the presence/absence of motifs indicative of translocation across the membrane. The Type I (S) clade group 1 [NiFe]-hydrogenase homolog is predicted to be located in the periplasm based on the presence of a twin-arginine translocation (tat) motif and to be a high affinity H_2 oxidation enzyme (group 1h) that functions in aerobic respiration (Søndergaard et al., 2016). In contrast, the Type II (D) clade group 1 [NiFe]-hydrogenase homolog is predicted to be cytoplasmic or inner membrane-associated (lack of tat motif) and is predicted to be involved in H_2 oxidation coupled to anaerobic respiration of sulfate, fumarate, nitrate, or metals (Søndergaard et al., 2016). Interestingly, homologs allowing for respiration of such oxidants were not identified among the Type II (D) clade MAGs.

In addition, of the 4,114 protein clusters, 1,196 were unique to the Type I (S) clade MAGs, and 749 were unique to the Type II (D) clade MAGs. Importantly, because these MAGs are incomplete (**Supplementary Table 2**) it cannot be known confidently that a protein sequence is necessarily unique to a clade. Nonetheless, that they were identified in three Type I (S) MAGs and no Type II (D) MAG and vice versa gives additional confidence to their uniqueness to a given clade. A far greater proportion of the proteins unique to the Type I (S) clade of BA1A *Meiothermus* MAGs were annotated in the KEGG categories of ABC transporters (26× as likely) and amino sugar and nucleotide sugar metabolism (10× as likely). Proteins unique to the Type I (S) clade of *Meiothermus* MAGs were also more likely annotated as two component regulatory systems (10× as likely) or as involved in quorum sensing (4× as likely). A number of protein encoding genes associated with sulfur metabolism were also identified in Type I (S) clade MAGs, including those encoding SoxABCDX that would potentially allow for oxidation

of thiosulfate/elemental sulfur. Intriguingly, while these genes are encoded by most non-Oman *Meiothermus* species, including those that are sister to the Oman *Meiothermus* clade (**Figure 2**), they are absent from the Type II (D) Oman clade. This suggests loss of these genes and the functionalities in the Type II (D) clade.

Proteins unique to the Type II (D) clade MAGs tended to be annotated in the KEGG categories of thiamine biosynthesis (3.5× as likely) and folate biosynthesis (5× as likely). Moreover, a complete thiamine biosynthesis pathway (ThiEMDLGOS and its regulator TenA) was identified exclusively in the Type II (D) clade MAGs. Based on close sequence homology of these subunits to *Acetothermia* and their absence in other non-Oman *Meiothermus* genomes, it is likely that the thiamine biosynthesis pathway was acquired via a horizontal gene transfer event from *Acetothermia* that tend to be enriched in Type II waters (Colman et al., 2022). Additionally, the Type II (D) clade encodes a copy of pyruvate ferredoxin oxidoreductase (PFOR; *porABC*), which, based on sequence homology, may have been obtained via HGT from cohabitating and anaerobic *Thermodesulfovibrio* that often predominates in Type II waters (Templeton et al., 2021). In addition, all six MAGs, regardless of whether they correspond to the shallow or the Type II (D) clade, encode pyruvate dehydrogenase (PDH) that typically facilitates oxidative conversion of pyruvate to acetyl CoA and CO_2 (unidirectional) in aerobes (de Kok et al., 1998).

SNV profiles of individual BA1A *Meiothermus* MAGs

To assess the extent of gene exchange among spatially or ecologically differentiated *Meiothermus* populations, a population biology study of MAGs via analyses of SNVs was undertaken. A total of 35,019 curated (see section "Materials and methods") SNVs were identified among the six BA1A *Meiothermus* MAGs, 22,476 of which were in ORFs (**Table 3**). SNVs were not distributed evenly across the MAGs. MAGs classified as rare [i.e., are the less abundant *Meiothermus* population in their respective community such as S-132 (**Table 2**)] had a significantly higher number of ORFs containing SNVs than their abundant counterparts (P = 0.00047; two tailed T-test). Further, they had a significantly higher total number of SNVs in ORFs (P = 0.012) and a significantly higher mean number of SNV's per ORF (P = 0.0013). There was no significant difference between the mean number of SNVs of MAGs that belonged to different clades [i.e., Type I (S) versus Type II (D)] or that were recovered from the different depths. However, the clade the MAG belonged to [i.e., Type I (S) versus Type II (D)] was a slightly stronger, albeit not significant, predictor of the mean number of SNVs across the MAGs (phylogenetic clade P = 0.075; abundance P = 0.20).

SNVs shared between MAGs

Of the 4,484 total protein clusters identified among the six *Meiothermus* MAGs, 369 protein clusters had no SNVs within their associated ORF, while 1,322 clusters had at least one SNV in an associated ORF for each *Meiothermus* MAG. The 369 invariable ORFs encode proteins that are highly conserved and/or that are essential (e.g., housekeeping proteins) (data not shown).

There was no significant difference in the number of shared SNVs by MAGs in the same clade or shared by MAGs with similar abundances (**Table 2**). Pairs of MAGs where both members came from the same depth interval, such as S-30/D-30, S-65/D-65, and S-132/D-132, have significantly fewer shared SNVs at the same site within a protein encoding gene than other pairs. The pairing of S-65/D-65 had no SNVs at the same site whereas the pairing of S-30/D-30 had two SNVs at the same site but with different base substitutions. Finally, the pairing of S-132/D-132 had three SNVs at the same site, two of which had the same base substitution. Surprisingly, two pairs of MAGs (S-65/D-132 and S-30/S-132) have a significantly higher number of shared SNVs in protein encoding ORFs than other pairs of MAGs, with 219 and 148 SNVs at the same site with the same base substitution, respectively (**Table 3**). This was despite the fact that the organisms with these MAGs have been evolutionarily/spatially more isolated from each other than those organisms from the same aquifer. The limited evidence for shared SNVs in MAGs recovered from the same depth is attributed at least in part to limitations associated with the approach utilized herein, where a given contig is only allowed to be present in a single bin due to the non-redundant nature of the contig binning process. As such, the results presented herein for co-inhabiting populations should be considered a conservative estimate of gene flow/recombination across phylogenetic lineages.

The only triplet sets of BA1A MAGs that had SNVs with the same substitution at the same site within a protein encoding gene occurred among MAGs that belonged to the same phylogenetic clade (**Table 3**). MAGs comprising the Type II (D) clade had ten SNVs at the same site of a protein encoding gene, two of which had the same base substitution. MAGs comprising the Type I (S) clade had five SNVs at the same site of a protein encoding gene, of which four had the same base substitution.

Correlation between shared SNVs and pairwise MAG genome similarity

The pairwise ANI between each contig in pairs of BA1A *Meiothermus* MAGs was calculated to determine if genomic regions containing shared SNVs at the same position were more similar than regions lacking shared SNVs. Importantly, it is also possible to calculate the ANI of individual protein coding genes (i.e., genes encoding proteins among protein clusters) that are shared between MAGs to identify those that likely arose from recent recombination (high ANI compared to average ANI). However, such an approach could confound an assessment of the influence of recombination due to potential differences in selective pressures on encoded proteins (i.e., false-positives among housekeeping genes under purifying selection, false-negatives among protein genes undergoing drift). A comparison of ANIs between contigs with shared SNVs among MAG pairs thus is a more conservative approach to identifying regions of MAGs that have been influenced by recombination and is the approach utilized herein.

Of the 10 MAG pairings that shared SNVs (**Table 3**), all exhibited higher genomic similarity in the regions containing those SNVs than in the other regions of the genome (**Figure 3** and **Table 3**). While there is a difference in the average length of contigs containing SNVs, there is no difference in the read depth and

10.3389/fmicb.2023.1138656

TABLE 3 Single nucleotide variants (SNVs) identified between the specified pair or triplet of metagenome assembled genomes (MAGs).

Metagenome assembled genome (MAG) pair or triplet	Shared SNVs at same site	Shared SNVs at same site with same substitution	Expected number of convergent SNVs[a]	Average ANI between contigs containing shared SNVs	Average ANI between contigs lacking shared SNVs
S-30, D-30	2	0	<1	NA[b]	81.0
S-65, D-65	0	0	0	NA[b]	81.8
S-132, D-132	3	2	<1	95.4	81.5
S-65, S-132	259	219	12.14	100	83.5
D-65, D-132	62	44	2.91	100	83.9
D-30, D-65	25	11	1.17	98.1	82.5
D-30, S-132	73	9	3.42	85.6	81.4
S-30, S-65	25	22	1.17	100	86.6
S-30, D-132	8	0	0.38	NA[b]	81.4
S-30, D-65	37	0	1.73	NA[b]	81.5
S-30, S-132	173	148	8.11	100	84.1
D-65, S-132	34	20	1.59	91.4	82.7
D-30, S-65	15	3	<1	93.8	80.9
D-30, D-132	27	15	1.27	98.4	83.5
S-65, D-132	1	0	<1	NA[b]	81.4
D-30, D-65, D-132 (*deep clade MAGs*)	10	2	<1	NA[c]	NA[c]
S-30, S-65, S-132 (*shallow clade MAGs*)	5	4	<1	NA[c]	NA[c]
S-30, D-65, D-132 (*common MAGs*)	0	0	0	NA[c]	NA[c]
D-30, S-65, S-132 (*rare MAGs*)	1	0	<1	NA[c]	NA[c]

MAGs are labeled as belonging to the Type I surface phylogenetic clade (S) or the Type II deep phylogenetic clade (D) followed by the maximum depth interval (m) from where they were recovered (30, 60, 132). The number of shared SNVs at the same site and those with the same substitution are reported, as is the expected number of SNVs that could arise through evolutionary convergence (see section "Materials and methods"). The average nucleotide identity (ANI) of contigs that share versus those that lack shared SNVs is provided. Bolded pairings or triplets denote MAGs that exhibit evidence for gene flow/recombination.

[a]The number SNVs that would theoretically be present in MAG pairs or triplets due to convergent evolution in the absence of gene flow/recombination as calculated based on substitution frequencies (see section "Materials and methods") multiplied by the number of SNVs shared by a pair or triplet of MAGs, as identified by InStrain (first column above). Values were rounded to the nearest integer.

[b]ANIs are not reported for pairs of MAGs with no shared SNVs.

[c]ANI calculations were not performed for triplets of MAGs.

overall sequence quality ($P = 0.12$; two tailed T-test). Further, while not every contig pair could be evaluated, as ANI is not reliable for sequences with less than 80% sequence similarity, the sample size of those contigs that were evaluated indicates that while the actual percentage similarities may not be accurate, the overall trend is accurate. In MAG pairs belonging to the same clade, much of this genomic similarity is likely a consequence of shared ancestry. Since the majority of contigs had shared SNVs, their high ANI reflects the overall high ANI between the MAG pairs. However, for the five pairs belonging to different clades but still exhibiting shared SNVs, this increase in genomic similarity near shared SNVs is likely to be a consequence of recombination in at least part of that contig.

Likelihood of SNVs arising convergently

A simple site substitution model was developed to evaluate the likelihood that SNVs in MAG pairs or MAG triplets arose convergently as opposed to having been either a property of their ancestor or result from gene flow/recombination (see section "Materials and methods" for model description). Ultimately, the model predicts that 12 out of 256 of all SNVs occurring at the same site between two MAGs and that 12 out of 4,096 of all SNVs occurring at the same site between three MAGs should have the same base substitution. In other words, the expected number of shared SNVs with the same substitution in a pair of MAGs in the absence of gene flow/recombination was calculated as: 12/256 × number of shared SNVs. As an example, the expected number of convergent SNVs between MAG pair D-65 and S-132 that have the same base substitution is ∼2 (12/256 × 34 = 1.59 or ∼2). However, 20 out of 34 shared SNVs at the same site in these two MAGs were found to have the same base substitution (Table 3). This suggests that convergent evolution alone (accounting for only ∼2 of the 20 observed shared SNVs with the same base substitution) is unlikely to explain the prevalence of shared SNVs with the same base substitution at the same site. This is the case for other MAG pairs from different clades (S versus D) (Table 3). This model is an oversimplification of mutation dynamics in natural

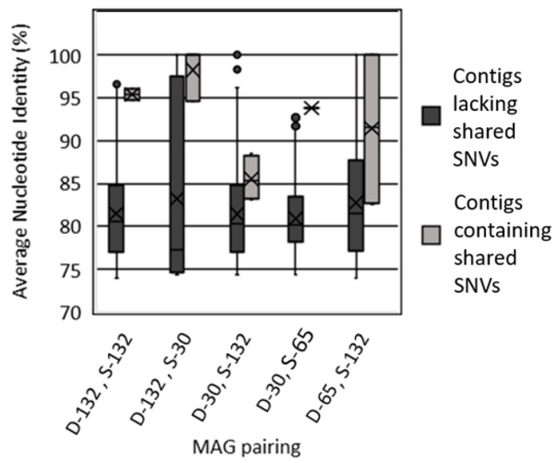

FIGURE 3
Average nucleotide identity of contigs between select pairs of metagenome assembled genomes (MAGs) that contain shared single nucleotide variants (SNVs) versus contigs from those pairs of MAGs that lack shared SNVs. MAGs are labeled as belonging to the Type I surface phylogenetic clade (S) or the Type II deep phylogenetic clade (D) followed by the maximum depth interval (m) from where they were recovered (30, 65, 132). Values for all MAG pairings are reported in **Table 3**.

systems since each base does not have an equal likelihood to mutate to any other base and different organisms and their genomes are not necessarily under the same selective pressures at any given time. Nonetheless, given the number of shared SNV observations, these probabilistic differences should become irrelevant.

Single nucleotide variants shared amongst MAGs belonging to the same clade were also examined (**Table 3**), as these SNVs were possibly present in the common ancestor of members of the clade, prior to their partitioning across different aquifers with differing chemistry that were intersected by BA1A. Alternatively, it is possible that these also arose from gene flow/recombination. Using the site substitution model (see section "Materials and methods"), the expected number of SNVs exhibiting the same base substitution for pairs of MAGs from the same clade could not be accounted for by convergent evolution alone in any set of MAG pairings, regardless of the clade from which they affiliate (**Table 3**). That the contigs where shared SNVs with the same base substitution had a higher ANI than regions of the MAGs where shared SNVs were not located could point to gene flow/recombination between these populations as well. However, given that the majority of contigs among MAG pairs contained shared SNVs, it is equally possible that these were inherited from their ancestral population.

The site substitution model was also applied to triplet MAGs from either the same clade or from different clades. In the case of the triplet MAGs from the Type I (S) clade, the expected number of SNVs exhibiting the same base substitution that arose convergently was estimated at < 1 ($12/4{,}096 \times 5$ shared SNVs $= 0.0146$ or <1; **Table 3**). Similarly, the expected number of SNVs exhibiting the same nucleotide for triplet MAGs from the Type II (D) MAGs that arose convergently is <1 ($12/4{,}096 \times 10$ shared SNVs $= 0.029$). These expected values are both less than the number of observed shared SNVs with the same base substitution [4 and 2 for Type I (S) and Type II (D) clades; **Table 3**] indicating that they are likely the result of gene flow/recombination or common ancestry rather than convergent evolution.

This same model was applied to each other MAG pair and MAG triplet to determine the likelihood that a SNV arose convergently, rather than being a result of gene flow/recombination or common ancestry. The number of expected convergent SNVs varied from near 0 (S-65/D-65 pairing) to 12 (S-65/D-132 pairing; **Table 3**). Ultimately, nine out of the total 15 possible pairs of *Meiothermus* MAGs exhibited probabilistic evidence for gene flow/recombination or shared ancestry as evidenced by observed shared SNVs with the same substitution exceeding expected values based on convergence alone. Seven of these nine pairs were from different depths and, more importantly, from different clades.

Identification of viral and non-viral integrated mobile genetic elements (IMGEs) in BA1A communities

Metagenome assembled genomes were evaluated for virus signatures and IMGEs. Within the BA1A30, BA1A65, and BA1A132 communities, 4,610, 7,969, and 4,482 viral sequences, respectively, were identified. However, none of the retrieved viral sequences were found on *Meiothermus* contigs. Nonetheless, 19 total IMGEs were identified on *Meiothermus* contigs, 13 of which were classified as insertion sequences (i.e., a transposase gene flanked by two inverted repeats) while the remaining six were classified as composite transposons or a composite mobile genetic element resulting from a transposase acting on the inverted repeat of a related mobile genetic element (MGE) that transposes both the original and new element together (Clark et al., 2019). *Meiothermus* MAGs from BA1A that comprised the Type II (D) clade consistently had more IMGEs than those that comprised the Type I (S) clade. Of the 19 IMGEs, four were present in more than one MAG from the Type II (D) clade. The first shared IMGE, ISGlo6, is present in D-132, D-65, and S-132. The sequence includes the transposase InsK, which may be able to act on additional insertion sequences besides ISGlo6 (Fernández De Henestrosa et al., 2000). The D-132 and D-65 sequences exhibited 100% identity (**Table 4**), but the S-132 MAG sequence is truncated and comprised only 131 residues compared to the full 214 residues in the other MAGs. Further, the S-132 MAG ISGlo6 sequence shared only 61% sequence identities with that of D-132 and D-65 MAGs. In the D-132 and D-65 MAGs, the insertion sequence is preceded by upwards of 10 kilo basepairs (kbp) that exhibited 100% sequence identity, which may constitute part of a larger transferred sequence.

The second shared IMGE, ISMyca1, was present in D-30, D-65, D-132, and S-132 MAGs (**Table 4**). The D-132 and D-65 MAG ISMyca1 sequences are identical. Moreover, the shorter D-132 MAG contig containing the ISMyca1 exhibited 100% sequence similarity to a portion of the larger D-65 MAG contig. The D-30 MAG ISMyca1 sequence, however, shared only 83% sequence identity with the D-132 and D-65 MAG ISMyca1 sequences. The S-132 MAG ISMyca1 sequence exhibited less than 50% similarity to the other three ISMyca1 sequences and lacked an identifiable transposase. The third potentially shared IMGE is ISPlu21 (**Table 4**), which is present in the D-30 MAG and that was duplicated in the D-132 MAG, one on the sense strand and one on

TABLE 4 Percent shared nucleic acid sequence identities between pairs of mobile genetic elements (MGE) retrieved from BA1A *Meiothermus* metagenome assembled genomes (MAGs).

	IS640	ISGlo6	ISMyca1	ISPa85	ISPlu21	ISUNCu3
D-132	NA	1.00	1.00	NA	1.00	NA
D-65	NA	1.00	1.00	NA	NA	NA
D-30	1.00	NA	0.83	1.00	1.00	NA
S-132	NA	0.61	0.42	NA	NA	1.00
S-65	NA	NA	NA	NA	NA	NA
S-30	NA	NA	NA	NA	NA	NA

MAGs are labeled as belonging to the Type I surface phylogenetic clade (S) or the Type II deep phylogenetic clade (D) followed by the maximum depth interval (m) from where they were recovered (30, 65, 132). The MAGs encoding MGEs are in rows and the individual MGEs are in columns. The percent nucleic acid identity of the specified MGE in each MAG is given in reference to the MGE from MAG D-132, or from whichever MAG encoded the MGE when it was absent from D-132. NA, not available.

the antisense strand. All three ISPlu21 sequences exhibited 100% sequence identity and are surrounded by upwards of 10 kbp also bearing 100% sequence identity.

The fourth sequence is Tn125, a common composite mobile genetic element with a wide phylogenetic distribution (Acman et al., 2022). One copy of Tn125 was detected in each of the six BA1A *Meiothermus* MAGs. Intriguingly, the degree of similarity between these Tn125 sequences does not recapitulate the presumed evolutionary history of the six BA1A *Meiothermus* MAGs, based on housekeeping genes or RpoB proteins (**Table 5** and **Figure 2**). The Tn125 sequences of the D-132 and D-65 MAGs are identical but exhibited only 43% sequence identity to the Tn125 sequence present in the D-30 MAG. Further, the D-132 and D-65 MAG Tn125 sequences exhibited 87% identity to the S-65 MAG Tn125 sequence. Similarly, S-132 and S-30 MAG Tn125 sequences exhibited 100% identity to each other, 44% identity to the S-65 MAG Tn125 sequence, and 87% identity to the D-30 MAG Tn125 sequence.

Discussion

Spatially segregated microbial communities from three depth intervals spanning 132 m in BA1A were shown to contain abundant populations of *Meiothermus*, a genus that thus far comprises only obligately aerobic cultivars (Mori et al., 2012). This was true even in the highly reduced Type II waters encountered at depth in BA1A (>132 m). While perhaps surprising, these observations align with previous 16S rRNA gene (Rempfert et al., 2017; Nothaft et al., 2021) and metagenomic sequencing studies (Fones et al., 2019, 2021; Kraus et al., 2021) that also revealed the presence of *Meiothermus* in anoxic Type II waters in the Samail Ophiolite. For example, sequences affiliated with *Meiothermus* were detected in highly reduced fluids from samples collected from depths of 85 m in well NSHQ14 where Type II waters are encountered (Rempfert et al., 2017; Fones et al., 2021). Like the Samail Ophiolite, investigations of highly reduced fluids from the Cedars, Zambales Ophiolite, and Lobios hot springs, all of which are influenced by serpentinization, also identified *Meiothermus* sequences (López-López et al., 2015; Woycheese et al., 2015; Suzuki et al., 2017).

Several non-mutually exclusive explanations were put forth to account for the presence of *Meiothermus* in highly reduced waters including (1) *Meiothermus* was present in Type II waters due to inadvertent mixing with Type I waters during their collection and thereby represent inactive cells in said waters, (2) distinct populations of *Meiothermus* exist in Type I and Type II waters in the Samail Ophiolite that are indistinguishable via the sequence of the conservative 16S rRNA marker gene, (3) *Meiothermus* in Type II waters are aerobes capable of generating endogenous O_2 to fuel their energy metabolism, (4) *Meiothermus* in Type II waters are facultative anaerobes, and/or (5) that there is more connectivity among the 0-30 m, 41-65 m, and 108-132 m aquifers than expected based on geochemical and hydrological data (Lods et al., 2020; Nothaft et al., 2021). More connectivity of aquifers (explanation 5) would potentially allow for movement/dispersal of *Meiothermus* cells, viruses, or DNA between surface and subsurface aquifers that could impact the extent of gene flow/recombination and shape patterns of speciation.

The use of packers to collect samples from discrete intervals in BA1A, combined with SMEG scores indicating that abundant Type II (D) MAGs are in an active state of genome replication at depth (albeit at low levels), discounts explanation 1 as a source of abundant *Meiothermus* in the 108-132 m depth interval community in BA1A (Nothaft et al., 2021). Importantly, the detection of Type I (S) *Meiothermus* (i.e., S-132), which was not in an active state of genome replication in the 108-132 m depth interval at the time of sample collection, could be due to residual water from mixing during drilling, small ambient downflow after drilling, or sources of vertical flow (other than from the borehole) from shallower aquifer levels during pumping with packers. This possibility is suggested based on a geochemical model that indicated that ~7.0% of the 108-132 m fluids are of the Type I, Mg-HCO_3 end member type (Nothaft et al., 2021). Regardless, such possibilities cannot explain the increased prevalence of Type II (D) *Meiothermus* with depth in BA1A.

Phylogenetic analyses of *Meiothermus* from the three depth intervals in BA1A, other previously sampled fractured fluids from the Samail Ophiolite (Fones et al., 2019, 2021; Kraus et al., 2021), and other serpentinite systems was performed to begin to evaluate explanation 2. Phylogenomic analysis of housekeeping genes recovered from Oman MAGs revealed a monophyletic clade comprising two sublineages, to the exclusion of *Meiothermus* from other environments. This was also found to be true when *Meiothermus* RpoB sequences from BA1A, additional wells in the Samail Ophiolite, and a single other serpentinite (Zambales Ophiolite) were examined. Unfortunately, attempts to do a similar analysis of 16S rRNA genes recovered from BA1A MAGs, from

TABLE 5 Percent nucleic acid identities between pairs of transposon 125 (Tn125) sequence homologs retrieved from BA1A *Meiothermus* metagenome assembled genomes (MAGs).

	D-132	D-65	D-30	S-132	S-65	S-30
D-132	1.00	1.00	0.42	0.44	0.86	0.43
D-65	–	1.00	0.41	0.43	0.87	0.42
D-30	–	–	1.00	0.88	0.44	0.87
S-132	–	–	–	1.00	0.43	1.00
S-65	–	–	–	–	1.00	0.44
S-30	–	–	–	–	–	1.00

MAGs are labeled as belonging to the Type I surface phylogenetic clade (S) or the Type II deep phylogenetic clade (D) followed by the maximum depth interval (m) from where they were recovered (30, 65, 132).

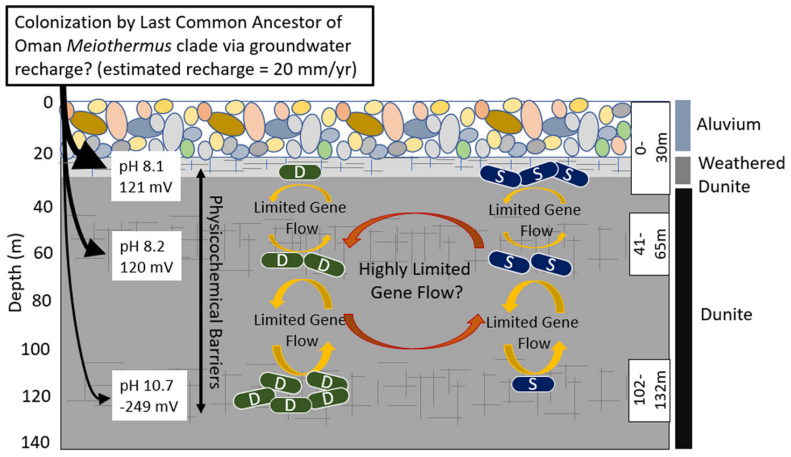

FIGURE 4
Schematic depicting proposed evolutionary dynamics of the Type I surface (S) populations and the Type II deep (D) populations of *Meiothermus* in three discrete depth intervals (fractures, indicated by hashed lines, isolated using a down borehole packer system) in well BA1A of the Samail Ophiolite and potential gene exchange/recombination between them and selective pressures indicated by arrows and text. The number of S and D cells at each depth interval is meant to depict the relative abundance of populations belonging to each clade at that depth. Characteristics of the waters and the predominant rock types that they interact with are indicated. The evidence for highly restricted gene flow/recombination (limited number of shared SVNs) between S and D *Meiothermus* populations from the same depth interval could be an artifact of the binning process, as discussed in the text, and the reader is cautioned of this possibility through the use of the question mark following this statement. Single cell genomics, in combination with other physiological approaches, would provide a more robust mechanism to evaluate whether the evidence for limited gene flow/recombination is artifactual or is due to selection against hybrid genotypes.

MAGs from other Oman wells, and those in the NCBI NR and SRA database were unsuccessful due to the highly fragmented nature of those genes in metagenome assemblies (data not shown). This indicates that distinct *Meiothermus* phylotypes exist in the Samail Ophiolite and that these were not distinguished in previous studies via analyses of the more conservative 16S rRNA marker gene. Together, these observations suggest that an ancestral *Meiothermus* population colonized the Samail Ophiolite or its geologic predecessor (**Figure 4**) and likely underwent speciation that led to two sublineages that have only been identified in the Samail Ophiolite to date. Additional metagenomic sequencing of other globally distributed ophiolites will be required to determine if these two sublineages are truly endemic to the Samail Ophiolite. These two sublineages of MAGs were termed Type I (S) and Type II (D) clades to reflect the water type (Type I versus Type II) and depth [Shallow (S) versus deep (D)] where they were most abundant (**Figure 4**).

To begin to investigate explanations (3 and 4) above, MAGs were compared and subjected to metabolic reconstruction, with the specific aim of determining if MAGs were capable of aerobic or anaerobic metabolism and/or generating their own endogenous O_2. Type II (D) MAGs are ~14% smaller than the Type I (S) MAGs, a finding that is potentially consistent with genome streamlining to reduce the nutrient and energetic costs associated with genome replication. Genome streamlining would presumably be advantageous in the carbon and oxidant limited Type II waters, such as has been suggested previously for populations inhabiting such waters in the Samail Ophiolite (Fones et al., 2019, 2021; Colman et al., 2022). Despite differences in genome sizes, MAGs from both *Meiothermus* clades encode Cox homologs, indicating an ability to respire O_2. Intriguingly, members of both clades also encode homologs of chlorite dismutase that, in other organisms, have been shown to function in the generation of endogenous O_2 via dismutation of chlorite (Bardiya and Bae, 2011; Mlynek et al., 2011; Hofbauer et al., 2014; Celis et al., 2015). Such a mechanism could conceivably be used to power aerobic metabolism in the presence of sufficient chlorine oxyanions. However, attempts to measure perchlorate and chlorite in Oman fracture waters have been unsuccessful to date (Templeton, unpublished data), suggesting they are either maintained at undetectable levels or

that these compounds are not present in the system. Further, attempts to cultivate *Meiothermus ruber* (ATCC strain 35948), which also encodes Cld, and to enrich *Meiothermus* from Oman fracture fluids under anaerobic conditions with a variety of electron donors/carbon sources and chlorite, chlorate, and perchlorate have been unsuccessful to date (Munro-Ehrlich, unpublished data). Together, these observations point to endogenous production of O_2 by *Meiothermus* (explanation 3) as being an unlikely reason for the abundance of *Meiothermus* sequence in BA1A132 communities.

The inferred proteomes indicate that the Type I (S) and Type II (D) *Meiothermus* are capable of aerobic, heterotrophic growth. However, the Type II (D) *Meiothermus* MAGs intriguingly encode several proteins suggestive of an ability to potentially grow anaerobically and/or autotrophically. This includes a group 1 [NiFe]-hydrogenase homolog that is predicted to provide reducing equivalents for the anaerobic respiration of sulfate, fumarate, nitrate, or metals (Søndergaard et al., 2016). Further, unlike Type I (S) MAGs, Type II (D) MAGs encode PFOR that allows for the anaerobic conversion of pyruvate to acetyl CoA and CO_2 (Furdui and Ragsdale, 2000; Fuchs, 2011; Mall et al., 2018; Witt et al., 2019). PFOR is a thiamine-dependent iron-sulfur ([Fe-S]) cluster-containing enzyme (Pieulle et al., 1995) which may, at least in part, explain why Type II (D) MAGs also encode a complete thiamine biosynthesis pathway, unlike Type I (S) MAGs.

Pyruvate ferredoxin oxidoreductase is reversible, allowing for the conversion of acetyl CoA and CO_2 to pyruvate (Furdui and Ragsdale, 2000; Fuchs, 2011; Mall et al., 2018; Witt et al., 2019). When operating in this direction, it is often termed pyruvate synthase and this enzyme/activity is required for three of the six known autotrophic pathways of CO_2 fixation including (i) the reductive acetyl CoA pathway [Wood-Ljungdahl pathway (Furdui and Ragsdale, 2000; Fuchs, 2011)], (ii) the reverse tricarboxylic acid (rTCA) cycle (Fuchs, 2011) and the more recently discovered functional reversal of the oxidative TCA cycle, termed the reverse oxidative TCA cycle or roTCA (Mall et al., 2018; Nunoura et al., 2018), and (iii) the dicarboxylate/hydroxybutyrate (DC/HB) cycle (Fuchs, 2011). In the anaerobe *Desulfurella acetivorans* when growing via the roTCA cycle, the directionality of PFOR is dictated by the availability of organic carbon. When acetate is present, heterotrophic growth (pyruvate oxidation) is favored whereas autotrophic growth is favored in its absence (Mall et al., 2018; Nunoura et al., 2018). The distribution and abundance of Type II (D) *Meiothermus* MAGs in anoxic waters in BA1A and in other waters impacted by serpentinization (discussed above), when combined with these MAGs uniquely encoding PFOR, oxidative [NiFe]-hydrogenase enzyme homologs that are typically involved in anaerobic respiration, and full TCA cycles that could potentially be reversed (e.g., roTCA) points to the intriguing possibility that these organisms are capable of anaerobic growth and/or autotrophy. Additional physiological and/or cultivation experiments are needed to further evaluate the plausibility that Type II (D) *Meiothermus* MAGs are facultative anaerobes (explanation 4) and possibly capable of autotrophic growth.

The recovery of Type II (D) MAGs in near-surface, less reacted aquifer waters (0–30 m, 41–65 m) and Type I (S) MAGs in deep, more reacted aquifer waters (108–132 m) suggested the possibility of dispersal between aquifers (explanation 5) and prompted a population-level analysis to examine the extent of gene flow/recombination among MAGs. Surprisingly, few shared SNVs with the same base substitution were identified among pairs of MAGs from different clades that co-occurred in the same depth. Interestingly, shared SNVs with the same base substitution were more prevalent among MAGs from different clades from differing depths. These shared SNVs could not be accounted for based on convergent (random) evolutionary processes alone indicating a potential role for limited gene flow/recombination among depth stratified populations despite chemical and physical barriers to dispersal (**Figure 4**). The role of gene flow/recombination, as opposed to shared ancestry, is potentially bolstered by the observation that contigs from MAG pairs where shared SNVs are located had, on average, significantly higher ANI than those contigs that did not share SNVs. While signatures of viruses were not evident in BA1A MAGs, several classes of IMGEs including the insertion sequences ISplu6 and the composite transposon Tn125 were detected thereby providing a potential mechanistic explanation for the observed but limited gene flow/recombination between *Meiothermus* populations comprising different clades. Intriguingly, the pattern of sequence identities among IMGEs, including that of Tn125, do not recapitulate the evolutionary history of the *Meiothermus* MAGs from which they derive. This provides further evidence for relatively recent gene flow/recombination between depth-stratified *Meiothermus* populations belonging to the same clade and, to a lesser extent, members of the different clades among depth intervals. The time scales over which gene flow/recombination occurred among spatially segregated *Meiothermus* is expected to be much shorter than the estimated residence times of Type II waters in the Samail Ophiolite [>20,000 years (Paukert Vankeuren et al., 2019)] based on the amount of time since they were in contact with the atmosphere. Such differences are likely a consequence of geochemical measurements made on bulk fluids as opposed to the resolution provided by the sensitive genomic techniques utilized herein.

Taken together, these findings suggest chemical and physical gradients in the subsurface of the Samail Ophiolite (or a geologically similar precursor) facilitated parapatric speciation of *Meiothermus* (**Figure 4**), a process where co-inhabiting populations speciate to inhabit specific ecological niches, with limited gene exchange between them (Butlin et al., 2008). In the case of *Meiothermus* in Oman, it is suggested that chemical variation generated by serpentinization creates opportunities for spatial variation between populations to develop (a form of geographic isolation), and this spatial variation of populations represents the starting point for further genetic divergence and speciation. As serpentinization of host rock progresses, the chemistry of deep fluids and near surface fluids further diverge, allowing for and/or promoting additional genetic divergence. Concomitantly, the porosity of host rocks (e.g., dunite, harzburgite), which likely become even less porous as serpentinization reactions progress (Klein and Le Roux, 2020), likely limits further dispersal and gene exchange. In this scenario, spatially and ecologically fragmented *Meiothermus* populations adapted to local environmental conditions and thereby independently accumulated distinct mutations, single nucleotide variants, and as illustrated above, differences in encoded functionalities. Parapatric speciation is thus likely to be a prominent mode of evolution in the Samail Ophiolite and other active subsurface geologic systems that have limited spatial connectivity and whose physical and chemical features are in actively evolving or changing.

Data availability statement

The datasets presented in this study can be found in online repositories. The names of the repository/repositories and accession number(s) can be found in the article/ **Supplementary material**.

Author contributions

DN and EB collected the samples. AT, JM, and EB designed the experiment. EF extracted DNA. MM-E conducted all bioinformatics analyses. EB and MM-E wrote the manuscript with help from other co-authors. All authors contributed to the article and approved the submitted version.

Funding

This work was supported by grants from NASA (NNA15BB02A and 80NSSC21K0489) to AT and EB. Drilling and research in the Oman Drilling Project were supported by the Alfred P. Sloan Foundation (in association with the Deep Carbon Observatory, DCO), the International Continental scientific Drilling Program (ICDP), US National Science Foundation (NSF) Research Grant NSF-EAR-1516300, the Japanese Marine Science and Technology Center (JAMSTEC), grant number 16H06347 from the Japanese Society for the Promotion of Science (JSPS), the US National Aeronautics and Space Administration (Rock Powered Life NASA Astrobiology Institute NNA15BB02A), the European Science Foundation, the German Science Foundation, the Swiss Science Foundation, and the International Ocean Discovery Program (IODP), with contributions from the Sultanate of Oman Ministry of Regional Municipalities and Water Resources, the Oman Public Authority of Mining, Sultan Qaboos University, CNRS, University of Montpellier, Columbia University of New York, and the University of Southampton.

Acknowledgments

We are grateful to the Sultanate of Oman Ministry of Regional Municipalities and Water Resources for allowing sampling and export of well waters. We are grateful to Philippe Gouze, Delphine Roubinet, Richard Leprovost, and Gérard Lods of CNRS, University of Montpellier for operating the packer system in 2018 and Amelia Paukert Vankeuren and Martin Stute for help with sample collection in 2019. We are grateful for two independent reviewers whose comments greatly improved this manuscript.

Conflict of interest

The authors declare that the research was conducted in the absence of any commercial or financial relationships that could be construed as a potential conflict of interest.

Publisher's note

Supplementary material

The Supplementary Material for this article can be found online at: https://www.frontiersin.org/articles/10.3389/fmicb.2023.1138656/full#supplementary-material

References

Acman, M., Wang, R., Van Dorp, L., Shaw, L. P., Wang, Q., Luhmann, N., et al. (2022). Role of mobile genetic elements in the global dissemination of the carbapenem resistance gene *blaNDM*. *Nat. Commun.* 13:1131. doi: 10.1038/s41467-022-28819-2

Anderson, R. E., Graham, E. D., Huber, J. A., and Tully, B. J. (2022). Microbial populations are shaped by dispersal and recombination in a low biomass subseafloor habitat. *mBio* 13:e0035422. doi: 10.1128/mbio.00354-22

Bardiya, N., and Bae, J.-H. (2011). Dissimilatory perchlorate reduction: A review. *Microb. Res.* 166, 237–254. doi: 10.1016/j.micres.2010.11.005

Barnes, I., and O'Neil, J. R. (1969). The relationship between fluids in some fresh alpine-type ultramafics and possible modern serpentinization, western United States. *Geo. Soc. Am. Bull.* 80, 1947–1960.

Bar-On, Y. M., Phillips, R., and Milo, R. (2018). The biomass distribution on Earth. *Proc. Natl. Acad. Sci. U.S.A.* 115, 6506–6511. doi: 10.1073/pnas.1711842115

Butlin, R. K., Galindo, J., and Grahame, J. W. (2008). Sympatric, parapatric or allopatric: The most important way to classify speciation? *Phil. Trans. R. Soc. B Biol. Sci.* 363, 2997–3007. doi: 10.1098/rstb.2008.0076

Celis, A. I., Geeraerts, Z., Ngmenterebo, D., Machovina, M. M., Kurker, R. C., Rajakumar, K., et al. (2015). A dimeric chlorite dismutase exhibits O_2-generating activity and acts as a chlorite antioxidant in *Klebsiella pneumoniae* MGH 78578. *Biochemistry* 54, 434–446. doi: 10.1021/bi501184c

Chaumeil, P.-A., Mussig, A. J., Hugenholtz, P., and Parks, D. H. (2019). GTDB-Tk: A toolkit to classify genomes with the genome taxonomy database. *Bioinformatics* 36, 1925–1927. doi: 10.1093/bioinformatics/btz848

Chung, A., Rainey, F., Nobre, M., Burghardt, J., and Da Costa, M. (1997). *Meiothermus cerbereus* sp. nov., a new slightly thermophilic species with high levels of 3-hydroxy fatty acids. *Int. J. Syst. Evol. Microbiol.* 47, 1225–1230. doi: 10.1099/00207713-47-4-1225

Clark, D. P., Pazdernik, N. J., and Mcgehee, M. R. (2019). "Mobile DNA," in *Molecular biology*, 3rd Edn, eds D. P. Clark, N. J. Pazdernik, and M. R. Mcgehee (Cambridge, MA: Academic Cell), 793–829.

Colman, D. R., Kraus, E. A., Thieringer, P. H., Rempfert, K., Templeton, A. S., Spear, J. R., et al. (2022). Deep-branching acetogens in serpentinized subsurface fluids of Oman. *Proc. Natl. Acad. Sci. U.S.A.* 119:e2206845119. doi: 10.1073/pnas.220684511

Darling, A. C. E., Mau, B., Blattner, F. R., and Perna, N. T. (2004). Mauve: Multiple alignment of conserved genomic sequence with rearrangements. *Gen. Res.* 14, 1394–1403. doi: 10.1101/gr.2289704

de Kok, A., Hengeveld, A. F., Fau, M. A., and Westphal, A. H. (1998). The pyruvate dehydrogenase multi-enzyme complex from Gram-negative bacteria. *Biochim. Biophys. Acta* 1385, 353–366. doi: 10.1016/s0167-4838(98)00079-x

El-Gebali, S., Mistry, J., Bateman, A., Eddy, S. R., Luciani, A., Potter, S. C., et al. (2018). The Pfam protein families database in 2019. *Nucl. Acids Res.* 47, D427–D432. doi: 10.1093/nar/gky995

Ellison, E. T., Templeton, A. S., Zeigler, S. D., Mayhew, L. E., Kelemen, P. B., Matter, J. M., et al. (2021). Low-temperature hydrogen formation during aqueous alteration of serpentinized peridotite in the Samail Ophiolite. *J. Geophys. Res. Solid Earth* 126:e2021JB021981. doi: 10.1029/2021JB021981

Emiola, A., Zhou, W., and Oh, J. (2020). Metagenomic growth rate inferences of strains in situ. *Sci. Adv.* 6:eaaz2299. doi: 10.1126/sciadv.aaz2299

Fernandes-Martins, M. C., Keller, L. M., Munro-Ehrlich, M., Zimlich, K. R., Mettler, M. K., England, A. M., et al. (2021). Ecological dichotomies arise in microbial communities due to mixing of deep hydrothermal waters and atmospheric gas in a circumneutral hot spring. *Appl. Environ. Microbiol.* 87:e0159821. doi: 10.1128/AEM.01598-21

Fernández De Henestrosa, A. R., Ogi, T., Aoyagi, S., Chafin, D., Hayes, J. J., Ohmori, H., et al. (2000). Identification of additional genes belonging to the LexA regulon in *Escherichia coli*. *Mol. Microbiol.* 35, 1560–1572. doi: 10.1046/j.1365-2958.2000.01826.x

Fones, E. M., Colman, D. R., Kraus, E. A., Nothaft, D. B., Poudel, S., Rempfert, K. R., et al. (2019). Physiological adaptations to serpentinization in the Samail Ophiolite, Oman. *ISME J.* 13, 1750–1762. doi: 10.1038/s41396-019-0391-2

Fones, E. M., Colman, D. R., Kraus, E. A., Stepanauskas, R., Templeton, A. S., Spear, J. R., et al. (2021). Diversification of methanogens into hyperalkaline serpentinizing environments through adaptations to minimize oxidant limitation. *ISME J.* 15, 1121–1135. doi: 10.1038/s41396-020-00838-1

Fones, E. M., Templeton, A. S., Mogk, D. W., and Boyd, E. S. (2022). Transformation of low-molecular-weight organic acids by microbial endoliths in subsurface mafic and ultramafic igneous rock. *Environ. Microbiol.* 24, 4137–4152. doi: 10.1111/1462-2920.16041

Frost, B. R., and Beard, J. S. (2007). On silica activity and serpentinization. *J. Petrol.* 48, 1351–1368. doi: 10.1093/petrology/egm021

Fu, L., Niu, B., Zhu, Z., Wu, S., and Li, W. (2012). CD-HIT: Accelerated for clustering the next-generation sequencing data. *Bioinformatics* 28, 3150–3152. doi: 10.1093/bioinformatics/bts565

Fuchs, G. (2011). Alternative pathways of carbon dioxide fixation: Insights into the early evolution of life? *Ann. Rev. Microbiol.* 65, 631–658. doi: 10.1146/annurev-micro-090110-102801

Furdui, C., and Ragsdale, S. W. (2000). The role of pyruvate ferredoxin oxidoreductase in pyruvate synthesis during autotrophic growth by the Wood-Ljungdahl pathway. *J. Biol. Chem.* 275, 28494–28499. doi: 10.1074/jbc.M003291200

Goordial, J., D'Angelo, T., Labonté, J. M., Poulton, N. J., Brown, J. M., Stepanauskas, R., et al. (2021). Microbial diversity and function in shallow subsurface sediment and oceanic lithosphere of the Atlantis Massif. *mBio* 12:e0049021. doi: 10.1128/mBio.00490-21

Henne, A., Brüggemann, H., Raasch, C., Wiezer, A., Hartsch, T., Liesegang, H., et al. (2004). The genome sequence of the extreme thermophile *Thermus thermophilus*. *Nat. Biotech.* 22, 547–553. doi: 10.1038/nbt956

Hofbauer, S., Schaffner, I., Furtmüller, P. G., and Obinger, C. (2014). Chlorite dismutases – a heme enzyme family for use in bioremediation and generation of molecular oxygen. *Biotech. J.* 9, 461–473. doi: 10.1002/biot.201300210

Imlay, J. A. (2002). What biological purpose is served by superoxide reductase? *J. Biol. Inorg. Chem.* 7, 659–663. doi: 10.1007/s00775-002-0361-3

Jain, C., Rodriguez-R, L. M., Phillippy, A. M., Konstantinidis, K. T., and Aluru, S. (2018). High throughput ANI analysis of 90K prokaryotic genomes reveals clear species boundaries. *Nat. Commun.* 9:5114. doi: 10.1038/s41467-018-07641-9

Johansson, M. H. K., Bortolaia, V., Tansirichaiya, S., Aarestrup, F. M., Roberts, A. P., and Petersen, T. N. (2021). Detection of mobile genetic elements associated with antibiotic resistance in *Salmonella enterica* using a newly developed web tool: MobileElementFinder. *J. Antimicrob. Chemother.* 76, 101–109. doi: 10.1093/jac/dkaa390

Jünemann, S. (1997). Cytochrome *bd* terminal oxidase. *Biochim. Biophys. Acta* 1321, 107–127. doi: 10.1016/s0005-2728(97)00046-7

Kanehisa, M., Furumichi, M., Sato, Y., Ishiguro-Watanabe, M., and Tanabe, M. (2020). KEGG: Integrating viruses and cellular organisms. *Nucl. Acids Res.* 49, D545–D551. doi: 10.1093/nar/gkaa970

Kelemen, P. B., Leong, J. A., Carlos de Obeso, J., Matter, J. M., Ellison, E. T., Templeton, A., et al. (2021). Initial results from the Oman Drilling Project Multi-Borehole Observatory: Petrogenesis and ongoing alteration of mantle peridotite in the weathering horizon. *J. Geophys. Res. Solid Earth* 126:e2021JB022729. doi: 10.1029/2021JB022729

Kieft, K., Zhou, Z., and Anantharaman, K. (2020). VIBRANT: Automated recovery, annotation and curation of microbial viruses, and evaluation of viral community function from genomic sequences. *Microbiome* 8:90. doi: 10.1186/s40168-020-00867-0

Klein, F., and Le Roux, V. (2020). Quantifying the volume increase and chemical exchange during serpentinization. *Geology* 48, 552–556.

Kraus, E. A., Nothaft, D., Stamps, B. W., Rempfert, K. R., Ellison, E. T., Matter, J. M., et al. (2021). Molecular evidence for an active microbial methane cycle in subsurface serpentinite-hosted groundwaters in the Samail Ophiolite, Oman. *Appl. Environ. Microbiol.* 87, e02068–20. doi: 10.1128/AEM.02068-20

Langmead, B., and Salzberg, S. L. (2012). Fast gapped-read alignment with Bowtie 2. *Nat. Methods* 9, 357–359. doi: 10.1038/nmeth.1923

Letunic, I., and Bork, P. (2021). Interactive tree of life (iTOL) v5: An online tool for phylogenetic tree display and annotation. *Nucl. Acids Res.* 49, W293–W296. doi: 10.1093/nar/gkab301

Lods, G., Roubinet, D., Matter, J. M., Leprovost, R., Gouze, P., and Oman Drilling Project Science Team (2020). Groundwater flow characterization of an ophiolitic hard-rock aquifer from cross-borehole multi-level hydraulic experiments. *J. Hydrol.* 589:125152. doi: 10.1016/j.jhydrol.2020.125152

López-López, O., Knapik, K., Cerdán, M. E., and González-Siso, M. I. (2015). Metagenomics of an alkaline hot spring in Galicia (Spain): Microbial diversity analysis and screening for novel lipolytic enzymes. *Front. Microbiol.* 6:1291. doi: 10.3389/fmicb.2015.01291

Ludwig, B. (1987). Cytochrome *c* oxidase in prokaryotes. *FEMS Microbiol Rev.* 3, 41–56. doi: 10.1111/j.1574-6968.1987.tb02451.x

Magnabosco, C., Lin, L.-H., Dong, H., Bomberg, M., Ghiorse, W., Stan-Lotter, H., et al. (2018). The biomass and biodiversity of the continental subsurface. *Nat. Geosci.* 11, 707–717. doi: 10.1038/s41561-018-0221-6

Mall, A., Sobotta, J., Huber, C., Tschirner, C., Kowarschik, S., Baènik, K., et al. (2018). Reversibility of citrate synthase allows autotrophic growth of a thermophilic bacterium. *Science* 359, 563–567. doi: 10.1126/science.aao2410

Malvoisin, B., Zhang, C., Müntener, O., Baumgartner, L. P., Kelemen, P. B., and Oman Drilling Project Science Party (2020). Measurement of volume change and mass transfer during serpentinization: Insights from the Oman Drilling Project. *J. Geophys. Res. Solid Earth* 125:e2019JB018877. doi: 10.1029/2019JB018877

McCollom, T. M., and Seewald, J. S. (2007). Abiotic synthesis of organic compounds in deep-sea hydrothermal environments. *Chem. Rev.* 107, 382–401. doi: 10.1021/cr0503660

McMahon, S., and Parnell, J. (2014). Weighing the deep continental biosphere. *FEMS Microb. Ecol.* 87, 113–120. doi: 10.1111/1574-6941.12196

Miller, H. M., Mayhew, L. E., Ellison, E. T., Kelemen, P., Kubo, M., and Templeton, A. S. (2017). Low temperature hydrogen production during experimental hydration of partially-serpentinized dunite. *Geochim. Cosmochim. Acta* 209, 161–183. doi: 10.1016/j.gca.2017.04.022

Minh, B. Q., Schmidt, H. A., Chernomor, O., Schrempf, D., Woodhams, M. D., Von Haeseler, A., et al. (2020). IQ-TREE 2: New models and efficient methods for phylogenetic inference in the genomic era. *Mol. Biol. Evol.* 37, 1530–1534. doi: 10.1093/molbev/msaa015

Mlynek, G., Sjöblom, B., Kostan, J., Füreder, S., Maixner, F., Gysel, K., et al. (2011). Unexpected diversity of chlorite dismutases: A catalytically efficient dimeric enzyme from *Nitrobacter winogradskyi*. *J. Bact.* 193, 2408–17. doi: 10.1128/JB.01262-10

Mori, K., Iino, T., Ishibashi, J. I., Kimura, H., Hamada, M., and Suzuki, K. I. (2012). *Meiothermus hypogaeus* sp. nov., a moderately thermophilic bacterium isolated from a hot spring. *Int. J. Syst. Evol. Microbiol.* 62, 112–117. doi: 10.1099/ijs.0.028654-0

Neal, C., and Stanger, G. (1985). "Past and present serpentinisation of ultramafic rocks; an example from the Semail Ophiolite Nappe of Northern Oman," in *The chemistry of weathering*, ed. J. I. Drever (Dordrecht: Springer), 249–275.

Nothaft, D. B., Templeton, A. S., Boyd, E. S., Matter, J. M., Stute, M., Paukert Vankeuren, A. N., et al. (2021). Aqueous geochemical and microbial variation across discrete depth intervals in a peridotite aquifer assessed using a packer system in the Samail Ophiolite, Oman. *J. Geophys. Res. Biogeosci.* 126:e2021JG006319. doi: 10.1029/2021JG006319

Nunoura, T., Chikaraishi, Y., Izaki, R., Suwa, T., Sato, T., Harada, T., et al. (2018). A primordial and reversible TCA cycle in a facultatively chemolithoautotrophic thermophile. *Science* 359, 559–563. doi: 10.1126/science.aao3407

Olm, M. R., Crits-Christoph, A., Bouma-Gregson, K., Firek, B. A., Morowitz, M. J., and Banfield, J. F. (2021). inStrain profiles population microdiversity from metagenomic data and sensitively detects shared microbial strains. *Nat. Biotech.* 39, 727–736. doi: 10.1038/s41587-020-00797-0

Paukert Vankeuren, A. N., Matter, J. M., Stute, M., and Kelemen, P. B. (2019). Multitracer determination of apparent groundwater ages in peridotite aquifers within the Samail Ophiolite, Sultanate of Oman. *Earth Plan. Sci. Lett.* 516, 37–48. doi: 10.1016/j.epsl.2019.03.007

Piccoli, F., Hermann, J., Pettke, T., Connolly, J. A. D., Kempf, E. D., and Vieira Duarte, J. F. (2019). Subducting serpentinites release reduced, not oxidized, aqueous fluids. *Sci. Rep.* 9:19573. doi: 10.1038/s41598-019-55944-8

Pieulle, L., Guigliarelli, B., Asso, M., Dole, F., Bernadac, A., and Hatchikian, E. C. (1995). Isolation and characterization of the pyruvate-ferredoxin oxidoreductase from

the sulfate-reducing bacterium *Desulfovibrio africanus*. *Biochim. Biophys. Acta* 1250, 49–59. doi: 10.1016/0167-4838(95)00029-t

Putman, L. I., Sabuda, M. C., Brazelton, W. J., Kubo, M. D., Hoehler, T. M., McCollom, T. M., et al. (2021). Microbial communities in a serpentinizing aquifer are assembled through strong concurrent dispersal limitation and selection. *mSystems* 6:e0030021. doi: 10.1128/mSystems.00300-21

Rempfert, K. R., Miller, H. M., Bompard, N., Nothaft, D., Matter, J. M., Kelemen, P., et al. (2017). Geological and geochemical controls on subsurface microbial life in the Samail Ophiolite, Oman. *Front. Microbiol.* 8:56. doi: 10.3389/fmicb.2017.00056

Seewald, J. S., Zolotov, M. Y., and McCollom, T. (2006). Experimental investigation of single carbon compounds under hydrothermal conditions. *Geochim. Cosmochim. Acta* 70, 446–460. doi: 10.1016/j.gca.2005.09.002

Sievers, F., Wilm, A., Dineen, D., Gibson, T. J., Karplus, K., Li, W., et al. (2011). Fast, scalable generation of high-quality protein multiple sequence alignments using Clustal Omega. *Mol. Syst. Biol.* 7:539. doi: 10.1038/msb.2011.75

Singh, R., Wiseman, B., Deemagarn, T., Jha, V., Switala, J., and Loewen, P. C. (2008). Comparative study of catalase-peroxidases (KatGs). *Arch. Biochem. Biophys.* 471, 207–214. doi: 10.1016/j.abb.2007.12.008

Søndergaard, D., Pedersen, C. N. S., and Greening, C. (2016). HydDB: A web tool for hydrogenase classification and analysis. *Sci. Rep.* 6:34212. doi: 10.1038/srep34212

Suzuki, S., Ishii, S. I., Hoshino, T., Rietze, A., Tenney, A., Morrill, P. L., et al. (2017). Unusual metabolic diversity of hyperalkaliphilic microbial communities associated with subterranean serpentinization at The Cedars. *ISME J.* 11, 2584–2598. doi: 10.1038/ismej.2017.111

Templeton, A. S., Ellison, E. T., Glombitza, C., Morono, Y., Rempfert, K. R., Hoehler, T. M., et al. (2021). Accessing the subsurface biosphere within rocks undergoing active low-temperature serpentinization in the Samail Ophiolite (Oman Drilling Project). *J. Geophys. Res. Biogeosci.* 126:e2021JG006315. doi: 10.1029/2021JG006315

Thannesberger, J., Hellinger, H. J., Klymiuk, I., Kastner, M. T., Rieder, F. J. J., Schneider, M., et al. (2017). Viruses comprise an extensive pool of mobile genetic elements in eukaryote cell cultures and human clinical samples. *FASEB J.* 31, 1987–2000. doi: 10.1096/fj.201601168R

Uritskiy, G. V., Diruggiero, J., and Taylor, J. (2018). MetaWRAP—a flexible pipeline for genome-resolved metagenomic data analysis. *Microbiome* 6:158. doi: 10.1186/s40168-018-0541-1

Witt, A., Pozzi, R., Diesch, S., Hädicke, O., and Grammel, H. (2019). New light on ancient enzymes – *in vitro* CO_2 fixation by pyruvate synthase of *Desulfovibrio africanus* and *Sulfolobus acidocaldarius*. *FEBS J.* 286, 4494–4508. doi: 10.1111/febs.14981

Woycheese, K. M., Meyer-Dombard, D. A. R., Cardace, D., Argayosa, A. M., and Arcilla, C. A. (2015). Out of the dark: Tansitional subsurface-to-surface microbial diversity in a terrestrial serpentinizing seep (Manleluag, Pangasinan, the Philippines). *Front. Microbiol.* 6:44. doi: 10.3389/fmicb.2015.00044

Zhang, Y., Horne, R. N., Hawkins, A. J., Primo, J. C., Gorbatenko, O., and Dekas, A. E. (2022). Geological activity shapes the microbiome in deep-subsurface aquifers by advection. *Proc. Nat. Acad. Sci. U.S.A.* 119:e2113985119. doi: 10.1073/pnas.2113985119

Zhu, B., Wang, J., Bradford, L. M., Ettwig, K., Hu, B., and Lueders, T. (2019). Nitric oxide dismutase (*nod*) genes as a functional marker for the diversity and phylogeny of methane-driven oxygenic denitrifiers. *Front. Microbiol.* 10:1577. doi: 10.3389/fmicb.2019.01577

frontiers | Frontiers in Microbiology

TYPE Original Research
PUBLISHED 21 April 2023
DOI 10.3389/fmicb.2023.1139633

OPEN ACCESS

EDITED BY
Marianne Quéméneur,
UMR7294 Institut Méditerranéen d'Océanographie (MIO), France

REVIEWED BY
James F. Holden,
University of Massachusetts Amherst, United States
Florence Schubotz,
University of Bremen, Germany

*CORRESPONDENCE
Kaitlin R. Rempfert
✉ kaitlin.rempfert@colorado.edu
Alexis S. Templeton
✉ alexis.templeton@colorado.edu

SPECIALTY SECTION
This article was submitted to Extreme Microbiology, a section of the journal Frontiers in Microbiology

RECEIVED 07 January 2023
ACCEPTED 15 March 2023
PUBLISHED 21 April 2023

CITATION
Rempfert KR, Nothaft DB, Kraus EA, Asamoto CK, Evans RD, Spear JR, Matter JM, Kopf SH and Templeton AS (2023) Subsurface biogeochemical cycling of nitrogen in the actively serpentinizing Samail Ophiolite, Oman. *Front. Microbiol.* 14:1139633. doi: 10.3389/fmicb.2023.1139633

Subsurface biogeochemical cycling of nitrogen in the actively serpentinizing Samail Ophiolite, Oman

Kaitlin R. Rempfert[1]*, Daniel B. Nothaft[1], Emily A. Kraus[2], Ciara K. Asamoto[1], R. Dave Evans[3], John R. Spear[2,4], Juerg M. Matter[5], Sebastian H. Kopf[1] and Alexis S. Templeton[1]*

[1]Department of Geological Sciences, University of Colorado, Boulder, CO, United States, [2]Department of Civil and Environmental Engineering, Colorado School of Mines, Golden, CO, United States, [3]School of Biological Sciences, Washington State University, Pullman, WA, United States, [4]Quantitative Biosciences and Engineering, Colorado School of Mines, Golden, CO, United States, [5]National Oceanography Centre, University of Southampton, Southampton, United Kingdom

Nitrogen (N) is an essential element for life. N compounds such as ammonium (NH_4^+) may act as electron donors, while nitrate (NO_3^-) and nitrite (NO_2^-) may serve as electron acceptors to support energy metabolism. However, little is known regarding the availability and forms of N in subsurface ecosystems, particularly in serpentinite-hosted settings where hydrogen (H_2) generated through water–rock reactions promotes habitable conditions for microbial life. Here, we analyzed N and oxygen (O) isotope composition to investigate the source, abundance, and cycling of N species within the Samail Ophiolite of Oman. The dominant dissolved N species was dependent on the fluid type, with Mg^{2+}-HCO_3^- type fluids comprised mostly of NO_3^-, and Ca^{2+}-OH^- fluids comprised primarily of ammonia (NH_3). We infer that fixed N is introduced to the serpentinite aquifer as NO_3^-. High concentrations of NO_3^- (>100 μM) with a relict meteoric oxygen isotopic composition ($\delta^{18}O \sim 22‰$, $\Delta^{17}O \sim 6‰$) were observed in shallow aquifer fluids, indicative of NO_3^- sourced from atmospheric deposition (rainwater NO_3^-: $\delta^{18}O$ of 53.7‰, $\Delta^{17}O$ of 16.8‰) mixed with NO_3^- produced *in situ* through nitrification (estimated endmember $\delta^{18}O$ and $\Delta^{17}O$ of ~0‰). Conversely, highly reacted hyperalkaline fluids had high concentrations of NH_3 (>100 μM) with little NO_3^- detectable. We interpret that NH_3 in hyperalkaline fluids is a product of NO_3^- reduction. The proportionality of the O and N isotope fractionation ($^{18}\varepsilon$ / $^{15}\varepsilon$) measured in Samail Ophiolite NO_3^- was close to unity ($^{18}\varepsilon$ / $^{15}\varepsilon \sim 1$), which is consistent with dissimilatory NO_3^- reduction with a membrane-bound reductase (NarG); however, abiotic reduction processes may also be occurring. The presence of genes commonly involved in N reduction processes (*narG*, *napA*, *nrfA*) in the metagenomes of biomass sourced from aquifer fluids supports potential biological involvement in the consumption of NO_3^-. Production of NH_4^+ as the end-product of NO_3^- reduction *via* dissimilatory nitrate reduction to ammonium (DNRA) could retain N in the subsurface and fuel nitrification in the oxygenated near surface. Elevated bioavailable N in all sampled fluids indicates that N is not likely limiting as a nutrient in serpentinites of the Samail Ophiolite.

KEYWORDS

serpentinization, water–rock interaction, deep subsurface biosphere, nitrate, nitrogen isotopes, nitrogen, Samail Ophiolite

1. Introduction

The terrestrial subsurface is known to host a substantial biosphere ($2–6 \times 10^{29}$ cells; 23–31 Pg carbon) of diverse microbial communities that likely play significant roles in biogeochemical cycling on a global scale (Nyyssönen et al., 2014; Magnabosco et al., 2018; Flemming and Wuertz, 2019). However, life in the continental subsurface is not uniformly distributed due to heterogeneity in energy availability resulting from differences in host rock lithology and the degree of hydrologic connectivity in the subsurface (Templeton and Caro, in press). Organic matter is scarce in hard-rock subsurface ecosystems, and thus, electron donors derived from minerals are the primary substrate for biological metabolism. Minerals can be directly dissolved by microorganisms, or energy can be released through abiotic chemical reactions (Escudero et al., 2018). For example, hydration and oxidation reactions that occur during the serpentinization of olivine and pyroxene in ultramafic rock can yield reducing power in the form of hydrogen gas (H_2) (McCollom and Bach, 2009). Thus, H_2 generation by serpentinization could fuel microbial life in peridotite rock, where sufficient oxidants are delivered hydrologically. Multiple studies have investigated the diversity and activity of microbial communities likely sustained by H_2 production in serpentinite aquifers (Rempfert et al., 2017; Fones et al., 2019; Sabuda et al., 2020; Seyler et al., 2020; Kraus et al., 2021; Nothaft et al., 2021; Templeton et al., 2021). However, the origins of nutrients and oxidants for these communities have not been sufficiently investigated, and so the broader habitability of subsurface serpentinizing environments remains unconstrained. In particular, the source and principal form of nitrogen (N) in terrestrial serpentinite-hosted ecosystems is unknown.

Nitrogen is essential to all life on Earth as it is required to synthesize proteins, nucleic acids, and many biological macromolecules. Accordingly, the availability of N may control the productivity of ecosystems or the structure of microbial communities where it is limiting. N exists in multiple oxidation states and thus can be utilized by life for energy metabolism in addition to biosynthesis. Reduced nitrogen species such as ammonia/ammonium (NH_3/NH_4^+) may act as electron donors, while N-oxides such as nitrate (NO_3^-) and nitrite (NO_2^-) can serve as electron acceptors. N-oxides are especially important in the deep biosphere because oxidants are often scarce (Jones et al., 2018; Meyer-Dombard and Malas, 2022; Mosley et al., 2022). Determining the source and speciation of N accessible to serpentinite-hosted subsurface life is crucial for understanding how N availability may influence the microbial habitability of subsurface environments. In particular, tracing the fate of NO_3^- could provide insight into the habitability of subsurface rock-hosted environments on other planetary bodies where NO_3^- is likely present, such as Mars (Stern et al., 2017).

We measured the N and oxygen (O) isotopic composition ($\delta^{15}N$ and $\delta^{18}O$, respectively) of dissolved NO_3^- and the N isotopic composition of NH_3/NH_4^+ to assess the origin and transformation of N in the subsurface of a terrestrial serpentinizing system in the Samail Ophiolite, Sultanate of Oman, the world's largest massif of serpentinized peridotite rock (Nicolas et al., 2000). Groundwater fluids were collected from deep boreholes hosted within peridotite and gabbro. The reaction histories of sampled fluids were inferred by geochemical composition, and the speciation and isotopic composition of fluid N were analyzed with the goals of: (1) identifying the major sources of N in the aquifer and (2) evaluating the subsequent biogeochemical cycling of N in the subsurface. In addition, we evaluated possible geologic sources of N by measuring the $\delta^{15}N$ of peridotite rock obtained from diamond drilling during Phase 2 of the Oman Drilling Project (Kelemen et al., 2020). Finally, the potential for microbial participation in the cycling of N at depth was assessed based on the presence of functional genes for N metabolisms in metagenomes derived from biomass collected from borehole fluids. This combined isotopic and functional gene approach yields new insights into the N dynamics of subsurface, serpentinite-hosted ecosystems, revealing how NO_3^- introduced into serpentinite aquifers is primarily converted to NH_4^+, and how NH_3/NH_4^+ is recycled, retaining a substantial pool of fixed N in this subsurface habitat.

2. Methods

2.1. Sampling and geochemical characterization of fluids

We obtained subsurface fluids over four annual field seasons (2015–2018) from 12 boreholes previously drilled by the Oman Ministry of Regional Municipalities and Water Resources. These boreholes are situated in crustal gabbros and mantle peridotites in the Wadi Tayin block of the Samail Ophiolite. We additionally sampled borehole BA1A of the Oman Drilling Project multi-borehole observatory during the 2018 field season; the hydrological properties of this borehole are described extensively in Lods et al. (2020). The lithologies, geographic coordinates, elevations, depths, and casing properties of the boreholes are listed in Table 1.

Detailed descriptions of fluid sampling and aqueous geochemical analyses are reported in Rempfert et al. (2017), Kraus et al. (2021), and Nothaft et al. (2021) for the 2015–2016, 2017, and 2018 field seasons, respectively, with key geochemical parameters summarized in Supplementary Table 1. Briefly, a Grundfos SQ-85 submersible pump was used to collect subsurface fluids for isotopic and metagenomic analyses. Water temperature, pH, and oxidation-reduction potential were measured in the field with a Hach (Loveland, CO) HQ40D Portable Multi Meter. Boreholes were pumped ~20 min prior to sampling until pH stabilized. Biomass was concentrated for DNA extraction on a 0.2-μm Millipore polycarbonate filter. Two aliquots of fluid for isotopic analyses were filtered through a 0.2-μm filter to remove cells and collected in acid-washed 15-ml Falcon tubes (Corning Inc., Corning, NY) (Granger and Sigman, 2009). One aliquot was acidified to a pH of <2 with concentrated hydrochloric acid for the analysis of $\delta^{15}N$ of reduced N (N_{red}) (U. S. Environmental Protection Agency, 1983); the other aliquot was left unacidified for $\delta^{15}N$ and $\delta^{18}O$ analyses of NO_3^- and NO_2^-. Filters for DNA extraction were flash-frozen, transferred in a liquid nitrogen dewar, and stored at −80°C until extraction. Fluid aliquots for isotopic analyses were stored in a cooler on ice in the field, transported *via* air cargo at room temperature, and then stored frozen at −20°C until analysis (Avanzino and Kennedy, 1993; Menchyk et al., 2014).

TABLE 1 Lithology, geographic location, elevation, depth, and borehole properties of wells sampled as previously reported by Rempfert et al. (2017) and Nothaft et al. (2021).

Well	Well depth (mbgl)	Casing extent (mbct)	Screened Interval (mbct)	Depth to water (mbct)	UTM Easting	UTM Northing	Elevation (mabsl)	Lithology
BA1A	400.0	22.0	Open below casing	13.47	674492	2531354	583	peridotite
CM2A	400.0	23.7	Open below casing	13.4	636988	2534284	713	gabbro
NSHQ04	304.0	5.8	Open below casing	4.7	670971	2531699	543	peridotite
NSHQ14	304.0	5.8	Open below casing	9.2	675495	2529716	526	peridotite
WAB103	101.0	101.0	90–98	15	648577	2530362	632	gabbro
WAB104	120.4	120.4	101–104	40	643099	2541124	842	peridotite
WAB105	120.5	120.5	110–117	16.5	644678	2536524	738	peridotite
WAB188	78.0	78.0	35–51	9.5	671123	2529798	514	gabbro
WAB55	102.0	102.0	8–97	7.5	634777	2506101	531	peridotite
WAB71	136.5	136.5	128–131	8.3	670322	2533981	608	peridotite
NSHQ3B	472.0	185.0	91–180	-	645068	2536069	688	alluvium
NSHQ10	304.0	5.8	Open below casing	14.3	645706	2502793	453	peridotite
NSHQ21	233.0	5.4	Open below casing	3.33	633569	2509105	514	gabbro

At BA1A, a packer system (Solexperts) was deployed to sample discrete depth intervals in the borehole. A detailed description of sampling with the packer system is provided by Nothaft et al. (2021).

A single rain event was sampled in 2017 for ~1 min of rainfall by holding an open, acid-washed 15-mL Falcon tube at ~5 ft over the ground. The tube was not opened until after the rain event had started in order to minimize the potential contamination of the sample with dust. The sample was immediately filtered through a 0.2-μm polycarbonate filter to remove cells and prevent the biological processing of N and then placed on ice in a cooler in the field. The sample was stored frozen at −20 °C until the analysis of $\delta^{15}N$ and $\delta^{17}O + \delta^{18}O$ of NO_3^-. Since the sample volume was limited, no second aliquot was acidified for the measurement of reduced N compounds. Because precipitation in Oman is scarce and sporadic (Weyhenmeyer et al., 2002), this sample was the only rainwater obtained during field sampling throughout the multiyear campaign.

2.2. Classification of fluid reaction histories

Serpentinized fluids were categorized as Mg^{2+}-HCO_3^- or Ca^{2+}-OH^- type compositions according to pH and concentrations of $\sum$Mg, $\sum$Ca, and $\sum CO_2$ (Supplementary Table 1) that reflect the extent of water–rock reaction (Barnes et al., 1967; Barnes and O'neil, 1969; Bruni et al., 2002; Paukert et al., 2012; Chavagnac et al., 2013). We infer that Mg^{2+}-HCO_3^- fluids reacted in an open system with atmospheric CO_2 over relatively short residence times, whereas Ca^{2+}-OH^- fluids reacted extensively over long residence times at depths closed to atmospheric inputs (Paukert et al., 2012; Paukert Vankeuren et al., 2019; Leong and Shock, 2020; Leong et al., 2021). The degree of mixing between Mg^{2+}-HCO_3^- and Ca^{2+}-OH^- fluid types was estimated using $\sum$Si as a conservative tracer because $\sum$Si is far more sensitive to mixing than pH in ophiolitic groundwater (Leong et al., 2021). Using the mixing model predictions published by Leong et al. (2021) for endmember Ca^{2+}-OH^- fluids containing 20 μmole/kg $\sum CO_2$, the modeled concentration of $\sum CO_2$ that most closely resembles $\sum CO_2$ measured in highly reacted fluids in this study (Supplementary Table 1), we applied a linear model of $\sum$Si and extent of mixing (%) to our measured fluid compositions (Supplementary Table 2).

2.3. Analysis of aqueous N species

NO_3^- and NO_2^- concentrations were quantified using a Griess reaction-VCl_3 sequential colorimetric assay (García-Robledo et al., 2014) on a BioTek Synergy 2 Microplate Reader. $\sum NH_3$ ($NH_3 + NH_4^+$) concentrations were also quantified spectrophotometrically on a microplate reader using a salicylate hypochlorite colorimetric assay (Ruppersberg et al., 2017).

The $\delta^{15}N$ and $\delta^{18}O$ of NO_3^- and NO_2^- as well as the ^{15}N composition of $\sum NH_3$ were determined using the denitrifier method (Sigman et al., 2001; Weigand et al., 2016) in the Sigman Lab at Princeton University using 20 nmol NO_3^- per analysis. Samples that exhibited >1% NO_2^- were subjected to NO_2^- removal through the sulfamic acid method prior to the analysis of the remaining NO_3^- (Granger and Sigman, 2009) and analyzed in parallel with untreated aliquots ($NO_3^- + NO_2^-$) to allow for the inference of NO_2^- isotopic composition by mass balance. Calibration of isotopic measurements was conducted with the IAEA-NO3 [$\delta^{15}N = 4.7‰$ vs. air, $\delta^{18}O = 25.6‰$ vs. Vienna Standard Mean Ocean Water (VSMOW)] and USGS34 ($\delta^{15}N = -1.8‰$ vs. air, $\delta^{18}O = -27.9‰$ vs. VSMOW) potassium nitrate standards at two concentrations (to correct for volumetric effects) every eight samples with analytical precision: 0.1‰ for $\delta^{15}N$ and

0.3‰ for $\delta^{18}O$ (1σ, $n = 122$). Prior to analysis with the denitrifier method, $\sum NH_3$ was oxidized to NO_3^- *via* the persulfate method using N-clean recrystallized potassium persulfate (Wang et al., 2015). These measurements are reported as $\delta^{15}N$ of N_{red} because persulfate oxidizes all reduced N in the sample. An additional suite of amino acid isotope standards was used to correct for NO_3^- contamination of persulfate (USGS 40, $\delta^{15}N = -4.5$‰; and USGS 41, $\delta^{15}N = 47.6$‰).

The $\delta^{17}O$ measurements of NO_3^- were conducted at the Stable Isotope Core Laboratory at Washington State University using the denitrifier method followed by thermal decomposition of nitrous oxide (N_2O) (Kaiser et al., 2007; Komatsu et al., 2008) with analytical precision 0.84‰ for $\delta^{18}O$ and 0.64‰ for $\delta^{17}O$ (1σ, $n = 5$) using the USGS34 and USGS35 ($\delta^{17}O = 51.50$‰ vs. VSMOW, $\delta^{18}O = 56.81$‰ vs. VSMOW) standards.

Isotopic data are reported with conventional delta notation vs. the international reference scales (air for N; VSMOW for O) in per mil (‰):

$$\delta^{15}N = ([^{15}N/^{14}N]_{sample}/[^{15}N/^{14}N]_{air} - 1)^* 1000 \quad (1)$$

$$\delta^{18}O = ([^{18}O/^{16}O]_{sample}/[^{18}O/^{16}O]_{VSMOW} - 1)^* 1000 \quad (2)$$

$$\delta^{17}O = ([^{17}O/^{16}O]_{sample}/[^{17}O/^{16}O]_{VSMOW} - 1)^* 1000 \quad (3)$$

2.4. Analysis of gaseous N species

The concentration of N_2O was determined from gas sampled by a modified bubble strip method (protocol available at: http://dx.doi.org/10.17504/protocols.io.2x5gfq6). The N_2O was measured with an HNU GC 301 gas chromatograph that was equipped with a Porapak N column under P-5 carrier gas (95% argon, 5% methane) at the USGS Water Mission Area Laboratories in Boulder as described in Repert et al. (2014) with a coefficient of variation for triplicate measurements of 11%.

2.5. Analysis of rock-N

Three peridotite rock core samples from the 280-meter depth interval in boreholes BA3A, BA4A, and BA1B of the multi-borehole observatory were obtained during Phase 2 of the Oman Drilling Project. Sampling procedures for clean retrieval of rock core are detailed in Templeton et al. (2021). Bulk $\delta^{15}N$ of powdered peridotite was measured *via* continuous-flow isotope ratio mass spectrometry using the sealed tube combustion method (Boocock et al., 2020) on a Thermo Finnigan MAT253 in the St Andrews Stable Isotope Geochemistry (STAiG) laboratory. All three samples exhibited a signal/blank ratio >10:1.

2.6. N-cycling functional gene analysis

Metagenomic data for this study were previously published by Fones et al. (2019) and Kraus et al. (2021), including procedures regarding DNA extraction, metagenomic library prep, and sequencing. In short, DNA extraction was conducted according to the manufacturer's instructions with a MoBio PowerSoil Kit or Zymo Research Xpedition Soil/Fecal DNA MiniPrep extraction kit for samples collected in 2015 and 2017, respectively. Triplicate extractions were pooled, quantified, and normalized to 1 ng before library preparation using the Nextera XT kit. After tagmentation and amplification, products were pooled equimolarly and sequenced on an Illumina MiSeq platform (2x150 bp) at the University of Colorado Next-Generation Sequencing Facility (2015 samples) or an Illumina HiSeq 2,500 platform (2 x 250 bp) at the Duke Center for Genomic and Computational Biology (2017 samples).

Demultiplexed metagenomic sequences were merged (minimum length of 30), low-quality bases were trimmed off read ends (<15), and reads of <100 bases were discarded using the AdapterRemoval v2 (Schubert et al., 2016). Reads were quality filtered and then aligned to the NCycDB database (95% clustering) (Tu et al., 2019) for the identification of N-cycling genes using the Diamond aligner (Buchfink et al., 2015). Gene homolog abundances were normalized to metagenome size, and results from the two sampling years were combined.

2.7. Calculations of ^{17}O difference ($\Delta^{17}O$)

The $\Delta^{17}O$ can be determined by the following equation provided by Miller (2002):

$$\Delta^{17}O = \left[\ln\left(1 + \frac{\delta^{17}O}{1000}\right) - 0.52 \cdot ln\left(1 + \frac{\delta^{18}O}{1000}\right) \cdot 1000\right] \quad (4)$$

The fraction of atmospheric endmember NO_3^- (f_{atm}) in an aquifer fluid can be calculated through a simple mass balance:

$$\Delta^{17}O_{mixed} = f_{biogeo}(\Delta^{17}O_{biogeo}) + f_{atm}(\Delta^{17}O_{atm}) \quad (5)$$

where $\Delta^{17}O_{mixed}$ is the ^{17}O difference of NO_3^- in a mixed aquifer fluid presumed to represent some fraction of atmospheric endmember NO_3^- ($\Delta^{17}O_{atm}$) and biogeochemical endmember NO_3^- ($\Delta^{17}O_{biogeo}$) ^{17}O. The $\Delta^{17}O_{biogeo}$ can be assumed to equal 0 because biogeochemical processes follow mass-dependent fractionation. Accordingly, equation (5) simplifies to:

$$f_{atm} = \Delta^{17}O_{mixed}/(\Delta^{17}O_{atm}) \quad (6)$$

For $\Delta^{17}O_{atm}$, we used the measured $\Delta^{17}O$ of sampled rainwater. We recognize a single rainwater sample may not be entirely representative of the isotopic composition of mean annual rainfall since the $\Delta^{17}O$ of dissolved NO_x in rainwater has been documented to fluctuate ~15‰ seasonally (Saud et al., 2022). The measured $\Delta^{17}O$ is in the lower range expected for atmospheric deposition (Savard et al., 2018), with $\Delta^{17}O$ values for atmospheric NO_x typically ranging between ~ 20–32‰ (Michalski et al., 2003). Accordingly, we applied an uncertainty of +15‰ for this endmember composition in mass balance calculations, using a $\Delta^{17}O_{atm}$ of 31.8‰ to conservatively estimate f_{atm}.

3. Results

3.1. Geochemical context of ophiolite fluids

Mg^{2+}-HCO_3^- fluids were characterized by alkaline pH (8.3–9.2) and relatively high ∑Mg and ∑CO_2 concentrations (0.37–3.3 mM and 1.3–3.6 mM, respectively) compared to the hyperalkaline pH (10–11.4) and high ∑Ca concentrations (0.43–7.8 mM) of Ca^{2+}-OH^- fluids (Supplementary Table 1). The Ca^{2+}-OH^- fluids also typically contained μM to mM concentrations of dissolved H_2 and CH_4. Of the wells sampled in this study, six wells hosted in peridotite were classified as Mg^{2+}-HCO_3^- type fluids, representing open-system water–rock reaction under relatively oxidized conditions (Eh 78 to 180 mV), and seven wells as Ca^{2+}-OH^- type fluids, representing closed-system water–rock reaction under highly reducing conditions (Eh as low as−415 mV).

To assess the degree of mixing of deep, reacted Ca^{2+}-OH^- fluids with less reacted Mg^{2+}-HCO_3^- fluids in the near surface, we applied the Leong et al. (2021) approach of using ∑Si as a conservative tracer for the mixing of reacted fluids in ophiolitic aquifers. The composition of fluids collected in this study is plotted along the Leong et al. (2021) reaction path model (Figure 1) for the progressive reaction of rainwater with peridotite during serpentinization. No Ca^{2+}-OH^- fluids sampled in this study displayed ∑Si concentrations as low as expected for chrysotile-brucite-calcite±diopside equilibrium, indicating some degree of mixing with Mg^{2+}-HCO_3^- fluids. From our calculations of endmember fluid mixing (Supplementary Table 2), most Ca^{2+}-OH^- fluids were mixed with <10% Mg^{2+}-HCO_3^- type fluids, except fluids sampled from BA1A from the 100–400 m packed interval and from well WAB56 which indicated mixing of ∼15% and 57–73% Mg^{2+}-HCO_3^- fluids, respectively. Fluids hosted within gabbro plotted with Mg^{2+}-HCO_3^- fluids, but with slightly higher ∑Si concentrations.

3.2. Concentration and isotopic composition of dissolved N species

The predominant dissolved N species was dependent on the fluid type, with alkaline Mg^{2+}-HCO_3^- type peridotite-hosted fluids and fluids hosted in gabbro comprised mostly of NO_3^-, and hyperalkaline Ca^{2+}-OH^- peridotite-hosted fluids comprised primarily of reduced N (∑NH_3) (Figure 2). The Mg^{2+}-HCO_3^- type fluids contained NO_3^- concentrations between 66 and 146 μM, while Ca^{2+}-OH^- fluids only contained up to 26 μM (Table 2). Conversely, Ca^{2+}-OH^- fluids were enriched in NH_3 (up to 114 μM), while ∑NH_3 concentrations were ∼5 μM in all Mg^{2+}-HCO_3^- type fluids (Table 3).

Fluids hosted within gabbros were also dominated by NO_3^-, but with higher concentrations (as high as 366 μM) than observed for Mg^{2+}-HCO_3^- fluids. Both Mg^{2+}-HCO_3^- and Ca^{2+}-OH^- type fluids had lower concentrations of NO_3^- than observed in rainwater (252 μM); however, gabbro well WAB103 demonstrated concentrations of NO_3^- greater than rainwater. NO_2^- was often detectable across fluid types, but in very low concentrations (∼1 μM) except for in a few fluids where NO_2^- was present at concentrations between ∼4 and 30 μM (Table 4). All wells where dissolved N_2O concentrations were analyzed contained detectable

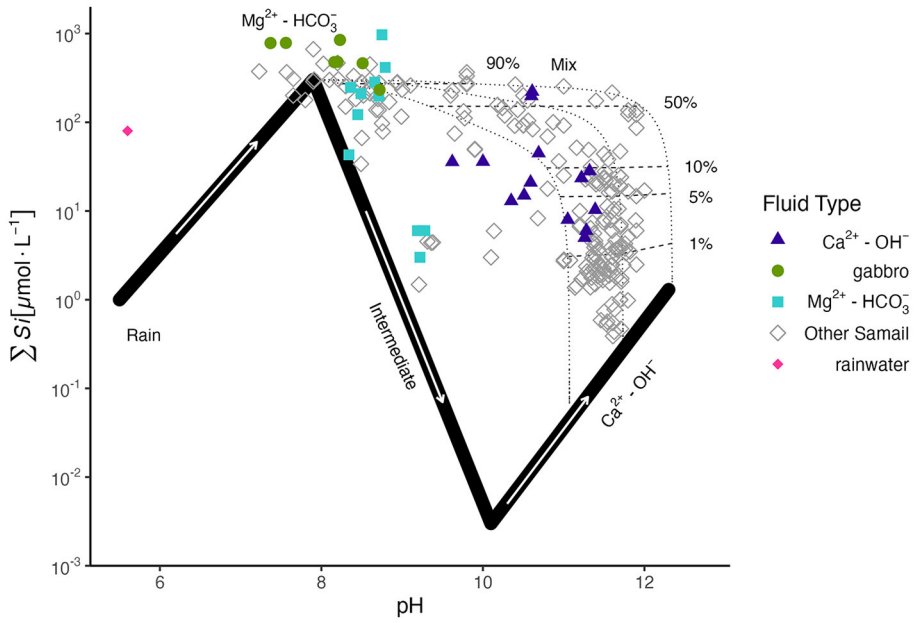

FIGURE 1
∑Si vs. pH of sampled fluids in this study, colored by fluid type, and of other Samail Ophiolite data (Stanger, 1986; Dewandel et al., 2004; Chavagnac et al., 2013; Rempfert et al., 2017; Leong et al., 2021) in gray, with the reaction path model of Leong et al. (2021) for the progressive reaction of rainwater with peridotite rock. Three potential Ca^{2+}-OH^- compositions of varying ∑CO_2 (8, 10, 20 μmole/kg from right to left) are plotted. ∑Si is used as a conservative tracer to distinguish the extent of mixing between Ca^{2+}-OH^- and Mg^{2+}-HCO_3^- fluids (shown in the plot as percentages next to mixing tie-lines). Mixing proportions are reported in Supplementary Table 2.

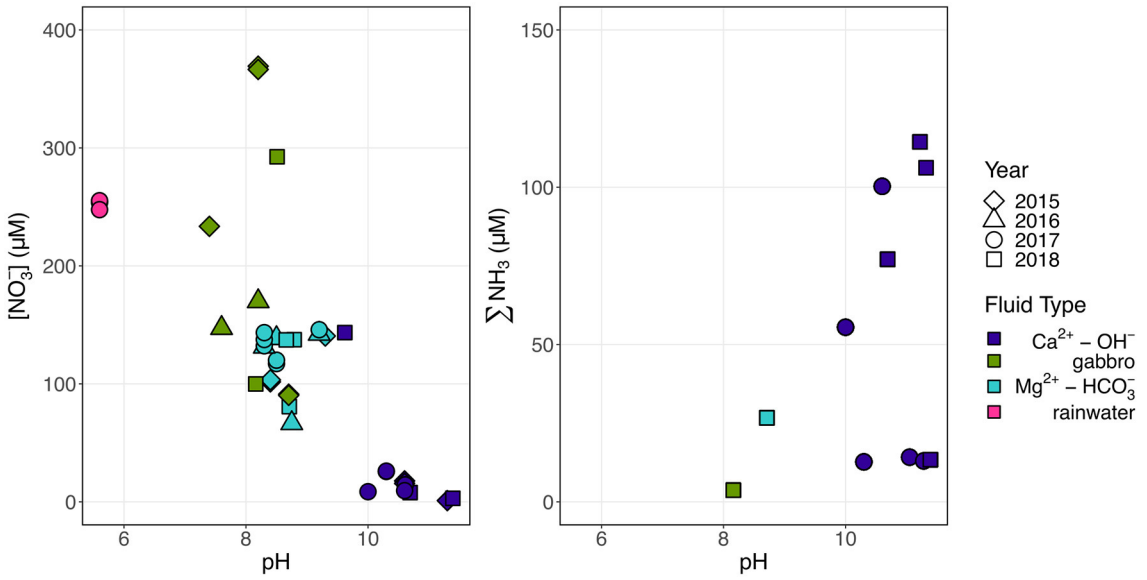

FIGURE 2
Trend of decreasing NO_3^- concentrations and increasing $\sum NH_3$ concentrations with pH. Colors indicate fluid composition and shapes indicate the year of sampling.

N_2O, which varied in concentration from 5 to 177 nM, with the highest concentration observed in the packed-off interval 55–66 m in borehole BA1A (Table 5).

The dual isotopic composition of NO_3^- ($\delta^{15}N$ and $\delta^{18}O$) offers valuable information on potential sources and subsequent transformations of NO_3^- in the subsurface, aquifer ecosystem. On a biplot of $\delta^{15}N$ and $\delta^{18}O$ of NO_3^- (Figure 3), Oman rainwater plots within the range expected for atmospheric deposition (Oman rainwater: $\delta^{15}N$ −2.2‰, $\delta^{18}O$ 55.6‰) (Kendall Carol, 1998; Kendall et al., 2007). A few Ca^{2+}-OH^- fluids, where NO_3^- concentrations are <26 μM, plot within the range expected for nitrification-derived NO_3^- ($\delta^{18}O$ < 10‰) (Kendall Carol, 1998; Kendall et al., 2007). However, most Samail ophiolite aquifer fluids exhibit $\delta^{18}O$ between these two sources, indicating the likely contribution of NO_3^- from both atmospheric and biological nitrification sources.

To investigate atmospheric deposition as a potential source of NO_3^- to the aquifer, we measured the $\delta^{17}O$ of oxidized aqueous N species ($NO_x = NO_2^- + NO_3^-$) in a subset of samples from the 2017 and 2018 field seasons. Atmospherically sourced NO_3^- and NO_2^- have $\delta^{17}O$ higher than predicted for mass-dependent fractionation due to photochemical reactions with ozone in the stratosphere (Thiemens, 1999, 2006; Lyons, 2001; Mauersberger et al., 2001; Michalski et al., 2002, 2003, 2004). Because subsequent biological fractionation of atmospherically derived NO_3^- should not impact the deviation of $\delta^{17}O$ in oxidized N species from expected mass-dependent fractionation ($\Delta^{17}O$ of NO_x), the $\Delta^{17}O$ of measured NO_x can be used to calculate the relative contribution of biogeochemical and atmospheric sources of NO_3^- (Michalski et al., 2003; Riha et al., 2014). Biogeochemical sources, such as nitrification-derived NO_3^-, are assumed to have a mass-dependent $\Delta^{17}O$ value of 0‰. We found that all measured fluids contained NO_3^- which reflected some contribution of a relict atmospheric source, with $\Delta^{17}O$ above 0‰ (Table 6). The $\Delta^{17}O$ was highest in Mg^{2+}-HCO_3^- type peridotite-hosted fluids (Figure 4) and generally correlated with the $\delta^{18}O$ and concentration of NO_3^-. These $\Delta^{17}O$ corresponded to estimated fractions of atmospheric endmember NO_3^- (f_{atm}) ranging from 0.09 to 0.41, accounting for uncertainty in the endmember $\Delta^{17}O_{atm}$ isotopic composition.

By mass balance, the isotopic composition of biogeochemically derived NO_3^-, $\delta^{18}O$ NO_3^- $_{biogeo}$, can be calculated (Supplementary Table 3). The $\delta^{18}O$ NO_3^- $_{biogeo}$ reflects NO_3^- produced by nitrification as well as processes that act to enrich the NO_3^- pool, such as nitrate reduction (NR) during biological assimilation or respiration. Most measured samples exhibited $\delta^{18}O$ NO_3^- $_{biogeo}$ <10‰, consistent with nitrification-derived NO_3^- (Kendall et al., 2007; Xue et al., 2009; Kaushal et al., 2011; Yi et al., 2017). However, fluids collected from borehole BA1A with the packer system to isolate deep Ca^{2+}-OH fluids below 100 m had $\delta^{18}O$ of 27‰, suggesting extensive NR. Biological NR causes the $\delta^{18}O$ and $\delta^{15}N$ of NO_3^- in the residual pool to increase in a relatively predictive pattern, with the proportionality of N and O isotopic fractionation varying between 0.5 and 1 (Böttcher et al., 1990; Sigman et al., 2005; Granger et al., 2008; Chen and MacQuarrie, 2011; Knöller et al., 2011; Granger and Wankel, 2016; Asamoto et al., 2021). We observed a general trend of coupled increase in $\delta^{18}O$ and $\delta^{15}N$ of NO_3^- with a proportionality of ~1 (Figure 3), consistent with NR.

The $\delta^{15}N$ of reduced nitrogen species (N_{red}) spanned a range of 30‰ (Table 4). In most samples, $\sum NH_3$ concentrations were comparable to the concentration of N_{red} measured *via* the mass balance of total N after persulfate oxidation compared to total oxidized nitrogen species ($NO_x = NO_3^- + NO_2^-$); however, this was not true in samples from WAB188 and NSHQ14 where concentrations of N_{red} were greater than

TABLE 2 $\delta^{15}N$ and $\delta^{18}O$ of NO_3^- with NO_3^- concentration measured by the denitrifier method.

Sample	Year	Fluid type	NO_3^- [μM]	$\delta^{15}N$ NO_3^- ‰	$\delta^{18}O$ NO_3^- ‰
BA1A_100_400m	2018	Ca^{2+}-OH^-	7.8 ± 0.1	25.2 ± 0.09	34.6 ± 0.5
BA1A_55_66m	2018	Mg^{2+}-HCO_3^-	80.7 ± 3.2	6.1 ± 0.06	26.8 ± 0.3
NSHQ10	2016	Mg^{2+}-HCO_3^-	66.6 ± 1.1	20.1 ± 0.05	24.3 ± 0.3
NSHQ14	2015	Ca^{2+}-OH^-	1 ± 0.1	15.9 ± 0.09	20.6 ± 0.7
NSHQ14	2018	Ca^{2+}-OH^-	3 ± 0.1	5.6 ± 0.06	12.7 ± 0.5
NSHQ14_18m	2017	Ca^{2+}-OH^-	25.8 ± 1.4	10.6 ± 0.24	9.5 ± 0.3
NSHQ21	2015	Gabbro	233 ± 2.5	9.0 ± 0.07	14.9 ± 0.2
NSHQ3B	2015	Mg^{2+}-HCO_3^-	102.5 ± 1.1	2.8 ± 0.05	21.7 ± 0.2
NSHQ4	2017	Ca^{2+}-OH^-	8.6 ± 0.5	4.0 ± 0.2	19.5 ± 0.3
rainwater	2017	rainwater	252.2 ± 9.0	−2.2 ± 0.2	55.6 ± 0.3
WAB103	2015	Gabbro	367.9 ± 4	8.9 ± 0.06	16.7 ± 0.2
WAB103	2016	Gabbro	169.9 ± 2.1	11.8 ± 0.04	18.9 ± 0.2
WAB103	2018	Gabbro	292.5 ± 4.9	10.5 ± 0.06	18.1 ± 0.3
WAB104	2016	Mg^{2+}-HCO_3^-	138.6 ± 2	1.4 ± 0.03	22.9 ± 0.2
WAB104	2017	Mg^{2+}-HCO_3^-	118.6 ± 5.9	2.3 ± 0.2	22.9 ± 0.3
WAB104	2018	Mg^{2+}-HCO_3^-	137.5 ± 3.4	1.1 ± 0.06	23.5 ± 0.3
WAB105	2016	Mg^{2+}-HCO_3^-	131.4 ± 1.5	2 ± 0.03	23.6 ± 0.2
WAB105	2017	Mg^{2+}-HCO_3^-	137.8 ± 4.9	2.5 ± 0.1	21.8 ± 0.6
WAB105	2018	Mg^{2+}-HCO_3^-	137.3 ± 3.1	2.2 ± 0.06	22 ± 0.3
WAB188	2015	Gabbro	90.7 ± 1	5.5 ± 0.05	22.5 ± 0.2
WAB188	2016	Gabbro	147.3 ± 1.7	3.3 ± 0.03	21.8 ± 0.2
WAB188	2017	Gabbro	135.9± 6.2	5.5 ± 0.04	22.5 ± 0.2
WAB188	2018	Gabbro	99.9 ± 3.1	3.2 ± 0.06	21.3 ± 0.3
WAB55	2015	Mg^{2+}-HCO_3^-	140 ± 1.5	7.4 ± 0.07	21.1 ± 0.2
WAB55	2016	Mg^{2+}-HCO_3^-	142.3 ± 1.7	7.5 ± 0.03	20.8 ± 0.2
WAB55	2017	Mg^{2+}-HCO_3^-	145.9 ± 0.9	8.8 ± 0.05	20.9 ± 0.2
WAB55	2018	Ca^{2+}-OH^-	143.5 ± 2.9	7.8 ± 0.06	20.5 ± 0.3
WAB56	2015	Ca^{2+}-OH^-	16.7 ± 0.3	20.7 ± 0.09	30.7 ± 0.2
WAB56	2017	Ca^{2+}-OH^-	14.4 ± 0.8	9.94 ± 0.23	22.8 ± 0.3
WAB71	2017	Ca^{2+}-OH^-	9.5 ± 0.5	13.2 ± 0.26	0.9 ± 0.3

Standard error is calculated from all experimental replicates.

measured $\sum NH_3$. In these wells, the $\delta^{15}N$ of N_{red} must be interpreted as a mixture of $\sum NH_3$ and other dissolved forms of reduced N, such as organic compounds. The $\delta^{15}N$ of N_{red} varied considerably, with the highest $\delta^{15}N$ (13.6‰) observed for borehole WAB71 where the concentration of NH_3 was greatest (114 μM).

3.3. Bulk rock N abundance and $\delta^{15}N$

Nitrogen can be stored in rocks as recalcitrant organic matter, NH_4^+ or NO_3^- salts, nitride minerals, substituted in hydrous minerals, incorporated into the structure of silicate minerals, or as gas within fluid inclusions (Holloway and Dahlgren, 2002; Loganathan and Kalinichev, 2013; Mysen, 2019). Because this N could be liberated or assimilated during water–rock reaction (Silver et al., 2012; Houlton et al., 2018), we measured the abundance of bulk N in peridotite rock using the sealed tube combustion method which allows for the measurement of even stably bound N within the silicate mineral structure (Bebout et al., 2007; Boocock et al., 2020). N abundances were low (11.3–13.9 ppm) in analyzed peridotite rock core samples and bulk $\delta^{15}N$ of peridotite samples varied from 3.5 to 6.7‰ (Table 7).

TABLE 3 $\delta^{15}N$ of N_{red} which represents the total reduced nitrogen in the sampled fluid (measured by the denitrifier method through mass balance after persulfate oxidation).

Sample	Fluid type	Year sampled	N_{red} [μM]	$\sum NH_3$ [μM]	$\delta^{15}N_{red}$ ‰
BA1A_100_400m	Ca^{2+}-OH^-	2018	80.2 ± 7.6	77.1 ± 10.0	−12.9 ± 1.5
BA1A_55_66m	Mg^{2+}-HCO_3^-	2018	32.0 ± 12.3	26.7 ± 0.5	−16.7 ± 6.5
CM2A	Ca^{2+}-OH^-	2018	99.1 ± 8.8	106.2 ± 5.9	6.9 ± 0.9
NSHQ14	Ca^{2+}-OH^-	2018	28.3 ± 2.4	13.4 ± 2.4	4.6 ± 0.5
NSHQ14_18m	Ca^{2+}-OH^-	2017	20.4 ± 1.2	12.7 ± 0.4	5.0 ± 0.6
NSHQ14_50m	Ca^{2+}-OH^-	2017	23.0 ± 0.4	14.2 ± 0.3	9.6 ± 0.2
NSHQ14_85m	Ca^{2+}-OH^-	2017	18.1 ± 0.3	13.0 ± 0.3	4.3 ± 0.2
NSHQ4	Ca^{2+}-OH^-	2017	50.7 ± 1.2	55.5 ± 5.0	0.9 ± 0.1
WAB188	Gabbro	2018	41.8 ± 14.5	3.7 ± 1.0	2.4 ± 1.4
WAB56	Ca^{2+}-OH^-	2017	141.6 ± 2.4	-	3.4 ± 0.1
WAB71	Ca^{2+}-OH^-	2017	109.6 ± 2.0	100.3 ± 1.9	11.2 ± 0.3
WAB71	Ca^{2+}-OH^-	2018	105.6 ± 11.1	114.4 ± 3.1	13.6 ± 2.0

Standard error is calculated from all experimental replicates. Concentrations of NH_3 via colorimetric assay are provided for comparison.

TABLE 4 δ15N and δ18O of NO_2^- with NO_2^- concentration measured by mass balance by the denitrifier method after NO_2^- removal with sulfamic acid.

Sample	Year	Fluid type	NO_2^- [μM]	$\delta^{15}N$ NO_2^- ‰	$\delta^{18}O$ NO_2^- ‰
NSHQ10	2016	Gabbro	30.3 ± 1.6	−17.9 ± 1.3	5.2 ± 1.7
NSHQ4	2017	Ca^{2+}-OH^-	4.8 ± 0.8	−4.4 ± 1.0	21.1 ± 3.1
WAB56	2015	Ca^{2+}-OH^-	3.8 ± 0.4	7.8 ± 2.3	22.5 ± 3.3

Errors reported are propagated errors for replicate analyses.

TABLE 5 Concentrations of dissolved N_2O measured in gases collected from the 2018 fluids *via* the bubble strip method.

Sample	Fluid type	$N_2O_{(g)}$ [nM]
BA1A-100-400m	Ca^{2+}-OH^-	5.05E00
BA1A-55-66m	Mg^{2+}-HCO_3^-	1.77E02
CM2A	Ca^{2+}-OH^-	5.13E00
NSHQ14	Ca^{2+}-OH^-	8.70E00
WAB103	gabbro	2.45E01
WAB104	Mg^{2+}-HCO_3^-	2.03E01
WAB105	Mg^{2+}-HCO_3^-	1.67E01
WAB188	gabbro	1.26E01
WAB55	Ca^{2+}-OH^-	1.87E01
WAB71	Ca^{2+}-OH^-	1.47E01

3.4. Presence of N-cycling genes

To assess the possibility of microbial involvement in the cycling of N within Samail Ophiolite aquifers, we used metagenomic sequencing of groundwater fluid biomass to probe for genes known to be involved in N utilization or transformation (Figure 5). N-cycling gene homologs were fairly ubiquitous across sampled fluids, albeit in low abundance (<2 gene homologs/Mb of sequence). Gene homologs associated with NR, both assimilatory *narB* and dissimilatory reductases *narG* and *napA*, were most abundant although homologs for the cytochrome c nitrite reductase (*nrfA*) involved in the reduction of NO_2^- to NH_4^+ in dissimilatory nitrate reduction to ammonium (DNRA) were also notably abundant across fluids. We did not observe any major trends in gene absence or presence by fluid type.

It is important to note that these methods only detect the presence of these genes in aquifer fluids, and do not indicate whether individual organisms possess all genes involved in any specific N-cycling pathway, or whether these genes are actively expressed or utilized. Nevertheless, the presence of gene homologs for N-cycling processes in Samail Ophiolite fluids suggests the potential for biological transformations.

4. Discussion

4.1. Rainwater delivers atmospheric N to Samail Ophiolite aquifers

The positive measured $\Delta^{17}O$ of NO_3^- for all sampled groundwaters suggests atmospheric deposition is a primary source of N to Samail Ophiolite aquifers. The degree to which NO_3^- is sourced from the atmosphere can be estimated using the $\delta^{17}O$ of NO_3^- as a conservative tracer. During ozone formation, the ratio of $^{18}O/^{16}O$ becomes equally elevated as the ratio of $^{17}O/^{16}O$, thus enriching both isotopes independent of their mass difference (Thiemens and Heidenreich, 1983; Thiemens et al., 2001;

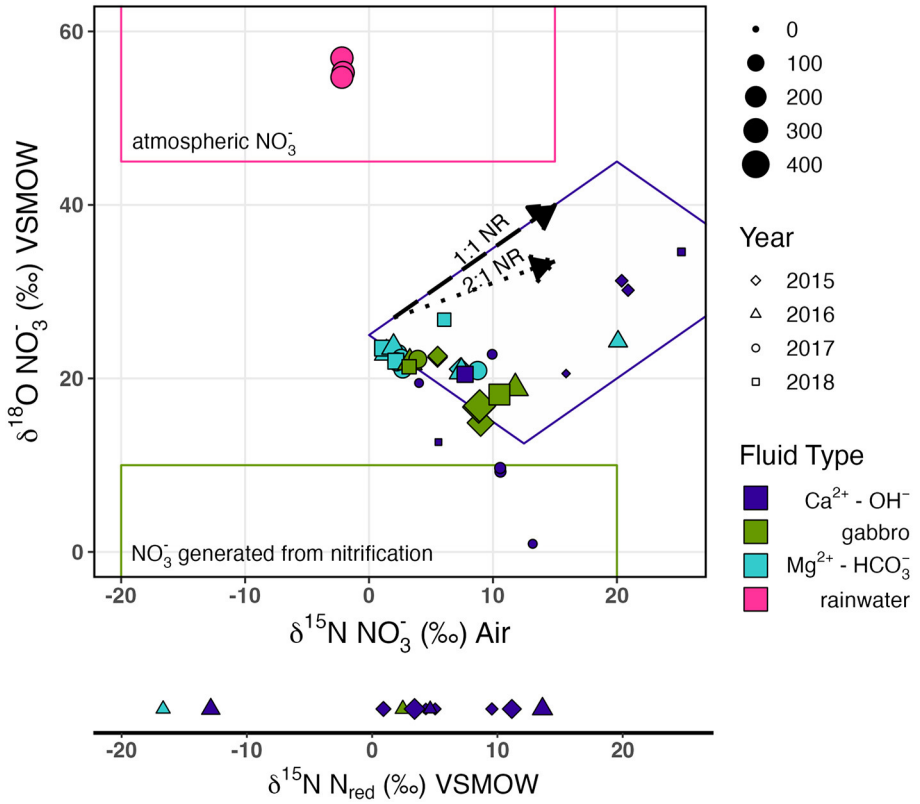

FIGURE 3
$\delta^{18}O$ vs. $\delta^{15}N$ of NO_3^- biplot, with the $\delta^{15}N$ of reduced N plotted on the same scale. Colors indicate fluid type, shapes indicate the year of sampling, and the size of points represents the concentration of N species in μM. Trends for NR with a slope of 1 (labeled 1:1; long dash) and 0.5 (labeled 2:1 with dotted arrow) are illustrated. The field outlined in pink represents the common isotopic composition for atmospheric NO_3^-, the field outlined in green represents the common isotopic composition of nitrified NO_3^-, and the field outlined in purple represents samples with ^{15}N- and ^{18}O-enriched isotopic compositions consistent with NR. Isotopic fields for common isotopic compositions were sourced from Kendall et al. (2007).

TABLE 6 $\delta^{17}O$ and $\delta^{18}O$ isotopic compositions of NO_3^-.

Sample	Year sampled	$\delta^{18}O\ NO_3^-$ (‰)	$\delta^{17}O\ NO_3^-$ (‰)	$\Delta^{17}O\ NO_3^-$ (‰)	f_{atm}
Rainwater	2017	53.7 (1.8)	44.7 (3.6)	16.8 (2.7)	1 [0.47]
WAB104	2018	19.6 (1.0)	17.1 (0.7)	6.9 (1.2)	0.41 [0.19]
BA1A 100-400m packed interval	2018	32.8	21.3	4.3	0.25 [0.12]
BA1A 55-66m packed interval	2018	26.4	20.7	6.9	0.41[0.19]
NSHQ14	2018	19.3	13.1	3.1	0.18 [0.09]
WAB104	2017	23.2	17.7	5.7	0.34 [0.16]
WAB105	2018	22.5	18.4	6.7	0.40 [0.19]
WAB188	2018	22.3	16.1	4.5	0.27 [0.13]
WAB55	2018	20.89	15.0	4.09	0.24 [0.11]

^{17}O difference ($\Delta^{17}O$) and corresponding calculated atmospheric endmember fractional contribution to the observed $\Delta^{17}O$ signatures of NO_3^- in borehole fluids are also reported. Errors (1σ, n = 2) for replicate measures are displayed in parentheses. Conservative estimates of f_{atm}, displayed in brackets, were calculated by applying an uncertainty of 15‰ for expected endmember $\Delta^{17}O_{atm}$ composition.

Miller, 2002). Ozone then transfers O atoms during oxidation reactions that result in a positive $\Delta^{17}O$ of many oxygen sources in the atmosphere (O_3, O_2, H_2O) which can be inherited by N-oxides during photochemical reaction (typically $\Delta^{17}O$ of 20–32‰) (Savarino et al., 2000, 2008; Lyons, 2001; Michalski et al., 2012). Mixing with biogeochemically sourced NO_3^- would lower $\Delta^{17}O$ toward 0‰ (Casciotti et al., 2002; Michalski et al., 2003; Ewing et al., 2007; Kendall et al., 2007; Dejwakh et al., 2012; Riha et al.,

TABLE 7 Bulk rock δ15N of peridotites sampled at the 280-m depth interval in boreholes BA1B, BA3A, and BA4A.

Borehole	Depth [m]	ppm N	$\delta^{15}N$ N_{bulk} ‰
BA1B	280	11.3	4.4
BA3A	280	13.9	3.54
BA4A	280	11.3	6.66

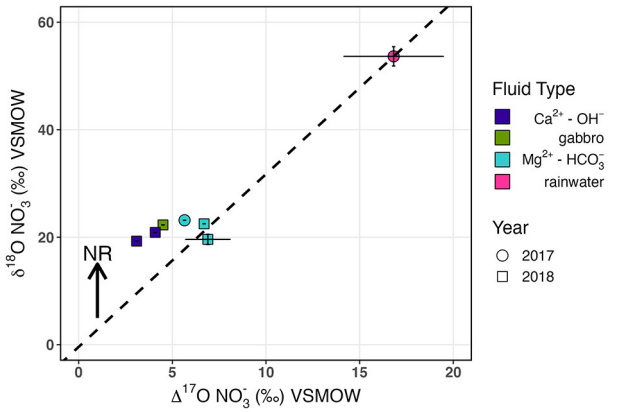

FIGURE 4
$\delta^{18}O$ vs. $\Delta^{17}O$ of NO_3^-. Mg^{2+}-HCO_3^- fluids (blue) plot on a theoretical mixing line with rainwater (pink) calculated for simple mixing of estimated end-member nitrified NO_3^- ($\delta^{18}O$ of−0.4‰ and $\Delta^{17}O$ of 0‰). NO_3^- reduction would lead to increased $\delta^{18}O$ with no change in $\Delta^{17}O$.

2014). We measured a range of $\Delta^{17}O$ for groundwater NO_3^- of 3.1 to 6.9‰, corresponding to estimated atmospheric endmember contributions of 18 to 41% using a simple two-member isotope mixing model (Table 6).

This atmospheric contribution represents both wet and dry deposition. The concentration of NO_3^- in rainwater was high (~255 μM), but precipitation in Oman is scarce and sporadic, with elevations below 1000 m typically receiving only 60–100 mm of rainfall per year from mostly Mediterranean frontal systems (Weyhenmeyer et al., 2002). Accordingly, dry deposition may contribute a more significant flux of N to Samail Ophiolite aquifers compared to wet deposition. While not well constrained, up to 82% of atmospheric NO_x deposition occurs as dry deposition in arid regions of central Asia (Li et al., 2013). An atmospheric origin of NO_3^- is consistent with reports for soil crusts in desert environments such as the Mojave and the Atacama as well as in catchments in the southwestern United States where 31 to 100% of soil nitrate and up to 82% of stream nitrate is atmospherically derived (Böhlke et al., 1997; Michalski et al., 2004; Lybrand et al., 2013; Riha et al., 2014).

A partial atmospheric source for the measured NO_3^- in shallow aquifer fluids would require effective transference of N to the subsurface. Despite low annual rainfall, the effective rainfall in the Samail Ophiolite is relatively high. In a hydrologic study conducted in the Ibra region of the Samail Ophiolite by Dewandel et al. (2005), 50 mm of rain per year was estimated to be effective rain, of which 18 ± 8 mm is presumed to recharge shallow peridotite aquifers. Estimated recharge into gabbro is predicted to be even higher (>20 mm/year) on account of the greater hydraulic conductivity of gabbros compared to peridotites in the Samail Ophiolite (10^{-5} to 10^{-6} for gabbro and 10^{-7} for serpentinized peridotite) and the likely additional input of surface runoff due to the moderate relief of gabbro outcrops, both of which could explain the higher NO_3^- concentrations observed in some gabbro wells (Dewandel et al., 2005). The absence of soil or major vegetation in this environment further facilitates the rapid transfer of rainwater to the subsurface before significant biological processing can remove N from the infiltrating fluids.

4.2. Nitrification-derived NO_3^- comprises the rest of the groundwater NO_3^- Pool

The remaining 59–91% of subsurface NO_3^- can be explained by biological nitrification. Nitrification is one of the two biological processes that produce NO_3^- during the biogeochemical cycling of N (Granger and Wankel, 2016). In this two-step process, NH_3 is oxidized to NO_2^- and then NO_3^-, coupled with aerobic respiration (Verstraete and Focht, 1977; Teske et al., 1994). Both bacteria and archaea mediate NH_3 oxidation, but only bacteria are known to carry out the NO_2^- oxidation step, with some bacterial taxa capable of completely oxidizing NH_3 to NO_3^- (comammox) (Daims et al., 2015; van Kessel et al., 2015). We detected both archaeal and bacterial functional markers for NH_3 oxidation (*amoA* gene), with no differential abundance by fluid type, despite $\sum NH_3$ concentration acting as a strong selector for NH_3 oxidizing taxa in other environments (Martens-Habbena et al., 2009; Bates et al., 2011; Verhamme et al., 2011; Lehtovirta-Morley, 2018). NH_3 oxidation is presumed to be primarily aerobic because we only sparsely detected gene homologs for hydrazine dehydrogenase (*hdh*), which encodes the key enzyme in anaerobic ammonia oxidation (anammox) for catalyzing hydrazine oxidation to N_2 gas (Kartal et al., 2007; Maalcke et al., 2016) (see Supplementary datasheet).

In NH_3 oxidation to NO_2^-, O is incorporated enzymatically from O_2 and H_2O in a 1:1 ratio, whereas in NO_2^- oxidation to NO_3^-, O is solely derived from H_2O (Andersson and Hooper, 1983; Buchwald and Casciotti, 2010). The $\delta^{18}O$ of nitrified NO_3^- has been shown to closely resemble the isotopic composition of ambient H_2O in both labeled nitrifying incubations (Boshers et al., 2019) and field observations (Buchwald and Casciotti, 2010; Buchwald et al., 2012). Accordingly, we presume that nitrified NO_3^- in Samail Ophiolite aquifers should have a $\delta^{18}O$ of−0.4‰, which represents the average $\delta^{18}O$ of aquifer H_2O measured from a subset of 2018 Mg^{2+}-HCO_3^- and Ca^{2+}-OH^- fluids (Supplementary Table 4). Utilizing this estimated value of−0.4‰ for $\delta^{18}O$ of NO_3^- along with a $\Delta^{17}O$ of 0‰ as a nitrification "end-member" for Samail Ophiolite fluids, we applied a simple two-member isotope mixing model with NO_3^- in rainwater (NO_3^- $\delta^{18}O$ 53.7‰, $\Delta^{17}O$ 16.8‰) (Figure 4). We can replicate the observed $\delta^{18}O$ and $\Delta^{17}O$ of shallow aquifer NO_3^- by solely mixing end-member atmospheric and nitrification sources, as all Mg^{2+}-HCO_3^- fluids plotted close to the predicted mixing line. Ca^{2+}-OH^- fluids plotted closer to the estimated nitrification source, which likely

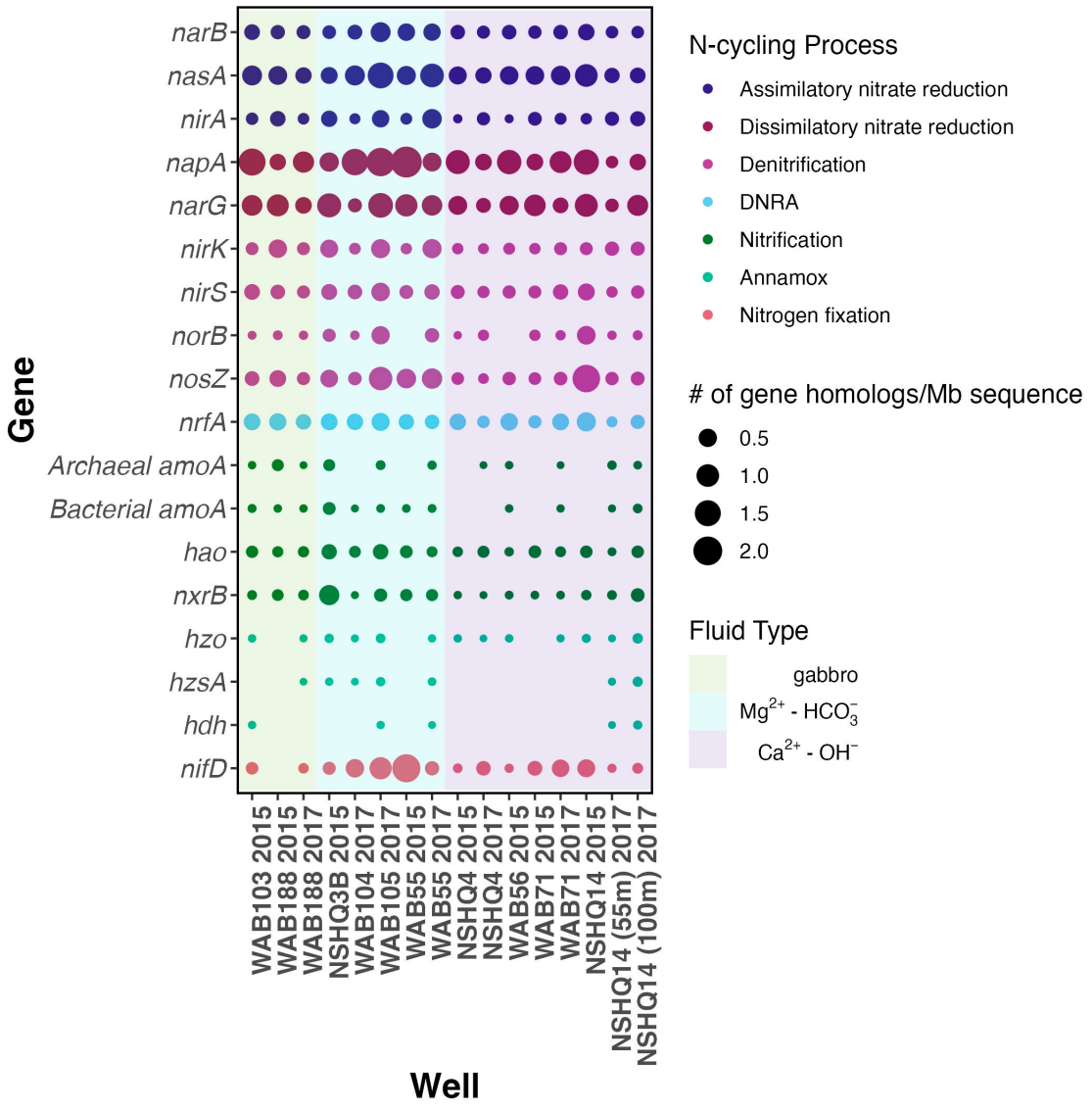

FIGURE 5
Dotplot of abundances of key N cycling genes, where the colors of the dots correspond to the type of N-cycling process, the size to the # of gene homologs detected per Mb sequence, and the background color representative of fluid type.

represents Ca^{2+}-OH^{-} fluids containing a greater proportion of nitrified NO_3^- than Mg^{2+}-HCO_3^- fluids.

4.3. NO_3^- is extensively reduced to NH_3 during progressive water–rock reaction

The concomitant decrease in NO_3^- concentration and increase in $\sum NH_3$ concentration with increasing pH (Figure 2) suggests a possible reduction of NO_3^- to $\sum NH_3$ during the progressive reaction of Mg^{2+}-HCO_3^- type fluids to reducing, Ca^{2+}-OH^{-} type fluids. We observed a trend of increasing $\delta^{15}N$ and $\delta^{18}O$ of NO_3^- with decreasing NO_3^- concentration (Figure 3) indicative of biological NR which characteristically enriches $\delta^{15}N$ and $\delta^{18}O$ of residual nitrate in approximately a 1:1 to 2:1 ratio (Casciotti and McIlvin, 2007; Casciotti et al., 2013; Gaye et al., 2013; Rafter et al., 2013; Bourbonnais et al., 2017). This trend implies ^{15}N isotopic discrimination of NR between −4.5‰ and −17.5‰ (Supplementary Figure 1) assuming Rayleigh kinetic fractionation dynamics. It is important to note that Samail Ophiolite aquifer fluids do not satisfy all assumptions for the Rayleigh fractionation model because nitrification and diffusion of NO_3^- from near-surface mixing may continually supply some NO_3^- during NO_3^- consumption.

In the Samail Ophiolite, reductants such as H_2 are produced during water-rock interactions, and most oxidants are highly limited in reacted hyperalkaline fluids. Thus, we would predict that NO_3^- introduced into the aquifer would act as an important electron acceptor for subsurface microbial metabolism. Accordingly, microbial NR through DNRA is a likely explanation for the presumed production of $\sum NH_3$ in

Samail Ophiolite aquifer fluids. DNRA is a common respiratory process in oligotrophic marine (Lam et al., 2009; Bonaglia et al., 2016), soil (Silver et al., 2001; Rütting et al., 2011; Zhang et al., 2015), and freshwater riparian to estuarine wetland environments (Welsh et al., 2001; Koop-Jakobsen and Giblin, 2010; Wang et al., 2020). The ubiquitous detection of *nrfA* gene homologs, the gene encoding the catalytic subunit for cytochrome c NO_2^- reductase for NO_2^- reduction to NH_4^+, further supports a biological role in the production of subsurface $\sum NH_3$.

While the isotope effect for DNRA has not been systematically evaluated, it is predicted to be similar to that of denitrification with an estimated maximum fractionation of ∼−30‰ (McCready et al., 2011). In both denitrification and DNRA, NO_3^- is first reduced by the periplasmic enzyme Nap (catalytic subunit encoded by *napA*) or the membrane-bound cytosolic enzyme Nar (catalytic subunit encoded by *narG*) which have $^{15}\varepsilon$ ranges of −11.4 to −39.8‰ and −6.6 to −31.6‰, respectively (Granger and Wankel, 2016; Asamoto et al., 2021; and references therein). There is an enzyme-specific coupling of O and N isotope fractionation during NR, with Nar reductases commonly imparting fractionation with a $^{18}\varepsilon/^{15}\varepsilon$ proportionality of approximately 0.91, and Nap reductases a $^{18}\varepsilon/^{15}\varepsilon$ proportionality of ∼ 0.55 (Asamoto et al., 2021). Accordingly, we presume if NR in Samail Ophiolite aquifer fluids is microbial, Nar reductases best explain the demonstrated proportionality of enrichment in $\delta^{18}O$ vs. $\delta^{15}N$ which was close to 1 (Figure 3). The observed discrimination for NR (−4.5 to −17.5‰) in Samail Ophiolite aquifers is largely consistent with dissimilatory NR with a Nar reductase, with reduced isotope effects due to NO_3^- uptake becoming the rate-limiting step at low concentrations of NO_3^- (Kritee et al., 2012) (see Supplementary datasheet). The predominance of Nap reductases in addition to Nar reductases in Samail Ophiolite aquifers could be explained by the functional diversity of Nap enzymes which can additionally be involved in the maintenance of cellular oxidation-reduction potential and NO_3^- scavenging (Potter and Cole, 1999; Potter et al., 1999; Richardson, 2000). Accordingly, the abundance of *napA* gene homologs does not necessarily indicate an active role in dissimilatory NR.

We do also consider that an abiotic reduction process could play a role in the conversion of NO_3^- to $\sum NH_3$. Although spontaneous NR in the presence of high H_2 concentrations is not expected to occur at the temperatures of the aquifer fluids (∼35° C), mineral-facilitated reduction by Fe-bearing phases could occur. For example, the quantitative conversion of NO_3^- to NH_4^+ can be catalyzed by green rust minerals at surface temperatures (Hansen et al., 1996). Similarly, Smirnov et al. (2008) reported the generation of NH_4^+ through NR in the presence of the FeNi alloys, such as awaruite ($Ni_{80}Fe_{20}$), although this reaction was highly temperature-dependent and proceeded almost negligibly at 22 °C (Smirnov et al., 2008). Yet, the detection of awaruite and Fe-bearing hydroxides in serpentinized peridotite in the Samail Ophiolite (Ellison et al., 2021) merits future investigation into the kinetics and associated isotope effects of these reactions under environmentally relevant conditions.

We note that other biological reduction pathways including denitrification to N_2 or assimilatory NR may have contributed to the observed NO_3^- consumption and loss from Samail Ophiolite aquifer fluids. We detected gene homologs for all major genes pertaining to denitrification (e.g., *nirS, nirK, norB,* and *nosZ*) (Philippot, 2002) in metagenomic sequencing of biomass from borehole fluids. High rates of denitrification have been reported in biological soil crusts in Oman associated with >300 μmol $N/m^2/h$ emissions of N_2O (Abed et al., 2013). We detected N_2O in nM concentrations (∼ 5–176 nM) in sampled aquifer fluids (Table 5). However, many other N cycling processes could produce N_2O, including the decomposition of intermediate hydroxylamine during NH_3 oxidation, reduction of NO_2^- by nitrifiers (nitrifier-denitrification), and reduction of NO_2^- through reaction with ferrous iron (chemodenitrification) (Wankel et al., 2017). Furthermore, DNRA would be expected to occur at higher rates than denitrification at alkaline pH (Yoon et al., 2015) and where NO_3^- is limited (Jørgensen, 1989; Kraft et al., 2014). In addition, the presence of assimilatory NR genes (e.g., *narB, nasA, nirA*) in aquifer fluids may indicate the potential for NR for assimilation into biomass instead of respiration (Moreno-Vivián et al., 1999); however, this process is unlikely to be the predominant NO_3^- consuming process in Ca^{2+}-OH^- type fluids where bioavailable N in the form of NH_3 is abundant and biomass is low (5×10^5 cells/mL) (Fones et al., 2019). The accompanying rise in $\sum NH_3$ concentrations with a decrease in NO_3^- concentrations and an increase in pH suggests that NR to $\sum NH_3$ is proportionally a more significant process, at least in Ca^{2+}-OH^- type fluids. However, additional measurements such as N_2/Ar ratios (Vogel et al., 1981), ^{15}N labeled assays, transcriptomics, and site-specific N_2O isotopic analyses should be carried out in future investigations of this system to more definitively assess the potential for alternative biological NR processes.

4.4. The isotopic composition of $\sum NH_3$ is highly variable in aquifer fluids

We observed a large range in $\delta^{15}N$ of $\sum NH_3$. We presume that $\delta^{15}N_{red}$ is equivalent to the $\delta^{15}N$ of $\sum NH_3$ for all boreholes except NSHQ14 and WAB188, as sampled fluids from these wells exhibited comparable N_{red} and $\sum NH_3$ concentrations (Table 3). The $\delta^{15}N < -12‰$ for $\sum NH_3$ measured in BA1A contrasts with positive values measured in other boreholes. This could be related to the collection of fluids with the packer system (see Supplementary datasheet), which discretely sampled the lower borehole (100–400 m), as this sampled pool of $\sum NH_3$ may reflect a pool that has undergone little oxidation by nitrifiers. The isotope effect for NH_3 oxidation can be as large as −38‰ for bacterial nitrification (Mariotti et al., 1981; Yoshida, 1988; Casciotti et al., 2003), and thus the partial oxidation of NH_3 in Ca^{2+}-OH^- fluids could enrich the residual $\sum NH_3$ pool, accounting in part for the higher $\delta^{15}N$ values of $\sum NH_3$ observed in other reacted fluids. In addition, there is a strong equilibrium isotope effect (−42.5‰) associated with $\sum NH_3$ speciation, volatilization, and degassing (Li et al., 2012). If ammonia is lost through degassing, the residual pool of NH_4^+, and thus $\sum NH_3$, should become increasingly enriched in ^{15}N. Finally, some variability in the $\delta^{15}N$ of $\sum NH_3$ can be explained by groundwater age. The $\delta^{15}N$ of NO_3^- in atmospheric deposition has decreased by approximately 15‰ over the past century due to the Haber–Bosch effect of increased anthropogenic

inputs from fertilizers (Yang and Gruber, 2016). Because Ca^{2+}-OH^- fluids in Oman are pre–H-bomb (older than 1952), whereas Mg-HCO_3^- are estimated to be only 4–40 years old (Paukert Vankeuren et al., 2019), the $\delta^{15}N$ composition of source NO_3^- was not consistent across fluids.

4.5. Other potential sources of $\sum NH_3$

Common sources of $\sum NH_3$ in aquifer catchments such as remineralized organic matter, fertilizer, or wastewater (Kendall Carol, 1998) are unlikely for the Samail Ophiolite aquifer system. Due to the location of the Samail Ophiolite in the Omani desert, there is little agriculture or even human inhabitation in the catchments that supply the subsurface aquifer. Furthermore, N_{red} is within the standard error for measured $\sum NH_3$ in most aquifer fluids. Dissolved organic N constitutes on average >80% of total N in anthropogenic runoff (Jani et al., 2020), thus we posit there is little contribution to reduced N from these sources where inorganic forms of N are predominant (see Supplementary datasheet for the discussion of samples where $N_{red} >> \sum NH_3$).

A major potential source of $\sum NH_3$ to Samail Ophiolite aquifers could be atmospheric deposition. Unfortunately, we did not acidify an aliquot of rainwater for analysis during the one rain event that coincided with our geochemical sampling, so the assessment of wet deposition was not possible. Whether through wet or dry deposition, atmospheric $\sum NH_3$ could be effectively transported to the subsurface aquifer through rainfall. However, despite the apparent atmospheric source for a significant fraction of shallow aquifer NO_3^-, the same cannot be presumed for $\sum NH_3$ because the atmospheric deposition of reduced nitrogen species (NH_x) is not necessarily correlated with the magnitude of N-oxide deposition. Sources of oxidized and reduced N in the atmosphere are quite different, with NH_x primarily originating from agricultural pollution such as emissions from livestock and volatilization of fertilizers (Reis et al., 2009).

Another source of $\sum NH_3$ to subsurface aquifers is biological N fixation. Although nitrogenase enzymes require high energetic costs to reduce N_2 gas to NH_4^+ (Broda and Peschek, 1980), this process has been hypothesized to occur in some oligotrophic, rock-hosted environments such as the Henderson Mine and the serpentinite-hosted Lost City hydrothermal field (Sahl et al., 2008; Swanner and Templeton, 2011; Lang et al., 2013). While we did detect *nifD* gene homologs (which encode the catalytic site for the nitrogenase enzyme), their detection did not correlate with $\sum NH_3$ concentrations. Alternatively, surficial $\sum NH_3$ produced by diazotrophic biological soil crusts could be transferred to the subsurface *via* recharging rainfall. N fixation by soil crusts commonly occurs in arid ecosystems, including Oman (Abed et al., 2010, 2013); however, aquifers in the Samail Ophiolite are hosted in alluvium and mafic to ultramafic bedrock without soil cover (Dewandel et al., 2005), likely limiting fixed soil N contributions to the aquifer. Regardless of where N fixation may occur, the fractionation imparted by nitrogenases cannot fully account for the ~30‰ variation in or the lowest (−16.7‰) $\delta^{15}N$ of $\sum NH_3$ observed. N fixation with common molybdenum–based nitrogenase enzymes only imparts a small isotopic effect of −2 to +1‰ (Macko et al., 1987), and less efficient vanadium and iron–based alternative nitrogenase enzymes a fractionation of −6 to −8‰ (Zhang et al., 2014). Accordingly, while N fixation may contribute $\sum NH_3$ to aquifer fluids, it seems unlikely as the primary source for the >100 μM $\sum NH_3$ observed in some Ca^{2+}-OH^- fluids.

Alternatively, rock-hosted N could be released during water–rock weathering reactions (Houlton et al., 2018). Although unaltered lithospheric peridotite has been found to have exceedingly low N concentrations (<1 ppm) (Yokochi et al., 2009), the substitution of NH_4^+ for potassium, calcium, or sodium in silicate minerals occurs widely (Holloway and Dahlgren, 2002), particularly as a result of water/rock interaction. We measured up to 13.9 ppm bulk N in serpentinized peridotite, which is within the range of concentrations (~1–20 ppm) measured for altered ophiolitic glasses (Bebout et al., 2017) and serpentinized metaperidotites (Philippot et al., 2007; Halama et al., 2010), where N is presumed to occur as silicate-bound NH_4^+ or trapped in fluid inclusions in sealed fractures produced during serpentinization reactions. Bulk $\delta^{15}N$ of our measured peridotite samples varied from 3.5 to 6.7‰, similar to values observed in altered basalts and peridotites (Busigny et al., 2005; Philippot et al., 2007; Halama et al., 2010; Bebout et al., 2017) and consistent of a mantle signature with some incorporation of NH_4^+ from reacted fluids (Busigny and Bebout, 2013). It is unclear whether the incorporation of NH_4^+ is ongoing through modern water–rock interactions, or if this N could be released into the fluids during rock dissolution. Future studies should investigate the potential for leaching of NH_4^+ from serpentinized peridotite, especially because on a microscale, fluid compositions in porewaters could be differentially enriched in dissolved N through this mechanism.

4.6. Recycling of $\sum NH_3$ in the near surface

NH_4^+ produced *via* DNRA in reacted fluids, in combination with $\sum NH_3$ from any aforementioned source, is recycled in the near surface through nitrification. Despite the highly reducing nature of Ca^{2+}-OH^- fluids (Eh typically below −100 mV), evidence for aerobic nitrification can be observed in some boreholes such as WAB71 where the $\delta^{18}O$ of NO_3^- measured was <10‰ across multiple years of sampling (Table 2). Nitrification is capable of proceeding at dissolved oxygen concentrations of 5–30 nM, or ~0.01% air saturation (Bristow et al., 2016), and thus NH_3 oxidation could occur in the shallow aquifer where Ca^{2+}-OH^- fluids come in contact with the atmosphere or mix with Mg-HCO_3^- type fluids.

Overall, the reduction of NO_3^- to NH_4^+, as opposed to N_2O or N_2 gas, retains N in the subsurface aquifer, thus preventing N from acting as a limiting nutrient for biological growth. The oxidation of $\sum NH_3$ produced by the reduction of atmospheric NO_3^- through nitrification would then allow for further recycling of N in the subsurface, serpentinite-hosted aquifer ecosystem to sustain microbial growth even when the aquifers are not actively recharged. This continued cycling of atmospherically sourced NO_3^- lends credence to the potential habitability of rock-hosted subsurface environments on other planetary bodies, such as Mars,

where surficial inputs of NO_3^- have been detected (Stern et al., 2017).

5. Conclusion

We employed dual N and O isotopic analysis of dissolved N species to probe the origin and subsequent cycling of NO_3^- in Samail Ophiolite aquifer fluids since NO_3^- is predicted to be a key electron acceptor for subsurface microbial life in terrestrial serpentinite ecosystems. NO_3^- in all measured aquifer fluids was characterized by a positive $\Delta^{17}O$ indicative of atmospheric deposition as a major source of oxidized N to the serpentinite-hosted aquifers. The $\Delta^{17}O$ and $\delta^{18}O$ of NO_3^- in shallow aquifer fluids were consistent with simple mixing of NO_3^- from atmospheric deposition with NO_3^- produced *via* nitrification. However, NO_3^- presumed to have formed through nitrification varied considerably in $\delta^{15}N$. In part, this is due to the ~30‰ variation of reactant $\sum NH_3$. Concentrations of $\sum NH_3$ increased concomitantly with a decrease in the concentration of NO_3^- in more deeply sourced fluids, implying that NR could be a major source of $\sum NH_3$ detected in Ca^{2+}-OH^- fluids. The isotopic fractionation imparted by NR seemingly varied with NO_3^- concentration, with greater fractionation ($\varepsilon^{15} \sim -17.5$‰) observed in shallow groundwaters, and less apparent fractionation ($\varepsilon^{15} \sim -4.5$‰) in deeper groundwaters where NO_3^- concentrations were $<30\,\mu M$. This difference in isotope effect could be explained if NO_3^- uptake becomes the rate-limiting step in NR in highly reacted fluids where NO_3^- is scarce. The relationship between O and N isotopic fractionation ($^{18}\varepsilon/^{15}\varepsilon$) during NO_3^- consumption was consistent with biological dissimilatory NR with a Nar reductase, although the possibility for abiotic reduction cannot be ruled out. Overall, the measured O and N isotopic compositions of NO_3^- in Samail Ophiolite aquifer fluids are consistent with the recycling of atmospherically derived N through the initial reduction of meteoric NO_3^- to NH_4^+ followed by partial (re)oxidation to NO_3^- during nitrification in the near surface. This mode of biogeochemical cycling has major implications for the habitability of these aquifers, as the reduction of NO_3^- to NH_4^+ retains N in the subsurface ecosystem.

Data availability statement

Raw isotopic data presented in this study and source code used to produce the figures and data tables in this manuscript are available at https://github.com/KopfLab/OmanN_Cycling. Metagenomic sequence files are available from the MG-RAST database under accession numbers mgm4795805.3 to mgm4795809.3 and mgm4795811.3.

Author contributions

AT, SK, JM, JS, and KR conceived the study. KR, DN, EK, JM, JS, and AT collected samples in the field. KR, DN, EK, CA, RDE, and SK analyzed samples and assisted in the data interpretation. KR wrote the manuscript. All authors critically revised the manuscript text and figures.

Funding

This research was directly supported by the Rock-Powered Life NASA Astrobiology Institute (NNA15BB02A). Samples were additionally provided by the Oman Drilling Project. The Oman Drilling Project is supported through combined funds from the International Continental Scientific Drilling Project, the Sloan Foundation–Deep Carbon Observatory (Grant 2014-3), the National Science Foundation (NSF-EAR), the NASA Astrobiology Institute (NNA15BB02A), the German Research Foundation (DFG), the Japanese Society for the Promotion of Science (JSPS), the European Research Council, the Swiss National Science Foundation, JAMSTEC, the TAMU-JR Science operator, and contributions from the Sultanate of Oman Ministry of Regional Municipalities and Water Resources, the Oman Public Authority of Mining, Sultan Qaboos University, CRNS-Univ. Montpellier II, Columbia University, and the University of Southampton.

Acknowledgments

We thank the Ministry of Regional Municipalities and Water Resources in the Sultanate of Oman for permits and access to boreholes for fluid sampling and export, the Oman Drilling Project for access to the Multi-Borehole Observatory, and Eric Ellison, Eric Boyd, Laura Bueter, and Lauren Seyler for assistance in field sampling. We would like to thank Daniel Sigman for access to analytical equipment at Princeton University and the entire Sigman Lab for support during isotopic analyses. In particular, we thank Emma Kast, Victoria Luu, Dario Marconi, Alexa Weigand, and Sergey Oleynik for guidance during sample preparation and assistance with isotopic measurements. We thank the Stüeken Lab at St. Andrews for the analysis of bulk $\delta^{15}N$ in peridotite rock, especially Toby Boocock for running the analyses, the Repert lab at the Boulder USGS offices for access to facilities for quantifying N_2O, and Benjamin Harlow at the Stable Isotope Core Lab at Washington State University for running the thermal decomposition triple oxygen isotopic analyses of nitrate. In addition, we thank Saroj Poudel for guidance in nitrogen functional gene analysis, Ben Johnson for discussions regarding rock-hosted nitrogen and arranging preliminary bulk $\delta^{15}N$ measurements with the Stüeken Lab, as well as Meaghan Petix and Katherine Gale for providing helpful comments to improve the manuscript.

Conflict of interest

The authors declare that the research was conducted in the absence of any commercial or financial relationships that could be construed as a potential conflict of interest.

Publisher's note

All claims expressed in this article are solely those of the authors and do not necessarily represent those of

their affiliated organizations, or those of the publisher, the editors and the reviewers. Any product that may be evaluated in this article, or claim that may be made by its manufacturer, is not guaranteed or endorsed by the publisher.

Supplementary material

The Supplementary Material for this article can be found online at: https://www.frontiersin.org/articles/10.3389/fmicb.2023.1139633/full#supplementary-material

References

Abed, R. M. M., Al Kharusi, S., Schramm, A., and Robinson, M. D. (2010). Bacterial diversity, pigments and nitrogen fixation of biological desert crusts from the Sultanate of Oman. *FEMS Microbiol. Ecol.* 72, 418–428. doi: 10.1111/j.1574-6941.2010.00854.x

Abed, R. M. M., Lam, P., de Beer, D., and Stief, P. (2013). High rates of denitrification and nitrous oxide emission in arid biological soil crusts from the Sultanate of Oman. *ISME J.* 7, 1862–1875. doi: 10.1038/ismej.2013.55

Andersson, K. K., and Hooper, A. B. (1983). O2 and H2O are each the source of one O in NO−2 produced from NH3 by Nitrosomonas: 15N-NMR evidence. *FEBS Lett.* 164, 236–240. doi: 10.1016/0014-5793(83)80292-0

Asamoto, C. K., Rempfert, K. R., Luu, V. H., Younkin, A. D., and Kopf, S. H. (2021). Enzyme-Specific Coupling of Oxygen and Nitrogen Isotope Fractionation of the Nap and Nar Nitrate Reductases. *Environ. Sci. Technol.* doi: 10.1021/acs.est.0c07816

Avanzino, R. J., and Kennedy, V. C. (1993). Long-term frozen storage of stream water samples for dissolved orthophosphate, nitrate plus nitrite, and ammonia analysis. *Water Resour. Res.* 29, 3357–3362. doi: 10.1029/93WR01684

Barnes, I., LaMarche, V. C., and Himmelberg, G. (1967). Geochemical evidence of present-day serpentinization. *Science.* 156, 830–832. doi: 10.1126/science.156.3776.830

Barnes, I., and O'neil, J. R. (1969). The relationship between fluids in some fresh alpine-type ultramafics and possible modern serpentinization, Western United States. *Geol. Soc. Am. Bull.* 80, 1947–1960. doi: 10.1130/0016-7606(1969)801947:TRBFIS2.0.CO;2

Bates, S. T., Berg-Lyons, D., Caporaso, J. G., Walters, W. A., Knight, R., and Fierer, N. (2011). Examining the global distribution of dominant archaeal populations in soil. *ISME J.* 5, 908–917. doi: 10.1038/ismej.2010.171

Bebout, G. E., Banerjee, N. R., Izawa, M. R. M., Kobayashi, K., Lazzeri, K., Ranieri, L. A. (2017). Nitrogen concentrations and isotopic compositions of seafloor-altered terrestrial basaltic glass: implications for astrobiology. *Astrobiology.* 18, 330–342. doi: 10.1089/ast.2017.1708

Bebout, G. E., Idleman, B. D., Li, L., and Hilkert, A. (2007). Isotope-ratio-monitoring gas chromatography methods for high-precision isotopic analysis of nanomole quantities of silicate nitrogen. *Chem. Geol.* 240, 1–10. doi: 10.1016/j.chemgeo.2007.01.006

Böhlke, J. K., Ericksen, G. E., and Revesz, K. (1997). Stable isotope evidence for an atmospheric origin of desert nitrate deposits in northern Chile and southern California, U.S.A. *Chem. Geol.* 136, 135–152. doi: 10.1016/S0009-2541(96)00124-6

Bonaglia, S., Klawonn, I., De Brabandere, L., Deutsch, B., Thamdrup, B., and Brüchert, V. (2016). Denitrification and DNRA at the Baltic Sea oxic-anoxic interface: Substrate spectrum and kinetics: denitrification and DNRA at the oxic-anoxic interface. *Limnol. Oceanogr.* 61, 1900–1915. doi: 10.1002/lno.10343

Boocock, T. J., Mikhail, S., Prytulak, J., Rocco, T. D., and Stüeken, E. E. (2020). Nitrogen mass fraction and stable isotope ratios for fourteen geological reference materials: evaluating the applicability of elemental analyser versus sealed tube combustion methods. *Geostand. Geoanalytical Res.* 44, 537–551. doi: 10.1111/ggr.12345

Boshers, D. S., Granger, J., Tobias, C. R., Böhlke, J. K., and Smith, R. L. (2019). Constraining the oxygen isotopic composition of nitrate produced by nitrification. *Environ. Sci. Technol.* 53, 1206–1216. doi: 10.1021/acs.est.8b03386

Böttcher, J., Strebel, O., Voerkelius, S., and Schmidt, H.-L. (1990). Using isotope fractionation of nitrate-nitrogen and nitrate-oxygen for evaluation of microbial denitrification in a sandy aquifer. *J. Hydrol.* 114, 413–424. doi: 10.1016/0022-1694(90)90068-9

Bourbonnais, A., Letscher, R. T., Bange, H. W., Échevin, V., Larkum, J., Mohn, J., et al. (2017). N2O production and consumption from stable isotopic and concentration data in the Peruvian coastal upwelling system. *Glob. Biogeochem. Cycles* 31, 678–698. doi: 10.1002/2016GB005567

Bristow, L. A., Dalsgaard, T., Tiano, L., Mills, D. B., Bertagnolli, A. D., Wright, J. J., et al. (2016). Ammonium and nitrite oxidation at nanomolar oxygen concentrations in oxygen minimum zone waters. *Proc. Natl. Acad. Sci.* 113, 10601–10606. doi: 10.1073/pnas.1600359113

Broda, E., and Peschek, G. A. (1980). Evolutionary considerations on the thermodynamics of nitrogen fixation. *Biosystems* 13, 47–56. doi: 10.1016/0303-2647(80)90004-0

Bruni, J., Canepa, M., Chiodini, G., Cioni, R., Cipolli, F., Longinelli, A., et al. (2002). Irreversible water–rock mass transfer accompanying the generation of the neutral, Mg–HCO3 and high-pH, Ca–OH spring waters of the Genova province, Italy. *Appl. Geochem.* 17, 455–474. doi: 10.1016/S0883-2927(01)00113-5

Buchfink, B., Xie, C., and Huson, D. H. (2015). Fast and sensitive protein alignment using DIAMOND. *Nat. Methods* 12, 59–60. doi: 10.1038/nmeth.3176

Buchwald, C., and Casciotti, K. L. (2010). Oxygen isotopic fractionation and exchange during bacterial nitrite oxidation. *Limnol. Oceanogr.* 55, 1064–1074. doi: 10.4319/lo.2010.55.3.1064

Buchwald, C., Santoro, A. E., McIlvin, M. R., and Casciotti, K. L. (2012). Oxygen isotopic composition of nitrate and nitrite produced by nitrifying cocultures and natural marine assemblages. *Limnol. Oceanogr.* 57, 1361–1375. doi: 10.4319/lo.2012.57.5.1361

Busigny, V., and Bebout, G. E. (2013). Nitrogen in the Silicate Earth: Speciation and Isotopic Behavior during Mineral–Fluid Interactions. *Elements* 9, 353–358. doi: 10.2113/gselements.9.5.353

Busigny, V., Laverne, C., and Bonifacie, M. (2005). Nitrogen content and isotopic composition of oceanic crust at a superfast spreading ridge: a profile in altered basalts from ODP Site (1256). Leg 206. Geochem. Geophys. Geosystems 6. doi: 10.1029/2005GC001020

Casciotti, K. L., Buchwald, C., and McIlvin, M. (2013). Implications of nitrate and nitrite isotopic measurements for the mechanisms of nitrogen cycling in the Peru oxygen deficient zone. *Deep Sea Res. Part Oceanogr. Res. Pap.* 80, 78–93. doi: 10.1016/j.dsr.2013.05.017

Casciotti, K. L., and McIlvin, M. R. (2007). Isotopic analyses of nitrate and nitrite from reference mixtures and application to Eastern Tropical North Pacific waters. *Mar. Chem.* 107, 184–201. doi: 10.1016/j.marchem.2007.06.021

Casciotti, K. L., Sigman, D. M., Hastings, M. G., Böhlke, J. K., and Hilkert, A. (2002). Measurement of the oxygen isotopic composition of nitrate in seawater and freshwater using the denitrifier method. *Anal. Chem.* 74, 4905–4912. doi: 10.1021/ac020113w

Casciotti, K. L., Sigman, D. M., and Ward, B. B. (2003). Linking diversity and stable isotope fractionation in ammonia-oxidizing bacteria. *Geomicrobiol. J.* 20, 335–353. doi: 10.1080/01490450303895

Chavagnac, V., Monnin, C., Ceuleneer, G., Boulart, C., and Hoareau, G. (2013). Characterization of hyperalkaline fluids produced by low-temperature serpentinization of mantle peridotites in the Oman and Ligurian ophiolites. *Geochem. Geophys. Geosystems* 14, 2496–2522. doi: 10.1002/ggge.20147

Chen, D. J. Z., and MacQuarrie, K. T. B. (2011). Correlation of δ15N and δ18O in NO3- during denitrification in groundwater. *J. Environ. Eng. Sci.* 4, 221–226. doi: 10.1139/s05-002

Daims, H., Lebedeva, E. V., Pjevac, P., Han, P., Herbold, C., Albertsen, M., et al. (2015). Complete nitrification by *Nitrospira bacteria*. *Nature.* 528, 504–509. doi: 10.1038/nature16461

Dejwakh, N. R., Meixner, T., Michalski, G., and McIntosh, J. (2012). Using 17O to investigate nitrate sources and sinks in a semi-arid groundwater system. *Environ. Sci. Technol.* 46, 745–751. doi: 10.1021/es203450z

Dewandel, B., Lachassagne, P., Boudier, F., Al-Hattali, S., Ladouche, B., Pinault, J.-L., et al. (2005). A conceptual hydrogeological model of ophiolite hard-rock aquifers in Oman based on a multiscale and a multidisciplinary approach. *Hydrogeol. J.* 13, 708–726. doi: 10.1007/s10040-005-0449-2

Dewandel, B., Lachassagne, P., and Qatan, A. (2004). Spatial measurements of stream baseflow, a relevant method for aquifer characterization and permeability evaluation. Application to a hard-rock aquifer, the Oman ophiolite. *Hydrol. Process.* 18, 3391–3400. doi: 10.1002/hyp.1502

Ellison, E. T., Templeton, A. S., Zeigler, S. D., Mayhew, L., Kelemen, P. B., and Matter, J. (2021). Iron mineralogy, hydrogen production, and brucite reactivity during

low-temperature serpentinization in the Samail ophiolite. *Journal of Geophysical Research: Solid Earth*. 126, e2021JB021981. doi: 10.1029/2021JB021981

Escudero, C., Oggerin, M., and Amils, R. (2018). The deep continental subsurface: the dark biosphere. *Int. Microbiol.* 21, 3–14. doi: 10.1007/s10123-018-0009-y

Ewing, S. A., Michalski, G., Thiemens, M., Quinn, R. C., Macalady, J. L., Kohl, S., et al. (2007). Rainfall limit of the N cycle on Earth. *Glob. Biogeochem. Cycles* 21. doi: 10.1029/2006GB002838

Flemming, H.-C., and Wuertz, S. (2019). Bacteria and archaea on Earth and their abundance in biofilms. *Nat. Rev. Microbiol.* 17, 247–260. doi: 10.1038/s41579-019-0158-9

Fones, E. M., Colman, D. R., Kraus, E. A., Nothaft, D. B., Poudel, S., Rempfert, K. R., et al. (2019). Physiological adaptations to serpentinization in the Samail Ophiolite, Oman. *ISME J.* 13, 1750–1762. doi: 10.1038/s41396-019-0391-2

García-Robledo, E., Corzo, A., and Papaspyrou, S. (2014). A fast and direct spectrophotometric method for the sequential determination of nitrate and nitrite at low concentrations in small volumes. *Mar. Chem.* 162, 30–36. doi: 10.1016/j.marchem.2014.03.002

Gaye, B., Nagel, B., Dähnke, K., Rixen, T., and Emeis, K.-C. (2013). Evidence of parallel denitrification and nitrite oxidation in the ODZ of the Arabian Sea from paired stable isotopes of nitrate and nitrite. *Glob. Biogeochem. Cycles.* 27, 1059–1071. doi: 10.1002/2011GB004115

Granger, J., and Sigman, D. M. (2009). Removal of nitrite with sulfamic acid for nitrate N and O isotope analysis with the denitrifier method. *Rapid Commun. Mass Spectrom.* 23, 3753–3762. doi: 10.1002/rcm.4307

Granger, J., Sigman, D. M., Lehmann, M. F., and Tortell, P. D. (2008). Nitrogen and oxygen isotope fractionation during dissimilatory nitrate reduction by denitrifying bacteria. *Limnol. Oceanogr.* 53, 2533–2545. doi: 10.4319/lo.2008.53.6.2533

Granger, J., and Wankel, S. D. (2016). Isotopic overprinting of nitrification on denitrification as a ubiquitous and unifying feature of environmental nitrogen cycling. *Proc. Natl. Acad. Sci.* 113, E6391–E6400. doi: 10.1073/pnas.1601383113

Halama, R., Bebout, G. E., John, T., and Schenk, V. (2010). Nitrogen recycling in subducted oceanic lithosphere: the record in high- and ultrahigh-pressure metabasaltic rocks. *Geochim. Cosmochim. Acta* 74, 1636–1652. doi: 10.1016/j.gca.2009.12.003

Hansen, H., Chr, B., Koch, C. B., Nancke-Krogh, H., Borggaard, O. K., and Sørensen, J. (1996). Abiotic nitrate reduction to ammonium: key role of green rust. *Environ. Sci. Technol.* 30, 2053–2056. doi: 10.1021/es950844w

Holloway, J. M., and Dahlgren, R. A. (2002). Nitrogen in rock: occurrences and biogeochemical implications. *Glob. Biogeochem. Cycles.* 16, 65-1 65–17. doi: 10.1029/2002GB001862

Houlton, B. Z., Morford, S. L., and Dahlgren, R. A. (2018). Convergent evidence for widespread rock nitrogen sources in Earth's surface environment. *Science* 360, 58–62. doi: 10.1126/science.aan4399

Jani, J., Yang, Y.-Y., Lusk, M. G., and Toor, G. S. (2020). Composition of nitrogen in urban residential stormwater runoff: concentrations, loads, and source characterization of nitrate and organic nitrogen. *PLoS ONE.* 15, e0229715. doi: 10.1371/journal.pone.0229715

Jones, R. M., Goordial, J. M., and Orcutt, B. N. (2018). low energy subsurface environments as extraterrestrial analogs. *Front. Microbiol.* 9, 01605. doi: 10.3389/fmicb.2018.01605

Jørgensen, K. S. (1989). Annual pattern of denitrification and nitrate ammonification in estuarine sediment. *Appl. Environ. Microbiol.* 55, 1841–1847. doi: 10.1128/aem.55.7.1841-1847.1989

Kaiser, J., Hastings, M. G., Houlton, B. Z., Röckmann, T., and Sigman, D. M. (2007). Triple oxygen isotope analysis of nitrate using the denitrifier method and thermal decomposition of N2O. *Anal. Chem.* 79, 599–607. doi: 10.1021/ac061022s

Kartal, B., Kuypers, M. M. M., Lavik, G., Schalk, J., Camp, H. J. M. O., den, Jetten, M. S. M., et al. (2007). Anammox bacteria disguised as denitrifiers: nitrate reduction to dinitrogen gas via nitrite and ammonium. *Environ. Microbiol.* 9, 635–642. doi: 10.1111/j.1462-2920.2006.01183.x

Kaushal, S. S., Groffman, P. M., Band, L. E., Elliott, E. M., Shields, C. A., and Kendall, C. (2011). Tracking nonpoint source nitrogen pollution in human-impacted watersheds. *Environ. Sci. Technol.* 45, 8225–8232. doi: 10.1021/es200779e

Kelemen, P. B., Matter, J. M., Teagle, D. A. H., Coggon, J. A., and Oman Drilling Project Science Team (2020). *Oman Drilling Project, Scientific Drilling in the Samail Ophiolite*. Sultanate of Oman: WWW Document.

Kendall Carol (1998). "Chapter 16 - Tracing Nitrogen Sources and Cycling in Catchments", in *Isotope Tracers in Catchment Hydrology*, Kendall, C., and McDONNELL, J.J. (eds.). Amsterdam: Elsevier.p. 519–576. doi: 10.1016/B978-0-444-81546-0.50023-9

Kendall, C., Elliott, E. M., and Wankel, S. D. (2007). "Tracing Anthropogenic Inputs of Nitrogen to Ecosystems", in *Stable Isotopes in Ecology and Environmental Science*. New York, NY: John Wiley and Sons, Ltd. p. 375–449. doi: 10.1002/9780470691854.ch12

Knöller, K., Vogt, C., Haupt, M., Feisthauer, S., and Richnow, H.-H. (2011). Experimental investigation of nitrogen and oxygen isotope fractionation in nitrate and nitrite during denitrification. *Biogeochemistry.* 103, 371–384. doi: 10.1007/s10533-010-9483-9

Komatsu, D. D., Ishimura, T., Nakagawa, F., and Tsunogai, U. (2008). Determination of the 15N/14N, 17O/16O, and 18O/16O ratios of nitrous oxide by using continuous-flow isotope-ratio mass spectrometry. *Rapid Commun. Mass Spectrom. RCM.* 22, 1587–1596. doi: 10.1002/rcm.3493

Koop-Jakobsen, K., and Giblin, A. E. (2010). The effect of increased nitrate loading on nitrate reduction via denitrification and DNRA in salt marsh sediments. *Limnol. Oceanogr.* 55, 789–802. doi: 10.4319/lo.2010.55.2.0789

Kraft, B., Tegetmeyer, H. E., Sharma, R., Klotz, M. G., Ferdelman, T. G., Hettich, R. L., et al. (2014). The environmental controls that govern the end product of bacterial nitrate respiration. *Science.* 345, 676–679. doi: 10.1126/science.1254070

Kraus, E. A., Nothaft, D., Stamps, B. W., Rempfert, K. R., Ellison, E. T., Matter, J. M., et al. (2021). Molecular evidence for an active microbial methane cycle in subsurface serpentinite-hosted groundwaters in the samail ophiolite, Oman. *Appl. Environ. Microbiol.* 87, e02068–20. doi: 10.1128/AEM.02068-20

Kritee, K., Sigman, D. M., Granger, J., Ward, B. B., Jayakumar, A., and Deutsch, C. (2012). Reduced isotope fractionation by denitrification under conditions relevant to the ocean. *Geochim. Cosmochim. Acta* 92, 243–259. doi: 10.1016/j.gca.2012.05.020

Lam, P., Lavik, G., Jensen, M. M., Vossenberg, J., van de, Schmid, M., Woebken, D., et al. (2009). Revising the nitrogen cycle in the Peruvian oxygen minimum zone. *Proc. Natl. Acad. Sci.* 106, 4752–4757. doi: 10.1073/pnas.0812444106

Lang, S. Q., Früh-Green, G. L., Bernasconi, S. M., and Butterfield, D. A. (2013). Sources of organic nitrogen at the serpentinite-hosted Lost City hydrothermal field. *Geobiology.* 11, 154–169. doi: 10.1111/gbi.12026

Lehtovirta-Morley, L. E. (2018). Ammonia oxidation: ecology, physiology, biochemistry and why they must all come together. *FEMS Microbiol. Lett.* 365, 9. doi: 10.1093/femsle/fny058

Leong, J. A. M., Howells, A. E., Robinson, K. J., Cox, A., Debes, R. V., Fecteau, K., et al. (2021). Theoretical predictions vs environmental observations on serpentinization fluids: Lessons from the Samail ophiolite in Oman [WWW Document]. *J. Geophy Reseach: Solid Earth*. 126, e2020JB020756.

Leong, J. A. M., and Shock, E. L. (2020). Thermodynamic constraints on the geochemistry of low-temperature, continental, serpentinization-generated fluids. *Am. J. Sci.* 320, 185–235. doi: 10.2475/03.2020.01

Li, K., Liu, X., Song, W., Chang, Y., Hu, Y., and Tian, C. (2013). Atmospheric nitrogen deposition at two sites in an arid environment of Central Asia. *PLoS ONE.* 8, e67018. doi: 10.1371/journal.pone.0067018

Li, L., Lollar, B. S., Li, H., Wortmann, U. G., and Lacrampe-Couloume, G. (2012). Ammonium stability and nitrogen isotope fractionations for NH4+-NH3(aq)–NH3(gas) systems at 20–70°C and pH of 2–13: applications to habitability and nitrogen cycling in low-temperature hydrothermal systems. *Geochim. Cosmochim. Acta.* 84, 280–296. doi: 10.1016/j.gca.2012.01.040

Lods, G., Roubinet, D., Matter, J. M., LEPROVOST, R., and Gouze, P. (2020). Groundwater flow characterization of an ophiolitic hard-rock aquifer from cross-borehole multi-level hydraulic experiments. *J. Hydrol.* 589, 125152. doi: 10.1016/j.jhydrol.2020.125152

Loganathan, N., and Kalinichev, A. G. (2013). On the hydrogen bonding structure at the aqueous interface of ammonium-substituted mica: a molecular dynamics simulation. *Z. Für Naturforschung A.* 68, 91–100. doi: 10.5560/zna.2012-0101

Lybrand, R. A., Michalski, G., Graham, R. C., and Parker, D. R. (2013). The geochemical associations of nitrate and naturally formed perchlorate in the Mojave Desert, California, USA. *Geochim. Cosmochim. Acta.* 104, 136–147. doi: 10.1016/j.gca.2012.10.028

Lyons, J. R. (2001). Transfer of mass-independent fractionation in ozone to other oxygen-containing radicals in the atmosphere. *Geophys. Res. Lett.* 28, 3231–3234. doi: 10.1029/2000GL012791

Maalcke, W. J., Reimann, J., de Vries, S., Butt, J. N., Dietl, A., Kip, N., et al. (2016). Characterization of anammox hydrazine dehydrogenase, a key N2-producing enzyme in the global nitrogen cycle. *J. Biol. Chem.* 291, 17077–17092. doi: 10.1074/jbc.M116.735530

Macko, S. A., Fogel, M. L., Hare, P. E., and Hoering, T. C. (1987). Isotopic fractionation of nitrogen and carbon in the synthesis of amino acids by microorganisms. *Chem. Geol. Isot. Geosci. Sect.* 65, 79–92. doi: 10.1016/0168-9622(87)90064-9

Magnabosco, C., Lin, L.-H., Dong, H., Bomberg, M., Ghiorse, W., Stan-Lotter, H., et al. (2018). The biomass and biodiversity of the continental subsurface. *Nat. Geosci.* 11, 707–717. doi: 10.1038/s41561-018-0221-6

Mariotti, A., Germon, J. C., Hubert, P., Kaiser, P., Letolle, R., Tardieux, A., et al. (1981). Experimental determination of nitrogen kinetic isotope fractionation: some principles; illustration for the denitrification and nitrification processes. *Plant Soil.* 62, 413–430. doi: 10.1007/BF02374138

Martens-Habbena, W., Berube, P. M., Urakawa, H., de la Torre, J. R., and Stahl, D. A. (2009). Ammonia oxidation kinetics determine niche separation of nitrifying Archaea and Bacteria. *Nature.* 461, 976–979. doi: 10.1038/nature08465

Mauersberger, K., Lämmerzahl, P., and Krankowsky, D. (2001). Stratospheric ozone isotope enrichments—revisited. *Geophys. Res. Lett.* 28, 3155–3158. doi: 10.1029/2001GL013439

McCollom, T. M., and Bach, W. (2009). Thermodynamic constraints on hydrogen generation during serpentinization of ultramafic rocks. *Geochim. Cosmochim. Acta.* 73, 856–875. doi: 10.1016/j.gca.2008.10.032

McCready, R. G. L., Gould, W. D., and Barendregt, R. W. (2011). Nitrogen isotope fractionation during the reduction of NO3– to NH4+ by Desulfovibrio sp. *Can. J. Microbiol.* 29, 231–234. doi: 10.1139/m83-038

Menchyk, N., Park, D., Moon, P. H., Unruh, J. B., and Trenholm, L. E. (2014). Freezing low volume aqueous solutions to preserve ammonia and nitrate plus nitrite. *Crop Sci.* 54, 2325–2327. doi: 10.2135/cropsci2013.12.0807

Meyer-Dombard, D. R., and Malas, J. (2022). Advances in defining ecosystem functions of the terrestrial subsurface biosphere. *Front. Microbiol.* 13, 891528. doi: 10.3389/fmicb.2022.891528

Michalski, G., Bhattacharya, S. K., and Mase, D. F. (2012). "Oxygen Isotope Dynamics of Atmospheric Nitrate and Its Precursor Molecules", in *Handbook of Environmental Isotope Geochemistry: Vol I, Advances in Isotope Geochemistry,* Baskaran, M. (ed.). Berlin, Heidelberg: Springer. p. 613–635. doi: 10.1007/978-3-642-10637-8_30

Michalski, G., Böhlke, J. K., and Thiemens, M. (2004). Long term atmospheric deposition as the source of nitrate and other salts in the Atacama Desert, Chile: New evidence from mass-independent oxygen isotopic compositions. *Geochim. Cosmochim. Acta* 68, 4023–4038. doi: 10.1016/j.gca.2004.04.009

Michalski, G., Savarino, J., Böhlke, J. K., and Thiemens, M. (2002). Determination of the total oxygen isotopic composition of nitrate and the calibration of a Δ17? nitrate reference material. *Anal. Chem.* 74, 4989–4993. doi: 10.1021/ac0256282

Michalski, G., Scott, Z., Kabiling, M., and Thiemens, M. H. (2003). First measurements and modeling of Δ17O in atmospheric nitrate. *Geophys. Res. Lett.* 30. doi: 10.1029/2003GL017015

Miller, M. F. (2002). Isotopic fractionation and the quantification of 17O anomalies in the oxygen three-isotope system: an appraisal and geochemical significance. *Geochim. Cosmochim. Acta* 66, 1881–1889. doi: 10.1016/S0016-7037(02)00832-3

Moreno-Vivián, C., Cabello, P., Martínez-Luque, M., Blasco, R., and Castillo, F. (1999). Prokaryotic nitrate reduction: molecular properties and functional distinction among bacterial nitrate reductases. *J. Bacteriol.* 181, 6573–6584. doi: 10.1128/JB.181.21.6573-6584.1999

Mosley, O. E., Gios, E., Close, M., Weaver, L., Daughney, C., and Handley, K. M. (2022). Nitrogen cycling and microbial cooperation in the terrestrial subsurface. *ISME J.* 16, 2561–2573. doi: 10.1038/s41396-022-01300-0

Mysen, B. (2019). Nitrogen in the Earth: abundance and transport. *Prog. Earth Planet. Sci.* 6, 38. doi: 10.1186/s40645-019-0286-x

Nicolas, A., Boudier, F., Ildefonse, B., and Ball, E. (2000). Accretion of Oman and United Arab Emirates ophiolite – Discussion of a new structural map. *Mar. Geophys. Res.* 21, 147–180. doi: 10.1023/A:1026769727917

Nothaft, D., Templeton, A. S., Boyd, E., Matter, J., Stute, M., and Vankeuren, A. N. P. (2021). Aqueous geochemical and microbial variation across discrete depth intervals in a peridotite aquifer assessed using a packer system in the Samail Ophiolite, Oman. *Jour of Geophy Research: Solid Earth.* 126, e2021JG006319. doi: 10.1029/2021JG006319

Nyyssönen, M., Hultman, J., Ahonen, L., Kukkonen, I., Paulin, L., Laine, P., et al. (2014). Taxonomically and functionally diverse microbial communities in deep crystalline rocks of the Fennoscandian shield. *ISME J.* 8, 126–138. doi: 10.1038/ismej.2013.125

Paukert Vankeuren, A. N., Matter, J. M., Stute, M., and Kelemen, P. B. (2019). Multitracer determination of apparent groundwater ages in peridotite aquifers within the Samail ophiolite, Sultanate of Oman. *Earth Planet. Sci. Lett.* 516, 37–48. doi: 10.1016/j.epsl.2019.03.007

Paukert, A. N., Matter, J. M., Kelemen, P. B., Shock, E. L., and Havig, J. R. (2012). Reaction path modeling of enhanced in situ CO2 mineralization for carbon sequestration in the peridotite of the Samail Ophiolite, Sultanate of Oman. Chem. Geol. 330–331, 86–100. doi: 10.1016/j.chemgeo.2012.08.013

Philippot, L. (2002). Denitrifying genes in bacterial and archaeal genomes. *Biochim. Biophys. Acta BBA - Gene Struct. Expr.* 1577, 355–376. doi: 10.1016/S0167-4781(02)00420-7

Philippot, P., Busigny, V., Scambelluri, M., and Cartigny, P. (2007). Oxygen and nitrogen isotopes as tracers of fluid activities in serpentinites and metasediments during subduction. *Mineral. Petrol.* 91, 11–24. doi: 10.1007/s00710-007-0183-7

Potter, L. C., and Cole, J. A. (1999). Essential roles for the products of the napABCD genes, but not napFGH, in periplasmic nitrate reduction by Escherichia coli K-12. *Biochem. J.* 344, 69–76. doi: 10.1042/bj3440069

Potter, L. C., Millington, P., Griffiths, L., Thomas, G. H., and Cole, J. A. (1999). Competition between Escherichia coli strains expressing either a periplasmic or a membrane-bound nitrate reductase: does Nap confer a selective advantage during nitrate-limited growth? *Biochem. J.* 344, 77–84. doi: 10.1042/bj3440077

Rafter, P. A., DiFiore, P. J., and Sigman, D. M. (2013). Coupled nitrate nitrogen and oxygen isotopes and organic matter remineralization in the Southern and Pacific Oceans. *J. Geophys. Res. Oceans* 118, 4781–4794. doi: 10.1002/jgrc.20316

Reis, S., Pinder, R. W., Zhang, M., Lijie, G., and Sutton, M. A. (2009). Reactive nitrogen in atmospheric emission inventories. *Atmospheric Chem. Phys.* 9, 7657–7677. doi: 10.5194/acp-9-7657-2009

Rempfert, K. R., Miller, H. M., Bompard, N., Nothaft, D., Matter, J. M., Kelemen, P., et al. (2017). Geological and geochemical controls on subsurface microbial life in the samail ophiolite, Oman. *Front. Microbiol.* 8, 00056. doi: 10.3389/fmicb.2017.00056

Repert, D. A., Underwood, J. C., Smith, R. L., and Song, B. (2014). Nitrogen cycling processes and microbial community composition in bed sediments in the Yukon River at Pilot Station. *J. Geophys. Res. Biogeosciences.* 119, 2328–2344. doi: 10.1002/2014JG002707

Richardson, D. J. (2000). Bacterial respiration: a flexible process for a changing environment. *Microbiol. Read. Engl.* 146, 551–571. doi: 10.1099/00221287-146-3-551

Riha, K. M., Michalski, G., Gallo, E. L., Lohse, K. A., Brooks, P. D., and Meixner, T. (2014). High atmospheric nitrate inputs and nitrogen turnover in semi-arid urban catchments. *Ecosystems.* 17, 1309–1325. doi: 10.1007/s10021-014-9797-x

Ruppersberg, H. S., Goebel, M. R., Kleinert, S. I., Wünsch, D., Trautwein, K., and Rabus, R. (2017). Photometric determination of ammonium and phosphate in seawater medium using a microplate reader. *Microb. Physiol.* 27, 73–80. doi: 10.1159/000454814

Rütting, T., Boeckx, P., Müller, C., and Klemedtsson, L. (2011). Assessment of the importance of dissimilatory nitrate reduction to ammonium for the terrestrial nitrogen cycle. *Biogeosciences.* 8, 1779–1791. doi: 10.5194/bg-8-1779-2011

Sabuda, M. C., Brazelton, W. J., Putman, L. I., McCollom, T. M., Hoehler, T. M., Kubo, M. D. Y., et al. (2020). A dynamic microbial sulfur cycle in a serpentinizing continental ophiolite. *Environ. Microbiol.* 22, 2329–2345. doi: 10.1111/1462-2920.15006

Sahl, J. W., Schmidt, R., Swanner, E. D., Mandernack, K. W., Templeton, A. S., Kieft, T. L., et al. (2008). Subsurface microbial diversity in deep-granitic-fracture water in Colorado. *Appl. Environ. Microbiol.* 74, 143–152. doi: 10.1128/AEM.01133-07

Saud, S., Fahad, S., and Hassan, S. (2022). Developments in the investigation of nitrogen and oxygen stable isotopes in atmospheric nitrate. *Sustain. Chem. Clim. Action.* 1, 100003. doi: 10.1016/j.scca.2022.100003

Savard, M. M., Cole, A. S., Vet, R., and Smirnoff, A. (2018). The $\Delta^{17}O$ and $\delta^{18}O$ values of atmospheric nitrates simultaneously collected downwind of anthropogenic sources – implications for polluted air masses. *Atmospheric Chem. Phys.* 18, 10373–10389. doi: 10.5194/acp-18-10373-2018

Savarino, J., Bhattacharya, S. K., Morin, S., Baroni, M., and Doussin, J.-F. (2008). The NO+O3 reaction: a triple oxygen isotope perspective on the reaction dynamics and atmospheric implications for the transfer of the ozone isotope anomaly. *J. Chem. Phys.* 128, 194303. doi: 10.1063/1.2917581

Savarino, J., Lee, C. C. W., and Thiemens, M. H. (2000). Laboratory oxygen isotopic study of sulfur (IV) oxidation: origin of the mass-independent oxygen isotopic anomaly in atmospheric sulfates and sulfate mineral deposits on Earth. *J. Geophys. Res. Atmospheres* 105, 29079–29088. doi: 10.1029/2000JD900456

Schubert, M., Lindgreen, S., and Orlando, L. (2016). AdapterRemoval v2: rapid adapter trimming, identification, and read merging. *BMC Res. Notes.* 9, 88. doi: 10.1186/s13104-016-1900-2

Seyler, L. M., Brazelton, W. J., McLean, C., Putman, L. I., Hyer, A., Kubo, M. D. Y., et al. (2020). Carbon assimilation strategies in ultrabasic groundwater: clues from the integrated study of a serpentinization-influenced aquifer. *mSystems.* 5, e00607–19. doi: 10.1128/mSystems.00607-19

Sigman, D. M., Casciotti, K. L., Andreani, M., Barford, C., Galanter, M., and Böhlke, J. K. (2001). A bacterial method for the nitrogen isotopic analysis of nitrate in seawater and freshwater. *Anal. Chem.* 73, 4145–4153. doi: 10.1021/ac010088e

Sigman, D. M., Granger, J., DiFiore, P. J., Lehmann, M. M., Ho, R., Cane, G., and Geen, A., van (2005). Coupled nitrogen and oxygen isotope measurements of nitrate along the eastern North Pacific margin. *Glob. Biogeochem. Cycles* 19. doi: 10.1029/2005GB002458

Silver, B. J., Raymond, R., Sigman, D. M., Prokopeko, M., Sherwood Lollar, B., Lacrampe-Couloume, G., et al. (2012). The origin of NO3– and N2 in deep subsurface fracture water of South Africa. *Chem. Geol.* 294–295, 51–62. doi: 10.1016/j.chemgeo.2011.11.017

Silver, W. L., Herman, D. J., and Firestone, M. K. (2001). Dissimilatory nitrate reduction to ammonium in upland tropical forest soils. *Ecology* 82, 2410–2416. doi: 10.1890/0012-9658(2001)0822410:DNRTAI2.0.CO;2

Smirnov, A., Hausner, D., Laffers, R., Strongin, D. R., and Schoonen, M. A. (2008). Abiotic ammonium formation in the presence of Ni-Fe metals and alloys and its implications for the Hadean nitrogen cycle. *Geochem. Trans.* 9, 5. doi: 10.1186/1467-4866-9-5

Stanger, G. (1986). *The hydrogeology of the Oman Mountains*. (Ph.D.). Alexandria, Virginia: Open University.

Stern, J. C., Sutter, B., Jackson, W. A., Navarro-González, R., McKay, C. P., Ming, D. W., et al. (2017). The nitrate/(per)chlorate relationship on Mars. *Geophys. Res. Lett*. 44, 2643–2651. doi: 10.1002/2016GL072199

Swanner, E. D., and Templeton, A. S. (2011). Potential for nitrogen fixation and nitrification in the granite-hosted subsurface at henderson mine, CO. *Front. Microbiol*. 2, 254. doi: 10.3389/fmicb.2011.00254

Templeton, A.S. and Caro, T. (in press). The rock hosted biosphere. *Annu. Rev. Earth Planet. Sci*. doi: 10.1146/annurev-earth-031920-081957

Templeton, A. S., Ellison, E. T., Glombitza, C., Morono, Y., Rempfert, K. R., Hoehler, T., et al. (2021). Accessing the subsurface biosphere within rocks undergoing active low-temperature serpentinization in the Samail ophiolite (Oman Drilling Project). *Jour of Geophy Rese: Solid Earth*. 126, e2021JG006315. doi: 10.1029/2021JG006315

Teske, A., Alm, E., Regan, J. M., Toze, S., Rittmann, B. E., and Stahl, D. A. (1994). Evolutionary relationships among ammonia- and nitrite-oxidizing bacteria. *J. Bacteriol*. 176, 6623–6630. doi: 10.1128/jb.176.21.6623-6630.1994

Thiemens, M. H. (1999). Mass-independent isotope effects in planetary atmospheres and the early solar system. *Science* 283, 341–345. doi: 10.1126/science.283.5400.341

Thiemens, M. H. (2006). History and applications of mass-independent isotope effects. *Annu. Rev. Earth Planet. Sci*. 34, 217–262. doi: 10.1146/annurev.earth.34.031405.125026

Thiemens, M. H., and Heidenreich, J. E. (1983). The mass-independent fractionation of oxygen: a novel isotope effect and its possible cosmochemical implications. *Science* 219, 1073–1075. doi: 10.1126/science.219.4588.1073

Thiemens, M. H., Savarino, J., Farquhar, J., and Bao, H. (2001). Mass-independent isotopic compositions in terrestrial and extraterrestrial solids and their applications. *Acc. Chem. Res*. 34, 645–652. doi: 10.1021/ar960224f

Tu, Q., Lin, L., Cheng, L., Deng, Y., and He, Z. (2019). NCycDB: a curated integrative database for fast and accurate metagenomic profiling of nitrogen cycling genes. *Bioinforma. Oxf. Engl*. 35, 1040–1048. doi: 10.1093/bioinformatics/bty,741

U. S. Environmental Protection Agency (1983). "Nitrogen, ammonia. Method 350.1 (colorimetric, automated phenate)", in *Methods for Chemical Analysis of Water and Wastes EPA-600/4–79–020*. Ohio, USA: USEPA. p. 350–1.1-250–1.4.

van Kessel, M. A. H. J., Speth, D. R., Albertsen, M., Nielsen, P. H., Op den Camp, H. J. M., Kartal, B., et al. (2015). Complete nitrification by a single microorganism. *Nature* 528, 555–559. doi: 10.1038/nature16459

Verhamme, D. T., Prosser, J. I., and Nicol, G. W. (2011). Ammonia concentration determines differential growth of ammonia-oxidising archaea and bacteria in soil microcosms. *ISME J*. 5, 1067–1071. doi: 10.1038/ismej.2010.191

Verstraete, W., and Focht, D. D. (1977). "Biochemical Ecology of Nitrification and Denitrification", in *Advances in Microbial Ecology, Advances in Microbial Ecology,* Alexander, M. (Ed.). Boston, MA: Springer US. p. 135–214. doi: 10.1007/978-1-4615-8219-9_4

Vogel, J. C., Talma, A. S., and Heaton, T. H. E. (1981). Gaseous nitrogen as evidence for denitrification in groundwater. *J. Hydrol*. 50, 191–200. doi: 10.1016/0022-1694(81)90069-X

Wang, S., Pi, Y., Song, Y., Jiang, Y., Zhou, L., Liu, W., et al. (2020). Hotspot of dissimilatory nitrate reduction to ammonium (DNRA) process in freshwater sediments of riparian zones. *Water Res*. 173, 115539. doi: 10.1016/j.watres.2020.115539

Wang, X. T., Sigman, D. M., Cohen, A. L., Sinclair, D. J., Sherrell, R. M., Weigand, M. A., et al. (2015). Isotopic composition of skeleton-bound organic nitrogen in reef-building symbiotic corals: A new method and proxy evaluation at Bermuda. *Geochim. Cosmochim. Acta* 148, 179–190. doi: 10.1016/j.gca.2014.09.017

Wankel, S. D., Ziebis, W., Buchwald, C., Charoenpong, C., de Beer, D., Dentinger, J., et al. (2017). Evidence for fungal and chemodenitrification based N 2 O flux from nitrogen impacted coastal sediments. *Nat. Commun*. 8, 15595. doi: 10.1038/ncomms15595

Weigand, M. A., Foriel, J., Barnett, B., Oleynik, S., and Sigman, D. M. (2016). Updates to instrumentation and protocols for isotopic analysis of nitrate by the denitrifier method. *Rapid Commun. Mass Spectrom*. 30, 1365–1383. doi: 10.1002/rcm.7570

Welsh, D., Castadelli, G., Bartoli, M., Poli, D., Careri, M., de Wit, R., et al. (2001). Denitrification in an intertidal seagrass meadow, a comparison of 15N-isotope and acetylene-block techniques: dissimilatory nitrate reduction to ammonia as a source of N2O? *Mar. Biol*. 139, 1029–1036. doi: 10.1007/s002270100672

Weyhenmeyer, C. E., Burns, S. J., Waber, H. N., Macumber, P. G., and Matter, A. (2002). Isotope study of moisture sources, recharge areas, and groundwater flow paths within the eastern Batinah coastal plain, Sultanate of Oman. *Water Resour. Res*. 38, 2–22. doi: 10.1029/2000WR000149

Xue, D., Botte, J., De Baets, B., Accoe, F., Nestler, A., Taylor, P., et al. (2009). Present limitations and future prospects of stable isotope methods for nitrate source identification in surface- and groundwater. *Water Res*. 43, 1159–1170. doi: 10.1016/j.watres.2008.12.048

Yang, S., and Gruber, N. (2016). The anthropogenic perturbation of the marine nitrogen cycle by atmospheric deposition: nitrogen cycle feedbacks and the 15N Haber-Bosch effect. *Glob. Biogeochem. Cycles*. 30, 1418–1440. doi: 10.1002/2016GB005421

Yi, Q., Chen, Q., Hu, L., and Shi, W. (2017). Tracking nitrogen sources, transformation, and transport at a basin scale with complex plain river networks. *Environ. Sci. Technol*. 51, 5396–5403. doi: 10.1021/acs.est.6b06278

Yokochi, R., Marty, B., Chazot, G., and Burnard, P. (2009). Nitrogen in peridotite xenoliths: Lithophile behavior and magmatic isotope fractionation. *Geochim. Cosmochim. Acta* 73, 4843–4861. doi: 10.1016/j.gca.2009.05.054

Yoon, S., Cruz-García, C., Sanford, R., Ritalahti, K. M., and Löffler, F. E. (2015). Denitrification versus respiratory ammonification: environmental controls of two competing dissimilatory NO 3 – /NO 2 – reduction pathways in Shewanella loihica strain PV-4. *ISME J*. 9, 1093–1104. doi: 10.1038/ismej.2014.201

Yoshida, N. (1988). 15 N-depleted N 2 O as a product of nitrification. *Nature* 335, 528–529. doi: 10.1038/335528a0

Zhang, J., Lan, T., Müller, C., and Cai, Z. (2015). Dissimilatory nitrate reduction to ammonium (DNRA) plays an important role in soil nitrogen conservation in neutral and alkaline but not acidic rice soil. *J. Soils Sediments* 15, 523–531. doi: 10.1007/s11368-014-1037-7

Zhang, X., Sigman, D. M., Morel, F. M. M., and Kraepiel, A. M. L. (2014). Nitrogen isotope fractionation by alternative nitrogenases and past ocean anoxia. *Proc. Natl. Acad. Sci*. 111, 4782–4787. doi: 10.1073/pnas.1402976111

frontiers | Frontiers in Microbiology

TYPE Original Research
PUBLISHED 04 May 2023
DOI 10.3389/fmicb.2023.1139333

OPEN ACCESS

EDITED BY
Nancy Merino,
Lawrence Livermore National Laboratory (DOE), United States

REVIEWED BY
Elizabeth Fones,
University of Washington, United States
John R. Spear,
Colorado School of Mines, United States

*CORRESPONDENCE
Alta E. G. Howells
✉ alta.howells@nasa.gov

†PRESENT ADDRESS
Alta E. G. Howells,
NASA Postdoctoral Program Fellow at NASA Ames, Mountain View, CA, United States

SPECIALTY SECTION
This article was submitted to Microbiological Chemistry and Geomicrobiology, a section of the journal Frontiers in Microbiology

RECEIVED 06 January 2023
ACCEPTED 30 March 2023
PUBLISHED 04 May 2023

CITATION
Howells AEG, De Martini F, Gile GH and Shock EL (2023) An examination of protist diversity in serpentinization-hosted ecosystems of the Samail Ophiolite of Oman. *Front. Microbiol.* 14:1139333. doi: 10.3389/fmicb.2023.1139333

An examination of protist diversity in serpentinization-hosted ecosystems of the Samail Ophiolite of Oman

Alta E. G. Howells[1*†], Francesca De Martini[1,2], Gillian H. Gile[1,3] and Everett L. Shock[3,4,5]

[1]School of Life Sciences, Arizona State University, Tempe, AZ, United States, [2]Mesa Community College, Mesa, AZ, United States, [3]Biodesign Center for Fundamental and Applied Microbiomics, Arizona State University, Tempe, AZ, United States, [4]School of Molecular Sciences, Arizona State University, Tempe, AZ, United States, [5]School of Earth and Space Exploration, Arizona State University, Tempe, AZ, United States

In the Samail Ophiolite of Oman, the geological process of serpentinization produces reduced, hydrogen rich, hyperalkaline (pH > 11) fluids. These fluids are generated through water reacting with ultramafic rock from the upper mantle in the subsurface. On Earth's continents, serpentinized fluids can be expressed at the surface where they can mix with circumneutral surface water and subsequently generate a pH gradient (~pH 8 to pH > 11) in addition to variations in other chemical parameters such as dissolved CO_2, O_2, and H_2. Globally, archaeal and bacterial community diversity has been shown to reflect geochemical gradients established by the process of serpentinization. It is unknown if the same is true for microorganisms of the domain Eukarya (eukaryotes). In this study, using 18S rRNA gene amplicon sequencing, we explore the diversity of microbial eukaryotes called protists in sediments of serpentinized fluids in Oman. We demonstrate that protist community composition and diversity correlate significantly with variations in pH, with protist richness being significantly lower in sediments of hyperalkaline fluids. In addition to pH, the availability of CO_2 to phototrophic protists, the composition of potential food sources (prokaryotes) for heterotrophic protists and the concentration of O_2 for anaerobic protists are factors that likely shape overall protist community composition and diversity along the geochemical gradient. The taxonomy of the protist 18S rRNA gene sequences indicates the presence of protists that are involved in carbon cycling in serpentinized fluids of Oman. Therefore, as we evaluate the applicability of serpentinization for carbon sequestration, the presence and diversity of protists should be considered.

KEYWORDS

protists, serpentinization, water-rock reaction, ecology, geochemistry

1. Introduction

Serpentinization, a subsurface geological process, involves reactions between water and ultramafic rock that produce reduced, hyperalkaline (>pH 11), H_2-rich fluids (McCollom, 2007; Leong and Shock, 2020). Serpentinized fluids can supply H_2 to archaea and bacteria whose metabolisms involve redox reactions including aerobic hydrogen oxidation,

sulfate reduction and methanogenesis (McCollom, 2007; Canovas et al., 2017) and many serpentinization-hosted ecosystems are populated by these organisms (Morrill et al., 2014; Miller et al., 2016; Brazelton et al., 2017; Crespo-Medina et al., 2017; Rempfert et al., 2017; Twing et al., 2017; Fones et al., 2019; Howells et al., 2022). During serpentinization, water alters minerals in ultramafic rocks and the resulting serpentinized fluids can mix with surface water to generate geochemical gradients (Leong et al., 2021).

Archaeal and bacterial community compositions vary along geochemical gradients in serpentinization-hosted ecosystems. For example, a study of an active submarine serpentinization site called Prony Hydrothermal Field, located at the southern end of New Caledonia in the Bay of Prony, demonstrated that community compositions differ by system type, submarine or intertidal (Frouin et al., 2018). At The Cedars, an active terrestrial serpentinization site located in California, community composition correlates with fluid types which include deep fluids that have reacted with ultramafic rock and marine sedimentary layers, shallow groundwater that has reacted only with the ultramafic rock, or fluids that are mixed to some extent with meteoric water (Suzuki et al., 2013). In the active terrestrial serpentinization system of the Samail Ophiolite in Oman archaeal and bacterial community compositions are related to the type of ultramafic rock with which the water interacts, and the degree to which the serpentinized fluid mixes with surrounding surface water or shallow subsurface water (Miller et al., 2016; Rempfert et al., 2017; Fones et al., 2019, 2021; Kraus et al., 2021; Howells et al., 2022). While drivers of archaeal and bacterial community composition in serpentinization-hosted ecosystems are being documented, it is unknown whether the factors that drive bacterial and archaeal diversity also drive microbial eukaryote diversity in these systems.

In this study the diversity of protists in serpentinization-hosted ecosystems in the Samail Ophiolite of Oman is explored through 18S rRNA gene amplicon sequencing. Additionally, the influence that geochemical and biological factors distinct to serpentinization in the Samail Ophiolite have on protist diversity are investigated. While there are many serpentinization-hosted ecosystems across the globe, the Samail Ophiolite in Oman offers serpentinized fluids that are easily accessible and relatively pristine due to the arid climate. Additionally, serpentinized fluid in the Samail Ophiolite can mix with surrounding surface water, which results in steep geochemical gradients that likely impact and shape the protist communities in the underlying sediments. **Figure 1** contains a schema adapted from Howells et al. (2022) of the geological and geochemical context of serpentinization in Oman. Path 1 illustrates that water from the surface can infiltrate the deep subsurface (>500 meters) and react with ultramafic rock. The resulting fluids are hyperalkaline (pH > 11), reduced and depleted in dissolved inorganic carbon (DIC) and silica. Path 2 shows that surface fluids can also seep into the shallower subsurface (<50 meters) and react with rocks that have undergone a greater extent of serpentinization due to their proximity to the surface. In comparison to fluids that reacted with rocks in the deep subsurface, path 2 fluids are only slightly alkaline (~ pH 8) and have higher concentrations of DIC and silica. As **Figure 1** illustrates, reacted fluids can make their way to the surface following fault lines and fissures. Once expressed at the surface, path 1 and path 2 fluids can mix, creating gradients in pH, silica, DIC, O_2 and H_2. It was demonstrated that the distribution of hydrogenotrophic prokaryote communities corresponds strongly to variations in these geochemical parameters (Howells et al., 2022). The purpose of this study is to determine if protist diversity also reflects these geochemical variations.

The pH gradient (~8 to >11) established by mixing between serpentinized fluid and surrounding surface water in Oman provides an opportunity to assess the influence alkaline pH has on microbial eukaryote diversity. In alkaline environments life can be proton limited, which has consequences for organisms acquiring energy through oxidative phosphorylation (Hicks et al., 2010). Therefore, alkaline environments can select for life that has adaptations for coping with proton limitation. While specific adaptations to alkaline pH have not been characterized in protists, ciliates are known to live in alkaline environments such as hypersaline soda lakes (Hu, 2014). In fact, the ciliate species *Frontonia anatolica* was discovered in the largest alkaline soda lake, Lake Van in Turkey (Yildiz and Şenler, 2013). In a study on ciliate populations living in two Kenyan soda lakes, Lake Bogoria (~pH 10) and Lake Nakuru (~pH 10), the species *Cyclidium glaucoma* was determined to be the most abundant ciliate and species of the genera *Frontonia*, *Condylostoma,* and *Holophyra* make up most of the biovolume (Ong'ondo et al., 2013). It should be noted that in addition to being alkaline, the Kenyan soda lakes are also hypersaline with Na^+ being the dominant cation, and carbonate rich, which makes them distinct from serpentinized fluids. Overall, the ability of ciliates to inhabit soda lakes suggests that microbial eukaryotes may live in diverse alkaline environments.

There is some evidence that protists can live in serpentinization-hosted ecosystems, specifically the deep-sea hydrothermal field, Lost City, located near the Mid-Atlantic Ridge. López-García et al. (2007) conducted 18S rRNA gene sequencing on DNA extracts from carbonate samples collected from vent chimney walls and from vent fluids. Ciliates were found to be the dominant protists in both sample types. Amaral-Zettler (2013) conducted a survey of microbial eukaryote community composition using 18S rRNA gene sequencing across systems ranging from a pH 2 to pH 11 and included pooled DNA extracts from Lost City chimney wall and biofilm samples. The dominant protist phylotype in the Lost City samples is of the ciliate genus, *Hypotrichia*. The detection of ciliates at Lost City implies that ciliates may be well suited for hyperalkaline serpentinizing systems on the ocean floor. Serpentinized fluids in Oman provide an opportunity to assess if the same is true in continental serpentinizing systems. Additionally, the pH of serpentinized fluids in Oman varies greatly within the alkaline range, which provides an opportunity to assess the influence pH may have on protist diversity.

In addition to pH, other environmental factors that change along the Samail Ophiolite mixing gradient were explored by focusing on the physiological requirements of protists that are governed by their lifestyles. Protists have diverse lifestyles, with lineages capable of carrying out oxygenic photosynthesis, aerobic heterotrophy, and fermentation under microaerophilic and anaerobic conditions. The physiological constraints and resource demands for sustaining these lifestyles may have consequences for the distribution of protists along chemical gradients in Oman. Factors that influence protist distribution patterns may in turn influence protist community assembly and diversity at our

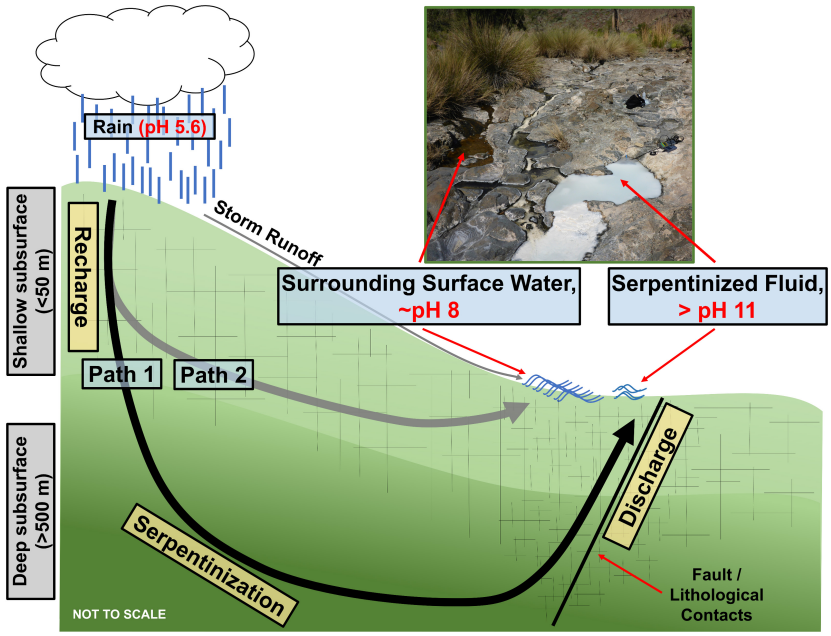

FIGURE 1
Conceptual model of serpentinization in the Samail Ophiolite of Oman adapted from Howells et al. (2022). Path 1 represents the generation of hyperalkaline (>pH 11) serpentinized fluid through infiltration of meteoric water to the deep subsurface where active serpentinization occurs. The reacted fluid is shown being expressed at the surface along faults and fissures. Path 2 represents meteoric water infiltrating the shallow subsurface and reacting to form ~ pH 8 fluid. The image is of a serpentinized fluid study site (140111F) flowing next to and mixing with a surrounding surface water study site (140111G).

sampling sites. For example, photosynthetic protists, like green algae and diatoms, have high demands for CO_2 (Sültemeyer et al., 1988; Hu and Gao, 2008; Yamano and Fukuzawa, 2009). CO_2 can be scarce in hyperalkaline serpentinized fluids and as a result may limit phototroph growth. Predatory heterotrophic protists are known to be selective in their prey (Straile, 1997; Seyler et al., 2019), feeding on smaller protists as well as bacterial and archaea (Pernthaler, 2005). In the sediments of serpentinized fluids of the Samail Ophiolite, bacterial and archaeal distributions are influenced by geochemical variations (Howells et al., 2022), which may have consequences for heterotrophic protists diversity. Some protists can carry out fermentation facultatively and some are strictly fermentative (Bernard and Fenchel, 1996). Either way, fermentation is an anaerobic process, and protists that depend on this metabolism are constrained to low oxygen environments (Fenchel and Finlay, 1990). We have demonstrated that factors including CO_2, O_2, and potential bacterial and archaeal foods sources change along the Samail Ophiolite mixing gradient (Howells et al., 2022). Guided by previous studies on the physiology and physiochemistry of phototrophic, heterotrophic, and anaerobic/fermentative protists, we assess whether the variations in the geochemical and biological factors observed in Howells et al. (2022) influence protist community composition and diversity. As there is increasing interest in the application of the natural process of serpentinization to carbon sequestration (Kelemen et al., 2011), understanding the diversity of microbial eukaryotes that both consume and produce CO_2 in serpentinizing systems will be key to determining the overall efficacy of serpentinization for carbon sequestration.

2. Materials and methods

2.1. Study sites

Geochemical and biological samples were collected at 19 fluidic sites located at 6 different locations within the Samail Ophiolite of Oman, as summarized in **Table 1**. Sites are described as serpentinized fluid [Type 2 fluids in Leong et al. (2021)], surrounding surface water [Type 1 fluids in Leong et al. (2021)] and mixing in **Table 1**. A geologic map of the Samail Ophiolite of Oman that shows the locations is in **Supplementary Figure 1**. This study includes a subset of sites described in Howells et al. (2022). Protists were not detected through 18S rRNA gene amplicon sequencing at some of the sites described in Howells et al. (2022).

2.2. Chemical analysis of fluids

Methods described by Leong et al. (2021) were used to measure temperature, pH, conductivity, dissolved oxygen (O_2), and total dissolved Si and sulfide in the field. Samples were collected for lab analysis of major anions (F^-, Cl^-, SO_4^{2-}, NO_3^-), major cations (Li^+, Na^+, K^+, Ca^{2+}, Mg^{2+}, NH_4^+), dissolved inorganic carbon (DIC), trace elements and dissolved gases. The concentrations of major ions, DIC, Si and H_2 can be found in **Table 2**. Howells et al. (2022) describes the methods for dissolved H_2 gas sample collection and analysis. Combined, the chemical data was used to calculate activities and solute speciation, as well as chemical affinities for mineral dissolution reactions with the geochemical modeling code

10.3389/fmicb.2023.1139333

TABLE 1 Overview of sites in this study.

Sample identification		Field measurements		Mixing indicator		Site description
Code	Location	Temp.	pH	Si	Percent	
		C°		μm	Serpentinized fluid	
140115Y	Al Bana	24.5	11.6	2.16[a]	99.7	Serpentinized fluid
140114V	Falaij North	24.4	11.4	2.75 [a]	99.5	Serpentinized fluid
140114T	Falaij North	27.2	11.4	1.84[a]	99.8	Serpentinized fluid
140113O	Falaij South	28.4	11.4	3.68[a]	99.2	Serpentinized fluid
140111G	Qafifah	22.6	8.9	276.35[a]	8.7	Visible mixing at surface
140111H	Qafifah	20.2	10.2	145[a]	52.3	Visible mixing at surface
140111I	Qafifah	18.8	10.9	100.25[a]	67.2	Visible mixing at surface
140111F	Qafifah	23.8	11.6	10.52[a]	96.9	Visible mixing at surface
140116B	Shumayt	26.5	7.9	302.59[a]	0.0	Surface water
140116D	Shumayt	27.1	9.1	260.49[a]	14.0	Visible mixing at surface
140117I	Shumayt	32.3	11.3	1.96[a]	99.8	Serpentinized fluid
140117G	Shumayt	30.5	11.4	1.50[a]	99.9	Serpentinized fluid
140117F	Shumayt	26.2	11.5	2.65[a]	99.5	Serpentinized fluid
140117H	Shumayt	29.6	11.5	1.66[a]	99.9	Serpentinized fluid
140110B	Dima	23.5	8.4	183.39[a]	39.6	Surface water
140112L	Dima	21.3	9.8	111.13[a]	63.5	Visible mixing at surface
140110D	Dima	21.8	10.4	91.38[a]	70.1	Visible mixing at surface
140112M	Dima	28.2	11.4	5.6[a]	98.6	Serpentinized fluid
140110C	Dima	27	11.4	4.26[a]	99.0	Serpentinized fluid
Geochemical model		40*	11.8*	1.39*	100	Chrysotile-brucite-diopside-calcite equilibria, 10 m*m* NaCl

This table is modified from Howells et al. (2022). The extent of mixing between surrounding surface water and serpentinized fluid is indicated by the calculated percent serpentinized fluid column. The site description notes locations where mixing between surrounding surface water and serpentinized fluid were visually observed. The locations of each of the sites can be found in the map in **Supplementary Figure 1**. The Geochemical model, reported in Leong et al. (2021), is of pristine serpentinized fluid derived from chrysotile-brucite-diopside-calcite equilibria and is used as our serpentinized fluid end member for calculating percent serpentinized fluid.

[a]Si values and methods for analyzing Si are reported in Leong et al. (2021).

*Values from model described in Leong et al. (2021).

EQ3 (Wolery and Jarek, 2003; Wolery and Jove-Colon, 2004), as described by Leong et al. (2021).

2.3. DNA sample collection and extraction

At each sampling site, sediments underlying the site fluid were collected using a stainless-steel spatula that was washed with ethanol and flame sterilized. Sediment composition ranged from small rocky granules to silt. Sediment was sampled to up to approximately one centimeter in depth. 50 mL sterile specimen cups were filled to approximately 40 mL with sediment, which was then homogenized by stirring with the spatula, followed by shaking the sealed specimen cup. Homogenized sediment was then aliquoted into 2 mL cryo vials, and frozen on liquid nitrogen in the field. Frozen sediment samples were shipped to the lab in a dry shipper (still frozen) and placed in a −80°C freezer for storage.

The protocol used for DNA extraction, modified from methods described in Huber et al. (2002), is described in Howells et al. (2022) and included both physical and chemical lysis. Briefly, excess fluid was removed from sediment samples by spinning the cryo vials at 8000 rpm for 20 min at 10°C and removing the supernatant using filtered pipette tips. After transferring and weighing sediment samples in DNAse/RNAase-free 15 mL falcon tubes, lysis buffer was added at 1 mL per gram of sediment, and the samples were subjected to three freeze-thaw cycles. After physical lysis, samples went through chemical lysis which involved a lysozyme treatment (18 μL of 50 mg/mL stock per mL of extraction volume) followed by a proteinase K plus sodium dodecyl sulfate (SDS) treatment (22.5 μL of 20 μg/mL proteinase K stock and 45 μL of 20% SDS stock per mL of extraction volume). DNA was purified using the phenol/chloroform/isoamyl alcohol (24:24:1) method, precipitated with ethanol, dried overnight and washed according to the washing step from MP Biomedicals FastDNA Spin Kit for Soil. A final clean-up step was conducted using MO BIO PowerClean DNA Clean-Up kit.

2.4. Sequencing library preparation and sequencing

Amplicons of 16S and 18S rRNA genes were sequenced using the Illumina MiSeq v3 2 × 300 platform at the Arizona State

TABLE 2 Geochemical parameters of this study.

Site	Conductivity	pH	Si	Ca^{+2}	H_2	O_2	DIC
ID	μS/cm		μmolality	μmolality	μmolality	μmolality	ppm C
140115Y	2778	11.6	2.16	1791.98	20.79	140.63	1.30
140114V	1803	11.4	2.75	1714.82	0.17	190.63	2.77
140114T	2061	11.4	1.84	1914.58	27.85	16.31	0.50
140113O	2329	11.4	3.68	2085.33	39.20	59.38	0.69
140111G	586	8.9	276.32	358.64	0.24	221.88	49.27
140111H	597	10.2	144.99	214.46	1.10	278.14	21.56
140111I	683	10.9	100.24	367.83	2.07	231.26	10.15
140111F	1470	11.6	10.52	1687.89	263.16	8.59	0.49
140116B	760	7.9	302.56	562.09	0.06	125.01	61.52
140116D	777	9.1	260.47	715.42	12.49	215.63	47.75
140117I	2000	11.3	1.96	1859.03	227.35	12.50	0.56
140117G	2015	11.4	1.50	1899.89	2.75	9.88	0.22
140117F	1868	11.5	2.65	1848.04	264.61	25.00	0.35
140117H	2067	11.5	1.66	2078.97	225.40	21.88	0.35
140110B	568	8.4	183.37	485.01	0.01*	243.76	43.60
140112L	659	9.8	111.12	312.81	0.01*	253.13	22.57
140110D	778	10.4	91.38	475.47	0.06	203.13	9.75
140112M	2058	11.4	5.60	1978.86	30.69	15.78	0.62
140110C	2011	11.4	4.26	1958.47	6.42	17.91	0.64

Geochemical parameters directly influenced by the process of serpentinization are pH, Si, Ca^{+2}, H_2, and DIC. pH, Si, O_2, and DIC are investigated in this study as factors that may influence protist diversity. Ca^{+2} is relevant to the chemical speciation of DIC. H_2 is relevant to potential interactions between anaerobic protists and hydrogenotrophic prokaryotes. Conductivity is provided for additional context.
*Denotes site where standard error on H_2 measurement is greater than 5%. DIC, dissolved inorganic carbon.

University (ASU) Biodesign Institute core facilities. Sequencing library preparation followed a two-step PCR protocol with dual indexing (Kozich et al., 2013). The first-step PCR for the 16S rRNA gene used the forward general archaeal and bacterial primer 341F 5′-CCTACGGGNBGCASCAG-3′ (Takahashi et al., 2014), and the reverse general bacterial and archaeal primer 806R 5′-GGACTACNVGGGTWTCTAAT-3′ from the Earth Microbiome Project (Caporaso et al., 2011; Apprill et al., 2015; Parada et al., 2016). During the first-step PCR for the 18S rRNA gene the general eukaryote primer set with forward primer TAREuk454FWD1 5′-CCAGCASCYGCGGTAATTCC-3′ and reverse primer TAREukREV3 5′-ACTTTCGTTCTTGATYRA-3′ was used (Stoeck et al., 2010). The gene-specific primers included the addition of an overhang that allowed for the addition of barcodes and Illumina adapters in the second PCR (Hamady and Knight, 2009).

In the first PCR the template DNA was taken from the same sediment DNA extract for both the 16S rRNA and 18S rRNA gene amplifications. The first PCR thermocycler conditions for the 16S rRNA gene amplification were one denaturation cycle at 94°C for 3 min, 30 cycles of denaturation at 94°C for 30 s, annealing at 48°C for 30 s, and elongation at 72°C for 50 s. A final elongation cycle followed at 72°C for 10 min. The first PCR thermocycler conditions for the 18S rRNA gene amplification were the same for 16S, except for primer annealing at 47°C. The thermocycler conditions for the second PCR were a denaturation cycle at 95°C for 3 min, 30 cycles of denaturation at 95°C for 30 s, annealing at 50°C for 30 s, and elongation at 72°C for 50 s. A final elongation cycle followed at 72°C for 10 min. For each amplification PCR reagent mixtures included 15 μL EconoTaq 2x Master Mix, 2.5 μL of each primer (forward and reverse) for a final concentration of 2 μM, 2.5 μL template DNA, and 7.5 μL of sterile, nuclease free water for a final reaction volume of 30 μL. The PCR products were purified at the DNA Shared Resource Facility at ASU using Ampure magnetic beads in combination with a Beckman Biomek NXp robot. Purified products were quantified using Invitrogen Qubit broad range dsDNA fluorescent dye and a Biotek HT1 Plate Reader. After quantification, 25 ng of each amplicon sample, now having a unique barcode and Illumina adapters, were pooled. The pooled sample was then submitted for sequencing.

2.5. Sequencing data analysis

Paired-end sequencing data were demultiplexed at the ASU Genomics Facility and returned with quality analysis in the Casava 1.8 format as ".fastqc.gz" (FASTQC) files. Sequencing data from this project can be found in the NCBI Sequence Read Archive under the BioProject ID, PRJNA919024. Bioinformatic analysis of the FASTQC files was done using the QIIME2-2019.7 (RRID:SCR_021258) program wrapper (Bolyen et al., 2019).

TABLE 3 Summary of Mann–Whitney U-tests conducted on the relative abundance and richness of protist and prokaryote microbial groups and fluid geochemistry.

	Factor	Test description	Min	Median	Max	Min	Median	Max	*U*-value	*Z*-value	Exact *p*-value
			Group 1 (G1), *N* = 12 >70% serpentinized fluid			Group 2 (G2), *N* = 7 <70% serpentinized fluid					
Geochemistry	pH	G1 > G2	10.4	11.4	11.6	7.9	9.1	10.9	83	3.4	4.0E−05
	Si (μmolality)	G1 < G2	1.5	2.7	91.4	100.2	183.4	302.6	0	−3.5	2.0E−05
	Ca^{+2} (μmolality)	G1 > G2	475.5	1879.5	2085.3	214.46	367.8	715.4	81	3.3	1.4E−04
	H_2 (μmolality)	G1 > G2	0.06	29.3	264.6	0.01	0.2	12.5	73	2.6	3.6E−03
	*DIC (μmolality)	G1 < G2	18.6	49.3	811.7	845.36	3630.5	5122.6	0	−3.5	2.0E−05
	O_2 (μmolality)	G1 < G2	8.6	19.9	203.1	125.01	231.3	278.1	3	−3.3	1.4E−04
Relative abundance	Phototrophic protists	G1 < > G2	0	6.6	62.8	31.6	65.1	75.1	9	−2.8	3.7E−03
	Heterotrophic protists	G1 < > G2	3.9	66.6	96.4	18.5	33.4	58.1	63	1.7	8.3E−02
	Anaerobic protists	G1 < > G2	0.5	11.9	87.3	0	0.2	3.5	81	3.3	2.8E−04
	Chlorophyceae	G1 < G2	0	0.1	5.4	0.2	1.9	13.4	15	−2.3	9.7E−03
	Cyclidium	G1 > G2	0.4	10.7	87.3	0	0	3.5	82	3.4	7.9E−05
	Ischnamoeba montana	G1 > G2	0.1	12.3	67.3	0	0	0.6	81	3.3	1.4E−04
	Diatomea	G1 < G2	0	0.1	10.4	6.2	29.4	54.6	1.5	−3.4	6.0E−05
Richness	All Protists	G1 < G2	9	18	111	103	154	179	1	−3.4	4.0E−05
	Phototrophic protists	G1 < G2	0	4	41	39	58	64	1	−3.4	4.0E−05
	Heterotrophic protists	G1 < G2	3	11.5	62	52	84	101	3	−3.3	1.4E−04
	Anaerobic protists	G1 < > G2	1	2	4	0	1	7	47.5	0.4	6.8E−01
	All prokaryotes	G1 < G2	67	97	200	67	504	831	11.5	−2.5	3.8E−03

Groupings include sites with > and <70% serpentinized fluid composition. Relative abundance refers to the relative abundance of the 16S or 18S rRNA gene ASVs. Richness refers to the observed number of ASVs. The *U*-value is the test statistic for the Mann–Whitney U test. The *Z*-value is the approximate normal test statistic derived from the *U*-value. *U* and *Z*-values were calculated using OriginPro Version 2019b.
*DIC, dissolved inorganic carbon. For an overview of the modeled inorganic carbon activities, see **Supplementary Table 1**.

10.3389/fmicb.2023.1139333

To generate amplicon sequence variants (ASVs), paired-end FASTQC files were quality filtered, trimmed, Illumina error corrected, merged and chimera checked using the program DADA2 (Callahan et al., 2016).

Taxonomic assignment of ASVs was done using a naïve Bayes trained classifier generated from the SILVA 132 99% OTU 16S and 18S databases (Quast et al., 2013) and the sklearn method in the QIIME 2 plugin, q2-feature-classifier (Pedregosa, 2011; Bokulich et al., 2018). After taxonomic assignment, 16S ASVs that occur only once were filtered out and 18S ASVs that occur less than 10 times across all sites were filtered out to be conservative in defining detectable phylotypes. 16S ASVs classified only to the domain level and those classified as species associated with the human microbiome were filtered out. 18S ASVs classified only to the domain level were filtered out. Because this study is focused on protist diversity, 18S ASVs classified as Opisthokonta and Magnoliophyta were filtered out. After filtering, sequence reads were rarefied for even sampling across sites; 16S reads were rarefied to 9,200 per site, and 18S reads were rarefied to 1,900 per site. Alpha rarefaction curves were made to ensure sufficient sampling of 16S and 18S diversity, as shown in **Supplementary Figure 2**. The rarefied reads were used to build a final frequency table of ASVs across all sites. Faith's phylogenetic diversity analysis was carried out on both 16S and 18S rarefied ASVs using the q2-diversity plugin (Faith, 1992), after aligning ASVs using MAFT within q2-align (Katoh et al., 2002). A phylogeny of the aligned ASVs was constructed with FastTree2 within q2-phylogeny (Price et al., 2010). The rarefied frequency table and phylogenetic diversity analysis were used in the following statistical analyses.

2.6. Statistical analyses and graphing

Non-metric multidimensional scaling (NMDS) ordination, Mantel correlation analysis, and analysis of similarity (ANOSIM) were carried out using the vegan package (version 2.5-6, RRID:SCR_011950) within R version 3.6.0 (R Core Team, 2019). A dendrogram heatmap was made using the pheatmap package in R. Additional ordinations and similarity percentage (SIMPER) analysis were carried out using the program Past 4.02 (Hammer et al., 2001). Scatter plots, Pearson correlation analyses, and Mann–Whitney U-tests were carried out using OriginPro, Version 2019b (RRID:SCR_014212) made by OriginLab Corporation, Northampton, MA, USA. Rarefied ASV frequencies were converted to relative abundances per site to assess variations in composition of 16S and 18S rRNA gene ASVs. Relative abundances were square-root transformed, and Bray-Curtis dissimilarity matrices were generated using the vegan package. To assess drivers of 18S and 16S compositional changes, Mantel correlation analyses with 999,999 permutations were done using the Bray-Curtis dissimilarity matrices and Manhattan dissimilarity of log transformed geochemical parameters. NMDS ordinations of the Bray-Curtis dissimilarity matrices were carried out with 1,000 permutations and two dimensions ($k = 2$). For both the 18S and 16S ASV NMDS plots, the stress was less than 0.1. The NMDS stress plot for 18S ASVs is shown in **Supplementary Figure 3A**. 95% concentration ellipses were drawn on principle coordinates analysis (PCO) and NMDS ordination of 18S ASVs in Past 4.02 (RRID:SCR_019129) to assess ASV-driven formation of site clusters as shown in **Supplementary Figures 3B, C**. Tests of correlations between geochemically defined groups and the observed clusters from the 95% concentration ellipse analyses were carried out with ANOSIM using 9,999 permutations. SIMPER analysis was used to evaluate the contribution of each 18S ASV to the Bray-Curtis dissimilarity between the 95% concentration ellipse clusters and sites grouped based on their geochemical composition. Mann–Whitney U-tests were conducted to test if differences in relative abundances of microbial groups correspond to differences in geochemical composition among sites. Correlations between geochemical parameters and the observed number of ASVs of microbial groups (richness) were evaluated using scatter plots and Pearson correlation analysis in Origin 2019b. Mann–Whitney U-tests were also conducted to assess the correspondence between variations in richness and the geochemically defined site groups.

3. Results

3.1. Geochemical composition of site fluids

Figure 1 illustrates that in Oman there are two distinct fluid compositions, one being what we call surrounding surface water, which is ~ pH 8, the other being serpentinized fluid, pH > 11. The sediments we sampled for characterization of protist diversity have overlaying fluids that include the two distinct fluid types as well as mixtures of the two. The fluid type at each of our sampling sites is noted in **Table 1** together with measurements of silicon (Si), which can be used as an indicator of the extent of serpentinization (Leong and Shock, 2020; Leong et al., 2021). Additionally, because the concentration of Si in serpentinized fluid expressed at the surface is nearly 3 orders of magnitude lower than the concentration in surrounding surface water, Si can be used as an indicator of the extent of mixing between the two (Leong et al., 2021). Therefore, we followed Howells et al. (2022) and used a linear mixing model with Si concentrations to calculate the percent contribution of serpentinized fluid to each sampling site. One end member of the model is a surface water site from this study with the highest concentration of Si (site 140116B) and the other is a geochemical model of a pristine serpentinized fluid reported in Leong et al. (2021). For results from this calculation, see **Table 1**. Percent serpentinized fluid is referenced throughout the text below to help define sampling along the mixing gradient in the Samail Ophiolite of Oman.

Measurements of conductivity, the concentrations of the calcium ion (Ca^{+2}), dissolved H_2, dissolved O_2 and dissolved inorganic carbon (DIC) are listed in **Table 2**, together with the pH and Si values reported in **Table 1**. Scatter plots of pH, DIC, O_2 and H_2 plotted as function so Si (indicator of mixing) can be found in **Supplementary Figure 4**. We include measurements of Ca^{+2} as chemical modeling shows that aqueous $CaCO_3$ and CO_3^{-2} are the most abundant inorganic carbon species in serpentinized fluids (see **Supplementary Figure 5** and **Supplementary Table 1**).

Howells et al. (2022) observed a distinct compositional change in sediment archaeal and bacterial (prokaryote) diversity and overlying fluid chemistry that corresponds to whether fluids with

10.3389/fmicb.2023.1139333

greater than or less than 70% serpentinized fluid. Therefore, we conducted non-parametric Mann–Whitney U-tests to assess whether pH, O_2 and DIC at sites above and below 70% serpentinized fluid composition are significantly different. Those results are summarized in **Table 3**.

3.2. Protist taxonomy

We classified the protist 18S rRNA gene ASVs taxonomically to explore variations in distribution and diversity of protist phylotypes grouped by taxa and lifestyle. An overview of the relative abundances of phylotypes grouped by the taxonomy reviewed in Adl et al. (2019) is given in **Figure 2A**. The bar chart is ordered by decreasing contribution of serpentinized fluid to each sampling site fluid composition. Stramenopiles and Chloroplastida phylotypes are the most abundant phylotypes at sites that have <70% serpentinized fluid. At sites with >70% serpentinized fluid, many communities are dominated by Amoebozoa phylotypes. Ciliophora phylotypes are present throughout the gradient and make up nearly 90% of the community at a site with 99.5% serpentinized fluid composition (site 140117F). Rhizaria and Apicomplexa are scattered along the gradient. At three sites with >70% serpentinized fluid (sites 140117I, 140114V, and 140110D) the protist communities have similarities to those from sites with <70% serpentinized fluid, having large relative abundances of Chloroplastida and in one case Stramenopile phylotypes. Having filtered out Opisthokonta for the diversity analyses we did exclude some protist ASVs taxonomically classified as Chanoflagellida. In the pre-filtered data set, these ASVs occur only at sites with <70% serpentinized fluid.

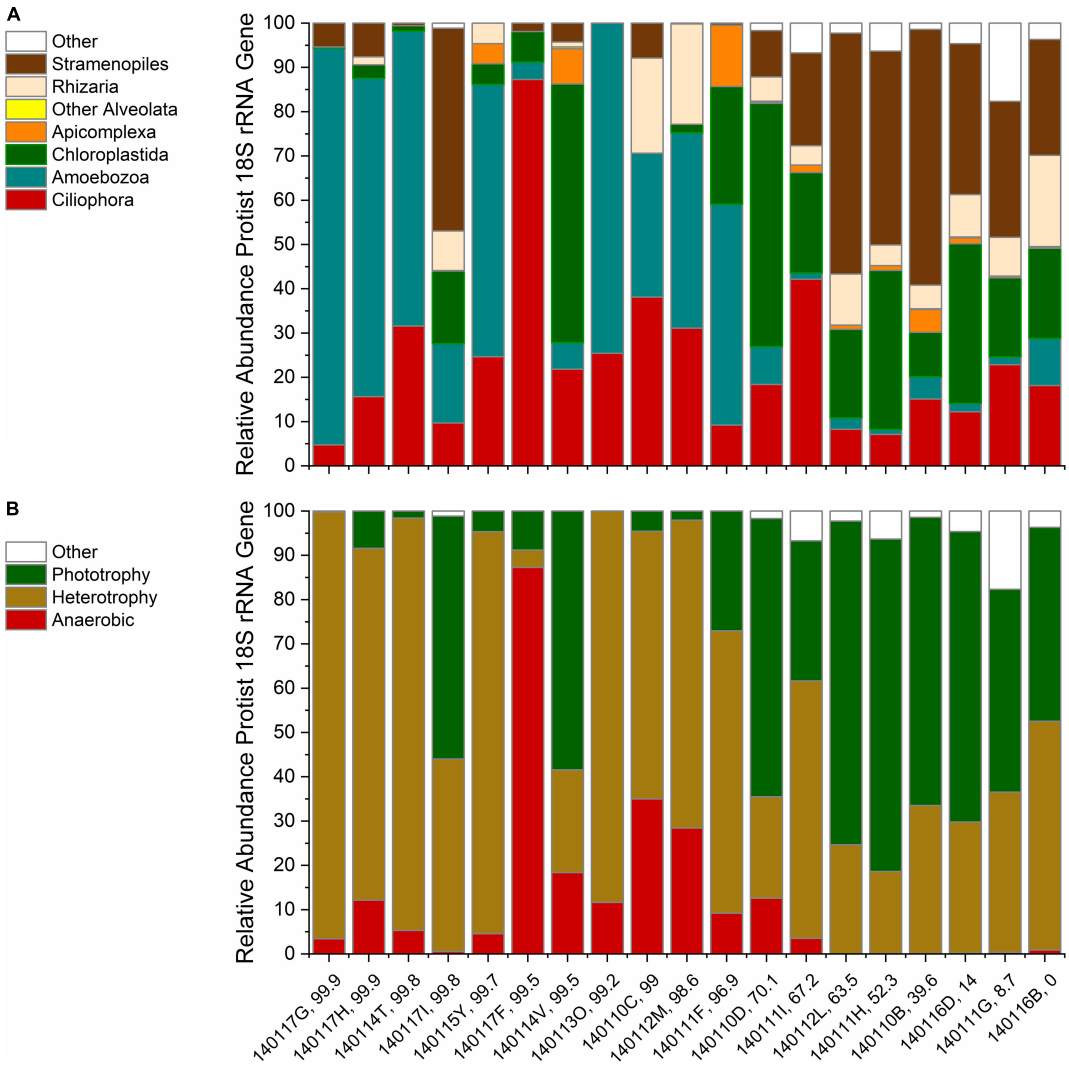

FIGURE 2
Rarefied protist ASV relative abundances. Each bar is labeled with the sampling site identification and the percent serpentinized fluid composition of the sampling site water. The bars are ordered by increasing percent serpentinized fluid from right to left. **(A)** Relative abundances arranged in order of decreasing contribution of serpentinized fluid to water composition at each site using taxonomic classification by major protist groups described in Adl et al. (2019) and the SILVA 32 database. Other Alveolata includes ASVs classified as Colpodellida and Perkinsidae. **(B)** Bar chart of ASV relative abundances grouped by lifestyles of the inferred taxa arranged as in panel **(A)**.

Protist phylotypes were grouped by their respective lifestyles, which was determined through descriptions of the taxonomic groups in the literature (Adl et al., 2019). For this study we focus on phototrophic, heterotrophic and anaerobic lifestyle types. **Figure 2B** shows the relative abundances of protist 18S rRNA gene ASVs grouped by lifestyle. Note that phototrophs are abundant at most sites with <70% serpentinized fluid. Anaerobic protists are most abundant at sites with >70% serpentinized fluid. Heterotrophs are distributed throughout the mixing gradient and show higher relative abundances in locations with elevated contributions of serpentinized fluid. The differences in distribution are reflected in **Table 3**, which reviews Mann–Whitney U-tests conducted to evaluate whether there are significant differences in the distribution between sites with greater than 70% and less than 70% serpentinized fluid.

3.3. Alpha diversity of protists

In this study we measured alpha diversity (richness) in two ways. One way is the count of the number of distinct 18S rRNA gene ASVs that occur at each site which we refer to as the observed number of ASVs. Another assessment of alpha diversity employed in this study is phylogenetic diversity calculated using the Faith method (Faith, 1992). This approach normalizes the richness of 18S rRNA gene sequences by the branch lengths of a phylogenetic tree constructed from the ASVs (see the section "2. Materials and methods"). While we report phylogenetic diversity, it is not a major focus of this study. Richness and phylogenetic diversity values at each site are reported in **Table 4**, which includes the initial count and counts of sequences at each stage of processing and filtering during sequence analysis. As noted in the section "2. Materials and methods" **Supplementary Figure 2** includes the rarefaction curves of filtered sequences at each site used to ensure sufficient sampling depth. Richness and phylogenetic diversity of 16S rRNA genes (prokaryotes) at each site are also reported in **Table 4**. The rarefaction curves for both the 18S and 16S rRNA gene reads indicate that the sites with the highest observed number of ASVs, 140111G, may not have sufficient sampling depth and therefore likely has more diversity than is represented in this study.

Using Pearson correlation analysis, protist richness was compared with geochemical and biological parameters that we hypothesize influence protist diversity in sediments of serpentinized fluid. Specifically, we evaluated correlations between overall observed number or protist ASVs and pH, Si (log transformed) and observed number of prokaryote ASVs, all of which are significant (Pearson r-value > 0.70 and ANOVA p-value > 0.005) as summarized in **Table 5**. We also evaluated correlations between 1) observed number of phototrophic protist ASVs and the concentration of DIC, and 2) observed number of heterotrophic protist ASVs with the concentration of O_2 and the observed number of prokaryote ASVs. Phototrophic protist richness was found to correlate significantly with DIC. Heterotrophic protist richness was found to correlate significantly both with the concentration of O_2 and to a greater extent, the observed number of prokaryote ASVs (see **Table 5** for Pearson r-values and ANOVA p-values).

Mann–Whitney U-tests were also carried out to determine if there is significant difference in protist richness between those sites with >70% serpentinized fluid and those with <70% serpentinized fluid. As summarized in **Table 3**, protist richness is significantly higher at sites with <70% serpentinized fluid than at sites with >70% serpentinized fluid. When examining protist richness grouped by lifestyle, the same holds true for phototrophic and heterotrophic protists. Anaerobic protist richness is overall much lower than phototrophic and heterotrophic richness and is not significantly different between sites with >70% serpentinized fluid and those with <70% serpentinized fluid.

3.4. Beta diversity of protists

We evaluated variations in community composition, or beta diversity, by conducting Bray-Curtis dissimilarity analysis of the relative abundances of protist 18S rRNA gene ASVs. The relative abundances were square-root transformed. We conducted Mantel correlation analysis between the protist dissimilarity matrix and (1) Manhattan dissimilarity of geochemical parameters and (2) Bray-Curtis dissimilarity of square-root transformed 16S rRNA gene relative abundances. The r-statistic and p-value for each Mantel correlation analysis are reported in **Table 6**. All Mantel correlations are significant with p-values < 0.005. The correlations with relatively lower r-statistics are between protists and pH (r-statistic $= 0.62$), phototrophic protists and dissolved inorganic carbon (DIC) (r-statistic $= 0.42$) and heterotrophic protists and dissolved O_2 (r-statistic $= 0.53$). Highest Mantel correlations are between protists and the concentration of Si (r-statistic $= 0.71$), prokaryotes and the concentration of Si (r-statistic $= 0.70$), heterotrophic protists and prokaryotes (r-statistic $= 0.71$) and protists and prokaryotes (r-statistic $= 0.73$).

4. Discussion

4.1. Protist diversity as a function of pH

The variation in pH along the mixing gradient observed is in large part due to the process of serpentinization and subsequent mixing between serpentinized fluids and surrounding surface water (Leong et al., 2021). In previous studies on microbial diversity of serpentinized fluid of the Samail Ophiolite, archaeal and bacterial diversity was shown to decrease as pH increases [reviewed in Howells et al. (2022)]. We found the observed number of protist ASVs (or richness) also significantly decreases with pH (Pearson r-value $= -0.86$ and ANOVA p-value < 0.005). A significant correlation between Bray-Curtis dissimilarity of square-root transformed protist ASV relative abundances and Manhattan dissimilarity of pH values was also observed (Mantel r-statistic $= 0.62$, p-value < 0.005), which indicates that variation in protist community composition significantly corresponds to pH.

The significant anti-correlation of protist richness and significant correspondence of protist community composition variation with pH may be explained by proton limitation experienced by protists under alkaline conditions. To overcome proton limitation, bacteria have adaptations such as increased expression of Na^+/H^+ antiporters or specialized adaptations in ATP synthase (Hu and Gao, 2008). It follows that hyperalkaline pH

10.3389/fmicb.2023.1139333

TABLE 4 Read depth, observed number of ASVs and phylogenetic diversity.

Site ID	Raw sequence frequency	DADA2 pipeline frequency	Non-chimeric frequency	Contaminants filtered frequency	*Observed number of ASVs (richness)	Faith's phylogenetic diversity
18S rRNA gene amplicon						
140117F	13850	6201	6201	5155	9	2.5
140117I	47452	38112	38102	13793	66	12.6
140116D	46408	37535	37316	12234	103	16.4
140117G	30809	24086	23935	7913	24	4.8
140116B	31831	24303	24139	12588	162	20.8
140113O	38718	27165	27143	5902	14	2.8
140115Y	27152	20089	19992	5315	19	5.3
140114T	23568	15160	15151	5711	17	3.5
140112L	36633	28460	28350	14448	130	18.3
140114V	45712	35596	34858	16928	44	5.7
140112M	29895	23347	22939	12288	23	5.2
140111I	152131	122182	113625	74206	154	18.6
140111H	43126	34155	33080	15734	126	18.1
140111G	86303	68413	68019	45861	179	24.4
140111F	32311	25667	24915	1932	14	4.1
140110C	43351	31847	25422	2198	11	3.4
140110D	18013	14036	13994	9808	111	15.7
140110B	48617	37795	36160	15770	156	21.8
140117H	26691	21440	21440	2262	16	4.4
16S rRNA gene amplicon						
140117F	44593	36561	35122	35114	91	16.1
140117I	31398	25253	24518	24239	200	30.1
140116D	52559	37017	34962	34466	451	47.9
140117G	28442	22341	20661	20659	116	18.7
140116B	64415	39181	38115	35828	831	78.0
140113O	26672	19437	17936	17844	67	15.1
140115Y	20065	15587	14471	14471	86	17.6
140114T	56169	43834	36543	36510	137	21.2
140112L	43196	24496	23400	22495	504	48.0
140114V	33551	25072	21807	21781	85	14.2
140112M	29764	22764	20979	20734	111	20.2
140111I	32875	17727	16836	16717	429	44.3
140111H	19067	9850	9662	9255	402	46.7
140111G	45400	27797	27400	25992	760	73.2
140111F	20835	16042	13522	13475	81	14.7
140110C	67207	53346	52903	52687	163	27.0
140110D	21339	16732	16163	16129	91	18.1
140110B	41080	24393	23506	20264	762	73.2
140117H	22711	17814	17058	17013	103	19.0

*Values for the observed number of ASVs are after rarefaction.

TABLE 5 Pearson correlations between geochemical and biological factors and observed number of protist (18S rRNA gene) ASVs.

Factors	Richness metric	Pearson *r*-value	ANOVA *p*-value
pH	Observed number protist ASVs	−0.86	2.5E−06
Si (log molality)	Observed number protist ASVs	0.92	4.0E−08
Si (log molality)	Phylogenetic diversity protist ASVs	0.91	5.5E−08
DIC (molality)	Observed number phototrophic protist ASVs	0.92	9.0E−09
O_2 (molality)	Observed number heterotrophic protist ASVs	0.77	1.2E−04
Si (log molality)	Observed number prokaryotic ASVs	0.84	9.1E−06
Observed number prokaryote ASVs	Observed number heterotrophic protist ASVs	0.85	5.1E−06
Observed number prokaryote ASVs	Observed number protist ASVs	0.9	3.4E−07

TABLE 6 Mantel correlations between dissimilarity of geochemical and biological factors and dissimilarity of protist 18S rRNA gene ASV relative abundances.

Factors	Microbial group	r-statistic	*p*-value
Manhattan, pH	Bray-Curtis, rarified protist ASV relative abundances (square-root transform)	0.62	2.0E−06
Manhattan, Si (log molality)	Bray-Curtis, rarified protist ASV relative abundances (square-root transform)	0.71	1.6E−05
Manhattan, DIC (log molality)	Bray-Curtis, rarified phototrophic protist ASV relative abundances (square-root transform)	0.42	5.3E−04
Manhattan, O_2 (molality)	Bray-Curtis, rarified heterotrophic protist ASV relative abundances (square-root transform)	0.53	1.2E−04
Manhattan, Si (log molality)	Bray-Curtis, rarified prokaryote ASV relative abundances (square-root transform)	0.70	1.0E−06
Bray-Curtis, rarified prokaryote ASV relative abundances (square-root transform)	Bray-Curtis, rarified heterotrophic protist ASV relative abundances (square-root transform)	0.71	2.0E−06
Bray-Curtis, rarified prokaryote ASV relative abundances (square-root transform)	Bray-Curtis, rarified protist ASV relative abundances (square-root transform)	0.73	2.0E−06

As noted in the table, Manhattan dissimilarity was applied to geochemical factors. Bray-Curtis dissimilarity was applied to protist ASV relative abundances. Any transformations applied to the data are noted. DIC stands for dissolved inorganic carbon.

requires specialized adaptations, some of which can be energetically costly to maintain. While there is not much known about protist capabilities for tolerating alkaline pH, it is possible only a few lineages are capable of surviving under such conditions. If true, this may explain the decrease in diversity, and differences in community composition, as pH increases.

4.2. Emerging ecotone

Howells et al. (2022) observed a distinct transition in archaeal and bacterial community composition in sediments in Oman at the point where the overlying water contains 70% serpentinized fluid. Specifically, sediments with overlying fluids that have >70% serpentinized fluid are populated by hydrogenotrophic bacteria and archaea that include aerobic hydrogen oxidizers, sulfate reducers and methanogens. The abundance of hydrogenotrophs drops off at sites with <70% serpentinized fluid and the overall bacterial and archaeal sediment community composition is significantly different among sites that fall above and below 70% serpentinized fluid. Additionally, bacterial and archaeal richness is significantly higher at sites with <70% serpentinized fluid. Howells et al. (2022) suggested the significant differences in pH, H_2 concentration, and concentrations of electron acceptors used by hydrogenotrophs translates to the distinct transition in archaeal and bacterial diversity between sampling sites that have greater than 70% serpentinized fluid and sites with less than 70% serpentinized fluid.

To investigate whether there is also a distinct transition in protist diversity we carried out NMDS ordination, as shown in **Figure 3A**, with Bray-Curtis dissimilarity of protist 18S rRNA gene ASV relative abundances (square-root transformed). The contours on the NMDS ordination show that variation along NMDS1 corresponds closely to the concentration of Si. A Mantel test between Manhattan dissimilarity of log Si concentration and Bray-Curtis dissimilarity of the relative abundances shows there is significant correlation between Si and community composition (Mantel r-statistic of 0.71, p-value < 0.005). As evident in **Figure 3A**, there are two distinct groups separated along NMDS1 that correspond to sites having less than (tan) or greater than (turquoise) 70% contribution from serpentinized fluid. Furthermore, ANOSIM shows that the transition in community composition at 70% serpentinized fluid is significant (ANOSIM r-statistic 0.93, P < 0.005), which also holds true for presence and absence of ASVs (Jaccard dissimilarity, ANOSIM r-statistic 0.93, p-value < 0.005). **Supplementary Figures 3B, C** show 95% concentration ellipses drawn on an NMDS plot and principal coordinate analysis (PCO) plot. The ellipses are estimates of where 95% of the ASVs are expected to fall based on their frequency and correspond to grouping of sites above and below 70% serpentinized fluid. In the NMDS plot, two sites with >70% serpentinized composition fall in the 95% ellipse that encompasses sites with <70% serpentinized fluid. This suggests that these two sites (140117I and 140110D), located centrally along NMDS1 in **Figure 3A**, are intermediate to the grouping above and below 70% serpentinized fluid composition.

Together with the ordination plots and the ANOSIM analysis, the ellipses suggest an overarching community type at sites with <70% serpentinized fluid and another type at sites with >70% serpentinized fluid, with some variability within the two groups. These results, along with observations made in

TABLE 7 List of protist taxa grouped at SILVA 32 level nine taxonomy whose average relative abundance across sites is greater than 1% and their metabolism.

Taxa	140117G	140117H	140114T	140117I	140115Y	140117F	140114V	140113O	140110C	140112M	140111F	140110D	140111I	140112L	140111H	140110B	140116D	140111G	140116B
Phototrophic, Chloroplastida, Charophyta																			
Spirogyra sp. clade H.CC.2012	0	0	0	0	0	0	0	0	0	0	0	0	0	1	0	0	33	0	0
Phototrophic, Chloroplastida, Chlorophyta																			
Characium saccatum	0	0	0	0	0	0	23	0	0	0	0	0	0	0	1	1	0	0	0
Chlamydomonadales	0	2	0	1	0	0	7	0	0	0	0	6	1	0	4	0	0	0	4
Nautococcus solutus	0	1	0	0	0	2	7	0	0	0	0	15	0	2	2	0	0	2	0
Chlorophyceae	0	0	0	1	0	1	3	0	0	0	0	5	13	1	12	2	0	1	2
Elongatocystis ecballocystiformis	0	0	0	4	4	2	5	0	0	0	15	3	0	0	0	0	0	0	0
Phototrophic, Stramenopiles, Diatomea																			
Achnanthidium minutissimum	0	0	0	0	0	0	0	0	0	0	0	0	1	4	2	6	0	7	9
Cymbella sp. TN.2014	0	0	0	6	0	0	0	0	0	0	0	1	3	14	12	0	0	1	0
Gomphonema sp. 12	0	0	0	0	0	0	0	0	0	0	0	0	0	11	11	10	3	2	6
Navicula	0	0	0	0	0	0	0	0	0	0	0	1	0	1	0	24	0	0	1
Ulnaria acus	0	0	0	3	0	0	0	0	5	0	0	2	0	15	1	2	14	6	0
Heterotrophic, Amoebozoa																			
Telaepolella sp. Tib190	3	2	48	0	7	0	3	10	21	10	36	0	0	0	0	0	0	0	0
Ischnamoeba montana	67	64	15	10	45	1	0	62	8	33	6	1	0	1	0	0	0	0	0
Echinamoeba exundans	3	2	0	7	0	2	0	0	4	0	1	5	0	0	0	0	1	0	0
Heterotrophic, other																			
Alveolata, *Eugregarinorida*	0	0	0	0	3	0	8	0	0	0	10	0	1	0	1	4	1	0	0
Ciliophora, *Hypotrichia*	1	2	26	0	11	0	3	13	0	0	0	0	0	0	0	0	0	0	0
Rhizaria, *Dimorpha* sp. ATCC PRA.54	0	2	0	0	5	0	1	0	18	23	0	0	0	0	0	0	0	0	0
Anaerobic (can be microaerophilic)																			
Ciliophora, *Cyclidium*	3	11	5	0	5	87	18	10	35	28	9	13	4	0	0	0	0	0	0

Values in the table are the relative abundances of the taxa at each sampling site.

10.3389/fmicb.2023.1139333

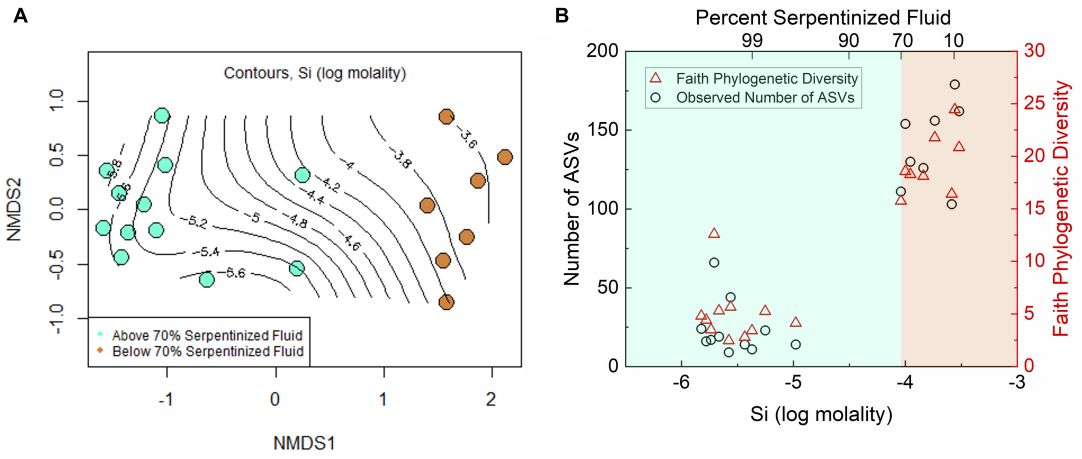

FIGURE 3
Diversity of protist ASVs along the Oman geochemical gradient. **(A)** Non-metric multidimensional scaling (NMDS) ordination of Bray-Curtis dissimilarity of rarefied, square-root transformed protist ASV relative abundances. Two dimensions were used. The stress is 0.094. The contours show Si concentration at each site and are drawn using a maximum likelihood method. Color indicates content of serpentinized fluid above and below 70%. Communities at sites above 70% serpentinized fluid composition are significantly different from those below (ANOSIM r-statistic = 0.93 and p-value < 0.001). **(B)** Richness, or the number of ASVs at each site, and Faith phylogenetic diversity of ASVs plotted against Si concentration. Communities at sites with water compositions <70% serpentinized fluid are significantly less rich than sites with >70% serpentinized fluid (Mann–Whitney U-test p-value < 0.05).

Howells et al. (2022), demonstrate a sharp transition in community composition. The space of transition, or merging, between two distinct communities connected in geographical space is called an ecotone. In our study, the sampling sites are in different geographical locations of the Samail Ophiolite, therefore an ecotone in this setting may reflect a transition between two community types in a chemical space that results from serpentinization and fluid mixing. Protist taxa within the sites located centrally along NMDS1 in Figure 3A may reflect the environmental and biological dynamics of a chemical ecotone. We acknowledge more sampling at sites with around 70% serpentinized fluid would increase the confidence in the presence of a chemical ecotone in this study. Now that Si can be used to determine percent serpentinized fluid composition, analysis of Si in the field can be used to target potential ecotone sites in future biodiversity studies.

Like the variation in protist community composition, protist ASV richness also significantly varies with the concentration of Si as indicated by the Pearson correlation analysis with log Si, r-value = 0.92 and ANOVA p-value < 0.005. Richness is plotted as a function of log Si in Figure 3B and illustrates that the observed number of protist ASVs at sites with <70% serpentinized fluid are significantly higher than the observed number of ASVs at sites with >70% serpentinized fluid, which is supported by the Mann–Whitney U-test p-value < 0.05 (see Table 3).

We hypothesize that the distinct differences in protist communities between sites with >70% serpentinized fluid and sites with <70% serpentinized fluid can be explained by the physiological differences of protists based on their lifestyle, which dictate the properties of the niche they occupy. To test this hypothesis, we constructed a dendrogram heatmap shown in Figure 4A of protist phylotypes grouped by SILVA taxonomic level 9 whose average relative abundance across sites is greater than 1%. The relative abundances of these phylotypes at each site is given in Table 7 and the overall contribution of these taxa to each community is illustrated in Supplementary Figure 6. The site-based dendrogram shown at the top of the heatmap in Figure 4A is derived from a cluster analysis, using the complete method, of Euclidean dissimilarity among sites based on the compositions of the taxa (defined by their occurrence and relative abundance) and illustrates *how similar the sites are* based on the composition of the protist taxa. The taxa-based dendrogram on the left of the heatmap uses differences in abundances of taxa among sites and illustrates *how similar taxa are* based on their distribution. The colors in the heatmap reflect the composition of the most abundant taxa at each site. For example, in the heatmap, the dark blue square at the site with 99.5% serpentinized fluid (site 140117F) indicates that the most abundant taxon at this site is of the genus, *Cyclidium*. The site-based dendrogram at the top of Figure 4 shows two distinct clusters on either side of the 70% serpentinized fluid transition, consistent with the NMDS ordination in Figure 3A and the ANOSIM analysis discussed above. Therefore, the compositions of the most abundant taxa correspond to overall protist community dissimilarity above and below 70% serpentinized fluids.

Insights into how the distributions of the most abundant taxa and their composition at each site contribute to the distinct community compositions above and below the 70% serpentinized fluid threshold can be gained from the taxa-based dendrogram and the heatmap coloration. Note that taxa that cluster together in the dendrogram tend to be similarly distributed across sites. As an example, the anaerobic protist genus *Cyclidium*, and the heterotrophs *Ischnamoeba montana*, *Telaepolella* sp. Tib190, and *Hypotrichia* compose cluster 1 in Figure 4A. As shown by the coloration in the heatmap, these taxa are often the most abundant taxa at sites with compositions that are >70% serpentinized fluid and are often the least abundant at sites with <70% serpentinized fluid. As emphasized by the break along the rows of the heatmap, this cluster is distinct from another cluster containing only phototrophic and heterotrophic taxa. Within this larger

10.3389/fmicb.2023.1139333

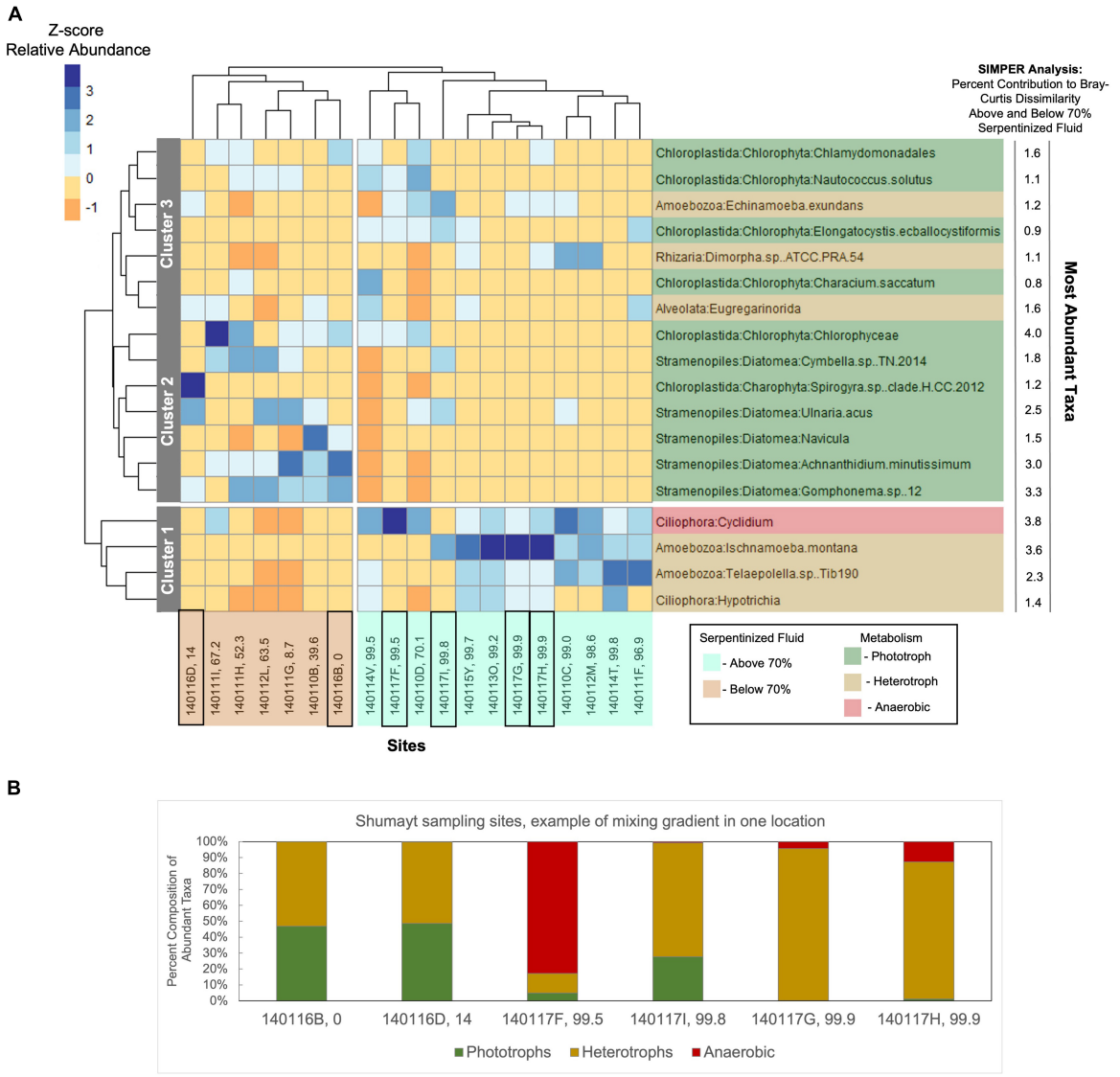

FIGURE 4
Heatmap of the most abundant taxa with cluster dendrogram analyses of both sites and taxa. **(A)** Taxa assigned at SILVA level 9 with >1% average relative abundance at all sites were included in the analysis. Relative abundances were square-root transformed. In the R package, pheatmap, Euclidean dissimilarity between sites was calculated based on the composition of the taxa and a complete cluster method was employed to construct the dendrogram shown at the top of the heatmap. For the dendrogram on the left of the heatmap, Euclidean dissimilarity between taxa was calculated based on the differences in distribution across sites and complete cluster analysis was used to construct the dendrogram. The coloration of the heatmap is scaled to z-scores of the relative abundances of taxa at each site. Two distinct clusters are revealed based on the composition of the most abundant taxa; one cluster composed of sites with water compositions that are >70% serpentinized fluid (cyan highlighted site labels) and the other composed of sites with <70% serpentinized fluid (brown highlighted site labels). Therefore, the compositions of the most abundant taxa align with overall community composition differences observed in the NMDS ordination of all protist 18S ASVs in Figure 3A. The taxa dendrogram on the left shows three distinct clusters. As shown by the heatmap coloration, cluster 1 is composed of taxa that are most abundant at sites with water containing >70% serpentinized fluid composition. Cluster 2 is composed of taxa that are most abundant at sites with <70% serpentinized fluid. Cluster 3 is composed of taxa that occur across the gradient regardless of water composition. Black squares around site IDs on the bottom of the dendrogram indicate Shumayt sampling sites. Shumayt is a location where serpentinized fluid and surrounding surface water co-occur and can mix, which may result in sites (e.g., 140117F and 140117I) with protist communities that reflect a chemical ecotone. **(B)** The composition of the most abundant taxa grouped by their lifestyles at Shumayt sampling sites.

cluster, there are two distinct subclusters designated 2 and 3 in Figure 4A. Cluster 2 is composed only of phototrophic protists, which are predominantly diatoms (Diatomea) with the addition of *Chlorophyceae* and *Spirogyra* sp. clade H CC 2012. Taxa within cluster 2 are often the most abundant at sites with compositions that are <70% serpentinized fluid. Cluster 3 is composed of both phototrophs and heterotrophs. Taxa within this cluster are never the most abundant at sites with <70% serpentinized fluid. The same is mainly true for sites with >70% serpentinized fluid as well, except for *Nautococcus solutus* and *Characium saccatum*, which are most abundant at sites with 70.1% (site 140110D) and 99.5% (site 140114V) serpentinized fluid, respectively. These taxa are green algae within the clade Chloroplastida. The dominance of Chloroplastida at these sites can be seen in Figure 2A. As

mentioned above, site 140110D is centrally located along NMDS1 in Figure 3A.

Next to each taxonomic group on the right side of the heatmap in Figure 4A is the contribution of each taxonomic group (in%) to the Bray-Curtis dissimilarity between communities at sites with water compositions above and below 70% serpentinized fluid as determined by SIMPER analysis. As shown by the SIMPER values in Figure 4A, the taxonomic group with the greatest contribution (4.0%) to Bray-Curtis dissimilarity above and below 70% serpentinized fluid is the phototrophic class *Chlorophyceae*, and ASVs classified as *Chlorophyceae* are significantly more abundant at sites with <70% serpentinized fluid (Mann–Whitney U-test p-value < 0.05, see Table 3). The taxonomic group of Figure 4A with the second highest contribution to variation above and below 70% serpentinized fluid is the Ciliophora genus *Cyclidium*. Species of this genus are microaerophilic to anaerobic. *Cyclidium* is significantly more abundant at sites with compositions that are >70% serpentinized fluid (Mann–Whitney U-test p-value < 0.05, see Table 3). The third highest contribution is from the heterotrophic Amoebozoa species *Ischnamoeba montana*. ASVs classified as this species are significantly more abundant at sites with compositions that are >70% serpentinized fluid according to the Mann–Whitney U-test p-value < 0.05. Combined, the ASVs of the Diatomea taxa in Figure 4A contribute 12% to the observed variation, with ASVs classified as diatom taxa significantly more abundant at sites with <70% serpentinized fluid as shown by the Mann–Whitney U-test p-value < 0.05.

The dendrogram heatmap illustrates further evidence for a chemical ecotone. As mentioned above, there are two taxa that are phototrophs, a lifestyle that is generally more prevalent at sites with <70% serpentinized fluid, that occur at sites that fall centrally along NMDS1. In the dendrogram heatmap, one of these sites 140110D, is within a site-based cluster that includes site 140117F and site 140114V. Sites within this cluster also have a relatively high abundance of phylotypes classified as *Cyclidium*. As mentioned above, *Cyclidium* phylotypes are prevalent at sites with >70% serpentinized fluid. The co-occurrence of phototrophs (a lifestyle associated with sites that have <70% serpentinized fluid) and *Cylclidum* (phylotypes of which are more prevalent at sites with >70% serpentinized fluid) suggest these sites represent a transition between two community types and the dynamics of these sites, biological, physical and/or chemical, allow for these taxa to co-occur. Site 140117F is located in Shumayt where surrounding surface water and serpentinized fluid are geographically co-located and can mix. Shumayt provides an example of where mixing between fluids in one geographical location may result in a chemical ecotone. Sampling sites from Shumayt are indicated by black boxes in Figures 4A, B shows the composition of the most abundant taxa grouped by their lifestyles at these sites. At Shumayt, sites 140116D (14% serpentinized fluid) and 140116B (0% serpentinized fluid) are representative of the <70% serpentinized fluid community type, with both phototrophic and heterotrophic protists. Sites 140117G and 140117H (both 99.9% serpentinized fluid) have both anerobic and heterotrophic protists and are representative of the >70% serpentinized fluid community type. Site 140017F and 140117I at Shumayt do not fall distinctly within either community type, with >70% serpentinized fluid and the occurrence of phototrophs at site 140117I (centrally located in the NMDS ordination of Figure 3A) and the co-occurrence of anaerobic protists (*Cylclidium*) and phototrophs at site 140117F. Sites 140117F and 140117I may represent systems where intermittent fluid mixing is more likely to occur and therefore may allow two distinct community types to merge, resulting in a chemical ecotone.

Overall, the dendrogram heatmap of the most abundant taxa across sites shown in Figure 4A, reveals that sites with compositions that are >70% serpentinized fluid are dominated by heterotrophs and the anaerobic protist genus, *Cyclidium*. Sites composed of <70% serpentinized fluid are dominated by phototrophs and heterotrophs. Diatoms are particularly distinct in their contribution to the difference in protist community composition above and below 70% serpentinized fluid. Unlike diatoms, species of Chloroplastida appear capable of surviving sites with >70% serpentinized fluid. The two distinct community types that are defined by greater than or less than 70% serpentinized fluid may reflect the physiological properties of the most abundant taxa shown in Figure 4A. Physiological requirements may constrain protists to the specific geochemical and biological conditions we observe at our sampling sites which result from the process of serpentinization and subsequent mixing between serpentinized fluid and surrounding surface water. With that in mind, in the following section we turn our attention to geochemical and biological factors that change along the mixing gradient and that may influence the composition and richness of phototrophic, heterotrophic, and anaerobic protist communities.

4.3. Protist diversity as functions of lifestyle requirements

We investigated several geochemical and biological parameters, in addition to pH, that may contribute to the distinct transition in protist community composition and richness at 70% serpentinized fluid. The parameters include dissolved inorganic carbon (DIC), dissolved O_2, the relative abundances of protists grouped by lifestyle, the richness of protists grouped by lifestyle, the relative abundances of prokaryotes grouped by metabolism type and the richness of prokaryote ASVs. Figure 5 contains a visual summary of the differences in these parameters above and below 70% serpentinized fluid composition. The violin plots in Figure 5 are kernel-fitted curves to the number of sites and their distribution across the range of data for each parameter. The larger the area under the curve, the higher the number of sites that fall within that data range. Within each violin plot is a box plot with the circle indicating the median, the ends of the box representing the 1^{st} (25%) and 3^{rd} (75%) quartiles of the data range, and the lines showing the total range of the data.

While there are many geochemical factors that are relevant to the survival of phototrophic protists, one that changes dramatically along the geochemical gradient is the availability of inorganic carbon, specifically CO_2, which is fixed by phototrophs for incorporation into cell mass and respired for energy (Spalding, 1989). Dissolved inorganic carbon is significantly lower at sites where the water contains >70% serpentinized fluid, as illustrated

10.3389/fmicb.2023.1139333

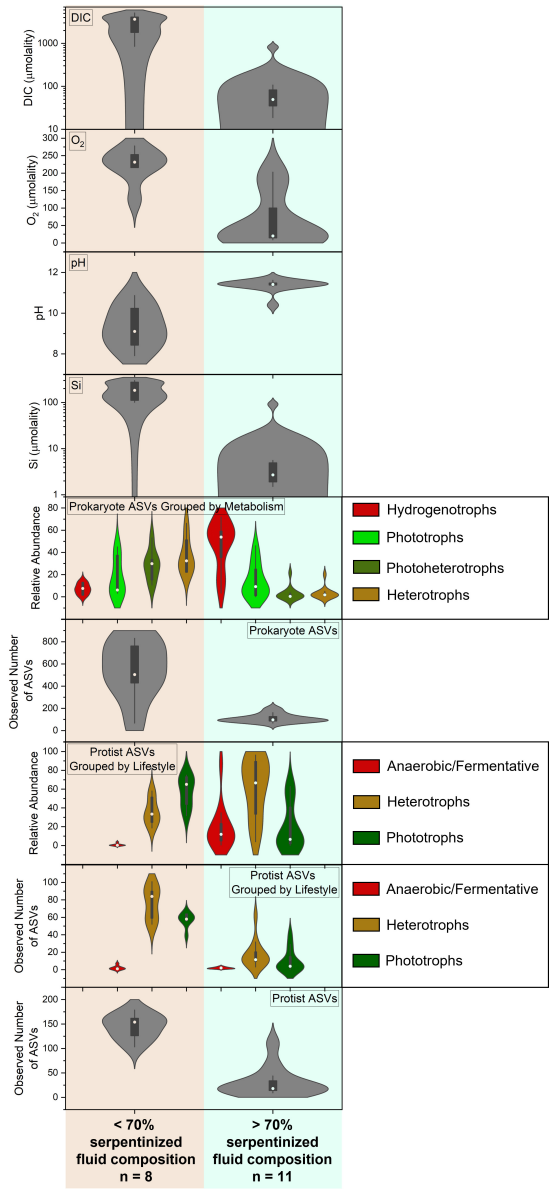

FIGURE 5
Summary of the variation in geochemical and microbial compositions of along the geochemical gradient of serpentinizing habitats in this study. Note the contrasts in protist diversity together with the geochemical and biological factors that correlate significantly with protist community composition and richness where water compositions are above and below 70% serpentinized fluid.

by the DIC violin plot in Figure 5 and confirmed by the Mann–Whitney p-value < 0.05 (see Table 3). Violin plots in Figure 5 also reflect that the relative abundance and richness of phototrophic protists are also significantly lower at sites with >70% serpentinized fluid (Mann–Whitney p-value < 0.05, see Table 3).

Variable DIC abundances can limit the effectiveness of photosynthesis. As an example, the growth rate of the green algae *Chlamydomonas reinhardtii* depends on the availability of DIC (Colman et al., 2002; Yamano and Fukuzawa, 2009), and kinetic studies indicate that its half saturation constant (K_m^{DIC}), or concentration required to reach half the maximum photosynthetic rate, is 100.5 ± 6.6 µM DIC when adapted to high CO_2 conditions. When adapted to low CO_2 conditions, the half saturation constant is 21.9 ± 3.03 µM DIC (Sültemeyer et al., 1988). In a separate study, K_m^{DIC} for the diatom *Nitzschia palea* was determined to be 92.4 ± 1.99 µM when adapted to high CO_2 conditions and 81.9 ± 4.7 µM when adapted to low CO_2 conditions (Hu and Gao, 2008). As shown in Figures 6A, B except for three locations, sites with more than 70% serpentinized fluid have DIC concentrations that are lower than the K_m^{DIC} values for *C. reinhardtii* and *N. palea* adapted to high abundances of CO_2. One of the exceptions, site 140115Y, is a site that occurs down an outflow from a spring of serpentinized fluid with elevated DIC obtained through reaction with the atmosphere. Site 140114V is another exception that is located in a region where surface water can mix with serpentinized fluid. And the third exception is site 140110D, which is a site where mixing between surface water and serpentinized fluid was visually observed at the time of sampling. Two of these exceptions, sites 140114V and 140110D, are a part of the site cluster in the dendrogram heatmap of Figure 4 that may reflect a chemical ecotone.

The influence the availability of DIC may have on protist diversity in serpentinizing systems is reflected in the distribution and diversity of phototrophic protist ASVs. As shown in Figure 6A, ASVs classified as belonging to the order Chlamydomonadales are predominantly absent from sites with >70% serpentinized fluid. The same is true of ASVs classified as belonging to the diatom genus *Nitzchia* as indicated in Figure 6B. A Mantel test shows that there is a significant positive correlation between Manhattan dissimilarity of log transformed DIC and Bray-Curtis dissimilarity of square-root transformed relative abundances of phototrophic protist ASVs, given the r-statistic = 0.44 and p-value < 0.005, which suggests the variation in phototrophic protist community composition is influenced by differences in DIC. As shown in Figure 6C, there is also a strongly significant correlation between DIC and phototroph richness, as indicated by the Pearson r-value = 0.92 and ANOVA p-value < 0.005.

The fact that DIC concentrations at most sites with >70% serpentinized fluid are lower than the known K_m^{DIC} for phototrophic microbial eukaryotes implies that these low concentrations are likely to limit photosynthetic activity and may explain the absence of Chlamydomonadales and *Nitzchia* ASVs at these sites. DIC correlation with richness suggests that an increased availability of inorganic carbon allows for more species to co-occur at sites with <70% serpentinized fluid and conversely, at sites with >70% serpentinized fluid, carbon limitation may enhance competitive interactions and therefore result in low phototrophic protist richness.

The correlation between the variation of phototrophic protist community composition and concentration of DIC may be explained by differences in carbon uptake and utilization between protist species. Phototrophic protists carry out photosynthesis with CO_2 (Colman et al., 2002). Additionally, phototrophic protists, such as species of the green algae genus, *Chlamydomonas*, have been shown to take up HCO_3^- and convert it to CO_2 for use (Colman et al., 2002; Miura et al., 2004). This requires an adaptation generally referred to as a carbon concentrating mechanism that

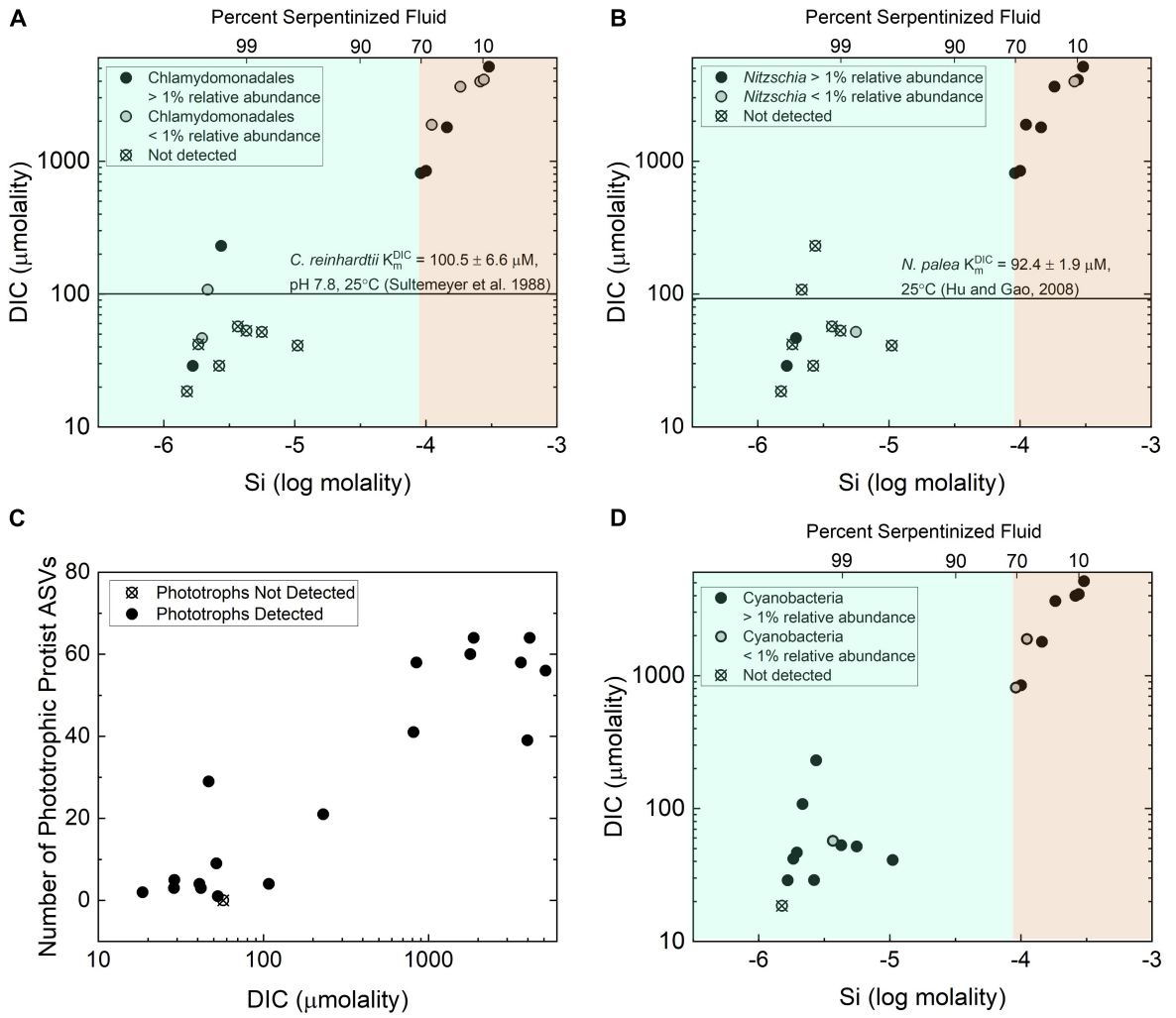

FIGURE 6
Distribution and richness of phototrophs with respect to inorganic carbon availability. **(A)** The distribution of protist phylotypes classified as belonging to the green algae order Chlamydomonadales as functions of total dissolved Si and DIC. The line shows the half saturation constant for DIC for photosynthetic activity by *Chlamydomas reinhardtii* reported in Sültemeyer et al. (1988). **(B)** The distribution of protist phylotypes classified as belonging to the diatom genus *Nitzschia*. The line is drawn to indicate the DIC half saturation constant for photosynthetic activity by *Nitzschia palea* reported in Hu and Gao (2008). **(C)** Richness quantified as the number of phototrophic protist ASVs, as a function of DIC. **(D)** The distribution of the prokaryote phylotypes classified as belonging to the phylum Cyanobacteria as functions of total dissolved Si and DIC.

includes bicarbonate transporters and carbonic anhydrase for the reversible conversion of HCO_3^- to CO_2 (Colman et al., 2002). As shown in **Supplementary Figure 5** the dominant aqueous species of inorganic carbon are $CaCO_3$(aq) and CO_3^{-2}. Inorganic carbon species known to be used by phototrophs, CO_2 and HCO_3^-, are far less abundant at sites where the water consists of >70% serpentinized fluid. While dissolved inorganic carbon is overall low and potentially limiting to phototrophic activity at sites with >70% serpentinized fluid, modeled chemical speciation of inorganic carbon along the gradient shows that CO_2 is ~6 orders of magnitude lower in abundance than HCO_3^-. While CO_2 is more abundant at sites with <70% serpentinized fluid, the thermodynamic activity (≅ concentration) of CO_2 is still ~1 order of magnitude lower than that of HCO_3^-. Therefore, differences in phototrophic protist community composition may reflect the selection for organisms with carbon concentrating mechanisms (uptake and utilization of HCO_3^-), particularly at sites with >70% serpentinized fluid. Furthermore, serpentinizing systems may select for protists with novel adaptations that have yet to be observed in nature for taking up and using the more abundant forms of inorganic carbon, CO_3^{-2} and aqueous $CaCO_3$.

Interactions with bacterial phototrophs may be another factor influencing the diversity of phototrophic protists. There has long been a hypothesis that photosynthetic bacteria, namely Cyanobacteria, can outcompete green algae for inorganic carbon because they have more effective carbon concentrating mechanisms (Beardall and Raven, 2017). More recently, through culture-dependent competition studies, some green algae were shown to outcompete Cyanobacteria under CO_2-poor conditions (Ji et al., 2017). The distribution along the geochemical gradient of 16S rRNA gene ASVs classified as belonging to the Cyanobacteria is shown in **Figure 6D**. At sites with compositions that are <70% serpentinized fluid,

Cyanobacteria phylotypes co-occur with Chlamydomonadales and *Nitzschia* phylotypes. At sites with >70% serpentinized fluid, where Chlamydomonadales and *Nitzschia* phylotypes are generally not detected, Cyanobacteria phylotypes are. These differences in distribution suggests that at sites in this study where the water is composed of >70% serpentinized fluid Cyanobacteria may have more effective carbon concentrating mechanisms than organisms of the order Chlamydomonadales and the genus *Nitzschia*. At sites with <70% serpentinized fluid there is likely to be sufficient DIC to enable coexistence of these phototrophs. However, it is worth noting that some eukaryotic phototrophs were detected at sites with >70% serpentinized fluid as shown in the **Figure 6C**. Perhaps these microbial phototrophic eukaryotes have adaptations that allow them to co-occur with Cyanobacteria.

The diversity of diatoms, which are among the phototrophic protists we detected at our study sites, may be influenced by an additional geochemical factor unrelated to dissolved inorganic carbon. Many diatoms have an amorphous silica shell, therefore, $SiO_2(aq)$ (also referred to as orthosilicic acid, $Si(OH)_4$) can be limiting to growth and survival (Martin-Jézéquel et al., 2000; Belton et al., 2012). Through the process of serpentinization, $SiO_2(aq)$, which is the dominant chemical species of Si in rain and circumneutral surface water, is removed as water infiltrates into the subsurface and reacts with rock, leaving serpentinized fluids relatively depleted in Si (Leong et al., 2021). While not all diatoms have silica shell, the availability of Si in serpentinized fluid may be a contributing factor to the overall diversity of diatoms in serpentinization-hosted ecosystems. The distribution and richness of diatom ASVs reflect the availability of Si with diatoms ASVs being present and most abundant as sites with <70% serpentinized fluid as shown in the NMDS plot of **Supplementary Figure 8A** and phylogenetic bar chart of **Supplementary Figure 6A**. At sites with >70% serpentinized fluid, diatoms are low in richness or absent as shown in **Supplementary Figure 8B**.

In the case of heterotrophic protists that may use O_2 as an electron acceptor for respiration we hypothesize that the availability of O_2 will influence the distribution and diversity. Heterotrophic protists have a wide range of O_2 demands with some being microaerophiles (Scholander et al., 1952; Fenchel, 2012a). Given that O_2 requirements vary among species of protists and that O_2 gradients are known to shape heterotrophic protist communities (Fenchel, 1982; Fenchel et al., 1990; Fenchel and Finlay, 2008), it is possible that O_2 abundance influences heterotrophic protist diversity along the geochemical gradient in the present study. As reflected in the O_2 violin plot in **Figure 5** sites with compositions that are >70% serpentinized fluid have significantly less dissolved O_2 (average = 60.1 μm, $n = 12$) than sites with <70% (average = 224.1 μm, $n = 7$) (Whitney U-test p-value < 0.05, see **Table 3**). As indicated by the Mantel r-statistic = 0.53 and p-value < 0.005 for Manhattan dissimilarity of dissolved O_2 concentration and Bray-Curtis dissimilarity of heterotrophic protist ASV square-root transformed relative abundances, there is a significant correlation between variations in O_2 concentrations and heterotrophic protist community composition. Richness of heterotrophic protist ASVs also significantly correlates with dissolved O_2, given the Pearson r-value = 0.77 and ANOVA p-value < 0.005. However, the abundance of heterotrophic protist is not significantly different between the two fluid types, which may reflect the potential for anaerobic respiration at sites with >70% serpentinized fluid.

In addition to O_2 variability, another factor that may influence heterotrophic protist diversity is the composition of potential food sources. Predatory heterotrophic protists graze upon smaller organisms such as archaea, bacteria and even smaller protists (Straile, 1997; Pernthaler, 2005). In a stable isotope study following carbon flow from bacterial versus archaeal ammonia oxidizers to predatory protists in the ocean water column, some protist populations were shown to preferentially eat archaeal over bacterial ammonia oxidizers and *vice versa* (Salcher et al., 2016). Additional experimental studies show that grazing patterns of protists were shown to shape the composition of bacterial communities (Rønn et al., 2002). It is difficult to observe the direct correspondence between protist feeding patterns and prey community composition in the natural environment. To bridge this gap, there is a conceptual model in protist ecology proposed by Šimek et al. (2002) and reviewed in Pernthaler (2005) for how environmental context and protist grazing can shape bacterial (and potentially archaeal) communities. One extreme in this model is a scenario where environmental resources for prey populations are limited. In this scenario, protist grazing would have a large effect on prey survival and the environment likely selects for defense specialists. This is known as top-down control where predation drives community composition of prey. At the other extreme, bottom-up control, there are sufficient resources for prey and prey biomass is high, therefore prey community composition is driven by resource availability and the environment selects for competition specialists (Pernthaler, 2005). Putting our geochemical gradient in this context, prey populations in serpentinized fluids may fit within the top-down scenario given that as few as 1.16×10^5 cells mL^{-1} were counted in a serpentinized fluid sample from a well (Fones et al., 2019). Surrounding surface water likely fits within the bottom-up scenario as high diversities of phototrophic ASVs, both bacterial and protist, imply these systems support relatively high productivity. Overall, with observed selectivity in protist grazing in other environments and the influence protist grazing may have in shaping prey communities, we expect that there will be correlations between heterotrophic protist community composition and the composition of potential food sources, archaea and bacteria, along this geochemical gradient.

We evaluated the composition of potential food sources for heterotrophic protists through 16S rRNA gene sequencing that captures both archaeal and bacterial (prokaryote) diversity and the resulting ASVs were classified using the SILVA database (Quast et al., 2013). 16S rRNA gene ASVs were grouped at the genus level, focusing on genera with average relative abundances across all sites >1%. Metabolisms were inferred based on 16S sequence homology with cultured archaea and bacteria, resulting in the list of taxa and assigned metabolisms in **Supplementary Table 2**, and the bar chart of taxa grouped by their metabolisms in **Figure 7**. As in the case of archaeal and bacterial metabolism types reported in Howells et al. (2022), there is a sharp transition in community composition at the point where water composition is ∼70% serpentinized fluid. As reflected in the prokaryote (archaea and bacteria) relative abundance violin plot of **Figure 5**, sites with <70% serpentinized

10.3389/fmicb.2023.1139333

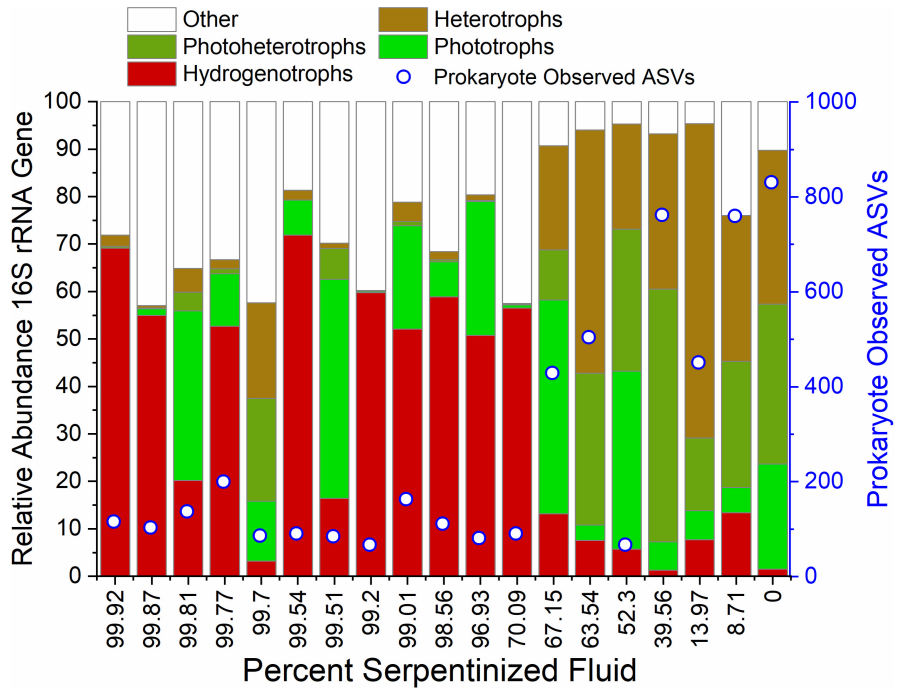

FIGURE 7
Diversity and inferred metabolic capacity of archea and bacteria in the Samail Ophiolite. 16S rRNA gene ASVs were taxonomically classified and grouped at the genus level and subsequently grouped by their potential metabolic capabilities. The bar-chart depicts only genera whose summed relative abundances at all sites is greater than 1%. Open circles indicate the number of 16S rRNA gene ASVs detected at each site.

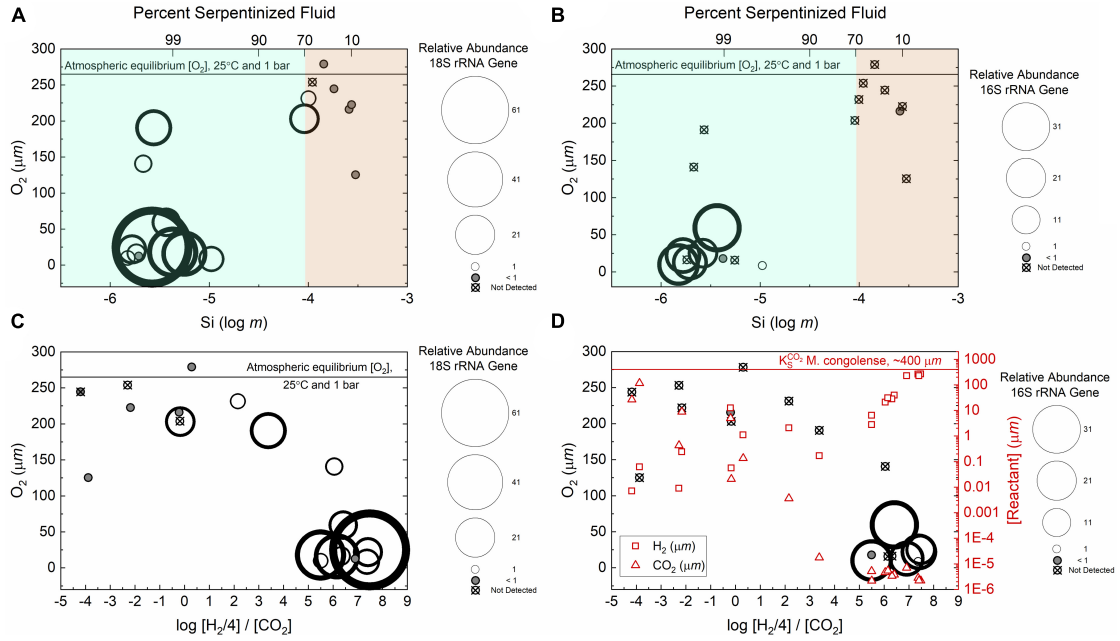

FIGURE 8
Relative abundances of anaerobic protists and the hydrogenotrophic methanogen, *Methanobacterium*. In these distribution plots the areas of the circles scale with the relative abundances of the 18S or 16S rRNA gene ASVs. **(A)** Relative abundances of the 18S rRNA gene ASVs classified as belonging to anaerobic protists as functions of dissolved O_2 and Si. **(B)** Relative abundances of 16S rRNA gene ASVs classified as belonging to *Methanobacterium* as functions of dissolved O_2 and Si. **(C)** Relative abundances of anaerobic protist ASVs as functions of dissolved O_2 and the stoichiometrically balanced ratio of H_2 and CO_2 concentrations. **(D)** Relative abundances of *Methanobacterium* ASVs as in panel **(C)** with reactant concentrations: CO_2 (triangles), H_2 (squares). The line shows the CO_2 half saturation constant for methanogenic activity by *Methanobacterium congolense* reported by Chen et al. (2019).

fluid are dominated by phototrophs, photoheterotrophs and heterotrophs. Sites with >70% serpentinized fluid are dominated by organisms that can use H_2 as an electron donor such as the aerobic hydrogen oxidizer genus, *Hydrogenophaga*, the hydrogenotophic methanogen, *Methanobacterium,* and sulfate reducers (Howells et al., 2022). A Mantel test between Bray-Curtis dissimilarity of square-root transformed prokaryote ASV relative abundances and Manhattan dissimilarity of log transformed Si concentration shows that there is a significant correlation between prokaryote ASV composition and the geochemical gradient, as indicated by the Mantel r-statistic = 0.70 and p-value < 0.005. Prokaryote communities at sites with <70% serpentinized fluid are significantly different from communities at sites with >70% serpentinized fluid, based on the ANOSIM r-statistic = 0.997 and p-value < 0.005. Prokaryote richness (number of ASVs) significantly correlates with log Si concentration (Pearson r-value = 0.84 and ANOVA p-value < 0.005) and richness is significantly higher at sites with <70% serpentinized fluid than at sites with >70% serpentinized fluid composition (Mann–Whitney U-test p-value < 0.05). For visualization of prokaryote community composition and richness changes along the gradient see **Supplementary Figure 9**.

A correlation between variations in potential food sources and heterotrophic protist community composition is revealed by a Mantel test between Bray-Curtis dissimilarity of square-root transformed relative abundances of prokaryote ASVs and heterotrophic protist dissimilarity. With a Mantel r-statistic of 0.71 and p-value < 0.005, there is a strong correlation between prokaryote and heterotrophic protist community composition dissimilarities. Pearson correlation analysis between the number of prokaryote and heterotrophic protist ASVs shows significant correlation between potential food source richness and heterotrophic protist richness, given the Pearson r-value = 0.85 and ANOVA p-value < 0.005. Overall, these correlations suggest that interactions among bacteria, archaea, and heterotrophic protists shape the microbial ecosystem dynamics along the geochemical gradient. It should be noted that both geochemical selectivity and the influence of predator-prey interactions can induce complex relations among the diversities of heterotrophic protists, bacteria, and archaea. The interactions themselves may be driven in part by the geochemical context, such as availability of oxygen. However, given the great interest in determining geochemical factors that shape bacterial and archaeal communities in serpentinization-hosted ecosystems, the observed correlations highlight the influence protist predation may have on shaping these communities.

The concentration of O_2 may also influence the diversity of anaerobic protists detected in serpentinized fluids of Oman. Strict anaerobic protists carry out fermentation for energy and facultative protists can switch to fermentation when O_2 is limited (Fenchel, 2012b). The exact cause of oxygen sensitivity in anaerobic protists is unknown, but it is hypothesized that anaerobic protists lack stress responses to O_2 exposure, such as provided by the enzyme superoxide dismutase (Fenchel and Finlay, 1990). Additionally, in order to carry out fermentation anaerobic protists have an organelle called a hydrogenosome that is rich in O_2-sensitive enzymes such as hydrogenases (Embley et al., 2003). In the present study, the most abundant anaerobic protist phylotype is classified as belonging to the genus *Cyclidium* (see **Supplementary Figure 6C**), whose members are known for their anaerobic capabilities. As an example, cultivation studies show that the species *Cyclidium porcatum* is a strict anaerobe (Clarke et al., 1993). Another species, *Cyclidium borrori*, isolated from a sulfur-rich microbial mat at Laguna Figueroa in Baja California, Mexico, can grow aerobically as well as under anaerobic, sulfide-rich conditions (Dyer, 1989). During anaerobic growth *C. borrori* mitochondria differentiate into smaller organelles (Dyer, 1989), which may be hydrogenosomes. Distribution studies of the species *Cyclidium citrullus* show that it lives in the oxyclines and anoxic zones of water-columns in Danish eutrophic fjords and is most abundant where O_2 is no longer detectable (Fenchel et al., 1990). In addition, a characterization of ciliate communities down the water column of a eutrophic pond showed that *Cyclidium portucatum* exists at a water-column depth where the concentration of O_2 is less than 50 μmolal (Guhl et al., 2006).

As discussed above, O_2 varies along the geochemical gradient, being highest at sites with water compositions that are <70% serpentinized fluid that approach equilibrium with atmosphere as indicated by the horizontal line in **Figure 8A**. The relative abundances of protist taxa, indicated by circle size, that we identify as having potential anaerobic requirements or capabilities are plotted as functions of total dissolved Si and dissolved O_2 in **Figure 8A**. Gray circles indicate sites where the relative abundance of fermentative protists is <1% and circles with an "x" correspond to sites where fermentative protists were not detected. The highest relative abundance of fermentative protist ASVs is at a site with 25 μmol O_2. At the majority (86%) of sites where the water composition is <70% serpentinized fluid ($n = 7$), anaerobic protists are present at less than 1% relative abundance or are absent. In contrast, the relative abundance of anaerobic protists ASVs is >1% at the majority (92%) of sites ($n = 12$) with >70% serpentinized fluid. While anaerobic protists seem to prefer sites with >70% serpentinized fluid, where the concentration of O_2 varies from 8.6 to 203.1 μmol, they are also detected in some of the sites with <70% serpentinized fluid where O_2 is nearly at equilibrium with the atmosphere. There is one site where the water is composed of >70% serpentinized fluid that is also nearly in equilibrium with the atmosphere, which is the same outflow site (140115Y) that is relevant to the distribution of the phototroph taxa discussed above. Overall, the distribution pattern suggests that anaerobic protists have a selective advantage at sites where fluids are more influenced by the process of serpentinization and therefore relatively O_2 limited.

Species of the genus *Cyclidium*, together with other anaerobic protist species, are known to have methanogen endosymbionts (Embley and Finlay, 1994; Esteban and Finlay, 1994). Methanogens are hypothesized to consume the fermentation product H_2, which renders fermentation more energetically favorable and therefore makes the symbiotic relationship beneficial for the protist (Fenchel and Finlay, 1991). This connection is supported by the observation that less H_2 evolves from protists with endosymbionts than free-living fermentative protists (Fenchel and Finlay, 1992). Endosymbiont methanogen species are within the orders Methanbacteriales, Methanosarcinales and Methanomicrobiales (Beinart et al., 2018). In our samples, the genus *Methanobacterium* (order Methanobacteriales) is most abundant at sites with water that is >70% serpentinized fluid (Howells et al., 2022) as indicated in **Figure 8B**, which shows

the distribution of the *Methanobacterium* phylotype as functions of dissolved Si and O_2. *Methanobacterium* phylotypes account for less than 1% of the relative abundance of ASVs or are absent from sites with water composed of <70% serpentinized fluid. *Methanobacterium* has greater relative abundance at many of the sites with >70% serpentinized fluid but is absent at sites with >~60 μmol O_2. While there is not complete correspondence with the distribution of the anaerobic protists, the relative abundance of *Methanobacterium* exceeds 1% at 5 of the 12 sites where the relative abundance of anaerobic protists also exceeds 1%. At these sites it is possible that *Methanobacterium* is living as an endosymbiont of anaerobic protists. In support of this hypothesis, the thermodynamic chemical activity of CO_2 at sites with >70% serpentinized fluid is ~8 orders of magnitude lower than the CO_2 half saturation constant reported by Chen et al. (2019) for methane production by *Methanobacterium congolense* (see **Figures 8C, D**). This suggests that the concentration of CO_2 in serpentinized fluids would be limiting to *M. congolense* activity and potentially other species of *Methanobacterium*. As CO_2 is a fermentation product, an endosymbiotic relationship with anaerobic protists has the potential to circumvent CO_2 limitation to species of *Methanobacterium* living in serpentinizing systems. At sites where *Methanobacterium* and *Cyclidium* phylotypes do not co-occur, it is possible that *Methanobacterium* strains are using formate as described by Fones et al. (2021).

Another advantage of the endosymbiotic relationship for methanogens is protection from an oxygenated atmosphere. A study on the response of the anaerobic protist *Metopus contortus*, which has methanogen endosymbionts, showed that methanogen viability within the protists was maintained upon prolonged exposure to O_2 tensions up to 2% of atmospheric saturation (Fenchel and Finlay, 1990). The endosymbiotic methanogen maintained viability even after a 5-min exposure to 100% atmospheric saturation (Fenchel and Finlay, 1990). Finally, if anaerobic protists detected in this study are truly sensitive to O_2, they are constrained to sites that are also relatively H_2-rich as shown in **Figures 8C, D**. Having an endosymbiotic relationship with an H_2 consumer is therefore beneficial for a protist carrying out fermentation as the endosymbiont can lower the internal concentration of H_2 making the metabolism more favorable.

Overall, while not conclusive, the co-occurrence of anaerobic protists and *Methanobacterium* highlights the potential for serpentinization-hosted ecosystems to support complex biological interactions. An additional factor that may contribute to the dominance of *Cyclidium* is the potential that organisms of this genus are carrying out fermentation (substrate level phosphorylation) and not oxidative phosphorylation, thereby bypassing the proton requirement for ATP synthesis. Fermentative protist may therefore have the advantage at sites with >70% serpentinized fluid, which also all have pH > 10.

5. Significance of protist diversity in serpentinizing systems

Correlations between heterotroph protist diversity and prokaryote diversity are observed in this study and the distribution of potential protist endosymbionts corresponds to anaerobic protist distribution. Looking at the data this way compels one to think that prokaryote diversity may drive protist diversity and *vice versa*. Indeed, correlation analysis between dissimilarity of all protist ASVs and dissimilarity of prokaryote ASVs reveals that overall protist community composition strongly and significantly correlates with prokaryote community composition, given the Mantel r-statistic = 0.73 and p-value < 0.005. Richness of protist and prokaryote ASVs are also strongly correlated, indicated by the Pearson r-value = 0.90 and ANOVA p-value < 0.005. While this may be due in part to predator-prey interactions and endosymbiosis, it may also reflect the selective nature of serpentinized fluid. As the contribution from serpentinized fluid increases, community compositions shift and less diversity is supported. Although there are complexities in disentangling the extent to which geochemical processes or biological interactions are driving protist diversity, the serpentinization gradient highlights the possibility that the environment may select for close associations between protists and prokaryotes. Furthermore, the process of serpentinization is thought to be ubiquitous in the solar system and may support life elsewhere such as the icy satellites of Jupiter and Saturn, Europa and Enceladus (McCollom, 1999; Glein et al., 2008; Waite et al., 2017). The potential for close associations between protists and bacteria and archaea in serpentinized fluids on Earth suggest that these satellites may support more complex biological interactions and complex life than originally anticipated.

With increased focus on the application of serpentinizing systems for energy, specifically H_2 production, and carbon sequestration, acknowledging the diversity of protists in these systems is key to understanding the efficacy of serpentinization for these applications. The presence of phototrophic protists is encouraging as photosynthetic activity may enhance CO_2 sequestration from the atmosphere. However, as discussed above, the greater the contribution of serpentinized fluid to the water composition, the lower the occurrence and richness of phototrophs. Given that the concentration of CO_2 at sites with >70% serpentinized fluid may potentially limit photosynthetic activity by protists, CO_2 limitation in sequestration efforts may be overcome by injections of CO_2 that increase the concentration to a point above protist requirements for photosynthesis. On the other hand, heterotrophic protists and protists that live in association with methanogens may enhance carbon release to the atmosphere and may render serpentinizing systems non-viable for carbon sequestration. Serpentinized fluid outflow channels may be a good target for carbon sequestration as O_2 from the atmosphere can limit methanogen growth and CO_2 from the atmosphere may allow organisms like *Chlamydomas reinhardtii* to survive as shown by investigations of site 140115Y in this study. Moving forward, now that the presence of protists in serpentinizing systems has been observed through 18S rRNA gene sequencing, we can consider their involvement in carbon cycling in these systems and give thought to what their presence in serpentinizing systems on Earth means for possibility of life elsewhere.

Data availability statement

The datasets presented in this study can be found in online repositories. The names of the repository/repositories and

accession number(s) can be found below: https://www.ncbi.nlm.nih.gov/, PRJNA919024.

Author contributions

The lab of GG at Arizona State University provided the supplies and the protocol for assembling the 18S rRNA gene amplicon sequencing library. FD helped AH to assemble the sequencing library. AH conducted the sequencing data processing, analysis, and interpretation with the advisement of FD and GG. AH conducted the geochemical sampling and analysis with the lab of ES at Arizona State University. AH conducted the aqueous chemical modeling with the advisement of ES. AH conducted the interpretation of sequencing and geochemical data and the write up of the results with the advisement of ES, GG, and FD. All authors contributed to the article and approved the submitted version.

Funding

This work was supported by NASA Exobiology grant NNX12AB38G, the NASA Astrobiology Institute Rock-Powered Life (RPL) project grant NNA 15BB02A, and NSF grant EAR-1515513. This work was also supported by the School of Life Sciences and College of Liberal Arts and Sciences (startup grant to GG). AH was supported by the National Science Foundation Graduate Research Fellowship Program.

Acknowledgments

Research presented in this manuscript first appeared in the dissertation of AH, see Howells (2020). Components of this research were presented at the Astrobiology Science Conference June, 2019 in Seattle, WA. Many people and institutions aided in the execution of this study. For field work in Oman, Alysia Cox, James Leong, and Kirt Robinson assisted in collecting water samples for chemical analyses and sediment samples for biological analyses. Peter Kelemen and Jürg Matter helped with the logistics of conducting research in Oman. James Leong also provided great insights into the geochemistry of silica in serpentinizing systems and inspired the investigation on the potential influence silica has on diatoms detected in our study. Juan Maldonado Ortiz and the ASU Genomics Facility made our sequencing efforts easy. As noted in previously published work, Vincent Debes, Kristopher Fecteau, and Michelle Santana conducted processing and analyses of samples in the lab. Tyler Thompson helped with sequencing data processing efforts. Peter Canovas developed the protocol for gas sampling and analysis. Tori Hoehler inspired investigation on the interplay between methanogen CO_2 requirements and the potential for endosymbiotic interactions between methanogens and protists. Lastly, this work would not have been possible without Rock Powered Life and P.I., Alexis Templeton.

Conflict of interest

The authors declare that the research was conducted in the absence of any commercial or financial relationships that could be construed as a potential conflict of interest.

Publisher's note

Supplementary material

The Supplementary Material for this article can be found online at: https://www.frontiersin.org/articles/10.3389/fmicb.2023.1139333/full#supplementary-material

References

Adl, S. M., Bass, D., Lane, C. E., Lukeš, J., Schoch, C. L., Smirnov, A., et al. (2019). Revisions to the classification, nomenclature, and diversity of eukaryotes. *J. Eukaryotic Microbiol.* 66, 4–119. doi: 10.1111/jeu.12691

Amaral-Zettler, L. A. (2013). Eukaryotic diversity at pH extremes. *Front. Microbiol.* 3:441. doi: 10.3389/fmicb.2012.00441

Apprill, A., Mcnally, S., Parsons, R., and Weber, L. (2015). Minor revision to V4 region SSU rRNA 806R gene primer greatly increases detection of SAR11 bacterioplankton. *Aquat. Microb. Ecol.* 75, 129–137. doi: 10.3354/ame01753

Beardall, J., and Raven, J. A. (2017). Cyanobacteria vs green algae: which group has the edge? *J. Exp. Bot.* 68, 3697–3699.

Beinart, R. A., Rotterová, J., Čepička, I., Gast, R. J., and Edgcomb, V. P. (2018). The genome of an endosymbiotic methanogen is very similar to those of its free-living relatives. *Environ. Microbiol.* 20, 2538–2551. doi: 10.1111/1462-2920.14279

Belton, D. J., Deschaume, O., and Perry, C. C. (2012). An overview of the fundamentals of the chemistry of silica with relevance to biosilification and technological advances. *FEBS J.* 279, 1710–1720. doi: 10.1111/j.1742-4658.2012.08531.x

Bernard, C., and Fenchel, T. (1996). Some microaerobic ciliates are facultative anaerobes. *Eur. J. Protistol.* 32, 293–297. doi: 10.1016/S0932-4739(96)80051-4

Bokulich, N. A., Kaehler, B. D., Rideout, J. R., Dillon, M., Bolyen, E., Knight, R., et al. (2018). Optimizing taxonomic classification of marker-gene amplicon sequences with QIIME 2's q2-feature-classifier plugin. *Microbiome* 6:90. doi: 10.1186/s40168-018-0470-z

Bolyen, E., Rideout, J. R., Dillon, M. R., Bokulich, N. A., Abnet, C. C., Al-Ghalith, G. A., et al. (2019). Reproducible, interactive, scalable and extensible microbiome data science using QIIME 2. *Nat. Biotechnol.* 37, 852–857. doi: 10.1038/s41587-019-0209-9

Brazelton, W. J., Thornton, C. N., Hyer, A., Twing, K. I., Longino, A. A., Lang, S. Q., et al. (2017). Metagenomic identification of active methanogens and methanotrophs in serpentinite springs of the Voltri Massif, Italy. *PeerJ* 5:e2945. doi: 10.7717/peerj.2945

Callahan, B. J., McMurdie, P. J., Rosen, M. J., Han, A. W., Johnson, A. J. A., and Holmes, S. P. (2016). DADA2: high-resolution sample inference from Illumina amplicon data. *Nat. Methods* 13, 581–583. doi: 10.1038/nmeth.3869

Canovas, P. A., Hoehler, T., and Shock, E. L. (2017). Geochemical bioenergetics during low-temperature serpentinization: an example from the Samail ophiolite, sultanate of Oman. *J. Geophys. Res. Biogeosci.* 122, 1821–1847. doi: 10.1002/2017JG003825

Caporaso, J. G., Lauber, C. L., Walters, W. A., Berg-Lyons, D., Lozupone, C. A., Turnbaugh, P. J., et al. (2011). Global patterns of 16S rRNA diversity at a depth of millions of sequences per sample. *Proc. Natl. Acad. Sci.* 108(Suppl._1), 4516–4522. doi: 10.1073/pnas.1000080107

Chen, X., Ottosen, L. D. M., and Kofoed, M. V. W. (2019). How low can you go: methane production of *Methanobacterium congolense* at low CO_2 concentrations. *Front. Bioeng. Biotechnol.* 7:34. doi: 10.3389/fbioe.2019.00034

Clarke, K. J., Finlay, J., Esteban, G., and Guhl, B. E. (1993). *Cyclidium porcatum* n. sp.: a free-living anaerobic Scuticociliate containing a stable complex of hydrogenosome, eubacteria and archaeobacteria. *Eur. J. Prostistol.* 29, 262–270. doi: 10.1016/S0932-4739(11)80281-6

Colman, B., Huertas, I. E., Bhatti, S., and Dason, J. S. (2002). The diversity of inorganic carbon acquisition mechanisms in eukaryotic microalgae. *Funct. Plant Biol.* 29, 261–270. doi: 10.1071/PP01184

Crespo-Medina, M., Twing, K. I., Sánchez-Murillo, R., Brazelton, W. J., McCollom, T. M., and Schrenk, M. O. (2017). Methane dynamics in a tropical serpentinizing environment: the Santa Elena Ophiolite, costa rica. *Front. Microbiol.* 8:916. doi: 10.3389/fmicb.2017.00916

Dyer, B. D. (1989). Metopus, Cyclidium and Sonderia: ciliates enriched and cultured from sulfureta of a microbial mat community. *BioSystems* 23, 41–45. doi: 10.1016/0303-2647(89)90007-5

Embley, T., Martin, van der Giezen, M., Horner, D. S., Dyal, P. L., Bell, S., et al. (2003). Hydrogenosomes, mitochondria and early eukaryotic evolution. *IUBMB Life* 55, 387–395. doi: 10.1080/1521654031000159283 4

Embley, T. M., and Finlay, B. J. (1994). The use of small subunit rRNA sequences to unravel the relationships between anaerobic ciliates and their methanogen endosymbionts. *Microbiology* 140, 225–235. doi: 10.1099/13500872-140-2-225

Esteban, G., and Finlay, B. J. (1994). A new genus of anaerobic scuticociliate with endosymbiotic methanogens and ectobiotic bacteria. *Archiv für Protistenkunde* 144, 350–356.

Faith, D. P. (1992). Conservation evaluation and phylogenetic diversity. *Biol. Conserv.* 61, 1–10. doi: 10.1016/0006-3207(92)91201-3

Fenchel, T. (1982). Ecology of heterotrophic microflagellates. III. adaptations to heterogeneous environments. *Mar. Ecol. Prog. Ser.* 9, 25–33. doi: 10.3354/meps009025

Fenchel, T. (2012a). Protozoa and oxygen. *Acta Protozoologica* 53, 3–12.

Fenchel, T. (2012b). "Anaerobic eukaryotes," in *Anoxia. Cellular Origin, Life in Extreme Habitats and Astrobiology, 21*, eds A. Altenbach, J. Bernhard, and J. Seckbach (Dordrecht: Springer). doi: 10.1007/978-94-007-1896-8_1

Fenchel, T., and Finlay, B. (2008). Oxygen and the spatial structure of microbial communities. *Biol. Rev.* 83, 553–569. doi: 10.1111/j.1469-185X.2008.00054.x

Fenchel, T., and Finlay, B. J. (1990). Oxygen toxicity, respiration and behavioural responses to oxygen in free-living anaerobic ciliates. *J. Gen. Microbiol.* 136, 1953–1959. doi: 10.1099/00221287-136-10-1953

Fenchel, T., and Finlay, B. J. (1991). Endosymbiotic methanogenic bacteria in anaerobic ciliates: significance for the growth efficiency of the host. *J. Protozool.* 38, 18–22. doi: 10.1016/S0932-4739(11)80143-4

Fenchel, T., and Finlay, B. J. (1992). Production of methane and hydrogen by anaerobic ciliates containing symbiotic methanogens. *Arch. Microbiol.* 157, 475–480. doi: 10.1007/BF00276765

Fenchel, T., Kristensen, L., and Rasmussen, L. (1990). Water column anoxia: vertical zonation of planktonic protozoa. *Mar. Ecol. Prog. Ser.* 62, 1–10. doi: 10.3354/meps062001

Fones, E. M., Colman, D. R., Kraus, E. A., Nothaft, D. B., Poudel, S., Rempfert, K. R., et al. (2019). Physiological adaptations to serpentinization in the Samail Ophiolite. *Oman. ISME J.* 13, 1750–1762. doi: 10.1038/s41396-019-0391-2

Fones, E. M., Colman, D. R., Kraus, E. A., Stepanauskas, R., Templeton, A. S., Spear, J. R., et al. (2021). Diversification of methanogens into hyperalkaline serpentinizing environments through adaptations to minimize oxidant limitation. *ISME J.* 15, 1121–1135. doi: 10.1038/s41396-020-00838-1

Frouin, E., Bes, M., Ollivier, B., Quéméneur, M., Postec, A., Debroas, D., et al. (2018). Diversity of rare and abundant prokaryotic phylotypes in the Prony hydrothermal field and comparison with other serpentinite-hosted ecosystems. *Front. Microbiol.* 9:102. doi: 10.3389/fmicb.2018.00102

Glein, C. R., Zolotov, M. Y., and Shock, E. L. (2008). The oxidation state of hydrothermal systems on early Enceladus. *Icarus* 197, 157–163. doi: 10.1016/j.icarus.2008.03.021

Guhl, B. E., Finlay, B. J., and Schink, B. (2006).). Seasonal development of hypolimnetic ciliate communities in a eutrophic pond. *FEMS Microbiol. Ecol.* 14, 293–306. doi: 10.1111/j.1574-6941.1994.tb00115.x

Hamady, M., and Knight, R. (2009). Microbial community profiling for human microbiome projects: tools, techniques, and challenges. *Genome Res.* 19, 1141–1152. doi: 10.1101/gr.085464.108

Hammer, O., Harper, D. A. T., and Ryan, P. D. (2001). *PAST: Paleontological Statistics Software Package for Education and Data Analysis the Cambrian Evolution of Brachiopods and Initiation of Constructing Early Paleozoic Marine Benthic Ecosystems View Project Lower Palaeozoic Stratigraphy of Greenland View project*. Available online at: http://palaeo-electronica.org/2001_1/past/issue1_01.htm (accessed May 25, 2020).

Hicks, D. B., Liu, J., Fujisawa, M., and Krulwich, T. A. (2010). F_1F_0-ATP synthases of alkaliphilic bacteria: Lessons from their adaptations. *Biochim. Biophys. Acta - Bioenerg.* 1797, 1362–1377. doi: 10.1016/j.bbabio.2010.02.028

Howells, A. E., Leong, J. A., Ely, T., Santana, M., Robinson, K., Esquivel-Elizondo, S., et al. (2022). Energetically informed niche models of hydrogenotrophs detected in sediments of serpentinized fluids of the Samail Ophiolite of Oman. *J. Geophys. Res. Biogeosci.* 127:e2021JG006317.

Howells, A. E. G. (2020). *A Combined Microbiome and Geochemical Approach, Assessing Drivers of Microbial Diversity, Distribution and Activity. Doctoral dissertation*. Tempe, AZ: Arizona State University.

Hu, H., and Gao, K. (2008). Impacts of CO2 enrichment on growth and photosynthesis in freshwater and marine diatoms. *Chin. J. Oceanol. Limnol.* 26, 407–414. doi: 10.1007/s00343-008-0407-7

Hu, X. (2014). Ciliates in extreme environments. *J. Eukaryotic Microbiol.* 61, 410–418. doi: 10.1111/jeu.12120

Huber, J. A., Butterfield, D. A., and Baross, J. A. (2002). Temporal changes in archaeal diversity and chemistry in a mid-ocean ridge subseafloor habitat. *Appl. Environ. Microbiol.* 68, 1585–1594. doi: 10.1128/AEM.68.4.1585-1594.2002

Ji, X., Verspagen, J. M. H., Stomp, M., and Huisman, J. (2017). Competition between cyanobacteria and green algae at low versus elevated CO_2: who will win, and why? *J. Exp. Bot.* 68, 3815–3828.

Katoh, K., Misawa, K., Kuma, K.-I., and Miyata, T. (2002). MAFFT: a novel method for rapid multiple sequence alignment based on fast fourier transform. *Nucleic Acids Res.* 30, 3059–3066. doi: 10.1093/nar/gkf436

Kelemen, P. B., Matter, J., Streit, E. E., Rudge, J. F., Curry, W. B., and Blusztajn, J. (2011). Rates and mechanisms of mineral carbonation in peridotite: natural processes and recipes for enhanced, in situ CO2 capture and storage. *Annu. Rev. Earth Planetary Sci.* 39, 545–576. doi: 10.1146/annurev-earth-092010-152509

Kozich, J. J., Westcott, S. L., Baxter, N. T., Highlander, S. K., and Schloss, P. D. (2013). Development of a dual-index sequencing strategy and curation pipeline for analyzing amplicon sequence data on the miseq illumina sequencing platform. *Appl. Environ. Microbiol.* 79, 5112–5120. doi: 10.1128/AEM.01043-13

Kraus, E. A., Nothaft, D., Stamps, B. W., Rempfert, K. R., Ellison, E. T., Matter, J. M., et al. (2021). Molecular evidence for an active microbial methane cycle in subsurface serpentinite-hosted groundwaters in the Samail Ophiolite. *Oman. Appl. Environ. Microbiol.* 87:e2068-20. doi: 10.1128/AEM.02068-20

Leong, J. A., Howells, A. E., Robinson, K. J., Cox, A., Debes, R. V., Fecteau, K., et al. (2021). Theoretical predictions versus environmental observations on serpentinization fluids: lessons from the Samail ophiolite in Oman. *J. Geophys. Res. Solid Earth* 126:e2020JB020756.

Leong, J. A. M., and Shock, E. L. (2020). Thermodynamic constraints on the geochemistry of low-temperature, continental, serpentinization-generated fluids. *Am. J. Sci.* 320, 185–235.

López-García, P., Vereshchaka, A., and Moreira, D. (2007). Eukaryotic diversity associated with carbonates and fluid–seawater interface in lost city hydrothermal field. *Environ. Microbiol.* 9, 546–554. doi: 10.1111/j.1462-2920.2006.01158.x

Martin-Jézéquel, V., Hildebrand, M., and Brzezinski, M. A. (2000). Silicon metabolism in diatoms: implications for growth. *J. Phycol.* 36, 821–840. doi: 10.1046/j.1529-8817.2000.00019.x

McCollom, T. M. (1999). Methanogenesis as a potential source of chemical energy for primary biomass production by autotrophic organisms in hydrothermal systems on Europa. *J. Geophys. Res. E Planets* 104, 30729–30742.

McCollom, T. M. (2007). Geochemical constraints on sources of metabolic energy for chemolithoautotrophy in ultramafic-hosted deep-sea hydrothermal systems. *Astrobiology* 7, 933–950. doi: 10.1089/ast.2006.0119

Miller, H. M., Matter, J. M., Kelemen, P., Ellison, E. T., Conrad, M. E., Fierer, N., et al. (2016). Modern water/rock reactions in Oman hyperalkaline peridotite aquifers and implications for microbial habitability. *Geochimica et Cosmochimica Acta* 179, 217–241.

Miura, K., Yamano, T., Yoshioka, S., Kohinata, T., Inoue, Y., Taniguchi, F., et al. (2004). Expression profiling-based identification of CO2-responsive genes regulated by CCM1 controlling a carbon-concentrating mechanism in Chlamydomonas reinhardtii. *Plant Physiol.* 135, 1595–1607. doi: 10.1104/pp.104.041400

Morrill, P. L., Brazelton, W. J., Kohl, L., Rietze, A., Miles, S. M., Kavanagh, H., et al. (2014). Investigations of potential microbial methanogenic and carbon

monoxide utilization pathways in ultra-basic reducing springs associated with present-day continental serpentinization: the tablelands, NL, CAN. *Front. Microbiol.* 5:613. doi: 10.3389/fmicb.2014.00613

Ong'ondo, G. O., Yasindi, A. W., Oduor, S. O., Jost, S., Schagerl, M., Sonntag, B., et al. (2013). Ecology and community structure of ciliated protists in two alkaline-saline rift valley lakes in Kenya with special emphasis on Frontonia. *J. Plankton Res.* 35, 759–771. doi: 10.1093/plankt/fbt044

Parada, A. E., Needham, D. M., and Fuhrman, J. A. (2016). Every base matters: assessing small subunit rRNA primers for marine microbiomes with mock communities, time series and global field samples. *Environ. Microbiol.* 18, 1403–1414. doi: 10.1111/1462-2920.13023

Pedregosa, V. (2011). Scikit-learn: machine learning in python. *J. Mach. Learn. Res.* 12, 2825–2830.

Pernthaler, J. (2005). Predation on prokaryotes in the water column and its ecological implications. *Nat. Rev. Microbiol.* 3, 537–546. doi: 10.1038/nrmicro1180

Price, M. N., Dehal, P. S., and Arkin, A. P. (2010). FastTree 2 - approximately maximum-likelihood trees for large alignments. *PLoS One* 5:e9490. doi: 10.1371/journal.pone.0009490

Quast, C., Pruesse, E., Yilmaz, P., Gerken, J., Schweer, T., Yarza, P., et al. (2013). The SILVA ribosomal RNA gene database project: improved data processing and web-based tools. *Nucleic Acids Res.* 41, 590–596. doi: 10.1093/nar/gks1219

R Core Team (2019). *R: a Language and Environment for Statistical Computing*. Vienna: R Foundation for Statistical Computing.

Rempfert, K. R., Miller, H. M., Bompard, N., Nothaft, D., Matter, J. M., Kelemen, P., et al. (2017). Geological and geochemical controls on subsurface microbial life in the Samail Ophiolite, Oman. *Front. Microbiol.* 8:56. doi: 10.3389/fmicb.2017.00056

Rønn, R., McCaig, A. E., Griffiths, B. S., and Prosser, J. I. (2002). Impact of protozoan grazing on bacterial community structure in soil microcosms. *Appl. Environ. Microbiol.* 68, 6094–6105. doi: 10.1128/AEM.68.12.6094-6105.2002

Salcher, M. M., Ewert, C., Šimek, K., Kasalickỳ, V., and Posch, T. (2016). Interspecific competition and protistan grazing affect the coexistence of freshwater betaproteobacterial strains. *FEMS Microbiol. Ecol.* 92:fiv156. doi: 10.1093/femsec/fiv156

Scholander, P. F., Claff, C. L., and Sveinsson, S. L. (1952). Respiration studies of single cells. II. observations on the oxygen consumption in single protozoans. *Biol. Bull.* 102, 178–184. doi: 10.2307/1538705

Seyler, L. M., Tuorto, S., McGuinness, L. R., Gong, D., and Kerkhof, L. J. (2019). Bacterial and archaeal specific-predation in the North Atlantic Basin. *Front. Mar. Sci.* 6:555.

Šimek, K., Nedoma, J., Pernthaler, J., Posch, T., and Dolan, J. R. (2002). Altering the balance between bacterial production and protistan bacterivory triggers shifts in freshwater bacterial community composition. *Antonie van Leeuwenhoek* 81, 453–463. doi: 10.1023/a:1020557221798

Spalding, M. H. (1989). Photosynthesis and photorespiration in freshwater green algae. *Aquat. Bot.* 34, 181–209. doi: 10.1016/0304-3770(89)90056-9

Stoeck, T., Bass, D., Nebel, M., Christen, R., Jones, M. D. M., Breiner, H. W., et al. (2010). Multiple marker parallel tag environmental DNA sequencing reveals a highly complex eukaryotic community in marine anoxic water. *Mol. Ecol.* 19(Suppl. 1), 21–31. doi: 10.1111/j.1365-294X.2009.04480.x

Straile, D. (1997). Gross growth efficiencies of protozoan and metazoan zooplankton and their dependence on food concentration, predator-prey weight ratio, and taxonomic group. *Limnol. Oceanogr.* 42, 1375–1385. doi: 10.4319/lo.1997.42.6.1375

Sültemeyer, D. F., Klöck, G., Kreuzberg, K., and Fock, H. P. (1988). Photosynthesis and apparent affinity for dissolved inorganic carbon by cells and chloroplasts of *Chlamydomonas reinhardtii* grown at high and low CO_2 concentrations. *Source Planta* 176, 256–260. doi: 10.1007/BF00392453

Suzuki, S., Ishii, S., Wu, A., Cheung, A., Tenney, A., Wanger, G., et al. (2013). Microbial diversity in the cedars, an ultrabasic, ultrareducing, and low salinity serpentinizing ecosystem. *Proc. Natl. Acad. Sci. U S A.* 110, 15336–15341. doi: 10.1073/pnas.1302426110

Takahashi, S., Tomita, J., Nishioka, K., Hisada, T., and Nishijima, M. (2014). Development of a prokaryotic universal primer for simultaneous analysis of Bacteria and Archaea using next-generation sequencing. *PLoS One* 9:e105592. doi: 10.1371/journal.pone.0105592

Twing, K. I., Brazelton, W. J., Kubo, M. D. Y., Hyer, A. J., Cardace, D., Hoehler, T. M., et al. (2017). Serpentinization-influenced groundwater harbors extremely low diversity microbial communities adapted to high pH. *Front. Microbiol.* 8:308. doi: 10.3389/fmicb.2017.00308

Waite, J. H., Glein, C. R., Perryman, R. S., Teolis, B. D., Magee, B. A., Miller, G., et al. (2017). Cassini finds molecular hydrogen in the Enceladus plume: evidence for hydrothermal processes. *Science* 356, 155–159. doi: 10.1126/science.aai8703

Wolery, T. J., and Jove-Colon, C. F. (2004). *Qualification of Thermodynamic Data for Geochemical Modeling Of Mineral-Water Interactions in Dilute Systems (No. ANL-WIS-GS-000003 REV 00) YMP*. Nevada: Yucca Mountain Project, Las Vegas. doi: 10.2172/850412

Wolery, T. W., and Jarek, R. L. (2003). *Software User's Manual Version, EQ3/6, version, 8, 376*.

Yamano, T., and Fukuzawa, H. (2009). Carbon-concentrating mechanism in a green alga, *Chlamydomonas reinhardtii*, revealed by transcriptome analyses. *J. Basic Microbiol.* 49, 42–51. doi: 10.1002/jobm.200800352

Yildiz, I., and Şenler, N. G. (2013). Frontonia anatolica n. sp., a new peniculid ciliate (Protista, Ciliophora) from lake van, Turkey. *Turkish J. Zool.* 37, 24–30. doi: 10.3906/zoo-1203-33

frontiers | Frontiers in Microbiology

TYPE Hypothesis and Theory
PUBLISHED 15 May 2023
DOI 10.3389/fmicb.2023.1145915

OPEN ACCESS

EDITED BY
Axel Schippers,
Federal Institute For Geosciences and Natural Resources, Germany

REVIEWED BY
Katja Laufer-Meiser,
GEOMAR Helmholtz Center for Ocean Research Kiel (HZ), Germany
Aurore Gorlas,
UMR9198 Institut de Biologie Intégrative de la Cellule (I2BC), France

*CORRESPONDENCE
Michael J. Russell
✉ Michael.J.Russell80@gmail.com

RECEIVED 16 January 2023
ACCEPTED 22 March 2023
PUBLISHED 15 May 2023

CITATION
Russell MJ (2023) A self-sustaining serpentinization mega-engine feeds the fougerite nanoengines implicated in the emergence of guided metabolism. *Front. Microbiol.* 14:1145915. doi: 10.3389/fmicb.2023.1145915

A self-sustaining serpentinization mega-engine feeds the fougerite nanoengines implicated in the emergence of guided metabolism

Michael J. Russell*

Dipartimento di Chimica, Università degli Studi di Torino, Torino, Italy

The demonstration by Ivan Barnes et al. that the serpentinization of fresh Alpine-type ultramafic rocks results in the exhalation of hot alkaline fluids is foundational to the submarine alkaline vent theory (AVT) for life's emergence to its 'improbable' thermodynamic state. In AVT, such alkaline fluids ≤150°C, bearing H_2 >CH_4 >HS^-—generated and driven convectively by a serpentinizing exothermic mega-engine operating in the ultramafic crust—exhale into the iron-rich, CO_2>>>NO_3^--bearing Hadean ocean to result in hydrothermal precipitate mounds comprising macromolecular ferroferric-carbonate oxyhydroxide and minor sulfide. As the nanocrystalline minerals fougerite/green rust and mackinawite (FeS), they compose the spontaneously precipitated inorganic membranes that keep the highly contrasting solutions apart, thereby maintaining redox and pH disequilibria. They do so in the form of fine chimneys and chemical gardens. The same disequilibria drive the reduction of CO_2 to $HCOO^-$ or CO, and the oxidation of CH_4 to a methyl group—the two products reacting to form acetate in a sequence antedating the 'energy-producing' acetyl coenzyme-A pathway. Fougerite is a 2D-layered mineral in which the hydrous interlayers themselves harbor 2D solutions, in effect constricted to ~1D by preferentially directed electron hopping/tunneling, and proton Gröthuss 'bucket-brigading' when subject to charge. As a redox-driven nanoengine or peristaltic pump, fougerite forces the ordered reduction of nitrate to ammonium, the amination of pyruvate and oxalate to alanine and glycine, and their condensation to short peptides. In turn, these peptides have the flexibility to sequester the founding inorganic iron oxyhydroxide, sulfide, and pyrophosphate clusters, to produce metal- and phosphate-dosed organic films and cells. As the feed to the hydrothermal mound fails, the only equivalent sustenance on offer to the first autotrophs is the still mildly serpentinizing upper crust beneath. While the conditions here are very much less bountiful, they do offer the similar feed and disequilibria the survivors are accustomed to. Sometime during this transition, a replicating non-ribosomal guidance system is discovered to provide the rules to take on the incrementally changing surroundings. The details of how these replicating apparatuses emerged are the hard problem, but by doing so the progenote archaea and bacteria could begin to colonize what would become the deep biosphere. Indeed, that the anaerobic nitrate-respiring methanotrophic archaea and the deep-branching *Acetothermia* presently comprise a portion of that microbiome occupying serpentinizing rocks offers circumstantial support for this notion. However, the inescapable, if jarring conclusion is drawn that, absent fougerite/green rust, there would be no structured channelway to life.

KEYWORDS

Acetothermia, double layer oxyhydroxides, entropy disproportionation, fougerite/green rust, serpentinization, submarine alkaline vent theory (AVT)

1. The submarine alkaline vent theory

The three founding facts underpinning the submarine "alkaline vent theory" for the emergence of life are:

1. Barnes and O'Neil's (1969) conclusion that: "convecting seawater at <200°C would have serpentinized the crust, becoming alkaline by this process of hydrolysis, much as today, hot springs involving ground-water circulating in ophiolite, have a pH of between 11.5 and 12″;
2. Dudley Foster's iconic photograph of the acidic ~380°C Black Smoker hydrothermal chimney with polychaete and tube worms on the East Pacific Rise (Ballard and Grassle, 1979; Spiess et al., 1980);
3. The smaller scale hydrothermal chimneys, chemical garden spires, and microbialites discovered in the ~340 million year old ore deposits in Ireland, inspired by the "Black Smoker" reports (Larter et al., 1981; Russell, 1996).

Jack Corliss et al. had calculated, on the basis of geochemical studies of basalts from the Mid-Atlantic Ridge and from the silica and magnesium chemistry of warm springs exhaling from the Galapagos submarine ridge, that 300°C metal-bearing hot springs should be found at ocean floor spreading centers (Corliss, 1971; Corliss et al., 1979). The discovery of acidic Black Smokers teaming with life met these predictions and led Corliss, John Baross and Sarah Hoffman to formulate a "hydrothermal origin-of-life hypothesis." Rejected from *Nature* and *Science*, they resorted to the "grey literature" to present their manuscript (Corliss et al., 1980, 1981; Baross and Hoffman, 1985; Levitt, 2023). As reported in Corliss et al. (1980), the hypothesis maintains that "Submarine hydrothermal systems provide all of the conditions necessary for the abiotic synthesis of organic compounds, polymers, and simple cell-like organisms. The continuous flow of circulating fluids in a hydrothermal system provides the thermal and chemical gradients which create the variation in conditions necessary for the successive reactions to take place. Other models for the origin of life fail to fulfill one or more of these requirements."

This "anaerobic chemoautotrophic" hypothesis riled those who had accultured to the Oparin–Haldane–Urey–Miller dogma of how life originated (Lahav, 1985; *cf.*, Lane et al., 2010). Indeed, Stanley Miller himself, with his colleague Jeffrey Bada, took to print in 1988, opining "The high temperatures in the vents would not allow synthesis of organic compounds, but would decompose them, unless the exposure time at vent temperatures was short… Even if the essential organic molecules were available in the hot hydrothermal waters, the subsequent steps of polymerization and the conversion of these polymers into the first organisms would not occur as the vent waters were quenched to the colder temperatures of the primitive oceans" (Miller and Bada, 1988). Their criticism prompted a response, in which it was argued from the discovery of fossil chimneys at Silvermines and the Tynagh base-metal ore deposit in Ireland (Larter et al., 1981; Boyce et al., 1983; Banks, 1985) that "similar, less extreme environments are known and could have provided suitable sources of chemical energy and nutrients as well as stable 'culture chambers'" (Russell et al., 1988).

However, a reading of Ivan Barne's studies and our field studies on Alpine-type ultramafic rocks in Southern Europe and Turkey (e.g., Fallick et al., 1991) led us to propose a substitution of the acidic hydrothermal spring models responsible for Black Smokers and exhalative orebodies, with a serpentinization-driven alkaline hydrothermal model that more appropriately explained the sources of fuel to feed life's 'origin' (Russell et al., 1989). Further development of the model had the alkaline hydrothermal solutions precipitating iron sulfide bubbles on contact with "the mildly oxidized, acidic and iron-bearing Hadean ocean water" (Russell et al., 1993). While this model could demonstrate the analogy with CO_2-based autotrophic metabolism—more fundamental was its explanation of the otherwise enigmatic origin of Peter Mitchell's *proton motive force* (PMF). How life could have invented the PMF had been a puzzle, so a key insight of AVT was that no invention of the 'force' was necessary—the PMF had been there from the beginning, freely developed from one aspect of the initial conditions, i.e., as a proton gradient imposed across mineral precipitate membranes—itself a result of the acidulous ocean interfacing the alkaline hydrothermal fluid as it exhales from the Hadean ocean floor (Mitchell, 1961; Russell et al., 1994; Figure 1).

Competing with AVT, though assuming only acidic conditions, is Günter Wächtershäuser's theory that the origin of life involves the reduction of copious volcanic CO_2 through the reductive acetyl coenzyme-A pathway to acetate (Wächtershäuser, 1988)—the pathway that is now broadly, but not universally, accepted for this role (Huber and Wächtershäuser, 1997; Peretó et al., 1999; Martin and Russell, 2003, 2007; Say and Fuchs, 2010; Martin, 2020; Boyd et al., 2023). That life was first engaged in the reduction of oceanic CO_2 through the acetyl coenzyme-A pathway was incorporated in AVT and expressed in the (grossly) oversimplified empirical Equation 1 (Russell and Martin, 2004)

$$2CO_2 + HSCoA + 4H_2 \rightarrow CH_3COSCoA + 3H_2O \qquad (1)$$

But more recently, we have argued for an alternative whereby the disequilibria across a ferrous–ferric oxyhydroxide membrane—with FeS now as a subordinate—are several and the potentials significantly greater, namely, the 'denitrifying methanotrophic acetogenic pathway' (DnMAP; Ducluzeau et al., 2009; Nitschke and Russell, 2013). This suggestion arises: (1) in consideration of methane emanations accompanying H_2 in some serpentinizing systems—an overlooked otherwise 'wasted' fuel and source of organic carbon (Kelley, 1996); (2) the 'energetic' requirement for an electron acceptor with a higher potential than CO_2 to order protometabolism (Russell and Hall, 1997; Nitschke and Russell, 2013); (3) in choosing the methanotrophic route, the steep uphill 'free' energy climb to the highly unstable formyl intermediate in the classic acetyl coenzyme-A pathway is avoided (Maden, 2000; Stojanowic and Hedderich, 2004); (4) to provide a source of ammonium, which otherwise is lacking (Nitschke and Russell, 2013); (5) and the ungainliness of the classic pathway's two 'legs', i.e., the disproportionate numbers of the reductive steps involved, one to reduce CO_2 to CO or formate, as against six to reduce it to a reactive methyl sulfide entity, is replaced by the more symmetrical, less complicated 'CO_2-reducing and denitrifying methanotrophic pathways' that converge to acetyl coenzyme-A (DNitAP; Nitschke and Russell, 2013). This pathway is also highly simplified to

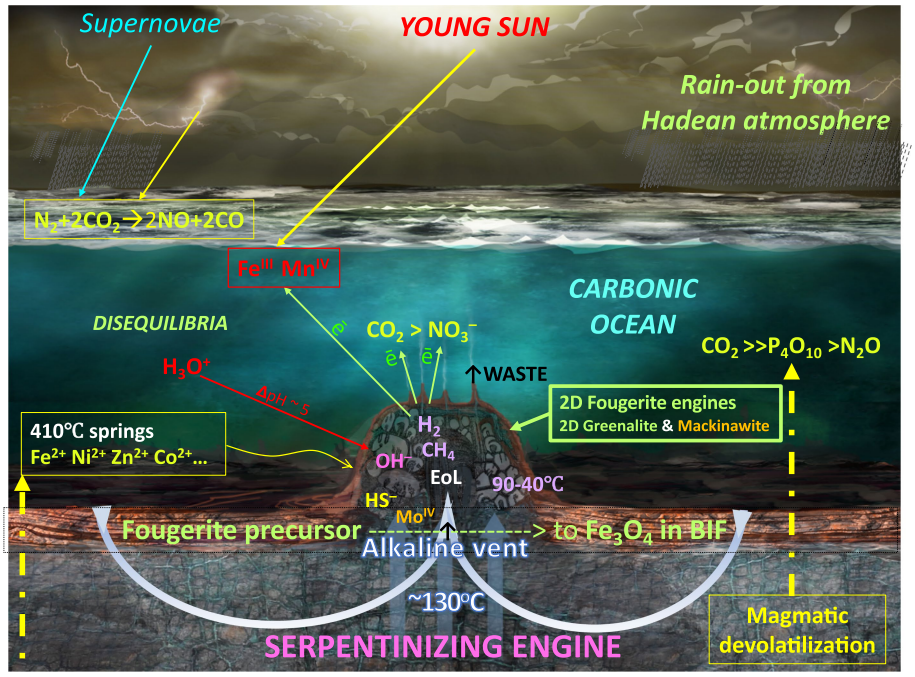

FIGURE 1
Initial conditions responsible for the emergence of life (EoL) according to the alkaline vent theory (AVT; Russell et al., 2013). Mantle-derived volcanic emanations (>700°C) and high temperature acidic hot springs (~410°C) inject CO_2, P_4O_{10}, some N_2O, and the transition elements directly through the Hadean ocean floor into the cool carbonic Hadean ocean (Yamagata et al., 1991; Javoy and Pineau, 1991; Macleod et al., 1994; Kasting and Siefert 2001; Wong et al., 2017; Mandon et al., 2019; Ueda and Shibuya, 2021; Brady et al., 2022; Buessecker et al., 2022; Heays et al., 2022; Nishizawa, 2022; Tatzel et al., 2022). At the ocean bottom, and diffusing laterally and upward, these volatiles and ions remain as saturated or supersaturated until meeting with alkaline hydrothermal solutions (at ≤130°C) produced by the serpentinization engine (Barnes and O'Neil, 1969; Russell et al. 1989; Branscomb and Russell, 2018; Shibuya and Takai., 2022). Fougerite, along with subordinate amorphous silica, greenalite, and subsidiary mackinawite spontaneously precipitate at the interface between the alkaline solution and the ocean solvent (Russell, 2018; Tosca et al., 2016, 2019; Borrego-Sánchez et al., 2022). These inorganic barriers maintain the pH and redox disequilibria that drive the emergence of life (EoL; Russell and Hall, 1997), so focusing the electrochemical disequilibria as native electrons, cations, anions, and dissolved gasses across the fougerite exteriors of the mound. Thus, these nanocrysts, assisted by the electron-conducting mackinawite, are forced into acting as nanoengines to resolve the disequilibria and thereby bring embryonic life into being (Arrhenius, 2003; Mielke et al., 2010; Nitschke and Russell, 2012, 2013; Barge et al., 2015a; Halevy et al. 2017; Russell and Nitschke, 2017; Wong et al., 2017; Yamamoto et al., 2017, 2022; Kitadai et al., 2018; Duval et al. 2019; Ooka et al., 2019; Hudson et al., 2020; Nitschke et al., 2022; Buessecker et al. 2022). [NB., The electron acceptors and the H^+ shown to be dissolved in the ocean are constantly delivered by the venturi effect to the outer barrier of the mound (Russell and Hall, 1997)]. Redrawn from Branscomb et al. (2017). An extensive aureole of the same minerals surround this and other vents, now altered to banded iron formation (BIF; Konhauser et al., 2007; Pons et al., 2011; Mloszewska et al., 2012). Not to scale. The serpentinite photograph was generously provided by Laura Barge.

$$\left\{4H^+ + CO_2 + N_2O\right\}_{\text{ocean}} + \left\{8H\bullet + CH_4 + HS^- + OH^-\right\}_{\text{hydrothermal}} \rightarrow \left\{CH_3COSH + 2NH_4^+\right\}_{\text{metabolism}} + 3H_2O_{\text{waste}} \quad (2)$$

Apart from the addition of methane, this alternative takes into account the disequilibria focused at a submarine alkaline vent as outlined in Russell and Hall (1997): the natural proton motive force and a 'respiratory' redox mechanism with electrons (some of them bifurcated) that H_2, *via* 2H•, provides, processing through a green rust (fougerite) nanoengine as electrons are conducted to high potential electron acceptors, e.g., nitrate (Nitschke and Russell, 2012, 2013; Barge et al., 2015a; Russell and Nitschke, 2017; Wong et al., 2017; Buessecker et al. 2022; Nitschke et al., 2022). We reiterate that this reductive mechanism also accounts for the required on-site source of ammonium for amino and nucleic acid synthesis, otherwise far from obvious (Barge et al., 2019).

Yet, a further change to AVT was the adoption of the term 'emergence', as we came to understand that the conventional 'origin of life' was an idiom devoid of evolutionary connotation (Russell et al., 1993)—this from the readings of Prigogine and Stengers' (1984) book "Order out of Chaos" and Wicken's (1987) volume "Evolution, Thermodynamics and Information." Indeed, contemplating life's 'emergence' forced a more serious consideration of the role of serpentinization in life's onset (Russell et al., 2013).

In the present theoretical contribution, life's emergence is traced from serpentinization to its fledging as a dynamic system that dramatically reduces entropy (thus substantially increasing the rate at which the driving disequilibria produce entropy). We conclude that the first proto-metabolic steps take place in the natural chemical garden spires that developed at a submarine alkaline hydrothermal vent sometime in the ~500 million year span of the Hadean era. Exothermic serpentinization is the mega-engine operating within the ultramafic oceanic crust that works to drive alkaline hydrothermal convective systems bearing $H_2 > CH_4$ fuels to exhale into the then carbonic, phosphate, nitrate, NO, and N_2O as well as metal complex-, and proton-bearing acidulous ocean—the disequilibria resulting in autotrophic metabolisms involving quinone-dependent NO reductase and membrane-bound N_2O reductase—supporting a primitive

aerobic respiration (Ducluzeau et al., 2009, 2014; Nitschke and Russell, 2013; Russell et al., 2013; Brady et al., 2022; Buessecker et al., 2022; Farr et al., 2022).

This is where the structural and ionic complexity of the 2D green rust mineral fougerite (~$Fe^{2+}{}_4Fe^{3+}{}_2(OH)_{12}CO_3.3H_2O$) moves to center stage in AVT. Initially precipitated as white rust (amakinite) under alkaline conditions, the oxidation by water to fougerite—with the concomitant evolution of H_2—is rapid (Trolard et al., 2022; Helmbrecht et al., 2022). Though more ordered, i.e., of lower entropy than those of the contributing solutes, amakinite/fougerite precipitation is entropy-driven (Van Santen, 1984). The structure of fougerite (formerly green rust) is complex but not "pre-designed," i.e., its growth is not algorithmic, it is merely self-ordered and requires no prescription (*cf.* Arrhenius, 2003; Abel and Trevors, 2006). It is the only macromolecular entity known to us with the chemical and physical flexibility and potential to respond to disequilibria at the vent. Thus, we propose that it has the wherewithal to act as the nanoengine to impel life into being. The iron sulfides mackinawite (FeS) and greigite (Fe_3S_4)—as subordinate components of the hydrothermal chimneys and spires—still hold vital support roles in their 'free energy' converting capacities and as conductors and semiconductors in AVT (Nitschke and Russell, 2009; Vasiliadou et al., 2019; Hudson et al., 2020).

2. Serpentinization—life's mother engine

The casting of exothermic serpentinization of ocean crust as a disequilibria- ("free energy"-) converting mega-engine (Russell et al., 2013) is based on an extensive literature (Barnes and O'Neil, 1969; Barnes et al., 1978; Neal and Stanger, 1983, 1984; Fallick et al., 1991; Kelley et al., 2001; Lowell and Rona, 2002; Russell and Arndt, 2005; Mielke et al., 2010; Paukert et al., 2012; Russell et al., 2013; Branscomb and Russell, 2018). Inspiration was rooted in the physics of materials, as considered by Cottrell (1979), whereby mechanical stress is converted through feedbacks, as in an engine, into physical and chemical disequilibria such as to result in "living things," themselves engines. How might we see such engines developing in the early Earth?

With Hadean days so short, the moon so close, and the Earth's mantle so soft, the mafic to ultramafic oceanic crust suffers pulses of incessant cracking, jointing, faulting, and brecciation that allow the invasion and gravitation of cool ocean water to depth (Miller et al., 2016; Heller et al., 2021; Tatzel et al., 2022). Once cracks form in a tensile stress regime near the surface, feedback ensures that smaller stresses are required to keep them ratcheting down through the crust as exothermic cracking engines (Cottrell, 1979; Lowell and Rona, 2002). Furthermore, the hydrostatic pressure so imposed increases the effective stress, though only after the crack has propagated at the nanoscale, feeding back to further cracking while the elasticity at the tip is converted to 'free energy'—a counter-intuitive realization (Cottrell, 1979). Such an autocatalytic feedback is further augmented by the hydrostatic pressure imposed on the mafic to ultramafic wallrock by the ocean waters gravitating to depth—a pressure that increases both the effective tensile and related sheer stresses (Cathles, 1990; Russell and Skauli, 1991). These couplings eventuate in the cracks reaching brittle-to-ductile transition zones in ultramafic rocks estimated from the hydrogen isotope work of Proskurowski et al. (2006) to bottom out at ~150°C, corresponding to an eventual maximum crustal depth of around 8–10 km (Macleod et al., 1994). This self-ordering and self-healing process continues until much of the upper crust is hydrated and carbonated, causing a lowering of density ($\gtrsim 2.6\,g\,cm^{-3}$) compared to the antecedent unaltered ultramafic crust ($3.3\,g\,cm^{-3}$), through expansion allowed for by crustal extension and/or domal uplift in processes leading to further cracking (Fujioka et al., 2002; Pons et al., 2011).

The exhaust from the serpentinizing system—as heat and solutes—is discharged in convective hydrothermal alkaline updrafts buffered to a pH of 10–11 units guided by approximately vertical fractures in a process that lasts a minimum of 30,000 years (~10^{21} nanoseconds; Früh-Green et al., 2003). The tectonic, thermal, and chemical disequilibria are resolved through hydrothermal convection to result in a hydrothermal fluid—initially carbonic ocean water—by being reduced to H_2 and short carboxylic acids and sparse methane (Früh-Green et al., 2003; Proskurowski et al., 2006; Ludwig et al., 2011; Tutolo et al. 2020; White et al., 2020; Albers et al., 2021; Figure 1; Equation. 3):

$$\begin{aligned}&\{12Ca_{0.25}Mg_{1.5}Fe_{0.25}Si_2O_6\}_{augite} + 16H_2O \rightarrow \\ &\{6Mg_3Si_2O_5(OH)_4 + 12SiO_2 + Fe_3O_4\}_{serpentinite} + \\ &+3Ca^{2+} + 6OH^- + H_2\uparrow\end{aligned} \quad (3)$$

Tidal and seismic pumping are additional inputs to the workings of this complex engine (Sibson et al., 1975; Davis and Becker, 1999; Glasby and Kasahara, 2001).

Spasmodic charges of methane, as well as of formate and acetate, are also recorded, both by a direct analysis and in laboratory experiments (Shock, 1992; Windman et al., 2007; White et al., 2020). However, it may be that much of the methane is derived through leaching from that generated in the lower crust and entrained in the same solutions (Shock, 1992; White et al., 2020). This thermal and chemical waste from serpentinization is now transported to the ocean floor in a hydrothermal solution that finds itself well out of thermal and electrochemical equilibrium with its new host, the iron-rich carbonic ocean water from which it first derives (Figure 1). Furthermore, the immediate effect of the meeting of the two contrasting solutions is the spontaneous precipitation of iron oxyhydroxides accompanied by silica and minor iron sulfides (Barge et al., 2015a,b, 2020; Helmbrecht et al., 2022). A portion of the precipitates makes up the hydrothermal chimneys and spires, while entrained flocs escape from this, and other alkaline springs, to disperse and lithify to banded iron formations comparable to those in Isua in the early Archean of western Greenland and in the Hadean Nuvvuagittuq greenstone belt in Canada (Appel, 1980; Papineau et al., 2011; Pons et al., 2011; Mloszewska et al., 2012; Halevy et al., 2017; Tosca et al., 2019; Bindeman and O'Neil, 2022).

The membranes precipitated at the hydrothermal mound have the effect of frustrating the release of the pent-up disequilibria, until a weakness can be found to guide interaction of the contrasting fluids. In the case of serpentinization and convection—the mega-engines just described—this was *via* chance cracks in the crust. However, at the nanoscale, the dissipative system finds a way to partial relaxation by the forced exploitation of nanochannels prized from hydrous cleavage cracks constituting fougerite interlayers (Figure 2). Furthermore, the redox- and pH-active nanochannels

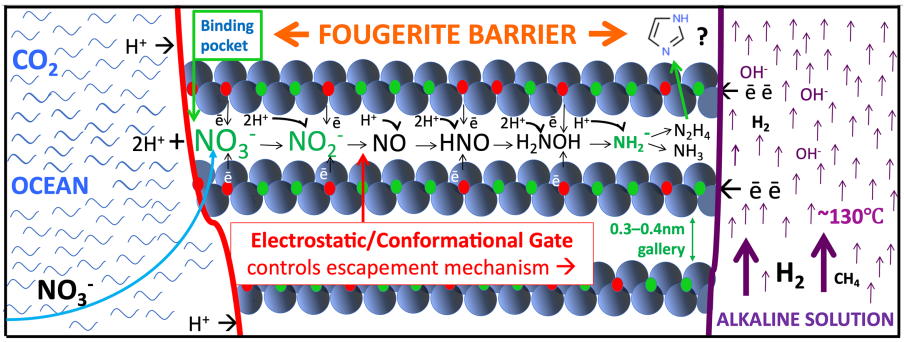

FIGURE 2
Fougerite modeled as a ready-made multifunctional motor enzyme/pump precursor set in the inorganic membrane, wherein it reduces nitrate drawn from the ocean (curved blue arrow to the left) to aminogen or ammonium, or nitrite to NO, N_2O, and N_2, vectored from 'left' to 'right' within the hydrate galleries (Hansen et al., 2001; Génin et al., 2005, 2006; Trolard et al., 2007, 2022; Trolard and Bourrié, 2012; Gerbois et al., 2014; Russell, 2018; Duval et al., 2019, 2020). At the same time and in theory, methane would be converted to a methyl group by NO (Kampschreur et al., 2011; Nitschke and Russell, 2013). Barge et al. (2019, 2020) show that in the same circumstances, pyruvate can be aminated to alanine and oxalate to glycine. Hydrazine is another speculative product (Duval et al., 2020). Note that an anion-binding pocket forms by the oxidation of the opposed iron molecules as they are confronted with nitrate which is thereby reduced (Nitschke and Russell, 2013). However, transmission ('escape') of a product to the interior is only permitted (ungated) when the nitrite is itself reduced to neutral NO and can be driven by the ionic gradients further into the interlayer. Note too that the flows (and counterflows) are vectorial, controlled by electron hopping rates (Wander et al., 2007). There is an expectation that short peptides will be produced within the interlayers (Muñoz-Santiburcio and Marx, 2017; Erastova et al., 2017; Grégoire et al., 2018; Holden et al. 2022) and partially extruded into the spire's interior. Further H_2 and organic molecules can be released to the hydrothermal flow by delamination and/or diagenetic alteration of fougerite to magnetite at depth in the mound (Asimakidou et al., 2020; Farr et al., 2022). The upward-directed arrows to the right signify the alkaline hydrothermal updraft, and the smaller arrows either side of the fougerite representing the inorganic membrane denote the direction of electron and proton flow. Not to scale.

within the interlayers might impose a vectorial two-way ordering—a primitive guidance system—along the reductive and oxidative synthetic steps of the denitrifying methanotrophic acetogenic pathway toward an incomplete reverse tricarboxylic acid cycle (TCA) (Hartman, 1975; Wander et al., 2007; Nitschke and Russell, 2013; *cf.*, Gatenby and Frieden, 2017; Figure 2).

Thus, a way is open, even at the nanoscale for a specialized dissipative (entropy-generating metabolizing) engine to materialize in obeyance to the Universe's predilection to 'produce' ever more disorder in its blind bid to continue its relaxation, independent of scale, from its initial excruciating disequilibrium at the origin of space–time (Nitschke and Russell, 2010; Russell et al., 2013; Carroll, 2016).

3. Life is, and was at its emergence, a disequilibria-converting macromolecular nanoengine

The series of orderly convection engines governed by physical transitions in the body of our planet, brought to a head by the serpentinization cracking engine, ultimately results in a long-lasting flow of reduced alkaline fluids into a highly contrasting relatively oxidized and mildly acidic Hadean seawater. Furthermore, the interactions of two solutions at the spontaneously precipitated membrane provide just the electrochemical disequilibria required to drive entropy-reducing metabolic pathways and reproductive cycles (Hitchcock and Lovelock, 1967; Russell and Hall, 1997; Russell and Arndt, 2005; Nitschke et al., 2022). However to bring these factors into play, disequilibria-converting engines are again required. Yet, the building components for construction are necessarily restricted to any inorganic materials at hand. Of course, at every step, engines must locally disproportionate entropy in such a ratio as to ensure its decrease in the driving of anabolic metabolism by an overall larger increase in entropy. This is achieved by the transportation of uncooperative molecules as waste from the partially open protometabolizing system.

Glaringly obvious is the requirement for the coupled hydrolysis of adenosine triphosphate, ATP, in present-day life—and thereby the need for its synthesis (Whicher et al., 2018; Pinna et al., 2022). To achieve such biosynthesis, Mitchell (1961) showed a pH gradient—a proton motive force—to be capable of driving the condensation of adenosine diphosphate (ADP) and inorganic phosphate (Pi) to adenine triphosphate (ATP) *via* the complex enzyme ATP synthetase situated in life's membranes. Thus, Mitchell apparently dispensed with the long-favored view that a 'high energy' intermediate molecule was responsible, calling his process 'chemiosmosis'. However, Boyer (1997) first made mechanical sense of Mitchell's finding, demonstrating that ATP synthetase is actually a rotating nanoengine involving 'binding-change' and gated escapement mechanisms driven by the proton gradient. In life, protons are delivered by the machinations of complex 1 and the like (Hedderich, 2004; Kaila, 2021). Boyer mapped out the stages the ATP synthetase rotatory enzyme took to complete the cycle, realizations now fundamental to an understanding of how life works and indicating how some, albeit simpler engine must have worked from the very beginning (Boyer, 1979, 1997; Astumian, 2012; Astumian et al., 2016; Anashkin, et al., 2021). For reasons of pedagogy, Yoshida et al. (2001) compare the ATPase to a Wankel engine, while Carter (2020) likens the binding change and reciprocally coupled gating mechanism to escapements in the workings of a mechanical clock.

Important though ATP is, clearly ATP synthetase itself is much too complicated to have been available at life's onset. Indeed, the discovery by Baltscheffsky et al. (1966) that inorganic pyrophosphate (PPi), situated in the membrane, can act as 'energy donor' in an

electron-transport phosphorylation system introduced the hypothesis that a proton pyrophosphatase (H^+-PPase) was a precursor to the ATP (Russell et al. 1994; Baltscheffsky et al., 1999). These reversible vacuolar pyrophosphatases are stochastic nanopumps (Lin et al., 2012, Li et al., 2016), in which a highly restricted number of water molecules within the axial region have the effect of dampening the flow of protons or cations. The protons make their way one-by-one through the gating mechanism, either inward or outward, depending on the ambient disequilibria (Branscomb and Russell, 2013, 2019; Scholz-Starke et al., 2019; Astumian et al., 2020).

However, PPi has strong competitors as a phosphorylating agent, e.g., acetyl phosphate [AcP]. Acetyl phosphate itself is readily generated from thioacetate and disodium phosphate under alkaline conditions (Heinen and Lauwers 1996; Huber and Wächtershäuser, 1997; Whicher et al., 2018). AcP is especially attractive as a precursor candidate of ATP (Pinna et al., 2022). Furthermore, Whicher et al. (2018) demonstrate the phosphorylation of ribose to ribose-5-phosphate and the phosphorylation of ADP to ATP also under alkaline conditions—the only nucleoside diphosphate to be thus phosphorylated—so explaining the primacy of ATP in bioenergetics (Pinna et al., 2022). Given that Wang et al. (2019) produce PPi from AcP and Pi, but not from 2Pi across an Fe-rich membrane in a microfluidic rig, would leave AcP as, perhaps, the major phosphate player in early metabolism. However, there are still other compounds such as the linear oligophosphates, glycolaldehyde phosphate (Arrhenius et al., 1993; Pitsch et al., 1995; Krishnamurthy et al., 1999), and the cyclic trimetaphosphate (TMP) shown by Etaix and Orgel (1978) to be capable of phosphorylating nucleosides in water—a discovery transferred into the 2D interlayers of the double-layer oxyhydroxides (DLHs; Yamanaka, 1988; Kuma et al., 1989; Yamagata et al., 1997; Kolb et al., 1997). Kolb et al. (1997), using TMP, induce phosphorylation of the glycolate ion in the interlayers of DLHs to glycolophosphate and diphosphate at a rate which is independent of the external concentration of glycolate ion in the range of 1–100 mM as measured—a remarkable and highly significant finding as we shall see. The phosphorylation can be followed by measuring the height of the interlayer; the initially absorbed hydroxyl height measures 0.29 nm, the glycolate replacement is 0.49 nm, and the trimetaphosphate (TMP) on its own is 0.68 nm, while adding TMP to glycolate to produce glycolophosphate plus the diphosphate generates a height of only 0.64 nm (Adam and Delbrück, 1968; Kolb et al., 1997).

Distinct from, and additional to the pyrophosphatase argument, and following Wächtershäuser (1990) and Peretó et al. (1999), the direct reduction of carbon dioxide *via* the reductive acetyl coenzyme-A pathway was next considered, though in terms of an inorganic FeS membrane rather than through the pyrite reaction (Russell and Martin, 2004). Branscomb and Russell (2013) modeled such a reduction involving the hydrogenation of CO_2 dissolved in, and sourced from, the most ancient ocean, combined with that ambient proton force in a membrane comprising iron monosulfide and fougerite. Several authors calculate that the proton motive force summing to 2 pH units or more (equivalent to ~120+ mV) will facilitate the reduction of CO_2 in alkaline waters (Russell and Hall, 1997; Schoepp-Cothenet et al., 2013; Sojo et al., 2016). Since then, and following Vasiliadou et al. (2019), Reuben Hudson and his coworkers have tested the latter hypothesis which is of direct relevance to the AVT using a microfluidic technique involving an iron sulfide membrane, duly demonstrating the requirement for "proticity" in such a reduction (Hudson et al., 2020). Whether fougerite, lightly dosed with sulfide, could achieve a similar result awaits experimental testing. However, fougerite's propensity to enforce redox reactions as well as its ability to interconvert redox and pH gradients is now well known (Hansen et al., 2001; Génin et al., 2005, 2006; Figure 2). Left hanging is fougerite's possible role as a precellular inorganic non-ribosomal peptide synthetase (Bernhardt, 2019).

4. The fougerite nanoengine and the drive to metabolism

Our realization that prebiotic chemistry could not explain the extreme reduction of entropy involved in the emergence of life focused attention on the ferroferric DLH, green rust—now named by its discoverer, Fabienne Trolard, 'fougerite' (Trolard et al., 2007). Arrhenius (1984, 2003) and Arrhenius et al. (1997) were the first to see the benefits of considering green rust/fougerite (and comparable non-redox but positively charged DLHs) in this precellular context, owing to, (1) its premetamorphic abundance in Archaean banded iron formations (Arrhenius et al., 1997; Halevy et al., 2017), (2) its propensity to selectively absorb anions where, in the 2D interlayers, the effective concentrations are increased up to a million-fold (Delbrück, 1970; Arrhenius et al., 1993; Pitsch et al., 1995), (3) its "structures"; capable of dynamic agency while limiting degrees of freedom (Pitsch et al., 1995; Kolb et al., 1997), (4) its potential, sited within and as a membrane separating two strongly contrasting solutions, to respond to environmental perturbations for the sake of continued growth, *cf.*, Mitchell, 1959), and (5) such arrangements might provide the governance required for the emergence of ordered reproduction (Popov, 1999; Arrhenius, 2003; Greenwell and Coveney, 2006; Galimov, 2014; Endres, 2017; Branscomb et al., 2017; Cartwright and Russell, 2019; Gribov et al., 2021). We might add the speculation, derived from other DLHs, that its variable pattern of cations could affect the configuration of any nucleic acids produced in the system, eventually resulting in a functional polymeric sequence of nucleic acids to govern the established metabolisms (Erastova et al., 2017; Grégoire et al., 2018).

That fougerite is conformationally flexible and responds reversibly and interactively to environmental pH and redox conditions as Génin et al. (2005, 2006), Ruby et al. (2010) demonstrate also supports the hypothesis that fougerite is the precursor to the 'free energy'/disequilibria-converting enzymes involved in conformational cycling (Nitschke et al., 2022; Equation 4):

$$Fe^{2+}{}_4Fe^{3+}{}_2(OH)_{12}CO_3.3H_2O + 2H^+(re)\text{protonation} \sim \text{reduction} \Leftrightarrow Fe^{2+}{}_2Fe^{3+}{}_4(OH)_{10}CO_3.3H_2O + (H_2O_2)\text{deprotonation} \sim \text{oxidation} \quad (4)$$

a view warranted in consideration of the remarkable experiments of Hansen et al. who demonstrate the power of fougerite to effect the ready reduction of nitrate to ammonia—a process involving the addition of eight separate electrons to the initial nitrate as fougerite is reduced to magnetite (Hansen et al., 1996; Génin et al. 2008; Russell, 2018; Asimakidou et al., 2020). Moreover using similar conditions, Gerbois et al. (2014) demonstrate the reduction of nitrite to NO, N_2O, and N_2. These capabilities demonstrate an enzyme-like agency of fougerite in out-of-equilibrium geochemical systems—engineering conversions not only comparable to the nitrate and nitrite reductases, but also comparable to the enzymes such as methane monooxygenase,

aminotransferase (transaminase), and acetyl phosphatase, an inorganic phosphoesterase, and, perhaps, a non-ribosomal peptide synthetase (Russell, 2018; Barge et al. 2019; Bernhardt, 2019; Branscomb and Russell, 2019; Duval et al., 2019; Huang, 2019, 2022; Wang et al., 2019).

An accompanying nickel-bearing iron sulfide mineral, mackinawite, is also planar conducting and can act as a hydrogenase ($H_2 \rightarrow 2\bar{e}$), ferredoxin, carbon-monoxide dehydrogenase, and acetyl coenzyme-A synthase (Hudson et al., 2020). Together, these are the conversions required to make the first ordered steps to autogenic life fed by H_2, CO_2, CH_4, HNO_3^-, HNO_2^-, NO, and PO_4^{3-} with an ambient steep proton gradient (Russell and Martin, 2004; Schoepp-Cothenet et al., 2013). Experiments grounded in the submarine alkaline vent model for life's emergence have largely demonstrated that these conversions—this "sucking of order" from the environment (Schrödinger, 1944)—had the capacity to get autotrophic (self-ordering, self-sufficient, self-sustaining, though not self-referencing) metabolism started (Russell et al., 2003; Nitschke et al., 2022).

Having some similar properties to enzymes, these minerals or their macromolecular precursors should give us a better understanding of biological phenomena (Smith, 1986; Branscomb and Russell, 2019). Indeed, the jarring conclusion is forced that only these two minerals together can execute most of the disequilibria conversions required by the first ordered steps to autogenic life fed by H_2, CO_2, CH_4, HNO_3^-, HNO_2^-, NO, and PO_4^{3-} with an ambient steep proton gradient (Barge et al. 2019; Hudson et al., 2020). In this view, the rates of synthesis would be governed independently of variations and fluctuations in chemical concentrations and pressure through the viscosity of water 'trapped' in the confined spaces of the interlayers, which consequentially severely restrict the degrees of freedom of the system (Kolb et al., 1997; Astumian, 2007; Muñoz-Santiburcio and Marx, 2017; Branscomb and Russell, 2019). Furthermore, although fougerite is a 2D mineral, motions within the interlayers would be generally restricted to 1D as the 0.56-nm iron-to-iron hopping rate to next-nearest neighbors is ~ 10^{10} s^{-1} at standard temperature and pressure (STP), 3 orders of magnitude faster than those of the other two symmetry-unique hops, thus imposing vectorial flow, as in modern cells, but through the 'green rust' interlayers (Wander et al. 2007). This electron tunneling activity would tend to pull the more laggardly protons in single file in the hydrous interlayers by the Grötthuss mechanism (Muñoz-Santiburcio and Marx, 2017).

5. Chemical garden setting

Fougerite, acting as the first nanoengine driving emergent metabolism, has to be mounted and secured in the inorganic membrane such as to cater for, and feed, order-for-order exchanges while concomitantly allowing for an entropy increase *via* waste disposal. In an attempt to resolve how this might turn out to be, we return to consider the natural chemical garden membranes comprising this ferroferric-carbonate DLH and subordinate iron sulfides, further buttressed, perhaps, by silica and/or greenalite (Mielke et al., 2011; Russell et al., 2013; McMahon, 2019; Tosca et al., 2019; Barge et al., 2020, 2015a; Rasmussen et al. 2021). These are the minerals comprising the Hadean to Archaean banded iron formations (Halevy et al., 2017; Tosca et al., 2019), which are presumed to be the overspill of hydrothermal exhalations (Russell, 1975; Pons et al., 2011; Mloszewska et al., 2012).

As usually understood, crystal-hydrate gardens are self-ordered structures driven by the osmotic flow of the external alkaline water across a spontaneously precipitated semipermeable barrier (inorganic membrane) drawn inward by the high concentrations of a hydrous acidic salt as it dissolves in its water of crystallization (Leduc, 1911; Cartwright et al., 2002; Barge et al. 2012, 2015b). Growth is generally limited to tens of minutes to a few hours by the initial crystal's mass as a result of the time taken to approach equalization of the ionic (and thereby the hydrostatic) pressures as inhibited by water stiction (Ding et al., 2016). Perret (1960) suggests that the spontaneous occurrence of expanding systems in a non-living environment such as a chemical garden might mark the first step toward the evolution of living organisms. However, in the case of the hydrothermal gardens, the expansion would mostly be the result of injection of alkaline into an ambient acidulous solution rather than osmosis (Russell et al., 1989, 1994; Russell, Hall, 1997; Mielke et al., 2011; Barge et al., 2015a). The chemical garden-like spires would continue to develop incrementally as the internal fluid perforates or breaks through, mostly at the top where the membrane is the thinnest, and reacts with the ambient fluid to produce a further segment (Barge et al., 2015b). The flow in this case is not osmotic, but 'chemiosmotic', where the inward transmission of individual protons via the Grötthuss mechanism (Muñoz-Santiburcio and Marx, 2017) is ~6 orders of magnitude faster than the outward velocity of hydroxyl ions as calculated for iron monosulfide membranes in the microfluidic experiments of Vasiliadou et al. (2019).

Extrapolation from similar microfluidic experiments involving chemical garden-like membranes comprising fougerite, as well as subsidiary mackinawite nanocrysts, is expected to reduce these external protons to hydrogen, and reduce carbonate to carbon monoxide and carboxylic acids; nitrate and nitrite to nitric oxide and ammonium; and furthermore, that the ammonium ion would aminate the carboxylic ions to the 'short' amino acids such as glycine, alanine, aspartate, serine, ornithine, and lysine (Hafenbradl et al., 1995; Huber and Wächtershäuser, 1998; Grégoire et al., 2016; Barge et al., 2019). Furthermore, there is some evidence to suggest that such amino acids would condense to short peptides within the confines of the interlayers of the fougerite and other DLHs where most of the water is not free, but is bound to the interior walls or even on their outer surfaces (Huber and Wächtershäuser, 1998; Rode, 1999; Huber et al., 2003; Grégoire et al., 2016, 2018; Erastova et al., 2017; Muñoz-Santiburcio and Marx, 2017; Branscomb and Russell, 2019; Rimola et al., 2022). In broad support of this view, Holden et al. (2022) show, using the electrospray mass spectrometry, that a substantial reduction in water activity does drive the condensation of glycine and alanine to dipeptide and, in droplet fusion reactions, protonated tri- and tetra-glycines. Additions of single glycines thereafter produced Gly_6, an introduction to a peptide 'world' (Holden et al. 2022). Moreover, Boigenzahn and Yin (2022) demonstrate the condensation of glycylglycine to oligoglycines driven by trimetaphosphate at low water activities (*cf.* Yamagata et al., 1997).

6. A peptide world sequestering inorganic anions with improvement in reproduction

The formation of peptide isomers on the microsecond timescale within the interlayers on fougerite could further support the potential

role of confined-volume systems in abiogenesis. That is, by membrane, cell-wall, and biofilm-like structures built from materials generated on site rather than from random organic molecules supposedly delivered haphazardly to the mound from Fischer–Tropsch reactions and the like, generated remotely at depth in the crust (Muñoz-Santiburcio and Marx, 2017; Holden et al., 2022; Römling, 2022). The addition of amino acids and short peptides to the inorganic membranes renders the chemical gardens significantly more durable (Russell et al. 1994; McGlynn et al. 2012; Barge et al., 2019; Hooks et al., 2020; Flores et al., 2021; Borrego-Sánchez et al., 2022). Moreover, as so generated, the backbone amides in short peptides would prove irresistible to inorganic ions and complexes through hydrogen bonding in the membrane—sequestering them to make enzyme-like structures such as hydrogenase and ferredoxin analogs (Nitschke and Russell 2013; Nitschke et al. 2022). Furthermore, being attractive to each other, they can produce robust peptide membranes involving the same ions—the beginning of the organic takeover (Zhang et al., 1993; Milner-White and Russell, 2005, 2008, 2011; Maury, 2009; Bianchi et al., 2012; Zhang, 2012; Kandemir et al., 2016).

Baranov et al. (2016) note that flexible linear peptides would have more structural uses and functions than cyclic molecules in the first stages of life. Moreover, Popov (1999) emphasizes that the peptide folding itself is a nonlinear non-equilibrium thermodynamic process. Intriguingly, H^+-PPases boast of a phosphate-binding site, a protein loop (P-loop) homologous with that of ATPases, that sequesters phosphate. And just such a peptide has since been assembled in the laboratory from a mixture of simple amino acids rich in glycine, whereby its flexible backbone is shown to cosset and sequester phosphate with two of the three main chain NH groups comprising the glycine-rich peptide backbone, that is, through hydrogen bonds to the phosphate ion which thereby bridges it to take the concave form (Milner-White and Russell, 2008; Bianchi et al., 2012).

The discoveries that both bacteria and archaea have prion-like domains allow the consideration of prions being pre-LUCA (Prusiner, 1998; Zajkowski et al., 2021). It is notable that uncoded peptides are self-recognizing and tend to arrange themselves as parallel α-sheets that can spontaneously convert into the more stable and insoluble amyloid β-sheet by plane flipping (Armen et al., 2004; Milner-White et al., 2006; Hayward and Milner-White, 2008, 2021; Milner-White, 2019). Such self-propagating and temperature-resistant sheets are much stronger than lipids and have the potential to act at the emergence of life in such roles as cell membrane/cell walls and biofilm analogs (Kosolapova et al., 2020). Furthermore, comprising membranes their backbones can sequester metals and phosphate without reliance on the side-chain order (Zhang et al., 1993; Milner-White and Russell, 2005; Childers et al., 2009, 2010; Maury, 2009; Greenwald and Riek, 2010; Li et al., 2010; Goodwin et al., 2012; Milner-White, 2019). Other short peptides that do involve side chains have shown similar or superior mastery over metal-ion chelation and, thereby, agency (Aithal et al., 2023; Timm et al. 2023).

Of course, the popular view is that lipids constituted the first organic membranes but there is no theoretical or experimental evidence to suggest how they would be produced in the protometabolic system autotrophically at plausible rates and temperature. What use would they have beyond acting, as they do today, as membrane fillers and lubricants? After all, in contrast to lipids, peptides and amyloids are, (i) interactively cooperative with other ions, (ii) stronger as in their involvement in a web-like role in cell walls, strong enough even to contain turgor pressures (Kandler and König, 1998; Desvaux et al., 2006), (iii) can be seen to have roles extending to the enzyme structure, proteins, and cofactors, (iv) as well as much of the membrane, and (v) as prions they seemingly offer autonomous and 'intentional exploration' of space and time for similar disequilibria (Chernoff, 2004; Lupi et al., 2006; Maury, 2009; Coca et al., 2021; Jheeta et al., 2021; Zajkowski et al., 2021).

Under alkaline vent conditions, amyloid peptides and amyloid fibrils would be expected to exude from the interlayers to produce organic molecular webs adhering to the spire's inner walls as metal-dosed organic films (Takahashi and Mihara, 2004; Larsen et al. 2007; Römling, 2022; Figure 3). Subject to entrainment in the hydrothermal updrafts, some of this amalgam is likely to spall off in the general direction of flow, eventually crowding and necking to form offspring capable of interacting and sharing the peptide film (Milner-White and Russell, 2005; Larsen et al. 2007; Greenwald and Riek, 2010; Greenwald et al., 2018; Römling, 2022). Yet, it is admitted that this speculation falls well short of how prions in membrane or cell-wall microbes could segue to a peptide–nucleotide world governing metabolic pathways and the reverse Krebs cycle (Gallardo and Rodhe, 1997; Schumann and Huntrieser, 2007; Carey et al. 2016; Weiss et al. 2016; Bromberg et al., 2022; Harrison et al., 2022; Lane, 2022; Palmeira et al., 2022). For this, we are forced to consider the emergence of an albeit imperfect genetic governance to get life into its historical and present role.

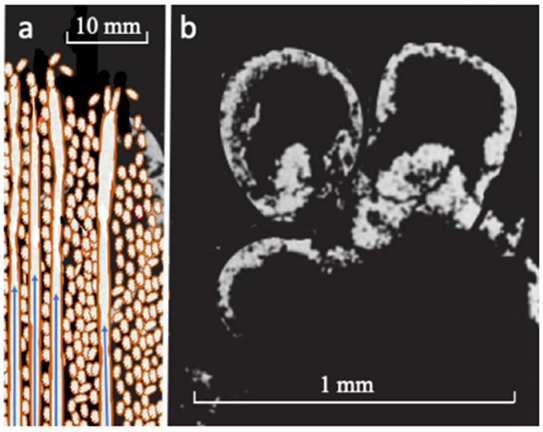

FIGURE 3
(A) Sketch of chemical garden spires comprising ferroferric oxyhydroxide and minor iron sulfide that spontaneously precipitate and continue to grow through injection at alkaline/acidic interfaces (Barge et al., 2015a, b; Helmbrecht et al., 2022; Akbari and Palsson, 2022b; see Figure 1). Short peptides produced in the fougerite interlayers are presumed to be gradient-driven vectorially through the fougerite nanocrysts from outside to the spire's inner surface where they are hypothesized to form metal-dosed organic films signified here by brown color (*cf.*, Oda and Fukuyoshi, 2015; Römling, 2022). Within certain limits of externally applied disequilibria, the fougerite or similar DLHs act like an enzyme, in that organic production rates remain constant in spite of fluctuations in supply (Pitsch et al., 1995; Hansen et al., 1996; Kolb et al., 1997; Branscomb et al., 2017). Continuation of the process leads to spalling and entrainment and eventual crowding at the growing spire's tip where necking-off produces organic/inorganic cells that gravitate to depth in a geode (also brown; Russell and Martin, 2004): **(B)** natural chemical garden sulfide bubbles by comparison in the 340Ma Tynagh orebody (Russell and Hall, 1997).

Furthermore, Abel and Trevors (2006) provide a cogent argument against the assumption that the complexification of peptide- and prion-assisted metabolisms is enough to initiate vertical evolution without the insertion of a rule-based physicochemical program. In other words, we have to face up to the introduction of a material program, which makes life distinct in being able to defend itself by exerting an autonomous choice, if surprised by external alterations beyond itself (Kordium, 2021). This is in contrast to ALL other simple self-ordering phenomena driven by the many varieties of known disequilibria (Russell et al., 2013; Ramstead et al., 2019).

However, there is at present no clearcut path from a putative fougerite–mackinawite–peptide reproducing system to a nucleotide-based replicative one.

7. Genome programming—from ordering to organization

Noting the main dilemma in the origin-of-life research, Freeman Dyson famously suggests that life must have originated twice "with two separate kinds of creatures, one kind capable of metabolism without exact replication and the other kind capable of replication without metabolism" (Dyson, 1986). Metabolism's creature seems to emerge through the synthesis and reproduction of amino acids and even peptides but has nowhere to go, while the replication creature is supposedly born whole in an age of information, yet cannot find the wherewithal to 'be'. These two creatures each have their champions and the regrettable outcome is the erection of an intellectual wall built between the 'computing replicationists/geneticists' and the 'engineers of metabolism'. What to do?

The 'metabolists' do need to find geologically informed ways to synthesize the nucleotides indispensable to making a code. The ball is in our court. Just how information was introduced early into the engines of metabolism is the 'hard problem of life' (Walker and Davies, 2017; Wong and Prabhu, 2023). From a crystallographic perspective, we might start with the size and shape, recalling Erwin Schrödinger's classification of the gene as an aperiodic crystal (Schrödinger 1944). Moreover 2 years later, Linus Pauling (1946) promulgated his views on the importance of complementarity of molecular shape as determinants of their interactions (Pauling, 1946), originally considered as the "lock and key" requirement for molecular interactions (Fischer, 1894) and the "side chain theory" of Ehrlich (1901). These articles set the scene for the self-assembly hypotheses of: (1) Dounce's (1953) nucleic acid template hypothesis, whereby the ribonucleic acids synthesized on the gene templates would, in turn, become templates for protein synthesis, (2) Gamow's (1954 and Gamow and Yčas, 1955) double coding hypothesis, in which "amino acid residues in proteins are selected by independent triplets of nucleotides," and (3) Nirenberg and Leder's (1964) "affinity method."

Woese et al. (1966) picked up on these ideas, framing the issue in terms of "whether or not amino acid-oligonucleotide steric interactions play or have played a role in determining these assignments, and if so, to what extent?" Their resounding and "essentially unavoidable conclusion" is that "codon assignments manifest an underlying codon-amino acid pairing"; a conclusion still resonating today (Woese et al., 1966; Russell et al., 2003; Yarus et al., 2005, 2009; Yarus, 2021; Harrison et al. 2022). Moreover, it leads to Massimo Di Giulio's (2008) hypothesis of an extension of the coevolution theory for the origin of the genetic code.

While these theories have been widely entertained, experimental exploration is limited. One notable success is due to Mellersh and Wilkinson (2000) who demonstrated, for example, how "polyadenylic acid immobilized on silica gel stereoselectively binds L-lysine from dilute aqueous solution"… and so facilitates "subsequent amide bond formation" (Russell et al., 2003). At the same time, Levy and Ellington (2003) expand upon their ideas regarding peptide-templated nucleic acid ligations. Mike Yarus (2017) confirms these affinities by demonstrating that the RNA–amino-acid interface logically relates triplets to the side chains of particular amino acids, concluding that "peptides may have been produced directly on an instructive amino acid binding RNA" (Yarus, 2017). We should also note the possibility that, given the degeneracy in the genetic code, the progenitors of the earliest genetic code were codons with four bases (or more)—the tessera codes of Baranov et al. (2009) and Gonzalez et al. (2012, 2019). Yarus (2011) also sees a way of "getting past the RNA world"—a world that never was according to Yockey (1995), Kurland (2010), and Wills and Carter (2018).

Wächtershäuser (1990), Martin and Russell (2007), and Harrison and Lane (2018) have made attempts at a "progression" but it might be argued, to use Stanley Miller's apothegm, that these erections are nothing more than "paper chemistry" (Hagmann, 2002, but see Polanyi (1962, p. 165) for a thoughtful defense of such 'speculations'). Abel and Trevors (2006) attempt to discipline the "metabolists," by pointing out that, absent a program, metabolic cycling is doomed to docile repetition as long as their particular driving disequilibria last, as per the laws of chemistry and physics. To animate metabolism and make it reflexive, we cannot expect complexification *per se* to answer the conundrum (Abel, 2011). The workings of life have to be understood in terms of their entirety and as Abel (2011) emphasizes, work itself "entails more than spontaneous phase transitions." Once metabolism's disequilibria-converting engines are up and running, to allow the system as a whole to progress and evolve they all must be algorithmically directed, and continually replaced (Trixler, 2021). Moreover, to last, any product stemming from the alkaline mound has to have its use as a component part of each metabolic engine; has to pay its way or be discarded (Branscomb et al., 2017). There seems nothing for it but to seek a non-ribosomal peptide synthetase that includes nucleotides in its structure (Kleinkauf and von Döhren, 1996; von Döhren et al., 1999; Fischbach and Walsh, 2006).

Attempts to assail this conceptual wall have been less than successful. However, just this year some 'cracks' have appeared on the metabolist-*cum*-chemical side. The Nick Lane–Stuart Harrison group at the Department of Genetics, Evolution and Environment, University College London, look to how randomly synthesized nuclear monomers could become involved in the very basis of metabolism—namely, as nucleotide catalysts in CO_2 hydrogenation and in amination of carboxylates to amino acids (Harrison et al. 2022; Palmeira et al., 2022; Pinna et al. 2022). This forward-looking approach can explain why ATP is universally conserved across life (Pinna et al., 2022). Moreover on this side, in a series of experiments, Joseph Moran's group at the Institut de Science et d'Ingénierie Supramoléculaires, Strasbourg, France, demonstrates the likely networks followed by the earliest non-enzymatic metabolic pathways,

for example, metal-ion transaminations (Mayer et al., 2021), the centrality of iron in catabolic as well as anabolic processes (Muchowska et al., 2019, 2020), and the abiotic conversion of aspartate to orotate and further reactions to produce all three of the pyrimidine nucleobases in water at 60°C catalyzed by a variety of metal ions along with an oxidant (Yi et al., 2022). Furthermore, Müller et al. (2022) explore 'palaeochemistry' in their search for a plausible scenario of an RNA–peptide world, while Akbari and Palsson (2022a) formulate how metabolic homeostasis and cellular growth might arise in the acetyl coenzyme-A pathway and the reductive TCA cycle, and Helmbrecht et al. (2022) demonstrate the accumulation of RNA in amakinite/fougerite chemical gardens.

How much of this might progress in the precellular DLH world? Pitsch et al. (1995) demonstrate how a weakly alkaline 20 μM solution of glycolaldehyde phosphate can, once absorbed within M^{2+}/M^{3+} oxyhydroxide interlayers of green rust, be transformed to hexose- and pentose-phosphates—the latter structurally related to the sugar phosphate units in RNA. Moreover, Krishnamurthy et al. (1996) demonstrate that the 'alternative' nucleic acid pyranosyl ribose-2,4-phosphate, the near-planar sugar phosphate structure formed in similar conditions, is a nucleic acid with exceptional base-pairing properties (Eschenmoser, 1994). Krishnamurthy et al. (1996) show that, on introducing formaldehyde and glyceraldehyde phosphate into the DLH interlayer, 40% of the product consists of pyranosyl ribose.

Perhaps, the secret of "The First Cell," the title of Azra Raza's book, which refers to the first cancer cell in an oncology case, is also the secret of the very first cell (Raza, 2019; Marshall, 2021; see Szent-Györgyi, 1968). According to Bernhardt and Patrick (2014), genetic code evolution started with the incorporation of glycine, followed by other small hydrophilic amino acids. Certainly, once the genetic code is sophisticated to the extent of being able to take on surprises and make choices and generate novel information (Marshall, 2021), there can be a rush to infest the entire hydrothermal mound. And life is ready for its diaspora. While relatively slow to colonize the ocean crust at first, as an entropy generator able to pick up any stray leftovers from other disequilibria generating systems, life takes over the surfaces on, and within, our planet eventuating in photosynthesis (Russell and Arndt, 2005; Figure 4).

8. The taproot and first branch of the evolutionary tree

In the present AVT, life is rooted in methanotrophic acetogenic microbes respiring nitrate (Nitschke and Russell, 2013). The taproot itself is grounded in fougerite, which sees to the harnessing of ambient H_2, CH_4, and CO_2 driven by the natural proton motive force and respiration of oxidized nitrogen entities (Barnes and O'Neil, 1969; Neal and Stanger, 1983; Ducluzeau et al., 2009, 2014). Once this system is up and running at the outer margins of the submarine alkaline hydrothermal mound, its requirements are, nevertheless, highly constricting. The evolutionary breakout ('break in') comes with metabolism's discovery of how to survive on the much reduced free energy from readily available H_2 and CO_2 within the mound itself. We speculate that Christian Schöne et al.'s (2022) exciting finding of the facile conversion of an archaeal methanogen to a carbon-monoxide-dependent acetogen through the removal of cellular function could be read as an indication of how "reverse methanotrophy" segued to an acetogenesis, perhaps related to the differentiation of the progenote into the archaea and bacteria (Russell and Nitschke, 2017; *cf.*, Lyu et al., 2022). This admittedly contentious suggestion sees a parallel in human society having to burn hydrocarbons while 'waiting for nuclear fusion(s)'.

9. Escape from the mound and the founding of the deep biosphere in serpentinizing ocean crust

Entrainment of the earliest microbes in a hydrothermal effluent to the ocean would lead to their immediate starvation. Thus, it is surmised that the only survivors are those who are caught up in an involuntary and random growth and expansion in a downward front to inaugurate the deep biosphere (Pedersen, 1993; Parkes et al., 1994; Parkes and Wellsbury, 2004; Russell and Arndt, 2005; Glasby, 2006; Schrenk et al., 2013). In such conditions, the 'law of natural rejection' would see all but the most efficient cells or cellular cooperatives die-off.

In the oceanic crust itself, these survivors would have missed the profusion of the mound and been drastically thinned out and stripped of non-essential genes (Fones et al., 2019, 2021). Fones et al. (2021) make the cogent argument that the absence of CO_2 in this new environment drives the adaptation of methanogens to generate their own. Discrete ocean downdrafts are another source of CO_2. Yet, the remaining feedstocks, while restricted, are otherwise not so different in the serpentinizing throat and ultramafic surrounds, perhaps also supplying the electron-donating H_2, CH_4, $HCOO^-$, CO, and CH_3COO^- (Windman et al., 2007; White et al., 2020). The latter four entities also supply the substrate carbon (White et al. 2020). Such alkaline fluids are known to support microbial nitrate and nitrite bacterial reduction (Albina et al., 2021).

Colman et al. (2022) offer a window into the effect of such conditions in their exhaustive study of the Semail ophiolite. Not only are reproduction rates much diminished but genetic diversity too is "streamlined" for survival (Colman et al., 2022). Furthermore, syntrophy, gene swapping both within and across domains, and the sharing of nutrients keep the microbiome operating (Wolin, 1982; Russell and Arndt, 2005; Tiago and Veríssimo, 2013; Kohl et al., 2016; Brazelton et al. 2017; Suzuki et al., 2017, 2018; Colman et al. 2022).

Extrapolating across the 4 billion years since life's onset, we gauge from Colman et al. (2022) that the autotrophic acetogenic analogs comparable to what they term type II *Acetothermia* would survive displacement from the mound into the hyperalkaline waters in equilibrium with incipient serpentinization. These types of *Acetothermia* employ an archaeal-like carbon-monoxide dehydrogenase and ferredoxin-based complexes to achieve acetogenesis. Moreover, they have the capacity for respiratory growth using nitrate (Youssef et al., 2019). Other bacteria revealed by metagenomics are the sulfate-reducing bacteria (Brazelton et al., 2017; Rempfert et al., 2017; Templeton et al., 2021).

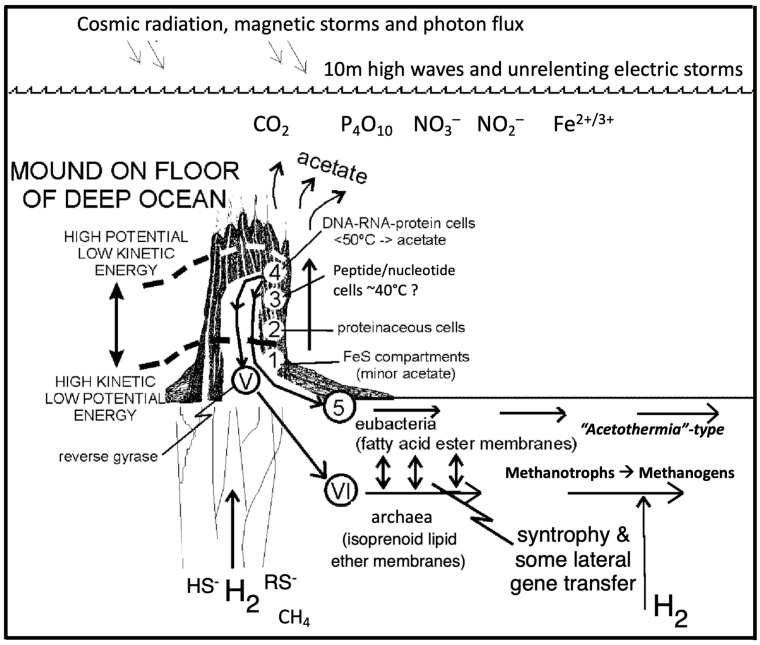

FIGURE 4
Emergence of the deep biosphere. Autotrophic life emerges and rapidly infects a hydrothermal alkaline mound (Figure 1) and differentiates interdependently into the precursors of the bacteria and archaea, grows by expansion downward and laterally into the surrounding sediments and serpentinizing ocean crust, thus initiating the deep biosphere, a hypothesis now broadly supported by recent research (Fones et al., 2019, 2021; Boyd et al., 2020; Berkemer and McGlynn, 2020; Leong et al., 2021; Colman et al., 2022). Numbers 1–3 relate to life's emergence, while 4 marks the supposed point of differentiation of the archaea and the bacteria. Roman numerals V–VI mark evolutionary stages of the archaea, and number 5 shows the stages of evolution of the bacteria in the deep biosphere (redrawn from Russell and Arndt, 2005).

Although apparently missing from the Semail ophiolite, sequences of an anaerobic Methanotroph group 1 (ANME-1) have been identified in the serpentinization-driven alkaline Cabeço de Vide aquifer in Portugal, and unclassified anaerobic methanotrophic euryarchaeota (ANME) MAG are recorded from Lost City (Tiago and Veríssimo, 2013; Nothaft et al., 2021). However, suggestions that these findings provide an inkling of support for the methanotrophy-first speculation of Nitschke and Russell (2013) are put on hold by the likelihood of the present-day "contamination from surface waters" (Merkel et al., 2013; Postec et al., 2015; Trutschel et al., 2022).

10. The submarine alkaline vent theory put to the test

Experiments on, and analyses of, AVT look to an evolutionary tree with its deepest roots in cosmogenesis—yet reaches upward and along the lowest branches of the acetyl coenzyme-A and an incomplete reverse TCA cycle (Nitschke and Russell, 2010; Russell et al., 2013; Carroll, 2016).

Findings and some predictions of AVT are that:

1. A natural proton disequilibria measuring between 2 to 5 pH units imposed across an FeS membrane separating a hydrogen-bearing alkaline solution from a carbonic ocean drives the hydrogenation of the CO_2 to formate/CO (Russell and Hall, 1997; Branscomb and Russell, 2013; Vasiliadou et al., 2019) is verified (Hudson et al., 2020), although most of the iron in the membrane is now argued to be in fougerite/green rust rather than in FeS (Russell et al., 2013).
2. An expectation of AVT is that methane derived from the lower mantle and entrained in the alkaline hydrothermal fluid will oxidize to a methyl group within green rust (Nitschke and Russell, 2013), itself (re)oxidized by NO and nitrate provided through …
3. appreciable volcanic and hurricane cloud-to-cloud lightning, bolide impacts, and photochemistry from the CO_2+N_2 atmosphere dissolved in the ocean as CO_2, NO_3^-, and NO_2^- (Mancinelli and McKay, 1988; Gallardo and Rodhe, 1997; Kasting and Siefert, 2001; Ducluzeau et al., 2009; Wong et al., 2017; Navarro-González et al., 2019).
4. Although conclusion 3 is challenged by Ranjan et al. (2019), the view that the nitrogen oxides were present in the Earth's early atmosphere and that their derivatives also invaded the ocean is now strongly reinforced by Buessecker et al. (2022) who suggest green rust to be responsible for carrying NO to depth bound as nitrosyl (and see Heays et al., 2022; Nishizawa, 2022) …
5. in turn supporting the denitrifying methanotrophic acetogenesis hypothesis as the first pathway to life, predating the more demanding acetyl coenzyme-A pathway (Nitschke and Russell, 2013; Russell and Nitschke, 2017) …
6. and that the amination of pyruvate and oxalate to alanine and glycine which can be accomplished *via* fougerite (Nitschke and Russell 2013) is verified by Barge et al. (2019, 2020) …
7. while the condensation of amino acids to peptides within the 2D interlayers of peptides has support from Muñoz-Santiburcio

and Marx (2017), Erastova et al. (2017), Grégoire et al. (2016, 2018), and Holden et al. (2022).

8. Fougerite interlayers are capable of dampening externally imposed disequilibria to produce an enzyme-like flux-force linearity to interactants (Branscomb and Russell, 2019), …
9. although indications of binding, binding-change, and disequilibria-conversion mechanisms (Russell, 2018) await experimentation using the operando X-ray absorption spectroscopy and allied techniques (Fracchia et al., 2018).
10. That the deep biosphere—initially the serpentinizing Hadean ocean crust—is first populated with respiring denitrifying methanotrophic archaea and acetogenic bacteria from their point of 'origin' (the progenote) in a submarine alkaline hydrothermal mound (Russell and Arndt, 2005; Nitschke and Russell, 2013; Ménez, 2020) is supported by circumstantial evidence; e.g., the bacterium *Acetothermia* is capable of respiration with nitrate (Fones et al., 2019, 2021; Youssef et al., 2019; Boyd et al., 2020; Colman et al., 2022) and an archaeon methanotroph, *cf.* ANME-1 (Tiago and Veríssimo, 2013; Brazelton et al., 2017). We might imagine these progenotes happening upon new locations with high concentrations of dissolved ions and gases, carried there passively by percolating solutions.

11. Conclusion

The production of alkaline hydrothermal waters through the serpentinization of mafic to ultramafic rocks, as introduced by Ivan Barnes et al., underpins AVT (Barnes and O'Neil, 1969; Barnes et al., 1972; Russell et al., 1989; Macleod et al., 1994). These authors also figure in the description of the Lost City vents discovered in 2000 (Kelley et al., 2001). The serpentinizing system that produces such alkaline submarine emissions has, through a reading of Cottrell (1979), since been described in terms of a disequilibria- ('free-energy'-) converting cracking engine (Russell et al., 2013). While AVT originally assumed a sulfide mound to be generated at the spring-to-ocean interface, it became apparent that the double-layer oxyhydroxide green rust (fougerite) would be the major ferroferric precipitate along with some sulfide and Mg-rich clays and silica (Russell and Hall, 1997; Russell and Arndt, 2005). Because of its physicochemical flexibility, this macromolecular 2D mineral could also be considered the necessary nanoengine/protomotor enzyme—in this case to convert the disequilibria between $H_2 + OH^- + CH_4$ and $CO_2 + NO_3^- + H^+$ to the rudiments of the denitrifying methanotrophic acetyl coenzyme-A pathway—the interlayers acting as precursor metabolic channels toward further downstream organic synthesis (Nitschke and Russell, 2013; *cf.* Srere, 1987).

The current AVT for life's emergence has it that fougerite-rich hydrothermal electrochemical gardens (fine chimney stalks and spires) mark the precellular stage [Russell et al., 2005, 2013 (Figure 3B); Barge et al., 2015b; Chin et al., 2020; Nitschke et al., 2022 (Figure 3)]. We imagine a well-ordered convective alkaline updraft feeding reductants to the also well-ordered macromolecular fougerite comprising the growing spires and chimneys, which in turn allows a well-ordered infiltration and vectorial flow of protons and anions from the ocean directed through the interlayers (Borrego-Sánchez et al., 2022). The result is an effusing tangle of organic molecules probably dominated by peptides to coat the inner wall of the spires (Akbari and Palsson, 2022b; Römling, 2022). Portions of this organic film spall off and are entrained in the flow, along with other organic molecules released by delamination and/or by diagenetic alteration to magnetite at depth in the mound. Some of this organic material may be 'attracted' to form cellular structures that are capable of sensing and responding to oscillations and fluctuations in supply and perhaps prove eventually to be self-sustaining, and, on the development of emerging genetic algorithms, would be able to make choices and generate novel information and rapidly infect the mound (Cain, 1949; Marshall, 2021).

Thus, beginning with the insights of Ivan Barnes et al., we argue that:

1. Serpentinization is the inescapable response of the Hadean Earth's ultramafic crust to the circulation of ocean water. Moreover, it is equally inescapable that the preorganized macromolecule fougerite is a prerequisite for the dissipation of the disequilibria resulting from the return of serpentinite's effluent to its original source, the Hadean carbonic ocean (Tatzel et al., 2022).
2. Just as cracks in the Hadean ocean floor are a prerequisite for priming serpentinization, so do aqueous interlayers within redox/pH-sensitive fougerite nanocrysts acquiesce to the forceful vectorial invasions from either flank of the precipitate membrane of pent-up ions, charged and uncharged fuels and oxidants, eventuating in protometabolisms (Nitschke and Russell, 2013).
3. However while fougerite may be considered to provide simple messages to govern a product, it is presumed that prion-like offspring may offer seemingly autonomous and 'intentional exploration' of space and time for similar disequilibria (Maury, 2009).
4. However, a second chapter on life's emergence awaits an understanding of the paths from the earliest coherent pregenetic governing algorithms of life to the emergence of the "modern synthesis"—both barely written introductions to the subsequent well-versed chapters of life's unitingly diversifying Gaian commonwealth where "everything is everywhere (though the environment selects)" (Baas Becking, 1931, 1934; Quispel, 1998; Abel and Trevors, 2006; Igamberdiev, 2021); *pace* (Martiny et al. 2006).

An understanding of how life both emerges and thrives requires the use of stochastic or trajectory thermodynamics—equilibrium thermodynamics is absolutely inappropriate for the task (Astumian, 2018, 2020; Bartlett and Beckett, 2019; Branscomb Russell, 2019; Horowitz and Gingrich, 2020; Feng et al., 2021; Ueltzhöffer et al., 2021). Furthermore, of course, experiments are required to test the hypothesis that self-sustaining hydrothermal 'electro-chemical gardens' comprising the minerals fougerite and mackinawite as nanoengines and nanoengine mountings are up to the task of engendering the earliest steps of life (Figures 2, 3). Thereafter, computer modeling and artificial intelligence beckon as ways of further resolving sequences of life's emergence (Ugliengo, 2019; Hassabis and Revell, 2021).

Data availability statement

The original contributions presented in the study are included in the article/supplementary material, further inquiries can be directed to the corresponding author.

Author contributions

The author confirms being the sole contributor of this work and has approved it for publication.

Acknowledgments

Eric Boyd, Elbert Branscomb, Steffen Buessecker, Simon Duval, Orion Farr, Emma Forrest, Wolfgang Nitschke, Piero Ugliengo, and Michael Wong are thanked for their help and discussions. Any mistakes or misconceptions are my own.

Conflict of interest

The author declares that the research was conducted in the absence of any commercial or financial relationships that could be construed as a potential conflict of interest.

Publisher's note

All claims expressed in this article are solely those of the authors and do not necessarily represent those of their affiliated organizations, or those of the publisher, the editors and the reviewers. Any product that may be evaluated in this article, or claim that may be made by its manufacturer, is not guaranteed or endorsed by the publisher.

References

Abel, D. L. (2011). Is life unique? *Life* 2, 106–134. doi: 10.3390/life2010106

Abel, D. L., and Trevors, J. T. (2006). Self-organization vs. self-ordering events in life-origin models. *Phys Life Rev* 3, 211–228. doi: 10.1016/j.plrev.2006.07.003

Adam, G., and Delbrück, M. (1968). Reduction of dimensionality in biological diffusion processes. *Struct. Chem. Mol. Biol.* 198, 198–215.

Aithal, A., Dagar, S., and Rajamani, S. (2023). Metals in prebiotic catalysis: a possible evolutionary pathway for the emergence of metalloproteins. *ACS Omega* 8, 5197–5208. doi: 10.1021/acsomega.2c07635

Akbari, A., and Palsson, B. O. (2022a). Positively charged mineral surfaces promoted the accumulation of organic intermediates at the origin of metabolism. *PLoS Comp. Biol.* 18:e1010377. doi: 10.1371/journal.pcbi.1010377

Akbari, A., and Palsson, B. (2022b). Metabolic homeostasis and growth in abiotic cells. *bioRxiv*. [Epub ahead of preprint]. doi: 10.1101/2022.10.16.512448

Albers, E., Bach, W., Pérez-Gussinyé, M., McCammon, C., and Frederichs, T. (2021). Serpentinization-driven H_2 production from continental break-up to mid-ocean ridge spreading: unexpected high rates at the West Iberia margin. *Front. Earth Sci.* 9:487. doi: 10.3389/feart.2021.673063

Albina, P., Durban, N., Bertron, A., Albrecht, A., Robinet, J. C., and Erable, B. (2021). Nitrate and nitrite bacterial reduction at alkaline pH and high nitrate concentrations, comparison of acetate versus dihydrogen as electron donors. *J. Envir. Manag.* 280:111859. doi: 10.1016/j.jenvman.2020.111859

Anashkin, V. A., Malinen, A. M., Bogachev, A. V., and Baykov, A. A. (2021). Catalytic asymmetry in homodimeric H+-pumping membrane pyrophosphatase demonstrated by non-hydrolyzable pyrophosphate analogs. *Internl J. molec. Sci.* 22:9820. doi: 10.3390/ijms22189820

Appel, P. W. U. (1980). On the early Archaean Isua iron-formation, West Greenland. *Precambrian Res.* 11, 73–87. doi: 10.1016/0301-9268(80)90081-9

Armen, R. S., Alonso, D. O., and Daggett, V. (2004). Anatomy of an amyloidogenic intermediate: conversion of β-sheet to α-sheet structure in transthyretin at acidic pH. *Structure* 12, 1847–1863. doi: 10.1016/j.str.2004.08.005

Arrhenius, G. (1984). "Minerals with channel structure as substrates for nucleotide and peptide synthesis" in *Fundamental Studies and the Future of Science*. ed. C. Wickramasinghe (Cardiff UK: University College Cardiff Press), 301–319.

Arrhenius, G. O. (2003). Crystals and life. *Helv. Chim. Acta* 86, 1569–1586. doi: 10.1002/hlca.200390135

Arrhenius, G., Gedulin, B., and Mojzsis, S. (1993). "Phosphate in models for chemical evolution" in *Chemical Evolution and Origin of Life*. eds. C. Ponnamperuma and J. Chela-Flores (Hampton, VA: A. Deepak Publishing), 25–50.

Arrhenius, G., Sales, B., Mojzsis, S., and Lee, T. (1997). Entropy and charge in molecular evolution—the case of phosphate. *J. Theor. Biol.* 187, 503–522. doi: 10.1006/jtbi.1996.0385

Asimakidou, T., Makridis, A., Veintemillas-Verdaguer, S., Morales, M. P., Kellartzis, I., Mitrakas, M., et al. (2020). Continuous production of magnetic iron oxide nanocrystals by oxidative precipitation. *Chem. Eng. J.* 393:124593. doi: 10.1016/j.cej.2020.124593

Astumian, R. D. (2007). Design principles for Brownian molecular machines: how to swim in molasses and walk in a hurricane. *Phys. Chem. Chem. Phys.* 9, 5067–5083. doi: 10.1039/b708995c

Astumian, R. D. (2012). Microscopic reversibility as the organizing principle of molecular machines. *Nat. Nanotech.* 7, 684–688. doi: 10.1038/nnano.2012.188

Astumian, R. D. (2018). Trajectory and cycle-based thermodynamics and kinetics of molecular machines: the importance of microscopic reversibility. *Acc. Chem. Res.* 51, 2653–2661. doi: 10.1021/acs.accounts.8b00253

Astumian, R. D., Mukherjee, S., and Warshel, A. (2016). The physics and physical chemistry of molecular machines. *ChemPhysChem* 17, 1719–1741. doi: 10.1002/cphc.201600184

Astumian, R. D., Pezzato, C., Feng, Y., Qiu, Y., McGonigal, P. R., Cheng, C., et al. (2020). Non-equilibrium kinetics and trajectory thermodynamics of synthetic molecular pumps. *Mat. Chem. Front.* 4, 1304–1314. doi: 10.1039/D0QM00022A

Baas Becking, L. G. M. (1931). *Gaia of leven en aarde. Oratie gewoon hoogleraar, Rijksuniv*. Leiden, Mart. Nijhoff's Gravenhage, 1–20.

Baas-Becking, L. G. M. (1934). *Geobiologie of inleiding tot de milieukunde*. Van Stockum & Zoon NV, The Hague.

Ballard, R. D., and Grassle, J. F. (1979). Incredible world of deep sea rifts. *Natl. Geogr.* 156, 680–705.

Baltscheffsky, M., Baltscheffsky, H., and Von Stedingk, L. V. (1966). "Light-induced energy conversion and the inorganic pyrophosphatase reaction in chromatophores from Rhodospirillum rubrum" in *Brookhaven Symposia in Biology*, 246–257.

Baltscheffsky, M., Schultz, A., and Baltscheffsky, H. (1999). H^+-PPases: a tightly membrane-bound family. *FEBS Lett.* 457, 527–533. doi: 10.1016/S0014-5793(99)90617-8

Banks, D. A. (1985). A fossil hydrothermal worm assemblage from the Tynagh lead–zinc deposit in Ireland. *Nature* 313, 128–131. doi: 10.1038/313128a0

Baranov, V. I., Gribov, L. A., and Mikhailov, I. V. (2016). Processes of the development of the molecular world at early stages of its formation: evidence from the investigation of the behavior of the vibrational entropy of molecules. *Geochem. Int.* 54, 929–935. doi: 10.1134/S0016702916110021

Baranov, P. V., Venin, M., and Provan, G. (2009). Codon size reduction as the origin of the triplet genetic code. *PLoS One* 4:e5708. doi: 10.1371/journal.pone.0005708

Barge, L. M., Abedian, Y., Russell, M. J., Doloboff, I. J., Cartwright, J. H., Kidd, R. D., et al. (2015a). From chemical gardens to fuel cells: generation of electrical potential and current across self-assembling iron mineral membranes. *Angew. Chem. Int. Ed.* 54, 8184–8187. doi: 10.1002/anie.201501663

Barge, L. M., Cardoso, S. S. S., Cartwright, J. H. E., Cooper, G. J. T., Cronin, L., De Wit, A., et al. (2015b). From chemical gardens to Chemobrionics. *Chem. Rev.* 115, 8652–8703. doi: 10.1021/acs.chemrev.5b00014

Barge, L. M., Doloboff, I. J., White, L. M., Russell, M. J., and Kanik, I. (2012). Characterization of iron-phosphate-silicate chemical garden structures. *Langmuir* 28, 3714–3721. doi: 10.1021/la203727g

Barge, L. M., Flores, E., Baum, M. M., VanderVelde, D. G., and Russell, M. J. (2019). Redox and pH gradients drive amino acid synthesis in iron oxyhydroxide mineral systems. *Proc. Natl. Acad. Sci. U. S. A.* 116, 4828–4833. doi: 10.1073/pnas.1812098116

Barge, L. M., Jones, J. P., Pagano, J. J., Martinez, E., and Bescup, J. (2020). Three-dimensional analysis of a simulated prebiotic hydrothermal chimney. *ACS Earth Space Chem.* 4, 1663–1669. doi: 10.1021/acsearthspacechem.0c00186

Barnes, I., and O'Neil, J. R. (1969). The relationship between fluids in some fresh alpine-type ultramafics and possible modern serpentinisation, Western United States. *Geol. Soc. Am. Bull.* 80, 1947–1960. doi: 10.1130/0016-7606(1969)80[1947:TRBFIS]2.0.CO;2

Barnes, I., O'Neil, J. R., and Trescases, J. J. (1978). Present day serpentinization in New Caledonia, Oman and Yugoslavia. *Geochim. Cosmochim. Acta* 42, 144–145. doi: 10.1016/0016-7037(78)90225-9

Barnes, I., Rapp, J. B., O'Neil, J. R., Sheppard, R. A., and Gude, A. J. (1972). Metamorphic assemblages and the direction of flow of metamorphic fluids in four instances of serpentinization. *Contrib. Min. Pet.* 35, 263–276. doi: 10.1007/BF00371220

Baross, J. A., and Hoffman, S. E. (1985). Submarine hydrothermal vents and associated gradient environments as sites for the origin and evolution of life. *Orig. Life Evol. Biosph.* 15, 327–345. doi: 10.1007/BF01808177

Bartlett, S. J., and Beckett, P. (2019). Probing complexity: thermodynamics and computational mechanics approaches to origins studies. *Interface Focus* 9:20190058. doi: 10.1098/rsfs.2019.0058

Berkemer, S. J., and McGlynn, S. E. (2020). A new analysis of archaea-bacteria domain separation: variable phylogenetic distance and the tempo of early evolution. *Mol. Biol. Evol.* 37, 2332–2340. doi: 10.1093/molbev/msaa089

Bernhardt, H. S. (2019). Making molecules with clay: layered double hydroxides, pentopyranose nucleic acids and the origin of life. *Life* 9:19. doi: 10.3390/life9010019

Bernhardt, H. S., and Patrick, W. M. (2014). Genetic code evolution started with the incorporation of glycine, followed by other small hydrophilic amino acids. *J. Mol. Evol.* 78, 307–309. doi: 10.1007/s00239-014-9627-y

Bianchi, A., Giorgi, C., Ruzza, P., Toniolo, C., and Milner-White, E. J. (2012). A synthetic hexapeptide designed to resemble a proteinaceous p-loop nest is shown to bind inorganic phosphate. *ProteinsStruct,Funct, Genet* 80, 1418–1424. doi: 10.1002/prot.24038

Bindeman, I. N., and O'Neil, J. (2022). Earth's earliest hydrosphere recorded by the oldest hydrothermally-altered oceanic crust: triple oxygen and hydrogen isotopes in the 4.3-3.8 Ga Nuvvuagittuq belt, Canada. *Earth Planet. Sci. Lett.* 586:117539. doi: 10.1016/j.epsl.2022.117539

Boigenzahn, H., and Yin, J. (2022). Glycine to oligoglycine via sequential trimetaphosphate activation steps in drying environments. *Orig. Life Evol. Biosph.* 52, 249–261. doi: 10.1007/s11084-022-09634-7

Borrego-Sánchez, A., Gutiérrez-Ariza, C., Sainz-Díaz, C. I., and Cartwright, J. H. (2022). The effect of the presence of amino acids on the precipitation of inorganic chemical-garden membranes: biomineralization at the origin of life. *Langmuir* 38, 10538–10547. doi: 10.1021/acs.langmuir.2c01345

Boyce, A. J., Coleman, M. L., and Russell, M. J. (1983). Formation of fossil hydrothermal chimneys and mounds from Silvermines, Ireland. *Nature* 306, 545–550. doi: 10.1038/306545a0

Boyd, E. S., Amenabar, M. J., Poudel, S., and Templeton, A. S. (2020). Bioenergetic constraints on the origin of autotrophic metabolism. *Phil. Trans. Roy. Soc. A* 378:20190151. doi: 10.1098/rsta.2019.0151

Boyd, E. S., Spietz, R. L., Kour, M., and Colman, D. R. (2023). A naturalist perspective of microbiology: examples from methanogenic archaea. *Environ. Microbiol.* 25, 184–198. doi: 10.1111/1462-2920.16285

Boyer, P. D. (1979). "The binding-change mechanism of ATP synthesis" in *Membrane Bioenergetics*. eds. C. P. Lee, G. Schatz and L. Ernster (Reading, MA: Addison-Wesley), 461–479.

Boyer, P. D. (1997). The ATP synthase—a splendid molecular machine. *Annu. Rev. Biochem.* 66, 717–749. doi: 10.1146/annurev.biochem.66.1.717

Brady, M. P., Tostevin, R., and Tosca, N. J. (2022). Marine phosphate availability and the chemical origins of life on earth. *Nat. Commun.* 13, 1–9. doi: 10.1038/s41467-022-32815-x

Branscomb, E., Biancalani, T., Goldenfeld, N., and Russell, M. (2017). Escapement mechanisms and the conversion of disequilibria; the engines of creation. *Phys. Rep.* 677, 1–60. doi: 10.1016/j.physrep.2017.02.001

Branscomb, E., and Russell, M. J. (2013). Turnstiles and bifurcators: the disequilibrium converting engines that put metabolism on the road. *Biochim. Biophys. Acta Bioenerg.* 1827, 62–78. doi: 10.1016/j.bbabio.2012.10.003

Branscomb, E., and Russell, M. J. (2018). Frankenstein or a submarine alkaline vent: who is responsible for abiogenesis? Part 2: as life is now, so it must have been in the beginning. *BioEssays* 40:1700182. doi: 10.1002/bies.201700182

Branscomb, E., and Russell, M. J. (2019). On the beneficent thickness of water. *Interface focus* 9:20190061. doi: 10.1098/rsfs.2019.0061

Brazelton, W. J., Thornton, C. N., Hyer, A., Twing, K. I., Longino, A. A., Lang, S. Q., et al. (2017). Metagenomic identification of active methanogens and methanotrophs in serpentinite springs of the Voltri massif, Italy. *Peer J* 5:e2945. doi: 10.7717/peerj.2945

Bromberg, Y., Aptekmann, A. A., Mahlich, Y., Cook, L., Senn, S., Miller, M., et al. (2022). Quantifying structural relationships of metal-binding sites suggests origins of biological electron transfer. *Sci. Adv.* 8:eabj3984. doi: 10.1126/sciadv.abj3984

Buessecker, S., Imanaka, H., Ely, T., Hu, R., Romaniello, S. J., and Cadillo-Quiroz, H. (2022). Mineral-catalysed formation of marine NO and N_2O on the anoxic early earth. *Nat. Geosci.* 15, 1056–1063. doi: 10.1038/s41561-022-01089-9

Cain, S. A. (1949). Plants and vegetation as exhaustible resources. *Sci. Monthly* 68, 321–328.

Carey, L. D., Koshak, W., Peterson, H., and Mecikalski, R. M. (2016). The kinematic and microphysical control of lightning rate, extent, and NOX production. *J. Geophys. Res. Atmosph.* 121, 7975–7989. doi: 10.1002/2015JD024703

Carroll, S. (2016). *The Big Picture on the Origins of Life, Meaning, and the Universe Itself*. Dutton, New York, NY.

Carter, C. W. (2020). Escapement mechanisms: efficient free energy transduction by reciprocally-coupled gating. *Proteins: Struct. Funct. Bioinf.* 88, 710–717. doi: 10.1002/prot.25856

Cartwright, J. H., García-Ruiz, J. M., Novella, M. L., and Otálora, F. (2002). Formation of chemical gardens. *J. Colloid Interf. Sci.* 256, 351–359. doi: 10.1006/jcis.2002.8620

Cartwright, J. H., and Russell, M. J. (2019). The origin of life: the submarine alkaline vent theory at 30. *Interface Focus* 9:20190104. doi: 10.1098/rsfs.2019.0104

Cathles, L. M. (1990). Scales and effects of fluid flow in the upper crust. *Science* 248, 323–329. doi: 10.1126/science.248.4953.323

Chernoff, Y. O. (2004). Amyloidogenic domains, prions and structural inheritance: rudiments of early life or recent acquisition? *Curr. Opin. Chem. Biol.* 8, 665–671. doi: 10.1016/j.cbpa.2004.09.002

Childers, W. S., Mehta, A. K., Ni, R., Taylor, J. V., and Lynn, D. G. (2010). Peptides organized as bilayer membranes. *Angew. Chemie.* 122, 4198–4201. doi: 10.1002/ange.201000212

Childers, W. S., Ni, R., Mehta, A. K., and Lynn, D. G. (2009). Peptide membranes in chemical evolution. *Curr. Opin. Chem. Biol.* 13, 652–659. doi: 10.1016/j.cbpa.2009.09.027

Chin, K., Pasalic, J., Hermis, N., and Barge, L. M. (2020). Chemical gardens as electrochemical systems: in situ characterization of simulated prebiotic hydrothermal vents by impedance spectroscopy. *ChemPlusChem* 85, 2619–2628. doi: 10.1002/cplu.202000600

Coca, J. R., Erana, H., and Castilla, J. (2021). Biosemiotics comprehension of PrP code and prion disease. *Biosystems* 210:104542. doi: 10.1016/j.biosystems.2021.104542

Colman, D. R., Kraus, E. A., Thieringer, P. H., Rempfert, K., Templeton, A. S., Spear, J. R., et al. (2022). Deep-branching acetogens in serpentinized subsurface fluids of Oman. *Proc. Natl. Acad. Sci. U. S. A.* 119:e2206845119. doi: 10.1073/pnas.2206845119

Corliss, J. B. (1971). The origin of metal-bearing submarine hydrothermal solutions. *J. Geophys. Res.* 76, 8128–8138. doi: 10.1029/JC076i033p08128

Corliss, J. B., Baross, J. A., and Hoffman, S. E. (1980). *Submarine Hydrothermal Systems—A Probable Site for the Origin of Life*. Corvallis, Oregon State University, School of Oceanography, Spec. Pub. 80–87.

Corliss, J. B., Baross, J. A., and Hoffman, S. E. (1981). An hypothesis concerning the relationship between submarine hot springs and the origin of life on earth. *Oceanol. Acta* 4, 59–69.

Corliss, J. B., Dymond, J., Gordon, L. I., Edmond, J. M., von Herzen, R. P., Ballard, R. D., et al. (1979). Submarine thermal springs on the Galápagos rift. *Science* 203, 1073–1083. doi: 10.1126/science.203.4385.1073

Cottrell, A. (1979). The natural philosophy of engines. *Contemp. Physics* 20, 1–10. doi: 10.1080/00107517908227799

Davis, E., and Becker, K. (1999). Tidal pumping of fluids within and from the oceanic crust: new observations and opportunities for sampling the crustal hydrosphere. *Earth Planet. Sci. Lett.* 172, 141–149. doi: 10.1016/S0012-821X(99)00197-1

Delbrück, M. (1970). A physicist's renewed look at biology: twenty years later. *Science* 168, 1312–1315. doi: 10.1126/science.168.3937.1312

Desvaux, M., and Hébraud, M. (2006). The protein secretion systems in listeria: inside out bacterial virulence. *FEMS Microbiol. Rev.* 30, 774–805. doi: 10.1111/j.1574-6976.2006.00035.x

Di Giulio, M. (2008). An extension of the coevolution theory of the origin of the genetic code. *Biol. Dir.* 3:37. doi: 10.1186/1745-6150-3-37

Ding, Y., Batista, B., Steinbock, O., Cartwright, J. H., and Cardoso, S. S. (2016). Wavy membranes and the growth rate of a planar chemical garden: enhanced diffusion and bioenergetics. *Proc. Natl. Acad. Sci. U. S. A.* 113, 9182–9186. doi: 10.1073/pnas.1607828113

Dounce, A. L. (1953). Nucleic acid template hypotheses. *Nature* 172:541. doi: 10.1038/172541a0

Ducluzeau, A. L., Schoepp-Cothenet, B., Baymann, F., Russell, M. J., and Nitschke, W. (2014). Free energy conversion in the LUCA: quo vadis? *Biochim. Biophys. Acta Bioenerg.* 1837, 982–988. doi: 10.1016/j.bbabio.2013.12.005

Ducluzeau, A. L., van Lis, R., Duval, S., Schoepp-Cothenet, B., Russell, M. J., and Nitschke, W. (2009). Was nitric oxide the first deep electron sink? *Trends Biochem. Sci.* 34, 9–15. doi: 10.1016/j.tibs.2008.10.005

Duval, S., Baymann, F., Schoepp-Cothenet, B., Trolard, F., Bourrié, G., Grauby, O., et al. (2019). Fougerite: the not so simple progenitor of the first cells. *Interface Focus* 9:20190063. doi: 10.1098/rsfs.2019.0063

Duval, S., Branscomb, E., Trolard, F., Bourrié, G., Grauby, O., Heresanu, V., et al. (2020). On the why's and how's of clay minerals' importance in life's emergence. *Appl. Clay Sci.* 195:105737. doi: 10.1016/j.clay.2020.105737

Dyson, F. (1986). *Origins of Life*. Cambridge, England: Cambridge University Press.

Ehrlich, P. (1901). Die seitenkettentheorie und ihre gegner. *Münchner Med Wochenschr* 52, 2123–2124.

Endres, R. G. (2017). Entropy production selects nonequilibrium states in multistable systems. *Sci. Rep.* 7, 1–13. doi: 10.1038/s41598-017-14485-8

Erastova, V., Degiacomi, M. T., Fraser, D. G., and Greenwell, H. C. (2017). Mineral surface chemistry control for origin of prebiotic peptides. *Nat. Commun.* 8, 1–9. doi: 10.1038/s41467-017-02248-y

Eschenmoser, A. (1994). Chemistry of potentially prebiological natural products. *Orig. Life Evol. Biosph.* 24, 389–423. doi: 10.1007/BF01582017

Etaix, L. E., and Orgel, L. E. (1978). Phosphorylation of nucleosides in aqueous solution using trimetaphosphate: formation of nucleoside triphosphates. *J. Carbohydr. Nucleosides Nucleotides* 5, 91–110.

Fallick, A. E., Ilich, M., and Russell, M. J. (1991). A stable isotope study of the magnesite deposits associated with the alpine-type ultramafic rocks of Yugoslavia. *Econ. Geol.* 86, 847–861. doi: 10.2113/gsecongeo.86.4.847

Farr, O., Elzinga, E. J., and Yee, N. (2022). Effect of Ni^{2+}, Zn^{2+}, and Co^{2+} on green rust transformation to magnetite. *Geochem. Trans.* 23:3. doi: 10.1186/s12932-022-00080-y

Feng, Y., Ovalle, M., Seale, J. S., Lee, C. K., Kim, D. J., Astumian, R. D., et al. (2021). Molecular pumps and motors. *J. Am. Chem. Soc.* 143, 5569–5591. doi: 10.1021/jacs.0c13388

Fischbach, M. A., and Walsh, C. T. (2006). Assembly-line enzymology for polyketide and nonribosomal peptide antibiotics: logic, machinery, and mechanisms. *Chem. Rev.* 106, 3468–3496. doi: 10.1021/cr0503097

Fischer, E. (1894). Einfluss der Configuration auf die Wirkung der Enzyme. *Ber. Dtsch. Chem. Ges.* 27, 2985–2993. doi: 10.1002/cber.18940270364

Flores, E., Martinez, E., Rodriguez, L. E., Weber, J. M., Khodayari, A., VanderVelde, D. G., et al. (2021). Effects of amino acids on phosphate adsorption onto iron (oxy) hydroxide minerals under early earth conditions. *ACS Earth Space Chem.* 5, 1048–1057. doi: 10.1021/acsearthspacechem.1c00006

Fones, E. M., Colman, D. R., Kraus, E. A., Nothaft, D. B., Poudel, S., Rempfert, K. R., et al. (2019). Physiological adaptations to serpentinization in the Samail ophiolite, Oman. *ISME J.* 13, 1750–1762. doi: 10.1038/s41396-019-0391-2

Fones, E. M., Colman, D. R., Kraus, E. A., Stepanauskas, R., Templeton, A. S., Spear, J. R., et al. (2021). Diversification of methanogens into hyperalkaline serpentinizing environments through adaptations to minimize oxidant limitation. *ISME J.* 15, 1121–1135. doi: 10.1038/s41396-020-00838-1

Fracchia, M., Visibile, A., Ahlberg, E., Vertova, A., Minguzzi, A., Ghigna, P., et al. (2018). α-And γ-FeOOH: stability, reversibility, and nature of the active phase under hydrogen evolution. *ACS Appl. Energ. Mater.* 1, 1716–1725. doi: 10.1021/acsaem.8b00209

Früh-Green, G. L., Kelley, D. S., Bernasconi, S. M., Karson, J. A., Ludwig, K. A., Butterfield, D. A., et al. (2003). 30,000 years of hydrothermal activity at the lost City vent field. *Science* 301, 495–498. doi: 10.1126/science.1085582

Fujioka, K., Yamanaka, T., Gamo, T., Inagaki, F., Miwa, T., Sato, H., et al. (2002). Serpentines as a capsule of the deep subsurface biosphere: evidence from the Chamorro seamount, Mariana forearc. *JAMSTECH J. Deep Sea Res.* 20, 1–16.

Galimov, E. M. (2014). Life is a product of molecular ordering "machine". *Geochem. Int.* 52, 1190–1196. doi: 10.1134/S0016702914130059

Gallardo, L., and Rodhe, H. (1997). Oxidized nitrogen in the remote Pacific: the role of electrical discharges over the oceans. *J. Atmos. Chem.* 26, 147–168. doi: 10.1023/A:1005738402496

Gamow, G. (1954). Lock and key. Possible relation between deoxyribonucleic acid and protein structures. *Nature* 173:318. doi: 10.1038/173318a0

Gamow, G., and Yčas, M. (1955). Statistical correlation of protein and ribonucleic acid composition. *Proc. Natl. Acad. Sci. U. S. A.* 41, 1011–1019. doi: 10.1073/pnas.41.12.1011

Gatenby, R. A., and Frieden, B. R. (2017). Cellular information dynamics through transmembrane flow of ions. *Sci. Rep.* 7:15075. doi: 10.1038/s41598-017-15182-2

Génin, J.-M. R., Aïssa, R., Géhin, A., Abdelmoula, M., Benali, O., Ernstsen, V., et al. (2005). Fougerite and Fe^{II-III} hydroxycarbonate green rust; ordering, deprotonation and/or cation substitution; structure of hydrotalcite-like compounds and mythic ferrosic hydroxide $Fe(OH)_{(2+x)}$. *Solid State Sci.* 7, 545–572. doi: 10.1016/j.solidstatesciences.2005.02.001

Génin, J.-M. R., Renard, A., and Ruby, C. (2008). Fougérite FeII-III oxyhydroxycarbonate in environmental chemistry and nitrate reduction. *Hyperfine Interac.* 186, 31–37. doi: 10.1007/s10751-008-9837-z

Génin, J.-M. R., Ruby, C., and Upadhyay, C. (2006). Structure and thermodynamics of ferrous, stoichiometric and ferric oxyhydroxycarbonate green rusts; redox flexibility and fougerite mineral. *Solid State Sci.* 8, 1330–1343. doi: 10.1016/j.solidstatesciences.2006.05.010

Gerbois, D., Ona-Nguema, G., Morin, G., Abdelmoula, M., Laverman, A. M., Mouchel, J.-M., et al. (2014). Nitrite reduction by biogenic hydrocarbonate Green rusts: evidence for hydroxy-nitrite Green rust formation as an intermediate reaction product. *Environ. Sci. Technol.* 48, 4505–4514. doi: 10.1021/es404009k

Glasby, G. P. (2006). Abiogenic origin of hydrocarbons: an historical overview. *Resour. Geol.* 56, 83–96. doi: 10.1111/j.1751-3928.2006.tb00271.x

Glasby, G. P., and Kasahara, J. (2001). Influence of tidal effects on the periodicity of earthquake activity in diverse geological settings with particular emphasis on submarine hydrothermal systems. *Earth-Sci. Rev.* 52, 261–297. doi: 10.1016/S0012-8252(00)00031-3

Gonzalez, D. L., Giannerini, S., and Rosa, R. (2012). On the origin of the mitochondrial genetic code: towards a unified mathematical framework for the management of genetic information. *Nat. Prec.* 7:1. doi: 10.1038/npre.2012.7136.1

Gonzalez, D. L., Giannerini, S., and Rosa, R. (2019). On the origin of degeneracy in the genetic code. *Interface Focus* 9:20190038. doi: 10.1098/rsfs.2019.0038

Goodwin, J. T., Mehta, A. K., and Lynn, D. G. (2012). Digital and analog chemical evolution. *Acc. Chem. Res.* 45, 2189–2199. doi: 10.1021/ar300214w

Greenwald, J., Kwiatkowski, W., and Riek, R. (2018). Peptide amyloids in the origin of life. *J. Mol. Biol.* 430, 3735–3750. doi: 10.1016/j.jmb.2018.05.046

Greenwald, J., and Riek, R. (2010). Biology of amyloid: structure, function, and regulation. *Struct.* 18, 1244–1260. doi: 10.1016/j.str.2010.08.009

Greenwell, H. C., and Coveney, P. V. (2006). Layered double hydroxide minerals as possible prebiotic information storage and transfer compounds. *Orig. Life Evol. Biosph.* 36, 13–37. doi: 10.1007/s11084-005-2068-2

Grégoire, B., Erastova, V., Geatches, D. L., Clark, S. J., Greenwell, H. C., and Fraser, D. G. (2016). Insights into the behaviour of biomolecules on the early earth: the concentration of aspartate by layered double hydroxide minerals. *Geochim. Cosmochim. Acta* 176, 239–258. doi: 10.1016/j.gca.2015.12.026

Grégoire, B., Greenwell, H. C., and Fraser, D. G. (2018). Peptide formation on layered mineral surfaces: the key role of brucite-like minerals on the enhanced formation of alanine dipeptides. *ACS Earth Space Chem.* 2, 852–862. doi: 10.1021/acsearthspacechem.8b00052

Gribov, L. A., Baranov, V. I., and Mikhailov, I. V. (2021). Some basic statements of the general theory of the universe evolution at the first stages of life. *Geochem. Int.* 59, 1106–1112. doi: 10.1134/S0016702921110021

Hafenbradl, D., Keller, M., Wächtershäuser, G., and Stetter, K. O. (1995). Primordial amino acids by reductive amination of α-oxo acids in conjunction with the oxidative formation of pyrite. *Tetrahed. Lett.* 36, 5179–5182. doi: 10.1016/00404-0399(50)10086-

Hagmann, M. (2002). Between a rock and a hard place. *Science* 295, 2006–2007. doi: 10.1126/science.295.5562.2006

Halevy, I., Alesker, M., Schuster, E. M., Popovitz-Biro, R., and Feldman, Y. (2017). A key role for green rust in the Precambrian oceans and the genesis of iron formations. *Nat. Geosci.* 10, 135–139. doi: 10.1038/ngeo2878

Hansen, H. C., Guldberg, S., Erbs, M., and Koch, C. B. (2001). Kinetics of nitrate reduction by green rusts—effects of interlayer anion and Fe (II): Fe (III) ratio. *Appl. Clay Sci.* 18, 81–91. doi: 10.1016/S0169-1317(00)00029-6

Hansen, H. C., Koch, C. B., Nancke-Krogh, H., Borggaard, O. K., and Sørensen, J. (1996). Abiotic nitrate reduction to ammonium: key role of green rust. *Environ. Sci. Technol.* 30, 2053–2056. doi: 10.1021/es950844w

Harrison, S. A., and Lane, N. (2018). Life as a guide to prebiotic nucleotide synthesis. *Nat. Commun.* 9:5176. doi: 10.1038/s41467-018-07220-y

Harrison, S. A., Palmeira, R. N., Halpern, A., and Lane, N. (2022). A biophysical basis for the emergence of the genetic code in protocells. *Biochim. Biophys. Acta Bioenerg.* 1863:148597. doi: 10.1016/j.bbabio.2022.148597

Hartman, H. (1975). Speculations on the origin and evolution of metabolism. *J. Mol. Evol.* 4, 359–370. doi: 10.1007/BF01732537

Hassabis, D., and Revell, T. (2021). With AI, you might unlock some of the secrets about how life works. *New Scientist* 249, 44–49. doi: 10.1016/S0262-4079(20)32269-7

Hayward, S., and Milner-White, E. J. (2008). The geometry of α-sheet: implications for its possible function as amyloid precursor in proteins. Proteins: Struct. *Funct. Bioinform.* 71, 415–425. doi: 10.1002/prot.21717

Hayward, S., and Milner-White, E. J. (2021). Determination of amino acids that favour the αL region using Ramachandran propensity plots. Implications for α-sheet as the possible amyloid intermediate. *J. Struct. Biol.* 213:107738. doi: 10.1016/j.jsb.2021.107738

Heays, A. N., Kaiserová, T., Rimmer, P. B., Knížek, A., Petera, L., Civiš, S., et al. (2022). Nitrogen oxide production in laser-induced breakdown simulating impacts on the hadean atmosphere. *J. Geophys. Res. Planets* 127:e2021JE006842. doi: 10.1029/2021JE006842

Hedderich, R. (2004). Energy-converting [NiFe] hydrogenases from archaea and extremophiles: ancestors of complex I. *J. Bioenerg. Biomembr.* 36, 65–75. doi: 10.1023/B:JOBB.0000019599.43969.33

Heinen, W., and Lauwers, A. M. (1996). Organic sulfur compounds resulting from the interaction of iron sulfide, hydrogen sulfide and carbon dioxide in an anaerobic aqueous environment. *Orig. Life Evol. Biosph.* 26, 131–150. doi: 10.1007/BF01809852

Heller, R., Duda, J. P., Winkler, M., Reitner, J., and Gizon, L. (2021). Habitability of the early earth: liquid water under a faint young Sun facilitated by strong tidal heating due to a closer moon. *Paläontol. Z.* 95, 563–575. doi: 10.1007/s12542-021-00582-7

Helmbrecht, V., Weingart, M., Klein, F., Braun, D., and Orsi, W. D. (2022). White and green rust chimneys accumulate RNA in a ferruginous chemical garden. arXiv preprint arXiv:2212.02793 [Epub ahead of preprint].

Hitchcock, D. R., and Lovelock, J. E. (1967). Life detection by atmospheric analysis. *Icarus* 7, 149–159. doi: 10.1016/0019-1035(67)90059-0

Holden, D. T., Morato, N. M., and Cooks, R. G. (2022). Aqueous microdroplets enable abiotic synthesis and chain extension of unique peptide isomers from free amino acids. *Proc. Natl. Acad. Sci. U. S. A.* 119:e2212642119. doi: 10.1073/pnas.2212642119

Hooks, M. R., Webster, P., Weber, J. M., Perl, S., and Barge, L. M. (2020). Effects of amino acids on iron-silicate chemical garden precipitation. *Langmuir* 36, 5793–5801. doi: 10.1021/acs.langmuir.0c00502

Horowitz, J. M., and Gingrich, T. R. (2020). Thermodynamic uncertainty relations constrain non-equilibrium fluctuations. *Nat. Phys.* 16, 15–20. doi: 10.1038/s41567-019-0702-6

Huang, X. L. (2019). "Iron oxide nanoparticles: an inorganic phosphatase" in *Nanocatalysts*. eds. I. Sinha and M. Shukla (London: IntechOpen), 97–124.

Huang, X. L. (2022). What are inorganic nanozymes? Artificial or inorganic enzymes. *New J. Chem.* 46, 15273–15291. doi: 10.1039/D2NJ02088B

Huber, C., Eisenreich, W., Hecht, S., and Wächtershäuser, G. (2003). A possible primordial peptide cycle. *Science* 301, 938–940. doi: 10.1126/science.1086501

Huber, C., and Wächtershäuser, G. (1997). Activated acetic acid by carbon fixation on (Fe, Ni)S under primordial conditions. *Science* 276, 245–247. doi: 10.1126/science.276.5310.245

Huber, C., and Wächtershäuser, G. (1998). Peptides by activation of amino acids with CO on (Ni,Fe)S. *Science* 281, 670–672. doi: 10.1126/science.281.5377.670

Hudson, R., de Graaf, R., Rodin, M. S., Ohno, A., Lane, N., McGlynn, S. E., et al. (2020). CO_2 reduction driven by a pH gradient. *Proc. Natl. Acad. Sci. U. S. A.* 117, 22873–22879. doi: 10.1073/pnas.2002659117

Igamberdiev, A. U. (2021). The drawbridge of nature: evolutionary complexification as a generation and novel interpretation of coding systems. *Biosystems* 207:104454. doi: 10.1016/j.biosystems.2021.104454

Javoy, M., and Pineau, F. (1991). The volatiles record of a "popping" rock from the mid-Atlantic ridge at 14 N: chemical and isotopic composition of gas trapped in the vesicles. *Earth Planet. Sci. Lett.* 107, 598–611. doi: 10.1016/0012-821X(91)90104-P

Jheeta, S., Chatzitheodoridis, E., Devine, K., and Block, J. (2021). The way forward for the origin of life: prions and prion-like molecules first hypothesis. *Life* 11:872. doi: 10.3390/life11090872

Kaila, V. R. K. (2021). Resolving chemical dynamics in biological energy conversion: long-range proton-coupled electron transfer in respiratory complex I. Acc. *Chem. Res.* 54, 4462–4473. doi: 10.1021/acs.accounts.1c00524

Kampschreur, M. J., Kleerebezem, R., de Vet, W. W., and van Loosdrecht, M. C. (2011). Reduced iron induced nitric oxide and nitrous oxide emission. *Water Res.* 45, 5945–5952. doi: 10.1016/j.watres.2011.08.056

Kandemir, B., Kubie, L., Guo, Y., Sheldon, B., and Bren, K. L. (2016). Hydrogen evolution from water under aerobic conditions catalyzed by a cobalt ATCUN metallopeptide. *Inorg. Chem.* 55, 1355–1357. doi: 10.1021/acs.inorgchem.5b02157

Kandler, O., and König, H. (1998). Cell wall polymers in archaea (Archaebacteria). *Cellul. Mol. Life Sci.* 54, 305–308. doi: 10.1007/s000180050156

Kasting, J. F., and Siefert, J. L. (2001). The nitrogen fix. *Nature* 412, 26–27. doi: 10.1038/35083660

Kelley, D. S. (1996). Methane-rich fluids in the oceanic crust. *J. Geophys. Res.-solid Earth* 101, 2943–2962.

Kelley, D. S., Karson, J. A., Blackman, D. K., Früh-Green, G. L., Butterfield, D. A., Lilley, M. D., et al. (2001). An off-axis hydrothermal vent field near the mid-Atlantic ridge at 30 N. *Nature* 412, 145–149. doi: 10.1038/35084000

Kitadai, N., Nakamura, R., Yamamoto, M., Takai, K., Li, Y., Yamaguchi, A., et al. (2018). Geoelectrochemical CO production: implications for the autotrophic origin of life. *Sci. Adv.* 4:eaao7265. doi: 10.1126/sciadv.aao7265

Kleinkauf, H., and von Döhren, H. (1996). A nonribosomal system of peptide biosynthesis. *Eur. J. Biochem.* 236, 335–351. doi: 10.1111/j.1432-1033.1996.00335.x

Kohl, L., Cumming, E., Cox, A., Rietze, A., Morrissey, L., Lang, S. Q., et al. (2016). Exploring the metabolic potential of microbial communities in ultra-basic, reducing springs at the cedars, CA, USA: experimental evidence of microbial methanogenesis and heterotrophic acetogenesis. *J. Geophys. Res. Biogeosci.* 121, 1203–1220. doi: 10.1002/2015JG003233

Kolb, V., Zhang, S., Xu, Y., and Arrhenius, G. (1997). Mineral induced phosphorylation of glycolate ion–a metaphor in chemical evolution. *Orig. Life Evol. Biosph.* 27, 485–503. doi: 10.1023/A:1006582526535

Konhauser, K. O., Lalonde, S. V., Amskold, L., and Holland, H. D. (2007). Was there really an Archean phosphate crisis? *Science* 315, 1234–2007. doi: 10.1126/science.1136328

Kordium, V. A. (2021). Defining life and evolution: essay on the origin, expansion, and evolution of living matter. *Biosystems* 209:104500. doi: 10.1016/j.biosystems.2021.104500

Kosolapova, A. O., Antonets, K. S., Belousov, M. V., and Nizhnikov, A. A. (2020). Biological functions of prokaryotic amyloids in interspecies interactions: facts and assumptions. *Intern. J. Mol. Sci.* 21:7240. doi: 10.3390/ijms21197240

Krishnamurthy, R., Arrhenius, G., and Eschenmoser, A. (1999). Formation of glycolaldehyde phosphate from glycolaldehyde in aqueous solution. *Orig. Life Evol. Biosph.* 29, 333–354. doi: 10.1023/A:1006698208873

Krishnamurthy, R., Pitsch, S., and Arrhenius, G. (1996). Mineral induced synthesis of ribose phosphates. *Orig. Life Evol. Biosph.* 26, 240–241. doi: 10.1007/BF02459734

Kuma, K., Paplawsky, W., Gedulin, B., and Arrhenius, G. (1989). Mixed-valence hydroxides as bioorganic host minerals. *Orig. Life Evol. Biosph.* 19, 573–601. doi: 10.1007/BF01808119

Kurland, C. G. (2010). The RNA dreamtime: modern cells feature proteins that might have supported a prebiotic polypeptide world but nothing indicates that RNA world ever was. *BioEssays* 32, 866–871. doi: 10.1002/bies.201000058

Lahav, N. (1985). The synthesis of primitive 'living' forms: definitions, goals, strategies and evolution synthesizers. *Orig. Life Evol. Biosph.* 16, 129–149. doi: 10.1007/BF01809467

Lane, N. (2022). *Transformer: The Deep Chemistry of Life and Death*. W. W. Norton & Company, New York, NY.

Lane, N., Allen, J. F., and Martin, W. (2010). How did LUCA make a living? Chemiosmosis in the origin of life. *BioEssays* 32, 271–280. doi: 10.1002/bies.200900131

Larsen, P., Nielsen, J. L., Dueholm, M. S., Wetzel, R., Otzen, D., and Nielsen, P. H. (2007). Amyloid adhesins are abundant in natural biofilms. *Environ. Microbiol.* 9, 3077–3090. doi: 10.1111/j.1462-2920.2007.01418.x

Larter, R. C., Boyce, A. J., and Russell, M. J. (1981). Hydrothermal pyrite chimneys from the Ballynoe baryte deposit, Silvermines, county Tipperary, Ireland. *Miner Depos* 16, 309–318. doi: 10.1007/BF00202742

Leduc, S. (1911). *The Mechanism of Life*. Rebman, London, 30–31.

Leong, J. A., Howells, A. E., Robinson, K. J., Cox, A., Debes, R. V., Fecteau, K., et al. (2021). Theoretical predictions versus environmental observations on serpentinization fluids: lessons from the Samail ophiolite in Oman. *J. Geophys. Res. Solid Earth* 126:e2020JB020756. doi: 10.1029/2020JB020756

Levitt, D. (2023). *What's Gotten Into You: The Story of Your Body's Atoms, From the Big Bang Through Last Night's Dinner*. New York: HarperCollins.

Levy, M., and Ellington, A. D. (2003). Peptide-templated nucleic acid ligation. *J. Mol. Evol.* 56, 607–615. doi: 10.1007/s00239-002-2429-7

Li, J., Browning, S., Mahal, S. P., Oelschlegel, A. M., and Weissmann, C. (2010). Darwinian evolution of prions in cell culture. *Science* 327, 869–872. doi: 10.1126/science.1183218

Li, K. M., Wilkinson, C., Kellosalo, J., Tsai, J. Y., Kajander, T., Jeuken, L. J., et al. (2016). Membrane pyrophosphatases from Thermotoga maritima and Vigna radiata suggest a conserved coupling mechanism. *Nat. Commun.* 7, 1–11. doi: 10.1038/ncomms13596

Lin, S. M., Tsai, J. Y., Hsiao, C. D., Huang, Y. T., Chiu, C. L., Liu, M. H., et al. (2012). Crystal structure of a membrane-embedded H^+-translocating pyrophosphatase. *Nature* 484, 399–403. doi: 10.1038/nature10963

Lowell, R. P., and Rona, P. A. (2002). Seafloor hydrothermal systems driven by serpentinization of peridotite. *Geophys. Res. Lett.* 29:1531. doi: 10.1029/2001GL014411

Ludwig, K. A., Shen, C. C., Kelley, D. S., Cheng, H., and Edwards, R. L. (2011). U–Th systematics and ^{230}Th ages of carbonate chimneys at the lost City hydrothermal field. *Geochim. Cosmochim. Acta* 75, 1869–1888. doi: 10.1016/j.gca.2011.01.008

Lupi, O., Dadalti, P., Cruz, E., and Sanberg, P. R. (2006). Are prions related to the emergence of early life? *Med. Hyp.* 67, 1027–1033. doi: 10.1016/j.mehy.2006.04.056

Lyu, Z., Rotaru, A. E., Pimentel, M., Zhang, C. J., and Simon, K. M. R. (2022). The methane moment-cross-boundary significance of methanogens: preface. *Front. Microbiol.* 13:1055494. doi: 10.3389/fmicb.2022.1055494

Macleod, G., Mckeown, C., Hall, A. J., and Russell, M. J. (1994). Hydrothermal and oceanic pH conditions at 4Ga relevant to the origin of life. *Orig. Life Evol. Biosph.* 24, 19–41. doi: 10.1007/BF01582037

Maden, B. (2000). Tetrahydrofolate and tetrahydromethanopterin compared: functionally distinct carriers in C1 metabolism. *Biochem. J.* 350, 609–629. doi: 10.1042/bj3500609

Mancinelli, R. L., and McKay, C. P. (1988). The evolution of nitrogen cycling. *Orig. Life Evol. Biosph.* 18, 311–325. doi: 10.1007/BF01808213

Mandon, C. L., Christenson, B. W., Schipper, C. I., Seward, T. M., and Garaebiti, E. (2019). Metal transport in volcanic plumes: a case study at White Island and Yasur volcanoes. *J. Volc. Geotherm. Res.* 369, 155–171. doi: 10.1016/j.jvolgeores.2018.11.024

Marshall, P. (2021). Biology transcends the limits of computation. *Progr. Biophys. Mol. Biol.* 165, 88–101. doi: 10.1016/j.pbiomolbio.2021.04.006

Martin, W. F. (2020). Older than genes: the acetyl CoA pathway and origins. *Front. Microbiol.* 11:817. doi: 10.3389/fmicb.2020.00817

Martin, W., and Russell, M. J. (2003). On the origin of cells: an hypothesis for the evolutionary transitions from abiotic geochemistry to chemoautotrophic prokaryotes, and from prokaryotes to nucleated cells. *Philos. Trans. R. Soc. Lond.* 358, 59–85. doi: 10.1098/rstb.2002.1183

Martin, W., and Russell, M. J. (2007). On the origin of biochemistry at an alkaline hydrothermal vent. *Philos. Trans. R. Soc. Lond.* 362, 1887–1926. doi: 10.1098/rstb.2006.1881

Martiny, J. B. H., Bohannan, B. J., Brown, J. H., Colwell, R. K., Fuhrman, J. A., Green, J. L., et al. (2006). Microbial biogeography: putting microorganisms on the map. *Nat. Rev. Microbiol.* 4, 102–112. doi: 10.1038/nrmicro1341

Maury, C. P. (2009). Self-propagating beta-sheet polypeptide structures as prebiotic informational molecular entities: the amyloid world. *Orig. Life Evol. Biosph.* 39, 141–150. doi: 10.1007/s11084-009-9165-6

Mayer, R. J., Kaur, H., Rauscher, S. A., and Moran, J. (2021). Mechanistic insight into metal ion-catalyzed transamination. *J. Am. Chem. Soc.* 143, 19099–19111. doi: 10.1021/jacs.1c08535

McGlynn, S. E., Kanik, I., and Russell, M. J. (2012). Peptide and RNA contributions to iron–Sulphur chemical gardens as life's first inorganic compartments, catalysts, capacitors and condensers. *Philos. Trans. R. Soc. Lond. A Phys. Sci.* 370, 3007–3022. doi: 10.1098/rsta.2011.0211

McMahon, S. (2019). Earth's earliest and deepest purported fossils may be iron-mineralized chemical gardens. *Proc. R. Soc. Lond. B* 286:20192410. doi: 10.1098/rspb.2019.2410

Mellersh, A. R., and Wilkinson, A.-S. (2000). RNA bound to a solid phase can select an amino acid and facilitate subsequent amide bond formation. *Orig. Life Evol. Biosph.* 30, 3–7. doi: 10.1023/A:1006620421068

Ménez, B. (2020). Abiotic hydrogen and methane: fuels for life. *Elements* 16, 39–46. doi: 10.2138/gselements.16.1.39

Merkel, A. Y., Huber, J. A., Chernyh, N. A., Bonch-Osmolovskaya, E. A., and Lebedinsky, A. V. (2013). Detection of putatively thermophilic anaerobic methanotrophs in diffuse hydrothermal vent fluids. *Appl. Environ. Microb.* 79, 915–923. doi: 10.1128/AEM.03034-12

Mielke, R. E., Robinson, K. J., White, L. M., McGlynn, S. E., McEachern, K., Bhartia, R., et al. (2011). Iron-sulfide-bearing chimneys as potential catalytic energy traps at life's emergence. *Astrobiology* 11, 933–950. doi: 10.1089/ast.2011.0667

Mielke, R. E., Russell, M. J., Wilson, P. R., McGlynn, S., Coleman, M., Kidd, R., et al. (2010). Design, fabrication and test of a hydrothermal reactor for origin-of-life experiments. *Astrobiology* 10, 799–810. doi: 10.1089/ast.2009.0456

Miller, S. L., and Bada, J. L. (1988). Submarine hot springs and the origin of life. *Nature* 334, 609–611. doi: 10.1038/334609a0

Miller, H. M., Matter, J. M., Kelemen, P., Ellison, E. T., Conrad, M. E., Fierer, N., et al. (2016). Modern water/rock reactions in Oman hyperalkaline peridotite aquifers and implications for microbial habitability. *Geochim. Cosmochim. Acta* 179, 217–241. doi: 10.1016/j.gca.2016.01.033

Milner-White, E. J. (2019). Protein three-dimensional structures at the origin of life. *Interface Focus* 9:20190057. doi: 10.1098/rsfs.2019.0057

Milner-White, E. J., and Russell, M. J. (2005). Sites for phosphates and iron-sulfur thiolates in the first membranes: 3 to 6 residue anion-binding motifs (nests): Orig. *Life Evol. Biosph.* 35, 19–27. doi: 10.1007/s11084-005-4582-7

Milner-White, E. J., and Russell, M. J. (2008). Predicting the conformations of proteins and peptides in early evolution. *Biol Dir.* 3:3. doi: 10.1186/1745-6150-3-3

Milner-White, E. J., and Russell, M. J. (2011). A peptide era heralding the emergence of life. *Genes* 2, 671–688. doi: 10.3390/genes2040671

Milner-White, E. J., Watson, J. D., Qi, G., and Hayward, S. (2006). Amyloid formation may involve α- to β-sheet interconversion via peptide plane flipping. *Structure* 14, 1369–1376. doi: 10.1016/j.str.2006.06.016

Mitchell, P. (1959). The origin of life and the formation and organizing functions of natural membranes. In: *Proceedings of the First International Symposium on the Origin of Life on the Earth*, A. I. Oparin, A.G. Pasynskiĭ, A.E. Brauntsteĭn and T.E. Pavlovskaya (Eds.). Moscow: House Academy of Science USSR, 1957; English Edition edited by F. Clark, and R.L.M. Synge, Pergamon Press, New York, 437–443.

Mitchell, P. (1961). Coupling of phosphorylation to electron and hydrogen transfer by a chemi-osmotic type of mechanism. *Nature* 191, 144–148. doi: 10.1038/191144a0

Mloszewska, A. M., Pecoits, E., Cates, N. L., Mojzsis, S. J., O'Neil, J., Robbins, L. J., et al. (2012). The composition of Earth's oldest iron formations: the Nuvvuagittuq Supracrustal Belt (Québec, Canada). *Earth Planet. Sci. Lett.* 317-318, 331–342. doi: 10.1016/j.epsl.2011.11.020

Muchowska, K. B., Varma, S. J., and Moran, J. (2019). Synthesis and breakdown of universal metabolic precursors promoted by iron. *Nature* 569, 104–107. doi: 10.1038/s41586-019-1151-1

Muchowska, K. B., Varma, S. J., and Moran, J. (2020). Nonenzymatic metabolic reactions and life's origins. *Chem. Rev.* 120, 7708–7744. doi: 10.1021/acs.chemrev.0c00191

Müller, F., Escobar, L., Xu, F., Węgrzyn, E., Nainytė, M., Amatov, T., et al. (2022). A prebiotically plausible scenario of an RNA–peptide world. *Nature* 605, 279–284. doi: 10.1038/s41586-022-04676-3

Muñoz-Santiburcio, D., and Marx, D. (2017). Chemistry in nanoconfined water. *Chem. Sci.* 8, 3444–3452. doi: 10.1039/C6SC04989C

Navarro-González, R., Navarro, K. F., Coll, P., McKay, C. P., Stern, J. C., Sutter, B., et al. (2019). Abiotic input of fixed nitrogen by bolide impacts to Gale crater during the Hesperian: insights from the Mars science laboratory. *J. Geophys. Res. Planets* 124, 94–113. doi: 10.1029/2018JE005852

Neal, C., and Stanger, G. (1983). Hydrogen generation from mantle source rocks in Oman. *Earth Planet. Sci. Lett.* 66, 315–320. doi: 10.1016/0012-821X(83)90144-9

Neal, C., and Stanger, G. (1984). Calcium and magnesium hydroxide precipitation from alkaline groundwaters in Oman, and their significance to the process of serpentinization. *Mineral. Mag.* 48, 237–241. doi: 10.1180/minmag.1984.048.347.07

Nirenberg, M., and Leder, P. (1964). RNA codewords and protein synthesis. I. the effect of trinucleotides upon the binding of sRNA to ribosomes. *Science* 145, 1399–1407. doi: 10.1126/science.145.3639.1399

Nishizawa, M. (2022). Abiotic path of Archean nitrogen. *Nat. Geosci.* 15, 962–963. doi: 10.1038/s41561-022-01072-4

Nitschke, W., and Russell, M. J. (2009). Hydrothermal focusing of chemical and chemiosmotic energy, supported by delivery of catalytic Fe, Ni, Mo/W, co, S and se, forced life to emerge. *J. Mol. Evol.* 69, 481–496. doi: 10.1007/s00239-009-9289-3

Nitschke, W., and Russell, M. J. (2010). Just like the universe the emergence of life had high enthalpy and low entropy beginnings. *J. Cosmol.* 10, 3200–3216.

Nitschke, W., and Russell, M. J. (2012). Redox bifurcations: mechanisms and importance to life now, and at its origin: a widespread means of energy conversion in biology unfolds…. *BioEssays* 34, 106–109. doi: 10.1002/bies.201100134

Nitschke, W., and Russell, M. J. (2013). Beating the acetyl coenzyme-a pathway to the origin of life. *Philos. Trans. R. Soc. Lond. Ser. B Biol. Sci.* 368:20120258. doi: 10.1098/rstb.2012.0258

Nitschke, W., Schoepp-Cothenet, B., Duval, S., Zuchan, K., Farr, O., Baymann, F., et al. (2022). Aqueous electrochemistry; the toolbox for life's emergence from redox disequilibria. *Electrochem. Sci. Adv.*:e2100192. doi: 10.1002/elsa.202100192

Nothaft, D. B., Templeton, A. S., Rhim, J. H., Wang, D. T., Labidi, J., Miller, H. M., et al. (2021). Geochemical, biological, and clumped isotopologue evidence for substantial microbial methane production under carbon limitation in serpentinites of the Samail ophiolite. *Oman. J. Geophys. Res: Biogeosci.* 126:e2020JG006025. doi: 10.1029/2020JG006025

Oda, A., and Fukuyoshi, S. (2015). Predicting three-dimensional conformations of peptides constructed of only glycine, alanine, aspartic acid, and valine. *Orig. Life Evol. Biosph.* 45, 183–193. doi: 10.1007/s11084-015-9418-5

Ooka, H., McGlynn, S. E., and Nakamura, R. (2019). Electrochemistry at deep-sea hydrothermal vents: utilization of the thermodynamic driving force towards the autotrophic origin of life. *Chem. Electro. Chem.* 6, 1316–1323. doi: 10.1002/celc.201801432

Palmeira, R. N., Colnaghi, M., Harrison, S. A., Pomiankowski, A., and Lane, N. (2022). The limits of metabolic heredity in protocells. *Proc. Roy. Soc. B.* 289:20221469. doi: 10.1098/rspb.2022.1469

Papineau, D., De Gregorio, B. T., Cody, G. D., O'Neil, J., Steele, A., Stroud, R. M., et al. (2011). Young poorly crystalline graphite in the >3.8-Gyr-old Nuvvuagittuq banded iron formation. *Nat. Geosci.* 4, 376–379. doi: 10.1038/ngeo1155

Parkes, R. J., Cragg, B. A., Bale, S. J., Getlifff, J. M., Goodman, K., Rochelle, P. A., et al. (1994). Deep bacterial biosphere in Pacific Ocean sediments. *Nature* 371, 410–413. doi: 10.1038/371410a0

Parkes, R. J., and Wellsbury, P. (2004). "Deep biospheres" in *Microbial Diversity and Bioprospecting*. ed. A. T. Bull (Washington, DC: ASM Press), 120–129.

Paukert, A. N., Matter, J. M., Kelemen, P. B., Shock, E. L., and Havig, J. R. (2012). Reaction path modeling of enhanced in situ CO_2 mineralization for carbon sequestration in the peridotite of the Samail ophiolite, Sultanate of Oman. *Chem. Geol.* 330-331, 86–100. doi: 10.1016/j.chemgeo.2012.08.013

Pauling, L. (1946). Molecular architecture and biological reactions. *Chem. Eng. News* 24, 1375–1377. doi: 10.1021/cen-v024n010.p1375

Pedersen, K. (1993). The deep subterranean biosphere. *Earth-Sci. Rev.* 34, 243–260. doi: 10.1016/0012-8252(93)90058-F

Peretó, J., Velasco, A. M., Becerra, A., and Lezcano, A. (1999). Comparative biochemistry of CO_2 fixation and the evolution of autotrophy. *Internatl. Microbiol.* 2, 3–10.

Perret, C. J. (1960). A new kinetic model of a growing bacterial population. *Microbiol.* 22, 589–617. doi: 10.1099/00221287-22-3-589

Pinna, S., Kunz, C., Halpern, A., Harrison, S. A., Jordan, S. F., Ward, J., et al. (2022). A prebiotic basis for ATP as the universal energy currency. *PLoS Biol.* 20:e3001437. doi: 10.1371/journal.pbio.3001437

Pitsch, S., Eschenmoser, A., Gedulin, B., Hui, S., and Arrhenius, G. (1995). Mineral induced formation of sugar phosphates. *Orig. Life Evol. Biosph.* 25, 297–334. doi: 10.1007/BF01581773

Polanyi, M. (1962). *Personal Knowledge*. London: Routledge & Kegan.

Pons, M. L., Quitté, G., Fujii, T., Rosing, M. T., Reynard, B., Moynier, F., et al. (2011). Early Archean serpentine mud volcanoes at Isua, Greenland, as a niche for early life. *Proc. Natl. Acad. Sci. U. S. A.* 108, 17639–17643. doi: 10.1073/pnas.1108061108

Popov, E. M. (1999). Protein folding as a nonlinear nonequilibrium thermodynamic process. *IUBMB Life* 47, 443–453. doi: 10.1080/15216549900201473

Postec, A., Quéméneur, M., Bes, M., Mei, N., Benaïssa, F., Payri, C., et al. (2015). Microbial diversity in a submarine carbonate edifice from the serpentinizing hydrothermal system of the Prony Bay (New Caledonia) over a 6-year period. *Front. Microbiol.* 6:857. doi: 10.3389/fmicb.2015.00857

Prigogine, I., and Stengers, I. (1984). *Order Out of Chaos*. Heinemann, London

Proskurowski, G., Lilley, M. D., Kelley, D. S., and Olson, E. J. (2006). Low temperature volatile production at the lost city hydrothermal field, evidence from a hydrogen stable isotope geothermometer. *Chem. Geol.* 229, 331–343. doi: 10.1016/j.chemgeo.2005.11.005

Prusiner, S. B. (1998). Nobel lecture: prions. *Proc. Natl. Acad. Sci. U. S. A.* 95, 13363–13383. doi: 10.1073/pnas.95.23.13363

Quispel, A. (1998). Lourens GM Baas Becking (1895–1963), inspirator for many (micro)biologists. *Int. Microbiol.* 1, 69–72.

Ramstead, M. J., Constant, A., Badcock, P. B., and Friston, K. J. (2019). Variational ecology and the physics of sentient systems. *Phys Life Rev* 31, 188–205. doi: 10.1016/j.plrev.2018.12.002

Ranjan, S., Todd, Z. R., Rimmer, P. B., Sasselov, D. D., and Babbin, A. R. (2019). Nitrogen oxide concentrations in natural waters on early earth. *Geochem. Geophys. Geosyst.* 20, 2021–2039. doi: 10.1029/2018GC008082

Rasmussen, B., Muhling, J. R., and Fischer, W. W. (2021). Greenalite nanoparticles in alkaline vent plumes as templates for the origin of life. *Astrobiology* 21, 246–259. doi: 10.1089/ast.2020.2270

Raza, A. (2019). *The First Cell: And the Human Costs of Pursuing Cancer to the Last*. New York: Basic Books.

Rempfert, K. R., Miller, H. M., Bompard, N., Nothaft, D., Matter, J. M., Kelemen, P., et al. (2017). Geological and geochemical controls on subsurface microbial life in the Samail ophiolite. *Oman. Front. Microbiol.* 8:56. doi: 10.3389/fmicb.2017.00056

Rimola, A., Balucani, N., Ceccarelli, C., and Ugliengo, P. (2022). Tracing the primordial chemical life of glycine: a review from quantum chemical simulations. *Internl J. Mol. Sci.* 23:4252. doi: 10.3390/ijms23084252

Rode, B. M. (1999). Peptides and the origin of life 1. *Peptides* 20, 773–786. doi: 10.1016/S0196-9781(99)00062-5

Römling, U. (2022). Is biofilm formation intrinsic to the origin of life? *Environl Microbiol.*:16179, 1462–2920. doi: 10.1111/1462-2920.16179

Ruby, C., Abdelmoula, M., Naille, S., Renard, A., Khare, V., Ona-Nguema, G., et al. (2010). Oxidation modes and thermodynamics of FeII–III oxyhydroxycarbonate green rust: dissolution–precipitation versus in situ deprotonation. *Geochim. Cosmochim. Acta* 74, 953–966. doi: 10.1016/j.gca.2009.10.030

Russell, M. J. (1996). The generation at hot springs of ores, microbialites and life. *Ore Geol. Rev.* 10, 199–214. doi: 10.1016/0169-1368(95)00023-2

Russell, M. J. (1975). Lithogeochemical environment of the Tynagh base-metal deposit, Ireland, and its bearing on ore deposition. *Trans. Instn. Min. Metall. (Appl. Earth Sci.: sect B)* 84, B128–133.

Russell, M. J. (2018). Green rust: the simple organizing 'seed' of all life? *Life* 8:35. doi: 10.3390/life8030035

Russell, M. J., and Arndt, N. T. (2005). Geodynamic and metabolic cycles in the hadean. *Biogeosciences* 2, 97–111. doi: 10.5194/bg-2-97-2005

Russell, M. J., Daniel, R. M., and Hall, A. J. (1993). On the emergence of life via catalytic iron sulphide membranes. *Terra Nova* 5, 343–347. doi: 10.1111/j.1365-3121.1993.tb00267.x

Russell, M. J., Daniel, R. M., Hall, A. J., and Sherringham, J. (1994). A hydrothermally precipitated catalytic iron sulphide membrane as a first step toward life. *J. Mol. Evol.* 39, 231–243. doi: 10.1007/BF00160147

Russell, M. J., and Hall, A. J. (1997). The emergence of life from iron monosulphide bubbles at a submarine hydrothermal redox and pH front. *J. Geol. Soc. Lond.* 154, 377–402. doi: 10.1144/gsjgs.154.3.0377

Russell, M. J., Hall, A. J., Boyce, A. J., and Fallick, A. E. (2005). 100th anniversary special paper: on hydrothermal convection systems and the emergence of life. *Econ. Geol.* 100, 419–438. doi: 0361-0128/01/3503/419-20

Russell, M. J., Hall, A. J., Cairns-Smith, A. G., and Braterman, P. S. (1988). Submarine hot springs and the origin of life. *Nature* 336:117. doi: 10.1038/336117a0

Russell, M. J., Hall, A. J., and Mellersh, A. R. (2003). "On the dissipation of thermal and chemical energies on the early earth: the onsets of hydrothermal convection, chemiosmosis, genetically regulated metabolism and oxygenic photosynthesis" in *Natural and Laboratory-simulated Thermal Geochemical Processes*. ed. R. Ikan (Dordrecht: Kluwer Academic Publishers), 325–388.

Russell, M. J., Hall, A. J., and Turner, D. (1989). In vitro growth of iron sulphide chimneys: possible culture chambers for origin-of-life experiments. *Terra Nova* 1, 238–241. doi: 10.1111/j.1365-3121.1989.tb00364.x

Russell, M. J., and Martin, W. (2004). The rocky roots of the acetyl coenzyme-a pathway. *Trends Biochem. Sci.* 29, 358–363. doi: 10.1016/j.tibs.2004.05.007

Russell, M. J., and Nitschke, W. (2017). Methane: fuel or exhaust at the emergence of life? *Astrobiology* 17, 1053–1066. doi: 10.1089/ast.2016.1599

Russell, M. J., Nitschke, W., and Branscomb, E. (2013). The inevitable journey to being. *Philos. Trans. R. Soc. B Biol. Sci.* 368:20120254. doi: 10.1098/rstb.2012.0254

Russell, M. J., and Skauli, H. (1991). A history of theoretical developments in carbonate-hosted base metal deposits and a new tri-level enthalpy classification. *Econ. Geol. Monogr.* 8, 96–116.

Say, R. F., and Fuchs, G. (2010). Fructose 1,6-bisphosphate aldolase/phosphatase may be an ancestral gluconeogenic enzyme. *Nature* 464, 1077–1081. doi: 10.1038/nature08884

Schoepp-Cothenet, B., van Lis, R., Atteia, A., Baymann, F., Capowiez, L., Ducluzeau, A.-L., et al. (2013). On the universal core of bioenergetics. *Biochim. Biophys. Acta Bioenerg.* 1827, 79–93. doi: 10.1016/j.bbabio.2012.09.005

Scholz-Starke, J., Primo, C., Yang, J., Kandel, R., Gaxiola, R. A., and Hirschi, K. D. (2019). The flip side of the Arabidopsis type I proton-pumping pyrophosphatase (AVP1): using a transmembrane H^+ gradient to synthesize pyrophosphate. *J. Biol. Chem.* 294, 1290–1299. doi: 10.1074/jbc.RA118.006315

Schöne, C., Poehlein, A., Jehmlich, N., Adlung, N., Daniel, R., von Bergen, M., et al. (2022). Deconstructing Methanosarcina acetivorans into an acetogenic archaeon. *Proc. Natl. Acad. Sci. U. S. A.* 119:e2113853119. doi: 10.1073/pnas.2113853119

Schrenk, M. O., Brazelton, W. J., and Lang, S. Q. (2013). Serpentinization, carbon, and deep life. *Rev. Mineral. Geochem.* 75, 575–606. doi: 10.2138/rmg.2013.75.18

Schrödinger, E. (1944). *What is Life? The Physical Aspect of the Living Cell*. Cambridge, England: Cambridge University Press.

Schumann, U., and Huntrieser, H. (2007). The global lightning-induced nitrogen oxides source. *Atmos. Chem. Phys.* 7, 3823–3907. doi: 10.5194/acp-7-3823-2007

Shibuya, T., and Takai, K. (2022). Liquid and supercritical CO_2 as an organic solvent in hadean seafloor hydrothermal systems: implications for prebiotic chemical evolution. *Progr. Earth Planet. Sci.* 9, 1–15. doi: 10.1186/s40645-022-00510-6

Shock, E. L. (1992). Chemical environments of submarine hydrothermal systems. *Orig. Life Evol. Biosph.* 22, 67–107. doi: 10.1007/BF01808019

Smith, J. M. (1986). *The Problems of Biology*. Oxford University Press, Oxford.

Sibson, R. H., Moore, J. M. M., and Rankin, A. H. (1975). Seismic pumping—a hydrothermal fluid transport mechanism. *J. Geol. Soc. Lond.* 131, 653–659. doi: 10.1144/gsjgs.131.6.0653

Sojo, V., Herschy, B., Whicher, A., Camprubí, E., and Lane, N. (2016). The origin of life in alkaline hydrothermal vents. *Astrobiology* 16, 181–197. doi: 10.1089/ast.2015.1406

Spiess, F. N., Macdonald, K. C., Atwater, T., Ballard, R., Carranza, A., Cordoba, D., et al. (1980). East Pacific rise: hot springs and geophysical experiments. *Science* 207, 1421–1433. doi: 10.1126/science.207.4438.1421

Srere, P. A. (1987). Complexes of sequential metabolic enzymes. *Annu. Rev. Biochem.* 56, 89–124. doi: 10.1146/annurev.bi.56.070187.000513

Stojanowic, A., and Hedderich, R. (2004). CO_2 reduction to the level of formylmethanofuran in Methanosarcina barkeri is non-energy driven when CO is the electron donor. *FEMS Microbiol. Lett.* 235, 163–167. doi: 10.1111/j.1574-6968.2004.tb09582.x

Suzuki, S., Ishii, S. I., Hoshino, T., Rietze, A., Tenney, A., Morrill, P. L., et al. (2017). Unusual metabolic diversity of hyperalkaliphilic microbial communities associated with subterranean serpentinization at the cedars. *ISME J.* 11, 2584–2598. doi: 10.1038/ismej.2017.111

Suzuki, S., Nealson, K. H., and Ishii, S. I. (2018). Genomic and in-situ transcriptomic characterization of the candidate phylum NPL-UPL2 from highly alkaline highly reducing serpentinized groundwater. *Front. Microbiol.* 9:3141. doi: 10.3389/fmicb.2018.03141

Szent-Györgyi, A. (1968). Bioelectronics: intermolecular electron transfer may play a major role in biological regulation, defense, and cancer. *Science* 161, 988–990. doi: 10.1126/science.161.3845.988

Takahashi, Y., and Mihara, H. (2004). Construction of a chemically and conformationally self-replicating system of amyloid-like fibrils. *Bioorg. Med. Chem.* 12, 693–699. doi: 10.1016/j.bmc.2003.11.022

Tatzel, M., Frings, P. J., Oelze, M., Herwartz, D., Lünsdorf, N. K., and Wiedenbeck, M. (2022). Chert oxygen isotope ratios are driven by Earth's thermal evolution. *Proc. Natl. Acad. Sci. U. S. A.* 119:e2213076119. doi: 10.1073/pnas.2213076119

Templeton, A. S., Ellison, E. T., Glombitza, C., Morono, Y., Rempfert, K. R., Hoehler, T. M., et al. (2021). Accessing the subsurface biosphere within rocks undergoing active low-temperature serpentinization in the Samail ophiolite (Oman drilling project). *J. Geophys. Res. Biogeosci.* 126:e2021JG006315. doi: 10.1029/2021JG006315

Tiago, I., and Veríssimo, A. (2013). Microbial and functional diversity of a subterrestrial high pH groundwater associated to serpentinization. *Environ. Microbiol.* 15, 1687–1706. doi: 10.1111/1462-2920.12034

Timm, J., Pike, D. H., Mancini, J. A., Tyryshkin, A. M., Poudel, S., Siess, J. A., et al. (2023). Design of a minimal di-nickel hydrogenase peptide. Science. *Advances* 9:eabq1990. doi: 10.1126/sciadv.abq1990

Tosca, N. J., Guggenheim, S., and Pufahl, P. K. (2016). An authigenic origin for Precambrian greenalite: implications for iron formation and the chemistry of ancient seawater. *Geol. Soc. Am. Bull.* 128, 511–530. doi: 10.1130/B31339.1

Tosca, N. J., Jiang, C. Z., Rasmussen, B., and Muhling, J. (2019). Products of the iron cycle on the early earth. *Free Radic. Biol. Medic.* 140, 138–153. doi: 10.1016/j.freeradbiomed.2019.05.005

Trixler, F. (2021). "Origin of nucleic acids" in *Prebiotic Chemistry and the Origin of Life*. eds. A. Neubeck and S. McMahon (Cham: Springer), 117–137.

Trolard, F., and Bourrié, G. (2012). "Fougerite a natural layered double hydroxide in gley soil: habitus, structure, and some properties" in *Clay Minerals in Nature: Their Characterization, Modification and Application*. eds. M. Valaskova and G. S. Martynkova (Rijeka, Croatia: InTech), 171–188.

Trolard, F., Bourrié, G., Abdelmoula, M., Refait, P., and Feder, F. (2007). Fougerite, a new mineral of the pyroaurite-iowaite group: description and crystal structure. *Clays Clay Miner.* 55, 323–334. doi: 10.1346/CCMN.2007.0550308

Trolard, F., Duval, S., Nitschke, W., Ménez, B., Pisapia, C., Nacib, J. B., et al. (2022). Mineralogy, geochemistry and occurrences of fougerite in a modern hydrothermal system and its implications for the origin of life. *Earth Sci. Rev.* 225:103910. doi: 10.1016/j.earscirev.2021.103910

Trutschel, L. R., Chadwick, G. L., Kruger, B., Blank, J. G., Brazelton, W. J., Dart, E. R., et al. (2022). Investigation of microbial metabolisms in an extremely high pH marine-like terrestrial serpentinizing system: Ney Springs. *Sci. Total Environ.* 836:155492. doi: 10.1016/j.scitotenv.2022.155492

Tutolo, B. M., Seyfried, W. E. Jr., and Tosca, N. J. (2020). A seawater throttle on H_2 production in Precambrian serpentinizing systems. *Proc. Natl. Acad. Sci. U. S. A.* 117, 14756–14763. doi: 10.1073/pnas.1921042117

Ueda, H., and Shibuya, T. (2021). Composition of the primordial ocean just after its formation: constraints from the reactions between the primitive crust and a strongly acidic, CO_2-rich fluid at elevated temperatures and pressures. *Fortschr. Mineral.* 11:389. doi: 10.3390/min11040389

Ueltzhöffer, K., Da Costa, L., Cialfi, D., and Friston, K. (2021). A drive towards thermodynamic efficiency for dissipative structures in chemical reaction networks. *Entropy* 23:1115. doi: 10.3390/e23091115

Ugliengo, P. (2019). The rise of computer modeling in prebiotic chemistry: comment on "prebiotic chemistry and origins of life research with atomistic computer simulations" by a. Pérez-villa et al. *Phys Life Rev* 34, 139–142. doi: 10.1016/j.plrev.2019.03.013

Van Santen, R. A. (1984). The Ostwald step rule. *J. Phys. Chem.* 88, 5768–5769. doi: 10.1021/j150668a002

Vasiliadou, R., Dimov, N., Szita, N., Jordan, S. F., and Lane, N. (2019). Possible mechanisms of CO_2 reduction by H_2 via prebiotic vectorial electrochemistry. *Interface Focus* 9:20190073. doi: 10.1098/rsfs.2019.0073

von Döhren, H., Dieckmann, R., and Pavela-Vrancic, M. (1999). The nonribosomal code. *Chem. Biol.* 6, R273–R279. doi: 10.1016/S1074-5521(00)80014-9

Wächtershäuser, G. (1988). Before enzymes and templates: theory of surface metabolism. *Microbio. Rev.* 52, 452–484. doi: 10.1128/mr.52.4.452-484.1988

Wächtershäuser, G. (1990). Evolution of the first metabolic cycles. *Proc. Natl. Acad. Sci. U. S. A.* 87, 200–204. doi: 10.1073/pnas.87.1.200

Walker, S. I., and Davies, P. C. (2017). "The "hard problem" of life" in *From matter to life: information and causality*. eds. S. I. Walker, P. C. Davies and G. F. Ellis (Cambridge, England: Cambridge University Press), 19–37.

Wander, M. C., Rosso, K. M., and Schoonen, M. A. (2007). Structure and charge hopping dynamics in green rust. *J. Phys. Chem. C* 111, 11414–11423. doi: 10.1021/jp072762n

Wang, Q., Barge, L. M., and Steinbock, O. (2019). Microfluidic production of pyrophosphate catalyzed by mineral membranes with steep pH gradients. *Chem. Eur. J.* 25, 4732–4739. doi: 10.1002/chem.201805950

Weiss, M. C., Sousa, F. L., Mrnjavac, N., Neukirchen, S., Roettger, M., Nelson-Sathi, S., et al. (2016). The physiology and habitat of the last universal common ancestor. *Nat. Microbiol.* 1:16116. doi: 10.1038/nmicrobiol.2016.116

Whicher, A., Camprubi, E., Pinna, S., Herschy, B., and Lane, N. (2018). Acetyl phosphate as a primordial energy currency at the origin of life. *Orig. Life Evol. Biosph.* 48, 159–179. doi: 10.1007/s11084-018-9555-8

White, L. M., Shibuya, T., Vance, S. D., Christensen, L. E., Bhartia, R., Kidd, R., et al. (2020). Simulating serpentinization as it could apply to the emergence of life using the JPL hydrothermal reactor. *Astrobiology* 20, 307–326. doi: 10.1089/ast.2018.1949

Wicken, J. S. (1987). *Evolution, Thermodynamics and Information: Extending the Darwinian Program*. Oxford University Press, New York, NY.

Wills, P. R., and Carter, C. W. (2018). Insuperable problems of the genetic code initially emerging in an RNA world. *BioSyst* 164, 155–166. doi: 10.1016/j.biosystems.2017.09.006

Windman, T., Zolotova, N., Schwandner, F., and Shock, E. L. (2007). Formate as an energy source for microbial metabolism in chemosynthetic zones of hydrothermal ecosystems. *Astrobiology* 7, 873–890. doi: 10.1089/ast.2007.0127

Woese, C. R., Dugre, D. H., Saxinger, W. C., and Dugre, S. A. (1966). The molecular basis for the genetic code. *Proc. Natl. Acad. Sci. U. S. A.* 55, 966–974. doi: 10.1073/pnas.55.4.966

Wolin, M. J. (1982). "Hydrogen transfer in microbial communities" in *Microbial Interactions and Communities*. eds. A. T. Bull and J. H. Slater (London: Academic Press), 323–356.

Wong, M. L., Charnay, B. D., Gao, P., Yung, Y. L., and Russell, M. J. (2017). Nitrogen oxides in early Earth's atmosphere as electron acceptors for life's emergence. *Astrobiology* 17, 975–983. doi: 10.1089/ast.2016.1473

Wong, M. L., and Prabhu, A. (2023). Cells as the first data scientists. *J. R. Soc. Interface* 20:20220081020220810. doi: 10.1098/rsif.2022.0810

Yamagata, Y., and Inomata, K. (1997). Condensation of glycylglycine to oligoglycines with trimetaphosphate in aqueous solution. II: catalytic effect of magnesium ion. *Orig. Life Evol. Biosph.* 27, 339–344. doi: 10.1023/A:1006529421813

Yamagata, Y., Watanabe, H., Saitoh, M., and Namba, T. (1991). Volcanic production of polyphosphates and its relevance to prebiotic evolution. *Nature* 352, 516–519. doi: 10.1038/352516a0

Yamamoto, M., Nakamura, R., Kasaya, T., Kumagai, H., Suzuki, K., and Takai, K. (2017). Spontaneous and widespread electricity generation in natural deep-sea hydrothermal fields. *Angew. Chemie* 129, 5819–5822. doi: 10.1002/ange.201701768

Yamamoto, M., Takaki, Y., Kashima, H., Tsuda, M., Tanizaki, A., Nakamura, R., et al. (2022). *In situ* electrosynthetic bacterial growth using electricity generated by a deep-sea hydrothermal vent. *ISME J.* 17, 12–20. doi: 10.1038/s41396-022-01316-6

Yamanaka, J., Inomata, K., and Yamagata, Y. (1988). Condensation of oligoglycines with trimeta- and tetrametaphosphate in aqueous solutions. *Orig. Life Evol. Biosph.* 18, 165–178. doi: 10.1007/BF01804669

Yarus, M. (2011). Getting past the RNA world: the initial Darwinian ancestor. *Cold Spring Harb. Perspect. Biol.* 3:a003590. doi: 10.1101/cshperspect.a003590

Yarus, M. (2017). The genetic code and RNA-amino acid affinities. *Life* 7:13. doi: 10.3390/life7020013

Yarus, M. (2021). Fitting the standard genetic code into its triplet table. *Proc. Natl. Acad. Sci. U. S. A.* 118:e2021103118. doi: 10.1073/pnas.2021103118

Yarus, M., Caporaso, J. G., and Knight, R. (2005). Origins of the genetic code: the escaped triplet theory. *Annu. Rev. Biochem.* 74, 179–198. doi: 10.1146/annurev.biochem.74.082803.133119

Yarus, M., Widmann, J. J., and Knight, R. (2009). RNA–amino acid binding: a stereochemical era for the genetic code. *J. Mol. Evol.* 69, 406–429. doi: 10.1007/s00239-009-9270-1

Yi, J., Kaur, H., Kazöne, W., Rauscher, S. A., Gravillier, L. A., Muchowska, K. B., et al. (2022). A nonenzymatic analog of pyrimidine nucleobase biosynthesis. *Angew. Chemie* 134:e202117211. doi: 10.1002/anie.202117211

Yockey, H. P. (1995). Comments on let there be life; thermodynamic reflections on biogenesis and evolution by Avshalom C. Elitzur. *J. Theor. Biol.* 176, 349–355. doi: 10.1006/jtbi.1995.0204

Yoshida, M., Muneyuki, E., and Hisabori, T. (2001). ATP synthase—a marvellous rotary engine of the cell. *Nat. Rev. Mol. Cell Biol.* 2, 669–677. doi: 10.1038/35089509

Youssef, N. H., Farag, I. F., Rudy, S., Mulliner, A., Walker, K., Caldwell, F., et al. (2019). The wood–Ljungdahl pathway as a key component of metabolic versatility in candidate phylum Bipolaricaulota (Acetothermia, OP1). *Envir. Microbiol. Rep.* 11, 538–547. doi: 10.1111/1758-2229.12753

Zajkowski, T., Lee, M. D., Mondal, S. S., Carbajal, A., Dec, R., Brennock, P. D., et al. (2021). The hunt for ancient prions: archaeal prion-like domains form amyloid-based epigenetic elements. *Mol. Biol. Evol.* 38, 2088–2103. doi: 10.1093/molbev/msab010

Zhang, S. (2012). Lipid-like self-assembling peptides. *Accounts Chem. Res.* 45, 2142–2150. doi: 10.1021/ar300034v

Zhang, S., Holmes, T., Lockshin, C., and Rich, A. (1993). Spontaneous assembly of a self-complementary oligopeptide to form a stable macroscopic membrane. *Proc. Natl. Acad. Sci. U. S. A.* 90, 3334–3338. doi: 10.1073/pnas.90.8.3334

frontiers | Frontiers in Microbiology

TYPE Original Research
PUBLISHED 15 June 2023
DOI 10.3389/fmicb.2023.1182497

OPEN ACCESS

EDITED BY
Marianne Quéméneur,
UMR7294 Institut Méditerranéen d'océanographie (MIO), France

REVIEWED BY
Daniel Colman,
Montana State University, United States
Okamoto Akihiro,
National Institute for Materials Science, Japan

*CORRESPONDENCE
Annette R. Rowe
✉ annette.rowe@uc.edu

RECEIVED 08 March 2023
ACCEPTED 24 May 2023
PUBLISHED 15 June 2023

CITATION
Trutschel LR, Kruger BR, Sackett JD, Chadwick GL and Rowe AR (2023) Determining resident microbial community members and their correlations with geochemistry in a serpentinizing spring.
Front. Microbiol. 14:1182497.
doi: 10.3389/fmicb.2023.1182497

Determining resident microbial community members and their correlations with geochemistry in a serpentinizing spring

Leah R. Trutschel[1], Brittany R. Kruger[2], Joshua D. Sackett[1], Grayson L. Chadwick[3] and Annette R. Rowe[1]*

[1]Department of Biological Sciences, University of Cincinnati, Cincinnati, OH, United States, [2]Division of Hydrologic Sciences, Desert Research Institute, Las Vegas, Las Vegas, NV, United States, [3]Department of Molecular and Cell Biology, University of California, Berkeley, Berkeley, CA, United States

Terrestrial serpentinizing systems allow us insight into the realm of alkaliphilic microbial communities driven by geology in a way that is frequently more accessible than their deep subsurface or marine counterparts. However, these systems are also marked by geochemical and microbial community variation due to the interactions of serpentinized fluids with host geology and the surface environment. To separate the transient from the endemic microbes in a hyperalkaline environment, we assessed the Ney Springs terrestrial serpentinizing system microbial community and geochemistry at six time points over the span of a year. Using 16S rRNA gene surveys we observed 93 amplicon sequence variants (ASVs) that were found at every sampling event. This is compared to ~17,000 transient ASVs that were detected only once across the six sampling events. Of the resident community members, 16 of these ASVs were regularly greater than 1% of the community during every sampling period. Additionally, many of these core taxa experienced statistically significant changes in relative abundance with time. Variation in the abundance of some core populations correlated with geochemical variation. For example, members of the *Tindallia* group, showed a positive correlation with variation in levels of ammonia at the spring. Investigating the metagenome assembled genomes of these microbes revealed evidence of the potential for ammonia generation via Stickland reactions within *Tindallia*. This observation offers new insight into the origin of high ammonia concentrations (>70mg/L) seen at this site. Similarly, the abundance of putative sulfur-oxidizing microbes like *Thiomicrospira*, *Halomonas*, and a *Rhodobacteraceae* species could be linked to changes observed in sulfur-oxidation intermediates like tetrathionate and thiosulfate. While these data supports the influence of core microbial community members on a hyperalkaline spring's geochemistry, there is also evidence that subsurface processes affect geochemistry and may impact community dynamics as well. Though the physiology and ecology of these astrobiologically relevant ecosystems are still being uncovered, this work helps identify a stable microbial community that impacts spring geochemistry in ways not previously observed in serpentinizing ecosystems.

KEYWORDS

serpentinization, Ney Springs, Illumina 16S rRNA, metagenome, sulfur oxidation intermediates

Introduction

Serpentinization is a globally relevant subsurface process caused by the hydration of iron and magnesium rich minerals within the Earth's crust which subsequently releases hydrogen gas (Mccollom and Seewald, 2013). The hydrogen produced, in addition to other reduced compounds generated, can serve as the energetic basis for microbial food webs. However, the high pH fluids overall have a profound effect on habitability. The degree of serpentinized fluid input can greatly alter microbial community composition, with pH in particular cited as a significant driver in systems that experience a range of pH values (Rempfert et al., 2017; Twing et al., 2017; Fones et al., 2021). The interaction of high pH serpentinized fluids with local geology and other water sources can also result in variation at the microbial community level, even within the same system (Morrill et al., 2013; Rempfert et al., 2017; Ortiz et al., 2018). Lastly, time scale can also have an effect on community composition, as sites undergoing active serpentinization are more impacted by high pH fluids than inactive ones (Schrenk et al., 2004; Szponar et al., 2013). Despite these known broad effects on microbial community composition, we still have limited insight into the specific geochemical drivers that explain the differences seen in the microbial communities across these systems.

Remarkable variation is seen across continental serpentinizing systems, even when comparing ones that are located within the same geologic formation (Woycheese et al., 2015; Trutschel et al., 2022). For example, Ney Springs and The Cedars are both a part of the Franciscan Subduction complex, but feature very different levels of salinity and are dominated by different microorganisms (Suzuki et al., 2017; Cook et al., 2021; Trutschel et al., 2022). Ney Springs is a terrestrial system notable for its extremely high pH (12.3–12.7) and abundance of ammonia, methane, and sulfide compared to other serpentinizing systems (Cook et al., 2021; Trutschel et al., 2022). Despite its continental location it also has marine-like levels of sodium, potassium, and boron which are likely the result of serpentinized fluids mixing with connate seawater and/or the Franciscan subduction complex marine deposit (Feth et al., 1961; Barnes et al., 1972). Ney Springs also contains incredibly high amounts of silica (>4,000 mg/L) which is likely due to the hyperalkaline fluids dissolving nearby silica-rich volcanic rocks (Feth et al., 1961; García-Ruiz et al., 2017). Ney Springs is dominated by members belonging to *Tindallia* and *Izimaplasma*, which are not typically abundant or even observed within other characterized serpentinizing systems (Trutschel et al., 2022). In comparison, The Cedars is known for its low conductivity fluids and a shallow groundwater microbial community that is dominated by the alkaliphilic and hydrogenotrophic *Serpentinomonas* (Morrill et al., 2013; Suzuki et al., 2013, 2017). Conductivity values at The Cedars are much lower compared to Ney Springs (0.8–3.0 mS/cm vs. 32–39 mS/cm, respectively), and The Cedars is limited for terminal electron acceptors such as sulfate and nitrate (Suzuki et al., 2013, 2017). The geochemical differences observed in these environments are likely explained by local variation in geology and hydrology, which in turn shape the microbial community composition and the challenges these microorganisms face.

Though surface exposed terrestrial systems are generally more easily accessed compared to their marine or purely deep subsurface counterparts, they are also subject to greater exogenous inputs and/or may be more impacted by seasonality (e.g., through precipitation, temperature, or photoperiod). Thus, they likely contain a mixture of microorganisms sustained solely by deep subsurface fluid chemistry, and microorganisms that utilize nutrient inputs and/or oxygen resulting from surface exposure. Long term geochemical and microbial community monitoring has been used to study temporal changes and the surface influence on the microbial community composition of mines and soda lake environments (Boros et al., 2017; Osburn et al., 2019). This approach allows one to determine what the endemic microbial community members of these interface environments are, how they utilize both subsurface and surface resources, and how they are impacted by temporal or seasonal changes in the environment.

In this work we assess the microbial community and aqueous geochemistry at Ney Springs over several points in a year (May 2021 – June 2022). This work identifies geochemical parameters at Ney Springs that change seasonally and those that vary temporally and are not associated with seasonality. We also present data identifying a core microbial community with an average seasonal relative abundance greater than 1%. Using metagenomics, we then investigated the potential metabolic features of this core community and how microbial metabolism may link to geochemical variation observed in this environment.

Materials and methods

Sample collection and analysis of aqueous geochemistry

Samples and field work were conducted at Ney Springs roughly every two months starting in May of 2021 through June of 2022 for a total of six trips. All Ney Springs fluids were collected from a 1 m × 1 m concrete cistern which captures the spring discharge (Supplementary Figure 1). A Mettler-Toledo multimeter (Columbus, OH, United States) was used to measure temperature, pH, conductivity, total dissolved solids (TDS), resistivity, and oxidation–reduction potential (ORP). Geochemical analyses conducted on site for dissolved oxygen (DO), S^{2-}, Fe^{2+}, tetrathionate ($S_4O_6^{2-}$), and thiosulfate ($S_2O_3^{2-}$) were done with a HACH (Loveland, CO, United States) portable spectrometer as described previously (Trutschel et al., 2022).

Fluid samples for ion chromatograph (IC) analysis of anions (F^-, Cl^-, NO_2^-, Br−, NO_3^-, PO_4^{3-}, and SO_4^{2-}) and cations (Li^+, Na^+, NH_4^+, K^+, Mg^{2+}, and Ca^{2+}) were collected using autoclaved MasterFlex® PharMed® BPT tubing (Cole-Palmer, Vernon Hills, IL, United States) with a Geopump™ peristaltic pump (GeoTech, Denver, CO, United States) to pump up water from the bottom of the cistern (Supplementary Figure 1). Fluids were passed through a polypropylene in-line filter housing (Millipore; Bedford, MA, United States) containing 0.1 µm polycarbonate membrane filters (47 mm diameter, Millipore, Tullagreen, Carrigtwohill Co. Cork, IRL) and kept on ice or refrigerated (4°C) until analysis on a Dionex Aquion Ion Chromatograph (Thermo Fisher Scientific, Waltham, MA, United States). All samples were run at a 1:10 dilution with MilliQ water, or at a 1:5 dilution after the sample had been mixed with Amberlite® MB20 H/OH resin beads (Sigma-Aldrich, United States, with a ratio of 80 mg of beads per 2 mL of sample) for chloride removal. This allowed for better detection of less abundant constituents such as NO_3^- and NO_2^-. Additional samples were

collected for external analysis through ACZ Laboratories (acz.com) (Steamboat Springs, CO, United States) for metals (silicon, iron, sodium, etc.) and ion species (nitrate, nitrite, phosphate, sulfate, and sulfide) using sample bottles and protocols provided by the company. Briefly, filtered, and unfiltered fluids were added to 250 mL HDPE bottles that were empty or contained 2 mL of 50% HNO_3. Bottles were kept on ice (~4°C) then shipped within 24 h and analyzed at ACZ. Inductively Coupled Plasma Spectroscopy (ICP) according to EPA Method 200.7 was used for metal analysis. EPA methods M353.2, M350.1 and M365.1 were used for nitrate/nitrite, ammonia, and phosphorous/phosphate, respectively. Methods D516-02/-07/-11 and SM4500s2-D were used for sulfate and sulfide (total sulfides or S). Samples for stable isotope analysis of hydrogen and oxygen in water were collected in glass exetainer vials filled without headspace or bubbles and capped to prevent evaporation and exchange of samples with atmospheric water vapor. Samples were analyzed at the Center for Stable Isotope Biogeochemistry at the University of California, Berkeley using Isotope Ratio Mass Spectrometry (IRMS). Stable isotope results were reported in parts per thousand (‰), using standard delta notation (δ^2H and $\delta^{18}O$) and are relative to VSMOW (Vienna Standard Mean Ocean Water).

Sample collection, DNA extraction, 16S rRNA gene and metagenomic sequencing

Microbial biomass was collected using the aforementioned peristaltic pump, 0.1 µm polycarbonate membrane filters, and filter setup. Filter housings were kept on ice in the dark while pumping water during summer collection periods. Water was pumped through the filters until they clogged, which occurred over a range of 2–12 L, then filters were promptly harvested and preserved on dry ice and then later at −20°C. At minimum three filters were obtained from the Ney Springs cistern at each collection period. DNA was extracted from preserved filters alongside an unused filter from the same pack to serve as a blank control using a Qiagen DNAeasy Powersoil kit. DNA was then quantified using a Qubit fluorometer (ThermoFisher Scientific, United States). Samples were then sent to Novogene (en.novogene.com) (Beijing, CHN) for 16S rRNA NovaSeq PE250 amplicon sequencing targeting the V4 region (515F-806R) using the Earth Microbiome project primers and protocol (Thompson et al., 2017) or for paired end 150 shotgun metagenomic sequencing.

16S rRNA analysis

Raw sequence data was trimmed, chimera checked, and quality filtered in DADA2 (V. 1.22) (Callahan et al., 2016) for R (V. 4.1.2). Taxonomic classification was performed using a compatible Naive Bayesian classifier trained using the SILVA_nr99_V138 training set implemented for DADA2 (McLaren, 2020). Phyloseq (V. 1.38.0) was used to generate taxonomic bar charts for 16S rRNA gene data (Mcmurdie and Holmes, 2013). Contamination sequences were determined by using the blank filter controls and were removed from the dataset using the prevalence based method in Decontam, which compares the presence/absence of taxa found in contaminated control samples to that in actual samples (Davis et al., 2018). For determination of core community Amplicon Sequence Variants (ASVs), 23 samples were first pooled into six categories based on time of sampling and then assessed for ASV detection. ASVs that were found within all six sampling events were deemed resident community members, while ASVs found during only one of the six sampling events were deemed transient. Microbial community composition and seasonal taxa overlap were visualized by generating an upset plot in UpSetR (V. 1.4.0) (Conway et al., 2017). Comparisons of mean relative abundance of core community ASVs was done using a Kruskal-Wallis test from the Vegan R package (V. 2.6-2) (Oksanen et al., 2022) followed by a Dunn test adjusted with Benjamini-Hochberg correction. The MicroViz R package (Barnett et al., 2021) was used to performed a redundancy analysis (RDA) on community samples with ASVs only detected once over the six sampling periods removed from the sample pool. Changes in the relative abundance of core community ASVs were compared with changes in various geochemical species overtime by calculating the correlation coefficient in Excel. 16S rRNA gene amplicon sequences are available under the NCBI BioProject accession number PRJNA739719.

Metagenome analysis

Metagenome sequencing data was pooled from the July 2021, January 2022, and March 2022 sampling trips as we were able to obtain sufficient biomass for metagenomics during these trips. Initial taxonomic classification of metagenome reads was performed with Kaiju (v1.7.4) (Menzel et al., 2016). Metagenomic reads were obtained and co-assembled by IDBA-ID (v1.1.3) (Peng et al., 2012), MEGAHIT (v1.2.9) (Li et al., 2015) and metaSPAdes (Nurk et al., 2017) (v 3.15.3) within the Kbase web platform (Arkin et al., 2018). The three assemblies were then binned using CONCOCT (v1.1) (Alneberg et al., 2014), MaxBin2 (V2.2.4) (Wu et al., 2016) and MetaBAT2 (v1.7) (Kang et al., 2019) for a total of nine different permutations. DAS tool (v1.1.2) (Sieber et al., 2018) was then used to merge any overlapping or redundant bins generated from CONCOCT, MaxBin2, and MetaBAT2 into one set of bins for each of the three assembly methods. These three assemblies were then classified using GTDB-tk (v1.7.0) (Parks et al., 2018) and extracted as bins. The bins were named for their number, taxonomic classification, and assembly method and were then merged as one large assembly set which was assessed in CheckM (v1.0.18) (Parks et al., 2015). A multiple sequence alignment (MSA) is generated in CheckM with HMMER[1], which uses 43 single copy phylogenetic marker genes to assess bin completeness (Parks et al., 2015). The MSA obtained from the CheckM output was then used to generate a tree using FastTree2 (v2.1.9) (Price et al., 2010). Using the phylogenetic tree along with CheckM stats, bins were manually selected based on phylogenic classification, completeness, and contamination. In most instances the phylogenetic tree nodes were grouped in sets of three, representative of each assembly method (i.e., IDBA-ID, MEGAHIT, and metaSPAdes), which all contained the same marker lineage designation, number of genomes, number of markers, and number of marker sets. The representative bin was then chosen based on highest completeness and lowest contamination. These finalized metagenome assembled genomes (MAGs) were

1 http://hmmer.janelia.org

combined with previously obtained MAGs associated with dominant Ney Springs taxa (Trutschel et al., 2022) to investigate the core microbial community members. All assemblies were annotated or re-annotated using the KEGG GhostKoala (v2.2.) online interface (Kanehisa et al., 2016). Metabolic pathway completeness was assessed using the KeggDecoder package (Graham et al., 2018) and via manual search of KO terms for genes of interest not included in the KeggDecoder package. Metagenome data is available under the NCBI BioProject accession number PRJNA739719.

Results and discussion

93 ASVs constitute Ney Springs' cistern resident community

Analysis of the pooled monthly seasonal samples revealed many transient ASVs found during only one of the sampling events, with approximately 17,000 out of the almost 20,000 ASVs detected falling into this category. These transient microorganisms are suspected to mostly come from input of debris from the surrounding environment (e.g., plants, insects, dust) into the cistern. The transient community is higher in diversity but much lower in abundance compared to the resident community, which was comprised of only 93 ASVs observed every sampling period. These 93 ASVs are referred to as the resident microbial members due to their persistent detection in the spring (Figure 1A). Notably, the resident community members were all bacteria, with Archaea only detected in low amounts in both the 16S RNA gene survey and metagenomic data for the cistern (Supplementary Datas 1, 2). This aligns with previous findings from Ney Springs which showed very little Archaeal presence (Trutschel et al., 2022). Of these resident community ASVs, the *Tindallia* and *Izimaplasma* genera consistently dominated the microbial community; seven *Tindallia* ASVs comprised 36–55% of the community and two *Izimaplasma* ASVs ranged from 3 to 36%. 16 of the resident community ASVs had an average annual abundance of greater than 1%. These 16 were deemed the core community ASVs and collectively comprised 63–87% of the community alone, while the 93 resident ASVs comprised 74–93% of the microbial community (Figure 1B).

The core community taxa found are from genera predominantly associated with alkaline environments, with many representatives previously detected in soda lakes. For example, the predominance of *Tindallia* and *Izimaplasma* species is distinct compared with other serpentinizing systems, though these taxa have been detected within soda lakes (Kevbrin et al., 1998; Vavourakis et al., 2018). Other predominant core community taxa are those belonging to the *Halomonas* and *Rhodobacteraceae* groups. Isolates from these groups have been cultured from multiple alkaline soda lake environments and have been shown to be heterotrophic sulfur oxidizers (Sorokin et al., 2000; Sorokin, 2003; Bryantseva et al., 2015; Kopejtka et al., 2017). Approximately 15% of the resident community ASVs belong to the *Rhodobacteraceae* and include the intermingled and poorly phylogenetically resolved *Paracoccus*, *Rhodobaca*, *Rhodobaculum*, *Roseibaca*, and *Roseinatronobacter* genera. The closest relative of the Gammaproteobacteria incertae sedis ASV is *Wenzhouxiangella*, another genus originally isolated from an alkaline soda lake (Sorokin et al., 2020). *Thioalkalimicrobium* (aka *Thiomicrospira*) is the only core community member also observed in high abundance in other serpentinizing system microbial communities-the Lost City and Prony Bay hydrothermal fields (Brazelton et al., 2012; Postec et al., 2015), though species have also been isolated from soda lakes as well (Sorokin et al., 2002). Ney Springs is located <640 km from Mono lake, a soda lake which shares many similar microbial members to those found in Ney Springs, such as *Halomonas, Thiomicrospira*, and *Roseinatronobacter* (Humayoun et al., 2003; Trutschel et al., 2022). The remaining core community taxa include *Planomicrobium* species, which are not known to be associated with alkaline environments, but the closely related *Planococcus* have been isolated from alkaline soils (Wang et al., 2015). There is also *Tyzzerella*, which is commonly found in the human gut microbiome, though the closest matches with our 16S rRNA sequence are from uncultured members detected in termite guts—which, are known for highly alkaline conditions that aid in digestion of plant material (Schmitt-Wagner et al., 2003). Overall, the core community taxa identified show precedence for being alkaliphiles, though this is the first time many have been detected in abundance within a serpentinizing system.

Seasonal evaporation occurs in the Ney Springs cistern

Our previous work used water isotopes to demonstrate that fluids from the Ney Springs primary cistern are distinct from other water sources in the Mt. Shasta/Dunsmuir, CA area as they diverge greatly from the meteoric water line (Trutschel et al., 2022). Our seasonal analysis has now identified fluctuations within the water isotope signatures, specifically within the $\delta^{18}O$ (‰ VSMOW) isotopes of H_2O (Figure 2). This change in oxygen isotope enrichment is likely due to evaporation as the highest $\delta^{18}O$ (‰ VSMOW) values are observed in July 2021 and June 2022, corresponding to the highest site temperatures, and the lowest $\delta^{18}O$ (‰ VSMOW) concentrations coinciding with the lowest temperature in January 2022 (Figures 2, 3A,B). The temperature extremes for the cistern were observed in January 2022 at 6°C (external daytime temperature −0.5 to 11.7°C) and in July 2021 at 13.9°C (external daytime temperature 13.3 to 32.8°C). A strong positive correlation is seen between $\delta^{18}O$ (‰ VSMOW) values and cistern temperature (correlation coefficient of 0.96) as well as $\delta^{18}O$ (‰ VSMOW) values when plotted alongside average monthly temperature for the region (correlation coefficient of 0.89) (Figure 3). When comparing average monthly precipitation to changes in water isotopes, we do not see a strong correlation. Very little precipitation is observed in the region, and a decrease in neither $\delta^{2}H$ (‰ VSMOW) nor $\delta^{18}O$ (‰ VSMOW) was observed in Ney water isotopes during October when precipitation was greatest (Figure 3). The cistern itself has a recharge rate of 3.88 L/h and its ability to refill quickly does not appear to be influenced by meteoric input. While evaporation appears to be the main driver of seasonal changes in water isotopic signatures, evaporation and precipitation do not appear to influence concentration in redox stable geochemical species such as silicon and sodium which may be more indicative of water rock-interactions (Figures 3E,F). Sodium levels at Ney Springs are elevated compared to typical marine geochemistry, making it a likely byproduct of subsurface water-rock interactions (Feth et al., 1961). At this point Ney Springs hydrogeology and specifically how this particular spring is isolated from meteoric water remains unknown. This in addition to the variation in geochemistry that may relate to active vs. mineralized

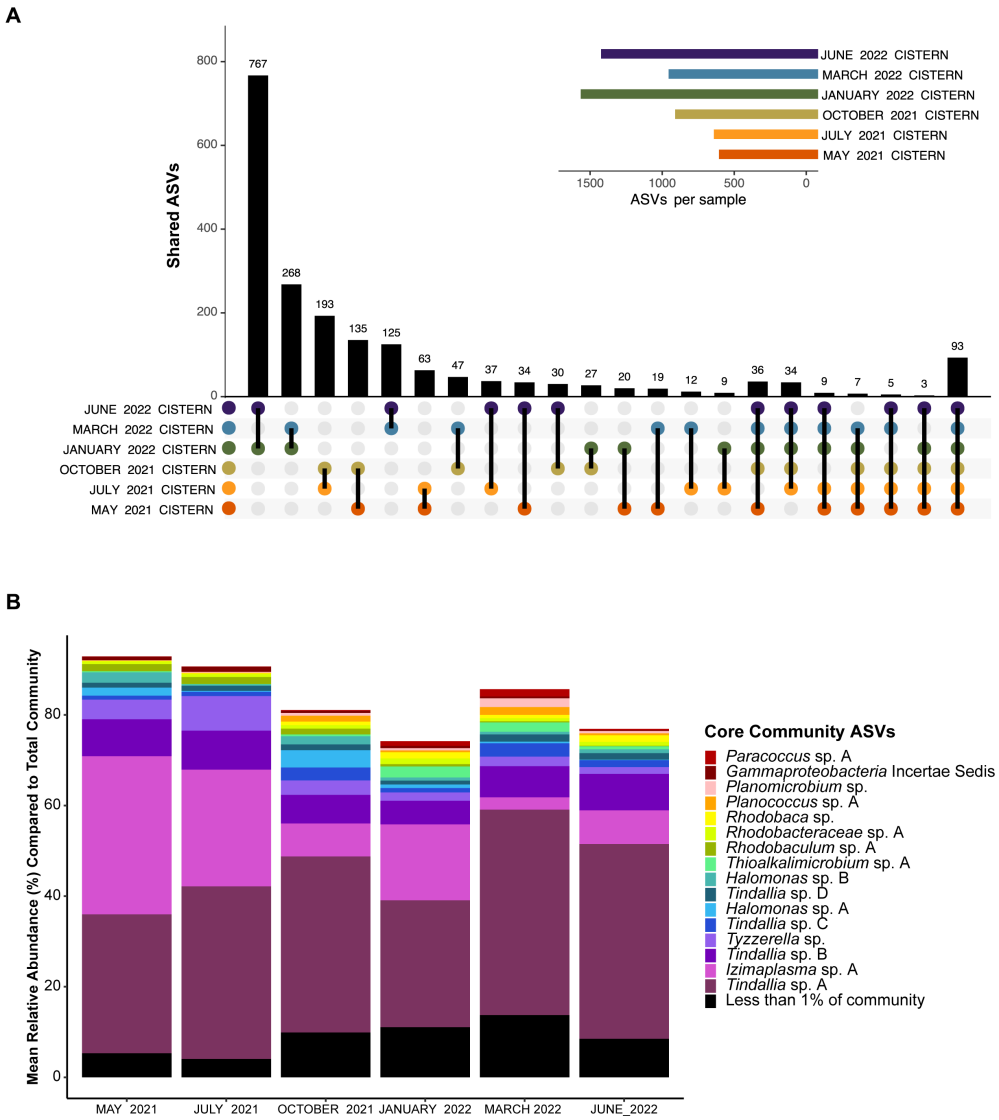

FIGURE 1
(A) UpSet plot showing how many unique ASVs overlap between pooled monthly samples. Plot shows overlap between all six months, at least five of the six months, and then ASVs which are only found in two of the six months sampled. The 93 ASVs found in all six months sampled represent the resident community members. The sample size for each month was $n \geq 3$. **(B)** Barplot showing the mean relative abundance of the 93 resident community ASVs compared to the total community. Only the top 16 with a mean relative abundance of >1% are shown, which represent the core community members. The remaining 77 resident community members are grouped together. A complete list of the resident community members can be found in Supplementary Data 1.

serpentinized fluids is in question, but at present there is no evidence for fluid mixing in the Ney Springs cistern.

Temporal variation is also observed in several redox active geochemical constituents, such as sulfur and nitrogen species. These species are more liable to be altered by microbial processes, and their variation may suggest that microbial community dynamics are driving changes that may or may not be related to other environmental parameters that change seasonally (i.e., temperature). In this system, sulfate is predicted to come from the connate nature of the deeper ground waters being influenced by the marine Franciscan subduction complex. It has previously been speculated that the sulfide present in the spring is potentially a product of microbial sulfate reduction, as it is not volcanic in nature (Feth et al., 1961). However, sulfur oxidation, which was previously shown to be a viable metabolism in this system, could also impact sulfate/sulfide concentrations (Trutschel et al., 2022). Interestingly, the balance of sulfur species changes over the course of our year sampling period. The abundance of sulfide vs. oxidized products supports the influence of microbial activity (Figure 4). While this change may be occurring at the surface level, deeper subsurface microbial activity and/or water-rock interactions could be influencing the sulfur species composition as well.

The high ammonia concentration (74–122 mg/L) in this system has been anomalous, especially compared to other characterized serpentinizing systems (Trutschel et al., 2022). It has been hypothesized that the high ammonia in Ney Springs may originate from decaying organic matter, though it is currently unclear if ancient or modern material could be the source (Waring, 1915; Feth et al., 1961). Ammonia concentrations vary over the sampling

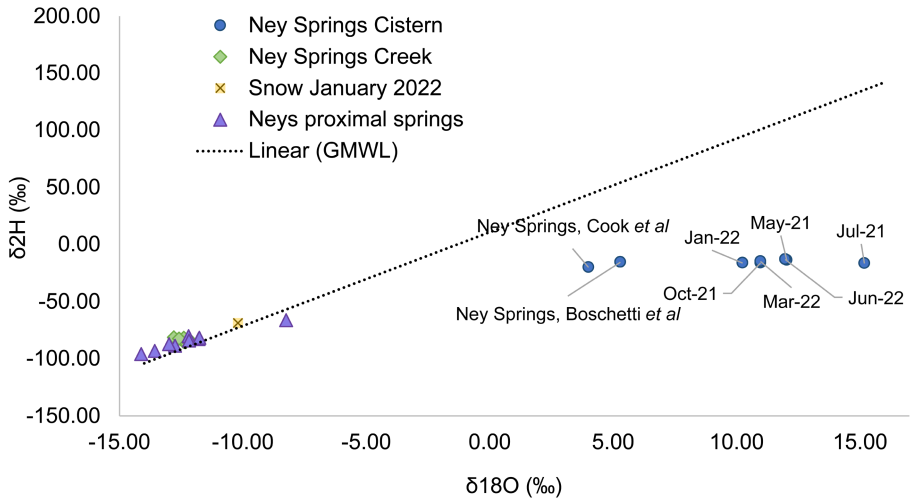

FIGURE 2
Water isotope plot showing Ney Springs cistern samples collected seasonally compared to surface water proximal springs, Ney Springs Creek, snow melt, and the global meteoric water line. Samples are differentiated by color and shape.

period, as do other detected nitrogen species. Nitrate (34–95 mg/L) and nitrite (0.01–51 mg/L) are also much higher than what is seen in other serpentinizing systems (Cardace et al., 2015; Crespo-Medina et al., 2017; Cook et al., 2021). The high concentration of nitrogen species within Ney Springs could come from interactions with the Franciscan Subduction Complex, but as the values are much higher than other serpentinizing systems within the same host geology (Morrill et al., 2013), this suggests the presence of additional nitrogen sources as well. Temporal variation in input from ancient marine sediment rich in organic matter could be contributing to nitrogen concentrations, as could subsurface microbial dissimilatory nitrate reduction to ammonia. However, it is also worth noting that within our system, we see particularly elevated amounts of nitrogen species during May and July of 2021, which may be due to seasonal changes in proximal environmental factors such as vegetation.

Changes in geochemistry and abundance of core microbial community members help explain seasonal variation

While the overall microbial community composition of Ney Springs changes seasonally, all of the samples collected across the six sampling events have a similar degree of variance. Permanova/adonis results on Bray-Curtis distances calculated for the monthly samples revealed there is a significant difference in the centroids of monthly samples (pr (>F) = 0.001), and they maintain a similar homogeneity of dispersion between them and are not significantly different in dispersal pattern (betadisper, pr (>F) = 0.224). Interestingly, community structure does not appear to be solely a function of season. For example, not all summer months cluster similarly. While May 2021 and July 2021 samples cluster, the June 2022 community samples cluster near March 2022 (Figure 5). Structure is also not simply a product of linear divergence over time due to the placement of the January 2022 and October 2021 samples in between these clusters. However, a longer sampling period would be needed to determine if the community follows any sort of cyclical or oscillating pattern.

The strongest correlations between taxa with particular sampling periods were seen in core community ASVs that experienced a significant increase in relative abundance within that sampling period (Figures 5, 6). Out of the 16 core community members, 12 underwent significant changes to their mean relative abundance seasonally (Kruskal-Wallis test, p value <0.05) (Figure 6). The greatest change in average relative abundance was observed in *Izimaplasma* sp. A, between May 2021 and March 2022 at 35% vs. 2.7% of the total microbial community, respectively, (Dunn test, p.adj. value = 0.0001). Previously, *Izimaplasma* had been observed as the most abundant microbial community member during the first sampling of Ney Springs in late May of 2019, reinforcing its observed strong association with the early summer month (Trutschel et al., 2022). Two other ASVs followed the inverse of this pattern, with their highest abundance and strongest correlation associated with March 2022 and their lowest abundance observed in May 2021. This included *Planococcus* sp. A (March 1.7% vs. May 0.05%) and the *Planomicrobium* sp. (March 1.91% vs. May 0.05%) (Dunn test, p.adj. values <0.01). Other ASVs experiencing a period of upsurge where their average relative abundance was significantly higher (Dunn test, p.adj. value<0.04) compared to two or more of the other sampling times included the *Tyzzerella* sp. during July 2021 with a maximum observed relative abundance of 7.6%, *Halomonas* sp. A in October 2021 at 3.84%, *Thioalkalimicrobium* sp. A in January 2022 at 2.41%, and *Tindallia* sp. C in March at 2.93%.

In addition to determining sampling periods' associations with specific ASVs, a redundancy analysis (RDA) was performed to determine how much seasonal variation within the microbial community may be explained by changes in geochemistry. Constrained elements were chosen based on their seasonal variation, potential for interaction with microbial metabolism, and on their unrelatedness to one another. These parameters included pH, temperature, sodium, ammonia, and sulfide. The five independent constrained variables explained 74.3% of the variation seen between

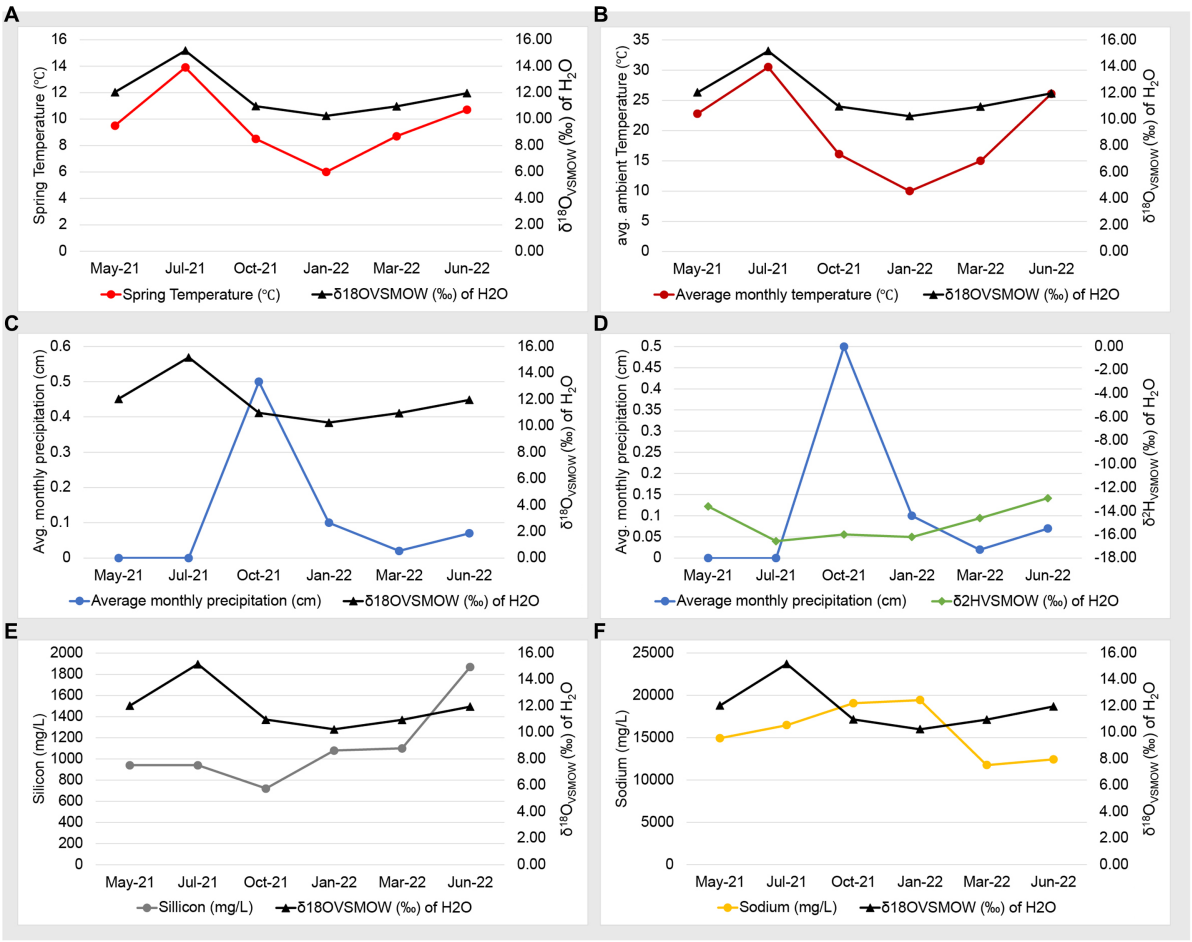

FIGURE 3
Geochemistry and water isotope time series plots. Plots consists of two *Y* axes, with data points listed in chronological order on the *X* axis. Panels are as follows: **(A)** Ney Springs cistern fluid temperature compared to $\delta^{18}O$ (‰ VSMOW) of H_2O. **(B)** Average ambient monthly temperature for greater Ney Springs area compared to $\delta^{18}O$ (‰ VSMOW) of H_2O. **(C)** Average monthly precipitation for greater Ney Springs area compared to $\delta^{18}O$ (‰ VSMOW) of H_2O. **(D)** Average monthly precipitation for greater Ney Springs area compared to $\delta^{2}H$ (‰ VSMOW) of H_2O. **(E)** Silicon concentration in Ney Springs cistern (mg/L) compared to $\delta^{2}H$ (‰ VSMOW) of H_2O. **(F)** Sodium concentration in Ney Springs cistern (mg/L) compared to $\delta^{2}H$ (‰ VSMOW) of H_2O.

the microbial community samples (Figure 5). This revealed several potential relationships between core community taxa and constrained elements associated with metabolism, such as *Tindallia* spp. with ammonia as well as *Thioalkalimicrobium* sp. A, and *Halomonas* sp. A with sulfide. Meanwhile, changes in pH, sodium, and temperature may cause a shift in favorable growth conditions for multiple core community members in a way that broadly alters structure. This could also explain why certain sampling periods are associated more closely with these parameters (e.g., sodium with January 2022).

Core community associated MAGs show adaptations to salinity and alkalinity

To understand the drivers of the observed correlations between species abundance, seasonality, and geochemistry, metagenome assembled genomes (MAGs) of the core microbial community were analyzed. In addition to seven previously obtained MAGs (Trutschel et al., 2022), we report nine additional MAGs used to investigate the metabolic potential of the core community members (Table 1). Three MAGs were below 95% complete (*Planococcus* bin 006, *Lachnospirales* bin 026, and *Roseinatronobacter* bin 022) and though all were present in the core microbial community, they have been omitted from further analysis due to the inability to confidently assess metabolism. *Tindallia* bin 004 was included despite its higher potential for contamination (9.27%) because it contained a 16S rRNA gene sequence that directly matched the most abundant ASV (*Tindallia* sp. A) and because all genes of interest matched *Tindallia* bin 001, which only contained 3% contamination. When assessing mechanisms for dealing with the stress of this environment, focus was placed on the organisms' genetic potential for tolerating salinity and alkalinity. While temperature is potentially a driving feature of seasonal variation of the spring community, genome level adaptations to temperature were not investigated as the cistern temperature remained in the low mesophilic to psychrophilic range all year (6–13.9°C), and as such, we would not expect a strong genome level signature for temperature.

Many of the MAGs encoded genes associated with salinity and alkalinity tolerance such as Na^+/H^+ antiporters Mrp and/or Nha (Figure 7). Mrp antiporters are often essential for maintaining an electrochemical gradient in alkaline and marine conditions by

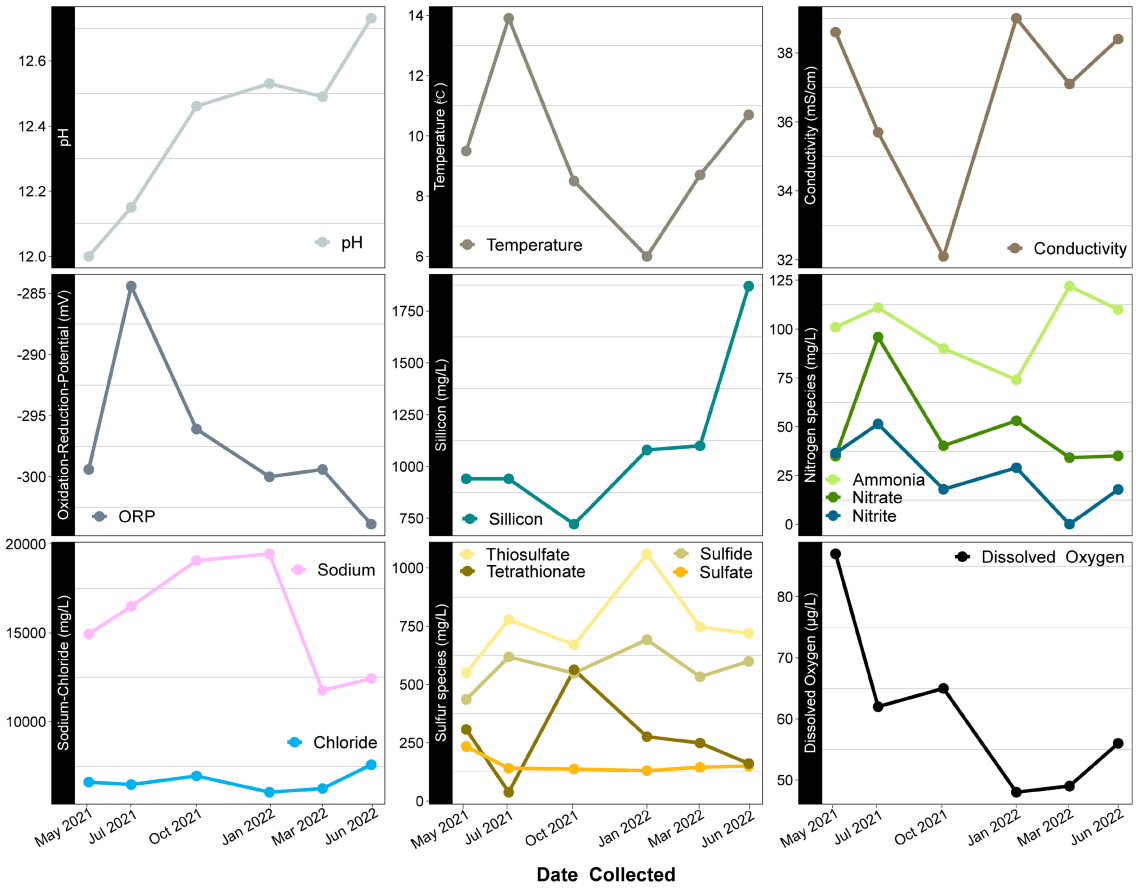

FIGURE 4
Time series scatter plots of geochemical constituents measured over a year at Ney Springs. *X* axis represents time sampled while *Y* axis specifies units for each constituent. Similar species likely to have relationships are grouped together.

pumping sodium ions out while pumping protons in (Ito et al., 2017). Homologs of the Na^+/H^+ antiporter NhaD found in the *Halomonas* MAG do not exhibit activity below pH 8 and have thus far only been found in alkaliphiles (Nozaki et al., 1998). NhaC homologs, which are detected in the *Tindallia* and *Wenzhouxiangella* MAGs, have been shown to be necessary for growth in alkaliphilic conditions for several *Bacillus* sp. (Ito et al., 1997; Krulwich et al., 1997). Putative sodium pumping NADH-coQ reductase (Nqr) was also observed in many of the MAGs, which can help maintain the electrochemical gradient under alkaline conditions in conjunction with the H^+/Na^+ antiporters by pumping sodium out (Vorburger et al., 2016). As described previously, most of the MAGs appear to encode for H^+ binding rather than Na^+ binding ATPases based on amino acid sequence despite the low concentrations of H^+ at pH 12 (Mulkidjanian et al., 2008; Trutschel et al., 2022). The exceptions to this are the *Tindalliaceae* and *Izemoplasmataceae* MAGs which are predicted to contain Na^+ binding F-type ATPases and are notably the most abundant taxa in the system (Figure 7). *Tindallia* sp. A and D exhibit a slight negative correlation with sodium respectively, but no other core community ASVs have a suggested strong relationship with sodium (Figure 8). Notably, the relative abundance of *Izimaplasma* sp. A is negatively correlated with pH, while only the *Rhodobaca* sp. A ASV was strongly positively correlated with an increase in pH (Figures 8, 9A,B). Previously an isolate from the *Roseinatronobacter-Rhodobaca* cluster of the *Rhodobacteraceae* family was isolated from Ney Springs and was found capable of growth in pH 12.4 media (Trutschel et al., 2022), suggesting that some members of this clade may be better at tolerating high pH conditions.

Metagenomic information shows potential for ammonia production by most abundant core community member

The source of ammonia within Ney Springs is unknown, but may be linked to current or past microbial activity. The potential for generation of ammonia through denitrification (DNRA) is observed in the *Rhodobacteraceae* and *Halomonas* MAGs, which each encode nitrate and nitrite reductases (NarGH/NapAB and NirBD) (Figure 7), however none of the *Rhodobacteraceae* or *Halomonas* ASVs exhibit a strong correlation coefficient with nitrite, nitrate, or ammonia (Figure 8). Only *Planococcus* sp. A and the *Planomicrobium* sp. were observed to have a relationship with nitrite (Figure 9G), while the *Tyzzerella* and Gammaproteobacteria Incertae Sedis spp. were the only ASVs positively correlated with nitrate (Figure 9H). Conversely, *Tindallia* sp. A, B and D are all positively correlated with ammonia (Figures 8, 9F). The *Tindallia* MAGs encode the enzymes necessary for Stickland reactions from glycine and ornithine (GrdABE and Ord), which have been shown to produce ammonia (Sangavai and Chellapandi, 2017). *Tindallia magadii*, the type-strain of the genus, has

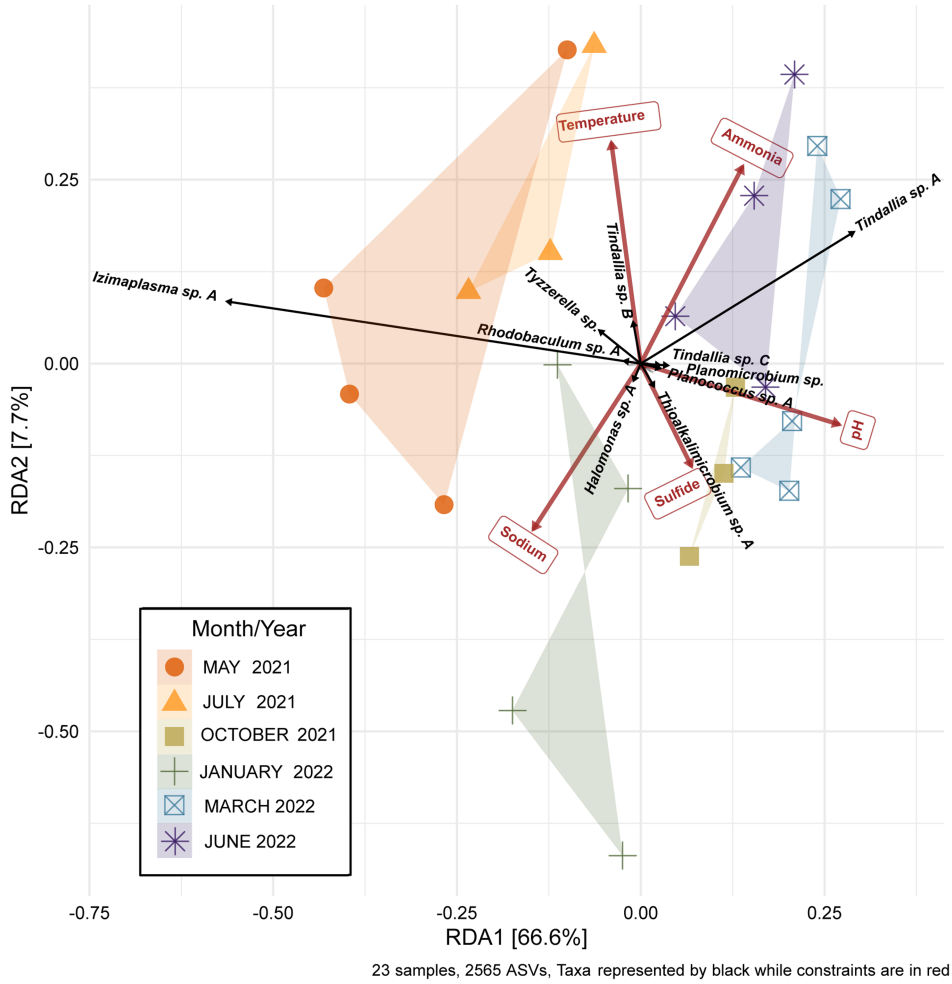

FIGURE 5
Redundancy analysis (RDA) plot of the Ney Springs cistern microbial community samples. 23 microbial community samples were collected during six different sampling events. Samples are devoid of transient ASVs, i.e., ASVs that were only encountered during one sampling event, in order to best represent the resident microbial community. Count data is transformed to be in terms of relative abundance per sample. Constrained elements were chosen based on their ability to explain variation within the microbial community and lack of overlap with one another.

been observed producing upwards of 30 mM of ammonium over a 60 h period when grown in culture with 2 g/L arginine and ornithine as the initial substrate (Kevbrin et al., 1998). Stickland reaction in members of the *Peptostreptococcaceae* are cited as the most abundant ammonia producing organisms within the rumen, with several strains capable of producing up to 0.4 mM per mg of protein per minute (Paster et al., 1993; Sangavai and Chellapandi, 2017). Given the high concentrations of ammonia generally produced by these groups, it is predicted that these organisms have adaptations for ammonia tolerance, though there is little insight into what these genetic adaptations may be.

Lack of hydrogen and methane metabolism amongst core community members

Ammonia is hypothesized to be one of key driving factors of community composition within this environment, and the likely reason we do not observe methanogens or methane oxidizers typically associated with serpentinizing systems within Ney Springs (Trutschel et al., 2022). The abundance of free molecular ammonia (NH_3 as opposed to NH_4^+) potentially places strong selective pressure on microbial inhabitants due to its increased membrane passivity (Kayhanian, 1999). Both ammonia and methane associated metabolisms are known to be inhibited by high ammonia concentrations (Lehtovirta-Morley, 2018; Yan et al., 2020). No evidence of potential ammonia oxidation (AmoA or Hzo), nor methanogenesis or methane oxidation (McrA, MmoA or PmoA) was observed within the core community MAGs (Figure 7), which concurs with previous results showing a lack of evidence for these metabolisms (Cook et al., 2021; Trutschel et al., 2022). Similarly, there were very few potential hydrogenases detected within the core community MAGs (Figure 7). Partially complete NAD (HoxFUY) and NADP-reducing (HndBCD or HndCD) hydrogenases were found in five of the MAGs. A partially complete NiFe hydrogenase (HyaBC) was found within *Rhodobacteraceae* bin 004, but it was missing the small subunit (HyaA). This could suggest a loss of gene function in these organisms. Hydrogen has been measured at exceptionally low concentrations at Ney Springs when compared to other serpentinizing systems. Bubbles that arise from the bottom of the cistern have consistently contained

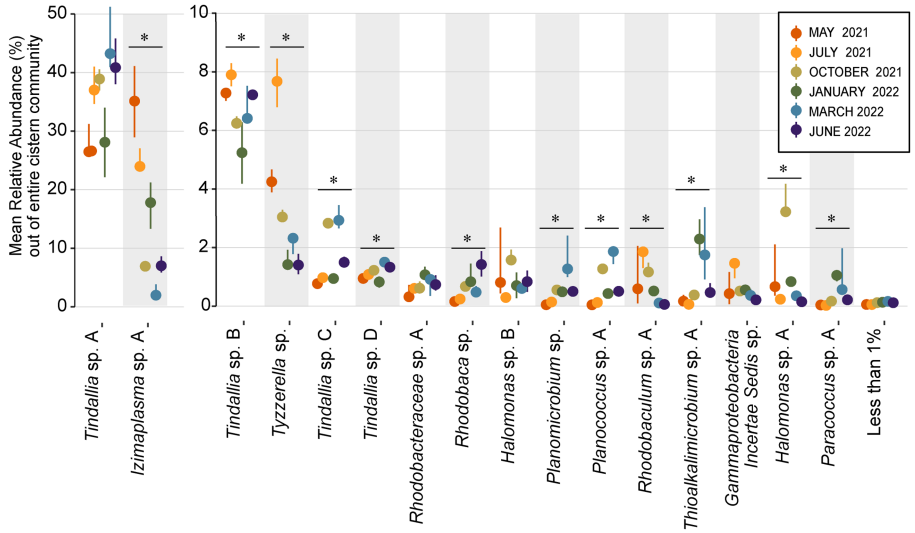

FIGURE 6
Dot plot showing change in mean relative abundance of sixteen core community ASVs that regularly comprise 1% or more of the total community. The remaining 77 resident community members are grouped together as the "Less than 1%" category. ASVs are organized by decreasing overall mean relative abundance, with groups split between two *Y* axes in order to better visualize changes in less abundant ASVs. The dots plotted represent the mean relative abundance of $n \geq 3$ samples each month, while lines emitting from the dots represent the 95% confidence interval. ASVs that had a significant change in relative abundance between months (Kruskal-Wallis test, *p* value <0.05) are denoted with a bar and "*" above them.

around 0.02 atm hydrogen by volume, while dissolved hydrogen was measured at <0.01 mg/L (Mariner et al., 2003; Trutschel et al., 2022). Although thermodynamically favorable in this system, hydrogen oxidation is likely limited due to the low concentration of hydrogen available within the cistern (Trutschel et al., 2022). Acetate and formate represent other potential energy sources that may be formed via serpentinization. Many of the MAGs did encode for putative formate dehydrogenases (FdoGHI) (Figure 7), with many of the *Rhodobacteraceae* MAGs containing multiple copies. The *Izemoplasmataceae/Tenericutes* MAGs also contained formate C-acetyltransferase (PflAD). Other than the *Tindalliaceae* and *Izemoplasmataceae/Tenericutes* MAGs, the core community members all contained Acetyl-CoA synthetase (ACS). *Rhodobacteraceae* and *Halomonas* spp. have been isolated from the system previously and have been observed using acetate as a carbon/energy source (Trutschel et al., 2022).

Temporal fluctuation in sulfur species concentrations associated with putative sulfur-oxidizing core community members

Another peculiar aspect of Ney Springs is the abundance of sulfide, which is not commonly found in terrestrial serpentinizing systems. Sulfide is found in marine serpentinizing systems such as the Lost City [2–32 mg/L (Schrenk et al., 2004)], but it is often orders of magnitude higher at Ney Springs (430–700 mg/L). Despite the abundance of sulfide and theoretical energy available for sulfate-reducing metabolic reactions, we have once again found little genetic evidence of microbial sulfide production via dissimilatory sulfate reduction or anaerobic methane oxidation using sulfate as a terminal electron acceptor (Trutschel et al., 2022). We did not detect methyl-coenzyme M reductase (McrA) or dissimilatory sulfate reductase (DsrAB) within the core microbial community associated MAGs, though a putative DsrAB was previously found in a MAG associated with resident community member *Desulfurivibrio* (Figure 7; Trutschel et al., 2022). Two *Rhodobacteraceae* MAGs putatively contain sulfate adenylyltransferase (Sat), which is likely to be involved in sulfur assimilation but has also been implicated in dissimilatory sulfur oxidation in this organism (Yu et al., 2007; Parey et al., 2013). Evidence of sulfur oxidation is much more prevalent in the core community members, as all the core community MAGs except those belonging to the *Tindalliaceae* and *Izemoplasmataceae* have the potential to engage in some form of sulfur species oxidation. The *Thiomicrospira/Thioalkalimicrobium* MAG contains Sqr (sulfide:quinone oxidoreductase) along with SoxXYZABCD (sulfur oxidation operon) and is predicted to oxidize sulfur species completely to sulfate. *Thioalkalimicrobium* sp. A relative abundance has a slight positive correlation with thiosulfate (Figure 8) and is most abundant when sulfide and thiosulfate are highest in January 2022. MAGs classified as *Rhodobacteraceae* all contain Sqr, have varying degrees of completeness of the Sox sulfur oxidation pathway, and all contain a complete or almost complete SoeABC (quinone sulfite dehydrogenase). Despite this putative evidence, only *Rhodobacteraceae* sp. A exhibits a positive correlation with sulfide and thiosulfate concentrations within the cistern (Figure 8), as its abundance is highest when thiosulfate and sulfide are also at their highest and conversely low when these concentrations are also low (Figures 9C,E). The *Halomonas* MAG only contains SoxZ (thiosulfate oxidation carrier protein), but does contain thiosulfate dehydrogenase (TsdA), an alternate thiosulfate oxidizing protein (Denkmann et al., 2012). This pathway produces tetrathionate as an end-product, which is not observed in organisms only utilizing the Sox system (Kelly et al., 1997; Grabarczyk and Berks, 2017). The changes in relative abundance of the *Halomonas* sp. A and B ASVs tracks well with changes in tetrathionate concentration within the

TABLE 1 Summary of MAGs relating to core microbial community.

MAG name	Phylum	Class	Order	Family	Genus	Completeness	Contamination	Contigs	Potential core community ASV match based on taxonomic classification	Source
March 2022-Tindalliaceae.bin004	Firmicutes_A	Clostridia	Peptostreptococcales	Tindalliaceae	JAABSW01	95.8	9.27	143	Direct match to *Tindallia* sp. A 16S rRNA	This work
May 2019-Tindalliaceae.bin001	Firmicutes_A	Clostridia	Peptostreptococcales	Tindalliaceae	–	97	3	275	*Tindallia* sp. B,C,D,	Trutschel et al. (2022)
January 2022-Izemoplasmataceae.bin006	Firmicutes	Bacilli	Izemoplasmatales	Izemoplasmataceae	CSBR16-87	98.67	0	75	*Izimaplasma* sp. A	This work
May 2019-Tenericutes.bin	Firmicutes	Bacilli	Izemoplasmatales	–	–	99	0	97	*Izimaplasma* sp. A	Trutschel et al. (2022)
[1]May 2019-Lachnospirales.bin026	Firmicutes_A	Clostridia	Lachnospirales	UBA5962	–	90	0	35	*Tyzzerella* sp.	Trutschel et al. (2022)
July 2021-Rhodobacteraceae.bin004	Proteobacteria	Alphaproteobacteria	Rhodobacterales	Rhodobacteraceae	Tabrizicola	95.52	5.19	330	*Paracoccus* sp. A	This work
July 2021-Rhodobacteraceae.bin017	Proteobacteria	Alphaproteobacteria	Rhodobacterales	Rhodobacteraceae	Yoonia	98.99	0.84	329	*Rhodobaculum* sp. A	This work
July 2021-Rhodobacteraceae.bin021	Proteobacteria	Alphaproteobacteria	Rhodobacterales	Rhodobacteraceae	Roseibaca	98.94	0.61	330	*Rhodobaculum* sp. A	This work
May 2019-Rhodobacteracea.bin019	Proteobacteria	Alphaproteobacteria	Rhodobacterales	Rhodobacteraceae	–	96	1.1	168	*Rhodobacteraceae* sp. A	Trutschel et al. (2022)
[1]March 2022-Roseinatronobacter.bin022	Proteobacteria	Alphaproteobacteria	Rhodobacterales	Rhodobacteraceae	Roseinatronobacter	74.14	8.75	58	*Rhodobacteraceae* sp. A	This work
May 2019-Halomonas.bin014	Proteobacteria	Gammaproteobacteria	Pseudomonadales	Halomonadaceae	Halomonas	99	6.1	229	*Halomonas* sp. A,B	Trutschel et al. (2022)
[1]March 2022-Planococcus.bin006	Firmicutes	Bacilli	Bacillales	Planococcaceae	Planococcus	54.52	4.52	275	*Planococcus sp*. A, *Planomicrobium* sp.	This work
[2]July 2021-Thiomicrospira.bin012	Proteobacteria	Gammaproteobacteria	Thiomicrospirales	Thiomicrospiraceae	Thiomicrospira	99.39	0	164	*Thioalkalimicrobium* sp. A	This work
March 2022-Wenzhouxiangella.bin008	Proteobacteria	Gammaproteobacteria	Xanthomonadales	Wenzhouxiangellaceae	Wenzhouxiangella	98.71	2.04	276	*Gammaproteobacteria Incertae Sedis* sp.	This work
May 2019-Wenzhouxiangella.bin008	Proteobacteria	Gammaproteobacteria	Xanthomonadales	Wenzhouxiangellaceae	Wenzhouxiangella	96	1.2	56	*Gammaproteobacteria Incertae Sedis* sp.	Trutschel et al. (2022)
May 2019-Wenzhouxiangella.bin027	Proteobacteria	Gammaproteobacteria	Xanthomonadales	Wenzhouxiangellaceae	Wenzhouxiangella	98	4.6	71	*Gammaproteobacteria Incertae Sedis* sp.	Trutschel et al. (2022)

[1]These MAGs omitted from metabolic discussion in paper due to less than 95% completeness.
[2]At the genus level this organism may be classified as Thiomicrospira or Thioalkalimicrobium.

10.3389/fmicb.2023.1182497

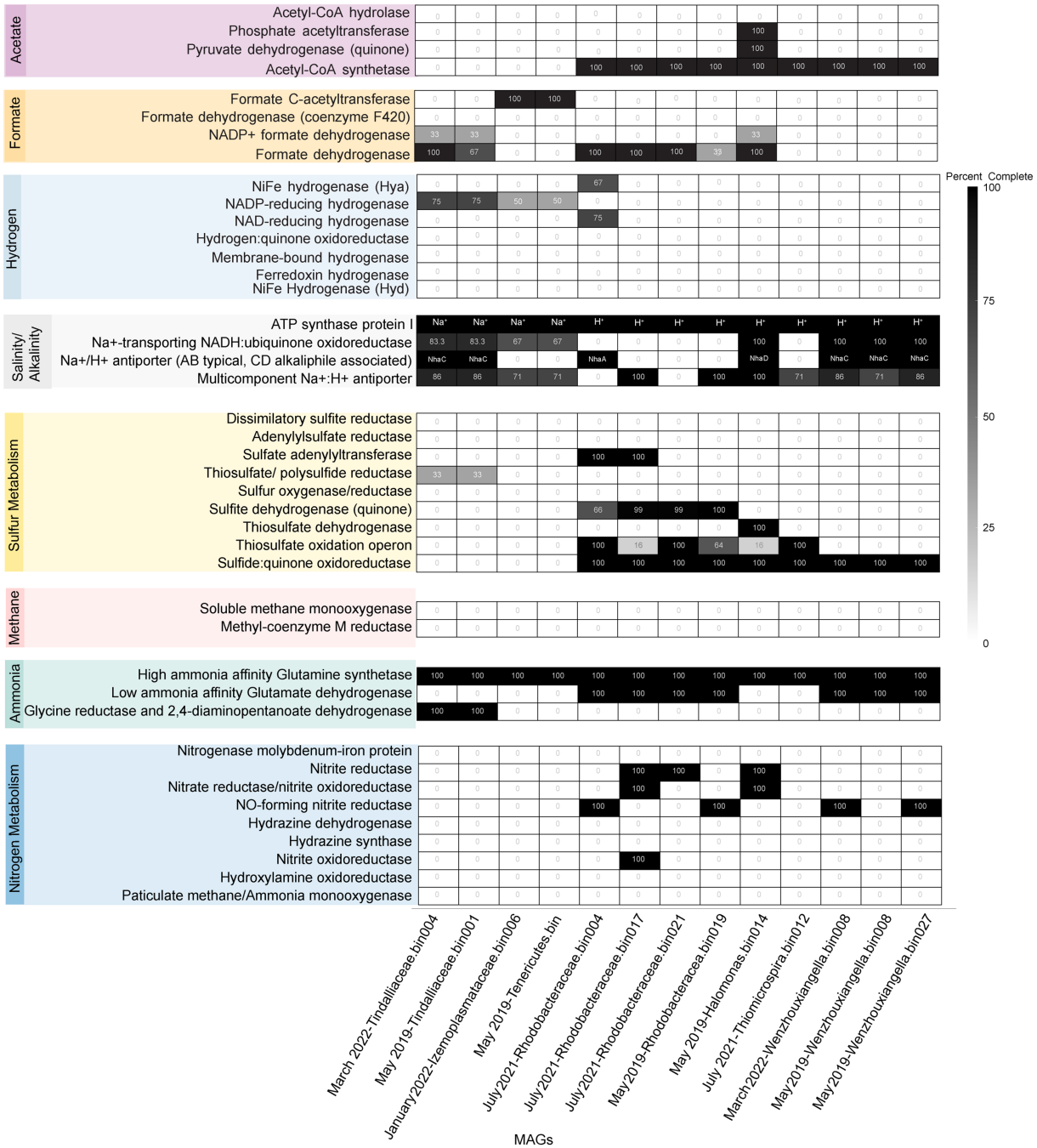

FIGURE 7
Heatmap of core community associated MAGs with selected marker proteins relating to nitrogen, sulfur, methane, hydrogen, formate, and acetate metabolism or are associated with alkalinity and salinity tolerance. Only MAGs that had greater than 95% completeness are shown within the Heatmap. The black boxes for ATP synthase protein I have all necessary subunits for an F-type ATPase (AtpFBCHGDAE) and instead specify whether an organism is likely to encode for a Na^+ or H^+ binding ATP synthase based on amino acid sequence. For organisms that do contain the gene homolog, the black boxes for the Na^+/H^+ antiporter specify if the organism is likely to contain NhaA, C or D, with Nha C and D originally characterized in and often associated with alkaliphiles.

cistern over time (Figure 9D) and *Halomonas* sp. A has a very high positive correlation coefficient with tetrathionate (Figure 8). A *Halomonas* isolate from Ney Springs has previously been shown to oxidize thiosulfate to tetrathionate *in vitro* as well, confirming this as a likely product produced by these organisms in the environment (Trutschel et al., 2022).

Implications

Since the discovery of active serpentinization in the Coast Range ophiolite many serpentinizing systems have been identified by Barnes in Northern California, including what is now the Coast Range Ophiolite Microbial Observatory, The Cedars, and Ney

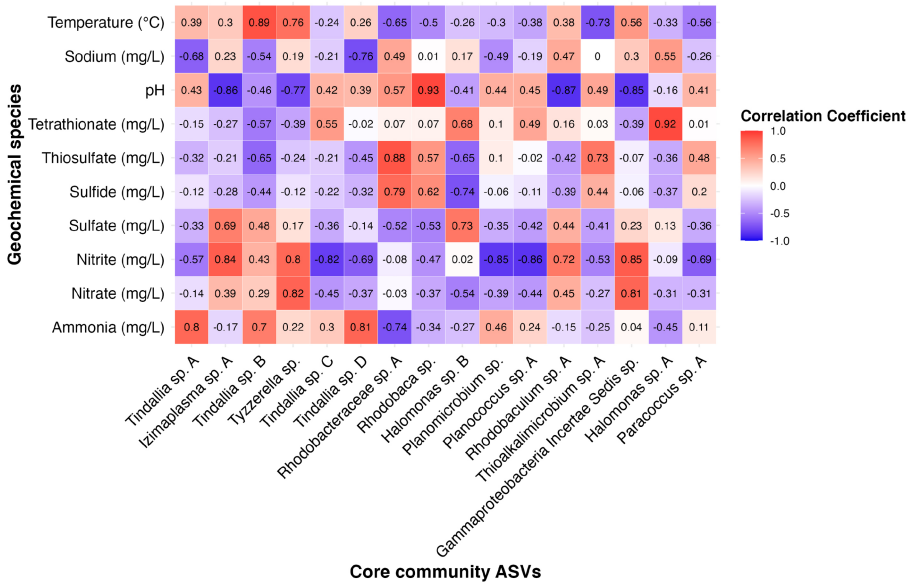

FIGURE 8
Heatmap showing correlation coefficient values between the relative abundance of 16 core community ASVs with geochemical constituents of interest as determined by results of RDA analysis.

Springs (Barnes et al., 1967, 1972; Barnes and O'Neil, 1969). The investigation of Ney Springs has allowed us greater insight into the ecology of terrestrial serpentinizing systems and the role host geology and microbial metabolism have on shaping geochemistry. Serpentinizing springs like Ney are commonly studied as windows into subsurface microbial communities and food webs that subsist on the reduced compounds generated by the serpentinzation reaction. Notably, these systems maintain their high pH and much of their geochemistry despite surface exposure, which results in a specialized microbial community. This can be seen within Ney Springs, with the resident community members making up the overwhelming majority of this interface microbial community. Using ASVs as the final denominator may produce an artifact of a seemingly large introduced community, but this more conservative method is preferred since it allowed us to focus on a limited number of well-established core taxa adapted to the polyextreme conditions of Ney Springs. By further identifying the putative adaptations and metabolic capabilities of these core community members, we could then assess the potential influence these organisms have on their environment and how that may explain temporal variation observed in the geochemistry.

The putative role of these core community members at Ney Springs is of interest, as they are likely driving temporal geochemical changes in the spring through their metabolisms. Within the core community, a few members had strong associations with changing geochemical parameters, and the metabolic potential we observed in their corresponding MAGs supports the capacity to use or produce these geochemical species. This was seen clearly with the *Tindallia* taxa and their correlation with ammonia concentrations. While additional experiments will be necessary to confirm that the *Tindallia* species detected are capable of excess ammonia generation, these findings represent the first plausible explanation with evidence for the profuse ammonia found within this environment. Though ammonia is a stressor, and is not common in many naturally occurring alkaline environments, it has been shown to inhibit microbial activities in bioreactors that experience ammonia buildup over time (Kayhanian, 1999; Leejeerajumnean et al., 2000). Similarly, while we have not yet observed this in other serpentinizing systems on Earth, the co-occurrence of high ammonia concentrations and serpentinization end products (e.g., hydrogen) have been detected on icy moons such as Enceladus (Vance et al., 2007; Waite et al., 2009). Understanding how ammonia impacts microbial metabolism and viability is an astrobiologically relevant question that could be further investigated at Ney Springs.

While the source of the sulfide at Ney Springs remains unclear, this work points to a metabolically diverse group of sulfur-oxidizing microbes that may use sulfide, thiosulfate, or elemental sulfur found within the spring. The complex role of sulfur intermediates within hyperalkaline environments is understudied, though many species, such as polysulfides and thiosulfate, have increased stability at high pH and are much more abundant and biologically available under these conditions (Van den Bosh et al., 2008; Findlay, 2016). Though best observed in the case of *Halomonas* and tetrathionate, other core community species may be producing and consuming these less studied sulfur intermediates. *Thiomicrospira* and members of the *Rhodobacteraceae* were more abundant when sulfide and thiosulfate were at their highest, supporting a potential link between the energy available for sulfur oxidation and these populations. Organisms like *Thiomicrospira* are obligate chemolithoautotrophs and the majority of *Rhodobacteraceae* from this environment are likely chemolithoheterotrophs. A *Rhodobacteraceae* isolate from this cistern, as well as closely related members of this family isolated from soda lakes, have been previously described as chemolithoheterotrophs and their ability to supplement energy through sulfur oxidation could explain their increased abundance during times of higher reduced sulfur species availability (Sorokin, 2003; Trutschel et al., 2022). As

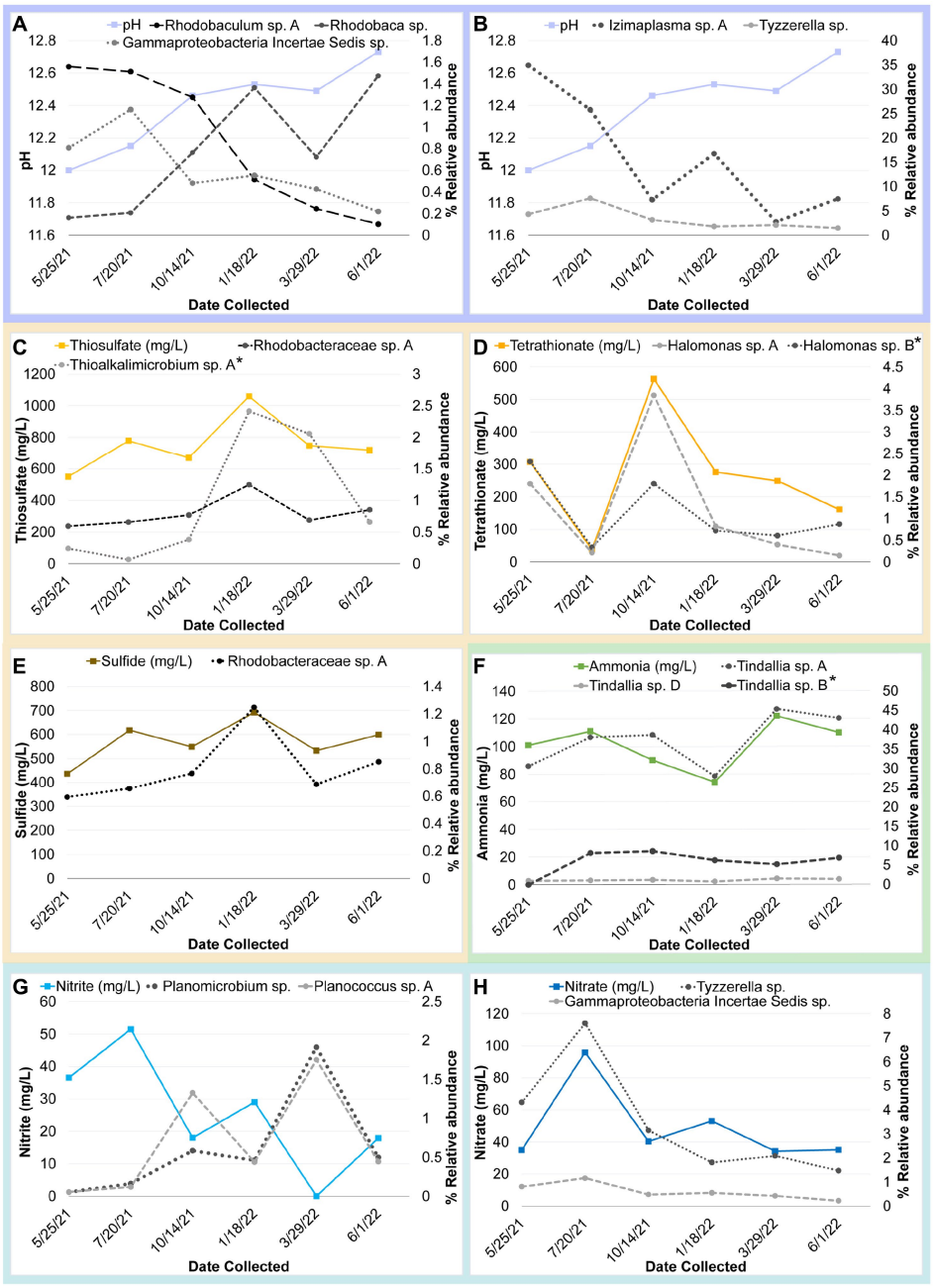

FIGURE 9
Timeseries plot of changes in core community ASV relative abundance that may be related seasonal changes in a geochemical constituent as identified by a correlation coefficient value at or above 0.80 unless otherwise noted (*). Each plot shows the relative abundance of one or more core community ASVs plotted alongside a different variable. Panels are as follows with correlation coefficient values for each ASV indicated in parentheses: **(A)** Change in pH compared to relative abundance of Gammaproteobacteria incertae Sedis sp. (−0.85), *Rhodobaculum* sp. (−0.87), and *Rhodobaca* sp. (0.93). **(B)** Change in pH compared to relative abundance of *Izimaplasma* sp. A (−0.86) and *Tyzzerella* sp. (−0.77) **(C)** Change in thiosulfate compared to relative abundance of *Thioalkalimicrobium/Thiomicrospira* sp. A (0.73*) and *Rhodobacteraceae* sp. A (0.88). **(D)** Change in tetrathionate compared to relative abundance of *Halomonas* sp. A and B (0.92 and 0.68*). **(E)** Change in sulfide compared to relative abundance of *Rhodobacteraceae* sp. A (0.79). **(F)** Change in ammonia compared to relative abundance of *Tindallia* sp. A, B and D (0.8, 0.7*, 0.81, respectively). **(G)** Change in nitrite compared to relative abundance of *Planococcus* sp. A (−0.86) and *Planomicrobium* sp. (−0.85). **(H)** Change in nitrate compared to relative abundance of *Tyzzerella* sp. (0.82) and Gammaproteobacteria incertae Sedis sp. (0.81).

such, *Rhodobacteraceae* populations may be more linked to carbon pools rather than sulfur species, though at present we have only low-resolution measurements for DOC/TOC from Ney Springs and cannot identify which carbon species are present and potentially bioavailable.

Future work within Ney Springs will focus on the role of carbon speciation and how it shapes the microbial community, as many of the core community species identified did not appear to have a strong association with the geochemical constraints chosen, such as seen with *Izimaplasma*. These organisms have been twice observed having

a period of significantly increased abundance within late May, but the driving factor for this bloom has yet to be identified. Potentially increased organic availability via exogenous carbon input from detritus could explain this, but further investigation is required. Other potential impacts on organism abundance are their relationships with one another. Organisms with similar metabolisms, like *Izimaplasma* and *Planococcaceae* species, which are both putative simple sugar fermenters, may face competition with one another. Similarly, a decrease in exogenous organic carbon input utilized by many of the abundant heterotrophic and/or fermentative taxa may then allow for the increased abundance of autotrophic organisms like *Thiomicrospira*. Additional work with enrichments and *in situ* activity assays may help identify which organisms are most active within this environment and are in direct competition with one another for resources. The role subsurface processes play in introducing or supporting different microbial taxa observed in this system remains to be explored. Certain geochemical parameters vary temporally with no seasonal pattern, and could be a function of differences in host rock interactions. In addition, subsurface microbial processes that are feasible but not observed in the surface community (e.g., sulfate reduction or anaerobic methane oxidation) could also be impacting the spring, though we currently lack evidence for these activities.

Data availability statement

The datasets presented in this study can be found in online repositories. The names of the repository/repositories and accession number(s) can be found in the article/Supplementary material.

Author contributions

LT, BK, JS, GC, and AR performed field sampling and data collection for Ney Springs. LT and BK performed geochemical analyses and interpretations. LT performed metagenomic analyses primarily with assistance from GC. LT performed statistical analyses and visualization. LT and AR are the primary authors of the manuscript with editing by BK, JS, and GC. AR and BK performed funding acquisition. All authors contributed to the article and approved the submitted version.

Funding

Funding and salary support for LT, BK, and AR have been provided by the NSF-EAR LowTemp Geochemistry Geobiology award 2025687 and NASA-Roses Exobiology Program grant number (80NSSC21K0482). LT received a Lewis and Clark Field work in Astrobiology fellowship and the University of Cincinnati Dr. Stacy Pfaller memorial scholarship.

Conflict of interest

The authors declare that the research was conducted in the absence of any commercial or financial relationships that could be construed as a potential conflict of interest.

Publisher's note

All claims expressed in this article are solely those of the authors and do not necessarily represent those of their affiliated organizations, or those of the publisher, the editors and the reviewers. Any product that may be evaluated in this article, or claim that may be made by its manufacturer, is not guaranteed or endorsed by the publisher.

Supplementary material

The Supplementary material for this article can be found online at: https://www.frontiersin.org/articles/10.3389/fmicb.2023.1182497/full#supplementary-material

References

Alneberg, J., Bjarnason, B. S., De Bruijn, I., Schirmer, M., Quick, J., Ijaz, U. Z., et al. (2014). Binning metagenomic contigs by coverage and composition. *Nat. Methods* 11, 1144–1146. doi: 10.1038/nmeth.3103

Arkin, A. P., Cottingham, R. W., Henry, C. S., Harris, N. L., Stevens, R. L., Maslov, S., et al. (2018). KBase: the United States department of energy systems biology knowledgebase. *Nat. Biotechnol.* 36, 566–569. doi: 10.1038/nbt.4163

Barnes, I., LaMarche, V. C. Jr., and Himmelberg, G. (1967). Geochemical evidence of present-day serpentinization. *Science* 156, 830–832. doi: 10.1126/science.156.3776.830

Barnes, I., and O'Neil, J. R. (1969). The relationship between fluids in some fresh alpine-type ultramafks and possible modern serpentinization, Western United States. *Geol. Soc. Am. Bull.* 80, 1947–1960. doi: 10.1130/0016-7606(1969)80[1947:TRBFIS]2.0.CO;2

Barnes, I., Rapp, J. B., O'Neil, J. R., Sheppard, R. A., and Gude, A. J. III (1972). Metamorphic assemblages and the direction of flow of metamorphic fluids in four instances of serpentinization. *Contrib. Mineral. Petrol.* 35, 263–276. doi: 10.1007/BF00371220

Barnett, D., Arts, I., and Penders, J. (2021). microViz: an R package for microbiome data visualization and statistics. *J. Open Source Softw.* 6:3201. doi: 10.21105/joss.03201

Boros, E., Balogh, K., Vörös, L., and Horváth, Z. (2017). Multiple extreme environmental conditions of intermittent soda pans in the Carpathian Basin (Central Europe). *Limnologica* 62, 38–46. doi: 10.1016/j.limno.2016.10.003

Brazelton, W. J., Nelson, B., Schrenk, M. O., Christner, B. C., and State, L. (2012). Metagenomic evidence for H 2 oxidation and H 2 production by serpentinite-hosted subsurface microbial communities. *Front. Microbiol.* 2:268. doi: 10.3389/fmicb.2011.00268

Bryantseva, I. A., Gaisin, V. A., and Gorlenko, V. M. (2015). *Rhodobaculum claviforme* gen. nov., sp. nov., a new alkaliphilic nonsulfur purple bacterium. *Microbiol* 84, 247–255. doi: 10.1134/S0026261715020022

Callahan, B. J., McMurdie, P. J., Rosen, M. J., Han, A. W., Johnson, A. J. A., and Holmes, S. P. (2016). DADA2: High-resolution sample inference from Illumina amplicon data. *Nat. Methods* 13, 581–583. doi: 10.1038/nmeth.3869

Cardace, D., Meyer-dombard, D. A. R., Woycheese, K. M., Arcilla, C. A., Brazelton, W., and Carolina, E. (2015). Feasible metabolisms in high pH springs of the Philippines. *Front. Microbiol.* 6, 1–16. doi: 10.3389/fmicb.2015.00010

Conway, J. R., Lex, A., and Gehlenborg, N. (2017). UpSetR: An R package for the visualization of intersecting sets and their properties. *Bioinformatics* 33, 2938–2940. doi: 10.1093/bioinformatics/btx364

Cook, M. C., Blank, J. G., Suzuki, S., Nealson, K. H., and Morrill, P. L. (2021). Assessing geochemical bioenergetics and microbial metabolisms at three terrestrial sites of serpentinization: The Tablelands (NL, CAN), The Cedars (CA, USA), and Aqua de Ney (CA, USA). *J. Geophys. Res. Biogeosciences* 126, 1–16. doi: 10.1029/2019jg005542

Crespo-Medina, M., Twing, K. I., Sánchez-Murillo, R., Brazelton, W. J., McCollom, T. M., and Schrenk, M. O. (2017). Methane dynamics in a tropical

serpentinizing environment: the Santa Elena Ophiolite, Costa Rica. *Front. Microbiol.* 8, 1–14. doi: 10.3389/fmicb.2017.00916

Davis, N. M., Proctor, D. M., Holmes, S. P., Relman, D. A., and Callahan, B. J. (2018). Simple statistical identification and removal of contaminant sequences in marker-gene and metagenomics data. *Microbiome* 6, 226–214. doi: 10.1186/s40168-018-0605-2

Denkmann, K., Grein, F., Zigann, R., Siemen, A., Bergmann, J., van Helmont, S., et al. (2012). Thiosulfate dehydrogenase: a widespread unusual acidophilic c-type cytochrome. *Environ. Microbiol.* 14, 2673–2688. doi: 10.1111/j.1462-2920.2012.02820.x

Feth, J. H., Rogers, S. M., and Roberson, C. E. (1961). Aqua de Ney, California, a spring of unique chemical character. *Geochim. Cosmochim. Acta* 26, 519–521. doi: 10.1016/0016-7037(62)90101-1

Findlay, A. J. (2016). Microbial impact on polysulfide dynamics in the environment. *FEMS Microbiol. Lett.* 363:fnw103. doi: 10.1093/femsle/fnw103

Fones, E. M., Colman, D. R., Kraus, E. A., Stepanauskas, R., Templeton, A. S., Spear, J. R., et al. (2021). Diversification of methanogens into hyperalkaline serpentinizing environments through adaptations to minimize oxidant limitation. *ISME J.* 15, 1121–1135. doi: 10.1038/s41396-020-00838-1

García-Ruiz, J. M., Nakouzi, E., Kotopoulou, E., Tamborrino, L., and Steinbock, O. (2017). Biomimetic mineral self-organization from silica-rich spring waters. *Sci. Adv.* 3, e1602285–e1602287. doi: 10.1126/sciadv.1602285

Grabarczyk, D. B., and Berks, B. C. (2017). Intermediates in the sox sulfur oxidation pathway are bound to a sulfane conjugate of the carrier protein SoxYZ. *PLoS One* 12:e0173395-15. doi: 10.1371/journal.pone.0173395

Graham, E. D., Heidelberg, J. F., and Tully, B. J. (2018). Potential for primary productivity in a globally-distributed bacterial phototroph. *ISME J.* 12, 1861–1866. doi: 10.1038/s41396-018-0091-3

Humayoun, S. B., Bano, N., and Hollibaugh, J. T. (2003). Depth distribution of microbial diversity in mono lake, a meromictic soda lake in California. *Appl. Environ. Microbiol.* 69, 1030–1042. doi: 10.1128/AEM.69.2.1030-1042.2003

Ito, M., Guffanti, A. A., Zemsky, J., Ivey, D. M., and Krulwich, T. A. (1997). Role of the nhaC-encoded Na+/H+ antiporter of alkaliphilic *Bacillus firmus* OF4. *J. Bacteriol.* 179, 3851–3857. doi: 10.1128/jb.179.12.3851-3857.1997

Ito, M., Morino, M., and Krulwich, T. A. (2017). Mrp antiporters have important roles in diverse bacteria and archaea. *Front. Microbiol.* 8:2325. doi: 10.3389/fmicb.2017.02325

Kanehisa, M., Sato, Y., and Morishima, K. (2016). BlastKOALA and GhostKOALA: KEGG tools for functional characterization of genome and metagenome sequences. *J. Mol. Biol.* 428, 726–731. doi: 10.1016/j.jmb.2015.11.006

Kang, D. D., Li, F., Kirton, E., Thomas, A., Egan, R., An, H., et al. (2019). MetaBAT 2: an adaptive binning algorithm for robust and efficient genome reconstruction from metagenome assemblies. *PeerJ* 7:e7359. doi: 10.7717/peerj.7359

Kayhanian, M. (1999). Ammonia inhibition in high-solids biogasification: an overview and practical solutions. *Environ. Technol.* 20, 355–365. doi: 10.1080/09593332008616828

Kelly, D. P., Shergill, J. K., Lu, W.-P., and Wood, A. P. (1997). Oxidative metabolism of inorganic sulfur compounds by bacteria. *Antonie Van Leeuwenhoek* 71, 95–107. doi: 10.1023/A:1000135707181

Kevbrin, V. V., Zhilina, T. N., Rainey, F. A., and Zavarzin, G. A. (1998). Tindallia magadii gen. nov., sp. nov.: An alkaliphilic anaerobic ammonifier from Soda Lake deposits. *Curr. Microbiol.* 37, 94–100. doi: 10.1007/s002849900345

Kopejtka, K., Tomasch, J., Zeng, Y., Tichý, M., Sorokin, D. Y., and Koblížek, M. (2017). Genomic analysis of the evolution of phototrophy among haloalkaliphilic rhodobacterales. *Genome Biol. Evol.* 9, 1950–1962. doi: 10.1093/gbe/evx141

Krulwich, T. A., Ito, M., Gimour, R., and Guffanti, A. A. (1997). Mechanisms of cytoplasmic pH regulation in alkaliphilic strains of Bacillus. *Extremophiles* 1, 163–170. doi: 10.1007/s007920050030

Leejeerajumnean, A., Ames, J. M., and Owens, J. D. (2000). Effect of ammonia on the growth of Bacillus species and some other bacteria. *Lett. Appl. Microbiol.* 30, 385–389. doi: 10.1046/j.1472-765x.2000.00734.x

Lehtovirta-Morley, L. E. (2018). Ammonia oxidation: ecology, physiology, biochemistry and why they must all come together. *FEMS Microbiol. Lett.* 365:fny058. doi: 10.1093/femsle/fny058

Li, D., Liu, C. M., Luo, R., Sadakane, K., and Lam, T. W. (2015). MEGAHIT: an ultra-fast single-node solution for large and complex metagenomics assembly via succinct de Bruijn graph. *Bioinformatics* 31, 1674–1676. doi: 10.1093/bioinformatics/btv033

Mariner, R. H., Evans, W. C., Presser, T. S., and White, L. D. (2003). Excess nitrogen in selected thermal and mineral springs of the Cascade Range in northern California, Oregon, and Washington: sedimentary or volcanic in origin? *J. Volcanol. Geotherm. Res.* 121, 99–114. doi: 10.1016/S0377-0273(02)00414-6

Mccollom, T. M., and Seewald, J. S. (2013). Serpentinites, hydrogen, and life. *Elements* 9, 129–134. doi: 10.2113/gselements.9.2.129

McLaren, M. R. (2020). Silva SSU taxonomic training data formatted for DADA2 (Silva version 138). *Zenodo*. doi: 10.5281/ZENODO.3986799

Mcmurdie, P. J., and Holmes, S. (2013). phyloseq: an R package for reproducible interactive analysis and graphics of microbiome census data. *PLoS One* 8:e61217. doi: 10.1371/journal.pone.0061217

Menzel, P., Ng, K. L., and Krogh, A. (2016). Fast and sensitive taxonomic classification for metagenomics with Kaiju. *Nat. Commun.* 7:11257. doi: 10.1038/ncomms11257

Morrill, P. L., Kuenen, J. G., Johnson, O. J., Suzuki, S., Rietze, A., Sessions, A. L., et al. (2013). Geochemistry and geobiology of a present-day serpentinization site in California: the cedars. *Geochim. Cosmochim. Acta* 109, 222–240. doi: 10.1016/j.gca.2013.01.043

Mulkidjanian, A. Y., Galperin, M. Y., Makarova, K. S., Wolf, Y. I., and Koonin, E. V. (2008). Evolutionary primacy of sodium bioenergetics. *Biol. Direct* 3, 1–19. doi: 10.1186/1745-6150-3-13

Nozaki, K., Kuroda, T., Mizushima, T., and Tsuchiya, T. (1998). A new Na+/H+ antiporter, NhaD, of *Vibrio parahaemolyticus*. *Biochim. Biophys. Acta Biomembr.* 1369, 213–220. doi: 10.1016/S0005-2736(97)00223-X

Nurk, S., Meleshko, D., Korobeynikov, A., and Pevzner, P. A. (2017). MetaSPAdes: a new versatile metagenomic assembler. *Genome Res.* 27, 824–834. doi: 10.1101/gr.213959.116

Oksanen, J., Blanchet, F. G., Friendly, M., Kindt, R., Legendre, P., McGlinn, D., et al. (2022). *Vegan: Community Ecology Package, R Package Version 2.6-2*. Available online: https://CRAN.R-project.org/package=vegan

Ortiz, E., Tominaga, M., Cardace, D., Schrenk, M. O., Hoehler, T. M., Kubo, M. D., et al. (2018). Geophysical characterization of serpentinite hosted hydrogeology at the McLaughlin natural reserve, coast range Ophiolite. *Geochem. Geophys. Geosyst.* 19, 114–131. doi: 10.1002/2017GC007001

Osburn, M. R., Kruger, B., Masterson, A. L., Casar, C. P., and Amend, J. P. (2019). Establishment of the deep mine microbial observatory (DeMMO), South Dakota, USA, a geochemically stable portal into the deep subsurface. *Front. Earth Sci.* 7:196. doi: 10.3389/feart.2019.00196

Parey, K., Demmer, U., Warkentin, E., Wynen, A., Ermler, U., and Dahl, C. (2013). Structural, biochemical and genetic characterization of dissimilatory ATP sulfurylase from *Allochromatium vinosum*. *PLoS One* 8:e74707. doi: 10.1371/journal.pone.0074707

Parks, D. H., Chuvochina, M., Waite, D. W., Rinke, C., Skarshewski, A., Chaumeil, P. A., et al. (2018). A standardized bacterial taxonomy based on genome phylogeny substantially revises the tree of life. *Nat. Biotechnol.* 36, 996–1004. doi: 10.1038/nbt.4229

Parks, D. H., Imelfort, M., Skennerton, C. T., Hugenholtz, P., and Tyson, G. W. (2015). CheckM: assessing the quality of microbial genomes recovered from isolates, single cells, and metagenomes. *Genome Res.* 25, 1043–1055. doi: 10.1101/gr.186072.114

Paster, B. J., Russell, J. B., Yang, C. M. J., Chow, J. M., Woese, C. R., and Tanner, R. (1993). Phylogeny of the ammonia-producing ruminal bacteria *Peptostreptococcus anaerobius*, *Clostridium sticklandii*, and *Clostridium aminophilum* sp. nov. *Int. J. Syst. Bacteriol.* 43, 107–110. doi: 10.1099/00207713-43-1-107

Peng, Y., Leung, H. C. M., Yiu, S. M., and Chin, F. Y. L. (2012). IDBA-UD: a de novo assembler for single-cell and metagenomic sequencing data with highly uneven depth. *Bioinformatics* 28, 1420–1428.

Postec, A., Quéméneur, M., Bes, M., Mei, N., and Benaïssa, F. (2015). Microbial diversity in a submarine carbonate edifice from the serpentinizing hydrothermal system of the Prony Bay (New Caledonia) over a 6-year period. *Front. Microbiol.* 6:857. doi: 10.3389/fmicb.2015.00857

Price, M. N., Dehal, P. S., and Arkin, A. P. (2010). FastTree 2 – approximately maximum-likelihood trees for large alignments. *PLoS One* 5:e9490. doi: 10.1371/journal.pone.0009490

Rempfert, K. R., Miller, H. M., Bompard, N., Nothaft, D., Matter, J. M., Kelemen, P., et al. (2017). Geological and geochemical controls on subsurface microbial life in the Samail Ophiolite, Oman. *Front. Microbiol* 8:56. doi: 10.3389/fmicb.2017.00056

Sangavai, C., and Chellapandi, P. (2017). Amino acid catabolism-directed biofuel production in *Clostridium sticklandii*: an insight into model-driven systems engineering. *Biotechnol. Rep.* 16, 32–43. doi: 10.1016/j.btre.2017.11.002

Schmitt-Wagner, D., Friedrich, M. W., Wagner, B., and Brune, A. (2003). Phylogenetic diversity, abundance, and axial distribution of bacteria in the intestinal tract of two soil-feeding termites (*Cubitermes* spp.). *Appl. Environ. Microbiol.* 69, 6007–6017. doi: 10.1128/AEM.69.10.6007-6017.2003

Schrenk, M. O., Kelley, D. S., Bolton, S. A., and Baross, J. A. (2004). Low archaeal diversity linked to subseafloor geochemical processes at the lost city hydrothermal field, mid-atlantic ridge. *Environ. Microbiol.* 6, 1086–1095. doi: 10.1111/j.1462-2920.2004.00650.x

Sieber, C. M. K., Probst, A. J., Sharrar, A., Thomas, B. C., Hess, M., Tringe, S. G., et al. (2018). Recovery of genomes from metagenomes via a dereplication, aggregation and scoring strategy. *Nat. Microbiol.* 3, 836–843. doi: 10.1038/s41564-018-0171-1

Sorokin, D. Y. (2003). Oxidation of inorganic sulfur compounds by obligately organotrophic bacteria. *Microbiology* 72, 641–653. doi: 10.1023/B:MICI.0000008363.24128.e5

Sorokin, D. Y., Gorlenko, V. M., Tourova, T. P., Tsapin, A. I., Nealson, K. H., and Kuenen, G. J. (2002). *Thioalkalimicrobium cyclium* sp. nov. and *Thioalkalivibrio jannaschii* sp. nov., novel species of haloalkaliphilic, obligately chemolithoautotrophic sulfur-oxidizing bacteria from hypersaline alkaline Mono Lake (California). *Int. J. Syst. Evol. Microbiol.* 52, 913–920. doi: 10.1099/ijs.0.02034-0

Sorokin, D. Y., Mosier, D., Zorz, J. K., Dong, X., and Strous, M. (2020). Wenzhouxiangella strain AB-CW3, a proteolytic bacterium from hypersaline Soda

Lakes that preys on cells of gram-positive Bacteria. *Front. Microbiol.* 11:597686. doi: 10.3389/fmicb.2020.597686

Sorokin, D. Y., Tourova, T. P., Kuznetsov, B. B., Bryantseva, I. A., and Gorlenko, V. M. (2000). *Roseinatronobacter thiooxidans* gen. nov., sp. nov., a new alkaliphilic aerobic bacteriochlorophyll a-containing bacterium isolated from a soda lake. *Microbiology* 69, 75–82. doi: 10.1007/BF02757261

Suzuki, S., Ishii, S., Hoshino, T., Rietze, A., Tenney, A., Morrill, P. L., et al. (2017). Unusual metabolic diversity of hyperalkaliphilic microbial communities associated with subterranean serpentinization at the cedars. *Nat. Publ. Gr.* 11, 2584–2598. doi: 10.1038/ismej.2017.111

Suzuki, S., Ishii, S., Wu, A., Cheung, A., Tenney, A., Wanger, G., et al. (2013). Microbial diversity in the cedars, an ultrabasic, ultrareducing, and low salinity serpentinizing ecosystem. *Proc. Natl. Acad. Sci.* 110, 15336–15341. doi: 10.1073/pnas.1302426110

Szponar, N., Brazelton, W. J., Schrenk, M. O., Bower, D. M., Steele, A., and Morrill, P. L. (2013). Geochemistry of a continental site of serpentinization, the Tablelands Ophiolite, Gros Morne National Park: a Mars analogue. *Icarus* 224, 286–296. doi: 10.1016/j.icarus.2012.07.004

Thompson, L. R., Sanders, J. G., Mcdonald, D., Amir, A., Ladau, J., Locey, K. J., et al. (2017). A communal catalogue reveals earth' s multiscale microbial diversity. *Nature* 551, 457–463. doi: 10.1038/nature24621

Trutschel, L. R., Chadwick, G. L., Kruger, B., Blank, J. G., Brazelton, W. J., Dart, E. R., et al. (2022). Investigation of microbial metabolisms in an extremely high pH marine-like terrestrial serpentinizing system: Ney Springs. *Sci. Total Environ.* 836:155492. doi: 10.1016/j.scitotenv.2022.155492

Twing, K. I., Brazelton, W. J., Kubo, M. D. Y., Hyer, A. J., Cardace, D., Hoehler, T. M., et al. (2017). Serpentinization-influenced groundwater harbors extremely low diversity microbial communities adapted to high pH. *Front. Microbiol.* 8:308. doi: 10.3389/fmicb.2017.00308

Van den Bosh, P. L. F., Sorokin, D. Y., Buisman, C. J. N., and Janssen, A. J. H. (2008). The effect of pH on thiosulfate formation in a biotechnological process for the removal of hydrogen sulfide from gas streams. *Environ. Sci. Technol.* 42, 2637–2642. doi: 10.1021/es7024438

Vance, S., Harnmeijer, J., Kimura, J., Hussmann, H., Demartin, B., and Brown, J. M. (2007). Hydrothermal systems in small ocean planets. *Astrobiology* 7, 987–1005. doi: 10.1089/ast.2007.0075

Vavourakis, C. D., Andrei, A. S., Mehrshad, M., Ghai, R., Sorokin, D. Y., and Muyzer, G. (2018). A metagenomics roadmap to the uncultured genome diversity in hypersaline soda lake sediments 06 biological sciences 0605 microbiology 06 biological sciences 0604 genetics. *Microbiome* 6, 1–18. doi: 10.1186/s40168-018-0548-7

Vorburger, T., Nedielkov, R., Brosig, A., Bok, E., Schunke, E., Steffen, W., et al. (2016). Role of the Na+−translocating NADH:quinone oxidoreductase in voltage generation and Na+ extrusion in *Vibrio cholerae*. *Biochim. Biophys. Acta Bioenerg.* 1857, 473–482. doi: 10.1016/j.bbabio.2015.12.010

Waite, J. H., Lewis, W. S., Magee, B. A., Lunine, J. I., McKinnon, W. B., Glein, C. R., et al. (2009). Liquid water on Enceladus from observations of ammonia and 40Ar in the plume. *Nature* 460, 487–490. doi: 10.1038/nature08153

Wang, K., Zhang, L., Li, J., Pan, Y., Meng, L., Xu, T., et al. (2015). *Planococcus dechangensis* sp. nov., a moderately halophilic bacterium isolated from saline and alkaline soils in Dechang Township, Zhaodong City, China. *Antonie van Leeuwenhoek* 107, 1075–1083. doi: 10.1007/s10482-015-0399-1

Waring, G. (1915). *Springs of California*. United States Geol. Surv. 338, 264–265.

Woycheese, K., Arcilla, C. A., Magnuson, T., and State, I. (2015). Out of the dark: transitional subsurface-to-surface microbial diversity in a terrestrial serpentinizing seep. *Front. Microbiol.* 6, 1–12. doi: 10.3389/fmicb.2015.00044

Wu, Y. W., Simmons, B. A., and Singer, S. W. (2016). MaxBin 2.0: an automated binning algorithm to recover genomes from multiple metagenomic datasets. *Bioinformatics* 32, 605–607. doi: 10.1093/bioinformatics/btv638

Yan, M., Treu, L., Zhu, X., Tian, H., Basile, A., Fotidis, I. A., et al. (2020). Insights into ammonia adaptation and methanogenic precursor oxidation by genome-centric analysis. *Environ. Sci. Technol.* 54, 12568–12582. doi: 10.1021/acs.est.0c01945

Yu, Z., Lansdon, E. B., Segel, I. H., and Fisher, A. J. (2007). Crystal structure of the bifunctional ATP sulfurylase – APS kinase from the chemolithotrophic thermophile

Aquifex aeolicus. *J. Mol. Biol.* 365, 732–743. doi: 10.1016/j.jmb.2006.10.035

frontiers | Frontiers in Microbiology

TYPE Original Research
PUBLISHED 06 July 2023
DOI 10.3389/fmicb.2023.1196516

OPEN ACCESS

EDITED BY
Federico Lauro,
Nanyang Technological University, Singapore

REVIEWED BY
Francesco Smedile,
National Research Council (CNR), Italy
Lauren M. Seyler,
Stockton University, United States

*CORRESPONDENCE
Marianne Quéméneur
✉ marianne.quemeneur@ird.fr

†PRESENT ADDRESSES
Julie Jeanpert,
Agence de l'eau Rhône,
Méditerranée Corse, Lyon, France

‡These authors have contributed equally to this work and share first authorship

RECEIVED 29 March 2023
ACCEPTED 20 June 2023
PUBLISHED 06 July 2023

CITATION
Quéméneur M, Mei N, Monnin C, Postec A, Guasco S, Jeanpert J, Maurizot P, Pelletier B and Erauso G (2023) Microbial taxa related to natural hydrogen and methane emissions in serpentinite-hosted hyperalkaline springs of New Caledonia.
Front. Microbiol. 14:1196516.
doi: 10.3389/fmicb.2023.1196516

Microbial taxa related to natural hydrogen and methane emissions in serpentinite-hosted hyperalkaline springs of New Caledonia

Marianne Quéméneur[1*‡], Nan Mei[2‡], Christophe Monnin[3], Anne Postec[1], Sophie Guasco[1], Julie Jeanpert[4†], Pierre Maurizot[4], Bernard Pelletier[5] and Gaël Erauso[1]

[1]Aix Marseille Univ, Université de Toulon, CNRS, IRD, MIO, Marseille, France, [2]School of Chemistry, Chemical Engineering, and Life Science, Wuhan University of Technology, Wuhan, China, [3]Géosciences Environnement Toulouse, UMR 5563 (CNRS/UPS/IRD/CNES), Toulouse, France, [4]Direction de l'Industrie, des Mines et de l'Energie, Nouméa, New Caledonia, [5]Centre IRD de Nouméa, Nouméa, New Caledonia

The southeastern part of New Caledonia main island (Grande Terre) is the location of a large ophiolitic formation that hosts several hyperalkaline springs discharging high pH (~11) and warm (<40°C) fluids enriched in methane (CH_4) and hydrogen (H_2). These waters are produced by the serpentinization of the ultrabasic rock formations. Molecular surveys had previously revealed the prokaryotic diversity of some of these New Caledonian springs, especially from the submarine chimneys of Prony Bay hydrothermal field. Here we investigate the microbial community of hyperalkaline waters from on-land springs and their relationships with elevated concentrations of dissolved H_2 (21.1–721.3 μmol/L) and CH_4 (153.0–376.6 μmol/L). 16S rRNA gene analyses (metabarcoding and qPCR) provided evidence of abundant and diverse prokaryotic communities inhabiting hyperalkaline fluids at all the collected springs. The abundance of prokaryotes was positively correlated to the H_2/CH_4 ratio. Prokaryotes consisted mainly of bacteria that use H_2 as an energy source, such as microaerophilic *Hydrogenophaga*/*Serpentinimonas* (detected in all sources on land) or anaerobic sulfate-reducing *Desulfonatronum*, which were exclusively found in the most reducing (E_h ref H_2 ~ -700 mV) and the most H_2-enriched waters discharging at the intertidal spring of the Bain des Japonais. The relative abundance of a specific group of uncultured Methanosarcinales that thrive in serpentinization-driven ecosystems emitting H_2, considered potential H_2-consuming methanogens, was positively correlated with CH_4 concentrations, and negatively correlated to the relative abundance of methylotrophic Gammaproteobacteria. Firmicutes were also numerous in hyperalkaline waters, and their relative abundance (e.g., *Gracilibacter* or *Dethiobacter*) was proportional to the dissolved H_2 concentrations, but their role in the H_2 budget remains to be assessed. The prokaryotic communities thriving in New Caledonia hyperalkaline waters are similar to those found in other serpentinite-hosted high-pH waters worldwide, such as Lost City (North Atlantic) and The Cedars (California).

KEYWORDS

bacteria, archaea, high-pH water, microbial diversity, natural hydrogen, methane, serpentinization, geothermal springs

1. Introduction

Serpentinization is a natural process of mantle rock alteration that transforms olivine into serpentine, with the parallel formation of dihydrogen (H_2) linked to water reduction and the oxidation of metals (principally iron) contained in the minerals (mainly olivine) (Sleep et al., 2004; Klein et al., 2013; Schrenk et al., 2013; Wang et al., 2014). This H_2 can react with carbon-bearing species such as carbonic acid to form methane (CH_4) as well as low-molecular-weight organic compounds such as acetate and formate (Schrenk et al., 2013; Wang et al., 2014; Konn et al., 2015). These organic compounds can be sources of energy (electron donors) and of carbon for microorganisms living in deep environments (McCollom and Seewald, 2013; Ménez, 2020). The environmental characteristics of serpentinizing environments are considered similar to those that have prevailed on the early Earth and on other rocky planets like Mars, thus providing a prebiotic chemistry that may have favored the emergence of life (Nealson et al., 2005; Russell et al., 2010). Thus, the study of these ecosystems allows to address fundamental questions such as the origin and limits of life on Earth, or more applied investigations such as the search of extremophiles (i.e., alkaliphiles) for biotechnological applications or the production of natural H_2 (also called native H_2) (Gaucher, 2020; Truche et al., 2020).

Several ecosystems found in such serpentinization-driven environments have been found in various areas around the world: (i) underwater, such as the shallow submarine Prony Bay hydrothermal field (PBHF) located at less than 50 meters below sea level (mbsl) in the southern lagoon of New Caledonia (South Pacific) (Monnin et al., 2014; Quéméneur et al., 2014; Postec et al., 2015), the deep submarine Lost City hydrothermal field (LCHF) near the Mid-Atlantic Ridge at 700–800 mbsl (Kelley et al., 2005), and the abyssal Old City hydrothermal field at 3,100 mbsl along the southwest Indian ridge (Lecoeuvre et al., 2021), or (ii) on-land, such as The Cedars spring system (CA, USA) (Suzuki et al., 2013), the Coast Range Ophiolite (CA, USA) (Twing et al., 2017), the Samail ophiolite (Oman) (Rempfert et al., 2017) and the Voltri ophiolitic springs (Italy) (Quéméneur et al., 2015). Phylogenetically and metabolically diverse microbial communities live inside the chimneys and concretions built by the venting of anoxic, high-pH fluids (Schrenk et al., 2013). Reactions involving H_2, CH_4, and sulfur compounds act as the energy source for these microbial communities, indicating that serpentinization-related fluids can sustain chemosynthesis rather than photosynthesis (McCollom and Seewald, 2013).

The southern part of the New Caledonia main island (Grande Terre) is covered by a large allochthonous sheet of oceanic lithosphere (ophiolite) thrusted over continental basement at the late Eocene (Avias, 1967; Cluzel et al., 2001; Pirard et al., 2013). There, a number of high-pH springs are located either on land, in the intertidal zone of the Prony Bay or at shallow depths in this bay (Cox et al., 1982; Monnin et al., 2014, 2021; Deville and Prinzhofer, 2016; Maurizot et al., 2020). In the Prony Bay, high-pH (up to 11.2) and warm (up to 42°C) fluids enriched in H_2 (12–30% vol of dry gas) and CH_4 (6–14% vol of dry gas) are currently venting into the lagoon (Monnin et al., 2014; Vacquand et al., 2018). Their mixing with seawater leads to the formation of brucite-carbonate chimneys and pinnacles, reaching heights up to tens of meters, as the 38-m high Aiguille de Prony (Launay and Fontes, 1985; Quéméneur et al., 2014). Previous molecular surveys have revealed the prokaryotic diversity of the coastal submarine PBHF, with diverse aerobic and anaerobic bacteria potentially involved in H_2 consumption (e.g., *Hydrogenophaga* and *Serpentinimonas*) or H_2 production (e.g., Clostridiales) (Quéméneur et al., 2014; Mei et al., 2016b). In addition, a low diversity of uncultured Methanosarcinales, potentially linked to CH_4 production or oxidation, was observed in PBHF chimneys (Quéméneur et al., 2014; Postec et al., 2015; Frouin et al., 2018), and was also found in other serpentinization-associated submarine and terrestrial sites such as The Cedars or Lost City (Kelley et al., 2005; Suzuki et al., 2013; Quéméneur et al., 2015). However, the microbial communities from on-land springs of the New Caledonia ophiolite have been only studied from the geothermal spring of La Crouen (Quéméneur et al., 2021), where bacteria potentially involved in sulfur cycle (e.g., *Candidatus* Desulfobacillus, *Thiofaba*, *Thiovirga*) and H_2 oxidation (e.g., *Hydrogenophaga*) dominated with *Ca*. Gracilibacteria in the waters depleted in H_2. The concentrations of H_2 and CH_4 in gases and waters emitted at the high-pH springs of New Caledonia are quite variable (Monnin et al., 2014, 2021; Deville and Prinzhofer, 2016) and likely to play a major role on the abundance and diversity of microorganisms.

This study used 16S rRNA gene analyses (metabarcoding and qPCR) to investigate the abundance and composition of prokaryotic communities inhabiting the high-pH fluids discharging at several on-land and intertidal springs of New Caledonia. We evaluated the relationship between the main taxa and the physicochemical characteristics of the high-pH fluids, including their contents in H_2 and CH_4. We also compared the dominant microbial members with those of other serpentinite-hosted hyperalkaline springs worldwide to uncover specific taxonomic bioindicators of this type of ecosystem and proxies of natural H_2 and CH_4 emissions.

2. Materials and methods

2.1. Study site

The studied high-pH thermal springs are all located in the southeastern part of the main island (**Figure 1**). The water samples were collected in November–December 2014 at five different sites : (i) a shallow (10-cm deep) pool of "La Coulée" (CL) spring, close to the town of Nouméa, (ii) the source of "Rivière des Pirogues" (PG), located halfway between the cities of Nouméa and Yaté, (iii) a natural 1-m deep pool of "Montagne des Sources" (MDS), located in a natural reserve close to the city of Nouméa, (iv) a shallow (10-cm) natural pool (RKB) and the spring captured in a cemented pool 1-m deep (RKH) of "Rivière des Kaoris," located in the Prony Bay, (v) the water venting at the "Bain des Japonais" (BJ), located in the intertidal zone of the Prony Bay (**Figure 1**). The spring locations have been previously described by Maurizot et al. (2020) and Monnin et al. (2021). All on-land springs are associated with carbonate deposits.

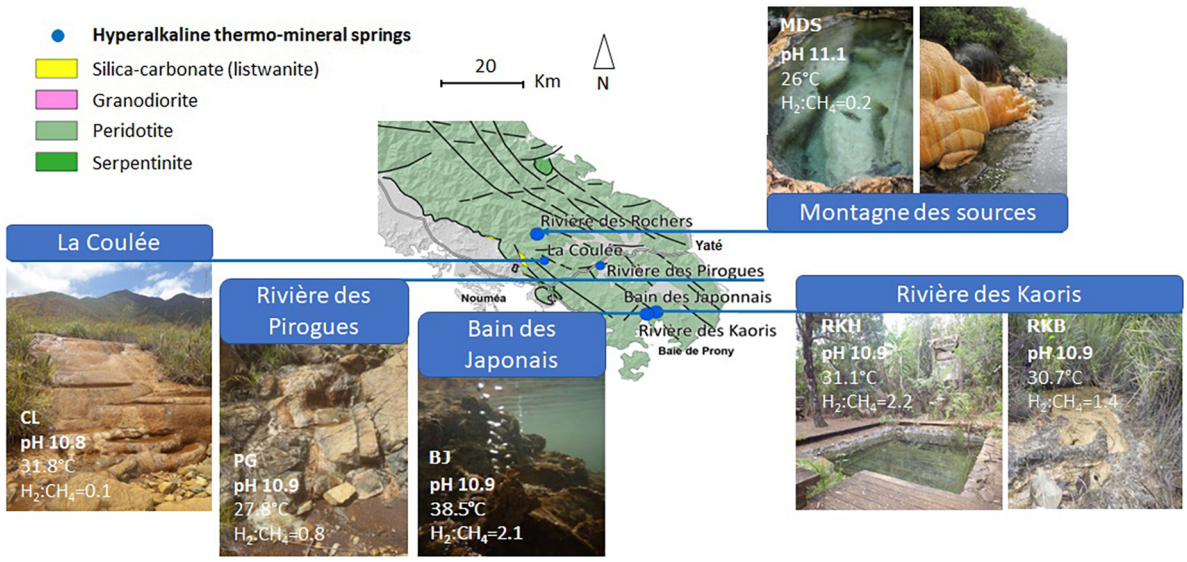

FIGURE 1
Location and photos of the high-pH springs of New Caledonia. CL corresponds to the highest pool of "La Coulée," MDS is a pool of the site "Montagne des Sources," PG indicates the source of the site "Rivière des Pirogues," RKB and RKH correspond to a natural and an artificial pool of the area "Rivière des Kaoris," respectively, and, BJ is a small intertidal vent of the site "Bain des Japonais" in the Prony Bay. The map is adapted from Maurizot et al. (2020). The H_2:CH_4 ratio is expressed in concentrations mol/mol.

2.2. Sample collection

Water samples were collected in cleaned 4-L plastic bottles using sterile and pre-rinsed syringes and stored in a portable icebox until arrival at the laboratory (about 2–3 h after sampling). Duplicate samples of two liters of water were filtered through 0.2 µm pore-size Isopore polycarbonate membrane filters 47-mm (Millipore). The filters were kept at -80°C before DNA extraction. Water samples dedicated to the chemical analyses were collected in duplicate in 120-ml glass bottles sealed with butyl-rubber stoppers. At springs where gas bubbles form, free gas samples were collected in 10-ml glass vials using the water displacement technique and sealed with butyl-rubber stoppers and aluminum caps in 10-ml glass vials these samples were kept at 4°C in the Nouméa (IRD) and Marseille (MIO) laboratories. The oxidation-reduction potential (E_h), dissolved oxygen (O_2), pH, temperature, and conductivity were measured *in situ* using a WTW Multi 3420® Multimeter with adequate probes (Monnin et al., 2021).

2.3. Dissolved gas analysis

Dissolved gas analysis was performed using a headspace equilibration method adapted from Magen et al. (2014). Briefly, a headspace representing 10% of the vial volume was created in the collection bottle by water displacement with argon, then the bottle was manually shaken for 1 min and placed on a shaker for 1 h. The composition of the headspace gas was determined using a Shimadzu GC 8A gas chromatograph equipped with a thermal conductivity detector (GC/TCD) and a concentric column CTR1 (Alltech, USA), as described previously (Mei et al., 2014). Argon was used as carrier gas at a flow rate of 60 mL/min; the injector and detector temperatures were fixed at 150°C. The concentrations of the dissolved gases were calculated using Henry's law (Sander, 2015).

2.4. DNA extraction

The filters were transferred to a sterile 2 mL tube containing a glass bead mixture (lysing matrix E from MP Biomedicals). The bacterial and archaeal cells of the filters were disrupted by a combination of mechanical (bead beating, according MP Biomedical recommendations) and chemical lyses by addition of 1 mL of sterile bacterial lysis buffer [100 mM NaCl, 100 mM Tris pH 8.0, 50 mM EDTA, 100 µL of 10 mg/mL lysozyme (Sigma-Aldrich, St. Louis, MO, USA), 20 µL of 10 µg/mL DNase-free RNase solutions] and incubation at 37°C for 15 min. Then, 100 µL of 10% SDS, 100 µL of 10% lauryl-sarkosyl and 50 µL of proteinase K (20 mg/mL were added to the mixture and incubated at 55°C for 1 h). DNA was extracted from the lysate with 1 volume of phenol:chloroform (1:1) mixture and then with 1 volume of chloroform. Total DNA was precipitated from the aqueous phase by adding 0.7 volume of isopropanol followed by centrifugation. The DNA pellet was washed in 75% ethanol and was again collected by centrifugation. The air-dried pellet was dissolved in 30 µL of TE buffer. The DNA concentrations were measured using a Qubit® fluorometer (Invitrogen).

2.5. Quantitative real-time PCR (qPCR)

The abundances of bacteria and archaea were determined by qPCR using, respectively, the primers set 341F/518R (Muyzer et al., 1993) and 344F/519R (Ovreås et al., 1997; Casamayor et al., 2002). The primer set used to quantify methanogens was

ME3MF/ME2r' targeting *mcrA* genes (Hales et al., 1996; Nunoura et al., 2008). The primer set used to quantify sulfate-reducers was DSRp2060f/DSR4R targeting *dsrB* genes (Wagner et al., 1998; Geets et al., 2006). The sequences of primers are given in **Supplementary Table 1**.

Each qPCR mixture (20 μL) contained 1X SsoAdvanced SYBR Green Supermix (Bio-Rad), 250 nM of each primer, 1 μl of DNA template (10-fold dilution series of standard PCR product or environmental DNA sample) or distilled water (negative control). All qPCR assays were performed in triplicate on a Bio-Rad CFX-96 real-time system (Bio-Rad). The qPCR cycling conditions were: 95°C for 2 min, followed by 40 cycles of a 2-step PCR protocol with a 15 sec denaturation phase at 95°C and a 15 sec annealing/elongation phase at 55°C. Fluorescence was measured at the end of each cycle. Following PCR, melt curves were generated between 65 and 95°C in 0.5°C increments, to verify PCR specificity.

qPCR standard curves were created from serial dilution of DNA standards of known concentration. For bacterial 16S rRNA and *dsrB* gene qPCR, standard DNA fragments were amplified from *Desulfovibrio vulgaris*^{T} DSM 644 using the primer sets 27F/907R (Lane, 1991) and DSR1F/DSR4R (Wagner et al., 1998), respectively. For archaeal 16S rRNA and *mcrA* gene qPCR, standard DNA fragments were amplified from *Methanosarcina barkeri*^{T} DSM 800 using the primer sets 109F/958R (Webster et al., 2006) and MLF/MLR (Luton et al., 2002), respectively. Triplicate PCR products were pooled and purified with the Nucleospin and PCR Clean-up kit (Macherey-Nagel), according to the manufacturer instructions. Purified PCR products were quantified using the BioSpec-nano Spectrophotometer (Shimadzu) and used as DNA standards. Copy number of DNA standards was calculated as described by Oldham and Duncan (2012). For each gene, the standard curve of C_T (threshold cycle) versus the gene copy numbers was generated by using a 10-fold dilution series from 10^8 to 10^1 copies per ng of DNA. For all standard curves, the coefficients of determination (R^2) were higher than 99.0%. The precision of the assay was measured by calculating the variation in Ct values across the three replicates. The abundance of targeted genes was reported as copy numbers per L of water.

2.6. 16S rDNA metabarcoding analyses of microbial communities

Bacterial and archaeal 16S rRNA gene V4 hypervariable regions were amplified by PCR using the 515F/806R universal primer set (Caporaso et al., 2011), with a barcode on the forward primer, as previously described by Dowd et al. (2008), and were sequenced by the MiSeq Illumina platform of the Molecular Research Laboratory (TX, USA). Sequence data were processed using the MR DNA analysis pipeline (MR DNA, Shallowater, TX, USA). In summary, sequences were joined (overlapping pairs) and grouped by samples following the barcodes before removing them. Short sequences (<150 bp) and sequences with ambiguous base calls were removed. Remaining sequences were denoised, operational taxonomic units (OTUs) were generated, and chimeras were checked using UCHIME and removed (Edgar et al., 2011). OTUs were clustered at 97% of similarity with USEARCH (Edgar, 2010) followed by removal of singleton sequences. Finally, OTUs were taxonomically classified using BLASTn against NCBI non-redundant (NR) reference database, and the top hit was taken as a taxonomic classification. The 16S rRNA gene sequences of the dominant OTUs have been deposited in the Genbank database under the accession numbers OQ551354-OQ551410. Raw sequence data were submitted to the NCBI SRA under BioProject PRJNA974011, BioSamples SAMN35158175–SAMN35158185.

2.7. Statistical analyses

All statistical analyses were performed using XLSTAT 2020.5.1 (Microsoft Excel add-in program; Addinsoft, Paris, France). The alpha diversity was calculated using the Shannon (1948) and Simpson (1949) indices from OTU abundance matrix. The beta diversity was based on Bray–Curtis's dissimilarities and a principal coordinate analysis (PCoA) (from phyla/classes) or a dendrogram (from dominant OTUs) was generated to group samples into clusters. Spearman correlations and principal component analyses (PCA) were used to evaluate the relationship between the relative abundance of microbial taxa (classes/phyla and dominant OTUs) and the physico-chemical parameters of water. P-values < 0.05 are statistically significant. The abundance of the dominant OTUs in the water samples was also visualized by heatmap.

3. Results

3.1. Physico-chemical parameters and dissolved gases of water samples

The water samples collected from the six spring sites had high pH values ranging from 10.8 (CLW) to 11.1 (MDSW), and their temperatures varied from 26.0°C (MDSW) to 38.5 °C (BJW) (**Table 1**), as previously reported (Monnin et al., 2021). The lowest E_h value (-697 mV, ref. H_2) was measured at the intertidal site of the "Bain des Japonais" (BJW). At this spring, very active gas bubbling is observed. The highest concentration of dissolved H_2 (721.3 μmol/L) is also measured from the BJ waters (**Table 1**). The lowest dissolved O_2 level (0.1 mg/L) was measured at the site of "Rivière des Kaoris" (RKB), also a site with intense gas bubbling (Monnin et al., 2014, 2021). There the concentration of dissolved CH_4 (376.6 μmol/L) is the highest of all the studied springs, while the highest ratio of H_2:CH_4 was observed at the site RKH (**Figure 2** and **Table 1**).

3.2. Abundance and diversity indices of prokaryotic communities

Real-time qPCR assays and 16S rDNA metabarcoding analyses were performed on the water samples collected from the six high-pH springs. The qPCR experiments revealed that the bacterial 16S rRNA gene abundances ranged between 3.1×10^7 (MDSW) and 3.3×10^8 (RKHW) copies/L. The archaeal 16S rRNA gene abundances varied from 4.6×10^6 (MDSW) to 5.1×10^7 (RKHW) copies/L (**Table 1**). The abundance of

10.3389/fmicb.2023.1196516

TABLE 1 *In situ* physicochemical parameters, diversity indices and gene abundances in water samples collected in the high-pH geothermal springs of New Caledonia.

Variables/samples	CLW	MDSW	PGW	RKHW	RKBW	BJW
pH*	10.8	11.1	10.9	10.9	10.9	10.9
Temperature (°C)*	31.8	26.0	27.8	31.1	30.7	38.5
O_2 (mg/L)*	0.4	3.0	0.3	2.2	0.1	0.2
E_h (mV; ref. H_2)*	324	42.0	−606.0	−176.0	−500.0	−697.0
H_2 (μmol/L)	21.1	68.4	247.4	342.2	510.7	721.3
CH_4 (μmol/L)	182.4	335.4	317.8	153.0	376.6	347.2
Bacterial 16S rDNA (copies/L)	3.7×10^7	3.1×10^7	6.3×10^7	3.3×10^8	1.1×10^8	2.2×10^8
Archaea 16S rDNA (copies/L)	8.2×10^6	4.6×10^6	5.1×10^6	5.1×10^7	2.5×10^7	1.4×10^7
dsrB (copies/L)	7.2×10^4	3.0×10^4	7.8×10^4	5.5×10^4	1.9×10^5	3.5×10^6
mcrA (copies/L)	3.9×10^5	2.4×10^6	3.1×10^6	1.0×10^7	1.7×10^7	1.8×10^6
Shannon index	5.29	4.84	5.25	4.58	5.23	4.10
Simpson index	0.98	0.97	0.97	0.93	0.97	0.92

*Data obtained from Monnin et al. (2021). CLW corresponds to the water collected from the highest pool of "La Coulée," MDSW is the water collected from a pool of the site "Montagne des Sources," PGW indicates the water of the source of the site "Rivière des Pirogues," RKBW and RKHW correspond to a natural and an artificial pool of the area "Rivière des Kaoris," respectively, and, BJW is the water collected from a small intertidal vent of the site "Bain des Japonais" in the Prony Bay.

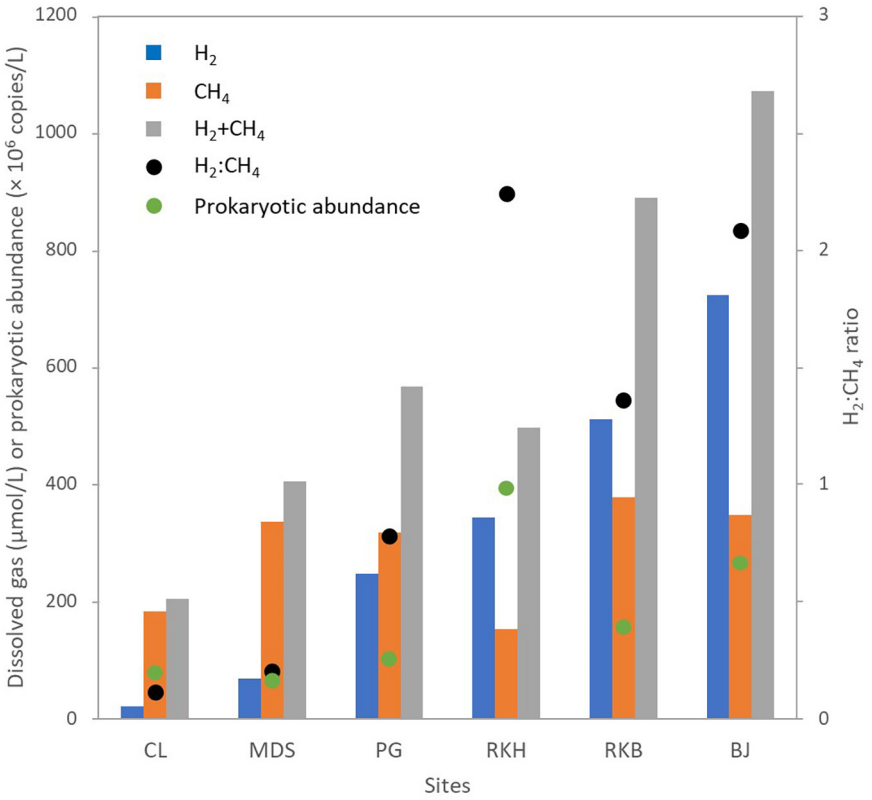

FIGURE 2
Dissolved gas (hydrogen and methane) and abundance of prokaryotes in water samples collected from the high-pH springs of New Caledonia. CL corresponds to the highest pool of "La Coulée," MDS is a pool of the "Montagne des Sources," PG indicates the source of the "Rivière des Pirogues," RKB and RKH correspond to a natural and an artificial pool of the "Rivière des Kaoris," respectively, and, BJ is a small intertidal vent of the "Bain des Japonais." Sum and ratio of hydrogen and methane concentrations (H_2:CH_4 ratio) and sum of the abundance of archaea and Bacteria (total quantity of prokaryotes obtained by real-time PCR) were indicated.

bacterial 16S rRNA genes was more than one order of magnitude higher than archaeal 16S rRNA genes, as previously observed in PBHF chimneys (Quéméneur et al., 2014; Postec et al., 2015). The highest abundances of prokaryotes were measured in the waters of the PBHF sites, with maximum values in the RKH pool (displaying the highest H_2 concentrations) (Figure 2). Prokaryotic

abundances increased with increasing H_2:CH_4 ratio (Figure 2 and Supplementary Figure 1). The *mcrA* genes (markers of methanoarchaea) were detected in all samples but were more abundant in the waters of the Rivière des Kaoris (> 10^7 copies/L of RKHW and RKBW). The *dsrB* genes (markers of sulfate reducers) were also detected in all samples. They were more abundant in the BJ waters (BJW), where sulfate concentrations range between 10 and 100 μM/L (Monnin et al., 2014).

The Simpson diversity indices (1-*D*) ranged between 0.92 and 0.98, while Shannon indices (*H*) varied from 4.1 to 5.2 (Table 1). Based on both indices, the lowest microbial diversity was observed in the most reducing water sample BJW (displaying the highest H_2 concentrations), while the highest diversity was found in CLW (displaying the highest E_h value and the lowest H_2 concentrations).

3.3. Global prokaryotic community composition

Variation in microbial community composition was observed in the spring waters with high-pH, which were different from each other (Figure 3). This was also observed in a principal coordinates analysis (PCoA), where the replicated samples from the same spring were closely grouped (with the exception of MDS water samples), but were situated far from each other on the PCoA plot (Supplementary Figure 1).

Twenty-six different phyla were identified by 16S rRNA metabarcoding analyses of the water samples collected from the six high-pH springs (Figure 3). However, only half of these phyla (n = 12) were considered dominant (representing each more than 1% of prokaryotic sequences and together more than 97% of prokaryotic sequences). Proteobacteria was predominant in all samples (37.5 ± 10.0%), followed by Bacteroidetes (11.0 ± 6.9%), Firmicutes (7.9 ± 5.1%), Cyanobacteria (7.8 ± 6.1%) and Euryarchaeota (6.5 ± 5.9%; Figure 3). These five major phyla (each > 5% on average) accounted for 85% of all prokaryotic sequences. The other dominant phyla ranged between 1 and 5% of prokaryotic phyla (in average) and included Actinobacteria (3.1 ± 1.8%), Deinococcus-Thermus (2.2 ± 1.7%), Nitrospirae (2.0 ± 1.3%), Chloroflexi (1.3 ± 0.9%), Planctomycetes (1.1 ± 0.9%), Spirochaetes (1.3 ± 1.2%), Verrucomicrobia (1.1 ± 1.1%), followed by minor phyla (0.1-1%): Acidobacteria, Bipolaricaulota (formerly known as Acetothermia or OP1), Thermotogae and Gracilibacteria (formerly designated GN02/BD1-5).

The highest content of Euryarchaeota (mainly represented by Methanosarcinales) was observed in Bain des Japonais (BJ) waters (19.1%), which also displayed the highest content of Deltaproteobacteria (mainly represented by *Desulfonatronum* species). Both Deinococcus-Thermus (*Meiothermus*) and Firmicutes (*Gracilibacter*) were also detected in significant amounts in BJ waters (> 10% of prokaryotes) and in Montagne des Sources (MDS) waters (> 10%). Firmicutes were ubiquitous and abundant in all waters (> 1%) and reached a maximum in CL waters (16.7 ± 1.0%), where *Dethiobacter* species mainly represented them. The PG waters were primarily dominated by Bacteroidetes (24%) and Cyanobacteria (16%). The MDS waters displayed the highest occurrences of Bipolaricaulota.

3.4. Distribution and diversity of abundant prokaryotic OTUs

Marked variations in the prokaryotic community of high-pH waters are also illustrated on a heatmap showing the most abundant OTUs (each > 1% on average) (Figure 4). Altogether, these 57 dominant OTUs represented almost 2/3 of the total prokaryotic sequences (60% in average).

In BJ waters (displaying the lowest E_h value and the highest H_2 content), the prokaryotes were dominated by: (i) potential H_2-oxidizing, sulfate-reducing *Desulfonatronum* OTUs (#21 and #7274, 19.5 and 1% of prokaryotes, respectively), closely related to *Desulfonatronum cooperativum* (96.7% identity; NR_043143), serpentinite-hosted PBHF clones (> 99% identity, KF886171; KT344938), and an uncultured deltaproteobacterium of deep groundwater (97.8%, LC055934), (ii) Methanosarcinales (OTU #12, 17.2% of prokaryotes) related to uncultured archaea from PBHF (KF886034 and KF886029; > 99.3% identity) and LCHF (SGYG644, SGYU755; 95.6% identity) classified as Lost City Methanosarcinales (LCMS); (iii) *Meiothermus* (OTU #37, 9.5%) closely related to *Meiothermus hypogaeus* (97.1% identity; NR_113226) and a PBHF clone (99.3% identity, KF886174), (iv) Bacteroidetes (OTU #65; 8.9%) related to uncultured bacteria from a deep subsurface gas storage aquifer (FJ168485, 90.2% identity) and deep groundwater from the Mizunami underground research laboratory (MIU) (LC055944, > 99% identity), (v) Firmicutes (OTUs #19 and #24203, 7.3 and 1.2%, respectively) affiliated with *Gracilibacter thermotolerans* (92–93%; NR_115692) and Firmicutes strains CE17 and CE8 (KX156793 and KX156784; > 95% identity) enriched from an *in situ* electrochemical experiment in a high-pH serpentinizing spring of The Cedars.

The RKH waters were dominated by: (i) H_2-oxidizing *Hydrogenophaga* OTUs (#6 and #23019; 24.6 and 3.3% of prokaryotes) closely related to *Hydrogenophaga aquatica* (97.5% identity) and *Serpentinimonas barnesii* (NR_181590; 99.3 and 97.1% identity), (ii) *Alteromonas* OTUs (#71 and #7774; 4.8 and 1.2%), (iii) Bacteroidetes OTUs (#87 and #65, 4.6 and 2.6%) closely related to those of carbonate precipitates from the Voltri serpentinite-hosted hyperalkaline springs (99% identity; KP097469). The RKB waters, similarly to the RKH ones, were also dominated by the *Hydrogenophaga* OTUs #6 and #23019, but in smaller quantities (about half as much, 13.3 and 1.7% of prokaryotes). Both *Alteromonas* and Bacteroidetes OTUs were also less represented (~2%), but Methanosarcinales OTUs #12 and #103 were more abundant in RKBW (6 and 0.5%), displaying higher CH_4 content than in RKHW (~0.5%). Bipolaricaulota OTU #3 related to *Acetothermus autotrophicum* (AP011801, 97% identity) accounted for 2.5% of RKBW prokaryotes. Cyanobacterial OTUs related to *Synechococcus* (#28, #365, and #2548) represented more than 5% of the prokaryotes.

In PG waters, the dominant OTUs were: (i) cyanobacterial *Leptolyngbya* (#4 and #13, 6.6 and 4.4% of prokaryotes) closely related to that of the mildly alkaline (pH 8.3–8.8) low-sulfur, low-carbonate Octopus hot spring (Yellowstone National Park, USA) (99% identity; KC236907, AY862014), (ii) Methanosarcinales (#12 and #103; 4.2 and 1.8%), (iii) *Hydrogenophaga* (#6; 2.7%), (iv) *Methylobacter* (#84; 1.3%).

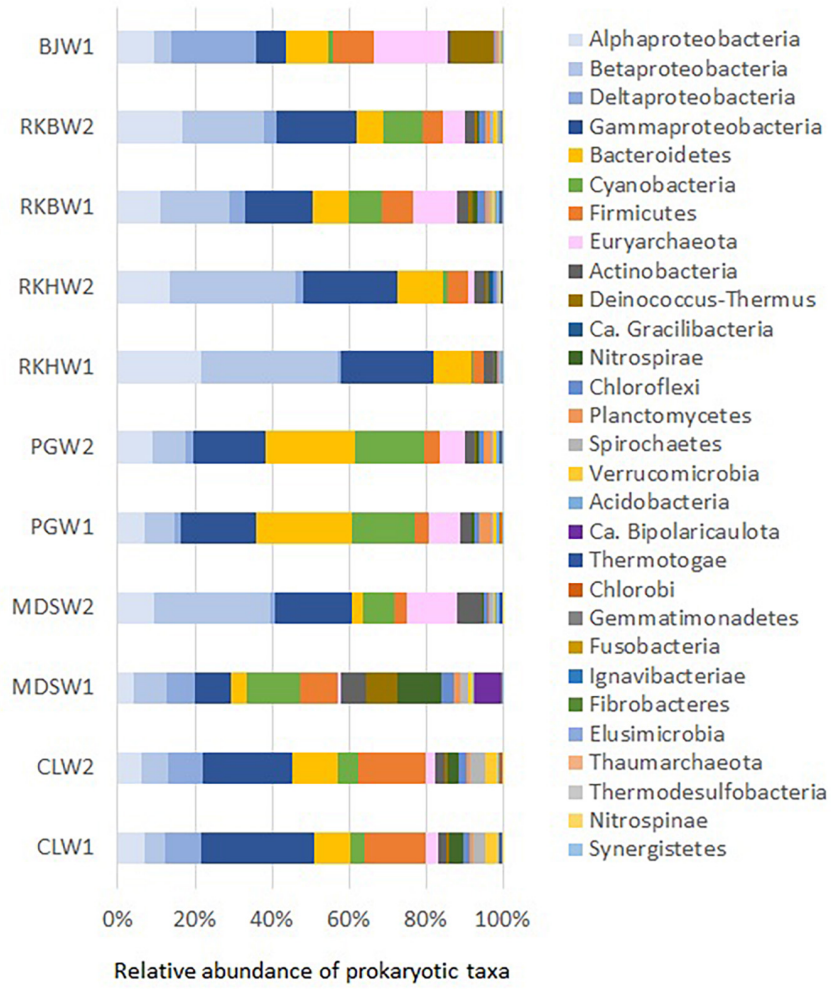

FIGURE 3
Prokaryotic phyla and proteobacterial classes (> 1% on average) in water samples collected from the high-pH springs of New Caledonia. CLW corresponds to the water of "La Coulée," MDSW is the water of "Montagne des Sources," PGW indicates the water of "Rivière des Pirogues," RKBW and RKHW correspond to the waters of "Rivière des Kaoris" and BJW is the water of "Bain des Japonais." Duplicated samples were indicated by numbers 1 or 2 (except for sample BJW).

In CL waters, the five dominant OTUs were affiliated with: (i) potential methylotrophic *Methyloglobus* (#17; 90% identity) and *Methylomonas* (#54), (ii) potential hydrocarbon-degrading *Syntrophus gentianae* (JQ346737; OTU #9; 95% identity), similar to uncultured deltaproteobacterium detected from deep groundwater (LC055948, > 98% identity), (iii) uncultured Firmicutes related to *Dethiobacter alkaliphilus* (OTUs #5, #18, #63; 94–96% identity), also detected from deep groundwater (LC055956) and from several serpentinite-hosted ecosystems (> 97% identity): PBHF (KJ149239, KF886127), Cabeço de Vide Aquifer (CVA) (AM777965), the hyperalkaline Allas Springs (Cyprus, 97.4% identity, JQ766804), the hyperalkaline spring GPS1 fed with deep groundwater at The Cedars (KC57503216S).

The MDS waters were dominated by six OTUs (representing more than 1/3 of the community) affiliated with (i) *Hydrogenophaga*/*Serpentinimonas* (#6 and #23019; 10.0 and 1.4% of prokaryotes), (ii) Methanosarcinales (#12 and #103; 10.0 and 1.1%), and (iii) sulfur-oxidizing *Thiofaba* (#10 and #23277, 8.2 and 2.4%).

3.5. Relationships between abundant taxa and environmental variables

Principal component analyses (PCA) was performed to identify the factors that affect the microbial community of New Caledonia high-pH spring waters (Figure 5). The first two principal components explained 63.6 and 76.1% of the data variability, for the phyla (Figure 5A) and major prokaryotic functional groups (Figure 5B), respectively. The first axis mostly separated the waters with the highest H_2 contents (BJW, RKBW, and RKHW) from the others. The second axis separated the more oxygenated waters RKHW and MDSW from the others. Spearman's rank correlation analyses examined the relationships between the microbial taxa, diversity indices and the environmental variables (Supplementary Tables 2–4).

At the phylum/class level, Gammaproteobacteria was positively correlated to E_h (r_S = 0.94, p < 0.05), and Deltaproteobacteria was positively correlated to temperature (r_S = 0.83, p < 0.05). Firmicutes were positively correlated to

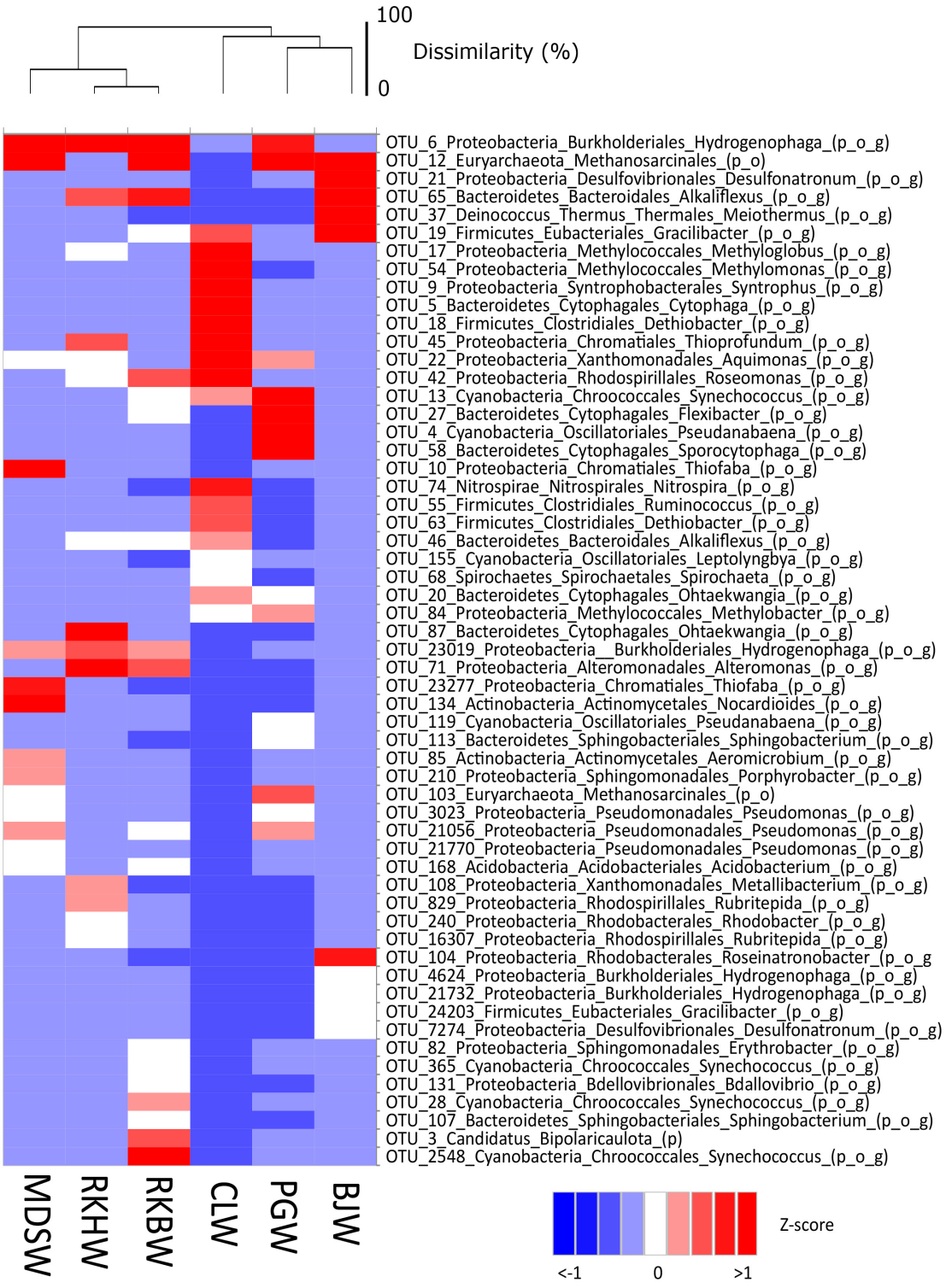

FIGURE 4
Heat map visualizing the Z-score distribution of the relative abundance of the dominant OTUs (> 1% on average) and their respective taxonomic affiliations in all water samples of the high-pH springs of New Caledonia. CLW corresponds to the water of "La Coulée," MDSW is the water of "Montagne des Sources," PGW indicates the water of "Rivière des Pirogues," RKBW and RKHW correspond to the waters of "Rivière des Kaoris" and BJW is the water of "Bain des Japonais." The average of replicates was calculated for each sampling site. The scale bar of the dendrogram represents the dissimilarity level (%) between microbial communities. The abbreviations of taxonomic ranks are p_ for phylum, o_ for order and g_ for genus.

H_2 (r_S = 0.96, p = 0.003), while the four phyla Elusimicrobia, Thermotogae, Ignavibacteria, and Thermodesulfovibrio were negatively correlated to H_2 (r_s = −0.89 to 0.99). Euryarchaeota (including methanogens) and Bipolaricaulota (Acetothermia) were positively correlated to CH_4 (r_s = 0.83 and 0.94, respectively; Supplementary Table 2).

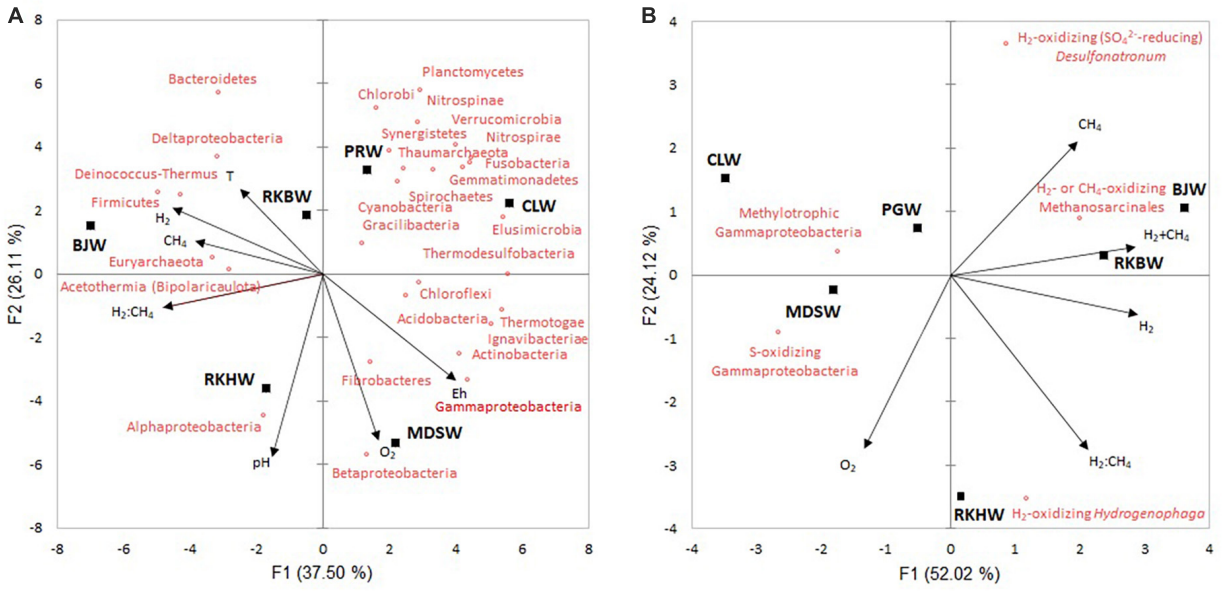

FIGURE 5
Principal component analysis (PCA) biplots show the variation among the high-pH water samples based on the physicochemical variables and the relative abundances of phyla (and proteobacterial classes) **(A)** and dominant prokaryotic functional groups **(B)**. Black squares represent water samples of high-pH springs of New Caledonia. Arrows indicate the direction of each variable's maximum increase and strength (through the length) to the overall distribution. CLW corresponds to the water of "La Coulée," MDSW is the water of "Montagne des Sources," PGW indicates the water of "Rivière des Pirogues," RKBW and RKHW correspond to the waters of "Rivière des Kaoris" and BJW is the water of "Bain des Japonais."

Among the dominant OTUs, four OTUs (*Gracilibacter* #19, *Meiothermus* #37, Bacteroidetes #65, *Roseinatronobacter* #104) were positively correlated with H_2. In comparison, five OTUs (Cyanobacteria #4, *Synthrophus* #9, *Dethiobacter* #63, Nitrospirae #74, *Leptolyngbya* #155) were negatively correlated with H_2, and only one OTU (Methanosarcinales #12) was positively correlated with CH_4 (**Supplementary Table 3**). Methanosarcinales (OTUs #12 and #103) were negatively correlated with methylotrophic gammaproteobacterial group ($r_S = -0.93$, $p < 0.02$). The sulfur-oxidizing gammaproteobacterial group was negatively correlated with H_2 ($r_S = -0.89$, $p < 0.05$) (**Supplementary Table 4** and **Supplementary Figure 2**). Prokaryotic abundances were positively correlated with H_2:CH_4 ratio ($r_S = 0.94$, $p < 0.02$). No significant correlation was observed between diversity indices and the environmental variables measured (**Supplementary Table 2**).

4. Discussion

The prokaryotic communities of the New Caledonian high-pH waters show several taxa previously detected in other ecosystems sustained by serpentinization, such as The Cedars and Lost City (Schrenk et al., 2013; Suzuki et al., 2013). These microbial taxa are represented by H_2-, CH_4-, and S-cycling prokaryotes (**Figure 6**), supporting the importance of oxidation or reduction of these compounds for the growth of microbial communities in New Caledonian springs.

Uncultured Methanosarcinales (OTUs #12 and #103) previously found in the submarine serpentinizing systems of PBHF (> 99% identity) (Quéméneur et al., 2014) and LCHF (> 95%) (Brazelton et al., 2010), could potentially anaerobically oxidize CH_4 or produce it using H_2 in an O_2-deprived environment. Methanosarcinales phylotypes are also detected in on-land high-pH (~11.5), H_2- and CH_4-rich springs of The Cedars (CA, USA) (Suzuki et al., 2013) and in the H_2-depleted Voltri springs (Italy) (Quéméneur et al., 2015). Our study shows that the uncultured Methanosarcinales (related to LCMS phylotypes) are abundant in most New Caledonian springs but are found in small quantities (~0.02% of the prokaryotes) in the CL waters, which have low CH_4 and H_2 contents. This was previously observed in the mildly alkaline (pH 9.3), CH_4 and H_2-poor waters of the La Crouen geothermal spring (Quéméneur et al., 2021). Moreover, the *Methanobacterium* phylotype was not detected in the hyperalkaline fluids of the studied on-land springs of New Caledonia. In contrast, this genus has been found in the alkaline geothermal spring of La Crouen (Quéméneur et al., 2021), where the novel species *Methanobacterium alkalithermotolerans* has been isolated (Mei et al., 2022), or in other on-land ecosystems sustained by serpentinization, such as the ophiolites of Samail (Oman) (Rempfert et al., 2017), Voltri (Northern Italy) (Quéméneur et al., 2015) and Zambales (Philippines) (Woycheese et al., 2015). On the other hand, in waters free from CH_4 (e.g., La Crouen or CL), the concentrations of potential aerobic methanotrophic Gammaproteobacteria (e.g., *Methylomonas*, *Methylobacter*, *Methylophaga*) were higher (> 5%) than in the CH_4-rich springs (<1%). These trends emphasize the importance of these potential methanogens and methanotrophs in the CH_4 budget.

Bacterial members of the aerobic H_2-oxidizing genera *Hydrogenophaga* (Lin et al., 2017) and *Serpentinimonas* (Bird et al., 2021) are also abundant in New Caledonian hyperalkaline springs, except in the BJ and CL waters (in which the H_2 concentrations are contrasted, high and low,

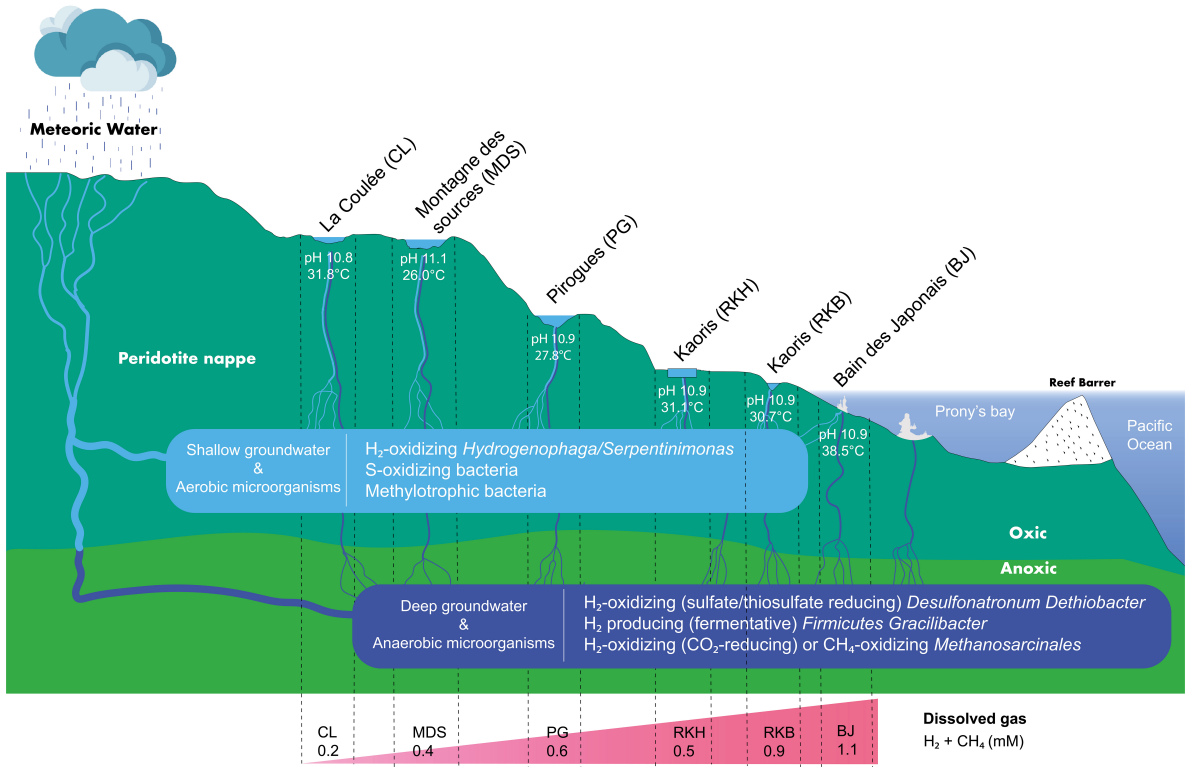

FIGURE 6
Schematic hydrothermal system diagram in southeastern New Caledonia's high-pH springs (not to scale). The meteoric water moves underground into the subsurface, where the process of serpentinization produces hyperalkaline H_2-rich fluids, before discharging at the geothermal springs of New Caledonia. Different microbial groups are observed depending on high-pH waters and their primary sources (shallow or deep).

respectively). Both genera were frequently detected in waters and sediments/concretions of on-land serpentinite-hosted springs, where anoxic H_2-rich subsurface fluids mix with oxygenated surface water (Suzuki et al., 2013; Quéméneur et al., 2015). They are present in the H_2-rich hyperalkaline waters of The Cedars springs (Suzuki et al., 2013), as well as in the H_2-depleted hyperalkaline waters of Voltri springs (Quéméneur et al., 2015), in the Cabeço de Vide Aquifer (Tiago and Veríssimo, 2013) and the H_2-depleted alkaline waters of La Crouen (Quéméneur et al., 2021). The low level of dissolved H_2 in these later spring waters could most likely be due to the high rate of H_2 consumption by the hyperalkaliphilic H_2-oxidizing *Serpentinimonas* (Marques et al., 2018).

BJ and CL waters displayed the lowest contents of *Hydrogenophaga*/*Serpentinimonas*, and the highest proportions of uncultured Firmicutes populations, previously identified from several serpentinizing systems. The dominant Firmicutes OTUs (#5 and #18) in CL waters were affiliated with *Dethiobacter alkaliphilus* (Sorokin et al., 2008), an anaerobic thiosulfate/polysulfide (not sulfate) reducer, polyextremophile, able to fix inorganic carbon through the Wood–Ljungdahl pathway using H_2 as an electron donor (Melton et al., 2017). *Dethiobacter* phylotypes were abundant at Cabeço de Vide (Tiago and Veríssimo, 2013), The Cedars (Suzuki et al., 2013), the Coast Range Ophiolite (Twing et al., 2017), and the PBHF sites (Mei et al., 2016b). The dominant Firmicutes OTUs (#19 and #24203) in BJ waters are affiliated with *Gracilibacter thermotolerans* (Lee et al., 2006), a strict anaerobe able to produce H_2 and acetate as a by-product of fermentation. *Gracilibacter* phylotypes were previously observed in the natural subsurface waters of the Coast Range Ophiolite (Twing et al., 2017) and the artificially enriched spring waters of The Cedars during an *in situ* electrochemical experiment (Rowe et al., 2017). Other potential acetogens and H_2-producers, positively correlated with H_2 and abundantly detected in MDS and RK waters, were affiliated with Bipolaricaulota (formerly known as Acetothermia and OP1). These microorganisms can transform low-molecular-weight organic compounds into H_2 and acetate in the subsurface aquifer (Kadnikov et al., 2019).

The hydrogenotrophic, alkaliphilic, sulfate-reducing bacterium, *D. cooperativum*, has been isolated from a syntrophic culture growing on acetate and enriched from soda lake samples (Zhilina et al., 2005). It dominated the highly reduced waters discharged by the intertidal BJ spring (OTUs #21 and #7274), as found in a previous study (Mei et al., 2016b). These anaerobic bacteria can use sulfate, thiosulfate, elemental sulfur, or polysulfide as terminal electron acceptors. They were detected in low abundance in other on-land high-pH springs of New Caledonia (this work) and previously found in subsurface fluids of the Samail Ophiolite (Oman) (Rempfert et al., 2017). In New Caledonian high-pH waters, *Desulfonatronum* bacteria were inversely correlated with sulfur-oxidizing Gammaproteobacteria (e.g., *Thiofaba*). This points to a link between microbial activity and the sulfur chemistry, constrained by the redox conditions of the local environment. This was previously observed in borehole fluids of the Samail

Ophiolite (Oman) (USA) and the California Coast Range Ophiolite (Glombitza et al., 2021).

5. Conclusion

The prokaryotic communities thriving in the hyperalkaline waters of several New Caledonia springs are mainly composed of microorganisms that use H_2 as an energy source. They consist mainly of microaerophilic bacteria belonging to *Hydrogenophaga*/*Serpentinimonas* (in on-land spring waters) or anaerobic archaea belonging to a specific phylotype (designated LCMS) of uncultured Methanosarcinales (potentially able to produce CH_4 using H_2), which are previously detected in both submarine (i.e., Lost City, Prony Bay) (Schrenk et al., 2013; Quéméneur et al., 2014; Postec et al., 2015) and on-land serpentinizing systems (e.g., The Cedars, Voltri ophiolite) (Schrenk et al., 2013; Suzuki et al., 2013; Quéméneur et al., 2015). Thus, the relative abundance of these H_2-consuming microorganisms could be used as signature-taxa (or taxonomic bioindicators) of serpentinite-hosted environments emitting natural H_2.

The low abundance of *Hydrogenophaga*/*Serpentinimonas* in the water of the intertidal site BJ of the Prony Bay, where anaerobic sulfate-reducing *Desulfonatronum* proliferate together with other abundant anaerobic and thermophilic bacterial taxa (e.g., Bacteroidetes, *Meiothermus*, or *Gracilibacter*), suggests different water origins between terrestrial and marine springs, or subsurface seawater infiltrations through rock fractures (Monnin et al., 2014). Moreover, the co-existence of aerobic and anaerobic microorganisms in the hyperalkaline waters of other terrestrial hyperalkaline springs of the New Caledonia ophiolite could result in a mixing of deep (anoxic and warm) and surface (oxygenated and cold) waters before surface discharge at the various springs (**Figure 6**). This would corroborate a circulation pattern of the hydrothermal systems in ophiolites where waters flow through oxic and anoxic zones (Leong and Shock, 2020).

The relative abundance of uncultured Methanosarcinales-like sequences (designated LCMS), exclusively detected in serpentinite-hosted ecosystems (Frouin et al., 2018), was negatively correlated with aerobic methylobacteria, able to use CH_4 as the sole source of carbon and energy in the waters of the hyperalkaline springs. This result suggests their implication in the consumption of CH_4, also measured in the anoxic water generated by the serpentinization of the New Caledonia ophiolite.

Other anaerobic microbial taxa previously found in serpentinite-hosted environments were detected in New Caledonia hyperalkaline waters. It is the case of two anaerobic Firmicutes phylotypes affiliated with *Dethiobacter* and *Gracilibacter* genera and correlated with H_2, which could also be considered as specific taxonomic bioindicators of H_2 emissions in serpentinite-hosted environments. Although some Firmicutes bacteria have been isolated from the hyperalkaline concretions of the New Caledonian sites of the PBHF (including H_2-producing bacteria) (Mei et al., 2014, 2016a,b; Postec et al., 2021), most remain uncultivated and their metabolisms unknown. Their role in the natural H_2 budget remains to be assessed.

Data availability statement

The datasets presented in this study can be found in online repositories. The names of the repository/repositories and accession number(s) can be found in this article/**Supplementary material**.

Author contributions

MQ, CM, and BP sampled water and gas during the H2NAT campaign. CM performed core parameter analyses. NM performed DNA extraction and PCR assays with the help of SG. MQ processed the MiSeq Illumina sequence data and wrote the first draft of the manuscript. All authors were involved in the critical revision and approval of the final version.

Funding

This project was financially supported by the French Institute of Research for Development (IRD), the INTERVIE CNRS INSU program, the H2NAT project funded by the Midi-Pyrénées Observatory (OMP, Toulouse), and the ANR MICROPRONY (N°19-CE02-0020-02).

Acknowledgments

We thank Jean Chatelier and the people at the IRD center and the DIMENC in Nouméa for their help on the field.

Conflict of interest

The authors declare that the research was conducted in the absence of any commercial or financial relationships that could be construed as a potential conflict of interest.

Publisher's note

Supplementary material

The Supplementary Material for this article can be found online at: https://www.frontiersin.org/articles/10.3389/fmicb.2023.1196516/full#supplementary-material

References

Avias, J. (1967). Overthrust structure of the main ultrabasic New Caledonian massives. *Tectonophysics* 4, 531–541. doi: 10.1016/0040-1951(67)90017-0

Bird, L. J., Kuenen, J. G., Osburn, M. R., Tomioka, N., Ishii, S., Barr, C., et al. (2021). Serpentinimonas gen. nov., Serpentinimonas raichei sp. nov., Serpentinimonas barnesii sp. nov. and Serpentinimonas maccroryi sp. nov., hyperalkaliphilic and facultative autotrophic bacteria isolated from terrestrial serpentinizing springs. *Int. J. Syst. Evol. Microbiol.* 71:004945. doi: 10.1099/ijsem.0.004945

Brazelton, W. J., Ludwig, K. A., Sogin, M. L., Andreishcheva, E. N., Kelley, D. S., Shen, C. C., et al. (2010). Archaea and bacteria with surprising microdiversity show shifts in dominance over 1,000-year time scales in hydrothermal chimneys. *Proc. Natl. Acad. Sci. U. S. A.* 107, 1612–1617. doi: 10.1073/pnas.0905369107

Caporaso, J. G., Lauber, C. L., Walters, W. A., Berg-Lyons, D., Lozupone, C. A., Turnbaugh, P. J., et al. (2011). Global patterns of 16S rRNA diversity at a depth of millions of sequences per sample. *Proc. Natl. Acad. Sci. U. S. A.* 108, 4516–4522. doi: 10.1073/pnas.1000080107

Casamayor, E. O., Massana, R., Benlloch, S., Øvreås, L., Díez, B., Goddard, V. J., et al. (2002). Changes in archaeal, bacterial and eukaryal assemblages along a salinity gradient by comparison of genetic fingerprinting methods in a multipond solar saltern. *Environ. Microbiol.* 4, 338–348. doi: 10.1046/j.1462-2920.2002.00297.x

Cluzel, D., Aitchison, J. C., and Picard, C. (2001). Tectonic accretion and underplating of mafic terranes in the late eocene intraoceanic fore-arc of New Caledonia (Southwest Pacific): Geodynamic implications. *Tectonophysics* 340, 23–59. doi: 10.1016/S0040-1951(01)00148-2

Cox, M. E., Launay, J., and Paris, J. (1982). "Geochemistry of low temperature geothermal systems in New Caledonia," in *Pacific geothermal conference and 4th NZ Geothermal Workshop*, (Vienna: International Atomic Energy Agency), 453–459.

Deville, E., and Prinzhofer, A. (2016). The origin of N2-H2-CH4-rich natural gas seepages in ophiolitic context: A major and noble gases study of fluid seepages in New Caledonia. *Chem. Geol.* 440, 139–147. doi: 10.1016/j.chemgeo.2016.06.011

Dowd, S. E., Callaway, T. R., Wolcott, R. D., Sun, Y., McKeehan, T., Hagevoort, R. G., et al. (2008). Evaluation of the bacterial diversity in the feces of cattle using 16S rDNA bacterial tag-encoded FLX amplicon pyrosequencing (bTEFAP). *BMC Microbiol.* 8:125. doi: 10.1186/1471-2180-8-125

Edgar, R. C. (2010). Search and clustering orders of magnitude faster than blast. *Bioinformatics* 26, 2460–2461. doi: 10.1093/bioinformatics/btq461

Edgar, R. C., Haas, B. J., Clemente, J. C., Quince, C., and Knight, R. (2011). UCHIME improves sensitivity and speed of chimera detection. *Bioinformatics* 27, 2194–2200. doi: 10.1093/bioinformatics/btr381

Frouin, E., Bes, M., Ollivier, B., Quéméneur, M., Postec, A., Debroas, D., et al. (2018). Diversity of rare and abundant prokaryotic phylotypes in the Prony Hydrothermal Field and comparison with other serpentinite-hosted ecosystems. *Front. Microbiol.* 9:102. doi: 10.3389/fmicb.2018.00102

Gaucher, E. C. (2020). New perspectives in the industrial exploration for native hydrogen. *Elements* 16, 8–9. doi: 10.2138/gselements.16.1.8

Geets, J., Borremans, B., Diels, L., Springael, D., Vangronsveld, J., van der Lelie, D., et al. (2006). DsrB gene-based DGGE for community and diversity surveys of sulfate-reducing bacteria. *J. Microbiol. Methods* 66, 194–205. doi: 10.1016/j.mimet.2005.11.002

Glombitza, C., Putman, L. I., Rempfert, K. R., Kubo, M. D., Schrenk, M. O., Templeton, A. S., et al. (2021). Active microbial sulfate reduction in fluids of serpentinizing peridotites of the continental subsurface. *Commun. Earth Environ.* 2:84. doi: 10.1038/s43247-021-00157-z

Hales, B. A., Edwards, C., Ritchie, D. A., Hall, G., Pickup, R. W., and Saunders, J. R. (1996). Isolation and identification of methanogen-specific DNA from blanket bog peat by PCR amplification and sequence analysis. *Appl. Environ. Microbiol.* 62, 668–675. doi: 10.1128/aem.62.2.668-675.1996

Kadnikov, V., Mardanov, A., Beletsky, A., Frank, Y., Karnachuk, O., and Ravin, N. (2019). Complete genome sequence of an uncultured bacterium of the candidate phylum bipolaricaulota. *Microbiology* 88, 461–468. doi: 10.1134/S0026261719040064

Kelley, D. S., Karson, J. A., Fruh-Green, G. L., Yoerger, D. R., Shank, T. M., Butterfield, D. A., et al. (2005). A serpentinite-hosted ecosystem: The Lost City hydrothermal field. *Science* 307, 1428–1434. doi: 10.1126/science.1102556

Klein, F., Bach, W., and McCollom, T. M. (2013). Compositional controls on hydrogen generation during serpentinization of ultramafic rocks. *Lithos* 178, 55–69. doi: 10.1016/j.lithos.2013.03.008

Konn, C., Charlou, J. L., Holm, N. G., and Mousis, O. (2015). The production of methane, hydrogen, and organic compounds in ultramafic-hosted hydrothermal vents of the Mid-Atlantic Ridge. *Astrobiology* 15, 381–399. doi: 10.1089/ast.2014.1198

Lane, D. (1991). "16S/23S rRNA sequencing," in *Nucleic acid techniques in bacterial systematics*, eds E. Stackebrandt and M. Goodfellow (New York, NY: Wiley).

Launay, J., and Fontes, J. C. (1985). Les sources thermales de Prony (Nouvelle Calédonie) et leurs précipités chimiques, exemple de formation de brucite primaire. *Geol. France* 1, 83–100.

Lecoeuvre, A., Ménez, B., Cannat, M., Chavagnac, V., and Gérard, E. (2021). Microbial ecology of the newly discovered serpentinite-hosted Old City hydrothermal field (southwest Indian ridge). *ISME J.* 15, 818–832. doi: 10.1038/s41396-020-00816-7

Lee, Y. J., Romanek, C. S., Mills, G. L., Davis, R. C., Whitman, W. B., and Wiegel, J. (2006). Gracilibacter thermotolerans gen. nov., sp. nov., an anaerobic, thermotolerant bacterium from a constructed wetland receiving acid sulfate water. *Int. J. Syst. Evol. Microbiol.* 56, 2089–2093. doi: 10.1099/ijs.0.64040-0

Leong, J. A. M., and Shock, E. L. (2020). Thermodynamic constraints on the geochemistry of low-temperature, continental, serpentinization-generated fluids. *Am. J. Sci.* 320, 185–235. doi: 10.2475/03.2020.01

Lin, S. Y., Hameed, A., Wen, C. Z., Hsu, Y. H., Liu, Y. C., Lai, W. A., et al. (2017). Hydrogenophaga aquatica sp. nov., isolated from a hot spring. *Int. J. Syst. Evol. Microbiol.* 67, 3716–3721. doi: 10.1099/ijsem.0.002146

Luton, P. E., Wayne, J. M., Sharp, R. J., and Riley, P. W. (2002). The mcrA gene as an alternative to 16S rRNA in the phylogenetic analysis of methanogen populations in landfill. *Microbiology* 148, 3521–3530. doi: 10.1099/00221287-148-11-3521

Magen, C., Lapham, L. L., Pohlman, J. W., Marshall, K., Bosman, S., Casso, M., et al. (2014). A simple headspace equilibration method for measuring dissolved methane. *Limnol. Oceanogr. Methods* 12, 637–650. doi: 10.1093/chromsci/36.5.253

Marques, J. M., Etiope, G., Neves, M., Carreira, P., Rocha, C., Vance, S., et al. (2018). Linking serpentinization, hyperalkaline mineral waters and abiotic methane production in continental peridotites: An integrated hydrogeological-bio-geochemical model from the Cabeço de Vide CH4-rich aquifer (Portugal). *Appl. Geochem.* 96, 287–301. doi: 10.1016/j.apgeochem.2018.07.011

Maurizot, P., Sevin, B., Lesimple, S., Collot, J., Jeanpert, J., Bailly, L., et al. (2020). Mineral resources and prospectivity of non-ultramafic rocks of New Caledonia. *Geol. Soc. Lond. Mem.* 51, 215–245. doi: 10.1144/M51-2016-9

McCollom, T. M., and Seewald, J. S. (2013). Serpentinites, hydrogen, and life. *Elements* 9, 129–134. doi: 10.2113/gselements.9.2.129

Mei, N., Postec, A., Bartoli, M., Vandecasteele, C., Wils, L., Gil, L., et al. (2022). Methanobacterium alkalithermotolerans sp. nov., a novel alkaliphilic and hydrogen-utilizing methanogen isolated from an alkaline geothermal spring (La Crouen, New Caledonia). *Int. J. Syst. Evol. Microbiol.* 72:005554. doi: 10.1099/ijsem.0.005554

Mei, N., Postec, A., Erauso, G., Joseph, M., Pelletier, B., Payri, C., et al. (2016a). Serpentinicella alkaliphila gen. nov., sp. nov., a novel alkaliphilic anaerobic bacterium isolated from the serpentinite-hosted Prony hydrothermal field, New Caledonia. *Int. J. Syst. Evol. Microbiol.* 66, 4464–4470. doi: 10.1099/ijsem.0.001375

Mei, N., Postec, A., Monnin, C., Pelletier, B., Payri, C. E., Ménez, B., et al. (2016b). Metagenomic and PCR-based diversity surveys of [FeFe]-hydrogenases combined with isolation of alkaliphilic hydrogen-producing bacteria from the serpentinite-hosted Prony Hydrothermal Field, New Caledonia. *Front. Microbiol.* 7:1301. doi: 10.3389/fmicb.2016.01301

Mei, N., Zergane, N., Postec, A., Erauso, G., Ollier, A., Payri, C., et al. (2014). Fermentative hydrogen production by a new alkaliphilic Clostridium sp.(strain PROH2) isolated from a shallow submarine hydrothermal chimney in Prony Bay, New Caledonia. *Int. J. Hydrogen Energy* 39, 19465–19473. doi: 10.1016/j.ijhydene.2014.09.111

Melton, E. D., Sorokin, D. Y., Overmars, L., Lapidus, A. L., Pillay, M., Ivanova, N., et al. (2017). Draft genome sequence of Dethiobacter alkaliphilus strain AHT1 T, a gram-positive sulfidogenic polyextremophile. *Standards Genomic Sci.* 12, 1–9. doi: 10.1186/s40793-017-0268-9

Ménez, B. (2020). Abiotic hydrogen and methane: Fuels for life. *Elements* 16, 39–46.

Monnin, C., Chavagnac, V., Boulart, C., Ménez, B., Gérard, M., Gérard, E., et al. (2014). Fluid chemistry of the low temperature hyperalkaline hydrothermal system of Prony Bay (New Caledonia). *Biogeosciences* 11, 5687–5706.

Monnin, C., Quéméneur, M., Price, R., Jeanpert, J., Maurizot, P., Boulart, C., et al. (2021). The chemistry of hyperalkaline springs in serpentinizing environments: 1. the composition of free gases in New Caledonia compared to other springs worldwide. *J. Geophys. Res. Biogeosci.* 126:e2021JG006243.

Muyzer, G., De Waal, E. C., and Uitterlinden, A. (1993). Profiling of complex microbial populations by denaturing gradient gel electrophoresis analysis of polymerase chain reaction-amplified genes coding for 16S rRNA. *Appl. Environ. Microbiol.* 59, 695–700. doi: 10.1128/aem.59.3.695-700.1993

Nealson, K. H., Inagaki, F., and Takai, K. (2005). Hydrogen-driven subsurface lithoautotrophic microbial ecosystems (SLiMEs): Do they exist and why should we care? *Trends Microbiol.* 13, 405–410. doi: 10.1016/j.tim.2005.07.010

Nunoura, T., Oida, H., Miyazaki, J., Miyashita, A., Imachi, H., and Takai, K. (2008). Quantification of mcrA by fluorescent PCR in methanogenic and methanotrophic microbial communities. *FEMS Microbiol. Ecol.* 64, 240–247.

Oldham, A. L., and Duncan, K. E. (2012). Similar gene estimates from circular and linear standards in quantitative PCR analyses using the prokaryotic 16S rRNA gene as a model. *PLoS One* 7:e51931. doi: 10.1371/journal.pone.0051931

Ovreås, L., Forney, L., Daae, F. L., and Torsvik, V. (1997). Distribution of bacterioplankton in meromictic Lake Saelenvannet, as determined by denaturing gradient gel electrophoresis of PCR-amplified gene fragments coding for 16S rRNA. *Appl. Environ. Microbiol.* 63, 3367–3373. doi: 10.1128/aem.63.9.3367-3373.1997

Pirard, C., Hermann, J., and O'Neill, H. S. C. (2013). Petrology and geochemistry of the crust–mantle boundary in a nascent arc, Massif du Sud ophiolite, New Caledonia, SW Pacific. *J. Petrol.* 54, 1759–1792.

Postec, A., Quéméneur, M., Bes, M., Mei, N., Benaïssa, F., Payri, C., et al. (2015). Microbial diversity in a submarine carbonate edifice from the serpentinizing hydrothermal system of the Prony Bay (New Caledonia) over a 6-year period. *Front. Microbiol.* 6:857. doi: 10.3389/fmicb.2015.00857

Postec, A., Quemeneur, M., Lecoeuvre, A., Chabert, N., Joseph, M., and Erauso, G. (2021). Alkaliphilus serpentinus sp. nov. and Alkaliphilus pronyensis sp. nov., two novel anaerobic alkaliphilic species isolated from the serpentinite-hosted Prony Bay Hydrothermal Field (New Caledonia). *Syst. Appl. Microbiol.* 44:126175. doi: 10.1016/j.syapm.2020.126175

Quéméneur, M., Bes, M., Postec, A., Mei, N., Hamelin, J., Monnin, C., et al. (2014). Spatial distribution of microbial communities in the shallow submarine alkaline hydrothermal field of the P rony Bay, New Caledonia. *Environ. Microbiol. Rep.* 6, 665–674. doi: 10.1111/1758-2229.12184

Quéméneur, M., Mei, N., Monnin, C., Postec, A., Wils, L., Bartoli, M., et al. (2021). Procaryotic Diversity and Hydrogenotrophic Methanogenesis in an Alkaline Spring (La Crouen, New Caledonia). *Microorganisms* 9:1360. doi: 10.3390/microorganisms9071360

Quéméneur, M., Palvadeau, A., Postec, A., Monnin, C., Chavagnac, V., Ollivier, B., et al. (2015). Endolithic microbial communities in carbonate precipitates from serpentinite-hosted hyperalkaline springs of the Voltri Massif (Ligurian Alps, Northern Italy). *Environ. Sci. Pollut. Res.* 22, 13613–13624. doi: 10.1007/s11356-015-4113-7

Rempfert, K. R., Miller, H. M., Bompard, N., Nothaft, D., Matter, J. M., Kelemen, P., et al. (2017). Geological and geochemical controls on subsurface microbial life in the Samail Ophiolite, Oman. *Front. Microbiol.* 8:56. doi: 10.3389/fmicb.2017.00056

Rowe, A. R., Yoshimura, M., LaRowe, D. E., Bird, L. J., Amend, J. P., Hashimoto, K., et al. (2017). In situ electrochemical enrichment and isolation of a magnetite-reducing bacterium from a high pH serpentinizing spring. *Environ. Microbiol.* 19, 2272–2285. doi: 10.1111/1462-2920.13723

Russell, M. J., Hall, A. J., and Martin, W. (2010). Serpentinization as a source of energy at the origin of life. *Geobiology* 8, 355–371.

Sander, R. (2015). Compilation of Henry's law constants (version 4.0) for water as solvent. *Atmosph. Chem. Phys.* 15, 4399–4981.

Schrenk, M. O., Brazelton, W. J., and Lang, S. Q. (2013). Serpentinization, carbon, and deep life. *Rev. Mineral. Geochem.* 75, 575–606.

Shannon, C. E. (1948). A mathematical theory of communication. *Bell Syst. Tech. J.* 27, 379–423.

Simpson, E. H. (1949). Measurement of diversity. *Nature* 163, 688–688.

Sleep, N., Meibom, A., Fridriksson, T., Coleman, R., and Bird, D. (2004). H2-rich fluids from serpentinization: Geochemical and biotic implications. *Proc. Natl. Acad. Sci. U. S. A.* 101, 12818–12823. doi: 10.1073/pnas.0405289101

Sorokin, D. Y., Tourova, T., Mußmann, M., and Muyzer, G. (2008). Dethiobacter alkaliphilus gen. nov. sp. nov., and Desulfurivibrio alkaliphilus gen. nov. sp. nov.: Two novel representatives of reductive sulfur cycle from soda lakes. *Extremophiles* 12, 431–439. doi: 10.1007/s00792-008-0148-8

Suzuki, S., Ishii, S., Wu, A., Cheung, A., Tenney, A., Wanger, G., et al. (2013). Microbial diversity in The Cedars, an ultrabasic, ultrareducing, and low salinity serpentinizing ecosystem. *Proc. Natl. Acad. Sci. U. S. A.* 110, 15336–15341. doi: 10.1073/pnas.1302426110

Tiago, I., and Veríssimo, A. (2013). Microbial and functional diversity of a subterrestrial high pH groundwater associated to serpentinization. *Environ. Microbiol.* 15, 1687–1706. doi: 10.1111/1462-2920.12034

Truche, L., McCollom, T. M., and Martinez, I. (2020). Hydrogen and abiotic hydrocarbons: Molecules that change the world. *Elements* 16, 13–18.

Twing, K. I., Brazelton, W. J., Kubo, M. D., Hyer, A. J., Cardace, D., Hoehler, T. M., et al. (2017). Serpentinization-influenced groundwater harbors extremely low diversity microbial communities adapted to high pH. *Front. Microbiol.* 8:308. doi: 10.3389/fmicb.2017.00308

Vacquand, C., Deville, E., Beaumont, V., Guyot, F., Sissmann, O., Pillot, D., et al. (2018). Reduced gas seepages in ophiolitic complexes: Evidences for multiple origins of the H2-CH4-N2 gas mixtures. *Geochim. Cosmochim. Acta* 223, 437–461.

Wagner, M., Roger, A. J., Flax, J. L., Brusseau, G. A., and Stahl, D. A. (1998). Phylogeny of dissimilatory sulfite reductases supports an early origin of sulfate respiration. *J. Bacteriol.* 180, 2975–2982. doi: 10.1128/JB.180.11.2975-2982.1998

Wang, X., Ouyang, Z., Zhuo, S., Zhang, M., Zheng, G., and Wang, Y. (2014). Serpentinization, abiogenic organic compounds, and deep life. *Sci. China Earth Sci.* 57, 878–887.

Webster, G., John Parkes, R., Cragg, B. A., Newberry, C. J., Weightman, A. J., and Fry, J. C. (2006). Prokaryotic community composition and biogeochemical processes in deep subseafloor sediments from the Peru Margin. *FEMS Microbiol. Ecol.* 58, 65–85.

Woycheese, K. M., Meyer-Dombard, D. A. R., Cardace, D., Argayosa, A. M., and Arcilla, C. A. (2015). Out of the dark: Transitional subsurface-to-surface microbial diversity in a terrestrial serpentinizing seep (Manleluag, Pangasinan, the Philippines). *Front. Microbiol.* 6:44. doi: 10.3389/fmicb.2015.00044

Zhilina, T. N., Zavarzina, D. G., Kuever, J., Lysenko, A. M., and Zavarzin, G. A. (2005). Desulfonatronum cooperativum sp. nov., a novel hydrogenotrophic, alkaliphilic, sulfate-reducing bacterium, from a syntrophic culture growing on acetate. *Int. J. Syst. Evol. Microbiol.* 55, 1001–1006. doi: 10.1099/ijs.0.63490-0

frontiers | Frontiers in Microbiology

TYPE Original Research
PUBLISHED 13 July 2023
DOI 10.3389/fmicb.2023.1179857

OPEN ACCESS

EDITED BY
Masahiro Ito,
Toyo University, Japan

REVIEWED BY
Isao Yumoto,
National Institute of Advanced Industrial Science and Technology (AIST), Japan
Daniel Colman,
Montana State University, United States

*CORRESPONDENCE
Nancy Merino
✉ merino4@llnl.gov

†These authors have contributed equally to this work and share first authorship

RECEIVED 05 March 2023
ACCEPTED 23 May 2023
PUBLISHED 13 July 2023

CITATION
Thompson J, Barr C, Babcock-Adams L, Bird L, La Cava E, Garber A, Hongoh Y, Liu M, Nealson KH, Okamoto A, Repeta D, Suzuki S, Tacto C, Tashjian M and Merino N (2023) Insights into the physiological and genomic characterization of three bacterial isolates from a highly alkaline, terrestrial serpentinizing system.
Front. Microbiol. 14:1179857.
doi: 10.3389/fmicb.2023.1179857

Insights into the physiological and genomic characterization of three bacterial isolates from a highly alkaline, terrestrial serpentinizing system

Jaclyn Thompson[1†], Casey Barr[1†], Lydia Babcock-Adams[2], Lina Bird[3], Eugenio La Cava[4], Arkadiy Garber[1,5], Yuichi Hongoh[6], Mark Liu[1], Kenneth H. Nealson[1], Akihiro Okamoto[7,8,9], Daniel Repeta[2], Shino Suzuki[10,11], Clarissa Tacto[1], Michelle Tashjian[1] and Nancy Merino[1,12,13]*

[1]Department of Earth Sciences, University of Southern California, Los Angeles, CA, United States, [2]Department of Marine Chemistry and Geochemistry, Woods Hole Oceanographic Institution, Woods Hole, MA, United States, [3]Center for Bio/Molecular Science and Engineering, Naval Research Laboratory, Washington, DC, United States, [4]National Institute for Materials Science, Tsukuba, Ibaraki, Japan, [5]Biodesign Center for Mechanisms of Evolution, Arizona State University, Tempe, AZ, United States, [6]School of Life Science and Technology, Tokyo Institute of Technology, Tokyo, Japan, [7]Research Center for Macromolecules and Biomaterials, National Institute for Materials Science, Tsukuba, Japan, [8]Graduate School of Chemical Sciences and Engineering, Hokkaido University, Sapporo, Hokkaido, Japan, [9]Graduate School of Science and Technology, University of Tsukuba, Tsukuba, Japan, [10]Institute of Space and Astronautical Science (ISAS), Japan Aerospace Exploration Agency (JAXA), Sagamihara, Sagamihara, Kanagawa, Japan, [11]Institute for Extra-cutting-edge Science and Technology Avant-garde Research (X-star), JAMSTEC, Yokosuka, Kanagawa, Japan, [12]Earth-Life Science Institute, Tokyo Institute of Technology, Tokyo, Japan, [13]Biosciences and Biotechnology Division, Lawrence Livermore National Laboratory, Livermore, CA, United States

The terrestrial serpentinite-hosted ecosystem known as "The Cedars" is home to a diverse microbial community persisting under highly alkaline (pH~12) and reducing (Eh<−550 mV) conditions. This extreme environment presents particular difficulties for microbial life, and efforts to isolate microorganisms from The Cedars over the past decade have remained challenging. Herein, we report the initial physiological assessment and/or full genomic characterization of three isolates: *Paenibacillus* sp. Cedars ('Paeni-Cedars'), *Alishewanella* sp. BS5-314 ('Ali-BS5-314'), and *Anaerobacillus* sp. CMMVII ('Anaero-CMMVII'). Paeni-Cedars is a Gram-positive, rod-shaped, mesophilic facultative anaerobe that grows between pH 7–10 (minimum pH tested was 7), temperatures 20–40°C, and 0–3% NaCl concentration. The addition of 10–20 mM $CaCl_2$ enhanced growth, and iron reduction was observed in the following order, 2-line ferrihydrite > magnetite > serpentinite ~ chromite ~ hematite. Genome analysis identified genes for flavin-mediated iron reduction and synthesis of a bacillibactin-like, catechol-type siderophore. Ali-BS5-314 is a Gram-negative, rod-shaped, mesophilic, facultative anaerobic alkaliphile that grows between pH 10–12 and temperatures 10–40°C, with limited growth observed 1–5% NaCl. Nitrate is used as a terminal electron acceptor under anaerobic conditions, which was corroborated by genome analysis. The Ali-BS5-314 genome also includes genes for benzoate-like compound metabolism. Anaero-CMMVII remained difficult to cultivate for physiological studies; however, growth was observed between pH 9–12, with the addition of 0.01–1% yeast extract. Anaero-CMMVII is a probable oxygen-tolerant anaerobic alkaliphile with hydrogenotrophic respiration coupled with nitrate reduction, as determined by genome analysis. Based on single-copy genes, ANI,

AAI and dDDH analyses, Paeni-Cedars and Ali-BS5-314 are related to other species (*P. glucanolyticus* and *A. aestuarii,* respectively), and Anaero-CMMVII represents a new species. The characterization of these three isolates demonstrate the range of ecophysiological adaptations and metabolisms present in serpentinite-hosted ecosystems, including mineral reduction, alkaliphily, and siderophore production.

KEYWORDS

serpentinization, extracellular electron transfer, alkaliphile, genome, siderophore, alkali-tolerant, facultative anaerobe

Introduction

Serpentinization is a geologic process involving the aqueous alteration of ultramafic rock, leading to the production of energy (e.g., hydrogen gas) and carbon (e.g., small organic molecules) sources for microbial life. However, ecosystems that host these reactions are highly alkaline and reducing, often with limited availability of terminal electron acceptors. These extreme geochemical conditions are challenging for microorganisms, but unique microbial communities have been discovered within them (Suzuki et al., 2013; Quéméneur et al., 2015; Twing et al., 2017; Trutschel et al., 2022). From an astrobiology perspective, serpentinite-hosted ecosystems are proposed to have supported the emergence and evolution of life, and could provide insight into potential life on other planetary bodies, including ocean worlds and Mars (NASEM, 2019). Moreover, terrestrial serpentinizing environments (i.e., ophiolites) provide more readily available access to subsurface fluids and their microbial communities, as compared to marine counterparts (e.g., Lost City). This access enables investigations into the biogeochemical processes and the microbial ecophysiology of these systems to further understand the limits of life on Earth and in a broader planetary context (Jones et al., 2018; Merino et al., 2019).

Although the geochemical underpinnings of the serpentinization reaction have been understood since the mid 1960's with Dr. Ivan Barnes' landmark publication (Barnes et al., 1967), the unique chemical and energetic constraints of the fluids within ophiolites present particular challenges in the cultivation and isolation of pure culture strains for formal laboratory investigations. Over the past decades, much knowledge has been gained through analysis of the geochemical composition and microbial diversity of these systems *in situ*; however, the limited number of isolated representatives available to study *in vitro* has stymied our understanding of the ecophysiological role of these organisms and the multifaceted adaptations required by life to survive and thrive in these hyperalkaline and extremely reducing environments (e.g., metabolic capabilities, ATP production, and iron and trace metal acquisition).

To date, the following microbes have been isolated for laboratory study from ophiolites: three strains of *Serpentinomonas* sp. from The Cedars (Suzuki et al., 2014; Bird et al., 2021), *Paenibacillus* sp. from The Cedars (Rowe et al., 2017), *Cellulomonas* sp. strain FA1 from The Cedars (Cohen et al., 2015; Kamennaya et al., 2020), *Phenylobacterium falsum* strain AC-49 from Cabeço de Vide (Tiago et al., 2005), *Methanobacterium* sp. strain NSHQ4 from Samail Ophiolite (Miller et al., 2018), and others from Cabeço de Vide (Tiago et al., 2004) and Zambales Ophiolite (Vallalar et al., 2019). Besides ophiolites, there are also microbes isolated from marine serpentinite-hosted ecosystems, such as *Alkalicella caledoniensis* (Quéméneur et al., 2021) and *Alkaliphilus* sp. (Postec et al., 2021).

In this study, we describe the preliminary physiological findings and in-depth genomic characterization of three isolates from The Cedars to commemorate the 55th anniversary of one of the first publications detailing serpentinization, published by Barnes et al. (1967). The Cedars is an active serpentinite-hosted ecosystem located in Northern California, which was first described by Drs. Barnes and James O'Neil (Barnes and O'Neil, 1969). Modern biogeochemical analysis and modeling of The Cedars spring system began in 2005, with initial biomass determinations (via filtration) for the various springs ranging from 10^2 to 10^3 cells/mL in the mixed fluid source springs and as low as 10 cells/mL in the deep serpentinization fluid system. Despite the extremely low biomass inherent to The Cedars' fluids, the results of the first *in situ* enrichment experiments yielded encouraging results (10^6–10^7 cells/cm^2) when glass slides were incubated in the springs for 3 weeks time (Morrill et al., 2013). That said, early attempts at cultivation and isolation of organisms for study in the laboratory proved unsuccessful, so focus turned towards identifying and describing the microbial community via 16S and 18S rRNA amplicon sequencing. This work (Suzuki et al., 2013) provided the first understanding of the diversity and composition of The Cedars microbial community, identified novel and uncultivated microorganisms, and provided evidence of both seasonal and spatial effects on the communities of the spring system.

Since then, hundreds-to-thousands of different cultivation conditions have been tested by several early career microbiologists, including undergraduate and graduate students and postdoctoral researchers in an effort to bring these elusive organisms into the laboratory. This initially led to the isolation and discovery of three species belonging to the novel genus *Serpentinomonas*, the dominant taxon in the mixed fluid springs (Suzuki et al., 2014). Members of the *Serpentinomonas* are hydrogen-utilizing obligate alkaliphiles, further characterized by Bird et al. (2021). Notably, *S. maccroryi* strain B1 holds the bacterial record for tolerating and growing at the highest pH (pH 12.5) (Merino et al., 2019).

Following the isolation of *Serpentinomonas* sp., a unique *in-situ* electrochemical enrichment approach led to the isolation of an alkali-tolerant microbe, *Paenibacillus* sp. Cedars, capable of extracellular electron transfer (EET) and reduction of magnetite (Rowe et al., 2017). However, as discussed by Rowe et al. (2017), other isolates were comparatively less robust than *Paenibacillus* sp. or exhibited loss of activity after several transfers, including one closely related to the *Alishewanella* lineage of the *Gammaproteobacteria*. Subsequent

isolation attempts led to the successful cultivation of *Alishewanella* sp. BS5-314 under alkaliphilic conditions, further described for the first time in this study. Multiple attempts have also targeted the cultivation of anaerobic alkaliphiles, and thus far, only one anaerobic alkaliphile from The Cedars is cultivable: *Cellulomonas* sp. strain FA1 (Cohen et al., 2015; Kamennaya et al., 2020). Another anaerobe remains difficult to grow but cultivable, *Anaerobacillus* sp. CMMVII, with the first in-depth genomic characterization and initial physiological description described in this study.

In celebration of the anniversary of Dr. Ivan Barnes' monumental work, we present our current progress, understanding and hypotheses into the nature and ecophysiology of three diverse isolates from The Cedars described above: *Paenibacillus* sp. Cedars ('Paeni-Cedars'), *Alishewanella* sp. BS5-314 ('Ali-BS5-314'), and *Anaerobacillus* sp. CMMVII ('Anaero-CMMVII'). Herein, we report on the growth conditions for Paeni-Cedars (ATCC BAA-3230) and Ali-BS5-314 (ATCC TSD-356). We then discuss the putative metabolic and energetic pathways present in the genomes of all three microbes. The isolation, description, and characterization of these isolates provides new insights into our understanding of the diversity of life in serpentinizing fluids, the adaptations of organisms to survive in high pH/extremely reducing environments, and ultimately, the possibilities of life beyond Earth on other planetary bodies where these geochemical reactions are thought to exist.

Experimental procedures

Isolation of the three microorganisms

Paeni-Cedars was enriched on a two-electrode *in-situ* electrochemical system incubated in a highly alkaline pool (pH ~ 11) called Mortar Bed Springs (previously named Campsite Spring; coordinates 38.6191396, −123.1330681) (Rowe et al., 2017). Afterwards, Paeni-Cedars was isolated in nutrient-rich mLA medium at pH 9, and the mineral- and electrode-reducing capabilities were evaluated by Rowe et al. (2017). In this study, Paeni-Cedars was cultivated in nutrient-rich (mLA) or minimal (CSM-A, Cedars Medium-A) media. mLA medium was previously described in Rowe et al. (2017). CSM-A medium contained 1× salts solution (100× consisted of 5 mM Na_2SO_4, 37.8 mM NH_4Cl, and 5 mM $MgCl_2$•$6H_2O$), 10 mM CAPS (pH 9), 0.1% yeast extract, and 2 mM $CaCO_3$. After autoclaving, filter-sterilized solutions were added to a final concentration of 0.086 mM K_2HPO_4 and 1× of vitamins and trace minerals previously described (Rowe et al., 2015). CSM-A was then dispensed to serum bottles to a liquid-to-gas ratio of 35:65 (liquid:gas phase). Each bottle was crimp sealed with rubber stoppers (Cat. No.: 309018, Misumi USA), and then sparged with N_2 gas for 5 min before overpressurizing with H_2 gas (~10 s).

Anaero-CMMVII was isolated from Grotto Pool Spring 1 (GPS1; coordinates 38.621133, −123.133567) water in CSM-L medium. CSM-L contained 1× salts solution (100× consisted of 5 mM Na_2SO_4, 37.8 mM NH_4Cl, and 5 mM $MgCl_2$•$6H_2O$), 5 mM CABS (pH 11.5), 7 mM NaCl, and 0.1% yeast extract. After autoclaving, filter-sterilized solutions were added to a final concentration of 5 mM $CaCl_2$, 0.3 mM sodium phosphate, 0.1× ATCC MD-TMS (trace mineral supplement), and 0.1× ATCC MD-VS (vitamin supplement). CSM-L was aseptically sparged with N_2 gas for at least 1 h and cultures were cultivated under anaerobic conditions (80/20% N_2/CO_2).

Ali-BS5-314 was enriched in laboratory microcosms containing 50:50 (v:v) CSM-N and Barnes Spring 5 (BS5; coordinates 38.621367, −123.133117) water (Morrill et al., 2013) with 90/10% N_2/Air. CSM-N medium contained 1× salts solution (100× consisted of 10 mM Na_2SO_4, 100 mM NH_4Cl, 55 mM $MgCl_2$•$6H_2O$, and 4.38 mM Na_2SiO_3•$5H_2O$), 10 mM CAPS (pH 11), 0.1% protease peptone, and 1.3 mM $CaCO_3$. After autoclaving, filter-sterilized solutions were added to a final concentration of 0.06 mM K_2HPO_4, 1× ATCC MD-TMS (trace mineral supplement), and 1× ATCC MD-VS (vitamin supplement). Enrichments were grown at 18–20°C without shaking. Within 2 weeks, several enrichments became cloudy, and 1% volume was transferred to fresh CSM-N. After three transfers, the enrichments were streaked onto R2A plates (pH 11) containing 3% gellan gum and colonies were picked for further isolation on R2A gellan gum plates, R2A liquid medium, and CSM-N liquid medium.

Physiological characterization

Physiological characterization of Ali-BS5-314 and Paeni-Cedars were conducted in 60 mL serum bottles (35:65 liquid:gas phase) crimped with rubber stoppers using CSM-N (Ali-BS5-314) and CSM-A (Paeni-Cedars) media. For physiological characterization, CSM-N medium gassing conditions were modified, similar to CSM-A medium, with the exception of overpressurizing with H_2/CO_2 (80/20%) gas. For Ali-BS5-314, air was then added to a final concentration of 10% as filter-sterilized air in serum bottles crimped with rubber stoppers. Prior to inoculation for physiological studies, cultures of each isolate from a glycerol stock were incubated at 30°C in nutrient-rich media (R2A for Ali-BS5-314; mLA for Paeni-Cedars) for 24 h. Subsequently, 0.1% of the culture was transferred to fresh nutrient-rich media and incubated at 30°C for 24 h. The cells were then washed three times with the respective minimal media and inoculated at ~10^6 cells/ml. The range and optimum temperature and pH growth conditions were examined by incubating cultures from 10 to 50°C (10°C increments) and from pH 7–12 (pH 1 increments). At select timepoints, cell counts were performed by filtering fixed cells (1% formalin) stained with SYBR green through a 0.2 µm filter. Cells were lightly sonicated for 45 s to ensure even distribution due to cells that clump to carbonate precipitates. A fluorescence microscope was used for cell counting on a 10 × 10 grid and counts were conducted for 10 discrete fields of view.

The range and optimum growth on salts (NaCl, $CaCl_2$, $MgCl_2$) and electron acceptors (fumarate, thiosulfate, sulfate, and nitrate) were determined by growth on minimal media (CSM-N for Ali-BS5-314; CSM-A for Paeni-Cedars) at optimum temperature and pH conditions. The optimum conditions for Ali-BS5-314 were determined as pH 11 and 30°C, and for Paeni-Cedars, the optimum conditions were pH 9 and 30°C. The concentrations tested for NaCl were 0, 1, 3, 5, 10, and 15%; and for $CaCl_2$ and $MgCl_2$ were 0, 0.1, 0.5, 1, 5, 10, 15, and 20 mM. The electron acceptors were tested in the respective anoxic minimal medium.

Catalase and oxidase activities were determined using 3% (v/v) hydrogen peroxide and Kovacs' reagent (Kovacs, 1956), respectively. Antibiotic susceptibility was tested using antibiotic disk diffusion assays on the respective nutrient-rich medium with 3% gellan gum at

30°C. After 48 h, the zone of inhibition was recorded as no inhibition (−) or zone of inhibition diameter < 3 cm (+), between 3–5 cm (++), >5 cm (+++), or unclear (+/−). Discs with no antibiotics were used as controls and the assay replicated two times. The following antibiotics were tested: kanamycin (50 mg/ml), gentamycin (20 mg/ml), ampicillin (1 mg/ml), rifampicin (25 mg/ml), chloramphenicol (29 mg/ml), bacitracin (20 mg/ml), neomycin sulfate (10 mg/ml), and penicillin (50 mg/ml). Gram-staining was performed with Crystal Violet stain (30 s), Gram's iodine (30 s), 95% ethanol (5–10 s) and safranin counterstain (30 s). Motility was assessed using swarm plates comprised of nutrient-rich media with either 0.3% gellan gum (to assess swimming behavior) or 0.5% gellan gum (to assess swarming behavior). Cultures were first grown in nutrient-rich media at 30°C overnight, and subsequently, 100 µl aliquot was added to the swarm plates. Plates were incubated at 30°C and checked 24 h later.

The capability for iron(III) reduction from minerals was examined for Paeni-Cedars. Minerals tested include magnetite, serpentinite, olivine, 2-line ferrihydrite, goethite, hematite, and chromite. Cultures were incubated under anaerobic conditions at 30°C and pH 9 in CSM-A medium supplemented with 1 mM glucose as the electron donor. After 160 h (magnetite) or 188 h (other minerals), samples were filtered through a 0.2 µm filter and centrifuged at 18,894 g for 2 min before conducting ferrozine analyses (Stookey, 1970; McBeth et al., 2011, 2013) to determine the Fe(II) concentrations.

DNA extraction and sequencing

DNA from Paeni-Cedars was extracted from a fresh cell pellet using Nucleobond AXG Column Kit (TakaraBio). The genome was sequenced by Takara Bio Inc. (Kusatsu, Japan) in a single-molecule real-time (SMRT) cell on a PacBio RSII sequencer (Pacific Bioscience, CA, USA) using a 15 kb insert library. This sequencing method consists of proprietary, long read, real-time detection sequencing based on terminal fluorophore attached nucleotides and zero-mode optical wave-guide detection system. A total of 90,234 inserts with a mean size of 16,260 bp (N50 22,314) were fully sequenced and assembled using the HGAP (Analysis Hierarchical Genome Assembly Process) protocol implemented in SMRT analysis (version 2.3, Pacific Bioscience). A total of three circular contigs were assembled: a 6,414,884 bp genomic contig with 181.03× mean coverage and two plasmids: 248,871 bp long with 208.87× mean coverage and 56,646 bp long with 113.26× mean coverage.

DNA from Anaero-CMMVII and Ali-BS5-314 were extracted from a fresh cell pellet using Qiagen AllPrep DNA/RNA Mini Kit. The genome was sequenced by MRDNA (TX, USA), using SMRT PacBio Sequel (Pacific Bioscience, CA, USA) with a 15 kb insert library. *De Novo* assembly of reads with mean size of 9.4 kb (Anaero-CMMVII) and 15.2 kb (Ali-BS5-314) was accomplished using HGAP implemented in SMRT analysis. For Anaero-CMMVII, a total of 24 polished reads were assembled (4,889,950 bp genome size) with 46× mean coverage using Falcon Assembler paired with Arrow polishing algorithm, and 80.15% of the bases were successfully realigned to the draft assembly with a mean concordance of 81.88%. For Ali-BS5-314, a total of 10 polished reads were assembled (3,747,989 bp genome size) with 2,234× mean coverage using Falcon Assembler paired with Arrow polishing algorithm, and 89.8% of the bases were successfully realigned to the draft assembly with a mean concordance of 89.7%.

Gene annotation

The PacBio assembled genomes were analyzed using Anvi'o version 4 (Eren et al., 2015), which determined the genome completeness and identified gene calls, single copy genes, and 16S rRNA sequences. We used tRNAscan-SE to identify tRNA sequences (Lowe and Eddy, 1997). Plasmids were checked by Platon (Schwengers et al., 2020), which uses PlasmidFinder (Carattoli et al., 2014), MOBscan (Garcillán-Barcia et al., 2020), and MOB-suite (Robertson and Nash, 2018) as dependencies. The ANI/AAI-matrices were calculated using http://enve-omics.ce.gatech.edu/g-matrix/index. Digital DNA–DNA hybridization (dDDH) was calculated using the Type (Strain) Genome Server (TYGS) (Meier-Kolthoff and Göker, 2019; Meier-Kolthoff et al., 2022). The 16S rRNA gene sequences were assessed against the SILVA database release 138 (Quast et al., 2013) using the SINA aligner and SINA "search and classify" ACT (Alignment, Classification and Tree) Service (Pruesse et al., 2012). Gene calls were annotated using several tools: InterProScan v5.28–67.0 with databases TIGRFAM, Pfam, and CDD (Jones et al., 2014; Finn et al., 2017), MAPLE v2.3.0 (Arai et al., 2018), AntiSMASH v4.1.0 (Blin et al., 2017), FeGenie v1.0 (Garber et al., 2020), PHASTER (Arndt et al., 2016), dbCAN (Yin et al., 2012; Zhang et al., 2018), SignalP v6 (Teufel et al., 2022), and HydDB (Søndergaard et al., 2016). AntiSMASH was used to identify secondary metabolites and the following options were used: --clusterblast --subclusterblast --knownclusterblast --smcogs --inclusive --borderpredict --full-hmmer --asf --tta. FeGenie identified heme-binding motifs and all iron-related genes, including those involved in iron acquisition, iron storage, iron gene regulation, and iron redox cycling. Localization prediction was done using PSORTb (Yu et al., 2010).

Phylogenetic tree

GTDB-Tk v1.1.0 (Chaumeil et al., 2020) on KBase (Arkin et al., 2018) was used to identify the taxonomic affiliation of all three isolates. Subsequently, GToTree v1.5.51 (Lee, 2019) was used to generate the phylogenetic tree by first identifying representative genomes for each genome from GTDB v202 with gtt-get-accessions-from-GTDB (Supplementary Tables S1, S2). Three phylogenetic trees were generated and displayed using Archaeopteryx (Han and Zmasek, 2009) and The Interactive Tree of Life v6 (Letunic and Bork, 2007, 2021): (1) a tree for Ali-BS5-314 using the default GToTree Gammaproteobacteria HMMs, and (2) a tree for Paeni-Cedars and Anaero-CMMVII using the default GToTree Firmicutes HMMs. GToTree relies on the following dependencies: HMMER3 v.3.3.2 (Eddy, 2011), Muscle v3.8.1551 (Edgar, 2004), TrimAl v1.4.rev15 (Capella-Gutierrez et al., 2009), Prodigal v2.6.3 (Hyatt et al., 2010), GTDB v202 (Parks et al., 2020), FastTree 2 v2.1.10 (Price et al., 2010), and GNU Parallel v20210422 (Tange, 2018). CIPRES Science Gateway (Miller et al., 2010) with parameters GTRGAMMA and autoMRE was also used to construct phylogenetic trees.

Isolate availability

Ali-BS5-314 (ATCC TSD-356) and Paeni-Cedars (ATCC BAA-3230) are deposited at ATCC. Anaero-CMMVII is available as an anaerobic glycerol stock from the Lawrence Livermore National Laboratory (LLNL) microbial culture collection.

Results and discussion

Potential abundance and relevance of the isolates in The Cedars

These three isolates are likely part of the rare biosphere within the microbial communities of The Cedars' fluids. Alignment of genomic reads from The Cedars metagenomes (Suzuki et al., 2017) against each isolate genome resulted in overall alignment rate percentages of: 0.07–0.11% for Paeni-Cedars, 0.08–0.11% for Anaero-CMMVII, and 0.04–0.22% for Ali-BS5-314. The rarity of these isolates may be an artifact of the sampling capabilities; for example, at The Cedars, it is not feasible to obtain sediment cores or to directly sample deeper fluids. Nevertheless, rare species can have a disproportionate impact on the biogeochemical cycles ongoing within various ecosystems, as reviewed by Jousset et al. (2017), and necessitates the need to enrich and isolate novel species for physiological and genomic characterization.

The isolation and characterization of microorganisms from terrestrial serpentinite-hosted ecosystems can reveal important ecophysiological functions and adaptations that are missed by metagenomic studies (e.g., Suzuki et al., 2017). For example, the isolation of Paeni-Cedars revealed that mineral reduction can occur in The Cedars' springs, potentially serving as an important terminal electron accepting process in the absence of oxygen (Rowe et al., 2017). EET-capable microorganisms, such as Paeni-Cedars, were initially not identified in metagenomic surveys of The Cedars (Rowe et al., 2017; Suzuki et al., 2017), likely because of low relative read abundances or unknown EET mechanisms. As discussed below, the putative EET mechanism used by Paeni-Cedars is actually related to that observed in *Listeria monocytogenes* 10403S (Light et al., 2018). There may be other potential unknown EET pathways within The Cedars and other serpentinite-hosted ecosystems; Paeni-Cedars is only one isolate among the EET-active community enriched by Rowe et al. (2017). The isolate Anaero-CMMVII may also be able to reduce minerals but further studies are needed to confirm this activity.

Rowe et al. (2017) also attempted to isolate an *Alishewanella* strain that seemed to have manganese reduction capabilities until the fifth round of transfer. However, the loss of growth and mineral reduction activity suggests the original culture may have included other microbial members responsible for manganese reduction. The isolation of Ali-BS5-314 (this study) further confirms that the *Alishewanella* species present in the spring waters of The Cedars cannot reduce minerals; however, this does not preclude the potential presence of other related *Alishewanella* strains with mineral reduction activity. Instead, the novelty of Ali-BS5-314, as discussed below, is its ability to grow at hyperalkaline pH > 10 and the potential for degrading aromatic compounds. Similarly, Anaero-CMMVII was observed to grow at pH > 9. The notable features of Anaero-CMMVII is that the isolate is likely an oxygen-tolerating anaerobe with the putative capability for hydrogenotrophic respiration. Further description of these three isolates is described below.

Taxonomic classification of the isolates

GTDB-Tk, ANI, AAI, and dDDH were used to confirm the taxonomic classification of the isolates. Alignment of the 16S rRNA gene sequences against related species resulted in inconclusive identification, with only the genus- or family-level association for Paeni-Cedars (>98% identity) and Ali-BS5-314 (>98% identity) (Supplementary Table S3). For Anaero-CMMVII, the 16S rRNA gene sequences are >95% related to *A. isosaccharinicus*; however, this is based on the GTDB database (Supplementary Table S3), and further analysis using GTDB-Tk identified that Anaero-CMMVII is a novel species, as described below.

Based on genome analysis, Paeni-Cedars and Ali-BS5-314 are related to other species while Anaero-CMMVII represents a new species (Supplementary Tables S4–S6 and Figure 1). GTDB-Tk identified that Paeni-Cedars is closely related to *P. glucanolyticus*, with closest placed alignment ANI of 98.89% and alignment fraction (AF) of 0.97 (Supplementary Table S4). Paeni-Cedars also shares dDDH >82.9% (Supplementary Table S5) and ANI and AAI of about 98% (Supplementary Table S6) with *P. glucanolyticus*.

Ali-BS5-314 is likely related to *A. aestuarii*, with GTDB-Tk ANI 95.99% and AF 0.85 (Supplementary Table S4). However, Ali-BS5-314 may represent a new species because of dDDH (54.2–69.3%) (Supplementary Table S5), ANI (>95%), AAI (>94%) (Supplementary Table S6) and phylogenetic placement (Figure 1A). The species boundary threshold is suggested to be 95% ANI, 90% AAI, and 70% dDDH (Konstantinidis and Tiedje, 2005; Richter and Rosselló-Móra, 2009). Further physiological characterization studies are needed to confirm whether Ali-BS5-314 is a new species.

Anaero-CMMVII is a new species according to all metrics used in this study. The closest placement reference for Anaero-CMMVII is *A. isosaccharinicus*, with GTDB-Tk ANI 80.82% and AF 0.42 (Supplementary Table S4). GTDB-Tk threshold for clustering is ANI >97% and AF 0.65. Furthermore, pairwise dDDH of Anaero-CMMVII against possible related species are <19.4% (Supplementary Table S5), and ANI ranges from about 76 to 81% and AAI ranges from 71 to 79% (Supplementary Table S6).

General physiological description of the isolates

The physiological characteristics of Paeni-Cedars, Ali-BS5-314, and Anaero-CMMVII are summarized in Table 1. Unfortunately, because of difficulties in consistent cultivation of Anaero-CMMVII (Supplementary Figure S1), the physiological investigations could not be completed. However, growth was observed between pH 9–12 and with the addition of 0.01–1% yeast extract. Initial tests also indicated that Anaero-CMMVII reduces Fe(III)-citrate and magnetite (data not shown).

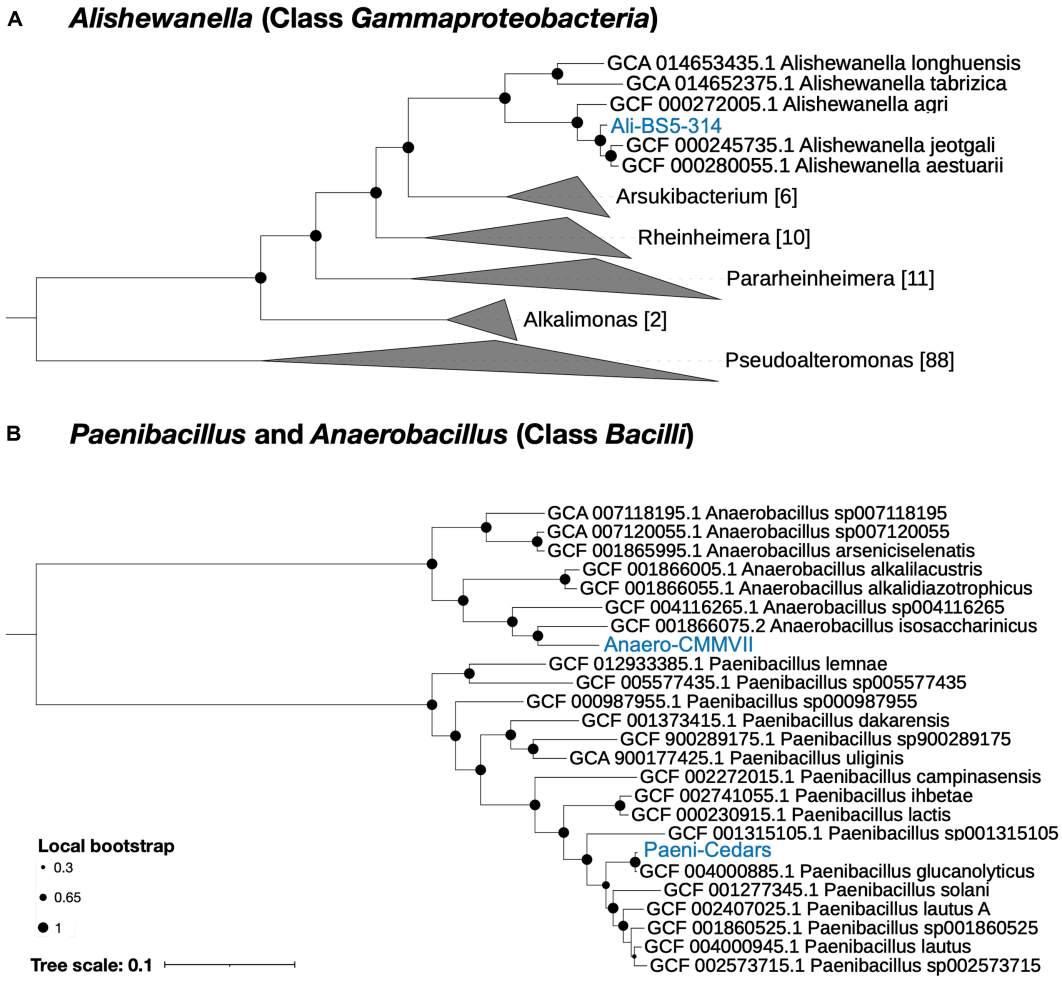

FIGURE 1
Phylogenetic tree for the three isolates. **(A)** Ali-BS5-314 and **(B)** Anaero-CMMVII and Paeni-Cedars. Representative genomes used to construct the phylogenetic trees are listed in Supplementary Tables S1, S2 and were retrieved via GToTree (Lee, 2019). FastTree (Price et al., 2010) via GToTree was used to generate the phylogenetic trees and viewed using the Interactive Tree of Life (iToL) v6 (Letunic and Bork, 2007). Local bootstrap values are depicted as circles at each node. Brackets indicate the number of genomes within a clade.

Ali-BS5-314 is a Gram-negative, rod-shaped (0.8–2 μm length by 0.4 μm diameter), mesophilic, facultative anaerobic alkaliphile (Figures 2A,B), with a cellular fatty acid composition mostly composed of $C_{16:0}$, $C_{16:1}$ ω7c, and $C_{18:1}$ ω7c (Table 2). Growth was observed between pH 10–12 (optimum pH 11) and temperatures 10–40°C (minimum temperature tested was 10°C; optimum between 20 and 30°C) (Figure 3 and Supplementary Figures S2, S3). No growth was observed below pH 9, above pH 12.1, or above 50°C. The addition of 10 mM nitrate to the original medium without oxygen supported growth, suggesting that nitrate can be used as a terminal electron acceptor under anaerobic conditions. Ali-BS5-314 also displays low salt tolerance, with ≥1% NaCl impacting growth and no growth was observed with ≥10% NaCl added (Figure 4A). More growth was also observed with less $CaCl_2$ added (0–0.5 mM $CaCl_2$; original media contains 1 mM) (Figure 4A) and grew optimally between 0 and 1 mM $MgCl_2$ (no growth observed ≥5 mM $MgCl_2$) (Figure 4A).

Paeni-Cedars is a Gram-positive, rod-shaped (2–6 μm length by 0.5 μm diameter), mesophilic facultative anaerobe (Figures 2C,D), with a cellular fatty acid composition mostly composed of anteiso-$C_{15:0}$ and $C_{16:0}$ (Table 2). Growth was observed between pH 7–10 (minimum pH tested was pH 7; optimum between pH 7–9) and temperatures 20–40°C (optimum between 20–30°C) (Figure 3). No growth was observed above pH 10, below 10°C, or above 50°C. Although the pH optimum is between 7 and 9 (Figure 3 and Supplementary Figures S2, S3), Rowe et al. (2017) demonstrated that pH 9 was optimal for mineral reduction and electrochemical activity. The addition of fumarate, thiosulfate, sulfate, or nitrate did not support growth under anaerobic conditions (Figure 4B). Similar to Ali-BS5-314, Paeni-Cedars displays relatively low salt tolerance and no growth was observed with ≥5% NaCl added (Figure 4B). In contrast to BS5-314, the addition of 5–20 mM $CaCl_2$ (original media contains 1 mM $CaCl_2$) enhanced growth of Paeni-Cedars (Figure 4B). However, increases in $MgCl_2$ impacted its growth and Paeni-Cedars grew optimally with 0 mM $MgCl_2$ (original media contains 0.1 mM $MgCl_2$) (Figure 4B).

Paeni-Cedars was previously reported to reduce magnetite with glucose as the electron donor (Rowe et al., 2017). We further examined its capability to reduce other Fe(III) minerals, such as 2-line ferrihydrite and Fe(III) minerals found at The Cedars and other serpentinite-hosted systems (e.g., serpentinite, olivine, chromite, hematite, and goethite).

TABLE 1 Physiological characteristics of Paeni-Cedars and Ali-BS5-314 compared to the closest relatives.

	1	2	3	4	5	6	7
Gram stain	+	+	−	−	−	N/A	+
Cell shape[a]	Rod (2–6 by 0.5)	Rod (>3 by <0.9)	Rod (0.8–2 by 0.4)	Rod (2–6 by 1)	Rod (N/A)	Rod (N/A)	Rod (2–5 by 0.5–0.7)
Motility	+[b]	+	+[b]	+	+	N/A	+
Temperature range (°C) (optimum)	20–40 (20–30)	15–37 (30)	<10[c]–40 (20–30)	4–40 (37)	18–44 (37)	Room Temp. (N/A)	10–40 (30)
pH range (optimum)	<7[d] – 10 (7–9)	6.5–11 (7)	10–12 (11)	6.5–9.5 (6.5–9)	N/A	9[d]–12 (N/A)	8.5–11 (9.8–10)
NaCl range (%) (optimum)	0–3	0–9 (0)	0–5	1–2 (1)	0–5	N/A	0–6 (2)
$CaCl_2$ range (mM)	0.1 – 20[e]	N/A	0–15	N/A	N/A	N/A	N/A
$MgCl_2$ range (mM)	0–1	N/A	0–1	N/A	N/A	N/A	N/A
Sensitivity to antibiotics[f]		N/A		N/A	N/A	N/A	N/A
Kanamycin	++		+++				
Gentamycin	++		++				
Ampicillin	−		+				
Tetracycline	++		++				
Rifampicin	+		−				
Chloramphenicol	+		++				
Bacitracin	+		+++				
Neomycin Sulfate	++		+/−				
Penicillin	+		+				
Catalase Test	+	N/A	+	+	+	N/A	+
Oxidase Test	+	N/A	+	+	+	N/A	+

(1) Paeni-Cedars, (2) *P. glucanolyticus* strain DSM 5162^T (data from Alexander and Priest, 1989; Shida et al., 1997; Priest, 2009; Liu et al., 2015), (3) Ali-BS5-314, (4) *A. jeotgali* strain MS1^T (=KCTC 22429^T = JCM 15561^T; data from Kim et al., 2009), (5) *A. aestuarii* strain B11^T (=KCTC 22051^T = DSM 19476^T; data from Roh et al., 2009), (6) Anaero-CMMVII, and *A. isosaccharinicus* strain NB2006^T (=DSM 100644^T = LMG 30032^T; data from Bassil and Lloyd, 2019). [a]Length µm by diameter µm. [b]Motility was assessed using swarm plates. [c]Lowest temperature tested 10°C. [d]Lowest pH tested pH 7 for Paeni-Cedars; Growth observed between pH 9–12 for Anaero-CMMVII. [e]Highest $CaCl_2$ concentration tested 20 mM. [f]Zone of inhibition 0 cm (−), <3 cm (+), 3–5 cm (++), >5 cm (+++), or unclear zone of inhibition (+/−).

Iron reduction was observed for 2-line ferrihydrite > magnetite > serpentinite ~ chromite ~ hematite (Table 3).

Both Ali-BS5-314 and Paeni-Cedars are oxidase and catalase positive. The isolates also displayed similar resistance to antibiotics, with the exception of ampicillin, rifampicin, bacitracin, and neomycin sulfate.

The physiological differences for Ali-BS5-314 and Paeni-Cedars suggests these two isolates may persist in separate niches within The Cedars springs fluids. Ali-BS5-314 seems to favor growth at conditions similar to the chemical composition of the fluids (pH 11.5–11.9, Ca^{2+} 0.94–1.3 mM, and Mg^{2+} 0.004–0.036 mM) (Morrill et al., 2013). In contrast, Paeni-Cedars grows pH < 10 and at much higher $CaCl_2$ concentrations. Along with the capability for mineral reduction, Paeni-Cedars may favor growth on or nearby solid substrates, including iron oxides and calcite precipitates. Rowe et al. (2017) also observed that EET activity was correlated with a drop in pH and that the optimal pH for mineral reduction was pH 9. One hypothesis suggested by Rowe et al. (2017) is that calcite precipitate microenvironments may accumulate protons and have lower pH, enabling Paeni-Cedars to persist. In contrast to Ali-BS5-314 and Paeni-Cedars, the isolate Anaero-CMMVII is likely found in anaerobic niches or deeper spring fluids that experience periodic exposure to oxygen.

Genome analyses: overview

The putative genome features for all three isolates are summarized in Table 4 and conceptual models are depicted in Figures 5–7. All gene annotations, including KEGG, InterProScan, and FeGenie, can be found in Supplementary Tables S8–S13.

Genome analyses: energy conservation and extracellular electron transport

Based on physiological observations and genome analyses, Ali-BS5-314 and Paeni-Cedars are facultative anaerobes, and Anaero-CMMVII is a probable oxygen-tolerant anaerobe. The respiratory electron transport chain (ETC) of all three isolates contains succinate dehydrogenase (*sdhABC* or *sdhABCD*), cytochrome bc_1 complex (*cytbc*$_1$), cytochrome c oxidase (*ccO*), and cytochrome *bd* (*cydAB* or *cydABCD*). All three microbes also use an H^+-coupled F-type ATPase for oxidative phosphorylation. Alignment of the *c*-subunit of the ATPase against other H^+ or Na^+ coupled F-type ATPases confirmed that the genomes of all three isolates encode for an H^+ coupled F-type ATPase (Supplementary Figure S4; Hicks et al., 2010). Besides these

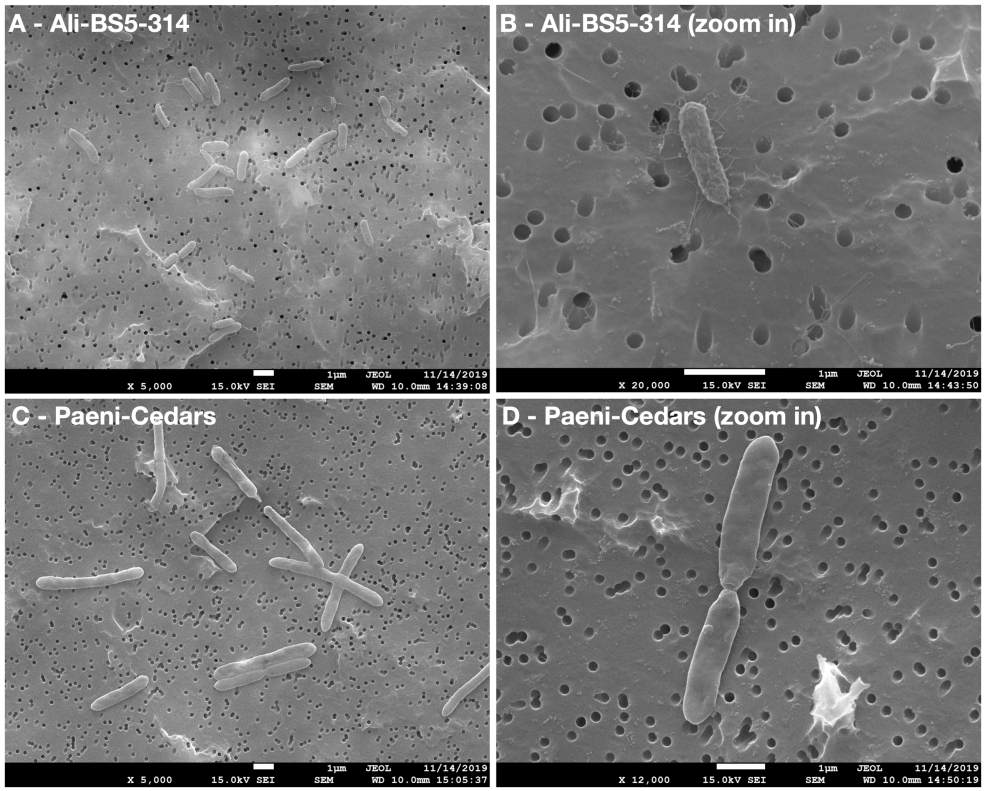

FIGURE 2
Scanning electron microscopy (SEM) images of Ali-BS5-314 and Paeni-Cedars. Panels **(A,C)** are zoomed out images with scale bar 1μm. Panels **(B,D)** are zoomed in images with scale bar 1μm.

similarities, the three isolates have differences in their energy conservation mechanisms.

The ETC of Ali-BS5-314 includes both nitrate reductase (NarGHJI) or fumarate reductase (FrdABCD). However, our physiological studies suggest that only nitrate can be used as a terminal electron acceptor during anaerobic respiration (Figure 4). This demonstrates that Ali-BS5-314 has flexibility for anaerobic or aerobic respiration, which may be required to persist in The Cedars. Dissolved oxygen is likely present in surface springs and shallow groundwater of The Cedars (Morrill et al., 2013), but there may be spatial and temporal changes resulting in anaerobic conditions or niches, requiring Ali-BS5-314 to rely on nitrate reduction in the environment. However, nitrate concentrations in The Cedars' springs fluids were low μM levels (Cook et al., 2021), potentially immediately utilized by the microbial community. The genome of Ali-BS5-314 lacks NADH dehydrogenase, indicating that other pathways are used for NADH oxidation, such as glutamate synthesis (van Heeswijk et al., 2013) or gluconeogenesis. NADH regeneration pathways include glycolysis and the action of the Rnf complex (*Rhodobacter* nitrogen fixation electron transport complex [*rnfABCDEG*]). The Rnf complex also results in the electrogenic pumping of Na^+/H^+ ions extracellularly, inducing an ion gradient that can be used for Na^+/H^+-dependent symporters and by the F-type ATPase. This complex may be important for Ali-BS5-314 to grow under hyperalkaline conditions, further discussed in the section "*Genome Analysis: adaptations to alkaliphily, osmotic stress, and radicals*".

The ETC of Anaero-CMMVII has NADH dehydrogenase (*nuoABCDHIJKLMN*), but the gene operon lacks the subunits *nuoEFG*. These subunits are known to contain the domain involved in NADH binding and oxidation (Sazanov, 2007). Instead, NADH dehydrogenase likely utilizes alternative electron donors, such as reduced ferredoxin. It is also unlikely that the *nuo* operon encodes for other closely related complexes, such as MBX (archaeal respiratory complex), FPO (methanogenic respiratory complex), and MBH ([NiFe] hydrogenase), as demonstrated by a maximum likelihood phylogenetic tree (Supplementary Figure S5) of the catalytic subunits in NUO, MBX, FPO, and MBH (Schut et al., 2016). Notably, the genome of Anaero-CMMVII does contain the genes *hyaABC*, which encode for group 1d [NiFe] hydrogenase (Peters et al., 2015). This suggests that energy conservation in Anaero-CMMVII likely involves hydrogenotrophic respiration by the action of the group 1d [NiFe] hydrogenase, HyaABC (Peters et al., 2015). The gene neighborhood of *hyaABC* includes nitrate reductase (*napGH-napABD-napG*), suggesting H_2 oxidation is coupled with the reduction of nitrate. Oxygen may also be used as an electron acceptor (Peters et al., 2015).

The ETC of Paeni-Cedars includes an additional terminal menaquinol oxidase, encoded by *qoxABCD*. This likely functions with the other terminal oxidases in aerobic respiration (Götz and Mayer, 2013). As mentioned above, Paeni-Cedars is capable of EET and reduction of magnetite (Rowe et al., 2017) and other iron minerals (Table 3). We inspected the genome of Paeni-Cedars for the presence of genetic markers gleaned from hypothesized EET mechanisms for Gram-positive and Gram-negative bacteria. We confirmed the presence of genes involved in EET mechanisms for Gram-positive bacteria only. Paeni-Cedars encodes an operon implicated in

TABLE 2 Cellular fatty acid composition (FA; %) of Paeni-Cedars and Ali-BS5-314.

	Paeni-Cedars	Ali-BS5-314
$C_{11:0}$ 3OH	n.d.	<1
$C_{12:0}$	1.48	1.62
$C_{12:0}$ 3OH	n.d.	5.26
$C_{14:0}$	5.35	2.11
$C_{14:0}$ 3OH	n.d.	5.11
iso-$C_{14:0}$	3.27	<1
$C_{15:0}$	<1	1.05
iso-$C_{15:0}$	5.26	n.d.
iso-$C_{15:0}$ 3OH	n.d.	<1
anteiso-$C_{15:0}$	**35.01**	<1
$C_{15:1}$ ω8c	n.d.	<1
$C_{16:0}$	**33.79**	**20.28**
iso-$C_{16:0}$	6.00	<1
$C_{16:1}$ ω7c	<1	**23.35**
$C_{16:1}$ ω11c	1.14	n.d.
$C_{17:0}$	n.d.	4.35
iso-$C_{17:0}$	1.20	**<1**
anteiso-$C_{17:0}$	2.34	<1
$C_{17:1}$ ω6c	n.d.	<1
$C_{17:1}$ ω8c	n.d.	8.94
$C_{18:0}$	3.22	1.91
iso-$C_{18:0}$	n.d.	<1
$C_{18:1}$ ω7c	n.d.	**17.27**
$C_{18:1}$ ω9c	<1	<1

FAs that represent ≥1% of the total FAs of at least one strain are shown. Bold values indicate major FA that are ≥10%. n.d., not detected or not reported.

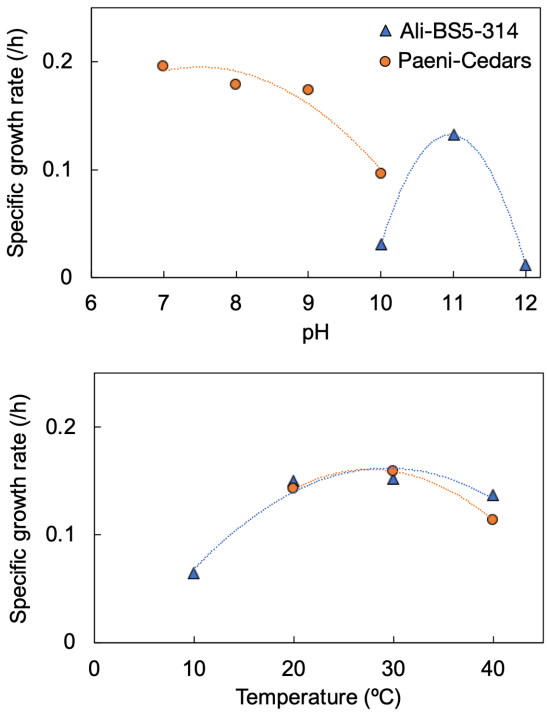

FIGURE 3
Specific growth rates of Ali-BS5-314 and Paeni-Cedars for pH **(top)** and temperature **(bottom)**. Supplementary Figures S2, S3 depict the growth curves.

flavin-mediated iron reduction in *Listeria monocytogenes* 10403S (Light et al., 2018). In *L. monocytogenes*, this operon consists of eight genes, including flavin transporters (*fmnB, fmnA*), cell surface electron transport proteins (*eetAB*, *pplA*), demethylmenaquinone synthases (*dmkA, dmkB*), and type II NADH dehydrogenases (*ndh2*). Homologs (*e*-value<1E-15) to seven of these genes are present in a single operon in Paeni-Cedars, while the eighth, one of the demethylmenaquinone (DMK) synthases (*dmkA*), is present elsewhere in the genome. The Paeni-Cedars EET operon also contains the genes for FAD transport via the ECF (energy-coupling factor) system, with the genes *ecfA1-ecfA2-ecfT* (*ecfT* is identified as *fmnA* in the *L. monocytogenes* EET operon) and an unknown gene for riboflavin transport (*ribU*) (Gutiérrez-Preciado et al., 2015). FAD transport is needed for FmnB to catalyze FMNylation of PplA, enabling electron transfer from DMK to FMN groups on PplA or free flavin shuttles for iron reduction (Light et al., 2018).

Genome analyses: carbon metabolism

All three microbes are capable of glycolysis and gluconeogenesis; and converting CO_2 to HCO_3 (or the reversible reaction) by the action of carbonic anhydrase. Carbonic anhydrase may be a necessary enzyme for microorganisms in The Cedars' springs given the high pH conditions and the presence of calcite precipitates. For glycolysis and gluconeogenesis, the Anaero-CMMVII genome lacks glucokinase (*glk*), which is involved in the phosphorylation of glucose to glucose-6-phosphate. Instead, Anaero-CMMVII likely relies on the phospho-enolpyruvate(PEP):carbohydrate phosphotransferase system (PTS) to catalyze the transport and phosphorylation of sugars (Deutscher et al., 2006).

Both Anaero-CMMVII and Paeni-Cedars are capable of transporting various sugars and complex carbohydrates, including the ATP-binding cassette (ABC) transporters GanOPQ-MsmX (galactose oligomer/maltooligosaccharide), MsmEFGK (raffinose/stachyose/melibiose), and LplABC (breakdown of cellulose, hemicellulose and transport of aldouronate). Notably, the Paeni-Cedars genome also has genes that encode the transport of other mono- and oligosaccharides, including CebEFG-MsiK (cellobiose), araNPQX (arabinooligosaccharide), and RhaSPQT (rhamnose), and contains 259 genes identified as carbohydrate-active enzymes (CAZyme), which breakdown complex carbohydrates. These CAZymes include 152 glycoside hydrolases (26 with signal peptides), 47 glycosyltransferases (0 with signal peptides), 7 polysaccharide lyases (3 with signal peptides), 34 carbohydrate esterases (4 with signal peptides), and 13 non-catalytic carbohydrate-binding modules (5 with signal peptides) (Wardman et al., 2022). This suggests Paeni-Cedars can secrete enzymes that degrade complex carbohydrates, similar to its closest relative *P. glucanolyticus* which can breakdown lignocellulose and beta-glucans (Alexander and Priest, 1989; Mathews et al., 2013, 2016).

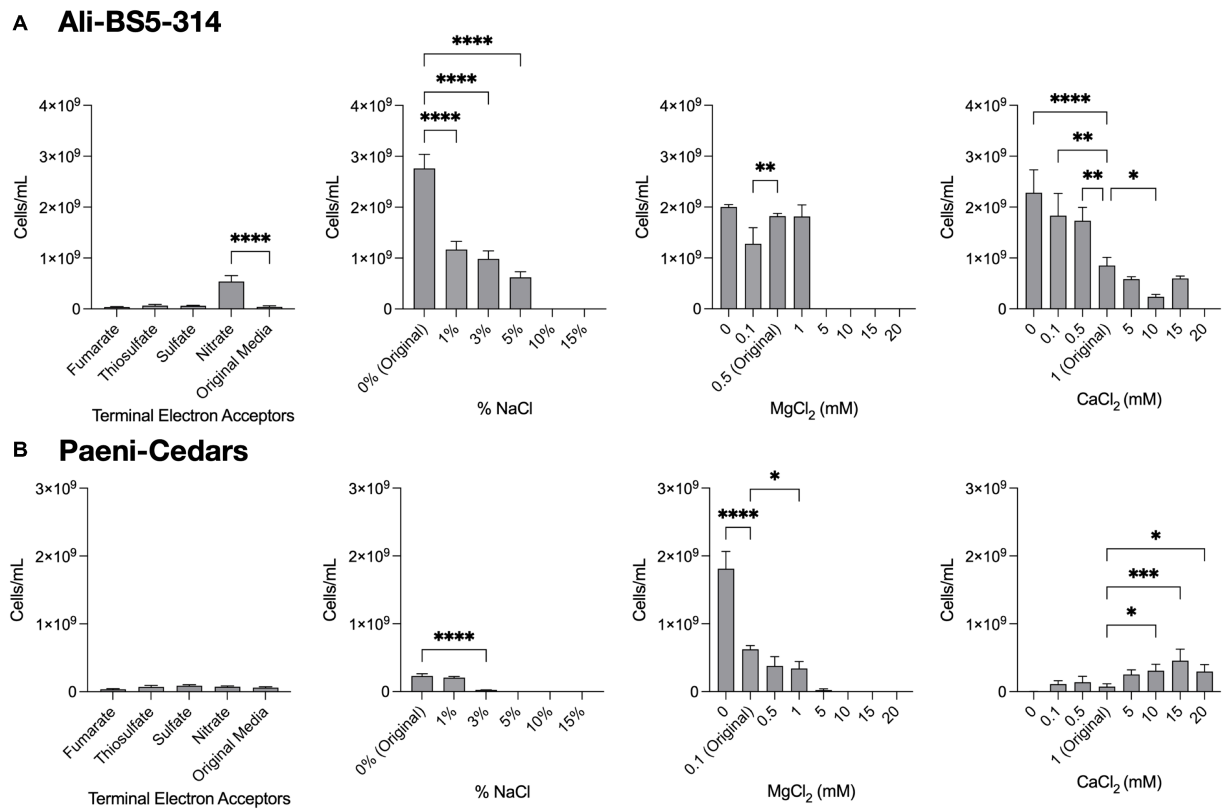

FIGURE 4
Growth under a range of conditions. The growth of **(A)** Ali-BS5-314 and **(B)** Paeni-Cedars was evaluated by varying the terminal electron acceptor (TEA) or by changing the concentration of NaCl (0–15%), $MgCl_2$ (0–20mM), or $CaCl_2$ (0–20mM). "Original" represents the original concentrations used to grow the isolate. When testing TEAs, both microbes were grown under anaerobic conditions. Asterisks (*) represent *p*-value of one-way ANOVA test comparing cell concentrations under different conditions against the original media: *p <0.05, **p <0.01, ***p <0.001, ****p <0.0001.

TABLE 3 Iron reduction by Paeni-Cedars.

Mineral	Fe(II) concentrations
Magnetite	++
Serpentinite	+
Chromite	+
Hematite	+
2-Line ferrihydrite	+++
Goethite	–
Olivine	–

Fe(II) was measured using the ferrozine assay at time 0 and after 160 h (magnetite) or 188 h (other minerals) of incubation. Cultures were incubated under anaerobic conditions at 30°C and pH 9 in CSM-A medium supplemented with 1 mM glucose as the electron donor. (–) indicates 0 mM Fe(II) was detected, (+) indicates <0.05 mM Fe(II) was detected, (++) indicates between 0.05–0.15 mM Fe(II) was detected, and (+++) indicates >0.15 mM Fe(II) was detected.

In contrast to the other two isolates, the Ali-BS5-314 genome likely encodes only two sugar-associated ABC transporters: AfuABC for the uptake of hexose/heptose-phosphate metabolites (e.g., glucose-6-phosphate) (Sit et al., 2015) and BenEK for the uptake of benzoate-like compounds (Patrauchan et al., 2005). Ali-BS5-314 may also catabolize benzoate-like compounds. In our growth studies, protease peptone was provided as a nutrient source, and it is likely that similar aromatic compounds are in The Cedars BS5 spring fluids, based on the observation of various aromatics in other marine (Pasini et al., 2013; Plümper et al., 2017) and terrestrial (Seyler et al., 2022) serpentinite-hosted ecosystems. After uptake by the transporter BenEK, these benzoate-like compounds can be degraded to catechol-like metabolites by the action of dioxygenase (BenABC) and dihydrodiol dehydrogenase (BenD) (Patrauchan et al., 2005). The gene neighborhood of the benzoate degradation pathway also includes genes (*catRBCA*) for catechol degradation by the 3-oxoadipate pathway (Harwood and Parales, 1996; Nojiri et al., 2002) and genes (*pcaIJFD*) for further degradation to acetyl-CoA by the protocatechuic acid degradation pathway (Clarkson et al., 2017).

Genome analyses: nitrogen metabolism

All three isolates have different nitrogen metabolisms. Ali-BS5-314 reduces nitrate and assimilates ammonia; Anaero-CMMVII is capable of dissimilatory nitrate reduction; and Paeni-Cedars uses the glycine cleavage and urea degradation pathways. However, in the natural setting of The Cedars, the isolates would likely experience limited nitrate and ammonia availability, with spring concentrations between 1 and 2 μM (Cook et al., 2021).

TABLE 4 Genome features for Paeni-Cedars, Anaero-CMMVII, and Ali-BS5-314.

Feature	Paeni-Cedars	Anaero-CMMVII	Ali-BS5-314
NCBI BioProject accession no.	PRJNA383291	PRJNA647468	PRJNA647464
Genome size	6,414,884 bp	4,889,950 bp	3,747,989 bp
N50	22,314 bp[a]	409,225 bp	2,153,191 bp
No. of contigs	3	24	10
GC (%)	49.0	36.9	51.4
No. of plasmids	2	1	0
Total Predicted Genes	6,216	5138	3412
16S rRNA	8	13	5
23S rRNA	8	13	7
tRNA[b]	77	115	80
Bacterial single copy genes	138	147	139
Genome Completeness (%)	99.3	100.0	98.6
No. of prophage regions	6	4	3
% The Cedars metagenomes[b]	0.07–0.11	0.08–0.11	0.04–0.22

Genome sequencing was done by PacBio, and analysis was conducted via Anvi'o v4 (Eren et al., 2015). [a]Read length from PacBio. [b]Reads from The Cedars metagenomes (Suzuki et al., 2017) were mapped to the isolate genomes. The metagenomes are under the DDBJ BioProject accession number PRJDB2971. The Bowtie2 (Langmead and Salzberg, 2012) overall alignment rate percentage is reported.

Genome analysis of Ali-BS5-314 identified that this microbe is capable of nitrate reduction by the action of nitrate reductase (NarGHJI). This is supported by the physiological studies, discussed above. Nitrate reduction occurs intracellularly, based on the localization of the catalytic subunit (*narG*) to the cytoplasm (Supplementary Figure S6; PSORTb localization prediction Supplementary Table S9) and the identification of nitrate/nitrite transporters (NarK1 and NarK2) (Sharma et al., 2006). Subsequent reduction to nitrogen or ammonia is likely not feasible. Instead, ammonia is transported intracellularly by the bidirectional ammonium transporter Amt and assimilated. For example, Ali-BS5-314 may use ammonia in the conversion of glutamate to glutamine (GlnA) and vice versa (GltB) (van Heeswijk et al., 2013). In Ali-BS5-314, ammonia could freely diffuse through the outer membrane into the periplasm for uptake by the transporter Amt (Andrade and Einsle, 2007). Potential buildup of ammonium intracellularly is prevented by regulation of Amt (Soupene et al., 2002; Andrade and Einsle, 2007).

For Anaero-CMMVII, dissimilatory nitrate reduction is feasible. The major facilitator superfamily proteins NarK1 and NarK2 are used to transport nitrate/nitrite (Sharma et al., 2006). Nitrate reduction is conducted by the action of nitrate reductase (NapABD). The gene operon for *napABD* does not contain *napC*, which encodes for a cytochrome needed for quinone cycling. Nitrite can then be converted to nitric oxide (NirK) or ammonia (NrfAH). Nitric oxide is a diffusible free radical gas that may be involved in oxidative stress response, cell signaling, and defense (Orsini et al., 2020). The genome also contains the gene *nmo*, which encodes for nitronate monooxygenase that acts to oxidize alkyl nitronates (e.g., nitroalkane) to nitrite or other compounds using molecular oxygen (Gadda and Francis, 2010).

Nitrogen metabolism in Paeni-Cedars may occur via the glycine cleavage system (GCS) and urea degradation. These two pathways result in the production of ammonia, which is needed for other metabolic pathways (e.g., glutamate synthesis). GCS is a multienzyme system which acts to oxidize glycine, resulting in CO_2, NH_3, 5,10-methylenetetrahydrofolate (5,10-CH_2-THF), and a reduced pyridine nucleotide (Okamura-Ikeda et al., 2010). In Paeni-Cedars, the GCS is feasible with the genes *gcvHT* (GCS proteins) and *gcvPAB* (glycine dehydrogenase). The genome also encodes the urea cycle via the arginine biosynthesis pathway, yielding urea. Urea can then breakdown into CO_2 and NH_3 by the action of urease. Paeni-Cedars may acquire arginine (or polyamines) and urea by ABC transporters. In particular, transported polyamines could be oxidized by the action of copper amine oxidase, releasing ammonia and hydrogen peroxide; other genes, discussed below, will then convert H_2O_2 to H_2O and O_2. The Paeni-Cedars genome also encodes for a nitrite or monovalent anion bi-directional transporter (NirC), which has been linked to the transport nitrite, formate, hydrosulfide, lactate, acetate, and bicarbonate (Atkovska and Hub, 2017). The reason for nitrite transport remains unknown, but could prevent nitrite build-up intracellularly as a result of nitroalkane breakdown by the action of Nmo.

Genome analyses: sulfur metabolism

All three microbes are capable of assimilatory sulfate reduction. Both Ali-BS5-314 and Paeni-Cedars transport sulfate into the cell by an ABC transporter, while Anaero-CMMVII uses sulfate permease (CysP). All three microbes convert sulfate to adenosyl phosphosulfate (APS) by the action of sulfate adenylyltransferase (CysND for Ali-BS5-314; Sat for Paeni-Cedars and Anaero-CMMVII). Subsequent conversion of APS to sulfide through multiple steps involves the genes *cysC* (adenylylsulfate kinase), *cysH* (phosphoadenosine phosphosulfate reductase), and *cysJI* (sulfite reductase). Sulfide can then be transformed to L-cysteine by the action of CysK (cysteine synthase A).

Paeni-Cedars may also acquire sulfur from alkanesulfonates or organosulfur compounds (Kahnert et al., 2000). Intracellular uptake

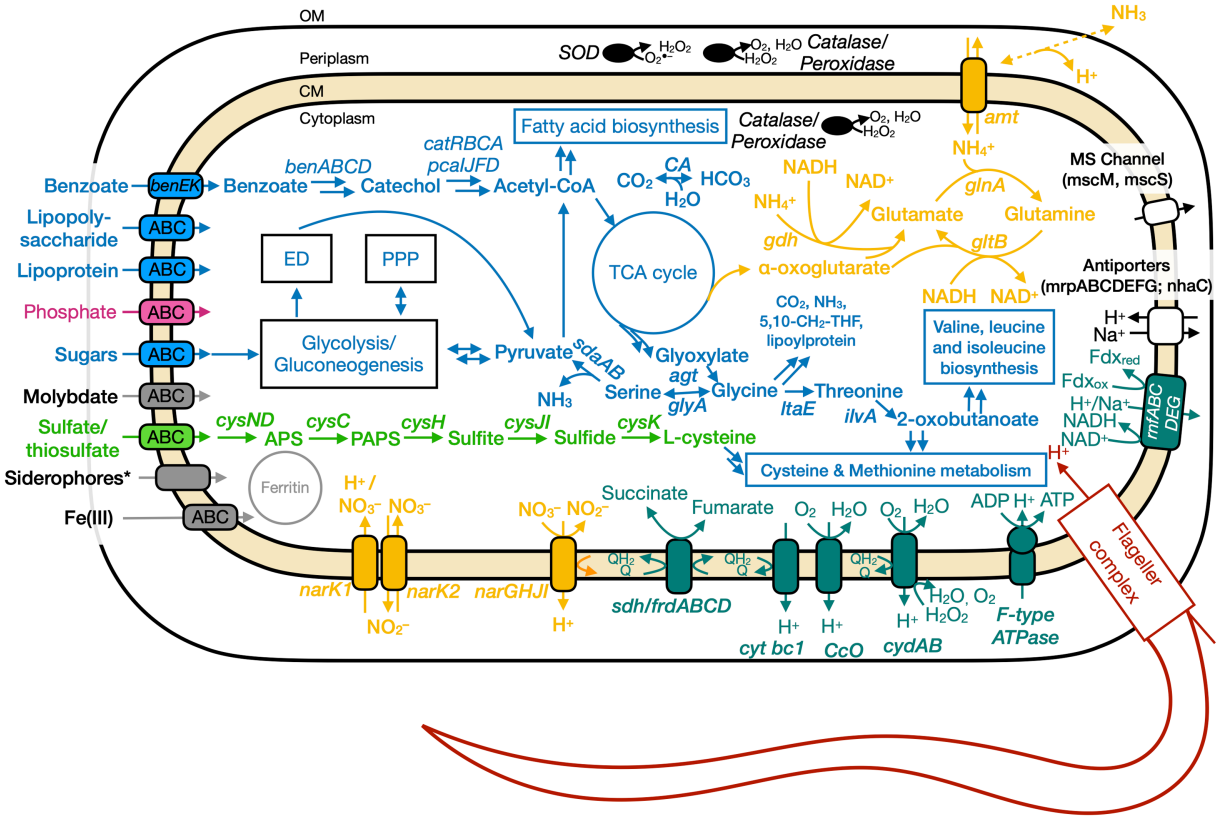

FIGURE 5
Conceptual cell model of Ali-BS5-314 based on genome analysis. Annotations for Ali-BS5-314 can be found in Supplementary Tables S8, S9, S13. 5,10-CH_2-THF, 5,10-methylenetetrahydrofolate; ABC, ATP-binding cassette; acetyl-CoA, acetyl coenzyme A; *agt*, aminotransferase/transaminase; *amt*, ammonium transporter; APS, adenosine-5′-phosphosulfate; *ben*, benzoate degradation genes; *cat*, catechol degradation genes; CA, carbonic anhydrase; CM, cytoplasmic membrane; cys, *cysND*, sulfate adenylyltransferase; *cysC*, adenylylsulfate kinase; *cysH*, phosphoadenosine phosphosulfate reductase; *cysJI*, sulfite reductase; *cysK*, cysteine synthase; cyt, cytochrome; *ccO*, cytochrome *c* oxidase; *cyd*, cytochrome *bd*; ED, Entner–Doudoroff pathway; *ilvA*, threonine dehydratase; *frd*, fumarate reductase; *gdh*, glutamate dehydrogenase; *glnA*, glutamine synthetase; *gltB*, glutamate synthase; *glyA*, glycine hydroxymethyltransferase; *ltaE*, threonine aldolase; *msc*, miniconductance mechanosensitive channel; *mrp*, antiporter complex; NAD(H), nicotinamide adenine dinucleotide; *nar*, nitrate reductase; *nha*, Na^+/H^+ antiporter; OM, outer membrane; *pca*, protocatechuate degradation genes; PPP, pentose phosphate pathway; rnf, Na^+-translocating ferredoxin:NAD^+oxidoreductase; *sdaAB*, L-serine dehydratase; *sdh*, succinate dehydrogenase; SOD, superoxide disumutase; TCA, tricarboxylic acid. Pink, phosphate transporter; gray, function related to metal transport or storage; blue, function related to the uptake, assimilation, or breakdown of sugars, amino acids, vitamin, fatty acids; orange, function related to the nitrogen cycle; dark red, flagellar complex; black, ROS/stress response; dark teal, oxidative phosphorylation; white/black, function related to ion homeostasis; green, function related to sulfur cycle; *Putative.

of alkanesulfonates occurs by the action of an ATP transporter, and the genome of Paeni-Cedars contains the genes *ssuBACC*. Subsequently, the alkanesulfonates can then be converted to sulfite by a gene encoding for a monooxygenase, which may function similarly as SsuD. The genome of Paeni-Cedars also contains several copies of *ssuE* (FMN reductase) and other genes for FMN reductase, although these genes are not in the same gene neighborhood as other *ssu* genes. This suggests that there is potential for Paeni-Cedars to have two sulfur metabolic pathways.

Genome analyses: iron and other trace metal acquisition

The genomes of all three microbes have genes for ABC transporters to uptake trace metals for growth and enzyme function. In the natural environment, The Cedars spring fluids contain low nM levels of iron, copper, nickel and cobalt (Supplementary Table S14), indicating that microorganisms require adaptations to transport metals from the surrounding minerals or fluids. Ali-BS5-314 is capable of iron (as Fe^{3+}) and molybdate uptake. In comparison, Paeni-Cedars and Anaero-CMMVII can uptake various metals, including iron (as Fe^{2+} or Fe^{3+}), molybdate, nickel, or zinc. Notably, the genome of Anaero-CMMVII also encodes an ABC transporter specifically for tungstate transport. Enzymes containing tungstate are often observed in prokaryotic obligate anaerobes (Hille, 2002), although Anaero-CMMVII is a likely oxygen-tolerant anaerobe.

Amongst the various metal acquisition pathways, genes for Fe(III) and molybdate uptake are present in all three genomes. In particular, Fe(III) is the likely dominating iron species in the highly alkaline fluids (Liu and Millero, 1999) of serpentinite-hosted ecosystems. Ali-BS5-314 and Anaero-CMMVII acquire Fe(III) by the action of an Fe(III) transporter (FutA1-FutB-FutC) (Katoh et al., 2001; Zappa and Bauer, 2017) or by the transport of Fe(III)-siderophore complexes. Siderophores are microbially-produced chelators that have a high affinity for binding ferric iron (Butler and

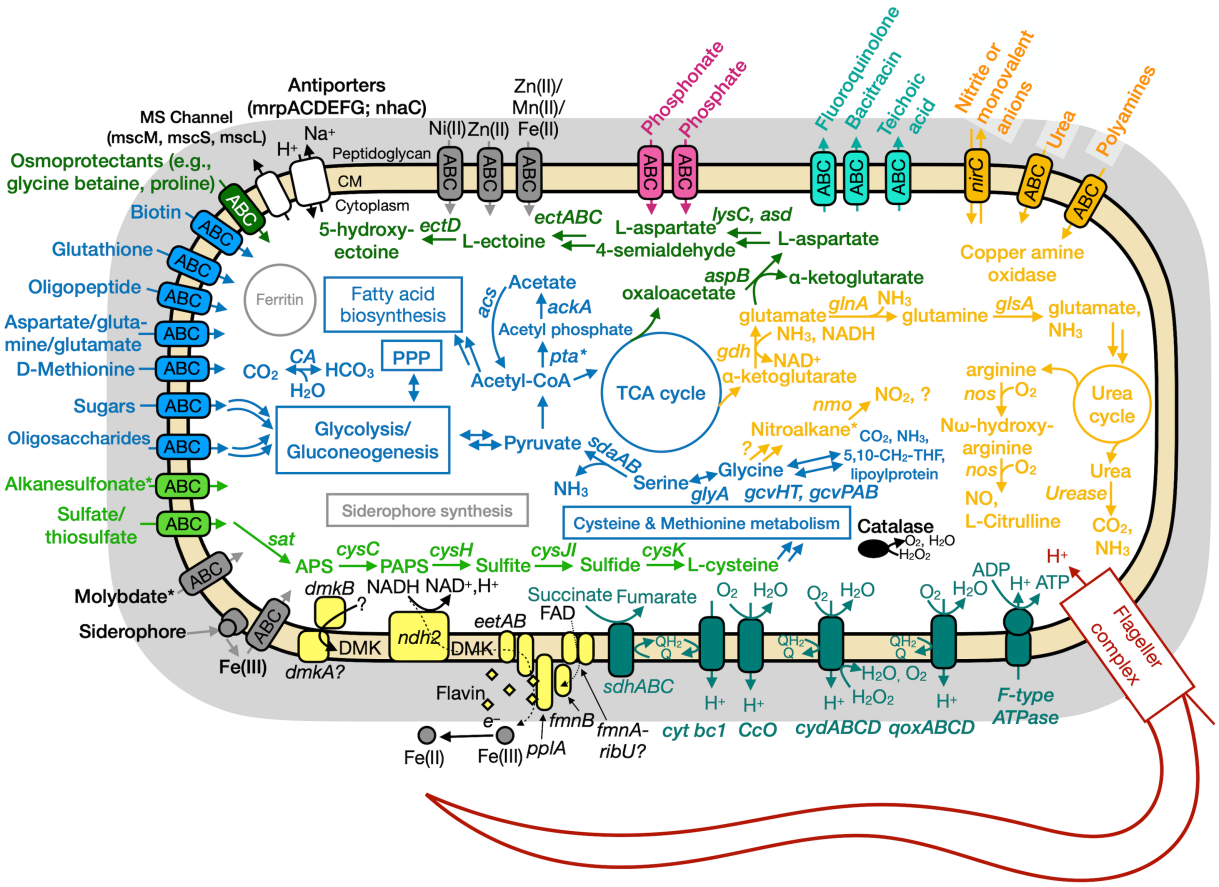

FIGURE 6
Conceptual cell model of Paeni-Cedars based on genome analysis. Annotations for Paeni-Cedars can be found in Supplementary Tables S8, S10, S13. Abbreviations also found in Figure 5 description. *Acs,* acetyl-CoA synthase; *ackA,* acetate kinase; *asd,* aspartate-semialdehyde dehydrogenase; *aspB,* aspartate aminotransferase; *dmkAB,* genes for demethylmenaquinone biosynthesis proteins; DMK, demethylmenaquinone; *ectA,* L-2,4-diaminobutyric acid acetyltransferase; *ectB,* diaminobutyrate-2-oxoglutarate transaminase; *ectC,* L-ectoine synthase; *ectD,* ectoine hydroxylase; *eetAB,* genes for extracellular electron transfer membrane proteins; FAD, flavin adenine dinucleotide; *fmnB,* flavin mononucleotide transferase; *lysC,* aspartate kinase; *nirC,* nitrite transporter; *pta,* phosphate acetyltransferase; *gcvHTPAB,* glycine cleavage system; *glsA,* glutaminase; *ndh2,* NADH dehydrogenase; *nos,* nitric oxide synthase; *pplA,* membrane-anchored lipoprotein; *sat,* ATP sulfurylase enzyme; *qoxABCD,* cytochrome aa3-600 menaquinol oxidase. Pink, phosphate transporter; gray, function related to metal transport or storage; blue, function related to the uptake, assimilation, or breakdown of sugars, amino acids, vitamin, fatty acids; orange, function related to the nitrogen cycle; dark red, flagellar complex; black, ROS/stress response; dark teal=oxidative phosphorylation; white/black, function related to ion homeostasis; yellow, extracellular electron transport; green, function related to sulfur cycle; *putative.

Theisen, 2010) and can acquire iron from minerals (Van Den Berghe et al., 2021). In contrast, Paeni-Cedars acquires iron by Fe(III)-siderophore complexes through the actions of a membrane-anchored binding protein and an ABC transporter (FbpABC). For all three microbes, once iron is transported into the cell, it can be stored in the iron storage protein ferritin (Andrews et al., 2003).

The siderophore uptake pathways suggests that microbes at The Cedars can synthesize these secondary metabolites. Moreover, putative siderophores were detected in spring BS5 and in river water by spring GPS1 (Supplementary Figure S7). However, only Paeni-Cedars is capable of synthesizing a siderophore, and the other two isolates likely rely on other microbial members for the production of this metabolite (Hibbing et al., 2010). The genome of Paeni-Cedars contains the full gene operon for a catechol-type siderophore, with a gene neighborhood that is 53% similar to the bacillibactin (*dhb*) neighborhood and 46% similar to the paenibactin (*pae*) neighborhood (Supplementary Figure S8). The gene operon also follows the bacillibactin and paenibactin synthesis operons: *dhbACEBF* (Wen et al., 2011). The gene *dhbF* is the non-ribosomal peptide synthetase (NRPS) module, which represents one pathway for producing siderophores and is responsible for synthesizing the peptide backbone of catechol-type siderophores. Overall, the presence of siderophore synthesis and uptake pathways demonstrates that unique secondary microbial metabolites remain undiscovered in serpentinizing fluids.

Genome analyses: adaptations to alkaliphily, osmotic stress, and radicals

The main adaptation of prokaryotes to alkaliphilic conditions is pH homeostasis (Hicks et al., 2010; Krulwich et al., 2014). It is

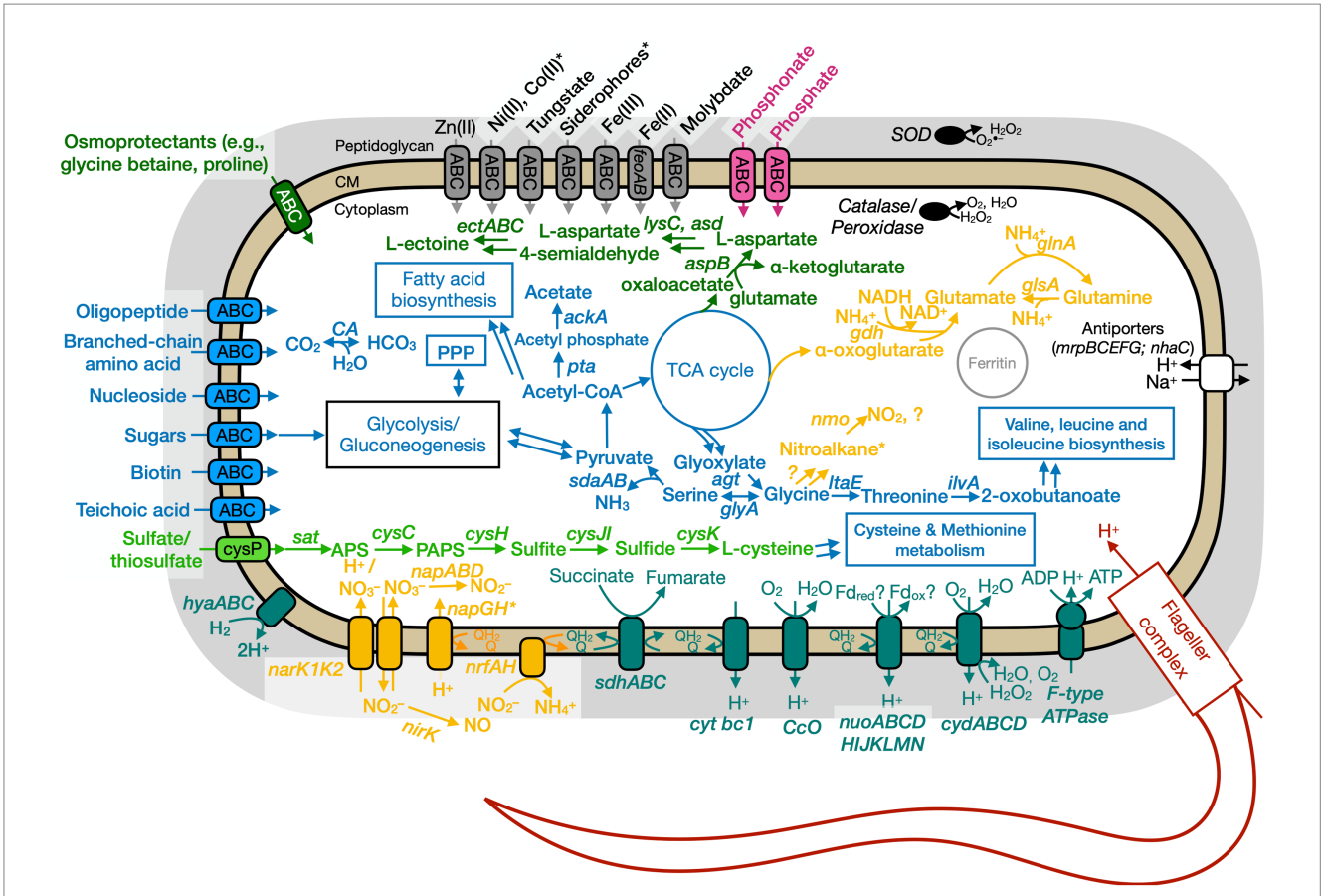

FIGURE 7
Conceptual cell model of Anaero-CMMVII based on genome analysis. Annotations for Anaero-CMMVII can be found in Supplementary Tables S8, S11, S13. Abbreviations also found in Figures 5, 6 description. *napABD,* nitrate reductase; *napGH,* genes for ferredoxin-type protein; *nrfAH,* nitrite reductase; *nirK,* nitrite reductase, NO forming; *nuo,* NADH dehydrogenase. Pink, phosphate transporter; gray, function related to metal transport or storage; blue, function related to the uptake, assimilation, or breakdown of sugars, amino acids, vitamin, fatty acids; orange, function related to the nitrogen cycle; dark red, flagellar complex; black, ROS/stress response; dark teal, oxidative phosphorylation; white/black, function related to ion homeostasis; green, function related to sulfur cycle; *putative.

well-known that alkaliphilic and alkali-tolerant microbes maintain an intracellular pH lower than the external pH through ion transport and/or synthesis of acidic compounds (Krulwich et al., 2014). All three genomes contain genes (*mrpABCDEFG* and *nhaC*) for Na^+/H^+ antiporters (Ito, 2017), in addition to proton pumping within the electron transport chain, oxidative phosphorylation, and flagellar rotation. Paeni-Cedars and Ali-BS5-314 also have genes (*mscM, mscS, and/or mscL*) for encoding mechanosensitive ion channels, which allow for osmotic adjustment (Cox et al., 2018).

Osmotic stress adaptations are used by all three microbes. These adaptations are needed in the natural environment of The Cedars, where the conductivity of spring fluids ranges from 740 and 3,010 µS/cm because of the high Ca^{2+}, Na^+ and Cl^- content (Morrill et al., 2013). Notably, all three microbes could synthesize glutamate as a primary organic osmolyte, as demonstrated in the halophile *Halobacillus halophilus* (Saum and Müller, 2008). In contrast, only Anaero-CMMVII and Paeni-Cedars may uptake osmoprotectants (e.g., glycine betaine and proline) by an ABC transporter. The ectoine biosynthesis pathway [*ectABC(D)*] is also present in the genomes of Anaero-CMMVII and Paeni-Cedars; ectoine is an osmolyte and is produced by microbes in response to osmotic stress (Czech et al., 2018). However, the genome of Anaero-CMMVII lacks *ectD*, indicating that ectoine cannot be subsequently transformed to the osmolyte 5-hydroxyectoine. The putative uptake and synthesis of osmolytes by Paeni-Cedars may enable growth under high $CaCl_2$ conditions (5–20 mM) (Figure 4).

All three microbes have adaptations against radicals and hydrogen peroxide, including genes encoding for superoxide dismutase, catalases, and peroxidases. In addition, the cytochrome *bd* complex (CydAB or CydABCD) is present in the three isolates, as described in the section "*Genome analyses: Energy conservation and extracellular electron transport*" and is also known to protect against oxidative and nitrosative stress conditions, potentially responding to high pH conditions (Giuffrè et al., 2014). Paeni-Cedars may also use transported polyamines, discussed above, to act as radical scavengers (Chattopadhyay et al., 2003; Shah et al., 2008), in addition to other biological functions (Khazaal et al., 2021).

Paeni-Cedars and Anaero-CMMVII may form endospores in response to adverse environmental conditions. The genomes of both isolates contain the sporulation master regulator gene, *spo0A*, and other genes involved in sporulation, including *sspA* (encodes for α/β-type small acid-soluble sporulation protein) and dipicolinate synthase (*dpaA* [*spoVFA*] and *dpaB* [*spoVFB*]) (Galperin et al., 2022). Spore formation may enable both isolates to survive in the

nutrient-limited and alkaliphilic conditions of fluids in The Cedars springs.

Conclusion

Serpentinite-hosted ecosystems are important locations to understand the origins and limits of life in a planetary context. The highly alkaline and reducing fluids are host to microbial communities that often persist under extreme conditions and nutrient limitations. However, the ecophysiology of these microbes remains elusive because of the lack of pure culture representatives available for investigation in the laboratory environment. In this study, we characterized three isolates (Ali-BS5-314, Paeni-Cedars, and Anaero-CMMVII) from The Cedars through physiological and genomic studies. These three isolates are each unique in their metabolic capacities and optimal growth conditions. Moreover, Ali-BS5-314 and Anaero-CMMVII are alkaliphiles, while Paeni-Cedars is alkali-tolerant. Further studies are needed to understand the mechanisms for alkaliphily and stress response. These isolates also have biotechnological potential for processes done at alkaline pH. Based on genome analyses, Ali-BS5-314 can putatively metabolize benzoate-like compounds, and Anaero-CMMVII can degrade complex carbohydrates. Notably, Paeni-Cedars has been demonstrated to perform EET, and is believed to be capable of synthesizing siderophores or metabolizing complex carbohydrates and alkanesulfonates. Overall, this work demonstrates how the enrichment, isolation, and investigation of novel microbes from serpentinizing systems in the laboratory setting is paramount to furthering our understanding of the nature of life in these unique systems and are necessary for studies in both astrobiology and biotechnology.

Data availability statement

This Whole Genome Shotgun project has been deposited at NCBI under the accession JACEHJ000000000 (Ali-BS5-314), JACEHK000000000 (Anaero-CMMVII), and CP020864.1 to CP020866.1 (Paeni-Cedars). The version described in this paper are version 1.

Author contributions

JT and CB contributed equally to the experimental design and physiological characterization of The Cedars microorganisms. NM, MT, ML, and CT supported the physiological characterization studies. NM isolated Ali-BS5-314 and analyzed the genomes of all isolates. LB isolated Anaero-CMMVII. ELC worked with Paeni-Cedars and sequenced the genome. SS, AO, LB, and KN advised the physiological and genomic characterization studies. YH advised the genomic analyses. LB-A and DR analyzed the siderophores from The Cedars. All authors contributed to the article and approved the submitted version.

Funding

JT, CB, MT, ML, CT, NM, LB, and KN were supported by NASA Grant NNA13AA92A and the Air Force Office of Scientific Research Grant FA9550-14-1-0114. NM was also supported by the Earth-Life Science Institute Origin of Life (EON) Postdoctoral Fellowship, the LLNL Postdoctoral Program, and LLNL Laboratory and Directed Research Development (LDRD, 22-LW-034). The EON fellowship is supported by a grant from the John Templeton Foundation. SS is partly supported by JSPS KAKENHI Grant Number 18H02501.

Acknowledgments

We thank Roger Raiche and David McCrory for site access and insight into The Cedars. We thank Gijs Kuenen for field sampling advice and discussion on iron solubility in serpentinizing ecosystems. We also thank Annette Rowe for advice on culturing Paeni-Cedars. We thank Kenneth Bolster for analyzing iron, copper, nickel, and cobalt in The Cedars springs and river (Supplementary Table 14).

Conflict of interest

The authors declare that the research was conducted in the absence of any commercial or financial relationships that could be construed as a potential conflict of interest.

Publisher's note

Author disclaimer

The opinions expressed in this publication are those of the author(s) and do not necessarily reflect the views of the John Templeton Foundation. LLNL, operated by LLN Security, for the U.S. Department of Energy, National Nuclear Security Administration under Contract DE-AC52-07NA27344 (LLNL-JRNL-844638).

Supplementary material

The Supplementary material for this article can be found online at: https://www.frontiersin.org/articles/10.3389/fmicb.2023.1179857/full#supplementary-material

References

Alexander, B., and Priest, F. G. (1989). *Bacillus glucanolyticus*, a new species that degrades a variety of p-Glucans. *Int. J. Syst. Bacteriol.* 39, 112–115. doi: 10.1099/00207713-39-2-112

Andrade, S. L. A., and Einsle, O. (2007). The Amt/Mep/Rh family of ammonium transport proteins. *Mol. Membr. Biol.* 24, 357–365. doi: 10.1080/09687680701388423

Andrews, S. C., Robinson, A. K., and Rodríguez-Quiñones, F. (2003). Bacterial iron homeostasis. *FEMS Microbiol. Rev.* 27, 215–237. doi: 10.1016/S0168-6445(03)00055-X

Arai, W., Taniguchi, T., Goto, S., Moriya, Y., Uehara, H., Takemoto, K., et al. (2018). MAPLE 2.3.0: an improved system for evaluating the functionomes of genomes and metagenomes. *Biosci. Biotechnol. Biochem.* 82, 1515–1517. doi: 10.1080/09168451.2018.1476122

Arkin, A. P., Cottingham, R. W., Henry, C. S., Harris, N. L., Stevens, R. L., Maslov, S., et al. (2018). KBase: the United States Department of Energy Systems Biology Knowledgebase. *Nat. Biotechnol.* 36, 566–569. doi: 10.1038/nbt.4163

Arndt, D., Grant, J. R., Marcu, A., Sajed, T., Pon, A., Liang, Y., et al. (2016). PHASTER: a better, faster version of the PHAST phage search tool. *Nucleic Acids Res.* 44, W16–W21. doi: 10.1093/nar/gkw387

Atkovska, K., and Hub, J. S. (2017). Energetics and mechanism of anion permeation across formate-nitrite transporters. *Sci. Rep.* 7:12027. doi: 10.1038/s41598-017-11437-0

Barnes, I., LaMarche, V. C., and Himmelberg, G. (1967). Geochemical evidence of present-day Serpentinization. *Science* 156, 830–832. doi: 10.1126/science.156.3776.830

Barnes, I., and O'Neil, J. R. (1969). The relationship between fluids in some fresh alpine-type ultramafics and possible modern serpentinization, Western United States. *GSA Bull.* 80, 1947–1960. doi: 10.1130/0016-7606(1969)80[1947:TRBFIS]2.0.CO;2

Bassil, N. M., and Lloyd, J. R. (2019). *Anaerobacillus isosaccharinicus* sp. nov., an alkaliphilic bacterium which degrades isosaccharinic acid. *Int. J. Syst. Evol. Microbiol.* 69, 3666–3671. doi: 10.1099/ijsem.0.002721

Bird, L. J., Kuenen, J. G., Osburn, M. R., Tomioka, N., Ishii, S., Barr, C., et al. (2021). *Serpentinimonas* gen. Nov., *Serpentinimonas raichei* sp. nov., *Serpentinimonas barnesii* sp. nov. and *Serpentinimonas maccroryi* sp. nov., hyperalkaliphilic and facultative autotrophic bacteria isolated from terrestrial serpentinizing springs. *Int. J. Syst. Evol. Microbiol.* 71:004945. doi: 10.1099/ijsem.0.004945

Blin, K., Wolf, T., Chevrette, M. G., Lu, X., Schwalen, C. J., Kautsar, S. A., et al. (2017). antiSMASH 4.0—improvements in chemistry prediction and gene cluster boundary identification. *Nucleic Acids Res.* 45, W36–W41. doi: 10.1093/nar/gkx319

Butler, A., and Theisen, R. M. (2010). Iron(III)–siderophore coordination chemistry: reactivity of marine siderophores. *Coord. Chem. Rev.* 254, 288–296. doi: 10.1016/j.ccr.2009.09.010

Capella-Gutierrez, S., Silla-Martinez, J. M., and Gabaldon, T. (2009). trimAl: a tool for automated alignment trimming in large-scale phylogenetic analyses. *Bioinformatics* 25, 1972–1973. doi: 10.1093/bioinformatics/btp348

Carattoli, A., Zankari, E., García-Fernández, A., Voldby Larsen, M., Lund, O., Villa, L., et al. (2014). *In Silico* detection and typing of plasmids using PlasmidFinder and plasmid multilocus sequence typing. *Antimicrob. Agents Chemother.* 58, 3895–3903. doi: 10.1128/AAC.02412-14

Chattopadhyay, M. K., Tabor, C. W., and Tabor, H. (2003). Polyamines protect *Escherichia coli* cells from the toxic effect of oxygen. *Proc. Natl. Acad. Sci.* 100, 2261–2265. doi: 10.1073/pnas.2627990100

Chaumeil, P.-A., Mussig, A. J., Hugenholtz, P., and Parks, D. H. (2020). GTDB-Tk: a toolkit to classify genomes with the genome taxonomy database. *Bioinformatics* 36, 1925–1927. doi: 10.1093/bioinformatics/btz848

Clarkson, S. M., Giannone, R. J., Kridelbaugh, D. M., Elkins, J. G., Guss, A. M., and Michener, J. K. (2017). Construction and optimization of a heterologous pathway for Protocatechuate catabolism in *Escherichia coli* enables bioconversion of model aromatic compounds. *Appl. Environ. Microbiol.* 83, e01313–e01317. doi: 10.1128/AEM.01313-17

Cohen, M. F., Hu, P., Nguyen, M. V., Kamennaya, N., Brown, N., Woyke, T., et al. (2015). Genome sequence of the alkaline-tolerant *Cellulomonas* sp., Strain FA1. *Genome Announc.* 3:e00646-15. doi: 10.1128/genomeA.00646-15

Cook, M. C., Blank, J. G., Rietze, A., Suzuki, S., Nealson, K. H., and Morrill, P. L. (2021). A geochemical comparison of three terrestrial sites of Serpentinization: the tablelands, the cedars, and aqua de Ney. *JGR Biogeosci* 126:e2021JG006316. doi: 10.1029/2021JG006316

Cox, C. D., Bavi, N., and Martinac, B. (2018). Bacterial mechanosensors. *Annu. Rev. Physiol.* 80, 71–93. doi: 10.1146/annurev-physiol-021317-121351

Czech, L., Hermann, L., Stöveken, N., Richter, A., Höppner, A., Smits, S., et al. (2018). Role of the extremolytes ectoine and hydroxyectoine as stress protectants and nutrients: genetics, phylogenomics, biochemistry, and structural analysis. *Genes* 9:177. doi: 10.3390/genes9040177

Deutscher, J., Francke, C., and Postma, P. W. (2006). How Phosphotransferase system-related protein phosphorylation regulates carbohydrate metabolism in Bacteria. *Microbiol. Mol. Biol. Rev.* 70, 939–1031. doi: 10.1128/MMBR.00024-06

Eddy, S. R. (2011). Accelerated profile HMM searches. *PLoS Comput. Biol.* 7:e1002195. doi: 10.1371/journal.pcbi.1002195

Edgar, R. C. (2004). MUSCLE: multiple sequence alignment with high accuracy and high throughput. *Nucleic Acids Res.* 32, 1792–1797. doi: 10.1093/nar/gkh340

Eren, A. M., Esen, Ö. C., Quince, C., Vineis, J. H., Morrison, H. G., Sogin, M. L., et al. (2015). Anvi'o: an advanced analysis and visualization platform for 'omics data. *PeerJ* 3:e1319. doi: 10.7717/peerj.1319

Finn, R. D., Attwood, T. K., Babbitt, P. C., Bateman, A., Bork, P., Bridge, A. J., et al. (2017). InterPro in 2017—beyond protein family and domain annotations. *Nucleic Acids Res.* 45, D190–D199. doi: 10.1093/nar/gkw1107

Gadda, G., and Francis, K. (2010). Nitronate monooxygenase, a model for anionic flavin semiquinone intermediates in oxidative catalysis. *Arch. Biochem. Biophys.* 493, 53–61. doi: 10.1016/j.abb.2009.06.018

Galperin, M. Y., Yutin, N., Wolf, Y. I., Vera Alvarez, R., and Koonin, E. V. (2022). Conservation and evolution of the sporulation gene set in diverse members of the Firmicutes. *J. Bacteriol.* 204:e0007922. doi: 10.1128/jb.00079-22

Garber, A. I., Nealson, K. H., Okamoto, A., McAllister, S. M., Chan, C. S., Barco, R. A., et al. (2020). FeGenie: a comprehensive tool for the identification of Iron genes and Iron gene neighborhoods in genome and Metagenome assemblies. *Front. Microbiol.* 11:37. doi: 10.3389/fmicb.2020.00037

Garcillán-Barcia, M. P., Redondo-Salvo, S., Vielva, L., and de la Cruz, F. (2020). MOBscan: automated annotation of MOB Relaxases, In *Horizontal gene transfer: Methods and protocols methods in molecular biology*., ed. CruzF. de la (New York, NY: Springer US), 295–308

Giuffrè, A., Borisov, V. B., Arese, M., Sarti, P., and Forte, E. (2014). Cytochrome bd oxidase and bacterial tolerance to oxidative and nitrosative stress. *Biochim. Biophys. Acta BBA Bioenerg.* 1837, 1178–1187. doi: 10.1016/j.bbabio.2014.01.016

Götz, F., and Mayer, S. (2013). Both terminal oxidases contribute to fitness and virulence during organ-specific *Staphylococcus aureus* colonization. *MBio* 4, e00976–e00913. doi: 10.1128/mBio.00976-13

Gutiérrez-Preciado, A., Torres, A. G., Merino, E., Bonomi, H. R., Goldbaum, F. A., and García-Angulo, V. A. (2015). Extensive identification of bacterial riboflavin transporters and their distribution across bacterial species. *PLoS One* 10:e0126124. doi: 10.1371/journal.pone.0126124

Han, M. V., and Zmasek, C. M. (2009). phyloXML: XML for evolutionary biology and comparative genomics. *BMC Bioinform.* 10:356. doi: 10.1186/1471-2105-10-356

Harwood, C. S., and Parales, R. E. (1996). The β-Ketoadipate pathway and the biology of self-identity. *Annu. Rev. Microbiol.* 50, 553–590. doi: 10.1146/annurev.micro.50.1.553

Hibbing, M. E., Fuqua, C., Parsek, M. R., and Peterson, S. B. (2010). Bacterial competition: surviving and thriving in the microbial jungle. *Nat. Rev. Microbiol.* 8, 15–25. doi: 10.1038/nrmicro2259

Hicks, D. B., Liu, J., Fujisawa, M., and Krulwich, T. A. (2010). F1F0-ATP synthases of alkaliphilic bacteria: lessons from their adaptations. *Biochim. Biophys. Acta BBA Bioenerg.* 1797, 1362–1377. doi: 10.1016/j.bbabio.2010.02.028

Hille, R. (2002). Molybdenum and tungsten in biology. *Trends Biochem. Sci.* 27, 360–367. doi: 10.1016/S0968-0004(02)02107-2

Hyatt, D., Chen, G.-L., LoCascio, P. F., Land, M. L., Larimer, F. W., and Hauser, L. J. (2010). Prodigal: prokaryotic gene recognition and translation initiation site identification. *BMC Bioinformatics* 11:119. doi: 10.1186/1471-2105-11-119

Ito, M. (2017). Mrp antiporters have important roles in diverse bacteria and archaea. *Front. Microbiol.* 8:12. doi: 10.3389/fmicb.2017.02325

Jones, P., Binns, D., Chang, H.-Y., Fraser, M., Li, W., McAnulla, C., et al. (2014). InterProScan 5: genome-scale protein function classification. *Bioinformatics* 30, 1236–1240. doi: 10.1093/bioinformatics/btu031

Jones, R. M., Goordial, J. M., and Orcutt, B. N. (2018). Low energy subsurface environments as extraterrestrial analogs. *Front. Microbiol.* 9:1605. doi: 10.3389/fmicb.2018.01605

Jousset, A., Bienhold, C., Chatzinotas, A., Gallien, L., Gobet, A., Kurm, V., et al. (2017). Where less may be more: how the rare biosphere pulls ecosystems strings. *ISME J.* 11, 853–862. doi: 10.1038/ismej.2016.174

Kahnert, A., Vermeij, P., Wietek, C., James, P., Leisinger, T., and Kertesz, M. A. (2000). The *ssu* locus plays a key role in organosulfur metabolism in *Pseudomonas putida* S-313. *J. Bacteriol.* 182, 2869–2878. doi: 10.1128/JB.182.10.2869-2878.2000

Kamennaya, N. A., Gray, J., Ito, S., Kainuma, M., Nguyen, M. V., Khilyas, I. V., et al. (2020). Deconstruction of plant biomass by a *Cellulomonas* strain isolated from an ultra-basic (lignin-stripping) spring. *Arch. Microbiol.* 202, 1077–1084. doi: 10.1007/s00203-020-01816-z

Katoh, H., Hagino, N., Grossman, A. R., and Ogawa, T. (2001). Genes essential to Iron transport in the Cyanobacterium *Synechocystis* sp. strain PCC 6803. *J. Bacteriol.* 183, 2779–2784. doi: 10.1128/JB.183.9.2779-2784.2001

Khazaal, S., Al Safadi, R., Osman, D., Hiron, A., and Gilot, P. (2021). Investigation of the polyamine biosynthetic and transport capability of *Streptococcus agalactiae*: the non-essential PotABCD transporter. *Microbiology* 167:001124. doi: 10.1099/mic.0.001124

Kim, M.-S., Roh, S. W., Nam, Y.-D., Chang, H.-W., Kim, K.-H., Jung, M.-J., et al. (2009). Alishewanella jeotgali sp. nov., isolated from traditional fermented food, and emended description of the genus Alishewanella. *Int. J. Syst. Evol. Microbiol.* 59, 2313–2316. doi: 10.1099/ijs.0.007260-0

Konstantinidis, K. T., and Tiedje, J. M. (2005). Genomic insights that advance the species definition for prokaryotes. *Proc. Natl. Acad. Sci.* 102, 2567–2572. doi: 10.1073/pnas.0409727102

Kovacs, N. (1956). Identification of *Pseudomonas pyocyanea* by the oxidase reaction. *Nature* 178:703. doi: 10.1038/178703a0

Krulwich, T. A., Hicks, D. B., Swartz, T., and Ito, M. (2014). "Bioenergetic adaptations that support Alkaliphily" in *Physiology and biochemistry of extremophiles*. eds. C. Gerday and N. Glansdorff (Washington, DC, USA: ASM Press), 311–329.

Langmead, B., and Salzberg, S. L. (2012). Fast gapped-read alignment with Bowtie 2. *Nat. Methods* 9, 357–359. doi: 10.1038/nmeth.1923

Lee, M. D. (2019). GToTree: a user-friendly workflow for phylogenomics. *Bioinformatics* 35, 4162–4164. doi: 10.1093/bioinformatics/btz188

Letunic, I., and Bork, P. (2007). Interactive tree of life (iTOL): an online tool for phylogenetic tree display and annotation. *Bioinformatics* 23, 127–128. doi: 10.1093/bioinformatics/btl529

Letunic, I., and Bork, P. (2021). Interactive tree of life (iTOL) v5: an online tool for phylogenetic tree display and annotation. *Nucleic Acids Res.* 49, W293–W296. doi: 10.1093/nar/gkab301

Light, S. H., Su, L., Rivera-Lugo, R., Cornejo, J. A., Louie, A., Iavarone, A. T., et al. (2018). A flavin-based extracellular electron transfer mechanism in diverse gram-positive bacteria. *Nature* 562, 140–144. doi: 10.1038/s41586-018-0498-z

Liu, X., and Millero, F. J. (1999). The solubility of iron hydroxide in sodium chloride solutions. *Geochim. Cosmochim. Acta* 63, 3487–3497. doi: 10.1016/S0016-7037(99)00270-7

Liu, Y., Zhai, L., Wang, R., Zhao, R., Zhang, X., Chen, C., et al. (2015). Paenibacillus zeae sp. nov., isolated from maize (Zea mays L.) seeds. *Int. J. Syst. Evol. Microbiol.* 65, 4533–4538. doi: 10.1099/ijsem.0.000608

Lowe, T. M., and Eddy, S. R. (1997). tRNAscan-SE: a program for improved detection of transfer RNA genes in genomic sequence. *Nucleic Acids Res.* 25, 955–964. doi: 10.1093/nar/25.5.955

Mathews, S. L., Ayoub, A. S., Pawlak, J., and Grunden, A. M. (2013). Methods for facilitating microbial growth on pulp mill waste streams and characterization of the biodegradation potential of cultured microbes. *J. Vis. Exp.* e51373. doi: 10.3791/51373

Mathews, S. L., Grunden, A. M., and Pawlak, J. (2016). Degradation of lignocellulose and lignin by *Paenibacillus glucanolyticus*. *Int. Biodeterior. Biodegrad.* 110, 79–86. doi: 10.1016/j.ibiod.2016.02.012

McBeth, J. M., Fleming, E. J., and Emerson, D. (2013). The transition from freshwater to marine iron-oxidizing bacterial lineages along a salinity gradient on the Sheepscot River, Maine, USA. *Environ. Microbiol. Rep.* 5, 453–463. doi: 10.1111/1758-2229.12033

McBeth, J. M., Little, B. J., Ray, R. I., Farrar, K. M., and Emerson, D. (2011). Neutrophilic Iron-oxidizing "Zetaproteobacteria" and mild steel corrosion in Nearshore marine environments. *Appl. Environ. Microbiol.* 77, 1405–1412. doi: 10.1128/AEM.02095-10

Meier-Kolthoff, J. P., Carbasse, J. S., Peinado-Olarte, R. L., and Göker, M. (2022). TYGS and LPSN: a database tandem for fast and reliable genome-based classification and nomenclature of prokaryotes. *Nucleic Acids Res.* 50, D801–D807. doi: 10.1093/nar/gkab902

Meier-Kolthoff, J. P., and Göker, M. (2019). TYGS is an automated high-throughput platform for state-of-the-art genome-based taxonomy. *Nat. Commun.* 10:2182. doi: 10.1038/s41467-019-10210-3

Merino, N., Aronson, H. S., Bojanova, D. P., Feyhl-Buska, J., Wong, M. L., Zhang, S., et al. (2019). Living at the extremes: extremophiles and the limits of life in a planetary context. *Front. Microbiol.* 10:780. doi: 10.3389/fmicb.2019.00780

Miller, H. M., Chaudhry, N., Conrad, M. E., Bill, M., Kopf, S. H., and Templeton, A. S. (2018). Large carbon isotope variability during methanogenesis under alkaline conditions. *Geochim. Cosmochim. Acta* 237, 18–31. doi: 10.1016/j.gca.2018.06.007

Miller, M. A., Pfeiffer, W., and Schwartz, T. (2010). "Creating the CIPRES science gateway for inference of large phylogenetic trees," in *Proceedings of the Gateway Computing Environments Workshop (GCE), 14 Nov. 2010*. New Orleans, LA, 1–8.

Morrill, P. L., Kuenen, J. G., Johnson, O. J., Suzuki, S., Rietze, A., Sessions, A. L., et al. (2013). Geochemistry and geobiology of a present-day serpentinization site in California: the cedars. *Geochim. Cosmochim. Acta* 109, 222–240. doi: 10.1016/j.gca.2013.01.043

NASEM (2019). *National Academies of sciences, engineering, and medicine. An astrobiology strategy for the search for life in the universe*. Washington, DC: The National Academies Press

Nojiri, H., Maeda, K., Sekiguchi, H., Urata, M., Shintani, M., Yoshida, T., et al. (2002). Organization and transcriptional characterization of catechol degradation genes involved in Carbazole degradation by *Pseudomonas resinovorans* strain CA10. *Biosci. Biotechnol. Biochem.* 66, 897–901. doi: 10.1271/bbb.66.897

Okamura-Ikeda, K., Hosaka, H., Maita, N., Fujiwara, K., Yoshizawa, A. C., Nakagawa, A., et al. (2010). Crystal structure of aminomethyltransferase in complex with dihydrolipoyl-H-protein of the glycine cleavage system. *J. Biol. Chem.* 285, 18684–18692. doi: 10.1074/jbc.M110.110718

Orsini, S. S., James, K. L., Reyes, D. J., Couto-Rodriguez, R. L., Gulko, M. K., Witte, A., et al. (2020). Bacterial-like nitric oxide synthase in the haloalkaliphilic archaeon *Natronomonas pharaonis*. *MicrobiologyOpen* 9:e1124. doi: 10.1002/mbo3.1124

Parks, D. H., Chuvochina, M., Chaumeil, P.-A., Rinke, C., Mussig, A. J., and Hugenholtz, P. (2020). A complete domain-to-species taxonomy for bacteria and archaea. *Nat. Biotechnol.* 38, 1079–1086. doi: 10.1038/s41587-020-0501-8

Pasini, V., Brunelli, D., Dumas, P., Sandt, C., Frederick, J., Benzerara, K., et al. (2013). Low temperature hydrothermal oil and associated biological precursors in serpentinites from Mid-Ocean ridge. *Lithos* 178, 84–95. doi: 10.1016/j.lithos.2013.06.014

Patrauchan, M. A., Florizone, C., Dosanjh, M., Mohn, W. W., Davies, J., and Eltis, L. D. (2005). Catabolism of benzoate and phthalate in *Rhodococcus* sp. strain RHA1: redundancies and convergence. *J. Bacteriol.* 187, 4050–4063. doi: 10.1128/JB.187.12.4050-4063.2005

Peters, J. W., Schut, G. J., Boyd, E. S., Mulder, D. W., Shepard, E. M., Broderick, J. B., et al. (2015). [FeFe]- and [NiFe]-hydrogenase diversity, mechanism, and maturation. *Biochim. Biophys. Acta BBA Mol. Cell Res* 1853, 1350–1369. doi: 10.1016/j.bbamcr.2014.11.021

Plümper, O., King, H. E., Geisler, T., Liu, Y., Pabst, S., Savov, I. P., et al. (2017). Subduction zone forearc serpentinites as incubators for deep microbial life. *Proc. Natl. Acad. Sci.* 114, 4324–4329. doi: 10.1073/pnas.1612147114

Postec, A., Quéméneur, M., Lecoeuvre, A., Chabert, N., Joseph, M., and Erauso, G. (2021). *Alkaliphilus serpentinus* sp. nov. and *Alkaliphilus pronyensis* sp. nov., two novel anaerobic alkaliphilic species isolated from the serpentinite-hosted Prony Bay hydrothermal field (New Caledonia). *Syst. Appl. Microbiol.* 44:126175. doi: 10.1016/j.syapm.2020.126175

Price, M. N., Dehal, P. S., and Arkin, A. P. (2010). FastTree 2 – approximately maximum-likelihood trees for large alignments. *PLoS One* 5:e9490. doi: 10.1371/journal.pone.0009490

Priest, F. G. (2009). Genus I. Paenibacillus. *Bergey's manual of systematic bacteriology* 3, 269–295.

Pruesse, E., Peplies, J., and Glöckner, F. O. (2012). SINA: accurate high-throughput multiple sequence alignment of ribosomal RNA genes. *Bioinformatics* 28, 1823–1829. doi: 10.1093/bioinformatics/bts252

Quast, C., Pruesse, E., Yilmaz, P., Gerken, J., Schweer, T., Yarza, P., et al. (2013). The SILVA ribosomal RNA gene database project: improved data processing and web-based tools. *Nucleic Acids Res.* 41, D590–D596. doi: 10.1093/nar/gks1219

Quéméneur, M., Erauso, G., Bartoli, M., Vandecasteele, C., Wils, L., Gil, L., et al. (2021). *Alkalicella caledoniensis* gen. Nov., sp. nov., a novel alkaliphilic anaerobic bacterium isolated from 'La Crouen' alkaline thermal spring, New Caledonia. *Int. J. Syst. Evol. Microbiol.* 71:004810. doi: 10.1099/ijsem.0.004810

Quéméneur, M., Palvadeau, A., Postec, A., Monnin, C., Chavagnac, V., Ollivier, B., et al. (2015). Endolithic microbial communities in carbonate precipitates from serpentinite-hosted hyperalkaline springs of the Voltri massif (Ligurian Alps, northern Italy). *Environ. Sci. Pollut. Res.* 22, 13613–13624. doi: 10.1007/s11356-015-4113-7

Richter, M., and Rosselló-Móra, R. (2009). Shifting the genomic gold standard for the prokaryotic species definition. *Proc. Natl. Acad. Sci.* 106, 19126–19131. doi: 10.1073/pnas.0906412106

Robertson, J., and Nash, J. H. E. (2018). MOB-suite: software tools for clustering, reconstruction and typing of plasmids from draft assemblies. *Microb. Genomics* 4. doi: 10.1099/mgen.0.000206

Roh, S. W., Nam, Y.-D., Chang, H.-W., Kim, K.-H., Kim, M.-S., Oh, H.-M., et al. (2009). *Alishewanella aestuarii* sp. nov., isolated from tidal flat sediment, and emended description of the genus *Alishewanella*. *Int. J. Syst. Evol. Microbiol.* 59, 421–424. doi: 10.1099/ijs.0.65643-0

Rowe, A. R., Chellamuthu, P., Lam, B., Okamoto, A., and Nealson, K. H. (2015). Marine sediments microbes capable of electrode oxidation as a surrogate for lithotrophic insoluble substrate metabolism. *Front. Microbiol.* 5. doi: 10.3389/fmicb.2014.00784

Rowe, A. R., Yoshimura, M., LaRowe, D. E., Bird, L. J., Amend, J. P., Hashimoto, K., et al. (2017). In situ electrochemical enrichment and isolation of a magnetite-reducing bacterium from a high pH serpentinizing spring: mineral reduction in a high pH serpentinizing spring. *Environ. Microbiol.* 19, 2272–2285. doi: 10.1111/1462-2920.13723

Saum, S. H., and Müller, V. (2008). Regulation of osmoadaptation in the moderate halophile *Halobacillus halophilus*: chloride, glutamate and switching osmolyte strategies. *Saline Syst.* 4:4. doi: 10.1186/1746-1448-4-4

Sazanov, L. A. (2007). Respiratory complex I: mechanistic and structural insights provided by the crystal structure of the hydrophilic domain. *Biochemistry* 46, 2275–2288. doi: 10.1021/bi602508x

Schut, G. J., Zadvornyy, O., Wu, C.-H., Peters, J. W., Boyd, E. S., and Adams, M. W. W. (2016). The role of geochemistry and energetics in the evolution of modern respiratory complexes from a proton-reducing ancestor. *Biochimica et Biophysica Acta (BBA) - Bioenergetics* 1857, 958–970. doi: 10.1016/j.bbabio.2016.01.010

Schwengers, O., Barth, P., Falgenhauer, L., Hain, T., Chakraborty, T., and Goesmann, A. (2020). Platon: identification and characterization of bacterial plasmid contigs in short-read draft assemblies exploiting protein sequence-based replicon distribution scores. *Microb. Genomics* 6. doi: 10.1099/mgen.0.000398

Seyler, L. M., Kraus, E. A., McLean, C., Spear, J. R., Templeton, A. S., and Schrenk, M. O. (2022). An untargeted metabolomics approach to characterize dissolved organic matter in groundwater of the Samail Ophiolite. *bioRxiv*. 2022.11.09.515806. doi: 10.1101/2022.11.09.515806

Shah, P., Romero, D. G., and Swiatlo, E. (2008). Role of polyamine transport in *Streptococcus pneumoniae* response to physiological stress and murine septicemia. *Microb. Pathog.* 45, 167–172. doi: 10.1016/j.micpath.2008.05.001

Sharma, V., Noriega, C. E., and Rowe, J. J. (2006). Involvement of NarK1 and NarK2 proteins in transport of nitrate and nitrite in the denitrifying bacterium *Pseudomonas aeruginosa* PAO. *Appl Env. Microbiol* 72, 695–701. doi: 10.1128/AEM.72.1.695-701.2006

Shida, O., Takagi, H., Kadowaki, K., Nakamura, L. K., and Komagata, K. (1997). Transfer of *Bacillus alginolyticus, Bacillus chondroitinus, Bacillus curdlanolyticus, Bacillus glucanolyticus, Bacillus kobensis*, and *Bacillus thiaminolyticus* to the Genus *Paenibacillus* and Emended Description of the Genus *Paenibacillus*. *Int. J. Bacteriol.* 47, 289–298. doi: 10.1099/00207713-47-2-289

Sit, B., Crowley, S. M., Bhullar, K., Lai, C. C.-L., Tang, C., Hooda, Y., et al. (2015). Active transport of phosphorylated carbohydrates promotes intestinal colonization and transmission of a bacterial pathogen. *PLoS Pathog.* 11:e1005107. doi: 10.1371/journal.ppat.1005107

Søndergaard, D., Pedersen, C. N. S., and Greening, C. (2016). HydDB: a web tool for hydrogenase classification and analysis. *Sci. Rep.* 6:34212. doi: 10.1038/srep34212

Soupene, E., Lee, H., and Kustu, S. (2002). Ammonium/methylammonium transport (Amt) proteins facilitate diffusion of NH_3 bidirectionally. *Proc. Natl. Acad. Sci.* 99, 3926–3931. doi: 10.1073/pnas.062043799

Stookey, L. L. (1970). Ferrozine---a new spectrophotometric reagent for iron. *Anal. Chem.* 42, 779–781. doi: 10.1021/ac60289a016

Suzuki, S., Ishii, S., Hoshino, T., Rietze, A., Tenney, A., Morrill, P. L., et al. (2017). Unusual metabolic diversity of hyperalkaliphilic microbial communities associated with subterranean serpentinization at the cedars. *ISME J.* 11, 2584–2598. doi: 10.1038/ismej.2017.111

Suzuki, S., Ishii, S., Wu, A., Cheung, A., Tenney, A., Wanger, G., et al. (2013). Microbial diversity in the cedars, an ultrabasic, ultrareducing, and low salinity serpentinizing ecosystem. *Proc. Natl. Acad. Sci.* 110, 15336–15341. doi: 10.1073/pnas.1302426110

Suzuki, S., Kuenen, J. G., Schipper, K., van der Velde, S., Ishii, S., Wu, A., et al. (2014). Physiological and genomic features of highly alkaliphilic hydrogen-utilizing Betaproteobacteria from a continental serpentinizing site. *Nat. Commun.* 5:3900. doi: 10.1038/ncomms4900

Tange, O. (2018). GNU Parallel 2018. *Ole Tange*. 112. doi: 10.5281/zenodo.1146014

Teufel, F., Almagro Armenteros, J. J., Johansen, A. R., Gíslason, M. H., Pihl, S. I., Tsirigos, K. D., et al. (2022). SignalP 6.0 predicts all five types of signal peptides using protein language models. *Nat. Biotechnol.* 40, 1023–1025. doi: 10.1038/s41587-021-01156-3

Tiago, I., Chung, A. P., and Veríssimo, A. (2004). Bacterial diversity in a nonsaline alkaline environment: heterotrophic aerobic populations. *Appl. Environ. Microbiol.* 70, 7378–7387. doi: 10.1128/AEM.70.12.7378-7387.2004

Tiago, I., Mendes, V., Pires, C., Morais, P. V., and Veríssimo, A. (2005). *Phenylobacterium falsum* sp. nov., an Alphaproteobacterium isolated from a nonsaline alkaline groundwater, and emended description of the genus *Phenylobacterium*. *Syst. Appl. Microbiol.* 28, 295–302. doi: 10.1016/j.syapm.2005.02.005

Trutschel, L. R., Chadwick, G. L., Kruger, B., Blank, J. G., Brazelton, W. J., Dart, E. R., et al. (2022). Investigation of microbial metabolisms in an extremely high pH marine-like terrestrial serpentinizing system: Ney Springs. *Sci. Total Environ.* 836:155492. doi: 10.1016/j.scitotenv.2022.155492

Twing, K. I., Brazelton, W. J., Kubo, M. D. Y., Hyer, A. J., Cardace, D., Hoehler, T. M., et al. (2017). Serpentinization-influenced groundwater harbors extremely low diversity microbial communities adapted to high pH. *Front. Microbiol.* 8. doi: 10.3389/fmicb.2017.00308

Vallalar, B., Meyer-Dombard, D. R., Cardace, D., and Arcilla, C. A. (2019). Multimetal resistant, alkalitolerant bacteria isolated from serpentinizing fluid-associated sediments and acid mine drainage in the Zambales Ophiolite, the Philippines. *Geomicrobiol J.* 36, 792–809. doi: 10.1080/01490451.2019.1628132

Van Den Berghe, M., Merino, N., Nealson, K. H., and West, A. J. (2021). Silicate minerals as a direct source of limiting nutrients: Siderophore synthesis and uptake promote ferric iron bioavailability from olivine and microbial growth. *Geobiology* 19, 618–630. doi: 10.1111/gbi.12457

van Heeswijk, W. C., Westerhoff, H. V., and Boogerd, F. C. (2013). Nitrogen assimilation in *Escherichia coli*: putting molecular data into a systems perspective. *Microbiol. Mol. Biol. Rev.* 77, 628–695. doi: 10.1128/MMBR.00025-13

Wardman, J. F., Bains, R. K., Rahfeld, P., and Withers, S. G. (2022). Carbohydrate-active enzymes (CAZymes) in the gut microbiome. *Nat. Rev. Microbiol.* 20, 542–556. doi: 10.1038/s41579-022-00712-1

Wen, Y., Wu, X., Teng, Y., Qian, C., Zhan, Z., Zhao, Y., et al. (2011). Identification and analysis of the gene cluster involved in biosynthesis of paenibactin, a catecholate siderophore produced by *Paenibacillus elgii* B69. *Environ. Microbiol.* 13, 2726–2737. doi: 10.1111/j.1462-2920.2011.02542.x

Yin, Y., Mao, X., Yang, J., Chen, X., Mao, F., and Xu, Y. (2012). dbCAN: a web resource for automated carbohydrate-active enzyme annotation. *Nucleic Acids Res.* 40, W445–W451. doi: 10.1093/nar/gks479

Yu, N. Y., Wagner, J. R., Laird, M. R., Melli, G., Rey, S., Lo, R., et al. (2010). PSORTb 3.0: improved protein subcellular localization prediction with refined localization subcategories and predictive capabilities for all prokaryotes. *Bioinformatics* 26, 1608–1615. doi: 10.1093/bioinformatics/btq249

Zappa, S., and Bauer, C. E. (2017). "The maintenance of Iron homeostasis among prokaryotic Phototrophs" in *Modern topics in the phototrophic prokaryotes: metabolism, bioenergetics, and omics*. ed. P. C. Hallenbeck (Cham: Springer International Publishing), 123–161.

Zhang, H., Yohe, T., Huang, L., Entwistle, S., Wu, P., Yang, Z., et al. (2018). dbCAN2: a meta server for automated carbohydrate-active enzyme annotation. *Nucleic Acids Res.* 46, W95–W101. doi: 10.1093/nar/gky418

frontiers | Frontiers in Microbiology

TYPE Mini Review
PUBLISHED 24 July 2023
DOI 10.3389/fmicb.2023.1197823

OPEN ACCESS

EDITED BY
William J. Brazelton,
The University of Utah, United States

REVIEWED BY
Daniel Colman,
Montana State University, United States
Leah Trutschel,
University of Cincinnati, United States

*CORRESPONDENCE
Gaël Erauso
✉ gael.erauso@mio.osupytheas.fr

RECEIVED 31 March 2023
ACCEPTED 29 June 2023
PUBLISHED 24 July 2023

CITATION
Popall RM, Postec A, Lecoeuvre A, Quéméneur M and Erauso G (2023) Metabolic challenges and key players in serpentinite-hosted microbial ecosystems. *Front. Microbiol.* 14:1197823. doi: 10.3389/fmicb.2023.1197823

Metabolic challenges and key players in serpentinite-hosted microbial ecosystems

Rabja Maria Popall, Anne Postec, Aurélien Lecoeuvre, Marianne Quéméneur and Gaël Erauso*

Aix-Marseille Univ, Univ Toulon, CNRS, IRD, MIO, Marseille, France

Serpentinite-hosted systems are amongst the most challenging environments for life on Earth. Serpentinization, a geochemical alteration of exposed ultramafic rock, produces hydrothermal fluids enriched in abiotically derived hydrogen (H_2), methane (CH_4), and small organic molecules. The hyperalkaline pH of these fluids poses a great challenge for metabolic energy and nutrient acquisition, curbing the cellular membrane potential and limiting electron acceptor, carbon, and phosphorous availability. Nevertheless, serpentinization supports the growth of diverse microbial communities whose metabolic make-up might shed light on the beginning of life on Earth and potentially elsewhere. Here, we outline current hypotheses on metabolic energy production, carbon fixation, and nutrient acquisition in serpentinizing environments. A taxonomic survey is performed for each important metabolic function, highlighting potential key players such as H_2 and CH_4 cycling *Serpentinimonas*, *Hydrogenophaga*, *Methanobacteriales*, *Methanosarcinales*, and novel candidate phyla. Methodological biases of the available data and future approaches are discussed.

KEYWORDS

serpentinization, alkaline hydrothermal system, alkaliphile, hydrogenotroph, lithotroph, submarine alkaline vent theory, origin of life

1. Introduction

The beginnings of life remain one of the most outstanding scientific issues and have been dubbed the "black hole at the heart of biology" (Lane, 2015). One of the central requirements for living systems is a continuous physicochemical disequilibrium driving biological activity (Russell et al., 1988). In marine alkaline hydrothermal systems, strong electrochemical gradients develop between the ultrabasic hydrothermal fluid rising from the deep subsurface, and the seawater. These gradients are maintained across the porous hydrothermal chimney wall, which can be compared to an osmotic membrane. It is hypothesized that this rudimentary proton motive force has driven chimney nanopores to develop into protocells at the emergence of life (Russell et al., 2010; Sojo et al., 2016). Modern ecosystems at hydrothermal vents might thus provide a glimpse into very early microbial life forms.

Most alkaline hydrothermal systems are formed in environments where mantle rocks have been tectonically uplifted and exposed, either above sea level or on the seafloor. Contact with water initiates serpentinization, a geochemical alteration of the ultramafic rock. This process

yields large amounts of hydrogen (H_2) and constitutes one of the most important sources of H_2 on Earth (Reaction 1) (Truche et al., 2020).

$$\underset{\text{Olivine}}{(MgFe)_2SiO_4} + H_2O \rightarrow \underset{\text{Serpentinite}}{Mg_3Si_2O_5(OH)_4} + \underset{\text{Brucite}}{Mg(OH)_2} + \underset{\text{Magnetite}}{Fe_3O_4} + H_2 \quad (1)$$

The oxidation of ferrous iron in olivine or pyroxene to ferric iron and magnetite by water creates reducing conditions. Catalyzed by minerals, this facilitates abiotic reactions of the produced H_2 with mantle-derived carbon dioxide (CO_2) or carbon monoxide (CO) (McCollom and Seewald, 2001). In Sabatier (Reaction 2) and Fischer-Tropsch (Reaction 3) type processes, methane (CH_4) and small organic molecules [C_n $H(2n+2)$] are enriched in the hydrothermal fluid (Barbier et al., 2020):

$$4H_2 + CO_2 \rightarrow CH_4 + 2H_2O \quad (2)$$

$$(3n+1)H_2 + nCO_2 \rightarrow C_nH_{2n+2} + 2nH_2O \quad (3)$$

The serpentinization reaction produces hydrothermal fluids with pH values commonly surpassing 12. In these ultrabasic conditions, the carbonate equilibrium is permanently shifted from CO_2 to carbonate species, removing most dissolved inorganic carbon (DIC) from the environment. Upon reaching the rock surface, much of the carbonate precipitates with fluid-derived calcium. Over time, calcium carbonate amalgamates with brucite and forms the chimneys or travertines typical for serpentinizing environments (Barnes et al., 1978; Früh-Green et al., 2004; McCollom and Seewald, 2013) (Figure 1A).

2. Serpentinite-hosted ecosystems

The products of serpentinization can support chemosynthetic microbial ecosystems growing independently from sunlight. Such serpentinite-hosted ecosystems are found in marine and continental environments, with hydrothermal fluids originating from marine, meteoric and/or groundwater sources.

Most marine serpentinizing ecosystems are located along rather slow-spreading mid-ocean ridges, where continuous tectonic activity facilitates frequent exposure of ultramafic rock (Schrenk et al., 2013; Albers et al., 2021). The most prominent example is the Lost City hydrothermal field near the Mid-Atlantic ridge (e.g., Kelley et al., 2005). A similar system, the Old City hydrothermal field, has recently been discovered along the Southwest Indian ridge (Lecoeuvre et al., 2021). Several other marine sites host mixed-type ecosystems that feature characteristics of both alkaline and acidic hydrothermal vents, such as the Rainbow (Flores et al., 2011), Logatchev (Perner et al., 2007), Ashadze (Fabri et al., 2011) and Kairei fields (Nakamura et al., 2009).

The most well-studied continental systems include the Samail ophiolite in Oman (Rempfert et al., 2017; Kraus et al., 2021), the Tablelands (Bay of Islands) ophiolite in Newfoundland (Brazelton et al., 2013), the Cabeço de Vide aquifer in Portugal (Tiago and Veríssimo, 2013), the Leka ophiolite complex in Norway (Daae et al., 2013), the Italian Gruppo di Voltri (Quéméneur et al., 2015), the Zambales ophiolite in the Philippines (Woycheese et al., 2015), The Cedars (Suzuki et al., 2013; Kohl et al., 2016) and Coast Range (Twing et al., 2017) ophiolites on the West Coast of the United States, the Chimaera (Tekirova) ophiolite in Turkey (Neubeck et al., 2017), the tropical Santa Elena ophiolite in Costa Rica (Crespo-Medina et al., 2017), the Del Puerto ophiolite in California (Blank et al., 2009) and the Troodos ophiolite in Cyprus (Rizoulis et al., 2016).

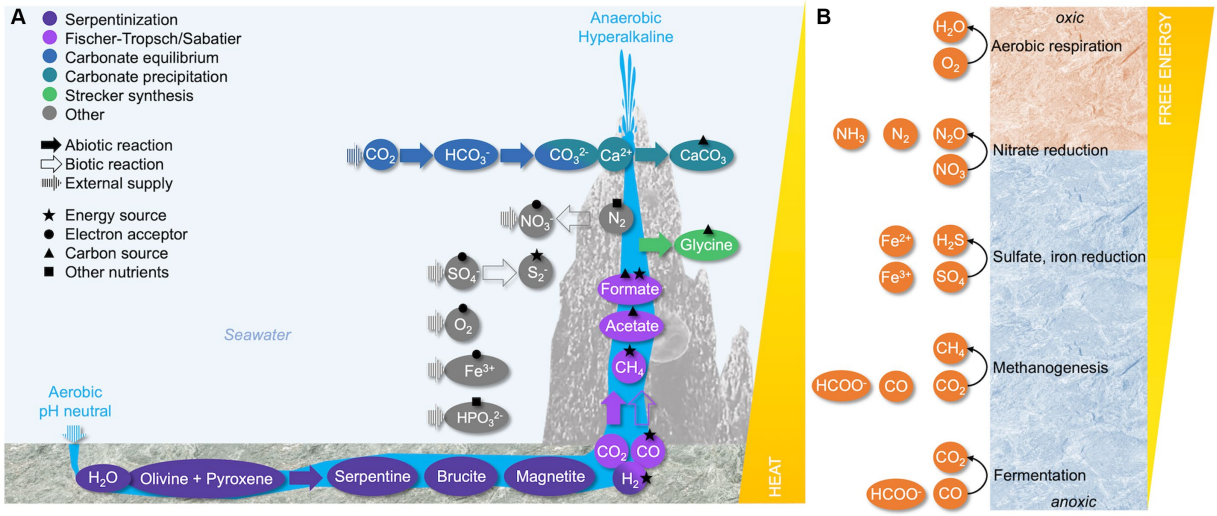

FIGURE 1
The biogeochemical environment of marine serpentinite-hosted systems. **(A)** Production of compounds of interest in microbial metabolism. Reactions are color-coded with solid arrows showing abiotic processes, empty arrows showing biotic processes, and striped arrows indicating external supply. The metabolic potential of shown compounds as an energy source, electron acceptor, carbon source, or other nutrient source is indicated with different shapes. Note that compound concentrations, external supply, temperature, and pH are strongly site dependent. In continental serpentinizing systems, travertines form instead of chimneys. **(B)** Redox potential of available electron acceptors along a gradient from the oxic surface to the anoxic interior of the chimney wall. Adapted from Boyd et al. (2014).

Terrestrial and marine serpentinizing systems are likely to differ in environmental variables such as salinity and the compounds available for microbial metabolism, which might influence the ecosystem's overall functioning. An exciting transition site between terrestrial and marine serpentinite-hosted ecosystems is the Prony Bay Hydrothermal field located on the Southern Coast of New Caledonia, South Pacific (Launay and Fontes, 1985; Monnin et al., 2014). Prony Bay features several venting sites along a gradient from land to sea with a maximum depth of 50 m. The Prony Bay springs are fed by meteoric water, implying a strong salinity gradient between the hydrothermal fluid and ambient seawater (Monnin et al., 2014; Postec et al., 2015). Inversely, the Ney Springs system in Northern California features marine-type hydrothermal fluids in a continental context (Trutschel et al., 2022). Prony Bay is geochemically and microbiologically reflective of both ophiolitic and deep marine sites (Quéméneur et al., 2014; Postec et al., 2015; Frouin et al., 2018, 2022; Trutschel et al., 2022).

3. Metabolic strategies of serpentinite-hosted ecosystems

Serpentinite-hosted ecosystems are subjected to very challenging environmental conditions. The elevated pH poses a fundamental energetic problem on the cellular level, as it inverts the transmembrane pH gradient that typically drives all cellular processes. Furthermore, the high pH also reduces the bioavailability of electron acceptors, carbon, and other macronutrients (McCollom and Seewald, 2013; Schrenk et al., 2013). The microbial adaptations to these challenges are essential to understand life in a serpentinization context.

3.1. The challenge of maintaining bioenergetics

3.1.1. Maintaining pH homeostasis and a proton motive force

The central challenge for life in hyperalkaline conditions revolves around maintaining intracellular pH homeostasis and, more critically, conserving an electrochemical proton gradient across the cell membrane, which is the main driving force of the cell. The so-called proton motive force has two components: A transmembrane pH gradient (ΔpH), which is usually alkaline inside the cell relative to the outside, and a transmembrane electrical potential (Δψ), which is negative as long as the inner membrane surface is negatively charged. Maintaining a circum-neutral intracellular pH is crucial to ensure the stability of nucleic acids and proteins. In hyperalkaline conditions, however, the ΔpH is inverted and very low due to H^+ limitation outside of the cell, as the concentration of H^+ decreases by 10^{-4} at pH 11 compared to pH 7. This reduces the proton motive force and jeopardizes pH homeostasis (Krulwich et al., 2011 and references therein). Most alkaliphiles employ mechanisms increasing the efficiency of H^+ uptake while maintaining a high Δψ, which is also essential for pH homeostasis. This is achieved via K^+/H^+ and Na^+/H^+ antiporters with high H^+ affinity, such as the Mrp complex in alkaliphilic *Bacillus* spp. (Ito et al., 2017). Those antiporters contribute to creating a transmembrane Na^+ gradient, generating a sodium motive force that requires specialized sodium-F_1F_0-ATP synthases or Na^+-dependent respiratory complexes (Krulwich et al., 2011; Kuhns et al., 2020). Based on varying Na^+ concentrations, it is likely that these mechanisms differ between terrestrial and marine serpentinization-influenced site microorganisms. In low salt environments, alkaliphiles might excrete Na^+ via V_1V_0-ATPases to maintain a sodium motive force (Suzuki et al., 2014; Ohlsson et al., 2019). Other alkaliphiles such as *Serpentinimonas* spp. isolated from The Cedars maintain a proton motive force using specialized H^+ binding F type ATPases (Hicks et al., 2010; Suzuki et al., 2014).

3.1.2. Energy conservation

The membrane potential generated via H^+ or Na^+ translocation depends on the redox potential of electron donors and acceptors. Serpentinization yields a range of reduced compounds that can serve as metabolic energy sources, most importantly H_2 and CH_4 (Figure 1A) (Boyd et al., 2014). The relative concentration of these gases varies significantly between sites (Etiope et al., 2011; Monnin et al., 2014), rendering generalized statements on a primary source of electrons provided by serpentinization difficult. While methanotrophs are more easily detected than hydrogenotrophs in many serpentinite-hosted environments (e.g., Brazelton et al., 2006; Kraus et al., 2021) (Table 1), the energetic potential of H_2 oxidation greatly surpasses the oxidation potential of CH_4. The detection of hydrogenotrophs may be limited by the methodological approach, as the metabolic potential to oxidize H_2 cannot be predicted from 16S rRNA sequences (Brazelton et al., 2012, 2022). Accordingly, metagenomic surveys show that many organisms in all types of serpentinite-hosted systems feature [FeFe]- and [NiFe]-hydrogenases (Brazelton et al., 2012; Mei et al., 2016; Kraus et al., 2021; Lecoeuvre et al., 2021; Frouin et al., 2022) (Table 1).

Another potential electron source in serpentinizing systems is constituted by compounds not directly created by serpentinization such as reduced sulfur species (Sabuda et al., 2020; Trutschel et al., 2022) and CO (Brazelton et al., 2012; Morrill et al., 2014; Fones et al., 2019) (Table 1). While the oxidation potential of CO is very low, the ability to use this energy source may provide a valuable ecological advantage. In surface exposed serpentinization-influenced waters, light constitutes an additional energy source used by cyanobacterial phototrophs (e.g., Kamran et al., 2020) (Table 1).

While serpentinization provides an abundance of electron donors, the availability of terminal electron acceptors is limited, especially in terrestrial serpentinizing systems, and mainly derived from the ambient environment (Figure 1A). Oxygen represents a very potent electron acceptor on the chimney or travertine surface. With increasing proximity to the reduced hydrothermal endmember, however, the availability of oxygen or alternative electron acceptors sharply decreases. The microbial community near the oxic-anoxic interphase may use nitrate (Frouin et al., 2022), even though data on nitrate reduction is scarce. In addition, organisms from the Troodos and The Cedars ophiolites have been shown to reduce metals such as iron or magnetite (Rizoulis et al., 2016; Rowe et al., 2017) (Table 1). Towards the anoxic interior of the hydrothermal carbonate chimneys or in deep ophiolite groundwaters, sulfate reduction is a dominant metabolic strategy in all types of serpentinite-hosted systems (Brazelton et al., 2006; Tiago and Veríssimo, 2013; Postec et al., 2015; Glombitza et al., 2021) (Table 1 and Figure 1B).

To deal with electron acceptor limitation, many microbes also perform fermentation of sugars, simple organic acids and amino

TABLE 1 Taxonomic survey for critical metabolic functions in all types of serpentinite-hosted environments, specifying the methodological approach including metagenome-assembled genomes (MAGs) and single-cell amplified genomes (SAGs).

Metabolism	Taxon	Site	Method	References
Hydrogen oxidation	Bacteria_Pseudomonadota_Alphaproteobacteria[1]	The Cedars (shallow waters)	MAGs	Suzuki et al. (2017)
	Bacteria_Pseudomonadota_Gammaproteobacteria	The Cedars (shallow waters)	MAGs; 16S rRNA	Suzuki et al. (2013, 2017)
	Bacteria_Pseudomonadota_Gammaproteobacteria_Betaproteobacteriales (formerly Betaproteobacteria)[2]	The Cedars (shallow waters)	MAGs	Suzuki et al. (2017)
	Bacteria_Pseudomonadota_Gammaproteobacteria_Burkholderiales_Burkholderiaceae_ Hydrogenophaga[3]	The Tablelands, Lost City (oxic/anoxic interface); Voltri; The Cedars (shallow waters); Prony Bay; Zambales	MAGs; 16S rRNA	Brazelton et al. (2012, 2017), Suzuki et al. (2013), Frouin et al. (2018), Woycheese et al. (2015)
	Bacteria_Pseudomonadota_Gammaproteobacteria_Burkholderiales_Burkholderiaceae_ Serpentinimonas[4]	Voltri; The Cedars (shallow waters/non-specified)	16S rRNA; cultivation	Quéméneur et al. (2015), Suzuki et al. (2014, 2017), Brazelton et al. (2017), Bird et al. (2021)
	Bacteria_Pseudomonadota_Gammaproteobacteria_Burkholderiales_Burkholderiaceae_ Serpentinimonas_S. raichei[5]	The Cedars	Cultivation	Bird et al. (2021)
	Bacteria_Pseudomonadota_Gammaproteobacteria_Burkholderiales_Burkholderiaceae_ Serpentinimonas_S. barnesii[6]	The Cedars	Cultivation	Bird et al. (2021)
	Bacteria_Pseudomonadota_Gammaproteobacteria_Burkholderiales_Burkholderiaceae_ Serpentinimonas_S. maccroryi[7]	The Cedars	Cultivation	Bird et al. (2021)
	Bacteria_Pseudomonadota_Gammaproteobacteria_Burkholderiales_Burkholderiaceae_ Cupriavidus_C. necator (formerly *Ralstonia eutropha*)[8]	The Tablelands, Lost City (oxic/anoxic interface)	MAGs	Brazelton et al. (2012)
	Bacteria_Former class Deltaproteobacteria	The Cedars (shallow waters)	MAGs; 16S rRNA	Suzuki et al. (2013, 2017)
	Bacteria_Desulfobacterota_Desulfovibrionia_Desulfovibrionales[9]	Voltri (deep subsurface)	MAGs	Brazelton et al. (2017)
	Bacteria_Desulfobacterota_Desulfovibrionia_Desulfovibrionales_Desulfonatronaceae_ Desulfonatronum[10]	Prony Bay	16S rRNA	Postec et al. (2015), Mei et al. (2016)
	Bacteria_BacillotaB_Desulfotomaculia_Desulfotomaculales_ Desulfotomaculaceae_ Desulfotomaculum_D. alkaliphilum[11]	Lost City	16S rRNA	Brazelton et al. (2006, 2010)
	Archaea_Methanobacteriota_Methanobacteria_Methanobacteriales_Methanobacteriaceae_ Methanobacterium_Lineage type I	Voltri; Samail (surface waters); Prony Bay	MAGs, SAGs, 14C labelling	Quéméneur et al. (2015, 2021, 2023), Fones et al. (2021)
Aerobic methane oxidation	Archaea_Methanobacteriota_Methanobacteria_Methanobacteriales_Methanobacteriaceae_ Methanobacterium_M. alkalithermotolerans strain DSM102889	La Crouen	Cultivation	Mei et al. (2022)
	Bacteria_Pseudomonadota_Gammaproteobacteria_Methylococcales_Methylococcaceae[12]	Voltri (shallow subsurface mixing zone)	16S rRNA, MAGs, 13C labelling	Brazelton et al. (2017)
	Bacteria_Pseudomonadota_Gammaproteobacteria_Methylococcales_Methylococcaceae_ Methylococcus	Samail	16S rRNA	Kraus et al. (2021)
	Bacteria_Pseudomonadota_Alphaproteobacteria_Rhizobiales_Beijerinckiaceae_ Methylosinus	Voltri	16S rRNA	Quéméneur et al. (2015)

(Continued)

10.3389/fmicb.2023.1197823

TABLE 1 (Continued)

Metabolism	Taxon	Site	Method	References
Methanogenesis/ anaerobic methane oxidation	Archaea_Halobacteriota_Methanomicrobia_Methanomicrobiales	Santa Elena	16S rRNA (MAGs)	Crespo-Medina et al. (2017)
	Archaea_Methanobacteriota_Methanobacteria_Methanobacteriales	Santa Elena; Voltri	16S rRNA (MAGs)	Crespo-Medina et al. (2017), Quéméneur et al. (2015)
	Archaea_Methanobacteriota_Methanobacteria_Methanobacteriales_Methanobacteriaceae[13]	Voltri (deep subsurface)	16S rRNA, MAGs, 13C labelling	Brazelton et al. (2017)
	Archaea_Methanobacteriota_Methanobacteria_Methanobacteriales_Methanobacteriaceae_ Methanobacterium	Samail (subsurface); Voltri; Zambales	16S rRNA; MAGs; SAGs; 13C labelling; 14C labelling	Kraus et al. (2021), Brazelton et al. (2017), Fones et al. (2021), Woycheese et al. (2015), Quéméneur et al. (2015)
	Archaea_Methanobacteriota_Methanobacteria_Methanobacteriales_Methanobacteriaceae_ Methanobacterium_M. alcaliphilum strain DSM3387	Del Puerto	16S rRNA	Blank et al. (2009)
	Archaea_Methanobacteriota_Methanobacteria_Methanobacteriales_Methanobacteriaceae_ Methanobacterium_M. alkalithermotolerans strain DSM102889	La Crouen	Cultivation	Mei et al. (2022)
	Archaea_Halobacteriota_Methanosarcinia_Methanosarcinales	Santa Elena; Voltri	16S rRNA (MAGs)	Crespo-Medina et al. (2017), Quéméneur et al. (2015), Suzuki et al. (2013)
	Archaea_Halobacteriota_Methanosarcinia_Methanosarcinales_LCMS phylotype[14]	Lost City (Brazelton et al. (2006): High-temperature); Prony Bay (intertidal and submarine); Old City	16S rRNA, MAGs; 13C labelling	Schrenk et al. (2004), Brazelton et al. (2006, 2011), Frouin et al. (2018), Lecoeuvre et al. (2021)
	Archaea_Halobacteriota_Methanosarcinia_Methanosarcinales_TCMS phylotype	The Cedars; Prony Bay (intertidal and submarine); Old City	16S rRNA, MAGs	Suzuki et al. (2013), Frouin et al. (2018), Lecoeuvre et al. (2021)
	Archaea_Halobacteriota_Syntropharchaeia_ANME-1	Lost City (low temperature); Santa Elena; Cabeço de Vide	16S rRNA (MAGs)	Brazelton et al. (2006), Crespo-Medina et al. (2017), Tiago and Veríssimo (2013)
Formate consumption	Bacteria_Pseudomonadota_Gammaproteobacteria_Methylococcales_Methylococcaceae[12]	Voltri (shallow subsurface mixing zone)	MAGs	Brazelton et al. (2017)
	Bacteria_Desulfobacterota_Desulfovibrionia_Desulfovibrionales[9]	Voltri (deep subsurface)	MAGs	Brazelton et al. (2017)
	Bacteria_Ca. Lithacetigena[15]	The Cedars, Hakuda Happo hot springs	MAGs	Nobu et al. (2022)
	Bacteria_Ca. Bipolaricaulota (OP1/MSBL6)[17]	Lost City	MAGs	Brazelton et al. (2022)
	Archaea_Methanobacteriota_Methanobacteria_Methanobacteriales_Methanobacteriaceae_ Methanobacterium_Lineage type II	Samail (subsurface)	MAGs, SAGs, 14C labelling	Fones et al. (2021)
Acetate consumption	Bacteria_Desulfobacterota_Desulfovibrionia_Desulfovibrionales[9]	Voltri (deep subsurface)	MAGs	Brazelton et al. (2017)
	Archaea_Halobacteriota_Methanosarcinia_Methanosarcinales_LCMS phylotype[14]	Lost City	MAGs	Brazelton et al. (2011)

(Continued)

10.3389/fmicb.2023.1197823

TABLE 1 (Continued)

Metabolism	Taxon	Site	Method	References
Glycine consumption	Bacteria_Ca. Lithacetigena[15]	The Cedars, Hakuda Happo hot springs	MAGs	Nobu et al. (2022)
Calcium carbonate consumption	Bacteria_Pseudomonadota_Gammaproteobacteria_Burkholderiales_Burkholderiaceae_Serpentinimonas[4]	The Cedars	Cultivation	Suzuki et al. (2014)
	Bacteria_Pseudomonadota_Gammaproteobacteria_Burkholderiales_Burkholderiaceae_Serpentinimonas_S. raichei[5]	The Cedars	Cultivation	Bird et al. (2021)
	Bacteria_Pseudomonadota_Gammaproteobacteria_Burkholderiales_Burkholderiaceae_Serpentinimonas_S. barnesii[6]	The Cedars	Cultivation	Bird et al. (2021)
	Bacteria_Pseudomonadota_Gammaproteobacteria_Burkholderiales_Burkholderiaceae_Serpentinimonas_S. maccroryi[7]	The Cedars	Cultivation	Bird et al. (2021)
	Bacteria_ NPL-UPA2 clade[18]	The Cedars, Prony Bay, Lost City	MAGs	Suzuki et al. (2018), Brazelton et al. (2022)
	Bacteria_Ca. Bipolaricaulota (OP1/MSBL6)[17]	Lost City	MAGs	Brazelton et al. (2022)
CO oxidation	Bacteria_Pseudomonadota_Gammaproteobacteria_Burkholderiales_Burkholderiaceae_Hydrogenophaga[3]	The Tablelands, Lost City (oxic/anoxic interface)	MAGs; 16S rRNA, 13C labelling	Brazelton et al. (2012), Morrill et al. (2014)
	Bacteria_Pseudomonadota_Gammaproteobacteria_Burkholderiales_Burkholderiaceae_Cupriavidus_C. necator (formerly *Ralstonia eutropha*)[8]	The Tablelands, Lost City (oxic/anoxic interface)	MAGs	Brazelton et al. (2012)
	Bacteria_Actinobacteriota_Ca. Hakubanella thermoalkaliphilus	Hakuda Happo hot springs	16S rRNA, SAGs	Merino et al. (2020)
	Archaea_Hadesarchaea (formerly SAGMEG)	Prony Bay	16S rRNA	Postec et al. (2015)
Sulfide/sulfur oxidation	Bacteria_Pseudomonadota_Gammaproteobacteria_Betaproteobacteriales (formerly Betaproteobacteria)[2]	Cabeço de Vide	16sS rRNA (DGGE)	Tiago and Veríssimo (2013)
	Bacteria_Pseudomonadota_Gammaproteobacteria_Thiomicrospirales_Thiomicrospiraceae_Hydrogenovibrio (formerly Thiomicrospira)	Lost City (low temperature)	16S rRNA	Brazelton et al. (2006)
	Bacteria_Pseudomonadota_Alphaproteobacteria_Rhodobacterales_Rhodobacteraceae	Ney Springs	MAGs, Cultivation	Trutschel et al. (2022)
	Bacteria_Pseudomonadota_Gammaproteobacteria_Pseudomonadales_Halomonadaceae_Halomonas	Ney Springs	MAGs, Cultivation	Trutschel et al. (2022)

(Continued)

10.3389/fmicb.2023.1197823

TABLE 1 (Continued)

Metabolism	Taxon	Site	Method	References
Sulfate reduction	Bacteria_BacillotaA_Clostridia[16]	Cabeço de Vide; The Cedars (deep subsurface)	16S rRNA (DGGE)	Tiago and Veríssimo (2013), Suzuki et al. (2013)
	Bacteria_BacillotaB_Desulfotomaculia_Desulfotomaculales_ Desulfotomaculaceae_ Desulfotomaculum_D. alkaliphilum[11]	Lost City	16S rRNA	Brazelton et al. (2006, 2010)
	Bacteria_BacillotaD_Dethiobacteria_Dethiobacterales_Dethiobacteraceae_Dethiobacter	The Tablelands, The Cedars, Cabeço de Vide, Prony Bay, Zambales		Brazelton et al. (2012), Suzuki et al. (2013), Tiago and Veríssimo (2013), Postec et al. (2015), Woycheese et al. (2015), Crespo-Medina et al. (2017), Trutschel et al. (2022), Twing et al. (2017)
	Bacteria_Desulfobacterota_Desulfovibrionia_Desulfovibrionales[9]	Voltri	MAGs	Brazelton et al. (2017)
	Bacteria_Desulfobacterota_Desulfovibrionia_Desulfovibrionales_Desulfonatronaceae_ Desulfonatronum[10]	Prony Bay	16S rRNA	Postec et al. (2015), Mei et al. (2016)
	Bacteria_Nitrospirota_Thermodesulfovibrionia_Thermodesulfovibrionales_ Thermodesulfovibrionaceae	Samail (subsurface fluids)	16S rRNA	Rempfert et al. (2017)
Nitrogen fixation	Bacteria_Pseudomonadota_Alphaproteobacteria_Azospirillales_Azospirillaceae_ Azospirillum	Voltri	16S rRNA	Quéméneur et al. (2015)
	Archaea_Methanobacteriota_Methanobacteria_Methanobacteriales_Methanobacteriaceae[13]	Voltri (deep subsurface)	16S rRNA, MAGs	Brazelton et al. (2017)
	Archaea_Halobacteriota_Methanosarcinia_Methanosarcinales_LCMS phylotype[14]	Lost City	MAGs	Brazelton et al. (2011)
Phosphonate catabolism	Bacteria_Proteobacteria_Alphaproteobacteria[1]	Prony Bay, Lost City	MAGs	Frouin et al. (2022)
	Bacteria_Proteobacteria_Gammaproteobacteria_Betaproteobacteriales (formerly Betaproteobacteria)[2]	Coast Range, Voltri, Santa Elena, Cabeço de Vide	MAGs	Frouin et al. (2022)
	Bacteria_ BacillotaA _Clostridia[16]	Prony Bay, Lost City	MAGs	Frouin et al. (2022)
Acetogenesis	Bacteria_Chloroflexota (formerly Chloroflexi)	The Cedars (deep subsurface); Prony Bay (submarine)	MAGs; 16S rRNA	Suzuki et al. (2013, 2017), Frouin et al. (2018)
	Bacteria_ NPL-UPA2 clade[18]	The Cedars; Prony Bay	16S rRNA; MAGs	Postec et al. (2015), Mei et al. (2016), Suzuki et al. (2018)
	Bacteria_BacillotaD_Dethiobacteria_Dethiobacterales_Dethiobacteraceae_Dethiobacter_D. alkaliphilus	The Cedars; Prony Bay; Cabeço de Vide	16S rRNA	Postec et al. (2015), Mei et al. (2016), Suzuki et al. (2013), Tiago and Veríssimo (2013)
	Bacteria_Ca. Bipolaricaulota (OP1/MSBL6)[17]	Samail (subsurface fluids)	MAGs	Colman et al. (2022)

(Continued)

10.3389/fmicb.2023.1197823

TABLE 1 (Continued)

Metabolism	Taxon	Site	Method	References
Fermentation	Bacteria_ BacillotaA _Clostridia	The Tablelands, Lost City	MAGs	Brazelton et al. (2012)
	Bacteria_ BacillotaA _Clostridia_Thermoanaerobacterales_Candidate Division OD1	The Cedars (deep subsurface); Voltri	16S rRNA, MAGs, 13C labelling	Suzuki et al. (2013, 2017), Brazelton et al. (2017)
	Bacteria_ BacillotaA _Clostridia_Lachnospirales_Vallitaleaceae_Vallitalea_V. pronyensis	Prony Bay	Cultivation	Ben Aissa et al. (2014), Mei et al. (2014)
	Bacteria_ BacillotaA _Clostridia_Peptostreptococcales_Natronincolaceae_Alkaliphilus_A. hydrothermalis	Prony Bay	Cultivation	Ben Aissa et al. (2015)
	Bacteria_ BacillotaA _Clostridia_Peptostreptococcales_Natronincolaceae_Alkaliphilus_A. serpentinus	Prony Bay	Cultivation	Postec et al. (2021)
	Bacteria_ BacillotaA _Clostridia_Peptostreptococcales_Natronincolaceae_Alkaliphilus_A. pronyensis	Prony Bay	Cultivation	Postec et al. (2021)
	Bacteria_ BacillotaA _Clostridia_Peptostreptococcales_Natronincolaceae_Serpentinicella_S. alkaliphila	Prony Bay	Cultivation	Mei et al. (2016)
	Bacteria_ BacillotaA _Clostridia_Peptostreptococcales_Peptostreptococcaceae_ Acetoanaerobium_A. pronyense	Prony Bay	Cultivation	Bes et al. (2015)
	Bacteria_Bacteroidetes_Bacteroidia_Bacteroidales_ML635J-40	Voltri	16S rRNA, MAGs, 13C labelling	Brazelton et al. (2017)
	Bacteria_BacillotaA_Clostridia_Peptostreptococcales_Peptostreptococcaceae	Ney Springs	MAGs, 16S rRNA	Trutschel et al. (2022)
	Bacteria_BacillotaA_Clostridia_Peptostreptococcales_Tindalliaceae_Tindallia	Ney Springs	MAGs, 16S rRNA	Trutschel et al. (2022)
	Bacteria_BacillotaB_Desulfotomaculia_Desulfotomaculales_ Desulfotomaculaceae_ Desulfotomaculum	The Tablelands, Lost City	MAGs	Brazelton et al. (2012)
	Bacteria_Bacilli_Bacillota_Erysipelotrichales_Erysipelotrichaceae	The Tablelands	MAGs	Brazelton et al. (2012)
Iron reduction	Bacteria_ BacillotaA _Clostridia_Peptostreptococcales_Natronincolaceae_Alkaliphilus	Troodos	Cultivation	Rizoulis et al. (2016)
	Bacteria_Bacillota_Bacilli_Paenibacillales_Paenibacillaceae_Paenibacillus	The Cedars	Cultivation	Rowe et al. (2017)
Photosynthesis	Bacteria_Cyanobacteria_Cyanobacteriia_Leptolyngbyales_Leptolyngbyaceae_Leptolyngbya	Voltri (surface); Del Puerto	16S rRNA	Kamran et al. (2020), Blank et al. (2009)
	Bacteria_Cyanobacteria_Cyanobacteriia_Synechococcales_Synechococcaceae_ Synechococcus	Prony Bay	16S rRNA	Mei et al. (2016)

Taxa appearing in several metabolic groups on the same taxonomic level are assigned with superscript numbers. The taxonomy is based on the Genome Taxonomy Database (GTDB Release 214).

10.3389/fmicb.2023.1197823

acids, including Stickland type reactions (Barker, 1981; Postec et al., 2021). Therefore, a large proportion of the anaerobic serpentinite-hosted community may not feature a *bona fide* electron transport chain with cytochromes or quinones (Table 1). Genomic analysis suggests that many serpentinite-hosted fermenters conserve energy by substrate-level phosphorylation (e.g., in glycolysis), or via bifurcative-confurcative [FeFe] H_2-producing hydrogenases, which balance the reducing equivalents NADH and ferredoxin produced by fermentation (Westphal et al., 2018). This is often associated with the Rnf complex, a respiratory enzyme that catalyzes the oxidation of reduced ferredoxin to the reduction of NAD^+. The negative free energy change of this reaction is used to generate a transmembrane H^+ or Na^+ gradient (Westphal et al., 2018). This system can be considered a primitive respiratory mechanism where the terminal electron acceptor is H^+ (Buckel and Thauer, 2018).

3.2. The challenge of coping with nutrient limitation

Next to maintaining energy-yielding reactions, microorganisms in serpentinite-hosted environments must cope with severe nutrient limitation resulting from the decreased solubility of essential macronutrients at high pH (McCollom and Seewald, 2013; Schrenk et al., 2013). Especially relevant for the metabolic functioning of the community are the carbon, nitrogen, and phosphorous sources for primary production (Figure 1A).

3.2.1. Carbon sources and carbon fixation

One of the most significant issues regarding primary production in serpentinite-hosted environments is the absence of DIC, which precipitates as calcium carbonate in hyperalkaline conditions. While calcium carbonate is mostly insoluble and thus unavailable as a carbon source, it has nevertheless been shown to support the growth of some serpentinite-hosted microorganisms. This might be the result of local redissolution into bicarbonate catalyzed by the carbonic anhydrase (Suzuki et al., 2014; Fones et al., 2019; Bird et al., 2021) (Table 1). Alternatively, small organic molecules may serve as primary source of carbon. These include organic acids such as formate and acetate produced in Fischer-Tropsch and Sabatier-type reactions (Barbier et al., 2020; Fones et al., 2021) or via acetogenesis and fermentation (Kohl et al., 2016; Suzuki et al., 2017), as well as amino acids such as glycine produced in Strecker synthesis (Ménez et al., 2018; Nobu et al., 2022) (Figure 1A). The abiotic origin of those organic carbon sources tackles the definition of heterotrophy, which normally refers to the consumption of organic compounds derived from organic sources (Schönheit et al., 2016).

While bicarbonate, formate, acetate, and glycine have been shown to support the growth of microorganisms associated with serpentinization, their metabolic route remains hypothetical. Transferred across the cell membrane via specialized transporters, formate can be oxidized to CO_2 via the formate dehydrogenase in the pH-neutral cytoplasm (Brazelton et al., 2022). Likewise, bicarbonate can be reduced to CO_2 via the carbonic anhydrase (Suzuki et al., 2014; Bird et al., 2021). The produced CO_2 is subsequently introduced to different carbon fixation pathways yielding acetyl-CoA. In serpentinite-hosted environments, the Wood-Ljungdahl pathway, reverse tricarboxylic acid cycle, and Calvin-Benson-Bassham cycle have been confirmed (Seyler et al., 2020). Based on a recent study expanding the phylogenetic range of most carbon fixation pathways, the 3-hydroxypropionate bi-cycle, dicarboxylate/4-hydroxybutyrate cycle, and 3-hydroxypropionate/4-hydroxybutyrate cycle might also be employed (Garritano et al., 2022). Contrary to formate and bicarbonate, glycine can be directly transformed into acetyl-phosphate and subsequently acetyl-coA via the lesser known reductive glycine pathway (Sánchez-Andrea et al., 2020). Genes encoding the glycine reductase are found in metagenomes from Lost City, The Cedars, and the Japanese Hakuba Happo hot springs (Brazelton et al., 2022; Nobu et al., 2022). Also acetate can be directly transformed into acetyl-phosphate and acetyl-CoA, rendering its metabolic route less complex (Rose et al., 1954).

3.2.2. Sources of other nutrients

Serpentinization also decreases the solubility of other macronutrients essential for microbial growth. Inorganic phosphorous is severely limited in serpentinizing environments because it is scavenged by the mineral brucite (Schrenk et al., 2013). A metagenomic survey revealed the high occurrence of genes involved in phosphonate catabolism in serpentinizing sites, suggesting that the microbial community might use phosphonates as an alternative phosphorous source (Frouin et al., 2022). The catabolism of methylphosphonate, the most commonly available phosphonate species in marine environments, may additionally contribute to the global carbon and energy budget in these ecosystems by releasing CH_4 (Frouin et al., 2022). On the contrary, the availability of nitrogen in serpentinizing environments remains controversial. While some authors suggest that concentrations are low (Schrenk et al., 2013), others propose that N_2 and nitrate are readily available to the serpentinite-hosted community (Lang et al., 2013; Rempfert et al., 2023). Potential nitrogen limitation may be alleviated by the fixation of N_2 derived from the endmember fluids or ambient seawater (Morrill et al., 2013; Monnin et al., 2014) (Figure 1A). While a recent study found the associated genetic marker *nifH* in 10 different serpentinite-hosted systems, its overall abundance was low (Frouin et al., 2022).

3.3. Metabolic links to the emergence of life

The biochemical characteristics of serpentinite-hosted ecosystems reinforce the presumed link between serpentinization and the beginnings of life. Serpentinization is an ancient process which likely occurred on early Earth (Russell et al., 2010). The abiotic production of organic acids associated with serpentinization is for instance supported by isotopic signatures (McCollom and Seewald, 2013). Likewise, amino acids such as glycine may be formed abiotically, which is especially interesting in prebiotic chemistry (Aubrey et al., 2009; Ménez et al., 2018). The metabolic use of these compounds is linked to very deep-branching functions, such as the reductive tricarboxylic acid cycle and the Wood-Ljungdahl pathway, which are likely the most ancient carbon fixation pathways on Earth (Sumi and Harada, 2021). Another primordial function preserved in serpentinizing environments is CO oxidation. CO is not only one of the most ancient energy sources exploited in metabolism but is also

suggested to have played a key role in several critical prebiotic reactions (King and Weber, 2007). It may thus constitute a direct link between abiotic and biotic chemistry.

4. Diversity of identified metabolic key players

The specific metabolic challenges posed by serpentinization suggest the presence of specialized taxonomic groups playing an important role in the trophic network. It might be possible that such "core" taxa are relevant in a wide variety of serpentinizing environments, even though the overall community structure can vary significantly in space and time (Suzuki et al., 2013; Postec et al., 2015; Fones et al., 2019; Brazelton et al., 2022; Trutschel et al., 2022).

The community of H_2 oxidizers appears to be dominated by Gammaproteobacteria (Table 1). This includes a major proportion of *Serpentinimonas* (formerly grouped under Betaproteobacteria). *Serpentinimonas* is one of the taxa most commonly associated with serpentinization, and represented by some of the few available isolates from serpentinite-hosted ecosystems (Suzuki et al., 2014; Bird et al., 2021). So far, all of those isolated strains originate from The Cedars. Still, 16S rRNA analysis confirms the presence of *Serpentinimonas* and its sister genus *Hydrogenophaga* in other terrestrial systems, as well as in Prony Bay and Lost City (e.g., Brazelton et al., 2012; Quéméneur et al., 2015; Woycheese et al., 2015; Frouin et al., 2018) (Table 1).

While aerobic methane oxidation is mostly performed by the bacterial *Methylococcales* (Brazelton et al., 2017; Kraus et al., 2021), anaerobic methanotrophy and methanogenesis feature exclusively archaea (Table 1). Hydrogenotrophic methanogens belonging to *Methanobacteriales* are often detected in serpentinite-hosted terrestrial ecosystems (Woycheese et al., 2015; Brazelton et al., 2017; Kraus et al., 2021; Quéméneur et al., 2021, 2023; Mei et al., 2022). In addition, there is a subgroup of *Methanosarcinales* which is probably endemic to serpentinizing environments and includes two distinct phylotypes (e.g., Schrenk et al., 2004; Brazelton et al., 2010; Suzuki et al., 2013). Next to their systems of origin, The Cedars *Methanosarcinales* (TCMS) and Lost City *Methanosarcinales* (LCMS) have been observed in Prony Bay (Frouin et al., 2018) and Old City (Lecoeuvre et al., 2021) (Table 1). However, attempts to culture them have been unsuccessful so far.

The fermenting community seems almost entirely dominated by *Clostridia* (Table 1), of which several novel species have been isolated from Prony Bay (Ben Aissa et al., 2014, 2015; Mei et al., 2014; Bes et al., 2015; Postec et al., 2021).

Other energy yielding metabolic strategies including CO oxidation, sulfur oxidation and sulfate reduction are performed by a broader diversity of taxonomic groups (Table 1). Notably, the community of sulfate reducers includes *Desulfovibrionales* and *Dethiobacter* species, which can be very abundant in serpentinizing environments (Brazelton et al., 2012; Suzuki et al., 2013; Tiago and Veríssimo, 2013; Postec et al., 2015; Woycheese et al., 2015; Mei et al., 2016) (Table 1).

Regarding carbon uptake, it might be especially interesting to further investigate certain candidate phyla that occur in various serpentinizing systems. For example, *Ca. Bipolaricaulota* can use bicarbonate and formate (Brazelton et al., 2022) and plays a role in acetogenesis (Colman et al., 2022). Likewise, *Ca.* NPL-UPA2 grows on bicarbonate (Brazelton et al., 2022) and performs acetogenesis via the Wood-Ljungdahl pathway (Suzuki et al., 2018) (Table 1). The Wood-Ljungdahl pathway is also employed by *Ca. Hakubanella thermoalkaliphilus*, a novel Actinobacteriota from the Hakuba Happo hot springs serpentinizing system (Merino et al., 2020). Finally, *Ca.* Lithacetigena was recently shown to perform glycine reduction (Nobu et al., 2022). These candidate phyla might play an important role in the trophic chain by supplying fixed carbon to the community.

5. Methodological shortcomings and future challenges

While several critical metabolic strategies and taxonomic groups could be identified, the scope of their distribution across serpentinizing ecosystems remains unclear due to methodological biases and shortcomings. Firstly, continental sites have been studied much more extensively than marine ones (Table 1). Our understanding of the latter is almost entirely based on the famous Lost City (Table 1) and most recently Old City (Lecoeuvre et al., 2021), which limits the generalization of findings on marine serpentinizing systems and reduces the meaningfulness of comparison with continental ones. This issue emphasizes the interest of the shallow marine transition field of Prony Bay. Its common characteristics with continental and marine sites may help establish the core metabolic properties of serpentinite-hosted ecosystems. In addition, the study of such shallow fields is facilitated by their geographical accessibility.

Another factor introducing bias is the methodological approach. Most studies rely on metabarcoding and metagenomic techniques (Table 1), which are strongly dependent on the scope of available reference databases. Moreover, the presence of a functional gene does not necessarily signify its activity. However, confirmation of gene expression is rare, notably due to technical difficulties in obtaining quality metatranscriptomes from such environments (Table 1). In addition, there is a lack of experimental evidence complementing bioinformatic hypotheses. Studies attempting to bridge this gap include activity measurements using ^{13}C and ^{14}C labeled substates in microcosms (Brazelton et al., 2011, 2017; Morrill et al., 2014; Fones et al., 2021), as well as isolation of *Serpentinimonas* and *Clostridia* species from cultures (e.g., Suzuki et al., 2014; Postec et al., 2021) (Table 1). Their small number is probably also associated with technical difficulties, including the cultivation of recalcitrant microorganisms such as obligate anaerobic chemolithoautotrophs. While combined omics approaches can provide valuable results, critical metabolic groups will eventually need to be cultivated to confirm their functional role in the ecosystem. This may be facilitated by implementing more sophisticated culture platforms to mimic the conditions associated with serpentinization in the laboratory.

6. Conclusion

Serpentinite-hosted environments are inhabited by microbial communities that cope with energetic challenges and severe nutrient limitation. It can be assumed that a significant proportion of those microorganisms yield energy from H_2 oxidation with electron acceptors derived from external sources or CO_2 degassed from mantle rocks. Calcium carbonate can serve as inorganic carbon source, and

formate, acetate and glycine as organic carbon sources for primary production. Bicarbonate, formate, and glycine may be fixed via different carbon fixation pathways such as the Wood-Ljungdahl pathway, the reverse tricarboxylic acid and Calvin-Benson-Bassham cycles and the reductive glycine pathway. Moreover, the microbial communities might cope with nitrogen and phosphorous limitation by fixing N_2 and breaking down phosphonates. The analysis of functional genes suggests that taxa such as *Gammaproteobacteria*, *Desulfovibrionales*, *Clostridia* and several candidate phyla play a crucial role in the trophic network and that the genera *Serpentinimonas*, *Hydrogenophaga*, and *Methanobacterium* as well as uncultivated *Methanosarcinales*, are characteristic for serpentinizing environments. However, the scope of research on serpentinite-hosted ecosystems needs to be broadened by including a greater diversity of marine and shallow transition sites. In addition, experimental evidence is needed to confirm the metabolic activity of hypothesized key players. A technological advancement of the methodological approach might not only contribute to the understanding of present serpentinite-hosted ecosystems, but also provide insights into the beginning of life on Earth and potentially elsewhere.

Author contributions

GE, AP, and RP: conceptualization. AL and MQ: validation. RP: investigation and writing of original draft. AL, MQ, AP, GE, and RP: review and edit of original draft. GE and AP: supervision. GE: project administration. All authors contributed to the article and approved the submitted version.

Funding

This project was financially supported by the ANR MICROPRONY (N°19-CE02-0020-02), the French Institute of Research for Development (IRD), and a Ph.D. fellowship granted to RP by the Aix-Marseille University's Doctoral School "Sciences de l'Environnement" (ED 251).

Acknowledgments

The authors thank all project partners, including MICROPRONY.

Conflict of interest

The authors declare that the research was conducted in the absence of any commercial or financial relationships that could be construed as a potential conflict of interest.

Publisher's note

References

Albers, E., Bach, W., Pérez-Gussinyé, M., McCammon, C., and Frederichs, T. (2021). Serpentinization-driven H2 production from continental break-up to mid-ocean ridge spreading: unexpected high rates at the West Iberia margin. *Front. Earth Sci.* 9:673063. doi: 10.3389/feart.2021.673063

Aubrey, A. D., Cleaves, H. J., and Bada, J. L. (2009). The role of submarine hydrothermal systems in the synthesis of amino acids. *Orig. Life Evol. Biosph.* 39, 91–108. doi: 10.1007/s11084-008-9153-2

Barbier, S., Huang, F., Andreani, M., Tao, R., Hao, J., Eleish, A., et al. (2020). A review of H2, CH4, and hydrocarbon formation in experimental serpentinization using network analysis. *Front. Earth Sci.* 8:209. doi: 10.3389/feart.2020.00209

Barker, H. A. (1981). Amino acid degradation by anaerobic bacteria. *Annu. Rev. Biochem.* 50, 23–40. doi: 10.1146/annurev.bi.50.070181.000323

Barnes, I., O'Neil, J. R., and Trescases, J. J. (1978). Present day serpentinization in New Caledonia, Oman and Yugoslavia. *Geochim. Cosmochim. Acta* 42, 144–145. doi: 10.1016/0016-7037(78)90225-9

Ben Aissa, F., Postec, A., Erauso, G., Payri, C., Pelletier, B., Hamdi, M., et al. (2015). Characterization of Alkaliphilus hydrothermalis sp. nov., a novel alkaliphilic anaerobic bacterium, isolated from a carbonaceous chimney of the Prony hydrothermal field, New Caledonia. *Extremophiles* 19, 183–188. doi: 10.1007/s00792-014-0697-y

Ben Aissa, F., Postec, A., Erauso, G., Payri, C., Pelletier, B., Hamdi, M., et al. (2014). Vallitalea pronyensis sp. nov., isolated from a marine alkaline hydrothermal chimney. *Int. J. Syst. Evol. Microbiol.* 64, 1160–1165. doi: 10.1099/ijs.0.055756-0

Bes, M., Merrouch, M., Joseph, M., Quéméneur, M., Payri, C., Pelletier, B., et al. (2015). Acetoanaerobium pronyense sp. nov., an anaerobic alkaliphilic bacterium isolated from a carbonate chimney of the Prony hydrothermal field (New Caledonia). *Int. J. Syst. Evol. Microbiol.* 65, 2574–2580. doi: 10.1099/ijs.0.000307

Bird, L. J., Kuenen, J. G., Osburn, M. R., Tomioka, N., Ishii, S., Barr, C., et al. (2021). Serpentinimonas gen. Nov., Serpentinimonas raichei sp. nov., Serpentinimonas barnesii sp. nov. and Serpentinimonas maccroryi sp. nov., hyperalkaliphilic and facultative autotrophic bacteria isolated from terrestrial serpentinizing springs. *Int. J. Syst. Evol. Microbiol.* 71:004945. doi: 10.1099/ijsem.0.004945

Blank, J. G., Green, S. J., Blake, D., Valley, J. W., Kita, N. T., Treiman, A., et al. (2009). An alkaline spring system within the Del Puerto ophiolite (California, USA): a Mars analog site. *Planet. Space Sci.* 57, 533–540. doi: 10.1016/j.pss.2008.11.018

Boyd, E. S., Schut, G. J., Peters, J. W., and Adams, M. W. W. (2014). Hydrogen metabolism and the evolution of biological respiration: two separate families of enzymes that oxidize hydrogen and also produce it arose through convergent evolution. *Microbe Mag.* 9, 361–367. doi: 10.1128/microbe.9.361.1

Brazelton, W. J., Ludwig, K. A., Sogin, M. L., Andreishcheva, E. N., Kelley, D. S., Shen, C.-C., et al. (2010). Archaea and bacteria with surprising microdiversity show shifts in dominance over 1,000-year time scales in hydrothermal chimneys. *Proc. Natl. Acad. Sci. USA* 107, 1612–1617. doi: 10.1073/pnas.0905369107

Brazelton, W. J., McGonigle, J. M., Motamedi, S., Pendleton, H. L., Twing, K. I., Miller, B. C., et al. (2022). Metabolic strategies shared by basement residents of the Lost City hydrothermal field. *Appl. Environ. Microbiol.* 88:e0092922. doi: 10.1128/aem.00929-22

Brazelton, W. J., Mehta, M. P., Kelley, D. S., and Baross, J. A. (2011). Physiological differentiation within a single-species biofilm fueled by serpentinization. *mBio* 2, e00127–e00111. doi: 10.1128/mBio.00127-11

Brazelton, W. J., Morrill, P. L., Szponar, N., and Schrenk, M. O. (2013). Bacterial communities associated with subsurface geochemical processes in continental serpentinite springs. *Appl. Environ. Microbiol.* 79, 3906–3916. doi: 10.1128/AEM.00330-13

Brazelton, W. J., Nelson, B., and Schrenk, M. O. (2012). Metagenomic evidence for H2 oxidation and H2 production by serpentinite-hosted subsurface microbial communities. *Front. Microbiol.* 2:268. doi: 10.3389/fmicb.2011.00268

Brazelton, W. J., Schrenk, M. O., Kelley, D. S., and Baross, J. A. (2006). Methane- and sulfur-metabolizing microbial communities dominate the Lost City hydrothermal field ecosystem. *Appl. Environ. Microbiol.* 72, 6257–6270. doi: 10.1128/AEM.00574-06

Brazelton, W. J., Thornton, C. N., Hyer, A., Twing, K. I., Longino, A. A., Lang, S. Q., et al. (2017). Metagenomic identification of active methanogens and methanotrophs in serpentinite springs of the Voltri massif, Italy. *PeerJ* 5:e2945. doi: 10.7717/peerj.2945

Buckel, W., and Thauer, R. K. (2018). Flavin-based electron bifurcation, ferredoxin, flavodoxin, and anaerobic respiration with protons (Ech) or NAD+ (Rnf) as electron acceptors: a historical review. *Front. Microbiol.* 9:401. doi: 10.3389/fmicb.2018.00401

Colman, D. R., Kraus, E. A., Thieringer, P. H., Rempfert, K., Templeton, A. S., Spear, J. R., et al. (2022). Deep-branching acetogens in serpentinized subsurface fluids of Oman. *Proc. Natl. Acad. Sci. USA* 119:e2206845119. doi: 10.1073/pnas.2206845119

Crespo-Medina, M., Twing, K. I., Sánchez-Murillo, R., Brazelton, W. J., McCollom, T. M., and Schrenk, M. O. (2017). Methane dynamics in a tropical serpentinizing environment: the Santa Elena ophiolite, Costa Rica. *Front. Microbiol.* 8:916. doi: 10.3389/fmicb.2017.00916

Daae, F. L., Økland, I., Dahle, H., Jørgensen, S. L., Thorseth, I. H., and Pedersen, R. B. (2013). Microbial life associated with low-temperature alteration of ultramafic rocks in the Leka ophiolite complex. *Geobiology* 11, 318–339. doi: 10.1111/gbi.12035

Etiope, G., Schoell, M., and Hosgörmez, H. (2011). Abiotic methane flux from the Chimaera seep and Tekirova ophiolites (Turkey): understanding gas exhalation from low temperature serpentinization and implications for Mars. *Earth Planet. Sci. Lett.* 310, 96–104. doi: 10.1016/j.epsl.2011.08.001

Fabri, M.-C., Bargain, A., Briand, P., Gebruk, A., Fouquet, Y., Morineaux, M., et al. (2011). The hydrothermal vent community of a new deep-sea field, Ashadze-1, 12°58′N on the mid-Atlantic ridge. *J. Mar. Biol. Assoc. U. K.* 91, 1–13. doi: 10.1017/S0025315410000731

Flores, G. E., Campbell, J. H., Kirshtein, J. D., Meneghin, J., Podar, M., Steinberg, J. I., et al. (2011). Microbial community structure of hydrothermal deposits from geochemically different vent fields along the mid-Atlantic ridge: microbial communities of hydrothermal vent deposits. *Environ. Microbiol.* 13, 2158–2171. doi: 10.1111/j.1462-2920.2011.02463.x

Fones, E. M., Colman, D. R., Kraus, E. A., Nothaft, D. B., Poudel, S., Rempfert, K. R., et al. (2019). Physiological adaptations to serpentinization in the Samail ophiolite, Oman. *ISME J.* 13, 1750–1762. doi: 10.1038/s41396-019-0391-2

Fones, E. M., Colman, D. R., Kraus, E. A., Stepanauskas, R., Templeton, A. S., Spear, J. R., et al. (2021). Diversification of methanogens into hyperalkaline serpentinizing environments through adaptations to minimize oxidant limitation. *ISME J.* 15, 1121–1135. doi: 10.1038/s41396-020-00838-1

Frouin, E., Bes, M., Ollivier, B., Quéméneur, M., Postec, A., Debroas, D., et al. (2018). Diversity of rare and abundant prokaryotic phylotypes in the Prony hydrothermal field and comparison with other serpentinite-hosted ecosystems. *Front. Microbiol.* 9:102. doi: 10.3389/fmicb.2018.00102

Frouin, E., Lecoeuvre, A., Armougom, F., Schrenk, M. O., and Erauso, G. (2022). Comparative metagenomics highlight a widespread pathway involved in catabolism of phosphonates in marine and terrestrial serpentinizing. *Ecosystems* 7:e0032822. doi: 10.1128/msystems.00328-22

Früh-Green, G. L., Connolly, J. A. D., Plas, A., Kelley, D. S., and Grobéty, B. (2004). "Serpentinization of oceanic peridotites: implications for geochemical cycles and biological activity" in *Geophysical monograph series*. eds. W. S. D. Wilcock, E. F. DeLong, D. S. Kelley, J. A. Baross and S. Craig Cary (Washington, D C: American Geophysical Union), 119–136. doi: 10.1029/144GM08

Garritano, A. N., Song, W., and Thomas, T. (2022). Carbon fixation pathways across the bacterial and archaeal tree of life. *PNAS Nexus* 1:pgac226. doi: 10.1093/pnasnexus/pgac226

Glombitza, C., Putman, L. I., Rempfert, K. R., Kubo, M. D., Schrenk, M. O., Templeton, A. S., et al. (2021). Active microbial sulfate reduction in fluids of serpentinizing peridotites of the continental subsurface. *Commun. Earth Environ.* 2:84. doi: 10.1038/s43247-021-00157-z

Hicks, D. B., Liu, J., Fujisawa, M., and Krulwich, T. A. (2010). F1F0-ATP synthases of alkaliphilic bacteria: lessons from their adaptations. *Biochim. Biophys. Acta BBA – Bioenerg.* 1797, 1362–1377. doi: 10.1016/j.bbabio.2010.02.028

Ito, M., Morino, M., and Krulwich, T. A. (2017). Mrp antiporters have important roles in diverse bacteria and archaea. *Front. Microbiol.* 8:2325. doi: 10.3389/fmicb.2017.02325

Kamran, A., Sauter, K., Reimer, A., Wacker, T., Reitner, J., and Hoppert, M. (2020). Cyanobacterial mats in calcite-precipitating serpentinite-hosted alkaline springs of the Voltri Massif, Italy. *Microorganisms* 9:62. doi: 10.3390/microorganisms9010062

Kelley, D. S., Karson, J. A., Früh-Green, G. L., Yoerger, D. R., Shank, T. M., Butterfield, D. A., et al. (2005). A serpentinite-hosted ecosystem: the Lost City hydrothermal field. *Science* 307, 1428–1434. doi: 10.1126/science.1102556

King, G. M., and Weber, C. F. (2007). Distribution, diversity and ecology of aerobic CO-oxidizing bacteria. *Nat. Rev. Microbiol.* 5, 107–118. doi: 10.1038/nrmicro1595

Kohl, L., Cumming, E., Cox, A., Rietze, A., Morrissey, L., Lang, S. Q., et al. (2016). Exploring the metabolic potential of microbial communities in ultra-basic, reducing springs at the cedars, CA, USA: experimental evidence of microbial methanogenesis and heterotrophic acetogenesis: methanogenesis at the cedars. *J. Geophys. Res. Biogeosci.* 121, 1203–1220. doi: 10.1002/2015JG003233

Kraus, E. A., Nothaft, D., Stamps, B. W., Rempfert, K. R., Ellison, E. T., Matter, J. M., et al. (2021). Molecular evidence for an active microbial methane cycle in subsurface serpentinite-hosted groundwaters in the Samail ophiolite, Oman. *Appl. Environ. Microbiol.* 87, e02068–e02020. doi: 10.1128/AEM.02068-20

Krulwich, T. A., Sachs, G., and Padan, E. (2011). Molecular aspects of bacterial pH sensing and homeostasis. *Nat. Rev. Microbiol.* 9, 330–343. doi: 10.1038/nrmicro2549

Kuhns, M., Trifunović, D., Huber, H., and Müller, V. (2020). The Rnf complex is a Na+ coupled respiratory enzyme in a fermenting bacterium, Thermotoga maritima. *Commun. Biol.* 3:431. doi: 10.1038/s42003-020-01158-y

Lane, N. (2015). *The vital question: energy, evolution, and the origins of complex life*. New York City: WW Norton & Company.

Lang, S. Q., Früh-Green, G. L., Bernasconi, S. M., and Butterfield, D. A. (2013). Sources of organic nitrogen at the serpentinite-hosted Lost City hydrothermal field. *Geobiology* 11, 154–169. doi: 10.1111/gbi.12026

Launay, J., and Fontes, J.-C. (1985). Les sources thermales de Prony (Nouvelle Calédonie) et leurs précipités chimiques, exemple de formation de brucite primaire. *Geol. Fr.* 1, 83–100.

Lecoeuvre, A., Ménez, B., Cannat, M., Chavagnac, V., and Gérard, E. (2021). Microbial ecology of the newly discovered serpentinite-hosted Old City hydrothermal field (southwest Indian ridge). *ISME J.* 15, 818–832. doi: 10.1038/s41396-020-00816-7

McCollom, T. M., and Seewald, J. S. (2001). A reassessment of the potential for reduction of dissolved CO 2 to hydrocarbons during serpentinization of olivine. *Geochim. Cosmochim. Acta* 65, 3769–3778. doi: 10.1016/S0016-7037(01)00655-X

McCollom, T. M., and Seewald, J. S. (2013). Serpentinites, hydrogen, and life. *Elements* 9, 129–134. doi: 10.2113/gselements.9.2.129

Mei, N., Postec, A., Bartoli, M., Vandecasteele, C., Wils, L., Gil, L., et al. (2022). Methanobacterium alkalithermotolerans sp. nov., a novel alkaliphilic and hydrogen-utilizing methanogen isolated from an alkaline geothermal spring (La Crouen, New Caledonia). *Int. J. Syst. Evol. Microbiol.* 72. doi: 10.1099/ijsem.0.005554

Mei, N., Postec, A., Monnin, C., Pelletier, B., Payri, C. E., Ménez, B., et al. (2016). Metagenomic and PCR-based diversity surveys of [FeFe]-hydrogenases combined with isolation of alkaliphilic hydrogen-producing bacteria from the serpentinite-hosted Prony hydrothermal field, New Caledonia. *Front. Microbiol.* 7:1301. doi: 10.3389/fmicb.2016.01301

Mei, N., Zergane, N., Postec, A., Erauso, G., Ollier, A., Payri, C., et al. (2014). Fermentative hydrogen production by a new alkaliphilic Clostridium sp. (strain PROH2) isolated from a shallow submarine hydrothermal chimney in Prony Bay, New Caledonia. *Int. J. Hydrog. Energy* 39, 19465–19473. doi: 10.1016/j.ijhydene.2014.09.111

Ménez, B., Pisapia, C., Andreani, M., Jamme, F., Vanbellingen, Q. P., Brunelle, A., et al. (2018). Abiotic synthesis of amino acids in the recesses of the oceanic lithosphere. *Nature* 564, 59–63. doi: 10.1038/s41586-018-0684-z

Merino, N., Kawai, M., Boyd, E. S., Colman, D. R., McGlynn, S. E., Nealson, K. H., et al. (2020). Single-cell genomics of novel actinobacteria with the Wood-Ljungdahl pathway discovered in a serpentinizing system. *Front. Microbiol.* 11:1031. doi: 10.3389/fmicb.2020.01031

Monnin, C., Chavagnac, V., Boulart, C., Ménez, B., Gérard, M., Gérard, E., et al. (2014). Fluid chemistry of the low temperature hyperalkaline hydrothermal system of Prony Bay (New Caledonia). *Biogeosciences* 11, 5687–5706. doi: 10.5194/bg-11-5687-2014

Morrill, P. L., Brazelton, W. J., Kohl, L., Rietze, A., Miles, S. M., Kavanagh, H., et al. (2014). Investigations of potential microbial methanogenic and carbon monoxide utilization pathways in ultra-basic reducing springs associated with present-day continental serpentinization: the tablelands, NL, CAN. *Front. Microbiol.* 5:613. doi: 10.3389/fmicb.2014.00613

Morrill, P. L., Kuenen, J. G., Johnson, O. J., Suzuki, S., Rietze, A., Sessions, A. L., et al. (2013). Geochemistry and geobiology of a present-day serpentinization site in California: the cedars. *Geochim. Cosmochim. Acta* 109, 222–240. doi: 10.1016/j.gca.2013.01.043

Nakamura, K., Morishita, T., Bach, W., Klein, F., Hara, K., Okino, K., et al. (2009). Serpentinized troctolites exposed near the Kairei hydrothermal field, central Indian ridge: insights into the origin of the Kairei hydrothermal fluid supporting a unique microbial ecosystem. *Earth Planet. Sci. Lett.* 280, 128–136. doi: 10.1016/j.epsl.2009.01.024

Neubeck, A., Sun, L., Müller, B., Ivarsson, M., Hosgörmez, H., Özcan, D., et al. (2017). Microbial community structure in a serpentine-hosted abiotic gas seepage at the Chimaera ophiolite, Turkey. *Appl. Environ. Microbiol.* 83, e03430–e03416. doi: 10.1128/AEM.03430-16

Nobu, M. K., Nakai, R., Tamazawa, S., Mori, H., Toyoda, A., Ijiri, A., et al. (2022). Unique H2-utilizing lithotrophy in serpentinite-hosted systems. *ISME J.* 17, 95–104. doi: 10.1038/s41396-022-01197-9

Ohlsson, J. I., Osvatic, J. T., Becraft, E. D., and Swingley, W. D. (2019). Microbial community in hyperalkaline steel slag-fill emulates serpentinizing springs. *Diversity* 11:103. doi: 10.3390/d11070103

Perner, M., Kuever, J., Seifert, R., Pape, T., Koschinsky, A., Schmidt, K., et al. (2007). The influence of ultramafic rocks on microbial communities at the Logatchev hydrothermal field, located 15Â°N on the mid-Atlantic ridge: influence of ultramafic rocks on microbial communities. *FEMS Microbiol. Ecol.* 61, 97–109. doi: 10.1111/j.1574-6941.2007.00325.x

Postec, A., Quéméneur, M., Bes, M., Mei, N., Benaïssa, F., Payri, C., et al. (2015). Microbial diversity in a submarine carbonate edifice from the serpentinizing

hydrothermal system of the Prony Bay (New Caledonia) over a 6-year period. *Front. Microbiol.* 6:857. doi: 10.3389/fmicb.2015.00857

Postec, A., Quéméneur, M., Lecoeuvre, A., Chabert, N., Joseph, M., and Erauso, G. (2021). Alkaliphilus serpentinus sp. nov. and Alkaliphilus pronyensis sp. nov., two novel anaerobic alkaliphilic species isolated from the serpentinite-hosted Prony Bay hydrothermal field (New Caledonia). *Syst. Appl. Microbiol.* 44:126175. doi: 10.1016/j.syapm.2020.126175

Quéméneur, M., Bes, M., Postec, A., Mei, N., Hamelin, J., Monnin, C., et al. (2014). Spatial distribution of microbial communities in the shallow submarine alkaline hydrothermal field of the Prony Bay, New Caledonia: microbial communities of Prony hydrothermal field. *Environ. Microbiol. Rep.* 6, 665–674. doi: 10.1111/1758-2229.12184

Quéméneur, M., Mei, N., Monnin, C., Postec, A., Guasco, S., Jeanpert, et al. (2023). Microbial taxa related to natural hydrogen and methane emissions in serpentinite-hosted hyperalkaline springs of New Caledonia. *Front. Microbiol.* 14:1196516. doi: 10.3389/fmicb.2023.1196516

Quéméneur, M., Mei, N., Monnin, C., Postec, A., Wils, L., Bartoli, M., et al. (2021). Procaryotic diversity and hydrogenotrophic methanogenesis in an alkaline spring (La Crouen, New Caledonia). *Microorganisms* 9:1360. doi: 10.3390/microorganisms9071360

Quéméneur, M., Palvadeau, A., Postec, A., Monnin, C., Chavagnac, V., Ollivier, B., et al. (2015). Endolithic microbial communities in carbonate precipitates from serpentinite-hosted hyperalkaline springs of the Voltri massif (Ligurian Alps, northern Italy). *Environ. Sci. Pollut. Res.* 22, 13613–13624. doi: 10.1007/s11356-015-4113-7

Rempfert, K. R., Miller, H. M., Bompard, N., Nothaft, D., Matter, J. M., Kelemen, P., et al. (2017). Geological and geochemical controls on subsurface microbial life in the Samail ophiolite, Oman. *Front. Microbiol.* 8:56. doi: 10.3389/fmicb.2017.00056

Rempfert, K. R., Nothaft, D. B., Kraus, E. A., Asamoto, C. K., Evans, R. D., Spear, J. R., et al. (2023). Subsurface biogeochemical cycling of nitrogen in the actively serpentinizing Samail ophiolite, Oman. *Front. Microbiol.* 14:1139633. doi: 10.3389/fmicb.2023.1139633

Rizoulis, A., Milodowski, A. E., Morris, K., and Lloyd, J. R. (2016). Bacterial diversity in the hyperalkaline allas springs (Cyprus), a natural analogue for cementitious radioactive waste repository. *Geomicrobiol J.* 33, 73–84. doi: 10.1080/01490451.2014.961107

Rose, I. A., Grunberg-Manago, M., Korey, S. R., and Ochoa, S. (1954). Enzymatic phosphorylation of acetate. *J. Biol. Chem.* 211, 737–756. doi: 10.1016/S0021-9258(18)71161-7

Rowe, A. R., Yoshimura, M., LaRowe, D. E., Bird, L. J., Amend, J. P., Hashimoto, K., et al. (2017). In situ electrochemical enrichment and isolation of a magnetite-reducing bacterium from a high pH serpentinizing spring. *Environ. Microbiol.* 19, 2272–2285. doi: 10.1111/1462-2920.13723

Russell, M. J., Hall, A. J., Cairns-Smith, A. G., and Braterman, P. S. (1988). Submarine hot springs and the origin of life. *Nature* 336:117. doi: 10.1038/336117a0

Russell, M. J., Hall, A. J., and Martin, W. (2010). Serpentinization as a source of energy at the origin of life: serpentinization and the emergence of life. *Geobiology* 8, 355–371. doi: 10.1111/j.1472-4669.2010.00249.x

Sabuda, M. C., Brazelton, W. J., Putman, L. I., McCollom, T. M., Hoehler, T. M., Kubo, M. D. Y., et al. (2020). A dynamic microbial sulfur cycle in a serpentinizing continental ophiolite. *Environ. Microbiol.* 22, 2329–2345. doi: 10.1111/1462-2920.15006

Sánchez-Andrea, I., Guedes, I. A., Hornung, B., Boeren, S., Lawson, C. E., Sousa, D. Z., et al. (2020). The reductive glycine pathway allows autotrophic growth of *Desulfovibrio desulfuricans*. *Nat. Commun.* 11:5090. doi: 10.1038/s41467-020-18906-7

Schönheit, P., Buckel, W., and Martin, W. F. (2016). On the origin of heterotrophy. *Trends Microbiol.* 24, 12–25. doi: 10.1016/j.tim.2015.10.003

Schrenk, M. O., Brazelton, W. J., and Lang, S. Q. (2013). Serpentinization, carbon, and deep life. *Rev. Mineral. Geochem.* 75, 575–606. doi: 10.2138/rmg.2013.75.18

Schrenk, M. O., Kelley, D. S., Bolton, S. A., and Baross, J. A. (2004). Low archaeal diversity linked to subseafloor geochemical processes at the Lost City hydrothermal field, mid-Atlantic ridge. *Environ. Microbiol.* 6, 1086–1095. doi: 10.1111/j.1462-2920.2004.00650.x

Seyler, L. M., Brazelton, W. J., McLean, C., Putman, L. I., Hyer, A., Kubo, M. D. Y., et al. (2020). Carbon assimilation strategies in ultrabasic groundwater: clues from the integrated study of a serpentinization-influenced aquifer. *mSystems* 5, e00607–e00619. doi: 10.1128/mSystems.00607-19

Sojo, V., Herschy, B., Whicher, A., Camprubí, E., and Lane, N. (2016). The origin of life in alkaline hydrothermal vents. *Astrobiology* 16, 181–197. doi: 10.1089/ast.2015.1406

Sumi, T., and Harada, K. (2021). Kinetics of the ancestral carbon metabolism pathways in deep-branching bacteria and archaea. *Commun. Chem.* 4:149. doi: 10.1038/s42004-021-00585-0

Suzuki, S., Ishii, S., Hoshino, T., Rietze, A., Tenney, A., Morrill, P. L., et al. (2017). Unusual metabolic diversity of hyperalkaliphilic microbial communities associated with subterranean serpentinization at the cedars. *ISME J.* 11, 2584–2598. doi: 10.1038/ismej.2017.111

Suzuki, S., Ishii, S., Wu, A., Cheung, A., Tenney, A., Wanger, G., et al. (2013). Microbial diversity in the cedars, an ultrabasic, ultrareducing, and low salinity serpentinizing ecosystem. *Proc. Natl. Acad. Sci. USA* 110, 15336–15341. doi: 10.1073/pnas.1302426110

Suzuki, S., Kuenen, J. G., Schipper, K., van der Velde, S., Ishii, S., Wu, A., et al. (2014). Physiological and genomic features of highly alkaliphilic hydrogen-utilizing betaproteobacteria from a continental serpentinizing site. *Nat. Commun.* 5:3900. doi: 10.1038/ncomms4900

Suzuki, S., Nealson, K. H., and Ishii, S. (2018). Genomic and in-situ transcriptomic characterization of the candida Monninte phylum NPL-UPL2 from highly alkaline highly reducing serpentinized groundwater. *Front. Microbiol.* 9:3141. doi: 10.3389/fmicb.2018.03141

Tiago, I., and Veríssimo, A. (2013). Microbial and functional diversity of a subterrestrial high pH groundwater associated to serpentinization: microbial and functional diversity of subsurface aquifer. *Environ. Microbiol.* 15, 1687–1706. doi: 10.1111/1462-2920.12034

Truche, L., McCollom, T. M., and Martinez, I. (2020). Hydrogen and abiotic hydrocarbons: molecules that change the world. *Elements* 16, 13–18. doi: 10.2138/gselements.16.1.13

Trutschel, L. R., Chadwick, G. L., Kruger, B., Blank, J. G., Brazelton, W. J., Dart, E. R., et al. (2022). Investigation of microbial metabolisms in an extremely high pH marine-like terrestrial serpentinizing system: Ney Springs. *Sci. Total Environ.* 836:155492. doi: 10.1016/j.scitotenv.2022.155492

Twing, K. I., Brazelton, W. J., Kubo, M. D. Y., Hyer, A. J., Cardace, D., Hoehler, T. M., et al. (2017). Serpentinization-influenced groundwater harbors extremely low diversity microbial communities adapted to high pH. *Front. Microbiol.* 8:308. doi: 10.3389/fmicb.2017.00308

Westphal, L., Wiechmann, A., Baker, J., Minton, N. P., and Müller, V. (2018). The Rnf complex is an energy-coupled transhydrogenase essential to reversibly link cellular NADH and ferredoxin pools in the acetogen *Acetobacterium woodii*. *J. Bacteriol.* 200:e00357. doi: 10.1128/JB.00357-18

Woycheese, K. M., Meyer-Dombard, D. R., Cardace, D., Argayosa, A. M., and Arcilla, C. A. (2015). Out of the dark: transitional subsurface-to-surface microbial diversity in a terrestrial serpentinizing seep (Manleluag, Pangasinan, the Philippines). *Front. Microbiol.* 6:44. doi: 10.3389/fmicb.2015.00044

frontiers | Frontiers in Microbiology

TYPE Review
PUBLISHED 02 October 2023
DOI 10.3389/fmicb.2023.1257597

OPEN ACCESS

EDITED BY
Marianne Quéméneur,
UMR7294 Institut Méditerranéen d'océanographie (MIO), France

REVIEWED BY
Gaël Erauso,
Aix-Marseille Université, France
Jeffrey M. Dick,
Central South University, China

*CORRESPONDENCE
Loraine Schwander
✉ loraine.schwander@hhu.de
William F. Martin
✉ bill@hhu.de

RECEIVED 12 July 2023
ACCEPTED 04 September 2023
PUBLISHED 02 October 2023

CITATION
Schwander L, Brabender M, Mrnjavac N, Wimmer JLE, Preiner M and Martin WF (2023) Serpentinization as the source of energy, electrons, organics, catalysts, nutrients and pH gradients for the origin of LUCA and life. *Front. Microbiol.* 14:1257597. doi: 10.3389/fmicb.2023.1257597

Serpentinization as the source of energy, electrons, organics, catalysts, nutrients and pH gradients for the origin of LUCA and life

Loraine Schwander[1]*, Max Brabender[1], Natalia Mrnjavac[1], Jessica L. E. Wimmer[1], Martina Preiner[2] and William F. Martin[1]*

[1]Institute of Molecular Evolution, Biology Department, Math. -Nat. Faculty, Heinrich-Heine-Universität, Düsseldorf, Germany, [2]Microcosm Earth Center, Max Planck Institute for Terrestrial Microbiology and Philipps-Universität, Marburg, Germany

Serpentinization in hydrothermal vents is central to some autotrophic theories for the origin of life because it generates compartments, reductants, catalysts and gradients. During the process of serpentinization, water circulates through hydrothermal systems in the crust where it oxidizes Fe (II) in ultramafic minerals to generate Fe (III) minerals and H_2. Molecular hydrogen can, in turn, serve as a freely diffusible source of electrons for the reduction of CO_2 to organic compounds, provided that suitable catalysts are present. Using catalysts that are naturally synthesized in hydrothermal vents during serpentinization H_2 reduces CO_2 to formate, acetate, pyruvate, and methane. These compounds represent the backbone of microbial carbon and energy metabolism in acetogens and methanogens, strictly anaerobic chemolithoautotrophs that use the acetyl-CoA pathway of CO_2 fixation and that inhabit serpentinizing environments today. Serpentinization generates reduced carbon, nitrogen and — as newer findings suggest — reduced phosphorous compounds that were likely conducive to the origins process. In addition, it gives rise to inorganic microcompartments and proton gradients of the right polarity and of sufficient magnitude to support chemiosmotic ATP synthesis by the rotor-stator ATP synthase. This would help to explain why the principle of chemiosmotic energy harnessing is more conserved (older) than the machinery to generate ion gradients via pumping coupled to exergonic chemical reactions, which in the case of acetogens and methanogens involve H_2-dependent CO_2 reduction. Serpentinizing systems exist in terrestrial and deep ocean environments. On the early Earth they were probably more abundant than today. There is evidence that serpentinization once occurred on Mars and is likely still occurring on Saturn's icy moon Enceladus, providing a perspective on serpentinization as a source of reductants, catalysts and chemical disequilibrium for life on other worlds.

KEYWORDS

serpentinization, hydrothermal vents, origin of life, microbial metabolism, astrobiology, hydrogen, methane, Lost City

1. Introduction

The question of how life arose is sometimes called, "the biggest question in science," which is possibly an exaggeration. What is true is that it is perhaps the only scientific question to which everyone would like to know the answer. The origin of living things has concerned humans since antiquity. Modern scientific approaches to the problem build on Pasteur's 19th century demonstration that life cannot be created spontaneously (Bulloch, 1938), except of course, at the origin of life from the elements of the early Earth, and Darwin's inference that we all originate from a single common ancestor (Darwin, 1859). Mereschkowsky et al. (1910) proposed that the first organisms on Earth were probably thermophilic chemolithoautotrophs, a concept that — for good reasons — is still current among microbiologists, while Oparin and Haldane proposed a theory involving a primordial soup (Haldane, 1929; Oparin, 1957) of the type that Miller synthesized in the famous 1953 experiment powered by electric discharge (Miller, 1953).

Oparin and Haldane as well as Miller worked under the assumption that the early Earth had a reducing atmosphere. More recent studies indicate that early Earth's mantle was oxidized, which in turn released oxidized compounds such as CO_2, N_2 and H_2O into the atmosphere such that the early Earth's atmosphere must have also been oxidizing (Sossi et al., 2020). However, reducing conditions are needed for the origin of life because, despite the coexistence of contradictory theories on origins, they all tend to concur that the carbon source for the first complex molecules was ultimately CO_2, which needs reducing conditions to react to more complex organic molecules. There are currently two general categories of solutions afloat in the literature as to where to obtain reductants at origins: the surface (the atmosphere) and the subsurface (the crust via serpentinization).

In surface reduction models, additional impactors subsequent to the Moon-forming impact are evoked as a source of native metals at the surface. These additional impactors generate (theoretical) transient phases of reducing conditions in the atmosphere, phases that are argued to reduce CO_2 and N_2 to cyanide that is, in turn, central to some models for the origin of life (Benner et al., 2020; Zahnle et al., 2020; Itcovitz et al., 2022). Notably, the additional impactors are not required to explain the composition of the early Earth or the early atmosphere, they are solely "required" as a source of transient supplies of gas phase ammonia, cyanide and nitriles as starting materials for the laboratory-style organic synthesis of RNA bases, under the dual assumption that i) RNA arose from cyanide and nitriles on the Earth's surface and that ii) something like an RNA world ever existed (Benner et al., 1989; Zahnle et al., 2007; Righter et al., 2008; Sleep, 2016; Sasselov et al., 2020; Grewal et al., 2023). Surface reduction models do not interface well with microbial metabolism, because there are neither cyanides nor nitriles in the biosynthetic pathways to bases, amino acids and cofactors and no microbe is known to require cyanide as a growth substrate. Geochemical sources of cyanide are not known, not even from volcanic exhalates (Rose et al., 2006).

In subsurface reduction models, the source of reductant for origins is geochemical and continuous: H_2 supplied by serpentinization. The electrons released by serpentinization reduce H_2O to H_2 which in turn reduces CO_2 to CH_4 and organics (Sleep et al., 2004; Martin et al., 2008; Sleep et al., 2011; McCollom and Seewald, 2013). The diffusible reductant, H_2, is generated within the crust, where suitable catalysts for CO_2 reduction such as awaruite (Ni_3Fe) and magnetite (Fe_3O_4) are synthesized (Preiner et al., 2018). If life originated in serpentinizing systems, it would not have needed anything from the Earth's early atmosphere except N_2 and CO_2, because serpentinizing systems create the reducing conditions essential for the origin of life (Russell et al., 2010). The initial products of H_2 dependent CO_2 reduction under serpentinizing conditions in the laboratory are formate, acetate, pyruvate and methane, which comprise the backbone of microbial carbon and energy metabolism in organisms that use the acetyl-CoA pathway (Preiner et al., 2020). Subsurface reduction models have good congruence with microbial carbon and energy metabolism. Nucleic acid synthesis that might underpin an RNA world is more challenging under hydrothermal vent conditions (Muchowska et al., 2020; Yi et al., 2022; Harrison et al., 2023) but at the same time, there is no clear evidence that an RNA world ever existed (Baross and Martin, 2015) and there are no self-replicating RNA molecules in any life form as far as we know. Here we will focus on subsurface reduction as it occurs in modern serpentinizing systems as a starting point for origins.

Isotope evidence suggests that the first forms of life existed at least 3.8 billion years ago because carbon with an isotope signature lighter than that of abiogenic reduced carbon appears in sediments of that age (Mojzsis et al., 1996). Such light isotope signatures ($\delta^{13}C$) in the range of −40‰ to −80‰ are generally interpreted to indicate the presence of methanogens (archaea) (Arndt and Nisbet, 2012), but acetogens (bacteria) have a similarly light isotopic signature (Blaser et al., 2013). Ultralight isotopes indicate the presence of the acetyl-CoA pathway of CO_2 fixation in primordial bacteria and archaea (Tashiro et al., 2017), in line with its exergonic nature (Berg, 2011), ancient physiology (Rühlemann et al., 1985; Fuchs, 2011), abundance of metal cofactors (Martin and Russell, 2003; Ragsdale, 2006) and carbon-metal bonds (Martin, 2020), its dual role as a pathway of carbon and energy metabolism in acetogens and methanogens (Martin and Russell, 2007) and in line with metabolic and phylogenetic reconstructions of LUCA (Weiss et al., 2016).

Methanogens and acetogens are chemolithoautotrophs and therefore grow anywhere where sufficient H_2 and CO_2 exists and where temperatures are biocompatible (Thauer et al., 2008; Schuchmann and Müller, 2014), from rumen to termite guts to anaerobic environments such as hydrothermal vents on the sea floor. Deep-sea hydrothermal vents were first discovered in 1977 near the Galapagos islands (Corliss et al., 1979) and since then they have been of interest for theories on the origin of life (Corliss et al., 1981; Baross and Hoffman, 1985). Criticism of vents as sites for the origin of life arose very quickly, however, because of the high temperature of black smokers (*ca.* 400°C) (Bada and Lazcano, 2002): the upper limit for life is currently 122°C (Takai et al., 2008). This is one reason why it was proposed that if life originated at a hydrothermal vent, it must have happened at a low-temperature, alkaline hydrothermal vent that undergoes serpentinization (Russell et al., 1994, 1997), a proposal that predated the discovery of the Lost City hydrothermal field (Kelley et al., 2001, 2005; Proskurowski et al., 2008) which contains multiple serpentinizing deep-sea alkaline hydrothermal vents. The Lost City hydrothermal field offers a window in time for the study of the origin of life (Martin and Russell, 2007) and fosters ideas for laboratory experiments that simulate the reducing and catalyst rich conditions of hydrothermal vents (McCollom, 2013; McCollom and Seewald, 2013;

Schrenk et al., 2013; Möller et al., 2017; Muchowska et al., 2017; Boyd et al., 2020; Preiner et al., 2020).

Serpentinization releases energy, generates reductants, and provides small organic compounds that directly interface with microbial metabolism. It occurs both in terrestrial systems (continental, on land) and in submarine systems on the sea floor, usually close to the borders of tectonic plates (Schrenk et al., 2013; Wang et al., 2014; Preiner et al., 2018). Continental serpentinizing systems, for example those hosted by ophiolites, are a valuable source of information about the process, as deep-sea hydrothermal vents are much harder to access and few Lost City type systems have been discovered so far (Lecoeuvre et al., 2021). Even more remote are, of course, environments outside Earth, but they are relevant in an astrobiology context, where serpentinization has come into focus as a source of energy and reductant. There is accumulating evidence to suggest that serpentinization has occurred on Mars and might still be occurring on Mars and Enceladus (a moon of Saturn). It is suspected to be an important process on other icy moons of the gas giants in our solar system, especially where their oceans have contact with the rocky core, such as Europa and Titan (Schulte et al., 2006; Zolotov, 2007; Ehlmann et al., 2010; Glein et al., 2015; Vance et al., 2016; Waite et al., 2017; Johnson et al., 2019; Steele et al., 2022). It is useful to collate and compare data from different serpentinizing systems, which will be shown in section 3.

2. The importance of gradients and catalysts

When the effluent of submarine hydrothermal vents interfaces with seawater at the ocean floor, two fluids with different physicochemical properties continuously mix, generating far from equilibrium conditions over the lifespan of the vent, which in the case of Lost City can be over 30,000 years (Früh-Green et al., 2003). Some very hot hydrothermal fields can also reach ages in excess of 30,000 years (Kuznetsov et al., 2006) but this does not necessarily describe the age of individual active chimneys. The continuous far from equilibrium state of serpentinizing systems produces pH-, temperature- and redox-gradients, which create a steady supply of chemical energy sources that are similar to those used by modern microbes to run metabolic reactions and synthesize ATP. The gradients at hydrothermal vents were recognized early on as harboring similarity to energy releasing processes of cells, providing links between chemical processes in the early Earth and early forms of life and hence conducive to origin of life processes (Corliss et al., 1981; Baross and Hoffman, 1985; Holm, 1992; Russell and Hall, 1997). Gradients are interesting in an origins context because all living cells generate gradients during life and growth.

Temperature gradients at hydrothermal vents have been extensively studied by Braun and coworkers in the context of thermophoresis, a physicochemical process that leads to chemical concentration gradients in physically confined compartments (Baaske et al., 2007; Möller et al., 2017; Hudson et al., 2020; Matreux et al., 2023). Thermophoresis can lead to orders of magnitude accumulation of organic compounds in compartments on scales the size of µm to cm. All theories for origins require sufficient concentrations of chemical reactants in order to react at a significant rate, generating enough products to react further and attain higher complexity. Naturally occurring networks of inorganic microcompartments that form at the vent-ocean interface of serpentinizing hydrothermal systems can serve as sites of natural chemical concentration processes (Russell and Hall, 1997; Martin and Russell, 2003) thermophoresis amplifies that effect by orders of magnitude (Baaske et al., 2007).

The pH gradients of serpentinizing systems are important in an origins context for two reasons. First, the alkaline nature of effluent in serpentinizing systems, in the range of pH 9–11, stemming from continuous Mg $(OH)_2$ synthesis during the serpentinization process (Chavagnac et al., 2013), together with high H_2 concentrations of 1–10 mM or more, generates extremely negative redox potentials, on the order of −435 to −830 mV which where both measured and calculated at and for serpentinizing systems (Suzuki et al., 2017; Boyd et al., 2020; Nobu et al., 2023; Quéméneur et al., 2023). Provided that enough catalysts are present (Preiner et al., 2018) these conditions are sufficient to abiotically reduce CO_2 (or solid phase inorganic carbon) to formate, with the result that formate of abiotic origin is a very common solute in the effluent of serpentinizing systems (Lang et al., 2010, 2018), continuously present in micromolar concentrations. Formate can serve as a substrate for growth of methanogens (Dolfing et al., 2008; Stams and Plugge, 2009) and acetogens (Moon et al., 2021), microbial groups that inhabit serpentinizing systems (Fones et al., 2021; Kraus et al., 2021; Lecoeuvre et al., 2021; Brazelton et al., 2022; Colman et al., 2022). The synthesis of formate in high mM amounts from H_2 and CO_2 is readily catalyzed by minerals such as awaruite (Ni_3Fe), magnetite (Fe_3O_4) and greigite (Fe_3S_4) under hydrothermal conditions in the laboratory (Preiner et al., 2020).

The second role of pH gradients in serpentinizing systems is that they generate a continuous and natural chemiosmotic gradient with the same polarity as cells. Modern oceans have a pH of 7.8–8.2 [...] with a calculated pH of 6.6 because of higher CO_2 concentrations (Schrenk et al., 2013; Krissansen-Totton et al., 2018). At the vent-ocean interface, this generated a natural proton gradient of roughly three pH units, a far greater gradient than the roughly one pH unit or less that modern cells require to power their rotor-stator ATP synthetase (Tran and Unden, 1998; Silverstein, 2014). Geochemically formed pH gradients could have been harnessed by cells before the origin of proton pumping proteins, which would explain why the ATP synthase and the principle of chemiosmotic energy conservation is universally conserved across all prokaryotic cells while the proteins that generate ion gradients are not (Martin and Russell, 2007; Lane et al., 2010; Lane and Martin, 2010).

It has been suggested that pH gradients might themselves be a source of chemical energy for CO_2 reduction (Sojo et al., 2019; Hudson et al., 2020). Hudson et al. (2020) reported *ca.* 1 µM formate in the presence of gradients, Sojo et al. (2019) obtained no gradient dependent CO_2 reduction. A number of recent studies of H_2-dependent CO_2 fixation under simulated hydrothermal vent conditions clearly show that no gradient or compartmentation is required for CO_2 reduction. Preiner et al. (2020) obtained 0.3 M formate, and up to 560 µM acetate and 10 µM pyruvate (C3 synthesis) from H_2 and CO_2 using alkaline vent conditions in free solution with no gradients or compartments. The key to organic synthesis in serpentinizing systems are not gradients but catalysts, for example hydrothermally formed minerals like awaruite, magnetite and greigite in the case of Preiner et al. (2020), or Ni or Fe metals (Muchowska et al., 2017). Recent work by the group of Harun Tüysüz in Mülheim has characterized in considerable detail the properties that influence

the efficiency of CO_2 reduction reactions with nanoparticular and silicate-supported solid state Fe, Ni and Co catalysts (Belthle et al., 2022; Beyazay et al., 2023a,b). For organic synthesis under simulated hydrothermal vent conditions, the catalytic properties of the solid phase and the right reactants are key, not the existence of gradients *per se*.

3. Serpentinizing systems and their similarities and differences

Serpentinization involves reactions of ultramafic rocks with water. Ultramafic rocks have low silicate (SiO_2) content (<45 %) and have a relatively high magnesium and iron content (the term *mafic* stems from *ma*gnesium and *f*errum rich). Olivine and orthopyroxene are the main minerals of ultramafic rocks (Proskurowski et al., 2008). Serpentinization produces hydrogen gas (H_2), which in Fischer-Tropsch type reactions (FTT) can lead to the production of methane (CH_4) and other hydrocarbons at low temperatures (<150°C) through the reduction of carbon dioxide (CO_2) (Etiope and Sherwood Lollar, 2013; Etiope and Schoell, 2014). The serpentinization reaction of olivine, an iron-magnesium silicate, and water to serpentinite and iron-rich brucite, with further reaction of the latter with silica to serpentinite, magnetite and hydrogen, can be written in several ways. Bach et al. (2006) summarize the reaction as:

$$2Mg_{1.8}Fe_{0.2}SiO_4 + 3H_2O \rightarrow Mg_{2.85}Fe_{0.15}Si_2O_5(OH)_4 + Mg_{0.75}Fe_{0.25}(OH)_2$$

$$57Mg_{0.75}Fe_{0.25}(OH)_2 + 30SiO_2(aq) \rightarrow 15Mg_{2.85}Fe_{0.15}Si_2O_5(OH)_4 + 23H_2O + 4Fe_3O_4 + 4H_2$$

while Chamberlain et al. (1965) summarize the reaction as follows:

$$6Mg_{1.5}Fe_{0.5}SiO_4(\text{olivine}) + 7H_2O \rightarrow 3Mg_3Si_2O_5(OH)_4(\text{serpentine}) + Fe_3O_4(\text{magnetite}) + H_2$$

whereby Sleep et al. (2011) simplify the reaction to the essential H_2-production process:

$$3FeO(\text{in rock}) + H_2O(\text{liquid}) \rightarrow H_2(\text{in solution}) + Fe_3O_4(\text{magnetite})$$

The H_2 produced by serpentinization can reduce CO_2 to organic compounds and methane, N_2 to ammonia, and divalent Fe and Ni ions to mineral alloys of native metals. Serpentinization is an abundant source of geological reducing power. Paul Sabatier first discovered the abiotic formation of methane in 1913 by letting CO_2 and H_2 react with metal catalysts. Franz Fischer and Hans Tropsch generated more complex hydrocarbons with CO and H_2 in 1925. Both are labeled Fischer-Tropsch-type (FTT) reactions (Etiope and Schoell, 2014). Large quantities of abiotic gas are generated on Earth by such reactions. As soon as a CO_2 source is available to a serpentinizing system, FTT reactions produce CH_4 by serpentinization (Etiope and Sherwood Lollar, 2013; Etiope and Schoell, 2014). Transition metals including Ni and Fe as well as transition metal minerals including magnetite (Fe_3O_4) and awaruite (Ni_3Fe) catalyze FTT reactions. The conversion of the gas occurs after chemisorption to the metal surface (Sleep et al., 2004; Etiope and Schoell, 2014; Holm et al., 2015; Preiner et al., 2018). Ni, Fe and Cr are the most abundant metals in ultramafic rock. Both serpentinization and FTT reactions are considered to be important for origin of life because they forge C–C bonds from CO_2 and CO as starting materials (Russell et al., 2010). In an astrobiological context, they are suspected to be involved in the production of hydrocarbons on other planets (Etiope and Schoell, 2014).

H_2 is a source of energy and an electron donor for microorganisms in modern serpentinizing systems, and it could have carried out the same role in prebiotic chemistry (Etiope, 2017). The generation of H_2 from serpentinization is itself exergonic and has been taking place on Earth ever since there was water present (Sleep et al., 2004; Preiner et al., 2018). On the early Earth the lithosphere was not yet differentiated and higher mantle temperatures allowed ultramafic lava to erupt on Earth's surface, such that ultramafic rocks were probably much more exposed to the surface oceans than today, meaning that serpentinization was almost certainly much more prevalent on early Earth than now (Sleep et al., 2004, 2011; McCollom and Seewald, 2013; Schrenk et al., 2013). Serpentinization can occur at temperatures lower than <100°C (Holm et al., 2015) and usually generates an alkaline pH, especially at lower temperatures (usually > pH 9) because protons are consumed and free OH^- is released during the process that leads to the production of H_2 (Mottl et al., 2003; Schrenk et al., 2013).

Products of serpentinization generate [...] formate and CH_4 as the main products of CO_2 reduction measured in modern vents. Methane is always present in continental serpentinization sites and usually in considerable amounts. Lang et al. (2010) reported acetate in the effluent of Lost City but suggested that it stemmed from microbial metabolism. Abiotically formed acetate has not been detected in the effluent of serpentinizing hydrothermal systems to our knowledge. A recent report detected 1.2 mM abiotic acetate in host rocks of the Canadian Shield (Sherwood Lollar et al., 2021), although there is no direct evidence of it being synthesized by serpentinization so far. In effluent samples, CH_4 concentrations range from 0.01 to 14 mg/L, while normal water in equilibrium with the atmosphere has a CH_4 concentration of roughly 0.00003 mg/L. Longer-chain hydrocarbons (ethane to pentane) are also abiotically produced in serpentinizing systems, both submarine (Proskurowski et al., 2008) and on the surface (Etiope and Schoell, 2014), however in much lower quantities than methane.

Continental serpentinization sites have been studied since at least the 1960s (Barnes et al., 1967) and some of them, such as Chimera in Turkey, have been known to humans for thousands of years (Etiope, 2015). There are three types of mafic host rocks that support continental serpentinizing systems: ophiolites (ultramafic mantle rocks obducted to the surface), orogenic peridotite massifs and igneous intrusions. Some continental serpentinizing systems have been well-studied with respect to microbiology, gas composition and geology. In studies of gas composition, the isotope compositions of CH_4 are particularly important to determine whether it has a biogenic or abiogenic origin (Etiope and Schoell, 2014). Differentiating the two is difficult because the gases in these systems can be a mix of both

abiotic and biotic gas, as for example, in The Cedars spring in California, where abiotic gas is present, but microbes also produce CH_4 through CO_2 reduction because of the abundant H_2 present as their energy source (Nealson, 2005; Morrill et al., 2013; Etiope and Schoell, 2014; Suzuki et al., 2017).

3.1. Hydrothermal vent types

Hydrothermal vents are often divided into two types — black and white smokers — but off ridge systems like Lost City belong to neither category because they do not emit "smoke." Both the smoke of black and white smokers comes from metal sulfide and calcium and barium precipitation, but white smokers vent slower and at slightly lower temperatures (220–330°C) than black smokers, which is why a greater percentage of the metals precipitates in the chimneys and is not vented out causing the white color of the smoke, Lost City type vents have carbonate chimneys but no smoke (Rona et al., 1986; Kelley et al., 2005). A map showing the geographical distribution of some vents discussed here is shown in Figure 1.

Black smokers are hydrothermal fumaroles with abundant sulfides usually located close to or directly on top of the spreading zones of mid-ocean ridges. Because of their proximity to magma, the water in them can be up to over 400°C hot. They are also characterized by a low pH, even though black smokers that are hosted in ultramafic rocks can host serpentinization, such as the Rainbow and Logatchev hydrothermal fields on the mid Atlantic ridge (MAR) (Schrenk et al., 2013). These serpentinizing black smokers, in contrast to Lost City type vents, have higher temperatures, higher metal concentrations and an acidic pH (3–4), but unlike hydrothermal vents hosted in basaltic rock, they have high hydrogen and methane concentrations like other serpentinizing systems. The Rainbow and Logatchev systems are the best studied vents of this type. They also vent C2–C5 hydrocarbons in trace amounts (Charlou et al., 2002; Schrenk et al., 2013). Serpentinization does not happen in basalt-hosted vents because of the higher silica content of the basaltic rock (McCollom and Seewald, 2013).

Off ridge vents, or Lost City type vents, are characterized by carbonate chimneys, a high effluent pH (9 to 11) and moderate temperatures (between 28 to 116°C) compared to black or white smokers (Proskurowski et al., 2008; Seyfried et al., 2015). They are mainly represented by the first system of its kind discovered: the Lost City hydrothermal field. Lost City is located 750 m below sea level, but 4 km above the sea floor on the Atlantis massif (Kelley et al., 2005). Submarine systems that are comparable to Lost City are Prony Bay in New Caledonia (Monnin et al., 2014), the Old City hydrothermal field in the Indian ocean (Lecoeuvre et al., 2021) and the Shinkai Seep Field on the Mariana arc (Okumura et al., 2016).

Prony Bay is in much shallower seawater than Lost City (only 16 to 47 m below the surface) and its water source is fresh water, not crustal circulated seawater as in Lost City (Kelley et al., 2001; Quéméneur et al., 2014; Postec et al., 2015; Twing et al., 2022). Other important differences between shallow seawater vents and deep-sea vents are the access to sunlight, the influence of tidal forces and the different pressures (Price and Giovannelli, 2017). However, in terms of effluent parameters, Prony Bay is more similar to Lost City than the black smokers or the continental serpentinizing systems. It has elevated concentrations of H_2 and CH_4, a high pH and low venting temperatures (see Table 1) (Monnin et al., 2014).

The main difference in effluent chemical composition between the high temperature black smokers that serpentinize like the Rainbow and Logatchev hydrothermal fields and the low temperature Lost City hydrothermal field, is that Rainbow and Logatchev have higher concentrations of CO_2 and metals and acidic pH in their effluent whereas Lost City has a high pH and is depleted in metals and CO_2 (Proskurowski et al., 2008).

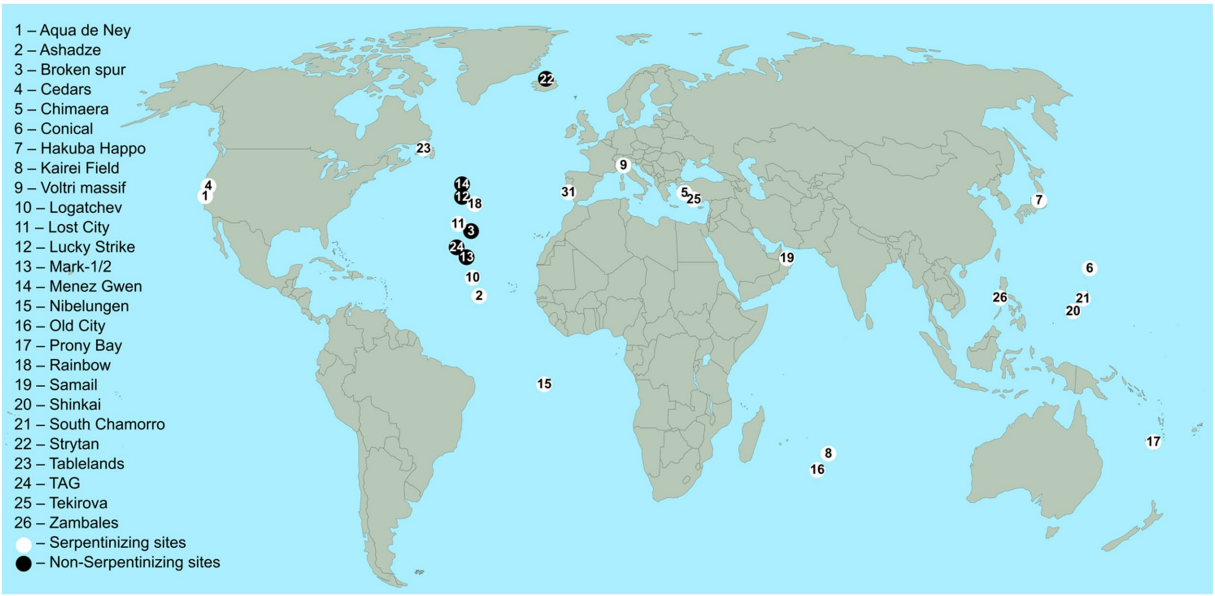

FIGURE 1
Locations of the serpentinizing and basalt hosted sites listed in Table 1. White circles indicate serpentinizing sites, black circles indicate non-serpentinizing sites. The sample of studies shown is not comprehensive and makes no statement about the relative frequencies of serpentinizing vs. non-serpentinizing sites. References: See Table 1.

TABLE 1 Parameters of different serpentinizing and basalt-hosted systems covered in this review.

Name	Loc/Water/ Serp	Temp [°C]	Depth [m]	pH	H_2	CH_4	CO_2
Aqua de Ney[1]	USA / f / Y	11.6	sur.	13	n.d.	1.92 mM	n.d.
Ashadze[2,3]	MAR / s / Y	296–372	–	3–4	19–26.5 mM	0.8–1.2 mM	n.d.–3.7 mM
Broken spur[4]	MAR / s / N	356–364	3,200	–	0.43–1.03 mM	65–130 µM	6.0–7.1 mM
Cedars[1]	USA / f / Y	17.4	sur.	12	157 µM	22 µM	44 µM
Chimaera[5]	Turkey / f / Y	–	sur.	–	9.82 vol%	85.33 vol%	trace
Conical[2]	MF / s / Y	–	3,083	12.5	–	2 mM	–
Hakuba Happo[6,7]	Japan / f / Y	50–60	500 (terr.)	>10	201–664 µM	124–201 µM	n.d.
Kairei Field[2]	CIR / s / Y	–	2,400	–	8 mM	500 µM	–
Voltri massif[2]	Italy / f / Y	10.5–23	sur.	10–12	–	6–867 µM	12–3,636 µM
Logatchev[2-4,8]	MAR / s / Y	320–352	3,000	3–4	11.1–12.5 mM	1.2–2.6 mM	4.4–10.1 mM
Lost City[2,3,9-11]	MAR / s / Y	40–116	7–800	9–12	0.5–16 mM	1–2 mM	trace
Lucky Strike[4]	MAR / s / N	170–364	1700	3.5	20–730 µM	0.5–0.97 mM	13–28 mM
Mark–1/2[4]	MAR / s / N	335–350	3,460	4	190–480 µM	23–62 µM	5.2–6.7 mM
Menez Gwen[4]	MAR / s / N	275–284	850	4.3	24–48 µM	1.35–2.63 mM	17–20 mM
Nibelungen[2]	MAR / s / Y	192–372	3,000	3	11.4 mM	1.4 mM	–
Old City[12,13]	CIR / s / Y	–	3,100	8	–	–	–
Prony Bay[2,14-16,22]	N.C. / f+s / Y	22–43	16–47	8–11	21.1–731.3 µM	153–376.6 µM	trace
Rainbow[4]	MAR / s / Y	365	2,300	3	12.9–16 mM	1.65–2.5 mM	16–17 mM
Samail[2,17]	Oman / f / Y	25–36.3	sur.	9–12	253 µM	0.1–483 µM	n.d.
Shinkai[18]	MF / s / Y	–	5,555	–	–	–	–
S. Chamorro[2]	MF / s / Y	–	2,960	12.5	–	2 mM	–
Strytan[13,19]	Iceland / f / N	70	16–70	<10	0.1–5.2 µM	0.5–1.4 µM	–
Tablelands[1,2]	Canada / f / Y	9.6	sur.	12–13	30–600 µM	23.7 µM	25–619 µM
TAG[4]	MAR / s / N	290–321	3,670	3	150–370 µM	124–147 µM	2.9–3.4 mM
Tekirova[2,5,20]	Turkey / f / Y	–	–	–	7.5–11.3 vol%	65–93 vol%	trace
Zambales[2,20,21]	Phillip. / f / Y	110–125	sur.	–	8.4–45.6 vol%	13–55 vol%	trace

Loc = Location; Water = Water source; f = freshwater source; s = seawater source; Serp = Serpentinizing system; Y = Yes (serpentinizing system); N = No (non-serpentinizing system, basalt hosted); MAR = Mid Atlantic Ridge = Atlantic Ocean; MF = Mariana Forearc, Pacific Ocean; CIR, Central Indian Ridge, Indian Ocean; N.C. = New Caledonia; Phillip = Phillippines; sur, surface = continental serpentinizing site; terr = terrestrial site, a hole was drilled 500 m into the ground; n.d. = not detected; trace = trace amounts detected; –, not reported.
[1](Cook et al., 2021), [2](Schrenk et al., 2013), [3](Konn et al., 2015), [4](Charlou et al., 2002), [5](Etiope et al., 2011b), [6](Suda et al., 2017), [7](Suda et al., 2014), [8](Proskurowski et al., 2008), [9](Kelley et al., 2001), [10](Kelley et al., 2005), [11](Seyfried et al., 2015), [12](Lecoeuvre et al., 2021), [13](Twing et al., 2022), [14](Monnin et al., 2014), [15](Postec et al., 2015), [16](Quéméneur et al., 2014), [17](Kraus et al., 2021), [18](Okumura et al., 2016), [19](Price and Giovannelli, 2017), [20](McCollom and Seewald, 2013), [21](Abrajano et al., 1988), [22](Quéméneur et al., 2023).

3.2. Conditions in hydrothermal vents

Continental serpentinizing systems have comparatively cool effluent under 100°C, and they also have hyperalkaline waters, although they are fed by fresh water (usually called meteoritic water, which is a complicated name for rainwater or snow) rather than altered sea water. Numerous continental serpentinization sites are known (Etiope et al., 2011b; Etiope and Schoell, 2014; Etiope, 2015). They are important analog sites to deep-sea serpentinizing sites because of their chemical similarities, and because they are easier to access. Like submarine serpentinizing systems, they also produce large amounts of H_2 and CH_4. They are the main source for abiotic gas on Earth (Etiope, 2017). Abiotic volatile hydrocarbons are still poorly understood but they can be generated by various inorganic mechanisms, including FTT. At some sites the amount of abiogenic methane can reach up to 90 vol% of the gas content (Etiope and Schoell, 2014), most of the remainder being H_2.

Abiogenic methane is widely discussed in the search for extraterrestrial life because methane is considered a potential biomarker, the sign of methanogenesis. But if Earth can generate large amounts of methane through abiotic processes, other wet, rocky planets and moons probably can as well, making methane itself problematic as a sign of life (Etiope, 2017). However, if biochemistry and life arose from exergonic H_2-dependent CO_2 reducing reactions, then abiotic methane serves as a proxy for the existence of geochemical conditions that are conducive to life's origin: exergonic reactions of H_2 and CO_2 under continuously far from equilibrium conditions.

The distinction between biotic and abiotic methane in usually made by isotope fractionation (Etiope et al., 2013; Etiope and Schoell, 2014). Abiotic methane is enriched in ^{13}C relative to biotic methane, which is isotopically light because of isotope discrimination in favor

of ^{12}C in the acetyl-CoA pathway (Blaser et al., 2013) of methyl synthesis from H_2 and CO_2 underpinning methanogenesis. However distinguishing biotic and abiotic methane by carbon isotope fractionation is not always straightforward (Horita and Berndt, 1999), which is why deuterium fractionation is also often taken into account (Etiope et al., 2011a) and often even combined (Miller et al., 2018) as shown in a study conducted in the Samail Ophiolite where it could be determined that biotic and abiotic methane mix (Nothaft et al., 2021).

Radiocarbon methods (^{14}C) can also be used to determine the source of C in CH_4 from serpentinizing systems. In the upper atmosphere, ^{14}C is constantly produced by neutron capture of ^{14}N to generate ^{14}C and a proton. The neutrons stem from cosmic radiation, the resulting ^{14}C has a half-life of 5,700 years. There is no radiocarbon in CH_4 of Lost City effluent. That is, CH_4 from Lost City is "radiocarbon dead," meaning that the carbon source cannot be bicarbonate from seawater, unless the circulation time exceeds 57,000 years (ten ^{14}C half-lives) because seawater contains ^{14}C that is constantly synthesized in the upper atmosphere. It is estimated that the entire volume of the ocean circulates through hydrothermal vents every 100,000–500,000 years (Fisher, 2005). The low CO_2 concentrations at Lost City together with its "radio-carbon-dead" CH_4 suggest that CH_4 in Lost City is likely derived from CO_2 of mantle origin that was reduced during serpentinization (Proskurowski et al., 2008).

3.3. CO_2 and H_2

Most of the carbon emitted from Lost City comes from the Earth's mantle in the form of formate (Lang et al., 2012, 2018). Formate can be used as a substrate for methanogenesis in environments where CO_2 is limiting. Methanogens can readily convert formate into CO_2 and H_2 or use it to reduce coenzyme F_{420} to $F_{420}H_2$, a flavin similar to FAD (Holden and Sistu, 2023). This allows them to access formate as a source of carbon and electrons for methanogenesis. This has been observed not only in Lost City but also in the Samail ophiolite (Fones et al., 2021). Formate forms abiotically under the high pH, reducing conditions of serpentinizing fluids. This can also be replicated in the laboratory (Preiner et al., 2020), where formate is typically the most abundant reduced carbon species under a variety of conditions (Belthle et al., 2022; Beyazay et al., 2023a,b). In Lost City, formate is the second most abundant carbon species after CH_4 and the second most available reductant after H_2 (Lang and Brazelton, 2020; Brazelton et al., 2022).

High concentrations of effluent H_2 are characteristic for serpentinizing systems, as summarized in Table 1. In terms of H_2 concentration, the non-serpentinizing Strytan hydrothermal field has the lowest out of all the systems where H_2 was detected. It is in the range of normal seawater. At first glance it might seem as if continental serpentinizing systems do not have high concentrations of H_2, however it should be mentioned that sometimes only the liquid phase was measured, not the actual gas phase emitted from the systems. In the Tekovira and Zambales ophiolite, where the gas phase composition was measured, H_2 can comprise 45 vol% of the emitted gas. High H_2 tends to correlate with high CH_4, but not strictly (see Supplementary Figure S1). Lost City and other serpentinizing systems of the mid Atlantic ridge (MAR) have high concentrations of CH_4 and H_2. The effluent at Prony Bay, a shallow sea vent with a fresh water source and similar microbial communities as continental ophiolites, has lower H_2 and CH_4 concentrations than Lost City of about a magnitude but still in significant amounts (Quéméneur et al., 2023). The Ashadze system on the MAR has very high H_2 concentration in its venting fluids of up to 26.5 mM. For CH_4 concentrations, many deep-sea hydrothermal vents, with a few exceptions, have a concentration of 1–3 mM. In continental serpentinizing sites CH_4 can reach between 20 vol% in New Zealand to 93 vol% of the gas phase in the Tekovira ophiolite (Etiope and Schoell, 2014). CH_4 is also extensively studied in continental serpentinization sites because they are the main contributor to abiotic gas (Etiope, 2017).

Alkaline serpentinizing systems are low in CO_2 because at high pH dissolved CO_2 turns into carbonate (CO_3^{2-}), which precipitate within the vent as Ca^{2+} and Mg^{2+} carbonates. This is the reason why hot and acidic hydrothermal vents such as Rainbow or Lucky Strike have very high CO_2 concentrations (up to 28 mM), while alkaline systems such as Lost City and Prony Bay harbor only have trace amounts of dissolved inorganic carbon. For continental serpentinization sites CO_2 was only detected in trace amounts in the gas phase. In the liquid phase CO_2 [often in the form of bicarbonate (HCO_3^-)] could sometimes be detected up to the mM range, but trace amounts are typical (Table 1). More complex organics than CH_4, when reported, were only detected in trace amounts both in ocean and continental serpentinization systems. Formate and acetate, when reported, were detected in Lost City in μM amounts and in the Conical Seamount of the Mariana Forearc in mM (formate) and μM (acetate) amounts, whereby the acetate at Lost City is likely biogenic (Lang et al., 2010).

Comparing different serpentinizing systems across studies is not straightforward because the sampling methods are often different and because of local heterogeneity: even in the same system values can differ greatly depending on where in the system the samples were taken. Cook et al. (2021) showed that the values measured in different samples, be it the temperature, the pH or the concentrations of the different compounds, can be vastly different depending on the sampling site. For example, if the groundwater, the well water or the surface water were sampled at three different sites — Tablelands, the Cedars, Aqua de Ney — the pH values could range between pH 8–9 in the surface water to pH 12–13 in the well water.

4. Microbiota of hydrothermal vents: a window into the past

Serpentinizing hydrothermal vents yield insights into primordial geochemical conditions, thereby providing a window in time into the nature of the environments that the first prokaryotic communities on the early Earth inhabited and the role of inorganic catalysts in the chemical setting of life's origin (Corliss et al., 1981; Baross and Hoffman, 1985). Serpentinizing systems also link the geochemistry of primitive environments to autotrophic theories for origins. It is estimated that about 60 % of all microbes inhabit Earth's crust: ~35 % in the submarine crust and ~25 % in the continental crust (Flemming and Wuertz, 2019). There is no sunlight, so primary production in the crust has to start with chemolithoautotrophs. The most prevalent (and obvious) source of energy for autotrophy is the H_2-CO_2 couple that

fuels acetogen and methanogen metabolism. Serpentinizing hydrothermal vents constantly generate H_2 and reducing conditions that mobilize nutrients.

Many reports have investigated the chemistry and microbial communities of hydrothermal vents, earlier reviews are provided by (Kelley et al., 2002; Martin et al., 2008; Lang and Brazelton, 2020). Serpentinizing hydrothermal systems were the topic of a recent special dedicated issue of the Philosophical Transactions of the Royal Society with contributions covering new insights from the serpentinite reactions at the Marianas trench (Fryer et al., 2020), the effect of pH on H_2 production (McCollom et al., 2020), hydrocarbons in fluid inclusions within olivine rich rocks (Grozeva et al., 2020), the role of serpentinite in the search for life beyond Earth (Vance and Daswani, 2020), the thermodynamics of the H_2-rich environments of serpentinizing systems and how that effects microbial CO_2 fixation (Boyd et al., 2020), a thorough review of microbial investigations at Lost City (Lang and Brazelton, 2020). Another worthy read is an in-depth study focusing on Prony Bay showing the relationship of microbial communities in hyperalkaline waters with high concentrations of H_2 (Quéméneur et al., 2023). A number of new reports shed light on the relationship between geochemical reactions at hydrothermal vents and autotrophic origins of microbial metabolism and life. In an origins context we can focus on anaerobic processes.

4.1. Carbon

Although CO_2 was very abundant on the early Earth (Sossi et al., 2020), modern serpentinizing systems are generally low in CO_2 because of magnesium carbonate and calcium carbonate precipitation at high pH. The effluent of serpentinizing systems can however be rich in formate ($HCOO^-$). Formate is readily converted by simple inorganic catalysts (Preiner et al., 2020; Belthle et al., 2022; Beyazay et al., 2023a,b) and by microbes into H_2 and CO_2 via the near-equilibrium reaction:

$$HCOO^- + H+ \rightarrow H_2 + CO_2$$

with $\Delta G_o' = -3.5\,kJ{\cdot}mol^{-1}$ (Maden, 2000). Microbes have a number of different enzymes for that reaction. The formate to CO_2 converting reaction is catalyzed by the enzyme hydrogen-dependent CO_2 reductase, HDCR (Schuchmann and Müller, 2013), or by NADH-dependent formate dehydrogenase (FDH), which is the typical enzyme of the acetyl-CoA pathway in acetogens (Schuchmann and Müller, 2013). In methanogens the reaction is catalyzed via hydrogenases that convert H_2 into reduced ferredoxin and the activity of formyl-methanofuran dehydrogenase, which contains a FDH domain and 46 [4Fe4S] clusters (Wagner et al., 2016). A third kind of formate dehydrogenase, HylABC-Fdh2, performs a reaction called electron bifurcation in which an electron pair is split, with the individual electrons being transferred to different acceptors with different redox potentials (Buckel and Thauer, 2013; Buckel and Thauer, 2018). HylABC-Fdh2 converts formate into CO_2 with one of the electrons being transferred to NAD^+ and the other being transferred to ferredoxin (Wang et al., 2013). Oxidation of two formate molecules via this reaction generates two CO_2, one NADH and two reduced ferredoxins. This bifurcating form of FDH is found in *Bipolaricaulota*, a deeply branching acetogen identified by metagenomics in the effluent of the hyperalkaline water of the Oman ophiolite (Colman et al., 2022). There are also cytochrome- dependent formate dehydrogenases (Sebban-Kreuzer et al., 1998). All formate dehydrogenases known so far, including HDCR, use Mo (in molybdopterin) or W (in tungstopterin) as a cofactor. The enzymatic mechanism of FDH is thought to involve binding of formate to Mo (or W) via its oxygen atoms (Hartmann et al., 2016), the abiotic mechanism is thought to involve bonding of the carbon atom in formate to Ni or Fe (Preiner et al., 2020).

The use of formate as a carbon source is a common theme in the effluent of serpentinizing systems. Although organisms have not yet been cultivated from hydrothermal vents that exhibit growth on formate, acetogens (Moon et al., 2021) and methanogens (Ferry et al., 1974) are known that use formate as their sole carbon and electron source, and some methanogens use formate as their sole carbon source (Costa et al., 2010; Lie et al., 2012). All indications are that formate based primary production is taking place at the submarine system of Lost City (Lang et al., 2018) and in some terrestrial serpentinizing systems including the Oman ophiolite (Colman et al., 2022), the Cedars (Suzuki et al., 2018), at Hakuba Happo (Nobu et al., 2023) and in the Prony Bay system, a freshwater fed submarine serpentinizing system that vents in seawater at a depth of about 50 m (Frouin et al., 2022), because there is no other carbon source reported to fuel primary production in these systems. For acetogens and methanogens living in these systems, formate is apparently the source of CO_2 and a source of electrons for primary production via the acetyl-CoA pathway, which generates reduced carbon to support the growth of fermenters that live from microbial cell mass (Schönheit et al., 2016) and other heterotrophs in the system.

The results of microbial sampling studies from different sites are not simple to compare directly because community composition within sites can vary, and at very small scales, depending on the specific position of the sample within the vent, effluent seawater mixing in the case of submarine vents, presence or absence of O_2 in the specific sample, the methods of analysis and other factors. For example, in the hyper-alkaline Strytan site, which has alkaline effluent but is not serpentinizing, anaerobes and the Wood Ljungdahl pathway of CO_2 fixation dominate in inner regions of vents while O_2-tolerant pathways dominate at the vent surfaces in contact with sea water (Twing et al., 2022). In the basement of Lost City alone, a broad diversity of phylotypes across sites sampled is observed (Brazelton et al., 2022). Methanogens are common in serpentinizing systems and can access carbon as formate (Fones et al., 2021). Quéméneur et al. (2023) showed that the abundance of certain prokaryotes is positively correlated to the H_2/CH_4 ratio in hyperalkaline springs and that bacteria that use H_2 as their main energy source are the most abundant among the microbial communities of Prony Bay.

A recent study by Frouin et al. (2022) stands out among surveys of microbial communities from different serpentinizing systems because the authors aimed to identify community and physiological properties that i) are shared among different serpentinizing systems and that ii) distinguish serpentinizing systems from hydrothermal vents in non-serpentinizing systems. They found that serpentinizing systems tend to be colonized by diverse communities, and that bacterial groups encountered often include acetogens (Firmicutes)

and methanogens like Methanosarcinales (Archaea), as originally discovered at Lost City. Frouin et al. (2022) found that Prony Bay was dominated by the acetogen *Bipolaricaulota*, which was also the main inhabitant of the Oman ophiolite community recently characterized by Colman et al. (2022) on the other side of the globe. Abundance of Firmicutes, which includes many acetogens, has been shown to be proportional to dissolved H_2, however why that is still has to be determined (Quéméneur et al., 2023).

A common physiological theme in serpentinizing systems is the ubiquitous presence of enzymes for the acetyl-CoA pathway (or Wood-Ljungdahl pathway) of CO_2 fixation. The Wood-Ljungdahl pathway is considered to be the most ancient pathway of carbon fixation (Fuchs and Stupperich, 1985; Fuchs and Stupperich, 1986; Berg, 2011; Fuchs, 2011). It is still the only exergonic pathway of CO_2 fixation known. The reaction to the level of the energy-rich thioester

$$2CO_2 + 8[H] + CoASH \rightarrow CH_3COSCoA + 3H_2O$$

is exergonic with $\Delta G_o' = -59.2$ kJ/mol if $2[H] = H_2$ and slightly endergonic with $\Delta G_o' = +13.2$ kJ/mol if $2[H] = NADH$ (Fuchs, 1994). The NADH forming reaction is slightly exergonic in the direction of CO_2, which is one reason that the pathway is so versatile among microbes (Fuchs, 1994; Zinder, 1994). It is the only pathway of CO_2 fixation that does not require net ATP input (Fuchs, 2011) and that occurs in both bacteria and archaea (Berg et al., 2010). It is a joined pathway of carbon and energy metabolism in which acetogens and methanogens obtain their ATP from ion gradients that they generate in the process of the exergonic reduction of CO_2 with electrons from H_2 at MtrA-H in methanogens (Thauer et al., 2008) and at Rnf in acetogens that lack cytochromes (Müller et al., 2018). In addition, acetogens and some methanogens can generate ATP in the acetyl-CoA pathway using substrate-level phosphorylation via acetyl-phosphate (Schöne et al., 2022). This kind of combined carbon and energy metabolism is so far unique to acetogens and methanogens. The acetyl-CoA pathway can be a dedicated pathway of CO_2 fixation (carbon metabolism) with no role in energy metabolism (ATP synthesis), for example in sulfate reducers that grow autotrophically, or in bacteria with phosphite-dependent energy metabolism (Mao et al., 2021). The acetyl-CoA pathway is a biochemical fossil that links acetogens and methanogens via functional, ecological and ancient evolutionary aspects (Martin, 2020; Schöne et al., 2022).

4.2. Electrons

The diffusible carrier electrons for reduction reactions in serpentinizing systems, H_2, is present in overabundance. At Lost City the effluent H_2 concentration is on the order of 10 mmol/kg [0.5 to 14 mmol/kg: (Proskurowski et al., 2008)], which is about 5–6 orders of magnitude more H_2 than is required to support methanogenesis (Thauer et al., 2008). Because of the high alkalinity and high H_2 concentration, the calculated redox potential of serpentinizing effluent can be in the range of −800 mV (Boyd et al., 2020), sufficient for most biologically relevant reduction as shown in Figure 2, with the exception of the phosphate/phosphite couple, where the midpoint potentials become more negative with increasing pH (Bernhard Schink, pers. comm.). Alkalinity favors the dissociation of H_2 into protons and electrons by consuming protons from the reaction $H_2 \rightarrow 2e^- + 2H^+$. Electrons from H_2 enter metabolism via hydrogenase. All hydrogenases except the Fe hydrogenase of methanogens (Thauer et al., 2008; Shima et al., 2011), reduce 4Fe4S clusters and most of them generate reduced ferredoxin as the reaction product. The redox potential needed to reduce ferredoxin as the source of electrons in metabolism is on the order of −500 mV. Suzuki et al. (2018) found no hydrogenases in metagenomes from The Cedars, raising the possibility that other routes of ferredoxin reduction might be possible under such reducing conditions. Studies of microbes that grow on native iron and on electrodes suggest that side activities of extracellular enzymes might be able to substitute for hydrogenases (Deutzmann et al., 2015). Early studies by Menon and Ragsdale (1996) indicated that acetyl-CoA synthase and pyruvate synthase have latent hydrogenase side activity, and the H_2-producing side reaction of nitrogenase (Hu and Ribbe, 2016) is well known. All of those side activity hydrogenases have FeS or NiFeS clusters that are likely candidates for the moonlighting active site. Metals (Fe, Ni, Co) and metal oxides can serve as hydrogenases, activating H_2 by splitting it into two metal bound hydrogen atoms for CO_2 reduction (Preiner et al., 2020; Belthle et al., 2022; Beyazay et al., 2023a,b) or for NAD^+ reduction (Henriques Pereira et al., 2022).

The highly reducing conditions of serpentinizing hydrothermal vents are key to origins because CO_2 has to be converted to organic carbon. There are, however, also alternative views about the source of energy at origins in serpentinizing hydrothermal systems. Duval et al. (2021), for example, argue that the energy required for the origin of metabolism was not exergonic H_2-dependent CO_2 reduction catalyzed by reduced transition metals as it occurs in the laboratory (Weiss et al., 2016; Preiner et al., 2020; Wimmer et al., 2021b; Beyazay et al., 2023a) and in acetogen and methanogen metabolism, but that instead the energy at origins stemmed from nitrate-dependent methane oxidation with the mixed valence iron oxide fougerite (green rust), acting as the catalyst (Duval et al., 2021) in alkaline hydrothermal systems. How energy release from methane oxidation is coupled to either prebiotic organic synthesis or carbon metabolism is not explained by Duval et al. (2021), changes in Gibbs free energy for the fougerite dependent reactions have not been presented, and abiotic laboratory versions of the fougerite dependent carbon assimilation reactions have not been reported. In laboratory versions of the acetyl-CoA pathway (Preiner et al., 2020; Beyazay et al., 2023a) and in acetogens and methanogens *in vivo* (Figure 3), energy for ATP synthesis is released in the exergonic H_2 dependent synthesis of acetate, pyruvate and methane from CO_2.

4.3. Nitrogen and sulfur

Frouin et al. (2022) looked carefully at sources and pathways for nitrogen but found no consistent trend. The source of nitrogen is still not well resolved in serpentinizing systems and might differ across systems. In very recent work, Shang et al. (2023a,b) found that experimental serpentinization reactions in the laboratory readily reduce N_2 to NH_3 in very large amounts and on time scales approaching 30 days. Cells are about 50% carbon and about 10% nitrogen by dry weight (Heldal et al., 1985), hence there has to be access to a nitrogen supply for primary production in serpentinizing systems. The simplest solution is that N_2 present in the water circulating through serpentinizing systems is reduced by nitrogenase. Most studies have detected nitrogenase genes among the microbiota

E_o for 1 µM H_2

T [°C]	pH 0	1	2	3	4	5	6	7	8	9	10	11	12	13	14
200	170	76	−18	−112	−206	−299	−393	−487	−581	−675	−769	−863	−957	−1051	−1144
150	154	70	−14	−98	−182	−265	−349	−433	−517	−601	−685	−769	−853	−937	−1021
100	139	65	−9	−83	−158	−232	−306	−380	−454	−528	−602	−676	−750	−824	−898
50	123	59	−5	−69	−134	−198	−262	−326	−390	−454	−518	−582	−647	−711	−775
25	115	56	−3	−62	−122	−181	−240	−299	−358	−417	−477	−536	−595	−654	−713
0	107	53	−1	−55	−110	−164	−218	−272	−326	−381	−435	−489	−543	−597	−652

E_o for 1 mM H_2

T [°C]	pH 0	1	2	3	4	5	6	7	8	9	10	11	12	13	14
200	−18	−112	−206	−299	−393	−487	−581	−675	−769	−863	−957	−1051	−1144	−1238	−1332
150	−14	−98	−182	−265	−349	−433	−517	−601	−685	−769	−853	−937	−1021	−1105	−1189
100	−9	−83	−158	−232	−306	−380	−454	−528	−602	−676	−750	−824	−898	−972	−1046
50	−5	−69	−134	−198	−262	−326	−390	−454	−518	−582	−647	−711	−775	−839	−903
25	−3	−62	−122	−181	−240	−299	−358	−417	−477	−536	−595	−654	−713	−772	−832
0	−1	−55	−110	−164	−218	−272	−326	−381	−435	−489	−543	−597	−652	−706	−760

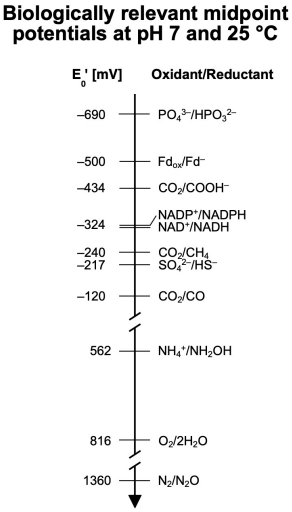

FIGURE 2
Range of redox potentials for two different concentrations of hydrogen (1 µM and 1 mM) over different pH ranges and temperatures. The pH has the biggest influence on the redox potential, followed by temperature and then hydrogen. Biologically relevant midpoint potentials are shown on the left, all of them measured at pH 7 (Vanysek, 2000; Schink et al., 2002; Lundblad and Macdonald, 2018; Martin et al., 2018; Madigan et al., 2021; Nelson and Cox, 2021).

of serpentinizing systems, though nitrate reduction can also be detected (Frouin et al., 2022). Trutschel et al. (2022) reported high concentrations of ammonia at Ney Springs. Ammonia has also been reported in the Oman ophiolite system (Rempfert et al., 2017), but in both cases the source of the ammonia is not resolved, with decaying organic matter within the system being the most widely discussed source. With the new report by Shang et al. (2023a), abiotic sources of NH_3 need to be considered in natural systems (Shang et al., 2023a).

The state of nitrogen in the primordial atmosphere was N_2 (Sossi et al., 2020). In an origins context, before the existence of biological N_2 fixation via nitrogenase, the source of nitrogen would have to be geochemical. Three sources are discussed: High pressure high temperature N_2 reduction by deep geochemical Haber-Bosch like processes (Brandes et al., 1998), low pressure low temperature FeS-mediated N_2 reduction processes (Dörr et al., 2003) and serpentinization-related geochemical processes. Ménez et al. (2018) reported the presence of abiotic tryptophan and other amino acids in the Atlantis massif that hosts the Lost City hydrothermal field. The exact route of synthesis is not yet known but might involve iron-dependent Friedel-Crafts like syntheses. The significance of amino acid synthesis in the crust for theories that life arose at hydrothermal vents is evident (Baross, 2018).

Lost City does not appear to emit abiotic amino acids in its effluent, but the terrestrial hydrothermal system Hakuba Happo does. Nobu et al. (2023) recently reported the presence of glycine (5 nM) in the effluent of Hakuba Happo which is likely of abiotic origin. Notably, there were no other amino acids in the effluent. Were glycine of biotic origin, the 19 other amino acids should be present. Some of the microbes that Nobu et al. characterized from Hakuba Happo, *ca.* Lithacetigenota, possessed genes for glycine reductase, an unusual selenoenzyme that synthesizes acetyl phosphate from glycine and P_i (Andreesen, 2004). The acetyl phosphate can be used for acetyl-CoA (carbon metabolism) or ATP synthesis via substrate level phosphorylation. Although the concentration of glycine in the Hakuba Happo effluent was low, it was sufficient to render the glycine reductase pathway thermodynamically favorable under the conditions of the vent. No archaea were detected in Hakuba Happo, but glycine reductase utilizing Lithacetigenota were detected at the Cedars (Nobu et al., 2023).

The glycine reductase variant of carbon assimilation and energy metabolism employed by Lithacetigenota starts with environmental glycine. It is distinct from the H_2-dependent glycine reductase pathway of autotrophic CO_2 fixation used by *Desulfovibrio desulfuricans* (Sánchez-Andrea et al., 2020). The findings of Ménez et al. (2018) indicate that geochemical nitrogen fixation to amino acids is possible. The findings of Nobu et al. (2023) suggest that it is ongoing today, continuously in the hyperalkaline serpentinizing environment of Hakuba Happo.

Sulfur is a trace element in cells. It is highly volatile in various oxidation states and readily eluted from rocks as H_2S or HS^- during serpentinization, but sulfate is also a common constituent of effluent and sulfate reducers are very common in serpentinizing systems (Reveillaud et al., 2016; Lang et al., 2018). Sulfur is an ancient substrate of energy metabolism (Rabus et al., 2006; Liu et al., 2012) and fulfills important catalytic functions in many cofactors (Kirschning, 2021). It is a component of ancient metabolism. Note however that the synthesis of formate, acetate and pyruvate from H_2 and CO_2 under simulated hydrothermal conditions using Ni_3Fe or Fe_3O_4 as catalysts requires no participation of sulfur (Preiner et al., 2020; Belthle et al., 2022; Beyazay et al., 2023a,b).

Today, nitrogen and sulfur compounds that occur in hydrothermal systems serve as terminal electron acceptors in anaerobic respiratory chains (Calisto and Pereira, 2021). At the origin of metabolism, CO_2 was arguably the most important electron acceptor because the synthesis of organic compounds was required in order to get metabolic pathways established. This underscores the evolutionary significance of the acetyl CoA pathway in acetogens and methanogens: it generates the starting compounds of metabolism while releasing energy that can

10.3389/fmicb.2023.1257597

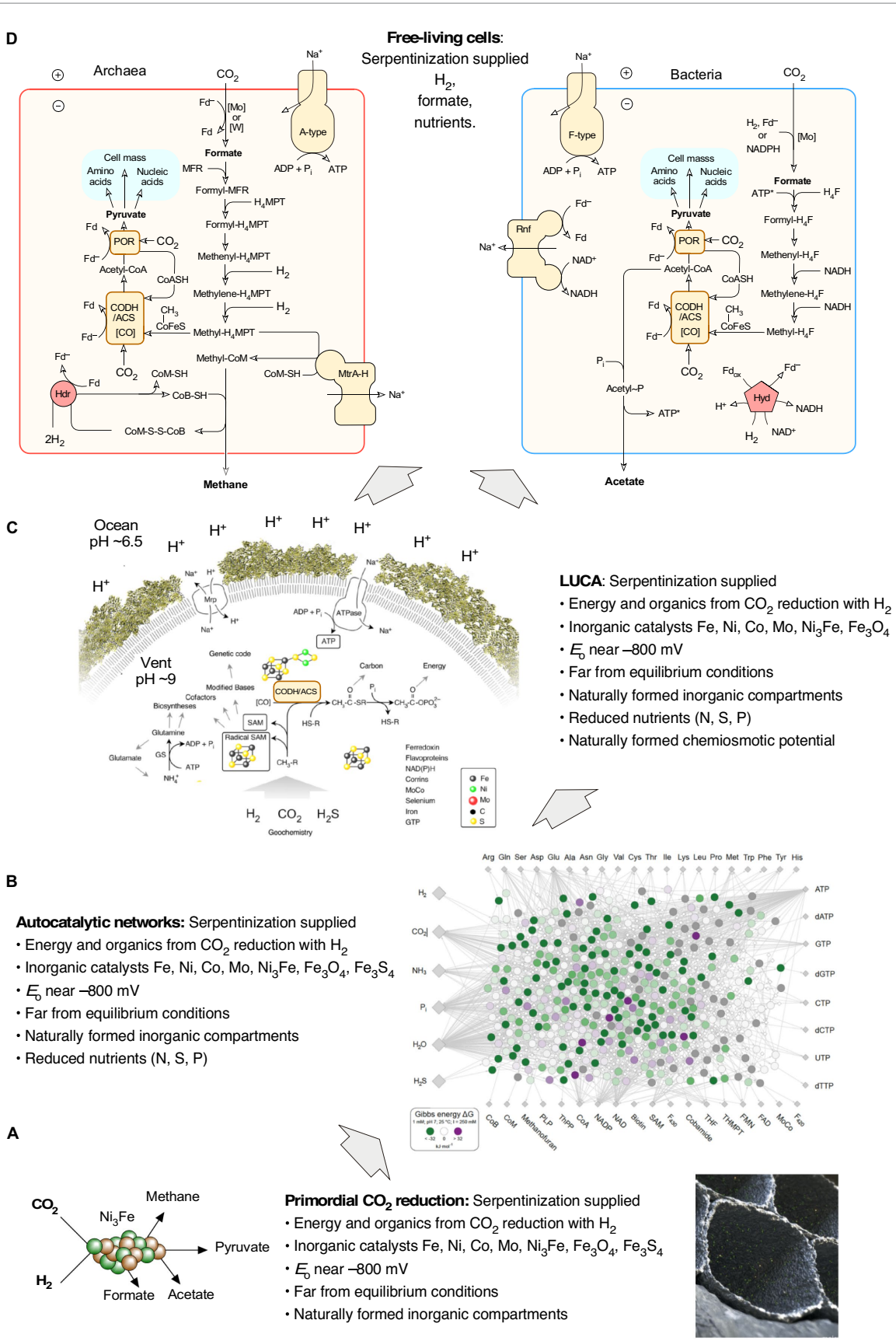

FIGURE 3
Contributions of serpentinization to the origin of free-living cells. **(A)** The H_2 produced in serpentinization synthesizes awaruite, Ni_3Fe (Preiner et al., 2018). Awaruite is a highly efficient catalyst for the conversion of H_2 and CO_2 into formate, acetate and pyruvate — the backbone of microbial

(Continued)

FIGURE 3 (Continued)
metabolism in anaerobic autotrophs that obtain their carbon and energy via the acetyl-CoA pathway — the reaction takes place overnight in water at pH 8-10 and 70-100°C in the dark using aqueous H_2 concentrations of 5 mM, similar to 10 millimolar H_2 observed at Lost City (Preiner et al., 2020). At that H_2 concentration and pH, the midpoint potential of the H_2/H^+ couple is on the order of −600 mV (see Figure 2), in Lost City the redox potential has been calculated to be in the order of −800 mV (Boyd et al., 2020), sufficient to reduce both CO_2 to formate ($E_o' = -450$ mV) and to reduce ferredoxin ($E_o = ca.$ −500 mV in cells). These low values of E_o are the reason why electron bifurcation is not required for CO_2 reduction with H_2 ($E_o' = -414$ mV) in the reaction shown in the panel (Martin, 2022), but is strictly required in enzyme based reduction in cells (Buckel and Thauer, 2018; Müller et al., 2018). Naturally formed inorganic microcompartments (an artist's impression is shown) can concentrate the organic products around their site of synthesis. **(B)** Autocatalytic networks are objects of molecular (self) organization. Because of the specificity and efficiency observed for their formation from H_2 and CO_2 using Ni_3Fe or Fe_3O_4, formate, acetate and pyruvate serve as elements of the food set (F) in food- (F-) generated reflexively autocatalytic networks, abbreviated as RAFs. RAFs can be identified in the metabolism of modern cells (Sousa et al., 2015; Xavier and Kauffman, 2022) and in acetogens and methanogens, cells that obtain their carbon and energy from H_2 dependent CO_2 reduction via the acetyl CoA pathway (Xavier et al., 2021). The reactions that are required to synthesize 20 amino acids, the (unmodified) bases of DNA and RNA, and 18 cofactors are called the autotrophic core (Wimmer et al., 2021a). Of the 400 reactions in the autotrophic core, 97 % reactions are exergonic under the reducing and far-from-equilibrium conditions of serpentinizing hydrothermal vents, as indicated by green dots on reactions of the network [image from Wimmer et al. (2021b)]. Serpentinization also provided reduced N, S and possibly P species as nutrients (see corresponding sections in the text). Natural inorganic compartments could have promoted the formation of autocatalytic networks by generating high reactant and product concentrations from specific food sets (Martin and Russell, 2007). Autocatalytic networks help to bridge the gap between reactions catalyzed by simple inorganic compounds and reactions catalyzed by peptides synthesized on ribosomes. **(C)** The last universal common ancestor, LUCA, possessed the universal genetic code and ribosomes was able to synthesize proteins as catalysts. Genomic reconstructions of LUCA (Weiss et al., 2016, 2018) indicate that the energy required for the synthesis of encoded peptide catalysts (protein synthesis cost 4 ATP per peptide bond) stemmed from substrate level phosphorylation, SLP (Weiss et al., 2016). Serpentinization provided H_2 for CO_2 reduction. The thermodynamics of laboratory scale bifurcation-independent acetate synthesis from H_2 and CO_2 are sufficient to enable SLP (Preiner et al., 2020). Serpentinization generates naturally occurring pH gradients between the alkaline effluent and the nearly neutral ocean water (see main text), the magnitude and polarity of the gradients are sufficient to drive an ATP synthase. The rotor stator ATP synthase is as universal among cells as the ribosome (Martin and Russell, 2003), it was present in LUCA (Weiss et al., 2016) and, inserted into a hydrophobic layer would provide the cytosol with a very high energy charge to support for protein synthesis. The origin of the genetic code is handled here as a given, not as an explanandum, it is not evident how serpentinization (or any other geochemical process) would specifically foster the origin of the genetic code, whose structure is determined by aminoacyl-tRNA synthetases (Carter and Wolfenden, 2015), bases in tRNA (Schimmel et al., 1993) and the peptidyl transferase site of the protoribosome (Bose et al., 2022). **(D)** By coupling H_2 dependent CO_2 reduction to the formation of ion gradients (pumping), and with the integration of flavin based electron bifurcation into the reduction of ferredoxin by H_2 in a stoichiometrically balanced energy metabolic reaction, the ancestors of acetogens (LBCA) and methanogens (LACA) could emerge as free-living cells. The lipids of bacteria and archaea are different in chemistry and biosynthesis, they evolved independently from LUCA en route to LACA and LBCA. See also Martin (2012, 2020) and Martin and Sousa (2016). Note the position of H_2, CO_2, formate, acetate, pyruvate and methane in panel A and panel D. In free living cells, various properties provided in different phases of biochemical evolution by serpentinization are replaced by biogenic molecules and catalysts. In all phases of the figure, the energy is supplied by serpentinization. In panel **(D)** the archaeal physiological map is for Methanothermobacter marburgensis, from Thauer et al. (2008), the bacterial map is for Acetobacterium woodii, from Schuchmann and Müller (2014).

be harnessed to synthesize ATP. In that sense, acetogenesis and methanogenesis are cytochrome-free and quinone-free anaerobic respirations that use CO_2 as the terminal acceptor in a reaction sequence that also generates a net gain of acetyl CoA. Anaerobic respirations that reduce sulfur and nitrogen compounds require siroheme, cytochromes and quinones, acetogenesis and methanogenesis do not, they are simpler in that regard. Coupled carbon and energy metabolism in the acetyl-CoA pathway using CO_2 as the electron acceptor probably preceded a differentiation into dedicated carbon metabolism and dedicated energy metabolism involving cytochrome dependent respiratory chains that use nitrogen and sulfur compounds as terminal acceptors.

4.4. Phosphorus: phosphate and phosphite

Phosphate has always presented problems in prebiotic chemistry because of its low solubility in contact with calcium to generate apatite, which is more or less insoluble, leading to various suggestions, that certain kinds of carbonate rich lakes existed on the primordial Earth that maintained phosphate in solution (Toner and Catling, 2020). The recent findings of Frouin et al. (2022) from Prony Bay place the phosphate problem in a fundamentally different light. They estimate that about half of the microbes that they sampled from Prony Bay possess the genes required for the metabolism of phosphonates and they found that phosphonate metabolism was fairly common in microbial communities from serpentinizing systems. What are phosphonates? Phosphonates are compounds that contain a C–P bond and are so far only known to be synthesized by microbes via a pathway that starts from phosphoenolpyruvate. Phosphonates can have concentrations in open ocean water that account for up to 25% of dissolved organic phosphorus (Acker et al., 2022). Their exact function is still not known, but they might represent a means of sequestering phosphorus among community members (Metcalf et al., 2012). That proposal has however recently been challenged because the phosphonate synthesis and utilization genes are so common: phosphonates might also mediate biological interactions at the cell surface (Acker et al., 2022). The question posed by Frouin et al. (2022) is: What are microbes from serpentinizing systems doing with a high frequency of phosphonate metabolizing enzymes?

Moreover, in some of the Prony Bay metagenomes, the gene for an additional enzyme, NAD^+-dependent phosphite oxidoreductase, *ptxD*, was often inserted into the phosphonate metabolizing operon (Frouin et al., 2022). The *ptxD* gene product converts phosphite and NAD^+ to phosphate and NADH (Vrtis et al., 2001). Frouin et al. (2022) noted the ability of Prony Bay microbes to utilize reduced phosphorous compounds. They were mainly concerned with the question of what the source of phosphonates in the Prony Bay fluid might be. While about half of the genomes from the Prony Bay vents contained genes related to phosphonate metabolism, metabolizing operons represent a frequency that is significantly higher than average for marine microbes (Frouin et al., 2022), it is not orders of magnitude higher: up to 30 % of marine microbial genomes have the potential for phosphonate degradation (Acker et al., 2022).

New findings by Pasek et al. (2022) suggest that the phosphite oxidase gene, *ptxD*, that Frouin et al. find inserted into the phosphonate (phn) operon might hold an important clue. Why is phosphite relevant? Two reasons: First, phosphite is much more soluble than phosphate. One solution to the "phosphate problem" of early evolution is that phosphorus in the ancient oceans was present in the form of the much more soluble phosphite ion (Schwartz, 2006). Studies by Pasek and colleagues have suggested that phosphite might have been more prevalent on the early Earth than it is today. Archaean oceans may have contained substantial amounts of phosphite in addition to phosphate (Pasek et al., 2013; Herschy et al., 2018). If phosphite was present in early environments but phosphate was needed, enzymatic phosphite oxidation would have been needed. Might the presence of phosphonates in the ocean, with P^{+3} oxidation state (like phosphite) and oxidation to phosphate (P^{+5}) in the cytosol, reflect a relic of ancestral marine environments? It is possible.

Second, where does phosphite in the environment come from such that so many microbes should have genes for phosphite metabolism (Schink et al., 2002)? In older papers, a source of ancient phosphite was originally suggested to be schreibersite from meteorite bombardments (Pasek et al., 2013). Schreibersite is a highly reactive phosphide mineral $(Ni, Fe)_3P$, that is indeed only known from meteorites (Pasek, 2008). But phosphite oxidation genes are commonplace today (Schink and Friedrich, 2000; Vrtis et al., 2001), being found in roughly 1.5 % of all genomes (Ewens et al., 2021), whereas huge schreibersite spreading impacts are rare at best. This clearly indicates that there are sources of phosphite in the environment that do not require bolide impacts.

The midpoint potential for the reduction of phosphate to phosphite is –690 mV at pH 7 and 25°C (Schink et al., 2002) (see Figure 2) but becomes more negative with higher pH (Bernhard Schink pers. comm.). Considering the measured and calculated reduction and midpoint potentials for serpentinizing systems is within the range of –435 to –830 mV, the reduction of phosphate to phosphite might not be within the range covered by H_2 in modern serpentinizing systems, [...] but might lie within the range of serpentinization processes that generate H_2 on early Earth. This brings us to a question relevant for modern microbial communities and for life's origins: do serpentinizing systems actually generate phosphite? The answer appears to be yes (Pasek et al., 2022), although phosphite has not been reported to be present directly in the effluent of serpentinizing systems. Pasek et al. (2022) measured phosphorus species in samples of rock from formations altered by serpentinization, they found that 20–50 % of the total P in some samples was phosphite (the remainder was phosphate). That corresponds to a substantial amount of phosphite stemming from serpentinization. The implications of i) genes for phosphite oxidation being present in microbes from serpentinizing systems (Frouin et al., 2022) and ii) phosphite being a component of rock in serpentinizing hydrothermal systems (Pasek et al., 2022) suggest that there is phosphite available in serpentinizing systems and that microbes that live there are using it. Could they be using this as a soluble source of P for enzymatic phosphate synthesis? If so, this would tie together some loose ends in phosphate metabolism and early evolution.

It is possible that genes for phosphite uptake and conversion into its biologically more useful form, phosphate, might reflect an ancient, possibly even ancestral state of phosphorus metabolism. As Buckel (2001) put it: "*At the time of the origin of life, about 3.8 billion years ago, phosphites could have been more important than today*." This would mean that the highly exergonic conversion of phosphite into its biologically relevant form, phosphate, occurred inside cells. But in early chemical evolution, before there were enzymes, was there a role for phosphite? This has not yet been extensively studied. Incorporation of phosphate into the fabric of early protobiochemical synthesis still presents a few sticking points in early metabolic evolution (Martin, 2020), environmental phosphite offers some alternative entry routes (Buckel, 2001).

Finally, the relevance of phosphite is underscored by the circumstance that it is a growth substrate for microbes, specifically for anaerobic autotrophs (Schink and Friedrich, 2000). Schink et al. (2002) characterized *Desulfotignum phosphitoxidans*, that grew autotrophically with phosphite as the sole electron donor and CO_2 as the sole electron acceptor. The energy-yielding metabolic reaction was the synthesis of phosphate with some acetate being produced as well. *D. phosphitoxidans* can also grow as a sulfate reducer that uses the acetyl-CoA pathway. In the absence of sulfate, its metabolism was that of an acetogen with energy generated by CO_2 reduction to acetate but using phosphite instead of H_2 as a source of electrons (Schink et al., 2002). Another phosphite oxidizer was recently isolated, but it was an autotrophic phosphite specialist — the strict anaerobe grew as a phosphite-dependent autotroph, using only phosphite as the electron donor and only CO_2 as the electron acceptor (Mao et al., 2021).

Buckel (2001) suggested that the highly exergonic process of phosphite oxidation might be coupled to substrate level phosphorylation, which is thermodynamically possible, but has not yet been shown so far. Phosphite in the environment appears to be derived from serpentinization. It is the only reductant other than H_2 that is known to fuel chemolithoautotrophic growth using the acetyl-CoA pathway. This links phosphite to serpentinization and ancient acetogenic physiology. Phosphite has a sufficiently negative midpoint potential that electron bifurcation would not be needed to reduce ferredoxin in cells that use phosphite, but its enzymatic oxidation product is NADH, which would require electron bifurcation for ferredoxin reduction.

5. Serpentinization, biochemical networks, physiology, and autotrophic origins

Under theories for autotrophic origins, the first free-living cells were able to synthesize all of their components from CO_2, a reductant (H_2), a nitrogen source and inorganic salts. It is a long way from the $H_2 + CO_2$-dependent synthesis of formate, acetate and pyruvate to the synthesis of free-living autotrophic cells, which require on the order of 1,500 genes and proteins to survive. Chemical reaction systems called autocatalytic networks are typically seen as intermediates in that evolutionary transition. Autocatalytic networks are objects of molecular (self-)organization. They involve catalytic properties of compounds within the network that act as simple catalysts to accelerate reactions within the network such that more products within the network, hence more catalysts, arise from the starting compounds (typically called the food set for the network) (Hordijk et al., 2011). Autocatalytic sets called RAFs (reflexively autocatalytic food-generated networks) are of particular interest for origins because they can be easily modeled on the computer (Hordijk and Steel, 2017)

and because they can be detected in the metabolic maps of modern microbes (Sousa et al., 2015). Xavier et al. (2020) detected RAFs in the metabolic maps of a well-curated acetogen and a well-curated methanogen. The sizes of those networks were 394 reactions (acetogen) and 209 reactions (methanogen) respectively. The acetogen and methanogen RAFs overlapped by 172 reactions that correspond to the RAF of their last common ancestor, which is effectively the RAF of the last universal common ancestor LUCA, which was highly enriched for transition metal catalysts and carbon metal bonds.

Note that the structure of RAFs (mathematical constructs) and the structure of real metabolic maps are not identical, such that a number of simplifying assumptions have to be made in order to apply RAF-detecting algorithms to real metabolic maps; Sousa et al. (2015) spelled out 11 simplifying assumptions that need to be taken into account when identifying RAFs in metabolic maps. The RAF of LUCA had the interesting property that RNA nucleobases arise from metabolic networks, but metabolic networks do not arise from bases, in line with a metabolism first view of origins as opposed to an RNA first view (Xavier et al., 2020). Xavier and Kauffman (2022) recently found that small-molecule autocatalytic networks are present in over 6,000 metabolic maps investigated, suggesting that autocatalytic networks are not only ancient, tracing to LUCA, but that they are also universal in metabolism.

The requirement for catalysis in RAFs means that cofactors are highly represented in RAFs detected computationally and that essential products that are required for life might not be included in a RAF. For example, the RAF of LUCA (Xavier et al., 2020) did not generate all amino acids or cofactors. How many reactions did primordial metabolism encompass? Autotrophs would need to synthesize all small molecules of metabolism themselves. Wimmer et al. (2021a) found that only 404 reactions are required to synthesize the 20 canonical amino acids, the bases of RNA and DNA (excluding modifications) and the 18 cofactors of ancient metabolism from H_2, CO_2, NH_3, H_2S, H_2O and P_i. Furthermore, 97 % of those reactions were exergonic under the conditions of a serpentinizing hydrothermal vent (alkaline, high pH, H_2 as a reductant), indicating that there is a natural tendency for reaction of metabolism to unfold under far from equilibrium hydrothermal conditions (Wimmer et al., 2021b). A theoretical study by Nunes Palmeira et al. (2022) involving autocatalysis in a simplified metabolic model concluded that various lines of evidence indicate that metabolism emerged from a geochemical protometabolism fueled by H_2 and CO_2.

Reconstructions of metabolism are also in line with an autotrophic origin of life at hydrothermal vents. Mei et al. (2023) and Williams et al. (2017) found that the ancestral physiology of archaea was likely hydrogen-dependent methanogenesis. Xavier et al. (2021) found that the ancestral physiology of bacteria was likely hydrogen-dependent acetogenesis. Coleman et al. (2021) found that the acetyl-CoA pathway reconstructs to the root of bacterial phylogeny although there is some discussion about the method they employed to infer the position of the root in the bacterial tree (Bremer et al., 2022). Schöne et al. (2022) found that with considerable genetic manipulation, a methanogen could be converted into acetogenic physiology, reflecting ancient physiological connections between the two groups and possibly uncovering an ancestral state of ATP synthesis via substrate level phosphorylation prior to the origin of chemiosmotic ATP synthesis. These findings that trace the exergonic reactions of H_2 with CO_2 in acetogenesis and methanogenesis to the first cells are consistent with genomic reconstructions of LUCA indicating that LUCA arose from similar reactions at a serpentinizing hydrothermal vent and that the most ancient lineages of anaerobes are acetogens and methanogens (Weiss et al., 2016). While there are numerous genomic reconstructions of LUCA present in the literature, they almost all focus on attributes and processes that are universal or nearly so among cells such as protein synthesis, ribosomal proteins, conserved pathways, and nucleic acids (Goldman et al., 2013) or genetics and lateral gene transfer (Crapitto et al., 2022). The studies of Weiss et al. (2016, 2018) took a different approach by looking carefully at physiology rather than universal gene distribution, in order to extract information about the environment in which LUCA arose and diversified and the presence of ancient physiological attributes such as transition metal catalysis, autotrophy, exergonic H_2-dependent CO_2 reduction, geochemical methyl groups, substrate level phosphorylation, and chemiosmotic ATP synthesis utilizing geochemical ion gradients. The studies of Weiss et al. (2016, 2018) are sometimes criticized for inferences about thermophily and use of the term "progenote "(Gogarten and Deamer, 2016), but no other study of LUCA makes a statement on the origin of ATP to drive any of the processes that are ascribed to LUCA by gene and genome-based inference. To drive ATP synthesis, exergonic chemical reactions of compounds in the environment have to be harnessed and the energy conserved as a biologically useful form such as thioesters, acyl anilides, acyl phosphates or ATP. In our model for LUCA and origins, LUCA's energy conservation and ATP synthesis comes from serpentinization.

5.1. Serpentinization: brimming with the energy of life

There are only two basic ways that cells conserve energy as high energy phosphate bonds: substrate level phosphorylation (Decker et al., 1970) and chemiosmotic energy harnessing using a rotor-stator ATP synthase (Walker et al., 1982; Walker, 2013). Serpentinizing systems provide a chemical environment that can support the origin of both forms of biological energy conservation.

Substrate level phosphorylation usually involves the generation of an acyl phosphate (or enol phosphate) bond during the oxidative breakdown of reduced carbon compounds. The classical example is the synthesis of the acyl phosphate bond in 1,3-bisphosphoglycerate at the reaction catalyzed by glyceraldehyde-3-phosphate dehydrogenase by oxidizing the aldehyde group on C1 of glyceraldehyde-3-phosphate with NAD^+ to form a thioester bond between the enzyme and the substrate, which is cleaved via phosphorolysis, generating the acyl phosphate bond at C1 which can phosphorylate ADP to generate ATP. There are also reductive routes of SLP, for example the conversion of the thioester bond in acetyl-CoA from the (reductive) acetyl-CoA pathway to acetyl phosphate, which can also phosphorylate ADP. Although the direct synthesis of acyl phosphates from thioesters has so far not been reported, it has long been known that acyl phosphates can phosphorylate ADP without enzymes (Kitani et al., 1991). More recently, Whicher et al. (2018) have shown that thioacetate can readily react with P_i to form acyl phosphates without enzymes, although thioacids are not known in central carbon or energy metabolism. The synthesis of acetate and pyruvate from H_2 and CO_2 under serpentinizing vent conditions using catalysts synthesized at hydrothermal vents — awaruite and magnetite

— is facile whereby there is furthermore enough energy released in the synthesis of acetate to energetically support SLP (Preiner et al., 2020; Belthle et al., 2022; Beyazay et al., 2023a,b). Reductive SLP also takes place via acetyl phosphate synthesis at the glycine reductase reaction (Andreesen, 2004) and the subsequent phosphorylation of ADP. Otherwise, net ATP synthesis involves either SLP via oxidation reactions of organic compounds (Müller, 2003; Martin and Thauer, 2017), which are thermodynamically unfavorable under the reducing conditions of serpentinizing systems, or it involves chemiosmotic ATP synthesis using the rotor-stator ATP synthase.

The rotor-stator ATP synthase is universal among cells. It generates ATP by the passage of protons (or Na^+) from the outside of the cell through the ATP synthase to the inside of the cell. The passage of protons through the ion channel of the stator subunit *a* and the subsequent protonation and deprotonation of an acidic residue in each of the c subunits of the ring-shaped rotor sets the rotor of the ATP synthase in rotation, inducing conformational changes in the catalytic subunits of the "head," changes that forge a phosphoanhydride bond between ADP and P_i and lead to release of ATP from the enzyme. Three ATP molecules are synthesized per complete 360° rotation of the head, this requires roughly 12 protons traversing the enzyme. This mechanism of ATP synthesis is universal in bacteria and archaea, it is furthermore reversible such that cells can expend ATP that they obtain from SLP to generate ion gradients for the import of small molecules (Franklin, 1986) or to generate reduced ferredoxin (Buckel and Thauer, 2013). The ion gradients that modern cells use to power chemiosmotic ATP synthesis are generated by membrane integral ion pumping proteins, or coupling sites, that pump protons (or Na^+) from the inside of the cell to the outside. There are two ways that pumping can be achieved: i) with the help of conformational changes within membrane-integral domains, and ii) with the help of what Mitchell called vectorial chemistry (Mitchell, 1991). In the former, the general mechanism (conformational change) is the same as that for the ATP synthase, except that the energy for conformational change and pumping stems from exergonic redox reactions that are part of the overall bioenergetic reactions of the cell, for example methane synthesis from H_2 and CO_2 (in methanogens) or acetate synthesis from H_2 and CO_2 (in acetogens). The second, evolutionarily more advanced mechanism (vectorial chemistry) requires the existence of quinones or quinone analogs (Berry, 2002), membrane soluble redox factors that can accept an electron pair and two protons on the cytosolic side and transfer the electron pair to an acceptor on the outside of the cell, thereby transferring protons from the inside of the cell to the outside merely by the relative position of hydride donor and hydride acceptor across the membrane. Ancient lineages of methanogens and acetogens lack quinones. They generate their ion gradients solely via conformational changes in membrane proteins (pumping).

It is a very curious observation that the principle of harnessing ion gradients for ATP synthesis and the enzyme that does it, the rotor-stator ATP synthase, are as universally conserved across all bacteria and archaea as the ribosome and the genetic code itself. This indicates that ion gradient harnessing was present in LUCA. LUCA could *use* ion gradients. Yet there is no similar form of conservation to indicate that LUCA could *generate* ion gradients. But if LUCA arose and existed at a serpentinizing vent, as much other evidence summarized above indicates, there is also no need to assume that LUCA had to generate ion gradients by itself, because serpentinization generates geochemical ion gradients continuously and for free that remain stable for the duration of the serpentinization process. Recalling that Lost City has been actively serpentinizing for roughly 100,000 years (Ludwig et al., 2011; Denny et al., 2016), a stable geochemically generated pH gradient of the right polarity (alkaline, lower proton concentration on the inside) and sufficient magnitude (cells synthesize ATP with the help of a pH difference of about one pH unit) (Tran and Unden, 1998; Silverstein, 2014) would present a continuous environmental setting in which natural chemiosmotic potential existed and could be harnessed (Martin and Russell, 2007; Martin, 2012).

This natural chemiosmotic energy source would have allowed the ancestral ATP synthase to function but would have required the evolution of protein based pumping mechanisms in the ancestors of the archaea and the bacteria in order for LACA (Last Archaeal Common Ancestor), (a methanogen) and LBCA (Last Bacterial Common Ancestor) (an acetogen) to make the transition to the free-living state. Methanogens without cytochromes pump with energy derived from H_2-dependent CO_2 reduction. The pumping reaction takes place at the methyl transferase step catalyzed by the membrane protein MtrA-H, which in a cobalamine-dependent reaction transfers a methyl group from a nitrogen atom in methyl-H_4MPT to a sulfur atom in coenzyme M; the free energy of the reaction $\Delta G_o'$ is $-30\,kJ{\cdot}mol^{-1}$ and pumps two Na^+ ions from the inside of the cell to the outside (Thauer et al., 2008). This energy conserving reaction is universal among H_2-dependent methanogens and likely represents their ancestral state. In acetogens without cytochromes, the pumping reaction is energetically driven by H_2-dependent CO_2 reduction and is catalyzed by the membrane protein Rnf, which pumps Na^+ from the inside of the cell to the outside while transferring electrons from reduced ferredoxin to NAD^+ (Biegel et al., 2011) with a $\Delta G_o'$ of $-34.7\,kJ{\cdot}mol^{-1}$ (Kuhns et al., 2020).

By coupling H_2-dependent CO_2 reduction to ion gradient formation, cells were able to generate their own ion gradients, were no longer dependent on geochemical ion gradients for ATP supply and could make the transition to the free-living state. The machinery to generate ion gradients by coupling exergonic reactions of H_2-dependent CO_2 reduction to ion pumping arose independently in the lineages leading to LBCA and LACA, because different steps were harnessed and unrelated enzymes were used. Note that both acetogens and methanogens require flavin based electron bifurcation to generate reduced ferredoxin for CO_2 reduction (Buckel and Thauer, 2018; Müller et al., 2018), but this is not required in CO_2 reduction promoted by metal catalysts (e.g., Ni_3Fe, Fe_3O_4) because of the very low midpoint potentials for H_2 oxidation that are generated by very high pH (Martin, 2022). A summary of energy inputs from serpentinization into the origin of biochemistry is given in Figures 3,4.

6. Serpentinization in our solar system

Since olivine is the most abundant silicate mineral that condensed during the formation of the solar system, ultramafic rocks are not unique to Earth and probably ubiquitous in most, if not all, rocky bodies of the solar system (McCollom and Seewald, 2013). Besides Earth there are currently two other solar system bodies where there is evidence for serpentinization: Mars and the Saturn moon Enceladus (Oze and Sharma, 2005; Glein et al., 2015). On Mars ultramafic and

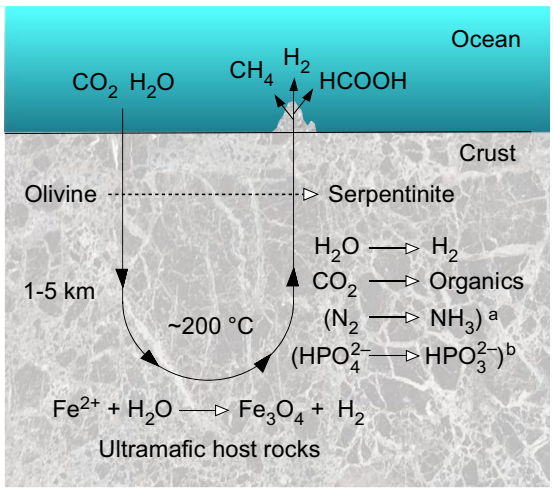

FIGURE 4
Serpentinization is a planetary scale reducing agent. The figure is modified from (Preiner et al., 2018). During serpentinization, surface water (seawater or freshwater) is drawn down into cracks in the crust where it reacts with ultramafic rocks at temperatures of about 200°C. During the reaction, Fe^{2+} in olivine is oxidized by water to Fe^{3+}, generating iron oxides in serpentinite and magnetite, Fe_3O_4, as well as H_2, diffusible reductant (Sleep et al., 2004; Bach et al., 2006; Lang et al., 2010). The reduction process converts water to H_2, CO_2 to formate and methane as well as other organics, and in newer studies of laboratory scale serpentinization, it converts N_2 to NH_3 (Shang et al., 2023b). Simulated geochemical systems using Co and Fe as catalysts can generate hydrocarbons from bicarbonate at high temperature and pressure (He et al., 2021). Although any kind of hydrophobic compounds could serve as insulators for the function of an ATP synthetase, long chain hydrocarbons are an option prior to the origin of genetically encoded enzymes for lipid synthesis. [a]The reduction of N_2 to NH_3 is indicated in parentheses because this has not been directly shown in modern serpentinizing systems, [...] but it occurs in laboratory scale serpentinization and very likely occurred in the Hadean crust [...] (Shang et al., 2023a,b). [b]Phosphate to phosphite is shown in parentheses because it is a recent discovery that serpentinzing systems might be able to generate it because naturally occurring serpentinized rocks can contain phosphite (Pasek et al., 2022); as with N_2 reduction to NH_3 the reaction has not been demonstrated in serpentinizing systems today.

serpentinized rocks have been found, with the olivine on Mars having an even higher iron content than that found on Earth (Hoefen et al., 2003; Christensen et al., 2004; Ehlmann et al., 2010; Holm et al., 2015; Tutolo and Tosca, 2023). Organic synthesis has been detected in Martian meteorites that date back 4 Ga which likely happened through serpentinization (McCollom and Seewald, 2013; Steele et al., 2022). Since water (in frozen form) has been detected on the surface of Mars, it is likely that it is also present in Mars' crust where it could interact with ultramafic material, which means that serpentinization could occur and H_2 and CH_4 could be produced (Etiope, 2017). Since both gases would disperse immediately in the Martian atmosphere [which mainly consists of CO_2 (Mahaffy et al., 2013)], direct monitoring is the only way these gases could be detected (Etiope and Sherwood Lollar, 2013; Holm et al., 2015). Such measurements have been conducted, for example with the Curiosity Rover (House et al., 2022) and on other missions (Lyons et al., 2005) and through observations from Earth (Mumma et al., 2009), however it is unclear if the detection of methane in some of these measurements originates from a contamination in the method employed by the rover (Schoell, 2022).

Using observational data from the Cassini spacecraft, Glein et al. (2015) constructed a model determining the pH and likely chemical composition of Enceladus. They found that Enceladus' ocean is a Na-Cl-CO_3 solution with a pH of 11–12. Zolotov (2007) also concluded in a different study that the ocean of Enceladus has a hyperalkaline pH. Enceladus shares the dominance of dissolved Na-Cl with Earth's oceans but the ubiquity of dissolved Na_2CO_3 is more comparable to soda lakes. The high pH is most likely a consequence of serpentinization and after the discovery of H_2 in the plume of Enceladus (Waite et al., 2017) it is even more likely that serpentinization is still actively occurring. CO_2 and CH_4 has also been detected in Enceladus plume and active serpentinization happening would also explain the presence of other organic species in Enceladus plume (Glein et al., 2015; Waite et al., 2017). In a recent study by Postberg et al. (2023) orthophosphates have been found in ice grains of Enceladus plume. The concentrations found indicates that Enceladus ocean has about a 100 times larger abundance of phosphates than Earth's oceans, with a phosphate: phosphite [...] 10:1, since phosphates are more stable under the alkaline conditions of Enceladus ocean. Of the elements considered essential for life (CHNOPS), phosphorus is found the least in astronomical observations and Enceladus is the first ocean world in our Solar System where it has been detected. The availability of phosphorus has been considered a bottle-neck for bio-essential elements on Enceladus and other icy moons and with the discovery of phosphorus in its oceans, Enceladus satisfies yet another requirement for potential habitability.

Other solar system bodies where it is strongly suspected that serpentinization might be happening are other icy moons of the gas giants (Jupiter, Saturn, Neptune, Uranus) (Vance et al., 2007; Schrenk et al., 2013; Vance et al., 2016; Lunine, 2017). Basically, wherever ultramafic rocks get in contact with circulating liquid water with temperatures below 350°C, serpentinization will occur (McCollom and Seewald, 2013). However, unlike with Enceladus, where we are lucky enough to have direct data from the plume because of the Cassini Mission, no direct measurement could be taken yet at these other icy moons and only theoretical models exist (Vance et al., 2007, 2016). It is however likely that we will have data of Europa soon, an icy moon of Jupiter, because missions have been planned from both ESA and NASA, with ESA's JUICE mission having launched earlier this year (ESA, 2023).

7. Conclusion

We return to the passage in the introduction of this paper about meteorite impacts as surface reduction processes vs. reduction in the crust. Available data indicate that the crust can generate reduced nitrogen in serpentinizing systems (Nobu et al., 2023; Shang et al., 2023b) and phosphite during serpentinization (Pasek et al., 2022), with carbon and sulfur reduction reactions being facile under serpentinizing conditions. From that it follows that all of the essential reduction reactions underlying the conversion of the elements on the early Earth from their ancestrally oxidized states (CO_2, N_2, HPO_4^{2-}, SO_2) to their biologically relevant state — reduced C, NH_3, H_2S, and in the case of P, the biochemically accessible state — now appear to lie within the range that serpentinizing systems can generate naturally (Russell et al., 2010; Boyd et al., 2020). In traditional cyanide-based RNA-world theories, the reducing functions required at origins are

attributed to meteorite impacts or UV-dependent reactions. In subsurface origins theories, serpentinization provides all the reducing power needed for organic synthesis and life. In the subsurface theory, the first organisms were anaerobic chemolithoautotrophs that arose, lived and diversified in complete darkness within the walls of serpentinizing, hence strongly reducing, hydrothermal vents. Such a scenario is much in line with what many microbiologists have thought for many decades. It would also be compatible with the environments presented by a growing number of moons and planets that lie beyond the confines of our atmosphere.

Serpentinization occurs at many sites on Earth and probably elsewhere in our solar system. It is relevant to the study of the origin of life and astrobiology for many reasons outlined here, but mainly because it is a source of a strong and diffusible reductant: H_2. It generates favorable conditions for organic synthesis and the emergence of life. It synthesizes catalysts that can act as the precursors to enzymes and electron donors that provide energy for metabolism and simple carbon compounds as a nutrient source. Microbial communities of serpentinizing systems, such as Lost City and Old City, provide what could be windows into the physiology of LUCA. The microbial communities of continental and shallow serpentinizing systems like Prony Bay might provide the same kind of window into the physiology of the first microbes as acetogens and methanogens serve as primary producers. Despite the differences between serpentinization sites on land and in the oceans, there is enough overlap between the geochemically produced compounds, the physiological conditions such as the pH and the temperature, as well as the microbial communities, that continental serpentinizing systems can serve as important proxies for the less easily accessible and less abundant deep-sea systems as well as the currently inaccessible serpentinizing systems beyond the confines of Earth.

Author contributions

LS: Conceptualization, Data curation, Visualization, Writing – original draft, Writing – review & editing. MB, Writing – review & editing. NM: Writing – review & editing. JW, Data curation, Visualization, Writing – review & editing. MP: Data curation, Visualization, Writing – review & editing. WM: Conceptualization, Data curation, Funding acquisition, Project administration, Visualization, Writing – original draft, Writing – review & editing.

Funding

The author(s) declare financial support was received for the research, authorship, and/or publication of this article. This project has received funding from the European Research Council (ERC) under the European Union's Horizon 2020 research and innovation program (grant agreement No. 101018894 to WM). This work was also supported by Volkswagen Foundation (96742 to WM).

Conflict of interest

The authors declare that the research was conducted in the absence of any commercial or financial relationships that could be construed as a potential conflict of interest.

Publisher's note

Supplementary material

The Supplementary material for this article can be found online at: https://www.frontiersin.org/articles/10.3389/fmicb.2023.1257597/full#supplementary-material

SUPPLEMENTARY FIGURE 1
Linear regression between the H_2 and CH_4 concentrations in the serpentinizing systems in this study. Here we show a linear regression of hydrogen and methane concentrations of the serpentinizing systems in this study when both compounds were reported or detected. Since mostly ranges of concentrations are reported in Table 1, the maximum concentrations reported were used for the linear regression shown in this figure for simplicity. During the analysis two data points stood out. (**A**) At first there seems to be no relationship between the hydrogen and methane concentrations between the different serpentinizing systems in this study, with $r^2 = 0.0551$ and $p = 0.4626$. However, the Prony Bay data reported by (Twing et al., 2022) in Table 4 of their study stands out in contrast to the others and after checking the sources that (Twing et al., 2022) used for Table 4, it seems like they accidentally reported mM amounts of hydrogen and methane for Prony Bay even though the two sources they cite for that data ((Quéméneur et al., 2014) (Postec et al., 2015)) report hydrogen and methane in vol% in their supplementary material. It also contradicts the data reported by (Quéméneur et al., 2023) where the hydrogen and methane concentrations are a magnitude lower, and the ratio of the abundances is also different. (**B**) Linear regression of the serpentinizing systems in this study without the Prony Bay data from (Twing et al., 2022) with $r^2 = 0.0596$ and $p = 0.0136$. This already suggests a high significance of the relationship between the concentrations for hydrogen and methane, however Ashadze still seems to be a clear outlier. (**C**) Linear regression of the serpentinizing systems without the data from Prony Bay (Twing et al., 2022) and Ashadze (Schrenk et al., 2013) with $r^2 = 0.8419$ and $p = 0.0002$.

References

Abrajano, T. A., Sturchio, N. C., Bohlke, J. K., Lyon, G. L., Poreda, R. J., and Stevens, C. M. (1988). Methane-hydrogen gas seeps, Zambales ophiolite, Philippines: deep or shallow origin? *Chem. Geol.* 71, 211–222. doi: 10.1016/0009-2541(88)90116-7

Acker, M., Hogle, S. L., Berube, P. M., Hackl, T., Coe, A., Stepanauskas, R., et al. (2022). Phosphonate production by marine microbes: exploring new sources and potential function. *Proc. Natl. Acad. Sci.* 119:e2113386119. doi: 10.1073/pnas.2113386119

Andreesen, J. R. (2004). Glycine reductase mechanism. *Curr. Opin. Chem. Biol.* 8, 454–461. doi: 10.1016/j.cbpa.2004.08.002

Arndt, N. T., and Nisbet, E. G. (2012). Processes on the young earth and the habitats of early life. *Annu. Rev. Earth Planet. Sci.* 40, 521–549. doi: 10.1146/annurev-earth-042711-105316

Baaske, P., Weinert, F. M., Duhr, S., Lemke, K. H., Russell, M. J., and Braun, D. (2007). Extreme accumulation of nucleotides in simulated hydrothermal pore systems. *Proc. Natl. Acad. Sci.* 104, 9346–9351. doi: 10.1073/pnas.0609592104

Bach, W., Paulick, H., Garrido, C. J., Ildefonse, B., Meurer, W. P., and Humphris, S. E. (2006). Unraveling the sequence of serpentinization reactions: petrography, mineral

chemistry, and petrophysics of serpentinites from MAR 15°N (ODP leg 209, site 1274). *Geophys. Res. Lett.* 33:L13306. doi: 10.1029/2006GL025681

Bada, J. L., and Lazcano, A. (2002). Some like it hot, But Not the First Biomolecules. *Science* 1979, 1982–1983. doi: 10.1126/science.1069487

Barnes, I., LaMarche, V. C., and Himmelberg, G. (1967). Geochemical Evidence of Present-Day Serpentinization. *Science.* 156, 830–832. doi: 10.1126/science.156.3776.830

Baross, J. A. (2018). The rocky road to biomolecules. *Nature* 564, 42–43. doi: 10.1038/d41586-018-07262-8

Baross, J. A., and Hoffman, S. E. (1985). Submarine hydrothermal vents and associated gradient environments as sites for the origin and evolution of life. *Orig. Life* 15, 327–345. doi: 10.1007/BF01808177

Baross, J. A., and Martin, W. F. (2015). The Ribofilm as a concept for Life's origins. *Cells* 162, 13–15. doi: 10.1016/j.cell.2015.06.038

Belthle, K. S., Beyazay, T., Ochoa-Hernández, C., Miyazaki, R., Foppa, L., Martin, W. F., et al. (2022). Effects of silica modification (mg, Al, ca, Ti, and Zr) on supported cobalt catalysts for H2-dependent CO2 reduction to metabolic intermediates. *J. Am. Chem. Soc.* 144, 21232–21243. doi: 10.1021/jacs.2c08845

Benner, S. A., Bell, E. A., Biondi, E., Brasser, R., Carell, T., Kim, H.-J., et al. (2020). When did life likely emerge on earth in an RNA-first process? *Chem Systems Chem* 2:e1900035. doi: 10.1002/syst.201900035

Benner, S. A., Ellington, A. D., and Tauer, A. (1989). Modern metabolism as a palimpsest of the RNA world. *Proc. Natl. Acad. Sci.* 86, 7054–7058. doi: 10.1073/pnas.86.18.7054

Berg, I. A. (2011). Ecological aspects of the distribution of different autotrophic CO2 fixation pathways. *Appl. Environ. Microbiol.* 77, 1925–1936. doi: 10.1128/AEM.02473-10

Berg, I. A., Kockelkorn, D., Ramos-Vera, W. H., Say, R. F., Zarzycki, J., Hügler, M., et al. (2010). Autotrophic carbon fixation in archaea. *Nat. Rev. Microbiol.* 8, 447–460. doi: 10.1038/nrmicro2365

Berry, S. (2002). The chemical basis of membrane bioenergetics. *J. Mol. Evol.* 54, 595–613. doi: 10.1007/s00239-001-0056-3

Beyazay, T., Belthle, K. S., Farès, C., Preiner, M., Moran, J., Martin, W. F., et al. (2023a). Ambient temperature CO2 fixation to pyruvate and subsequently to citramalate over iron and nickel nanoparticles. *Nat. Commun.* 14:570. doi: 10.1038/s41467-023-36088-w

Beyazay, T., Ochoa-Hernández, C., Song, Y., Belthle, K. S., Martin, W. F., and Tüysüz, H. (2023b). Influence of composition of nickel-Iron nanoparticles for abiotic CO2 conversion to early prebiotic organics. *Angew. Chem. Int. Ed.* 62:e202218189. doi: 10.1002/anie.202218189

Biegel, E., Schmidt, S., González, J. M., and Müller, V. (2011). Biochemistry, evolution and physiological function of the Rnf complex, a novel ion-motive electron transport complex in prokaryotes. *Cell. Mol. Life Sci.* 68, 613–634. doi: 10.1007/s00018-010-0555-8

Blaser, M. B., Dreisbach, L. K., and Conrad, R. (2013). Carbon isotope fractionation of 11 Acetogenic strains grown on H2 and CO2. *Appl. Environ. Microbiol.* 79, 1787–1794. doi: 10.1128/AEM.03203-12

Bose, T., Fridkin, G., Davidovich, C., Krupkin, M., Dinger, N., Falkovich, A. H., et al. (2022). Origin of life: protoribosome forms peptide bonds and links RNA and protein dominated worlds. *Nucleic Acids Res.* 50, 1815–1828. doi: 10.1093/nar/gkac052

Boyd, E. S., Amenabar, M. J., Poudel, S., and Templeton, A. S. (2020). Bioenergetic constraints on the origin of autotrophic metabolism. *Philos. Trans. R. Soc. A Math. Phys. Eng. Sci.* 378:20190151. doi: 10.1098/rsta.2019.0151

Brandes, J. A., Boctor, N. Z., Cody, G. D., Cooper, B. A., Hazen, R. M., and Yoder, H. S. (1998). Abiotic nitrogen reduction on the early earth. *Nature* 395, 365–367. doi: 10.1038/26450

Brazelton, W. J., McGonigle, J. M., Motamedi, S., Pendleton, H. L., Twing, K. I., Miller, B. C., et al. (2022). Metabolic strategies shared by basement residents of the lost City hydrothermal field. *Appl. Environ. Microbiol.* 88:e0092922. doi: 10.1128/aem.00929-22

Bremer, N., Knopp, M., Martin, W. F., and Tria, F. D. K. (2022). Realistic gene transfer to gene duplication ratios identify different roots in the bacterial phylogeny using a tree reconciliation method. *Life* 12:995. doi: 10.3390/life12070995

Buckel, W. (2001). Inorganic chemistry in marine sediments. *Angew. Chem. Int. Ed.* 40, 1417–1418. doi: 10.1002/1521-3773(20010417)40:8<1417::AID-ANIE1417>3.0.CO;2-V

Buckel, W., and Thauer, R. K. (2013). Energy conservation via electron bifurcating ferredoxin reduction and proton/Na+ translocating ferredoxin oxidation. *Biochim. Biophys. Acta - Bioenerg.* 1827, 94–113. doi: 10.1016/j.bbabio.2012.07.002

Buckel, W., and Thauer, R. K. (2018). Flavin-based Electron bifurcation, a new mechanism of biological energy coupling. *Chem. Rev.* 118, 3862–3886. doi: 10.1021/acs.chemrev.7b00707

Bulloch, W. (1938). *The history of bacteriology*. London: Oxford University Press.

Calisto, F., and Pereira, M. M. (2021). Modularity of membrane-bound charge-translocating protein complexes. *Biochem. Soc. Trans.* 49, 2669–2685. doi: 10.1042/BST20210462

Carter, C. W., and Wolfenden, R. (2015). tRNA acceptor stem and anticodon bases form independent codes related to protein folding. *Proc. Natl. Acad. Sci.* 112, 7489–7494. doi: 10.1073/pnas.1507569112

Chamberlain, J. A., McLeod, C. R., Traill, R. J., and Lachance, G. R. (1965). Native metals in the muskox intrusion. *Can. J. Earth Sci.* 2, 188–215. doi: 10.1139/e65-017

Charlou, J. L., Donval, J. P., Fouquet, Y., Jean-Baptiste, P., and Holm, N. (2002). Geochemistry of high H2 and CH4 vent fluids issuing from ultramafic rocks at the rainbow hydrothermal field (36°14′N, MAR). *Chem. Geol.* 191, 345–359. doi: 10.1016/S0009-2541(02)00134-1

Chavagnac, V., Monnin, C., Ceuleneer, G., Boulart, C., and Hoareau, G. (2013). Characterization of hyperalkaline fluids produced by low-temperature serpentinization of mantle peridotites in the Oman and Ligurian ophiolites. *Geochem. Geophys. Geosyst.* 14, 2496–2522. doi: 10.1002/ggge.20147

Christensen, P. R., Ruff, S. W., Fergason, R. L., Knudson, A. T., Anwar, S., Arvidson, R. E., et al. (2004). Initial results from the Mini-TES experiment in Gusev crater from the Spirit rover. *Science* 1979, 837–842. doi: 10.1126/science.1100564

Coleman, G. A., Davín, A. A., Mahendrarajah, T. A., Szánthó, L. L., Spang, A., Hugenholtz, P., et al. (2021). A rooted phylogeny resolves early bacterial evolution. *Science* 372:eabe 0511. doi: 10.1126/science.abe0511

Colman, D. R., Kraus, E. A., Thieringer, P. H., Rempfert, K., Templeton, A. S., Spear, J. R., et al. (2022). Deep-branching acetogens in serpentinized subsurface fluids of Oman. *PNAS* 119:e2206845119. doi: 10.1073/pnas

Cook, M. C., Blank, J. G., Rietze, A., Suzuki, S., Nealson, K. H., and Morrill, P. L. (2021). A geochemical comparison of three terrestrial sites of Serpentinization: the tablelands, the cedars, and aqua de Ney. *J. Geophys. Res. Biogeosci.* 126:e2021JG006316. doi: 10.1029/2021JG006316

Corliss, J. B., Baross, J. A., and Hoffman, S. E. (1981). An hypothesis concerning the relationships between submarine hot springs and the origin of life on earth. *Oceanol. Acta.* 26, 59–70.

Corliss, J. B., Dymond, J., Gordon, L. I., Edmond, J. M., von Herzen, R. P., Ballard, R. D., et al. (1979). Submarine thermal springs on the Galápagos rift. *Science* 1979, 1073–1083. doi: 10.1126/science.203.4385.1073

Costa, K. C., Wong, P. M., Wang, T., Lie, T. J., Dodsworth, J. A., Swanson, I., et al. (2010). Protein complexing in a methanogen suggests electron bifurcation and electron delivery from formate to heterodisulfide reductase. *Proc. Natl. Acad. Sci.* 107, 11050–11055. doi: 10.1073/pnas.1003653107

Crapitto, A. J., Campbell, A., Harris, A. J., and Goldman, A. D. (2022). A consensus view of the proteome of the last universal common ancestor. *Ecol. Evol.* 12:e8930. doi: 10.1002/ece3.8930

Darwin, C. R. (1859). *The origin of species*. PF Collier & Son New York.

Decker, K., Jungermann, K., and Thauer, R. K. (1970). Energy production in anaerobic organisms. *Angew. Chem. Int. Ed. Engl.* 9, 138–158. doi: 10.1002/anie.197001381

Denny, A. R., Kelley, D. S., and Früh-Green, G. L. (2016). Geologic evolution of the lost City hydrothermal field. *Geochem. Geophys. Geosyst.* 17, 375–394. doi: 10.1002/2015GC005869

Deutzmann, J. S., Sahin, M., and Spormann, A. M. (2015). Extracellular enzymes facilitate Electron uptake in biocorrosion and Bioelectrosynthesis. *MBio* 6. doi: 10.1128/mbio.00496-15

Dolfing, J., Jiang, B., Henstra, A. M., Stams, A. J. M., and Plugge, C. M. (2008). Syntrophic growth on Formate: a new microbial niche in anoxic environments. *Appl. Environ. Microbiol.* 74, 6126–6131. doi: 10.1128/AEM.01428-08

Dörr, M., Käßbohrer, J., Grunert, R., Kreisel, G., Brand, W. A., Werner, R. A., et al. (2003). A possible prebiotic formation of Ammonia from dinitrogen on Iron sulfide surfaces. *Angew. Chem. Int. Ed.* 42, 1540–1543. doi: 10.1002/anie.200250371

Duval, S., Zuchan, K., Baymann, F., Schoepp-Cothenet, B., Branscomb, E., Russell, M. J., et al. (2021). "*5 minerals and the emergence of LIFE*," in, eds. P. Kroneck and M. S. Torres (D. Gruyter), 135–158.

Ehlmann, B. L., Mustard, J. F., and Murchie, S. L. (2010). Geologic setting of serpentine deposits on Mars. *Geophys. Res. Lett.* 37. doi: 10.1029/2010gl042596

ESA (2023). JUICE Mission. Available at: https://www.esa.int/Science_Exploration/Space_Science/Juice

Etiope, G. (2015). *Natural gas seepage: The Earth's hydrocarbon degassing*. Springer International Publishing. New York.

Etiope, G. (2017). Abiotic methane in continental Serpentinization sites: an overview. *Procedia Earth Planet. Sci.* 17, 9–12. doi: 10.1016/j.proeps.2016.12.006

Etiope, G., Baciu, C. L., and Schoell, M. (2011a). Extreme methane deuterium, nitrogen and helium enrichment in natural gas from the Homorod seep (Romania). *Chem. Geol.* 280, 89–96. doi: 10.1016/j.chemgeo.2010.10.019

Etiope, G., Ehlmann, B. L., and Schoell, M. (2013). Low temperature production and exhalation of methane from serpentinized rocks on earth: a potential analog for methane production on Mars. *Icarus* 224, 276–285. doi: 10.1016/j.icarus.2012.05.009

Etiope, G., and Schoell, M. (2014). Abiotic gas: atypical, but not rare. *Elements* 10, 291–296. doi: 10.2113/gselements.10.4.291

Etiope, G., Schoell, M., and Hosgörmez, H. (2011b). Abiotic methane flux from the Chimaera seep and Tekirova ophiolites (Turkey): understanding gas exhalation from low temperature serpentinization and implications for Mars. *Earth Planet. Sci. Lett.* 310, 96–104. doi: 10.1016/j.epsl.2011.08.001

Etiope, G., and Sherwood Lollar, B. (2013). Abiotic methane on earth. *Rev. Geophys.* 51, 276–299. doi: 10.1002/rog.20011

Ewens, S. D., Gomberg, A. F. S., Barnum, T. P., Borton, M. A., Carlson, H. K., Wrighton, K. C., et al. (2021). The diversity and evolution of microbial dissimilatory phosphite oxidation. *Proc. Natl. Acad. Sci.* 118:e2020024118. doi: 10.1073/pnas.2020024118

Ferry, J. G., Smith, P. H., and Wolfe, R. S. (1974). Methanospirillum, a new genus of methanogenic Bacteria, and characterization of Methanospirillum hungatii sp. nov. *Int. J. Syst. Bacteriol.* 24, 465–469. doi: 10.1099/00207713-24-4-465

Fisher, A. T. (2005). Marine hydrogeology: recent accomplishments and future opportunities. *Hydrogeol. J.* 13, 69–97. doi: 10.1007/s10040-004-0400-y

Flemming, H.-C., and Wuertz, S. (2019). Bacteria and archaea on earth and their abundance in biofilms. *Nat. Rev. Microbiol.* 17, 247–260. doi: 10.1038/s41579-019-0158-9

Fones, E. M., Colman, D. R., Kraus, E. A., Stepanauskas, R., Templeton, A. S., Spear, J. R., et al. (2021). Diversification of methanogens into hyperalkaline serpentinizing environments through adaptations to minimize oxidant limitation. *ISME J.* 15, 1121–1135. doi: 10.1038/s41396-020-00838-1

Franklin, H. M. (1986). *Bioenergetics extended: The vital force. A study of bioenergetics*. New York: Freeman.

Frouin, E., Lecoeuvre, A., Armougom, F., Schrenk, M. O., and Erauso, G. (2022). Comparative metagenomics highlight a widespread pathway involved in catabolism of phosphonates in marine and terrestrial Serpentinizing ecosystems. *mSystems*:7:e0032822. doi: 10.1128/msystems.00328-22

Früh-Green, G. L., Kelley, D. S., Bernasconi, S. M., Karson, J. A., Ludwig, K. A., Butterfield, D. A., et al. (2003). 30, 000 years of hydrothermal activity at the lost City vent field. *Science* 1979, 495–498. doi: 10.1126/science.1085582

Fryer, P., Wheat, C. G., Williams, T., Kelley, C., Johnson, K., Ryan, J., et al. (2020). Mariana serpentinite mud volcanism exhumes subducted seamount materials: implications for the origin of life. *Philos. Trans. R. Soc. A Math. Phys. Eng. Sci.* 378:20180425. doi: 10.1098/rsta.2018.0425

Fuchs, G. (1994). "Variations of the acetyl-CoA pathway in diversely related microorganisms that are not acetogens" in *Acetogenesis*. ed. H. L. Drake (New York: Springer), 507–520.

Fuchs, G. (2011). Alternative pathways of carbon dioxide fixation: insights into the early evolution of life? *Annu. Rev. Microbiol.* 65, 631–658. doi: 10.1146/annurev-micro-090110-102801

Fuchs, G., and Stupperich, E. (1985). "Evolution of autotrophic CO2 fixation" in *Evolution of Prokaryotes, FEMS Symposium No. 29*. eds. K. H. Schleifer and E. Stackebrandt (London: Academic Press).

Fuchs, G., and Stupperich, E. (1986). Carbon assimilation pathways in archaebacteria. *Syst. Appl. Microbiol.* 7, 364–369. doi: 10.1016/S0723-2020(86)80035-2

Glein, C. R., Baross, J. A., and Waite, J. H. (2015). The pH of Enceladus' ocean. *Geochim. Cosmochim. Acta* 162, 202–219. doi: 10.1016/j.gca.2015.04.017

Gogarten, J. P., and Deamer, D. (2016). Is LUCA a thermophilic progenote? *Nat. Microbiol.* 1:16229. doi: 10.1038/nmicrobiol.2016.229

Goldman, A. D., Bernhard, T. M., Dolzhenko, E., and Landweber, L. F. (2013). LUCApedia: a database for the study of ancient life. *Nucleic Acids Res.* 41, D1079–D1082. doi: 10.1093/nar/gks1217

Grewal, D. S., Dasgupta, R., Sun, C., Tsuno, K., and Costin, G. (2023). Delivery of carbon, nitrogen, and sulfur to the silicate earth by a giant impact. *Sci. Adv.* 5:eaau 3669. doi: 10.1126/sciadv.aau3669

Grozeva, N. G., Klein, F., Seewald, J. S., and Sylva, S. P. (2020). Chemical and isotopic analyses of hydrocarbon-bearing fluid inclusions in olivine-rich rocks. *Philos. Trans. R. Soc. A Math. Phys. Eng. Sci.* 378:20180431. doi: 10.1098/rsta.2018.0431

Haldane, J. B. S. (1929). The origin of life. *Rationalist Ann* 148, 3–10.

Harrison, S. A., Webb, W. L., Rammu, H., and Lane, N. (2023). Prebiotic Synthesis of Aspartate Using Life's Metabolism as a Guide. *Life* 13:1177. doi: 10.3390/life13051177

Hartmann, T., Schrapers, P., Utesch, T., Nimtz, M., Rippers, Y., Dau, H., et al. (2016). The molybdenum active site of Formate dehydrogenase is capable of catalyzing C–H bond cleavage and oxygen atom transfer reactions. *Biochemistry* 55, 2381–2389. doi: 10.1021/acs.biochem.6b00002

He, D., Wang, X., Yang, Y., He, R., Zhong, H., Wang, Y., et al. (2021). Hydrothermal synthesis of long-chain hydrocarbons up to C24 with NaHCO3-assisted stabilizing cobalt. *Proc. Natl. Acad. Sci.* 118:e2115059118. doi: 10.1073/pnas.2115059118

Heldal, M., Norland, S., and Tumyr, O. (1985). X-ray microanalytic method for measurement of dry matter and elemental content of individual bacteria. *Appl. Environ. Microbiol.* 50, 1251–1257. doi: 10.1128/aem.50.5.1251-1257.1985

Henriques Pereira, D. P., Leethaus, J., Beyazay, T., do Nascimento Vieira, A., Kleinermanns, K., Tüysüz, H., et al. (2022). Role of geochemical protoenzymes (geozymes) in primordial metabolism: specific abiotic hydride transfer by metals to the biological redox cofactor NAD+. *FEBS J.* 289, 3148–3162. doi: 10.1111/febs.16329

Herschy, B., Chang, S. J., Blake, R., Lepland, A., Abbott-Lyon, H., Sampson, J., et al. (2018). Archean phosphorus liberation induced by iron redox geochemistry. *Nat. Commun.* 9:1346. doi: 10.1038/s41467-018-03835-3

Hoefen, T. M., Clark, R. N., Bandfield, J. L., Smith, M. D., Pearl, J. C., and Christensen, P. R. (2003). Discovery of olivine in the Nili fossae region of Mars. *Science* 1979, 627–630. doi: 10.1126/science.1089647

Holden, J. F., and Sistu, H. (2023). Formate and hydrogen in hydrothermal vents and their use by extremely thermophilic methanogens and heterotrophs. *Front. Microbiol.* 14:1093018. doi: 10.3389/fmicb.2023.1093018

Holm, N. G. (1992). *Marine hydrothermal systems and the origin of life*. Springer. New York.

Holm, N. G., Oze, C., Mousis, O., Waite, J. H., and Guilbert-Lepoutre, A. (2015). Serpentinization and the formation of H2 and CH4 on celestial bodies (planets, moons, comets). *Astrobiology* 15, 587–600. doi: 10.1089/ast.2014.1188

Hordijk, W., Kauffman, S. A., and Steel, M. (2011). Required levels of catalysis for emergence of autocatalytic sets in models of chemical reaction systems. *Int. J. Mol. Sci.* 12, 3085–3101. doi: 10.3390/ijms12053085

Hordijk, W., and Steel, M. (2017). Chasing the tail: the emergence of autocatalytic networks. *Biosystems* 152, 1–10. doi: 10.1016/j.biosystems.2016.12.002

Horita, J., and Berndt, M. E. (1999). Abiogenic methane formation and isotopic fractionation under hydrothermal conditions. *Science* 1979, 285, 1055–1057. doi: 10.1126/science.285.5430.1055

House, C. H., Wong, G. M., Webster, C. R., Flesch, G. J., Franz, H. B., Stern, J. C., et al. (2022). Depleted carbon isotope compositions observed at Gale crater, Mars. *Proc. Natl. Acad. Sci.* 119:e2115651119. doi: 10.1073/pnas.2115651119

Hu, Y., and Ribbe, M. W. (2016). Nitrogenases—a tale of carbon atom(s). *Angew. Chem. Int. Ed.* 55, 8216–8226. doi: 10.1002/anie.201600010

Hudson, R., de Graaf, R., Rodin, M. S., Ohno, A., Lane, N., McGlynn, S. E., et al. (2020). CO2 reduction driven by a pH gradient. *Proc. Natl. Acad. Sci.* 117, 22873–22879. doi: 10.1073/pnas.2002659117

Itcovitz, J. P., Rae, A. S. P., Citron, R. I., Stewart, S. T., Sinclair, C. A., Rimmer, P. B., et al. (2022). Reduced atmospheres of post-impact worlds: the early earth. *Planet. Sci. J.* 3:115. doi: 10.3847/PSJ/ac67a9

Johnson, P. V., Hodyss, R., Vu, T. H., and Choukroun, M. (2019). Insights into Europa's ocean composition derived from its surface expression. *Icarus* 321, 857–865. doi: 10.1016/j.icarus.2018.12.009

Kelley, D. S., Baross, J. A., and Delaney, J. R. (2002). Volcanoes, fluids, and life at Mid-Ocean ridge spreading centers. *Annu. Rev. Earth Planet. Sci.* 30, 385–491. doi: 10.1146/annurev.earth.30.091201.141331

Kelley, D. S., Karson, J. A., Blackman, D. K., Früh-Green, G. L., Butterfeld, D. A., Lilley, M. D., et al. (2001). An off-axis hydrothermal vent field near the mid-Atlantic ridge at 30° N. *Nature* 412, 145–149. doi: 10.1038/35084000

Kelley, D. S., Karson, J. A., Früh-Green, G. L., Yoerger, D. R., Shank, T. M., Butterfield, D. A., et al. (2005). A Serpentinite-hosted ecosystem: the lost City hydrothermal field. *Science* 307, 1428–1434. doi: 10.1126/science.1102556

Kirschning, A. (2021). Coenzymes and their role in the evolution of life. *Angew. Chem. Int. Ed.* 60, 6242–6269. doi: 10.1002/anie.201914786

Kitani, A., Tsunetsugu, S., and Sasaki, K. (1991). Fe-ion-catalysed non-enzymatic transformation of ADP in to ATP. *J. Chem. Soc. Perkin Trans.* 2, 329–331. doi: 10.1039/P29910000329

Konn, C., Charlou, J. L., Holm, N. G., and Mousis, O. (2015). The production of methane, hydrogen, and organic compounds in ultramafic-hosted hydrothermal vents of the mid-Atlantic ridge. *Astrobiology* 15, 381–399. doi: 10.1089/ast.2014.1198

Kraus, E. A., Nothaft, D., Stamps, B. W., Rempfert, K. R., Ellison, E. T., Matter, J. M., et al. (2021). Molecular evidence for an active microbial methane cycle in subsurface Serpentinite-hosted Groundwaters in the Samail ophiolite, Oman. *Appl. Environ. Microbiol.* 87, 1–18. doi: 10.1128/AEM.02068-20

Krissansen-Totton, J., Arney, G. N., and Catling, D. C. (2018). Constraining the climate and ocean pH of the early earth with a geological carbon cycle model. *Proc. Natl. Acad. Sci.* 115, 4105–4110. doi: 10.1073/pnas.1721296115

Kuhns, M., Trifunović, D., Huber, H., and Müller, V. (2020). The Rnf complex is a Na+ coupled respiratory enzyme in a fermenting bacterium, Thermotoga maritima. *Commun. Biol.* 3:431. doi: 10.1038/s42003-020-01158-y

Kuznetsov, V., Cherkashov, G., Lein, A., Shilov, V., Maksimov, F., Stepanova, T., et al. (2006). 230Th/U dating of massive sulfides from the Logatchev and rainbow hydrothermal fields (mid-Atlantic ridge). *Geochronometria* 8, 72–76. doi: 10.2478/s13386-011-0001-1

Lane, N., Allen, J. F., and Martin, W. (2010). How did LUCA make a living? Chemiosmosis in the origin of life. *Bio Essays* 32, 271–280. doi: 10.1002/bies.200900131

Lane, N., and Martin, W. (2010). The energetics of genome complexity. *Nature* 467, 929–934. doi: 10.1038/nature09486

Lang, S. Q., and Brazelton, W. J. (2020). Habitability of the marine serpentinite subsurface: a case study of the lost City hydrothermal field. *Philos. Trans. R. Soc. A Math. Phys. Eng. Sci.* 378:20180429. doi: 10.1098/rsta.2018.0429

Lang, S. Q., Butterfield, D. A., Schulte, M., Kelley, D. S., and Lilley, M. D. (2010). Elevated concentrations of formate, acetate and dissolved organic carbon found at the

lost City hydrothermal field. *Geochim. Cosmochim. Acta* 74, 941–952. doi: 10.1016/j.gca.2009.10.045

Lang, S. Q., Früh-Green, G. L., Bernasconi, S. M., Brazelton, W. J., Schrenk, M. O., and McGonigle, J. M. (2018). Deeply-sourced formate fuels sulfate reducers but not methanogens at lost City hydrothermal field. *Sci. Rep.* 8:755. doi: 10.1038/s41598-017-19002-5

Lang, S. Q., Früh-Green, G. L., Bernasconi, S. M., Lilley, M. D., Proskurowski, G., Méhay, S., et al. (2012). Microbial utilization of abiogenic carbon and hydrogen in a serpentinite-hosted system. *Geochim. Cosmochim. Acta* 92, 82–99. doi: 10.1016/j.gca.2012.06.006

Lecoeuvre, A., Ménez, B., Cannat, M., Chavagnac, V., and Gérard, E. (2021). Microbial ecology of the newly discovered serpentinite-hosted Old City hydrothermal field (southwest Indian ridge). *ISME J.* 15, 818–832. doi: 10.1038/s41396-020-00816-7

Lie, T. J., Costa, K. C., Lupa, B., Korpole, S., Whitman, W. B., and Leigh, J. A. (2012). Essential anaplerotic role for the energy-converting hydrogenase Eha in hydrogenotrophic methanogenesis. *Proc. Natl. Acad. Sci.* 109, 15473–15478. doi: 10.1073/pnas.1208779109

Liu, Y., Beer, L. L., and Whitman, W. B. (2012). Methanogens: a window into ancient sulfur metabolism. *Trends Microbiol.* 20, 251–258. doi: 10.1016/j.tim.2012.02.002

Ludwig, K. A., Shen, C.-C., Kelley, D. S., Cheng, H., and Edwards, R. L. (2011). U–Th systematics and 230Th ages of carbonate chimneys at the lost City hydrothermal field. *Geochim. Cosmochim. Acta* 75, 1869–1888. doi: 10.1016/j.gca.2011.01.008

Lundblad, R., and Macdonald, F. (2018) in *Handbook of biochemistry and molecular biology*. eds. R. Lundblad and F. Macdonald. *5th* ed (Boca Raton, FL: CRC Press)

Lunine, J. I. (2017). Ocean worlds exploration. *Acta Astronaut.* 131, 123–130. doi: 10.1016/j.actaastro.2016.11.017

Lyons, J. R., Manning, C., and Nimmo, F. (2005). Formation of methane on Mars by fluid-rock interaction in the crust. *Geophys. Res. Lett.* 32, 1–4. doi: 10.1029/2004GL022161

Maden, E. (2000). Tetrahydrofolate and tetrahydromethanopterin compared: functionally distinct carriers in C1 metabolism. *Biochem. J.* 352:935. doi: 10.1042/bj3520935u

Madigan, M., Bender, K., Buckley, D., Sattley, W., and Stahl, D. (2021). Brock biology of microorganisms, global edition. Pearson Deutschland Available at: https://elibrary.pearson.de/book/99.150005/9781292405063

Mahaffy, P. R., Webster, C. R., Atreya, S. K., Franz, H., Wong, M., Conrad, P. G., et al. (2013). Abundance and isotopic composition of gases in the Martian atmosphere from the curiosity rover. *Science* 1979, 263–266. doi: 10.1126/science.1237966

Mao, Z., Gräßle, F., Frey, J., Franchini, P., Schleheck, D., Müller, N., et al. (2021). Phosphitispora fastidiosa gen. Nov. sp. nov., a new dissimilatory phosphite-oxidizing anaerobic bacterium isolated from anaerobic sewage sludge. *Int. J. Syst. Evol. Microbiol.* 71. doi: 10.1099/ijsem.0.005142

Martin, W. F. (2012). Hydrogen, metals, bifurcating electrons, and proton gradients: the early evolution of biological energy conservation. *FEBS Lett.* 586, 485–493. doi: 10.1016/j.febslet.2011.09.031

Martin, W. F. (2020). Older than genes: the acetyl CoA pathway and origins. *Front. Microbiol.* 11:817. doi: 10.3389/fmicb.2020.00817

Martin, W. F. (2022). Narrowing gaps between earth and life. *Proc. Natl. Acad. Sci.* 119:e2216017119. doi: 10.1073/pnas.2216017119

Martin, W., Baross, J., Kelley, D., and Russell, M. J. (2008). Hydrothermal vents and the origin of life. *Nat. Rev. Microbiol.* 6, 805–814. doi: 10.1038/nrmicro1991

Martin, W. F., Bryant, D. A., and Beatty, J. T. (2018). A physiological perspective on the origin and evolution of photosynthesis. *FEMS Microbiol. Rev.* 42, 205–231. doi: 10.1093/femsre/fux056

Martin, W., and Russell, M. J. (2003). On the origins of cells: a hypothesis for the evolutionary transitions from abiotic geochemistry to chemoautotrophic prokaryotes, and from prokaryotes to nucleated cells. *Philos. Trans. R. Soc. Lond. Ser. B Biol. Sci.* 358, 59–85. doi: 10.1098/rstb.2002.1183

Martin, W., and Russell, M. J. (2007). On the origin of biochemistry at an alkaline hydrothermal vent. *Philos. Trans. R. Soc. Lond., B, Biol. Sci.* 362, 1887–1926. doi: 10.1098/rstb.2006.1881

Martin, W. F., and Sousa, F. L. (2016). Early microbial evolution: the age of anaerobes. *Cold Spring Harb. Perspect. Biol.* 8:a018127. doi: 10.1101/cshperspect.a018127

Martin, W. F., and Thauer, R. K. (2017). Energy in ancient metabolism. *Cells* 168, 953–955. doi: 10.1016/j.cell.2017.02.032

Matreux, T., Altaner, B., Raith, J., Braun, D., Mast, C. B., and Gerland, U. (2023). Formation mechanism of thermally controlled pH gradients. *Commun. Phys.* 6:14. doi: 10.1038/s42005-023-01126-y

McCollom, T. M. (2013). Laboratory simulations of abiotic hydrocarbon formation in earth's deep subsurface. *Rev. Mineral. Geochem.* 75, 467–494. doi: 10.2138/rmg.2013.75.15

McCollom, T. M., Klein, F., Solheid, P., and Moskowitz, B. (2020). The effect of pH on rates of reaction and hydrogen generation during serpentinization. *Philos. Trans. R. Soc. A Math. Phys. Eng. Sci.* 378:20180428. doi: 10.1098/rsta.2018.0428

McCollom, T. M., and Seewald, J. S. (2013). Serpentinites, hydrogen, and life. *Elements* 9, 129–134. doi: 10.2113/gselements.9.2.129

Mei, R., Kaneko, M., Imachi, H., and Nobu, M. K. (2023). The origin and evolution of methanogenesis and Archaea are intertwined. *PNAS Nexus* 2:pgad023. doi: 10.1093/pnasnexus/pgad023

Ménez, B., Pisapia, C., Andreani, M., Jamme, F., Vanbellingen, Q. P., Brunelle, A., et al. (2018). Abiotic synthesis of amino acids in the recesses of the oceanic lithosphere. *Nature* 564, 59–63. doi: 10.1038/s41586-018-0684-z

Menon, S., and Ragsdale, S. W. (1996). Unleashing hydrogenase activity in carbon monoxide dehydrogenase/acetyl-CoA synthase and pyruvate: ferredoxin oxidoreductase. *Biochemistry* 35, 15814–15821. doi: 10.1021/bi9615598

Mereschkowsky, K., Kowallik, K. V., and Martin, W. F. (1910). The origin of symbiogenesis: an annotated English translation of Mereschkowsky's 1910 paper on the theory of two plasma lineages. *Curr. Mod. Biol.* 199:104281. doi: 10.1016/j.biosystems.2020.104281

Metcalf, W. W., Griffin, B. M., Cicchillo, R. M., Gao, J., Janga, S. C., Cooke, H. A., et al. (2012). Synthesis of Methylphosphonic acid by marine microbes: a source for methane in the Aerobic Ocean. *Science* 1979, 1104–1107. doi: 10.1126/science.1219875

Miller, S. L. (1953). A production of amino acids under possible primitive earth conditions. *Science* 117, 528–529. doi: 10.1126/science.117.3046.528

Miller, H. M., Chaudhry, N., Conrad, M. E., Bill, M., Kopf, S. H., and Templeton, A. S. (2018). Large carbon isotope variability during methanogenesis under alkaline conditions. *Geochim. Cosmochim. Acta* 237, 18–31. doi: 10.1016/j.gca.2018.06.007

Mitchell, P. (1991). Foundations of vectorial metabolism and osmochemistry. *Biosci. Rep.* 11, 297–346. doi: 10.1007/BF01130212

Mojzsis, S. J., Arrhenius, G., McKeegan, K. D., Harrison, T. M., Nutman, A. P., and Friend, C. R. L. (1996). Evidence for life on earth before 3, 800 million years ago. *Nature* 384, 55–59. doi: 10.1038/384055a0

Möller, F. M., Kriegel, F., Kieß, M., Sojo, V., and Braun, D. (2017). Steep pH gradients and directed colloid transport in a microfluidic alkaline hydrothermal pore. *Angew. Chem. Int. Ed.* 56, 2340–2344. doi: 10.1002/anie.201610781

Monnin, C., Chavagnac, V., Boulart, C., Ménez, B., Gérard, M., Gérard, E., et al. (2014). Fluid chemistry of the low temperature hyperalkaline hydrothermal system of Prony Bay (New Caledonia). *Biogeosciences* 11, 5687–5706. doi: 10.5194/bg-11-5687-2014

Moon, J., Dönig, J., Kramer, S., Poehlein, A., Daniel, R., and Müller, V. (2021). Formate metabolism in the acetogenic bacterium Acetobacterium woodii. *Environ. Microbiol.* 23, 4214–4227. doi: 10.1111/1462-2920.15598

Morrill, P. L., Kuenen, J. G., Johnson, O. J., Suzuki, S., Rietze, A., Sessions, A. L., et al. (2013). Geochemistry and geobiology of a present-day serpentinization site in California: the cedars. *Geochim. Cosmochim. Acta* 109, 222–240. doi: 10.1016/j.gca.2013.01.043

Mottl, M. J., Komor, S. C., Fryer, P., and Moyer, C. L. (2003). Deep-slab fluids fuel extremophilic Archaea on a Mariana forearc serpentinite mud volcano: ocean drilling program leg 195. *Geochem. Geophys. Geosyst.* 4. doi: 10.1029/2003GC000588

Muchowska, K. B., Varma, S. J., Chevallot-Beroux, E., Lethuillier-Karl, L., Li, G., and Moran, J. (2017). Metals promote sequences of the reverse Krebs cycle. *Nat. Ecol. Evol.* 1, 1716–1721. doi: 10.1038/s41559-017-0311-7

Muchowska, K. B., Varma, S. J., and Moran, J. (2020). Nonenzymatic metabolic reactions and Life's origins. *Chem. Rev.* 120, 7708–7744. doi: 10.1021/acs.chemrev.0c00191

Müller, V. (2003). Energy conservation in Acetogenic Bacteria. *Appl. Environ. Microbiol.* 69, 6345–6353. doi: 10.1128/AEM.69.11.6345-6353.2003

Müller, V., Chowdhury, N. P., and Basen, M. (2018). Electron bifurcation: a long-hidden energy-coupling mechanism. *Annu. Rev. Microbiol.* 72, 331–353. doi: 10.1146/annurev-micro-090816-093440

Mumma, M. J., Villanueva, G. L., Novak, R. E., Hewagama, T., Bonev, B. P., DiSanti, M. A., et al. (2009). Strong release of methane on Mars in northern summer 2003. *Science* 1979, 1041–1045. doi: 10.1126/science.1165243

Nealson, K. H. (2005). Hydrogen and energy flow as "sensed" by molecular genetics. *Proc. Natl. Acad. Sci.* 102, 3889–3890. doi: 10.1073/pnas.0500211102

Nelson, D. L., and Cox, M. M. (2021). *Lehninger principles of biochemistry*. *8th* Macmillan Learning. New York, NY.

Nobu, M. K., Nakai, R., Tamazawa, S., Mori, H., Toyoda, A., Ijiri, A., et al. (2023). Unique H2-utilizing lithotrophy in serpentinite-hosted systems. *ISME J.* 17, 95–104. doi: 10.1038/s41396-022-01197-9

Nothaft, D. B., Templeton, A. S., Rhim, J. H., Wang, D. T., Labidi, J., Miller, H. M., et al. (2021). Geochemical, biological, and clumped Isotopologue evidence for substantial microbial methane production under carbon limitation in Serpentinites of the Samail ophiolite, Oman. *J. Geophys. Res. Biogeosci.* 126:e2020JG006025. doi: 10.1029/2020JG006025

Nunes Palmeira, R., Colnaghi, M., Harrison, S. A., Pomiankowski, A., and Lane, N. (2022). The limits of metabolic heredity in protocells. *Proc. R. Soc. B Biol. Sci.* 289:20221469. doi: 10.1098/rspb.2022.1469

Okumura, T., Ohara, Y., Stern, R. J., Yamanaka, T., Onishi, Y., Watanabe, H., et al. (2016). Brucite chimney formation and carbonate alteration at the Shinkai seep field, a

serpentinite-hosted vent system in the southern Mariana forearc. *Geochem. Geophys. Geosyst.* 17, 3775–3796. doi: 10.1002/2016GC006449

Oparin, A. I. (1957). *The origin of life on the earth*. The University of Chicago Chicago, IL.

Oze, C., and Sharma, M. (2005). Have olivine, will gas: Serpentinization and the abiogenic production of methane on Mars. *Geophys. Res. Lett.* 32. doi: 10.1029/2005GL022691

Pasek, M. A. (2008). Rethinking early earth phosphorus geochemistry. *Proc. Natl. Acad. Sci.* 105, 853–858. doi: 10.1073/pnas.0708205105

Pasek, M. A., Harnmeijer, J. P., Buick, R., Gull, M., and Atlas, Z. (2013). Evidence for reactive reduced phosphorus species in the early Archean Ocean. *Proc. Natl. Acad. Sci.* 110, 10089–10094. doi: 10.1073/pnas.1303904110

Pasek, M. A., Omran, A., Feng, T., Gull, M., Lang, C., Abbatiello, J., et al. (2022). Serpentinization as a route to liberating phosphorus on habitable worlds. *Geochim. Cosmochim. Acta* 336, 332–340. doi: 10.1016/j.gca.2022.09.027

Postberg, F., Sekine, Y., Klenner, F., Glein, C. R., Zou, Z., Abel, B., et al. (2023). Detection of phosphates originating from Enceladus's ocean. *Nature* 618, 489–493. doi: 10.1038/s41586-023-05987-9

Postec, A., Quéméneur, M., Bes, M., Mei, N., Benaïssa, F., Payri, C., et al. (2015). Microbial diversity in a submarine carbonate edifice from the serpentinizing hydrothermal system of the Prony Bay (New Caledonia) over a 6-year period. *Front. Microbiol.* 6:857. doi: 10.3389/fmicb.2015.00857

Preiner, M., Igarashi, K., Muchowska, K. B., Yu, M., Varma, S. J., Kleinermanns, K., et al. (2020). A hydrogen-dependent geochemical analogue of primordial carbon and energy metabolism. *Nat. Ecol. Evol.* 4, 534–542. doi: 10.1038/s41559-020-1125-6

Preiner, M., Xavier, J. C., Sousa, F. L., Zimorski, V., Neubeck, A., Lang, S. Q., et al. (2018). Serpentinization: connecting geochemistry, ancient metabolism and industrial hydrogenation. *Life* 8, 1–22. doi: 10.3390/life8040041

Price, R. E., and Giovannelli, D. (2017). *A review of the geochemistry and microbiology of marine shallow-water hydrothermal vents, in Reference module in earth systems and environmental sciences* (Elsevier Amsterdam).

Proskurowski, G., Lilley, M. D., Seewald, J. S., Früh-Green, G. L., Olson, E. J., Lupton, J. E., et al. (2008). Abiogenic hydrocarbon production at lost City hydrothermal field. *Science* 1979, 604–607. doi: 10.1126/science.1151194

Quéméneur, M., Bes, M., Postec, A., Mei, N., Hamelin, J., Monnin, C., et al. (2014). Spatial distribution of microbial communities in the shallow submarine alkaline hydrothermal field of the Prony Bay, New Caledonia. *Environ. Microbiol. Rep.* 6, 665–674. doi: 10.1111/1758-2229.12184

Quéméneur, M., Mei, N., Monnin, C., Postec, A., Guasco, S., Jeanpert, J., et al. (2023). Microbial taxa related to natural hydrogen and methane emissions in serpentinite-hosted hyperalkaline springs of New Caledonia. *Front. Microbiol.* 14:14:1196516. doi: 10.3389/fmicb.2023.1196516

Rabus, R., Hansen, T. A., and Widdel, F. (2006). "Dissimilatory sulfate- and sulfur-reducing prokaryotes," in *The prokaryotes: Volume 2: Ecophysiology and biochemistry*, Martin Dworkin, Stanley Falkow, Eugene Rosenberg, Karl-Heinz Schleifer, Erko Stackebrandt (New York, NY: Springer), 659–768.

Ragsdale, S. W. (2006). "Nickel Enzymes & Cofactors" in *Encyclopedia of inorganic chemistry.*

Rempfert, K. R., Miller, H. M., Bompard, N., Nothaft, D., Matter, J. M., Kelemen, P., et al. (2017). Geological and geochemical controls on subsurface microbial life in the Samail ophiolite, Oman. *Front. Microbiol.* 8:56. doi: 10.3389/fmicb.2017.00056

Reveillaud, J., Reddington, E., McDermott, J., Algar, C., Meyer, J. L., Sylva, S., et al. (2016). Subseafloor microbial communities in hydrogen-rich vent fluids from hydrothermal systems along the mid-Cayman rise. *Environ. Microbiol.* 18, 1970–1987. doi: 10.1111/1462-2920.13173

Righter, K., Humayun, M., and Danielson, L. (2008). Partitioning of palladium at high pressures and temperatures during core formation. *Nat. Geosci.* 1, 321–323. doi: 10.1038/ngeo180

Rona, P. A., Klinkhammer, G., Nelsen, T. A., Trefry, J. H., and Elderfield, H. (1986). Black smokers, massive sulphides and vent biota at the mid-Atlantic ridge. *Nature* 321, 33–37. doi: 10.1038/321033a0

Rose, W. I., Millard, G. A., Mather, T. A., Hunton, D. E., Anderson, B., Oppenheimer, C., et al. (2006). Atmospheric chemistry of a 33–34 hour old volcanic cloud from Hekla volcano (Iceland): insights from direct sampling and the application of chemical box modeling. *J. Geophys. Res. Atmos.* 111. doi: 10.1029/2005JD006872

Rühlemann, M., Ziegler, K., Stupperich, E., and Fuchs, G. (1985). Detection of acetyl coenzyme a as an early CO2 assimilation intermediate in Methanobacterium. *Arch. Microbiol.* 141, 399–406. doi: 10.1007/BF00428856

Russell, M. J., Daniel, R. M., Hall, A. J., and Sherringham, J. A. (1994). A hydrothermally precipitated catalytic Iron Sulphide membrane as a first step toward life. *J. Mol. Evol.* 39, 231–243. doi: 10.1007/BF00160147

Russell, M. J., and Hall, A. J. (1997). The emergence of life from iron monosulphide bubbles at a submarine hydrothermal redox and pH front. *J. Geol. Soc. Lond.* 154, 377–402. doi: 10.1144/gsjgs.154.3.0377

Russell, M. J., Hall, A. J., and Martin, W. (2010). Serpentinization as a source of energy at the origin of life. *Geobiology* 8, 355–371. doi: 10.1111/j.1472-4669.2010.00249.x

Sánchez-Andrea, I., Guedes, I. A., Hornung, B., Boeren, S., Lawson, C. E., Sousa, D. Z., et al. (2020). The reductive glycine pathway allows autotrophic growth of Desulfovibrio desulfuricans. *Nat. Commun.* 11:5090. doi: 10.1038/s41467-020-18906-7

Sasselov, D. D., Grotzinger, J. P., and Sutherland, J. D. (2020). The origin of life as a planetary phenomenon. *Sci. Adv.* 6:eaax3419. doi: 10.1126/sciadv.aax3419

Schimmel, P., Giegé, R., Moras, D., and Yokoyama, S. (1993). An operational RNA code for amino acids and possible relationship to genetic code. *Proc. Natl. Acad. Sci.* 90, 8763–8768. doi: 10.1073/pnas.90.19.8763

Schink, B., and Friedrich, M. (2000). Phosphite oxidation by sulphate reduction. *Nature* 406:37. doi: 10.1038/35017644

Schink, B., Thiemann, V., Laue, H., and Friedrich, M. W. (2002). Desulfotignum phosphitoxidans sp. nov., a new marine sulfate reducer that oxidizes phosphite to phosphate. *Arch. Microbiol.* 177, 381–391. doi: 10.1007/s00203-002-0402-x

Schoell, M. (2022). Methane 13 C/ 12 C isotope analyses with the SAM-EGA pyrolysis instrument suite on Mars curiosity rover: a critical assessment. *Proc. Natl. Acad. Sci. U. S. A.* 119:e2205344119. doi: 10.1073/pnas.2205344119

Schöne, C., Poehlein, A., Jehmlich, N., Adlung, N., Daniel, R., von Bergen, M., et al. (2022). Deconstructing Methanosarcina acetivorans into an acetogenic archaeon. *Proc. Natl. Acad. Sci.* 119:e2113853119. doi: 10.1073/pnas.2113853119

Schönheit, P., Buckel, W., and Martin, W. F. (2016). On the origin of heterotrophy. *Trends Microbiol.* 24, 12–25. doi: 10.1016/j.tim.2015.10.003

Schrenk, M. O., Brazelton, W. J., and Lang, S. Q. (2013). Serpentinization, carbon, and deep life. *Rev. Mineral. Geochem.* 75, 575–606. doi: 10.2138/rmg.2013.75.18

Schuchmann, K., and Müller, V. (2013). Direct and reversible hydrogenation of CO2 to Formate by a bacterial carbon dioxide reductase. *Science* 1979, 1382–1385. doi: 10.1126/science.1244758

Schuchmann, K., and Müller, V. (2014). Autotrophy at the thermodynamic limit of life: a model for energy conservation in acetogenic bacteria. *Nat. Rev. Microbiol.* 12, 809–821. doi: 10.1038/nrmicro3365

Schulte, M., Blake, D., Hoehler, T., and Mccollom, T. (2006). Serpentinization and its implications for life on the early earth and Mars. *Astrobiology* 6, 364–376. doi: 10.1089/ast.2006.6.364

Schwartz, A. W. (2006). Phosphorus in prebiotic chemistry. *Philos. Trans. R. Soc. Lond., B, Biol. Sci.* 361, 1743–1749. doi: 10.1098/rstb.2006.1901

Sebban-Kreuzer, C., Dolla, A., and Guerlesquin, F. (1998). The formate dehydrogenase-cytochrome c553 complex from Desulfovibrio vulgaris Hildenborough. *Eur. J. Biochem.* 253, 645–652. doi: 10.1046/j.1432-1327.1998.2530645.x

Seyfried, W. E., Pester, N. J., Tutolo, B. M., and Ding, K. (2015). The lost City hydrothermal system: constraints imposed by vent fluid chemistry and reaction path models on subseafloor heat and mass transfer processes. *Geochim. Cosmochim. Acta* 163, 59–79. doi: 10.1016/j.gca.2015.04.040

Shang, X., Huang, R., and Sun, W. (2023a). An ammonia-methane dominated atmosphere in the hadean eon. *Solid Earth Sci.* 8, 191–194. doi: 10.1016/j.sesci.2023.05.005

Shang, X., Huang, R., and Sun, W. (2023b). Formation of ammonia through serpentinization in the hadean eon. *Sci. Bull. (Beijing)* 68, 1109–1112. doi: 10.1016/j.scib.2023.04.038

Sherwood Lollar, B., Heuer, V. B., McDermott, J., Tille, S., Warr, O., Moran, J. J., et al. (2021). A window into the abiotic carbon cycle – acetate and formate in fracture waters in 2.7 billion year-old host rocks of the Canadian shield. *Geochim. Cosmochim. Acta* 294, 295–314. doi: 10.1016/j.gca.2020.11.026

Shima, S., Schick, M., and Tamura, H. (2011). "Chapter seven - preparation of [Fe]-hydrogenase from methanogenic Archaea" in *Methods in methane metabolism, part a methods in enzymology*. eds. A. C. Rosenzweig and S. W. Ragsdale (Cambridge, MA: Academic Press), 119–137.

Silverstein, T. P. (2014). An exploration of how the thermodynamic efficiency of bioenergetic membrane systems varies with c-subunit stoichiometry of F1F0 ATP synthases. *J. Bioenerg. Biomembr.* 46, 229–241. doi: 10.1007/s10863-014-9547-y

Sleep, N. H. (2016). Asteroid bombardment and the core of Theia as possible sources for the Earth's late veneer component. *Geochem. Geophys. Geosyst.* 17, 2623–2642. doi: 10.1002/2016GC006305

Sleep, N. H., Bird, D. K., and Pope, E. C. (2011). Serpentinite and the dawn of life. *Philos. Trans. R. Soc. Lond., B, Biol. Sci.* 366, 2857–2869. doi: 10.1098/rstb.2011.0129

Sleep, N. H., Meibom, A., Fridriksson, T., Coleman, R. G., and Bird, D. K. (2004). H 2-rich fluids from serpentinization: geochemical and biotic implications. *PNAS* 101, 12818–12823. doi: 10.1073/pnas.0405289101

Sojo, V., Ohno, A., McGlynn, S. E., Yamada, Y. M. A., and Nakamura, R. (2019). Microfluidic reactors for carbon fixation under ambient-pressure alkaline-hydrothermal-vent conditions. *Life* 9:16. doi: 10.3390/life9010016

Sossi, P. A., Burnham, A. D., Badro, J., Lanzirotti, A., Newville, M., and O'Neill, H. S. (2020). Redox state of earth’ s magma ocean and its Venus-like early atmosphere. *Sci. Adv.* 6:eabd 1387. doi: 10.1126/sciadv.abd1387

Sousa, F. L., Hordijk, W., Steel, M., and Martin, W. F. (2015). Autocatalytic sets in E. coli metabolism. *J. Syst. Chem.* 6:4. doi: 10.1186/s13322-015-0009-7

Stams, A. J. M., and Plugge, C. M. (2009). Electron transfer in syntrophic communities of anaerobic bacteria and archaea. *Nat. Rev. Microbiol.* 7, 568–577. doi: 10.1038/nrmicro2166

Steele, A., Benning, L. G., Wirth, R., Schreiber, A., Araki, T., McCubbin, F. M., et al. (2022). Organic synthesis associated with serpentinization and carbonation on early Mars. *Science* 1979, 172–177. doi: 10.1126/science.abg7905

Suda, K., Gilbert, A., Yamada, K., Yoshida, N., and Ueno, Y. (2017). Compound– and position–specific carbon isotopic signatures of abiogenic hydrocarbons from on–land serpentinite–hosted Hakuba Happo hot spring in Japan. *Geochim. Cosmochim. Acta* 206, 201–215. doi: 10.1016/j.gca.2017.03.008

Suda, K., Ueno, Y., Yoshizaki, M., Nakamura, H., Kurokawa, K., Nishiyama, E., et al. (2014). Origin of methane in serpentinite-hosted hydrothermal systems: the CH4–H2–H2O hydrogen isotope systematics of the Hakuba Happo hot spring. *Earth Planet. Sci. Lett.* 386, 112–125. doi: 10.1016/j.epsl.2013.11.001

Suzuki, S., Ishii, S., Hoshino, T., Rietze, A., Tenney, A., Morrill, P. L., et al. (2017). Unusual metabolic diversity of hyperalkaliphilic microbial communities associated with subterranean serpentinization at the cedars. *ISME J.* 11, 2584–2598. doi: 10.1038/ismej.2017.111

Suzuki, S., Nealson, K. H., and Ishii, S. (2018). Genomic and in-situ transcriptomic characterization of the candidate phylum NPL-UPL2 from highly alkaline highly reducing Serpentinized groundwater. *Front. Microbiol.* 9:3141. doi: 10.3389/fmicb.2018.03141

Takai, K., Nakamura, K., Toki, T., Tsunogai, U., Miyazaki, M., Miyazaki, J., et al. (2008). Cell proliferation at 122°C and isotopically heavy CH 4 production by a hyperthermophilic methanogen under high-pressure cultivation. *PNAS* 105, 10949–10954. doi: 10.1073/pnas.0712334105

Tashiro, T., Ishida, A., Hori, M., Igisu, M., Koike, M., Méjean, P., et al. (2017). Early trace of life from 3.95 Ga sedimentary rocks in Labrador, Canada. *Nature* 549, 516–518. doi: 10.1038/nature24019

Thauer, R. K., Kaster, A.-K., Seedorf, H., Buckel, W., and Hedderich, R. (2008). Methanogenic archaea: ecologically relevant differences in energy conservation. *Nat. Rev. Microbiol.* 6, 579–591. doi: 10.1038/nrmicro1931

Toner, J. D., and Catling, D. C. (2020). A carbonate-rich lake solution to the phosphate problem of the origin of life. *Proc. Natl. Acad. Sci.* 117, 883–888. doi: 10.1073/pnas.1916109117

Tran, Q. H., and Unden, G. (1998). Changes in the proton potential and the cellular energetics of Escherichia coli during growth by aerobic and anaerobic respiration or by fermentation. *Eur. J. Biochem.* 251, 538–543. doi: 10.1046/j.1432-1327.1998.2510538.x

Trutschel, L. R., Chadwick, G. L., Kruger, B., Blank, J. G., Brazelton, W. J., Dart, E. R., et al. (2022). Investigation of microbial metabolisms in an extremely high pH marine-like terrestrial serpentinizing system: Ney Springs. *Sci. Total Environ.* 836:155492. doi: 10.1016/j.scitotenv.2022.155492

Tutolo, B. M., and Tosca, N. J. (2023). Observational constraints on the process and products of Martian serpentinization. *Sci. Adv.* 9:eadd8472. doi: 10.1126/sciadv.add8472

Twing, K. I., Ward, L. M., Kane, Z. K., Sanders, A., Price, R. E., Pendleton, H. L., et al. (2022). Microbial ecology of a shallow alkaline hydrothermal vent: Strýtan hydrothermal field, Eyjafördur, northern Iceland. *Front. Microbiol.* 13:960335. doi: 10.3389/fmicb.2022.960335

Vance, S. D., and Daswani, M. (2020). Serpentinite and the search for life beyond earth. *Philos. Trans. R. Soc. A Math. Phys. Eng. Sci.* 378:20180421. doi: 10.1098/rsta.2018.0421

Vance, S. D., Hand, K. P., and Pappalardo, R. T. (2016). Geophysical controls of chemical disequilibria in Europa. *Geophys. Res. Lett.* 43, 4871–4879. doi: 10.1002/2016GL068547

Vance, S., Harnmeijer, J., Kimura, J., Hussmann, H., Demartin, B., and Brown, J. M. (2007). Hydrothermal systems in small ocean planets. *Astrobiology* 7, 987–1005. doi: 10.1089/ast.2007.0075

Vanysek, P. (2000). "Electrochemical series" in *Handbook of chemistry and physics* (Boca Raton, FL: CRC Press), 23–33.

Vrtis, J. M., White, A. K., Metcalf, W. W., and van der Donk, W. A. (2001). Phosphite dehydrogenase: an unusual phosphoryl transfer reaction. *J. Am. Chem. Soc.* 123, 2672–2673. doi: 10.1021/ja004301k

Wagner, T., Ermler, U., and Shima, S. (2016). The methanogenic CO2 reducing-and-fixing enzyme is bifunctional and contains 46 [4Fe-4S] clusters. *Science* 1979, 114–117. doi: 10.1126/science.aaf9284

Waite, J. H., Glein, C. R., Perryman, R. S., Teolis, B. D., Magee, B. A., Miller, G., et al. (2017). Cassini finds molecular hydrogen in the Enceladus plume: evidence for hydrothermal processes. *Science* 356, 155–159. doi: 10.1126/science.aai8703

Walker, J. E. (2013). The ATP synthase: the understood, the uncertain and the unknown. *Biochem. Soc. Trans.* 41, 1–16. doi: 10.1042/BST20110773

Walker, J. E., Saraste, M., Runswick, M. J., and Gay, N. J. (1982). Distantly related sequences in the alpha- and beta-subunits of ATP synthase, myosin, kinases and other ATP-requiring enzymes and a common nucleotide binding fold. *EMBO J.* 1, 945–951. doi: 10.1002/j.1460-2075.1982.tb01276.x

Wang, S., Huang, H., Kahnt, J., and Thauer, R. K. (2013). Clostridium acidurici Electron-Bifurcating Formate Dehydrogenase. *Appl. Environ. Microbiol.* 79, 6176–6179. doi: 10.1128/AEM.02015-13

Wang, X., Ouyang, Z., Zhuo, S., Zhang, M., Zheng, G., and Wang, Y. (2014). Serpentinization, abiogenic organic compounds, and deep life. *Sci. China Earth Sci.* 57, 878–887. doi: 10.1007/s11430-014-4821-8

Weiss, M. C., Preiner, M., Xavier, J. C., Zimorski, V., and Martin, W. F. (2018). The last universal common ancestor between ancient earth chemistry and the onset of genetics. *PLoS Genet.* 14, 1–19. doi: 10.1371/journal.pgen.1007518

Weiss, M. C., Sousa, F. L., Mrnjavac, N., Neukirchen, S., Roettger, M., Nelson-Sathi, S., et al. (2016). The physiology and habitat of the last universal common ancestor. *Nat. Microbiol.* 1, 1–8. doi: 10.1038/nmicrobiol.2016.116

Whicher, A., Camprubi, E., Pinna, S., Herschy, B., and Lane, N. (2018). Acetyl phosphate as a primordial energy currency at the origin of life. *Orig. Life Evol. Biosph.* 48, 159–179. doi: 10.1007/s11084-018-9555-8

Williams, T. A., Szöllősi, G. J., Spang, A., Foster, P. G., Heaps, S. E., Boussau, B., et al. (2017). Integrative modeling of gene and genome evolution roots the archaeal tree of life. *Proc. Natl. Acad. Sci.* 114, E4602–E4611. doi: 10.1073/pnas.1618463114

Wimmer, J. L. E., Vieira, A. D. N., Xavier, J. C., Kleinermanns, K., Martin, W. F., and Preiner, M. (2021a). The autotrophic core: an ancient network of 404 reactions converts H2, CO2, and NH3 into amino acids, bases, and cofactors. *Microorganisms* 9, 1–16. doi: 10.3390/microorganisms9020458

Wimmer, J. L. E., Xavier, J. C., Vieira, A., Pereira, D. P. H., Leidner, J., Sousa, F. L., et al. (2021b). Energy at origins: favorable thermodynamics of biosynthetic reactions in the last universal common ancestor (LUCA). *Front. Microbiol.* 12:793664. doi: 10.3389/fmicb.2021.793664

Xavier, J. C., Gerhards, R. E., Wimmer, J. L. E., Brueckner, J., Tria, F. D. K., and Martin, W. F. (2021). The metabolic network of the last bacterial common ancestor. *Commun. Biol.* 4:413. doi: 10.1038/s42003-021-01918-4

Xavier, J. C., Hordijk, W., Kauffman, S., Steel, M., and Martin, W. F. (2020). Autocatalytic chemical networks at the origin of metabolism. *Proc. R. Soc. B Biol. Sci.* 287:20192377. doi: 10.1098/rspb.2019.2377

Xavier, J. C., and Kauffman, S. (2022). Small-molecule autocatalytic networks are universal metabolic fossils. *Philos. Trans. R. Soc. A Math. Phys. Eng. Sci.* 380:20210244. doi: 10.1098/rsta.2021.0244

Yi, J., Kaur, H., Kazöne, W., Rauscher, S. A., Gravillier, L.-A., Muchowska, K. B., et al. (2022). A nonenzymatic analog of pyrimidine nucleobase biosynthesis. *Angew. Chem. Int. Ed.* 61:e202117211. doi: 10.1002/anie.202117211

Zahnle, K., Arndt, N., Cockell, C., Halliday, A., Nisbet, E., Selsis, F., et al. (2007). Emergence of a habitable planet. *Space Sci. Rev.* 129, 35–78. doi: 10.1007/s11214-007-9225-z

Zahnle, K. J., Lupu, R., Catling, D. C., and Wogan, N. (2020). Creation and evolution of impact-generated reduced atmospheres of early earth. *Planet. Sci. J.* 1:11. doi: 10.3847/PSJ/ab7e2c

Zinder, S. H. (1994). "Syntrophic acetate oxidation and 'reversible acetogenesis'" in *Acetogenesis*. ed. H. L. Drake (New York, NJ: Springer), 386–415.

Zolotov, M. Y. (2007). An oceanic composition on early and today's Enceladus. *Geophys. Res. Lett.* 34:L23203. doi: 10.1029/2007GL031234

Frontiers in Microbiology

Explores the habitable world and the potential of microbial life

The largest and most cited microbiology journal which advances our understanding of the role microbes play in addressing global challenges such as healthcare, food security, and climate change.

Discover the latest Research Topics

See more →

Frontiers

Avenue du Tribunal-Fédéral 34
1005 Lausanne, Switzerland
frontiersin.org

Contact us

+41 (0)21 510 17 00
frontiersin.org/about/contact